MCEER
EARTHQUAKE ENGINEERING TO EXTREME EVENTS

ISSN 1520-295X

Seismic Analysis of Multi-story Unreinforced Masonry Buildings with Flexible Diaphragms

by
Juan Aleman, Gilberto Mosqueda and Andrew Whittaker



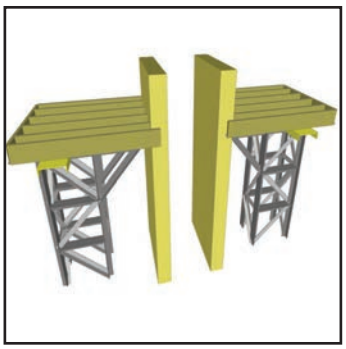


Technical Report MCEER-15-0001

June 12, 2015

This research was conducted at the University at Buffalo, State University of New York,
and was supported by MCEER Thrust Area 2, Sustainable and Resilient Buidlings.

NOTICE

This report was prepared by the University at Buffalo, State University of New York, as a result of research sponsored by MCEER. Neither MCEER, associates of MCEER, its sponsors, the University at Buffalo, State University of New York, nor any person acting on their behalf:

a. makes any warranty, express or implied, with respect to the use of any information, apparatus, method, or process disclosed in this report or that such use may not infringe upon privately owned rights; or

b. assumes any liabilities of whatsoever kind with respect to the use of, or the damage resulting from the use of, any information, apparatus, method, or process disclosed in this report.

Any opinions, findings, and conclusions or recommendations expressed in this publication are those of the author(s) and do not necessarily reflect the views of MCEER, or other sponsors.

Seismic Analysis of Multi-story Unreinforced Masonry Buildings with Flexible Diaphragms

by

Juan Aleman,[1] Gilberto Mosqueda[2] and Andrew Whittaker[3]

Publication Date: June 12, 2015
Submittal Date: November 19, 2014

Technical Report MCEER-15-0001

MCEER Thrust Area 2, Sustainable and Resilient Buildings

1 Engineer, Structures, Arup, Los Angeles and former Graduate Student, Department of Civil, Structural and Environmental Engineering, University at Buffalo, State University of New York
2 Associate Professor, Department of Structural Engineering, University of California, San Diego
3 Professor and Chair, Department of Civil, Structural and Environmental Engineering, University at Buffalo, State University of New York

MCEER
University at Buffalo, State University of New York
212 Ketter Hall, Buffalo, NY 14260
E-mail: *mceer@buffalo.edu*; WWW Site: *http://mceer.buffalo.edu*

PREFACE

MCEER is a national center of excellence dedicated to the discovery and development of new knowledge, tools and technologies that equip communities to become more disaster resilient in the face of earthquakes and other extreme events. MCEER accomplishes this through a system of multidisciplinary, multi-hazard research, education and outreach initiatives.

Headquartered at the University at Buffalo, State University of New York, MCEER was originally established by the National Science Foundation (NSF) in 1986, as the first National Center for Earthquake Engineering Research (NCEER). In 1998, it became known as the Multidisciplinary Center for Earthquake Engineering Research (MCEER), from which the current name, MCEER, evolved.

Comprising a consortium of researchers and industry partners from numerous disciplines and institutions throughout the United States, MCEER's mission has expanded from its original focus on earthquake engineering to one which addresses the technical and socioeconomic impacts of a variety of hazards, both natural and man-made, on critical infrastructure, facilities, and society.

MCEER investigators derive support from the State of New York, National Science Foundation, Federal Highway Administration, National Institute of Standards and Technology, Department of Homeland Security/Federal Emergency Management Agency, other state governments, academic institutions, foreign governments and private industry.

The main goal of this study was to develop simulation capabilities supported by experimental testing to evaluate the seismic performance of typical unreinforced masonry buildings with flexible diaphragms located in NYC. Simplified nonlinear macro-models of wood diaphragms, masonry walls and floor-to-wall connections were developed and validated individually using data from past experiments. The models are implemented in both commercial and research software to demonstrate their practical use. In particular, a new approach for modeling flexible diaphragms is proposed that is shown to provide similar accuracy to detailed finite element models at a fraction of the computation cost. The models developed were also validated at the system level, through shake table testing of two full-scale specimens conducted as part of this study. The specimens were designed and constructed to represent the expected loading conditions of a central portion of a one-story URM building and constructed of materials representative of older masonry construction. The tests provide a unique data set that captures the interaction between flexible floors, out-of-plane walls and their connections at full scale.

ABSTRACT

Studies regarding the regional seismicity of New York City (NYC) indicate that earthquakes of magnitude greater than or equal to 5 have a 20-40% probability of occurring in a 50 year period. Considering that more than 50% of the large population of the region (19.1 million) is living in an area where 80% of the buildings are of old Unreinforced Masonry (URM) construction, it is likely that even a moderate earthquake could have critical consequences on public safety and the economy of this area.

The main goal of this study was to develop simulation capabilities supported by experimental testing to evaluate the seismic performance of typical unreinforced masonry buildings with flexible diaphragms located in NYC. Simplified nonlinear macro-models of wood diaphragms, masonry walls and floor-to-wall connections were developed and validated individually using data from past experiments. The models are implemented in both commercial and research software to demonstrate their practical use. In particular, a new approach for modeling flexible diaphragms is proposed that is shown to provide similar accuracy to detailed finite element models at a fraction of the computation cost. The models developed were also validated as at the system level, through shake table testing of two full-scale specimens conducted as part of this study. The specimens were designed and constructed to represent the expected loading conditions of a central portion of a one-story URM building and constructed of materials representative of older masonry construction. The tests provide a unique data set that captures the interaction between flexible floors, out-of-plane walls and their connections at full scale.

The validated macro-models can be used for performance-based seismic assessment of unreinforced masonry buildings in NYC and elsewhere. To demonstrate their use, preliminary studies were conducted to develop out-of-plane URM fragility curves, a building-specific collapse fragility function, and to estimate the seismic response of the building when subjected to a ground shaking intensity similar to the 2011 Virginia Earthquake. The probabilistic framework and new performance definitions provided by the FEMA P58 project were used to conduct a performance-based seismic assessment for an archetype unreinforced masonry building in New York City with an emphasis on out-of-plane behavior. This preliminary study served to demonstrate the applicability of the proposed models for applications in performance-based design.

ACKNOWLEDGEMENTS

Financial support for this research was provided by the Multidisciplinary Center for Earthquake Engineering Research, Buffalo, NY and partial funding to the first author was also provided by the US Fulbright Scholarship Program. Their support is gratefully acknowledged. The experimental portion of this research was benefited from donations of material and workmanship by The International Masonry Institute, John H. Black Co. and Bricklayers of Local 3 Buffalo. Their support is deeply appreciated. The authors also thank Dr. David Peralta and Mr. Michael Schuller for providing experimental data for wood diaphragms and in-situ flatjack tests, respectively.

TABLE OF CONTENTS

LIST OF FIGURES

LIST OF TABLES

SECTION 1
INTRODUCTION

1.1 Motivation

Unreinforced masonry (URM) buildings are one of the most seismically vulnerable building types in the world (Spence 2007). The URM building inventory accounts for more than 60% of the buildings in some countries like Italy, Mexico, Indonesia and Australia (Jaiswal and Wald 2008).

Studies conducted by Tantala et al. (2003) regarding the regional seismicity of New York City (NYC) indicate that earthquakes of magnitude greater than or equal to 5 have a 20-40% probability of occurring in a 50 year period (See Figure 1-1). Considering that more than 50% of the total population of the region (19.1 million) is living in an area where 80% of the buildings are of old URM construction, it is likely that even a moderate earthquake could have critical consequences on public safety and the economy of this area.

The consequences of a moderate earthquake in NYC can be estimated by the FEMA P-58 seismic assessment guidelines (FEMA P58-1 2012), which can be used to evaluate in a more rational way the performance of URM buildings when subjected to future earthquake shaking. Also, FEMA P-58 uses performance measures that can be easily understood by owners and other decision-makers (i.e. number of casualties, downtime and repair costs). Moreover, it is easier to show the impact of cost-effective retrofitting methods if an increased performance level is desired.

The next generation of performance based seismic design guidelines require well-validated, computationally efficient numerical models that can be used to conduct numerous response-history analyses. A thorough review of the literature reveals that conducting reliable seismic analysis of multi-story URM buildings remains a challenging task within the earthquake and structural engineering field. Although several numerical methods have been proposed, the combination of highly nonlinear material and structural component behavior, complex geometric configurations and lack of experimental data makes the problem difficult to solve. Even more, as of today there are no reported attempts to capture the nonlinear seismic response of full multi-story URM buildings with flexible diaphragms at the system level. In order to conduct such

studies, there is a need to develop and validate numerical macro-models of the diaphragm, masonry wall and floor-to wall connections able to capture the full dynamic characteristics at the system level within reasonable analysis time.

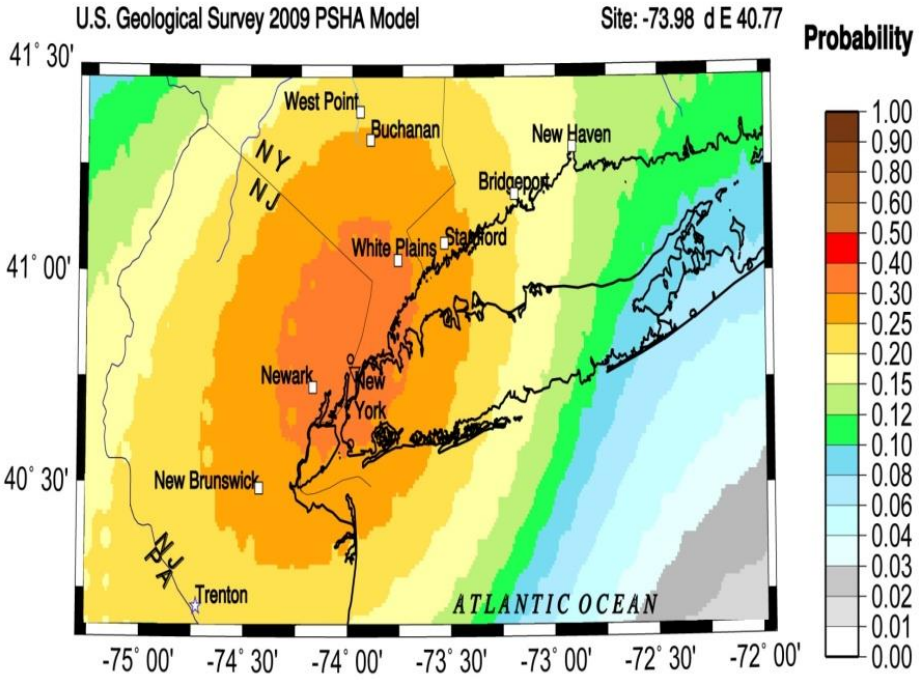

Figure 1-1 Probability of having an earthquake with Mw>5 in NYC (USGS 2009)

1.2 Research Objectives

The main goal of this study is to develop and validate numerical macro-models to evaluate the seismic performance of typical URM buildings located in New York City. Simplified numerical macro-models of wood diaphragms, masonry walls and floor-to-wall connections are first developed and validated individually using data from past experiments. These models are also validated at the system level, through shake table testing of two full-scale specimens of wall slices with flexible diaphragms conducted as part of this study. The specimens are designed and constructed to simulate the conditions expected in the central portion of a one-story URM building.

The specific objectives of this report are summarized as follow:

- Collaborate with the NYC structural engineering community to address the lack of knowledge in modeling and analyzing older URM buildings under seismic loads.

- Understand the building inventory in NYC, develop a representative archetype building and identify critical vulnerabilities of structural components.
- Propose new simplified, reliable and robust macro-models to address critical vulnerabilities previously identified. These models must be well-validated analytical tools accessible to practicing engineers and the design community.
- Conduct material tests on actual URM specimens from NYC buildings, to better understand the material properties that should be used in laboratory testing.
- Perform shake table tests to better understand the seismic behavior and interaction between flexible diaphragms and out of plane walls, which are some of least understood components.
- Assess the robustness of the numerical models under moderate and strong ground motion based on the shake table test data.
- Initiate preliminary studies to conduct an intensity-based assessment of the archetype URM building using the FEMA P-58 methodology and develop expected dollar and casualty loss for NYC.

1.3 Report Outline

This report is organized in ten sections and three appendices. Following this introductory section, Section 2 presents a review of the literature focusing on seismic behavior of low-rise multi-story URM buildings with flexible diaphragms. Theoretical, actual and experimental global response of this type of buildings during earthquake loading is discussed.

After characterizing the building stock in New York City, a representative URM building is identified in Section 3. Structural vulnerabilities for the archetype URM building are also defined and discussed. Flexible diaphragms, floor-to-wall connections and out-of-plane masonry walls are identified as the main structural components requiring further investigations to better understand their seismic behavior and develop reliable models.

In Section 4, suitable numerical models of wood diaphragms with similar structural characteristics to those found in older URM buildings in NYC are identified and evaluated for performance-based seismic design applications. The models were implemented in SAP2000 and OpenSees. A novel 3D nonlinear macro-model of the diaphragm, able to capture the full dynamic characteristic while significantly reducing analysis time is proposed and validated.

Comparison with previous numerical models and key experimental results from the literature are provided.

A 3D nonlinear macro-model of a typical floor-to-wall connection in URM buildings is proposed and validated in Section 5. The SAP2000 model accounts for friction, impact and potential nonlinear behavior of anchors or nails. The model is validated with previous experiments available in the literature.

In Section 6, simplified, robust non-linear macro-models for in-plane and out-of-plane walls were developed in SAP2000 and validated using previous experiments found in the literature. The numerical models are suitable for pushover or nonlinear response history analysis. These models can be easily combined with the models developed in Section 4 and 5, to analyze multi-story URM buildings subjected to seismic loads.

The experimental program is presented in Section 7 and 8. A full scale structural system including a simulated flexible wood diaphragm with realistic wood-to-wall connections, and out-of-plane masonry walls is designed, constructed and tested until collapse under seismic loads. The results of these tests are used to refine and validate the computer models developed in previous sections.

In Section 7, material characterization tests are conducted to determine all mechanical properties for masonry units, mortar and masonry walls that better represent actual conditions of the building stock in the New York City region. In Section 8, the data obtained from Section 7 is used as a reference to build two full-scale masonry walls that represent the central portion of a first story URM building in NYC. The walls are tested for out-of-plane dynamic loads using a shake table in the Structural Engineering and Earthquake Simulation Laboratory (SEESL) of the University at Buffalo.

In Section 9, a preliminary performance-based seismic assessment is conducted for an archetype URM building in NYC with an emphasis on out-of-plane behavior. The validated numerical models are used to develop out-of-plane URM fragility curves, a building-specific collapse fragility function, and estimate the seismic response of the building when subjected to moderate intensity ground shaking. The probabilistic framework and new performance definitions provided by the FEMA P58 project are used to conduct the assessment. Sample results are

presented from the performance calculations that illustrate the probable loss and repair time for the archetype building.

Section 10 gives an overview of the main original contributions, provides a summary of each section and highlights potential future work. Alternative modeling techniques developed in Ruamoko, OpenSees and SAP2000 for in-plane walls and further applications are provided in Appendix A and B. The results of preliminary numerical analysis in SAP2000 and LS-DYNA for two-way bending behavior of URM walls is presented in Appendix C. A set of structural drawings of the test specimens are included in Appendix D.

SECTION 2
BACKGROUND ON SEISMIC BEHAVIOR OF URM

The seismic behavior of URM has been the focus of a large number of studies throughout the world, due to its high use and vulnerability (Spence 2007). In developing a comprehensive research program for seismic assessment of URM masonry structures, it is important to consider all fundamental aspects of URM building response. The seismic assessment of an URM building involves an effective combination of experimental testing, numerical analysis and in-situ testing.

Research oriented testing is required to define material properties and structural components seismic behavior and to assess the global response accounting for the interaction between different structural members. Also, it provides necessary data for the development of analytical or numerical models.

Materials tests are typically conducted to determine compression strength of units, compressive strength of mortar, joint shear strength/tensile strength, interface friction coefficient, and compression strength of masonry prisms. Structural component tests are needed to characterize the in-plane and out-of-plane behavior of masonry walls subjected to both static and dynamic loads. Flexible diaphragms also need to be investigated, along with the connection between diaphragms and masonry walls. Different wall aspect and slenderness ratios, boundary conditions, and loading protocols must be considered. Structural system tests such as shaking table tests and static tests are both required for a complete understanding of the performance of complex structures.

Numerical simulation is essential to extend the scope of the research program, conduct seismic risk assessment, sensitivity and reliability analysis.

Finally, in-situ testing is important to assess the condition of existing buildings, define critical parameters of masonry behavior and characterize the material and component properties. This general framework for testing of masonry structures for seismic assessment is summarized in Table 2-1 but extensively discussed in Calvi et al. (1996).

Table 2-1 General framework for seismic assessment of URM buildings (Calvi et al. 1996)

Laboratory Testing	Material tests	• Compression strength of units • Compression strength of mortar • Joint shear strength/tensile strength • Friction coefficient • Compression strength of masonry prisms
	Structural component tests	• In-Plane walls • Out-of-Plane walls • Diaphragms • Connections
	Structural system tests	• Quasi-static • Pseudo-dynamic • Shake table
Numerical Simulation	Micro-scale models	• Discrete element • Rigid body spring • Interface elements • Homogenization
	Macro-Scale models	• Equivalent frame • Fiber elements • Zero-length springs • Rigid body models
	Analytical models	• Limit analysis • Code based equations • Empirical equations
In-Situ Testing	Material tests	• Flatjack test • In-place shear triplet test
	Non-destructive techniques	• Acoustic emission • Ultrasonic pulse velocity • Spectroscopy/Photogrammetry • Lasser Doppler Vibrometer • Thermography

The main goal of this section is to acquire a deeper understanding on the global seismic behavior of multi-story URM buildings with flexible diaphragms. To this end, the theoretical, actual and experimental response of this type of buildings during earthquakes loading is discussed in the following sections. Additional background on research conducted on materials and structural components is provided in subsequent sections

2.1 Theoretic Seismic Behavior of URM Medium-rise Buildings

When studying dynamics of multi-story buildings, it is commonly assumed that lateral deformation is taken by flexible columns, whereas floor and beams are infinitely stiff in flexure. As shown in Figure 2-1, in this so-called shear type building model, all the mass of each story is lumped at the floor level and the columns are considered massless. These simple assumptions have been proven to be convenient to develop the equations of motions of MDOF systems and determine its dynamic response (Chopra 2007).

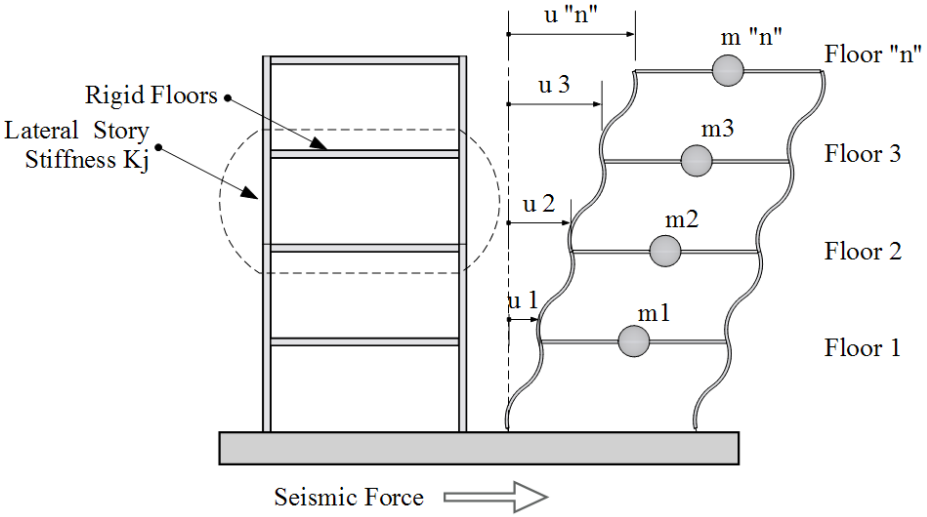

Figure 2-1 Typical idealization of MDOF systems (Chopra 2007)

Unfortunately, URM buildings cannot be idealized in that way due to its fundamentally different structure. In addition to the brittle nature of bricks and mortar, typical URM buildings have stiff walls to resist lateral forces and flexible diaphragms as illustrated in Figure 2-2. Floor mass is not significant when compared to wall mass and therefore, it is not appropriate to lump it at each floor level. A better formulation, for instance, would estimate the seismic response based on systems with distributed mass and elasticity (Cohen et al. 2004).

Due to the URM building characteristics, several complementary formulations have been proposed along the years to better understand its seismic response. A summary of most relevant formulations is discussed in the following section.

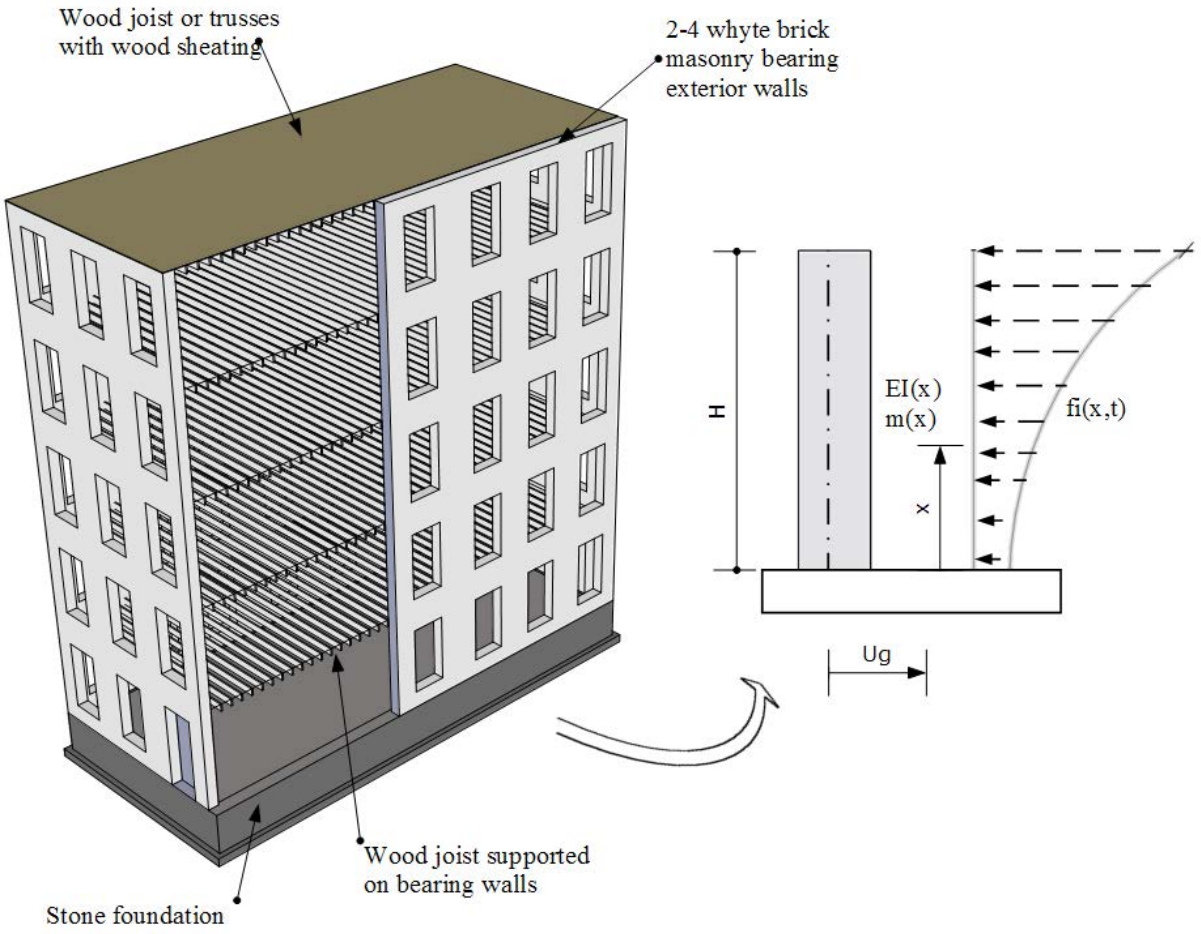

Figure 2-2 Typical URM building components and distributed mass and elasticity idealization (Adapted from FEMA 547 and Chopra 2007)

Although URM masonry research in North America has been published since early 1900's (Allen 1958; Duke 1951), first efforts to provide a comprehensive description of the URM buildings seismic behavior date back to the 1980's, when the Agbabian Associates, S.B. Barnes and Associates, and Kariotis and Associates (ABK) proposed a methodology to mitigate the seismic hazard in this type of buildings (ABK 1984). In short, the methodology suggests that when floor diaphragms are seismically excited by the end-walls parallel to the earthquake direction, perpendicular walls accelerate and vibrate in the out-of-plane direction. A visual representation of this behavior considering an archetype building is shown in Figure 2-3. As indicated by Bruneau (1994b), this particular seismic behavior implies several major assumptions. First, note that the ground motion is assumed to be transmitted unmodified to each

floor by the end-walls, which are in turn assumed to be infinitely rigid in-plane. For multi-story buildings with significant amount of openings this may not be the case. Second, a perfect tie between walls and diaphragms is considered so that an effective transfer of forces and accelerations is guaranteed and out-of-plane collapse is prevented during an earthquake.

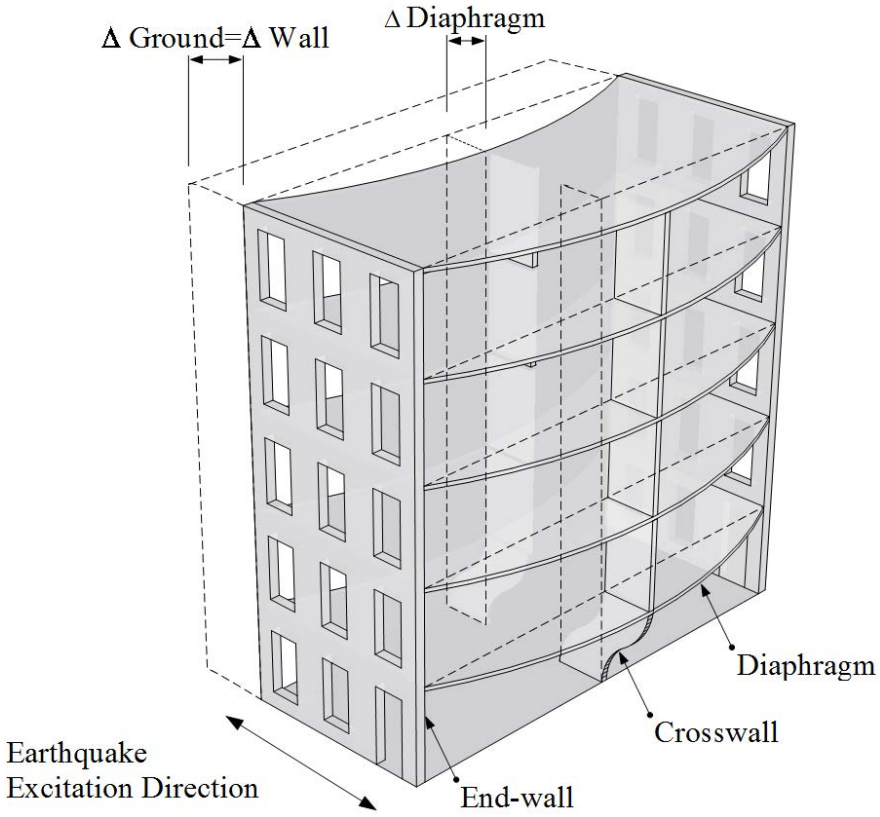

Figure 2-3 ABK behavior philosophy on URM buildings in New York City

In these conditions, it is clear that the dynamic characteristic of diaphragms play a fundamental role since they control the final response of out-of-plane walls and the strength demands of the wall to floor connection.

A more comprehensive description of the seismic response of URM buildings during severe earthquakes was provided by Paulay and Priestley (1992). As shown in Figure 2-4, the in-plane walls respond to the ground acceleration due to its larger stiffness in the earthquake direction. They vibrate depending on the building total mass. Then, in-plane accelerations are transmitted to the floor diaphragms which deforms and finally deliver modified accelerations to the out-of-plane walls. These accelerations could have different magnitude, and as pointed out by Paulay and Priestley, they may be out of phase with significantly different frequency composition.

A conservative solution for estimating peak floor level accelerations was proposed in terms of response spectra. Using this approach it was found that in general, resonance response could occur at in-plane walls with potential high amplifications. In particular, the roof level walls are the most vulnerable since they will be subjected to the maximum accelerations.

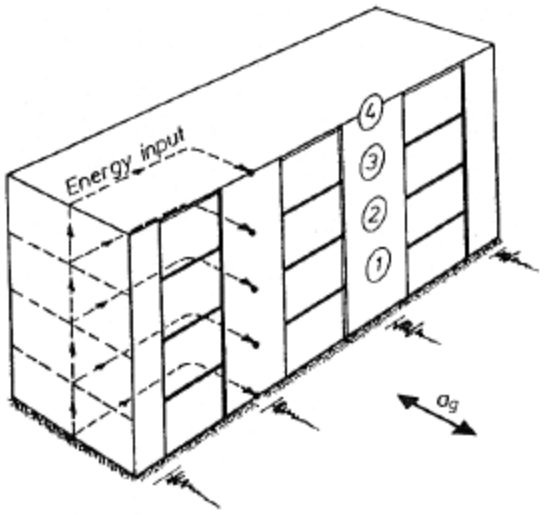

(a) Seismic load path for unreinforced masonry building

Figure 2-4 Seismic response of URM buildings (Paulay and Priestley 1992)

The effects of this amplified accelerations on out-of-plane walls was described by proposing the rigid body mechanism shown in Figure 2-5 and it will be further discussed in subsequent sections.

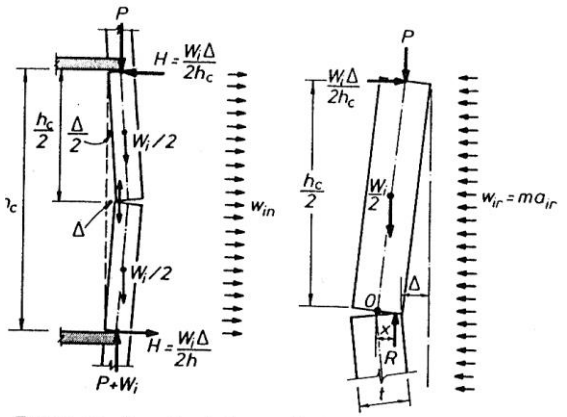

Forces on face-loaded wall including lateral reactions

(b) Moment equilibrium for face-loaded wall

Figure 2-5 Rigid body mechanism proposed by Paulay and Priestley (1992)

Similarly, Tomazevic (1999) recognized that vibration of URM buildings is tridimensional due to the earthquake ground motion nature that induces both vertical and horizontal inertial forces. At very small amplitudes of vibration, in the elastic range, URM buildings behave as a monolithic box. However, their behavior changes completely as the ground motion intensity increases and the structure moves into the nonlinear zone. At this point, the interconnection of the walls and type of floor plays a fundamental role in the seismic response. Besides, local effects of inertial forces are significantly different from those expected on concrete or steel building members because the distributed mass of each wall is big enough to induce forces perpendicular to the wall plane. This results in a complex local out-of-plane vibration of structural and nonstructural walls that must be resisted simultaneously with the global in-plane vibration induced by the seismic ground motion. Under these conditions, the following three events might characterize the final response. First, accelerations are amplified and maximized at the top floors due to a predominant first mode response. Second, out-of-plane excitation is filtered by the nonlinear response of the main structure and no longer similar to the input ground motion. Finally, the out-of-plane vibration can be further amplified due to local resonance effects with potential higher natural modes in the floor response (See Figure 2-6).

At the final stage, collapse mechanisms will occur when the structure consecutively reaches the maximum resistance and it is unstable to resist lateral loads. Partial or complete collapse will develop according to the number of elements exhibiting severe nonlinear behavior.

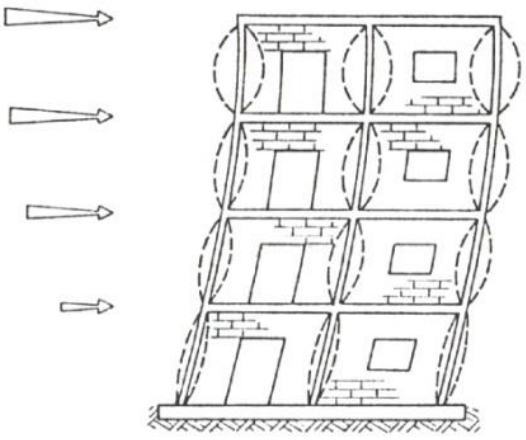

Figure 2-6 Seismic behavior of URM buildings (Tomazevic 1999)

After the 1989 Loma Prieta earthquake, Tena-Colunga and Abrams (1996) investigated the actual performance of three URM buildings which survived the earthquake without major damage. Because those buildings were instrumented with accelerometers at key locations, it was possible to compare actual response with numerical simulations. Interestingly, the best prediction was obtained with the simplified 10-DOF and 8-DOF models shown in Figure 2-7 that assumed linear behavior of masonry and flexible diaphragms. More important, this model considered soil-structure interaction by including rotational and translational springs at the base. Note that this assumption was not evident in the field, since the soil was identified as stiff and the structure was on shallow foundations. Under these conditions, surprisingly, large amplifications of ground acceleration were properly predicted at the top level on both directions of shaking. Displacement amplifications in both analysis directions were considerable too, but this did not affect significantly the out-of-plane behavior. Observe that in general, this building may be considered as a box-type structure, where potential separation between walls and floors induced by earthquake was prevented years before the event by standard retrofitting methods.

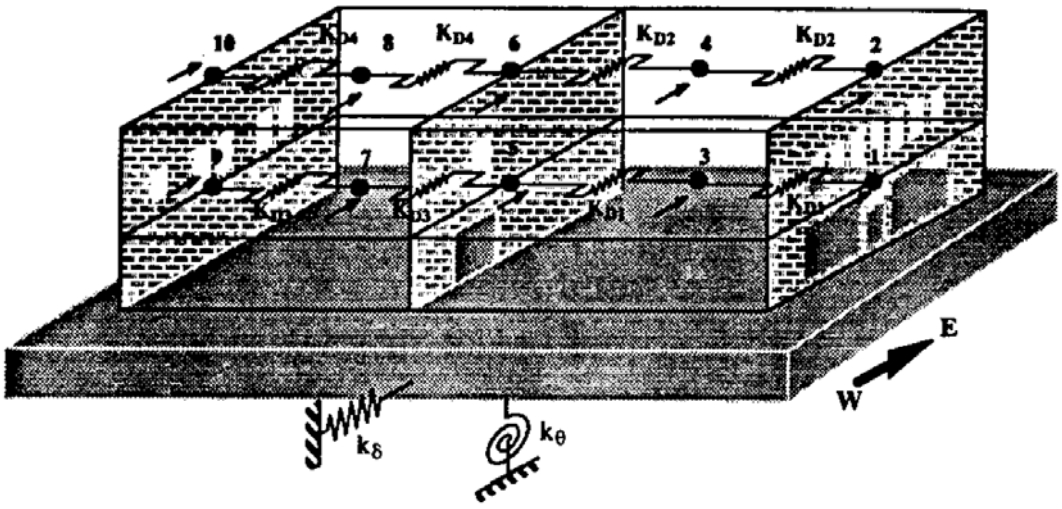

Figure 2-7 Simplified 10-DOF and 6-DOF with soil-structure interaction (Tena-Colunga and Abrams 1996)

Although mainly applicable to low-rise masonry buildings, the work by Cohen et al. (2004) includes interesting assumptions that deserve consideration. This research comprises shaking table tests, quasi-static tests and analytical evaluation of two half-scale one story reinforced masonry buildings with flexible diaphragms. They suggested that these buildings perform as a

system with two independent DOF; with one associated to the in-plane response of shear walls and another related to the in-plane diaphragm deformation. Figure 2-8 illustrates those assumptions. Noteworthy, walls and diaphragms were considered as systems with distributed mass and stiffness. However, note that out-of-plane walls are not explicitly considered in this formulation but are included in the diaphragm response. Also, it is important to mention that the in-plane wall behavior was considered completely elastic. Despite good agreement achieved between analytical models and experimental results it is not clear if previous assumptions could be extended to a multi-story building with in-plane walls that might present potential nonlinear behavior. Additionally, several shortcoming of this research will be further discussed in subsequent sections.

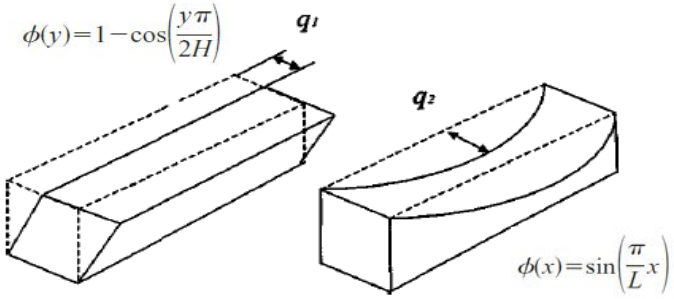

Figure 2-8 Two DOF system and associated mode shapes proposed by Cohen et al. (2004)

In summary, during an earthquake, any URM wall in a building will respond initially as in-plane wall, presenting a box-type behavior. As the magnitude increases, the behavior of the system is strongly related to the flexibility of the diaphragms and its connection to the wall. In the worst case scenario, poorly connected flexible diaphragms will generate larger deformation to the transverse walls, which in turn, will behave as tall unrestrained cantilevers. As described in the following section, this behavior has been observed during past earthquakes in parapets, upper walls in multi-story buildings and gables of churches.

Yet, the complex interaction between global in-plane inertial forces and local out-of-plane mechanisms that must be resisted by the same wall, remains poorly understood.

2.2 Actual Response of URM Building During Earthquakes

The seismic performance of North American URM buildings has been thoroughly reviewed by Bruneau (1994a). Failure modes listed included in-plane failures, out-of-plane failures and a combination of both (See Figure 2-9 through Figure 2-13). Note that in general, in-plane failures have not endanger the gravity load carrying capacity of the walls even with significant visible cracking. On the other hand, out-of-plane failures modes were aggravated by lack/failure of anchorage between wall and floors, and diaphragms excessive flexibility. In general, buildings were most vulnerable to this unstable and catastrophic failure mode. Those observations have been extensively confirmed by other reconnaissance teams around the world; see for instance reports on Cairo earthquake in 1992 by Hamid (1993); Kobe earthquake in 1995 by Bruneau and Yoshimura (1996) and more recently in Darfield byIngham and Griffith (2010).

Regarding the combined in-plane and out-of-plane failure mode, as noted by Bruneau (1994a), this failure mode is difficult to identify in the field and most of the time it will be erroneously considered as pure out-of-plane failure. Figure 2-9 and Figure 2-10, shows this particular failure mode.

Figure 2-9 Combined in-plane and out-of-plane collapse during 1989 Loma Prieta Earthquake (Bruneau 1994a)

Figure 2-10 Combined in-plane and out-of-plane failure mode during the 2005 Kashmir Earthquake in Pakistan (Naseer et al. 2010)

Figure 2-11 Piers and spandrel failures (Ingham 2011)

Figure 2-12 Pounding damage between URM buildings (Ingham 2011)

Figure 2-13 Unsuccessful parapet strengthening in URM buildings (Ingham 2011)

Considering current vulnerabilities in New York City, widely recognized by SEAoNY (Eschenasy 2011), such as out-of-plane demand on bearing walls (rotation) induced by rotted wood joists simple supported on masonry with poor mortar, it is clear that the out-of-plane failure mode typically observed during an earthquake is a critical issue in the area. Moreover, as the typical archetype URM building in NYC is four to five-story high, with flexible diaphragms spanning over long horizontal transverse walls, and many openings at the façade, it is expected that high simultaneous in-plane and out-of-plane demands can occur despite the low seismic risk.

2.3 Experimental Seismic Behavior

Since the overarching goal of this research is provide an accurate seismic evaluation of most common medium-rise URM buildings in New York City, critical parameters that determine the final seismic response of this type of buildings must be considered. Specifically, the most critical failure due to seismic loading discussed in previous sections will be investigated. Therefore, this section focuses on previous experimental research on seismic behavior of out-of-plane walls in multi-story URM buildings with flexible diaphragms. Secondly, a thorough revision of previous research on simultaneous bidirectional seismic behavior of URM walls will be discussed.

Unreinforced masonry buildings are considered to be one of the most dangerous structural systems. In particular, the high vulnerability of unreinforced masonry walls with parapets and flexible wood diaphragms to out-of-plane damage and collapse has been consistently observed in past earthquakes. Most common failures include parapets and chimneys falling to the ground and masonry walls collapsing due to failure in the connection with wood diaphragms (FEMA P547 2006), as illustrated in Figure 2-14.

Figure 2-14 Out-of-plane failure of a building during the 2011 New Zealand Earthquake (Ingham 2011)

The seismic out-of-plane behavior of individual URM walls has been investigated both experimentally and analytically. Experimental studies can be mainly classified according to the loading system and boundary conditions considered. Table 2-2 lists previous experiments on out-of-plane URM walls. Shake table tests, quasi-static tests and airbag tests have been used along the years. Walls simple supported at the top and the bottom, at all sides, in cantilever and with fix boundary conditions can also be found among those previous studies.

Table 2-2 Previous experimental research on out-of-plane masonry walls

Researcher	Wall dimensions (mm)				Category										
	t	h	l	h/t	a	b	c	d	e	f	g	h	i	j	k
Ewing et al. (1981)	300	4267	1800		x					x			x	x	x
Tomazevic et al. (1990)					x						x		x		x
Gulkan et al. (1990)	150	2640	2440	18	x					x		x		x	
Costley and Abrams (1996)	94	1671	1084		x						x		x		x
Benedetti et al. (1998)	225	1500	2200		x						x		x		x
(Paquette et al. 2001)	95	1500	1200	16	x					x					x
Simsir (2004)	93	1938	988	21	x					x			x	x	
(Griffith et al. 2004)	50	1500		30	x	x				x					x
Paquette and Bruneau (2006)	190	2724	5690	14		x		x			x		x		x
Vaculik and Griffith (2007)		1232	1840	0	x						x				x
Griffith et al. (2007)	110	2500	4000	23			x	x			x				x
Mosallam (2007)	100	2640	2640	26			x		x	x					x
Bean Popehn et al. (2007)	90	3610	800	40		x			x	x				x	x
Meisl et al. (2007)	355	4250	1500	12	x					x					x
Lazzarini et al. (2008)	209	3380	1090	16		x		x		x					x
Willis et al. (2009)	110	2500	4000	23			x		x		x				x
Derakhshan et al. (2009)	220	4100	1150	19			x		x	x					x
Hamed and Rabinovitch (2010)	200	2100	1203	11		x			x	x				x	
Ismail (2011)	220	3900	1170	18			x		x	x					x
Penner and Elwood (2012)	Several dimensions														

a-Shake table test, b-Quasi-static loads, c-Airbags, d-Cyclic, e-Monotonic, f-One-way bending, g-Two way bending h-Cantiliver, i-Flexible diaphragms, j-CMU, k-Clay bricks

More recently, Krawinkler et al. (2012) developed fragility functions of parapets and chimneys based on a combination of engineering judgment, empirical data and sophisticated numerical models subjected to the ATC-63 far-field ground motion set. Yet, experimental data on the seismic behavior of URM walls with parapets accounting for diaphragm flexibility, and the effectiveness of strengthened parapets and floor-to-wall connections has not been experimentally tested. In particular, the seismic vulnerability of URM buildings with parapets and flexible diaphragms in medium and low seismic hazard areas, similar to New York City, remains unexplored although is expected to be high. Hence, there is a pressing need to obtain experimental data to verify and validate simplified numerical models that can be used by

structural engineering practitioners to understand the most likely behavior and interaction between components of this complex, poorly-understood system.

2.3.1 Seismic Behavior of Out-of-plane Walls in Multi-story URM buildings with Flexible Diaphragms

On-site observations after the San Fernando earthquake in 1971, revealed serious shortcomings in the connections between walls and diaphragms of many URM buildings in Los Angeles area (MSJC 2008). This led to an extensive research program founded by NSF in 1977 and carried out by ABK. As previously mentioned the final goal was to develop a new methodology to mitigate the seismic hazard in URM buildings.

In one particular task, 22 full scale walls representative of typical URM buildings were subjected to dynamic out-of-plane excitation in order to provide data about its resistance to collapse, to evaluate different retrofit techniques and lastly to calibrate and verify analytical models. As previous field survey showed that several boundary conditions existed for out-of-plane walls, single and multi-story buildings (up to 3 stories) with rigid or flexible diaphragm were considered as prototype. In addition, several combinations of height to thickness ratio (h/t) and overburden were examined. As shown in Figure 2-15, floor response motions for multi-story buildings were developed based on dynamic analysis of analytical models that account for the non-linear hysteretic behavior of the wall/diaphragm system. Input motions applied simultaneously at the top and the bottom of the wall ranged between 0.1g to 0.4g accounting for the most part of seismic hazard in the US. Figure 2-15 illustrate the test set up used in this research. Note that a perfect anchorage between floor and walls was assumed, although walls were free to rotate at both ends.

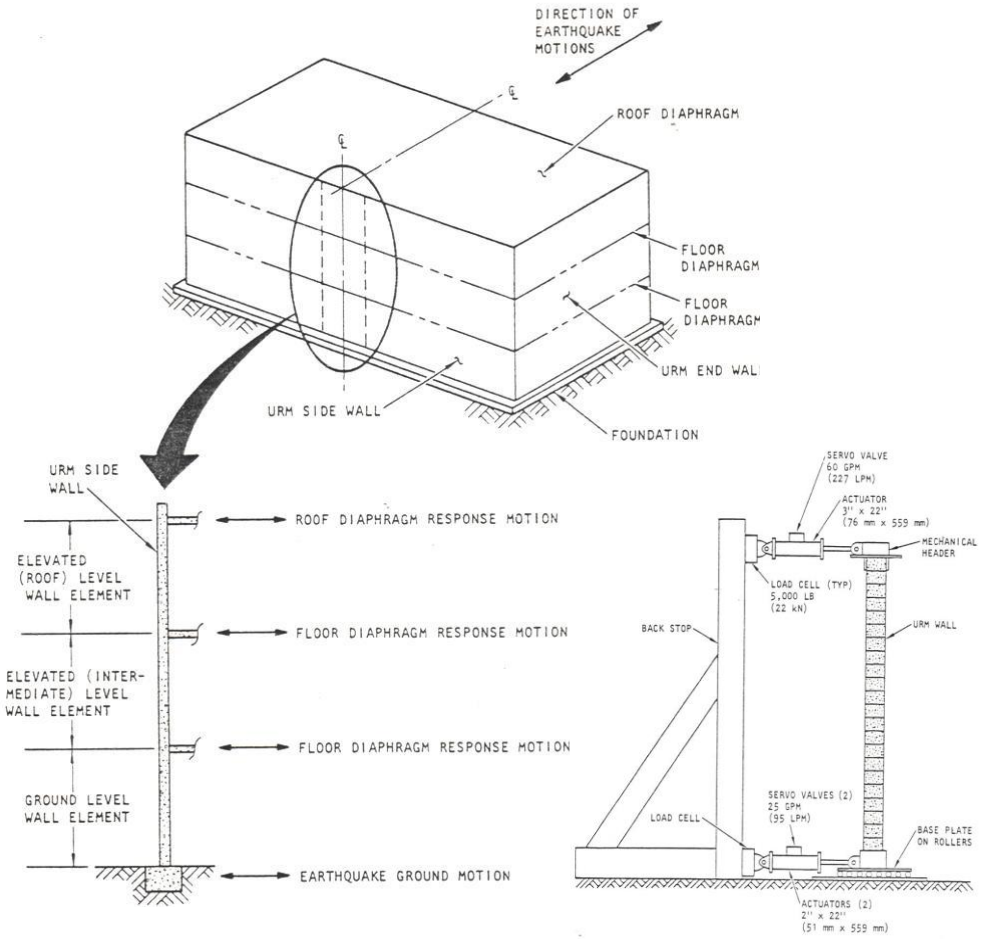

Figure 2-15 Multi-story buildings: Out-of-plane walls and test setup (Ewing and Kariotis 1981)

Under those loading and boundary conditions, most of the walls cracked horizontally at mid-height and close to the base before collapse. Moreover, a stable rigid body rotation around cracking surfaces was noticed during medium intensity excitations. This key observation led to recommendations on acceptable slenderness ratios as function of overburden load and peak input excitations at the top and the base. Additionally, limits on diaphragm span that prevent high amplification on out-of-plane walls were recommended. In 1998, those results were incorporated in FEMA 307 as guidelines to prevent out-of-plane failure. Despite of the limitations discussed in section 2.1, current ASCE 41-06 guidelines are still based on this cornerstone research program.

In 1990, a comprehensive testing program on URM buildings was carried out by Tomazevic et al. (1990) at the Institute for Testing and Research Materials and Structures (ZRMK) in Slovenia. In this study, four 1:4 scale two-story URM buildings were dynamically tested on shake table to investigate the influence of floor flexibility and its connections to walls on the seismic resistance of old brick and stone masonry houses. Two different diaphragms configurations and materials were investigated as well as several retrofit techniques. Remarkably, although an identical structural layout was used for all models, out-of-plane vibration was only observed in the model with wooden floors without strong connections to the walls. At very early stages of the test sequence, ground motion intensity as low as 0.20g induced separation of the wall in the second floor. Then, at higher intensity levels produce partial collapse in the upper floor as seen in Figure 2-16. Although diaphragm gravity and inertial loads were supported only by in-plane walls without openings, the final response was not determined by in-plane response but rather by the out-of-plane walls acting in cantilever.

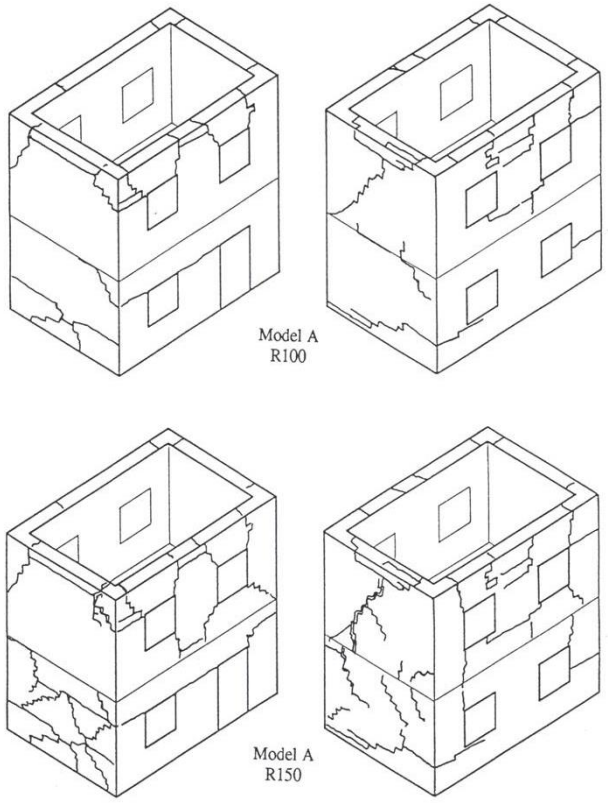

Figure 2-16 Final crack pattern after 100% and 150% intensity level test (Tomazevic 1990)

On the other hand, an extensive US research program mainly carried out by Costley and Abrams (1996) in collaboration with Italian researchers Calvi and Magenes (1997), did not find significant out-of-plane behavior in a 3:8 scale two-story URM masonry building with flexible diaphragms. The previously discussed work done by Tena-Colunga and Abrams (1996) on an instrumented URM building which survived the Loma Prieta Earthquake in 1989 led to this research program and it was used as a comparison reference. As in that research, several relevant observations were verified. First, significant amplification of ground accelerations was found prior to cracking at the top of the in-plane walls and the roof diaphragm (i.e. about 1.4 and 2.7 respectively). Moreover, due to the presence of flexible diaphragms, a uniform lateral force distribution between two floors was observed instead of the inverted-triangular distribution typically used for shear-type buildings with rigid diaphragms. As said before, out-of-plane failure was not observed during the test, mainly due to its short horizontal span, connection details used to prevent pounding against roof and floor and a full height vertical joint at one side of the wall that avoided transfer of forces with one in-plane wall. These observations are confirmed by Benedetti et al. (1998), in which fourteen 1:2 scale URM two-story houses were tested on a shaking table to compare effectiveness of several retrofit techniques. Although wooden slabs supported by wooden beams were used in this research, a box-type behavior was predominantly observed due to the short horizontal span of out-of-plane walls.

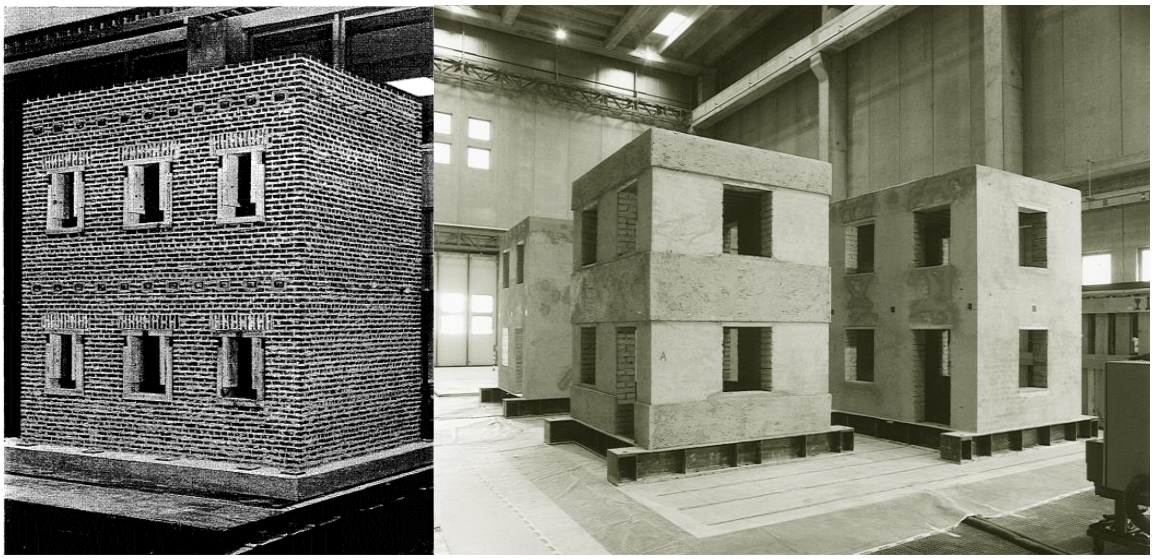

Figure 2-17 a) Building at 3:8 scale by Costley and Abrams (1996) and b) Building at 1:2 scale by Benedetti et al. (1998)

Although Costley and Abrams (1996) and Benedetti et al. (1998) investigated the dynamic behavior of a whole URM building through shake table testing, their research was inconsistent with field observations since a 38% and 50% scale models were utilized due to laboratory constraints. Thus, as recognized by Benedetti et al. (1998), to fully satisfy similitude relationships additional masses were added at the floors and this modified the seismic response mechanisms. To complement this researches, Paquette et al. (2004) conducted the very first full scale URM building pseudo-dynamic test in the U.S. This research had three objectives, namely, a) investigate the effects of flexible and weak diaphragms on URM shear walls, b) investigate the influence of building corners in the global response and c) investigate benefits of a potential retrofit technique. Interestingly, although a flexible wooden diaphragm was used, it did not produce significant out-of-plane instability effects when subjected to accelerations as high as 1.80g. As expected, due to in-plane walls with stable rocking/sliding mechanisms, large deformations were sustained without strength degradation. Furthermore, corner effects did not modified the final response of the system during high seismic excitations.

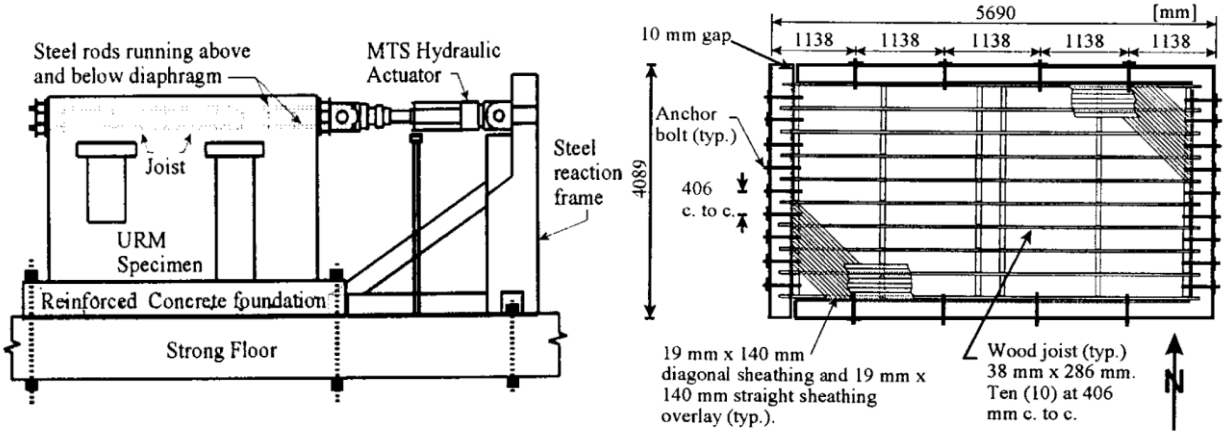

Figure 2-18 Test setup and plan view of experiment conducted by Paquette and Bruenau (1994)

Similarly, as previously discussed in section 2.1, the work done by Cohen et al. (2004) focused on the seismic response of wood diaphragms rather than investigating out-of-plane walls. The common idea behind these research studies was to investigate the interaction between diaphragms and in-plane walls, and provide upper bound performance limits that would lead to recommendations to mitigate the out-of-plane wall failure mode.

Because past shaking testing programs neglected the response of out-of-plane URM bearing walls excited by flexible diaphragms, Simsir et al. (2004) investigated this characteristic by testing 2 out-of-plane walls on the shaking table of the University of Illinois at Urbana-Champaign. Several key parameters were considered in this study, namely, the axial stress on the out-of-plane walls, the diaphragm stiffness and the stiffness contribution of in-plane walls. Figure 2-19 illustrate the specimen and test setup utilized. Note that in this configuration, the mass of the floor is mainly resisted by the out-of-plane walls while the in-plane walls are taking the inertial force generated. This is different from previous research where in-plane walls usually resist the diaphragm gravity force and out-of-plane walls take inertial forces generated during seismic excitation. Using this test setup, large drift ratios (up to 3.5%) and high amplified acceleration (up to 4.5 times the ground acceleration) were recorder at the top of the wall with slight damage in the specimen, suggesting that larger wall slenderness limit than those specified by FEMA 356 could be safely used.

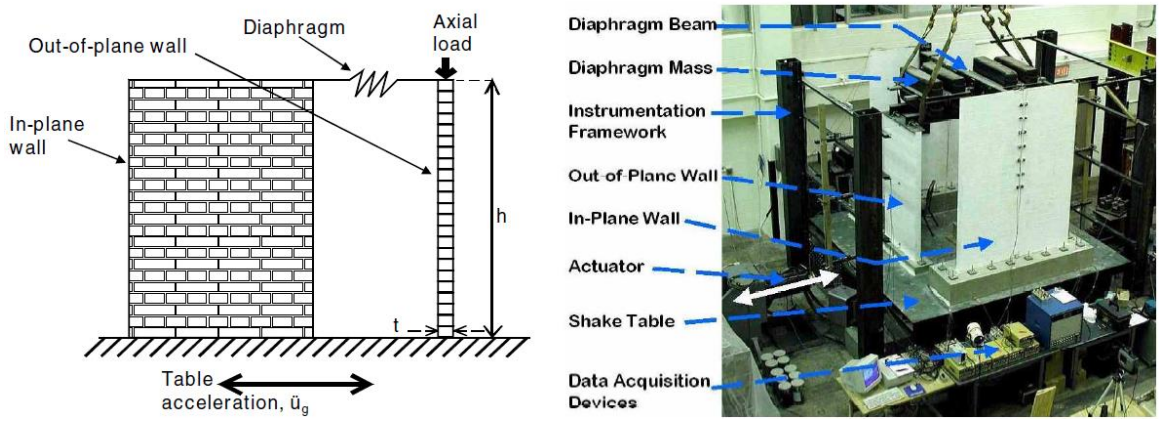

Figure 2-19 Shake table testing configuration (Simsir 2004)

Several shortcomings can be identified in this research. Firstly, there was no prototype building for this model. As a result, the global response obtained (e.g. Fundamental period, maximum displacement at diaphragm and walls) cannot be verified in a rigorous way. Second, in-plane walls were strengthened with horizontal and vertical steel reinforcement bars and a strong Type S mortar, whereas out-of-plane walls were made of unreinforced concrete blocks with a weak Type O mortar. This unusual combination prevents the applicability of this research result to a broader range of buildings, since most of them usually have the same type of masonry construction. Third, even though a good wall performance was obtained despite the ground

motion intensity and wall slenderness, it is important to notice that small inertial force was sustained out-of-plane. A different test diaphragm setup may yield different results.

2.3.2 Bidirectional Seismic Behavior of Out-of-plane Walls in Multi-story URM buildings with Flexible Diaphragms

While it has been recognized that combined in-plane and out-of-plane effects constitute a serious life safety hazard in URM buildings with flexible diaphragms, experimental and analytical research to better understand the seismic behavior is scarce in the literature. Angel et al. (1994) conducted experimental and analytical studies regarding the loss of out-of-plane strength for URM masonry infill panels as a result of in-plane damage. They reported that out-of-plane capacity decrease by as much as half depending on the in-plane damage. Additionally, the effect of in-plane cracking on the out-of-plane capacity increases proportionally to the slenderness of the wall.

Flanagan and Bennett (1999) conducted a series of bidirectional tests on a single bay clay infill wall. Three load sequences were used, namely: in-plane load following out-of-plane load, out-of-plane load following in-plane load and simultaneous in-plane and out-of-plane loads. In the first load case, a 25 % reduction of in-plane capacity was observed after the test. In contrast, when the out-of-plane load was applied first, a significant reduction of in-plane stiffness was observed, but the strength remained almost unaffected. Finally, combining both loadings tended to reduce the out-of-plane capacity.

Some of these observations have been confirmed through numerical simulations. Minaie (2009) performed a parametric study to examine the influence of bi-directional loading on partially grouted masonry shear walls. Variables investigated include wall aspect ratio, axial stress, and out-of-plane displacement amplitude. As seen in Figure 2-20, for each analysis, a constant out-of-plane drift was applied to the wall followed by cyclic in-plane drift. Main outcomes reflected that the reduction of in-plane capacity due to out-of-plane drift is higher for low axial loads. (i.e., up to 25%). Moreover, the reduction of capacity is higher for walls with high aspect ratio and low axial stress. In summary, out-of-plane load affected the in-plane capacity of the wall; however, the post peak response is not greatly affected even with significant presence of cracks in the wall. Therefore, the author concluded that bidirectional effects most likely does not affect

the global seismic performance. Those results have been recently confirmed by Dolatshahi et al. (2014) and Najafgholipour et al. (2014), who investigated the experimental and numerical bidirectional behavior of slender URM wall panels under simulated seismic loads.

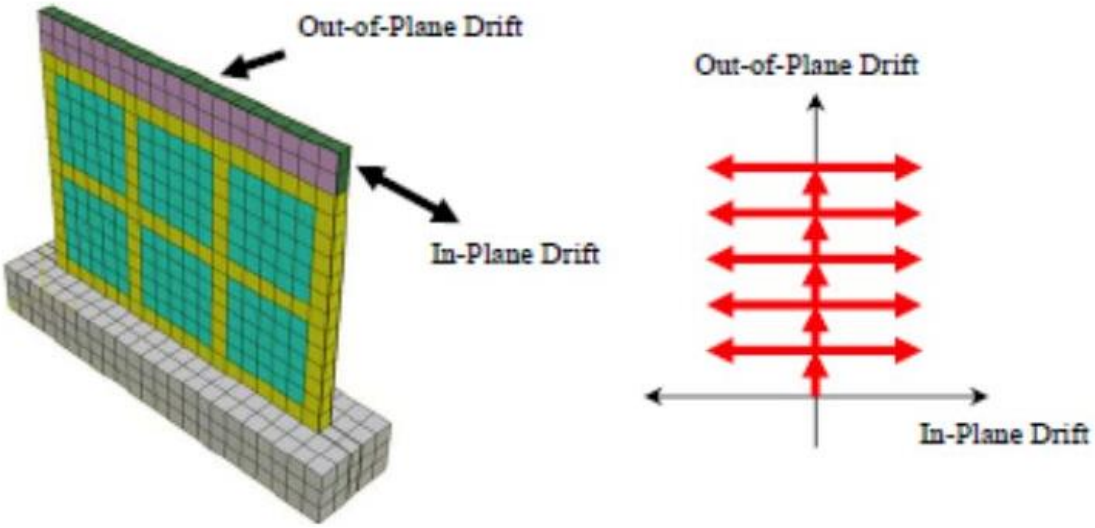

Figure 2-20 Illustration of combined in-plane and out-of-plane excitations (Minaie 2009)

SECTION 3
ARCHETYPE BUILDING FOR NEW YORK CITY

3.1 Introduction

Large variations in masonry constructions techniques and architectural forms can be found across the United States (Abrams 1994). Therefore, conducting a reliable seismic evaluation of masonry buildings in New York City requires defining an archetype building representative of typical construction in the area.

In this section, after characterizing the building stock in New York City, a representative URM building is identified. Statistical information about the current building stock in New York City was obtained from a database developed by the NYCEM Project (Tantala et al. 2003). This information was used, together with relevant architectural and historical books, to select a first target archetype URM building. Additional construction details and characteristics relevant to this building were obtained from the literature and information provided by the Structural Engineering Association of New York City (SEAoNY) and the Department of Buildings (DOB). Finally, current structural vulnerabilities for the archetype URM building were identified and discussed at the end of this section. Identifying these vulnerabilities was a key component in selecting the structural elements or components that need to be further investigated.

3.2 Characterization of Building Stock in New York City

Information about the current building stock in New York City was obtained from the NYCEM Project (Tantala et al. 2003). This project developed a comprehensive building inventory database of the New York City metropolitan area that was used to estimate key parameters of the archetype building model. Plan dimensions, type of structural system, occupancy and qualitative description of exterior conditions and existing damage were estimated for 649 buildings. The survey was mainly conducted in Manhattan, Queens and Brooklyn. It was found that about 80% of the buildings in the area of interest are unreinforced masonry type, as illustrated in the building count by structural type and neighborhood shown in Figure 3-1. Most of these buildings were constructed before 1940's, as explained in the next section. The percentage of other structural systems is also shown in Figure 3-2.

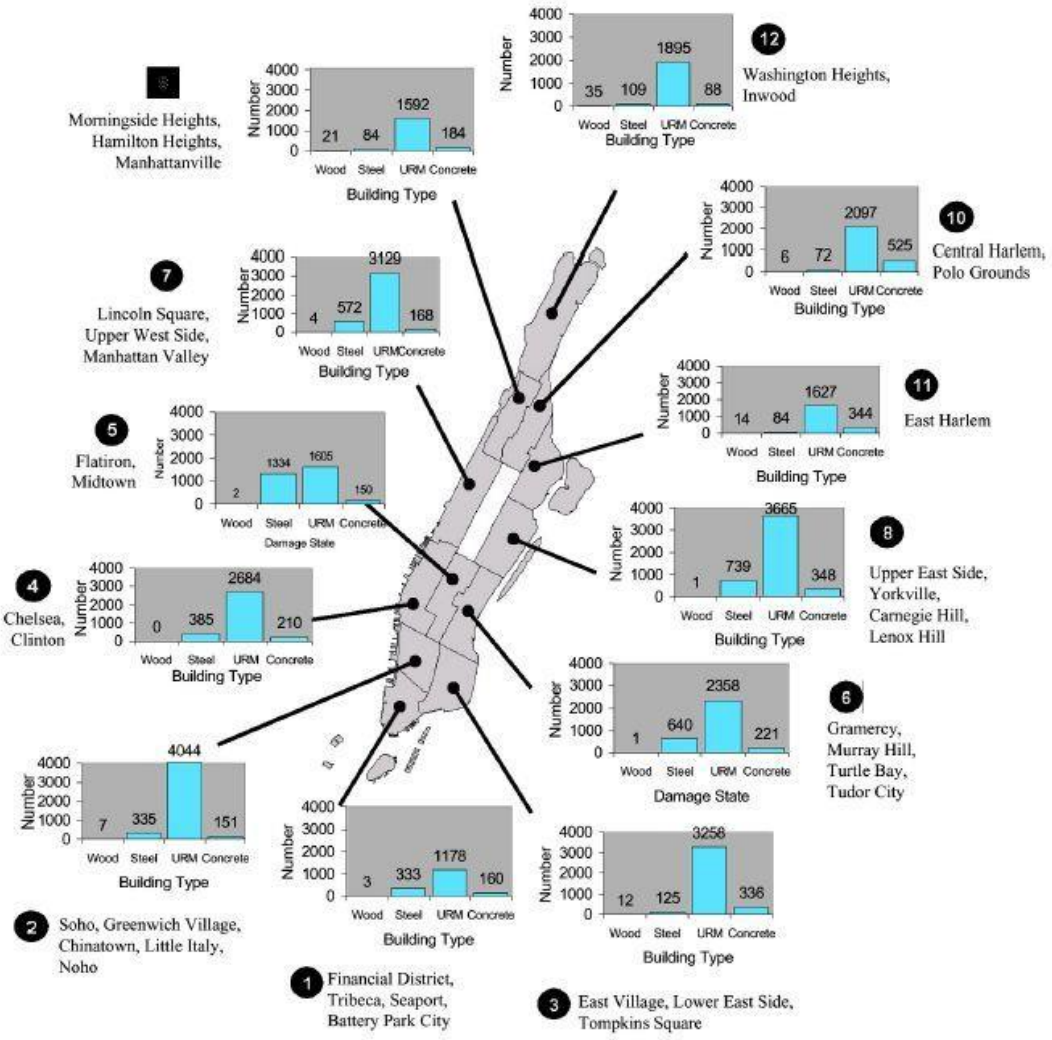

Figure 3-1 Building count by structural type and neighborhood (Tantala et al. 2003)

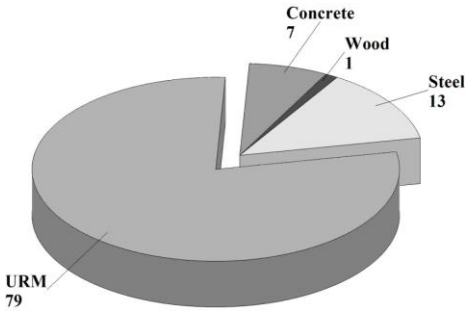

Figure 3-2 Types of buildings in the NYC metropolitan area

3.3 Characterization of URM Buildings in New York City

Average key architectural and structural characteristics of the URM building stock in NYC were determined and used to define an archetype building. Specifically, information regarding type of structure, width, length, number of stories, occupancy, masonry wall thickness, masonry materials and floor properties most representative of the stock was defined.

3.3.1 Structural Type

Based on the building codes that have governed NYC construction practice since 1700's, the DOB has identified four types of URM building construction, namely 1) Federal Era buildings that were constructed from 1765 to 1789, 2) Row-Houses that were built in the 1830 to 1940 period, 3) Larger buildings such as Mercantile Loft style that were built between 1845 and 1895, and 4) Old/New Law tenements that were built in the 1880-1930 period. Figure 3-3 illustrates representative buildings of each type of construction and Figure 3-4 presents the age distribution of these buildings in Manhattan.

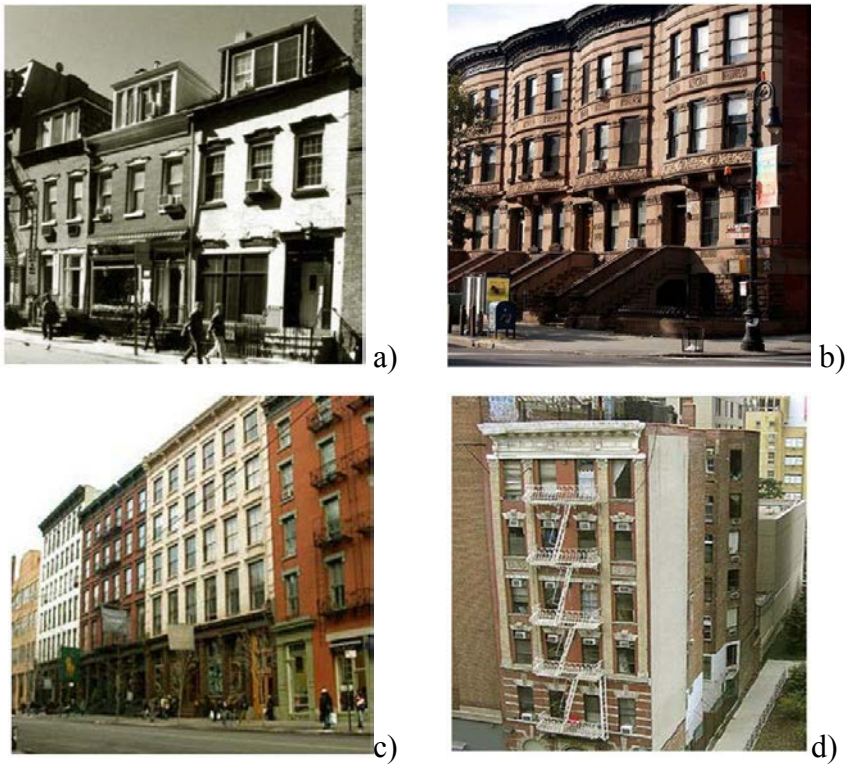

Figure 3-3 Type of URM buildings a) Federal Era b) Row Houses c) Mercantile Loft and c) Old/New Law Tenements

Because URM buildings were ruled by construction codes, there is a remarkable uniformity in its architectural configuration. Since Row-Houses have been constructed for the longest period of time, the first stage of this research will focus on this type of construction. In general, Row-Houses or Brownstones, were constructed 18 to 25 feet wide, with wood joist simple spanning between brick party walls between the houses in a row and no taller that five stories above their basements (Ramsey 1998).

New York City construction details for Row-Houses such as wall thickness, diaphragm configuration, windows and door sizes were obtained from architectural and historical books related to NYC (Friedman 1995; Radford 1983; Ramsey 1998; Reynolds 1994).

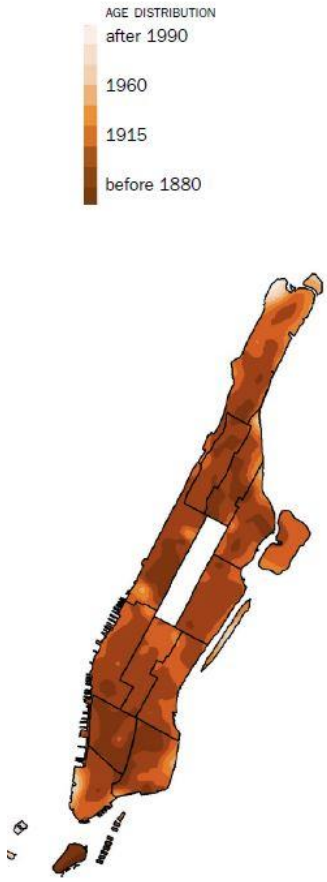

Figure 3-4 Age distribution of buildings in Manhattan (Tantala et al. 2003)

3.3.2 Width, Length and Number of Stories

Figure 3-5 presents the histograms of number of stories, length and width that were obtained after conducting a statistical analysis of the database generated by NYCEM. A five story building with plan dimensions of 25 ft by 60 ft will be the average structure. These general average values of length and width were expected since the layout of Manhattan follows pretty close the 1811 Commissioner's report that created the characteristic grid of avenues and streets in the city (Friedman 1995). Figure 3-6 illustrates the URM archetype building defined using the average dimensions obtained from the histograms.

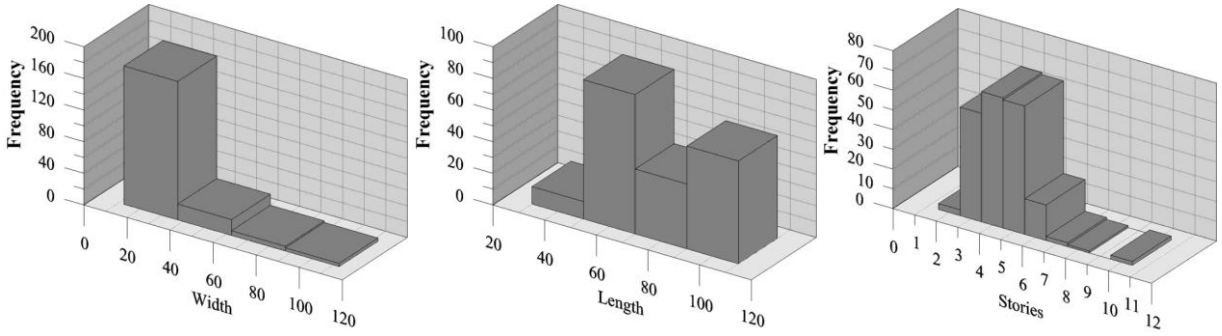

a) b) c)

Figure 3-5 Histogram of a) width (m), b) length (m) and c) number of stories

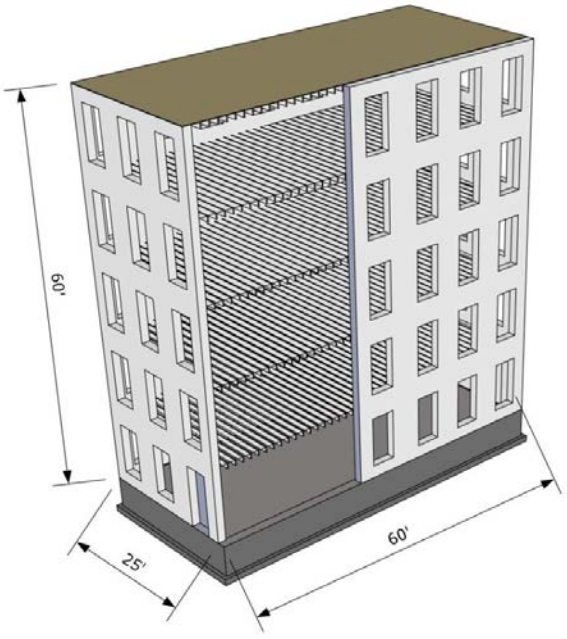

Figure 3-6 URM building archetype of New York City

3.3.3 Occupancy

Occupancy of URM buildings was found to be mainly residential and a mix of residential and commercial. Figure 3-7 describes the distribution of occupancy within the URM building stock. A thorough inspection in Google Earth of the surveyed areas by NYCEM revealed that a significant portion of URM buildings use the first floor for commercial purposes.

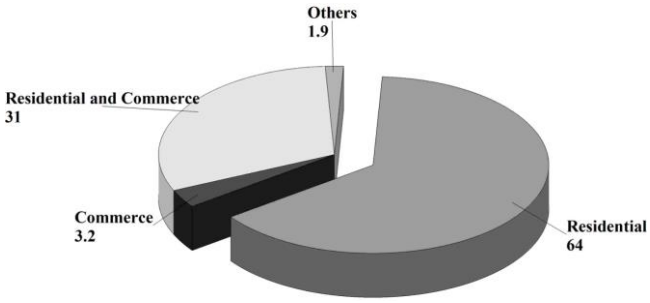

Figure 3-7 URM buildings occupancy

3.3.4 Masonry Wall Thickness

Masonry wall thickness is an important characteristic since the main structural system of URM construction is based on bearing walls. Thickness of the walls of businesses, residences and public buildings were specified to be 16 inches up to 20 feet and then reduced to 12 inches as shown in Figure 3-8. Note that this rule of thumb was applied regardless the width and depth of the building.

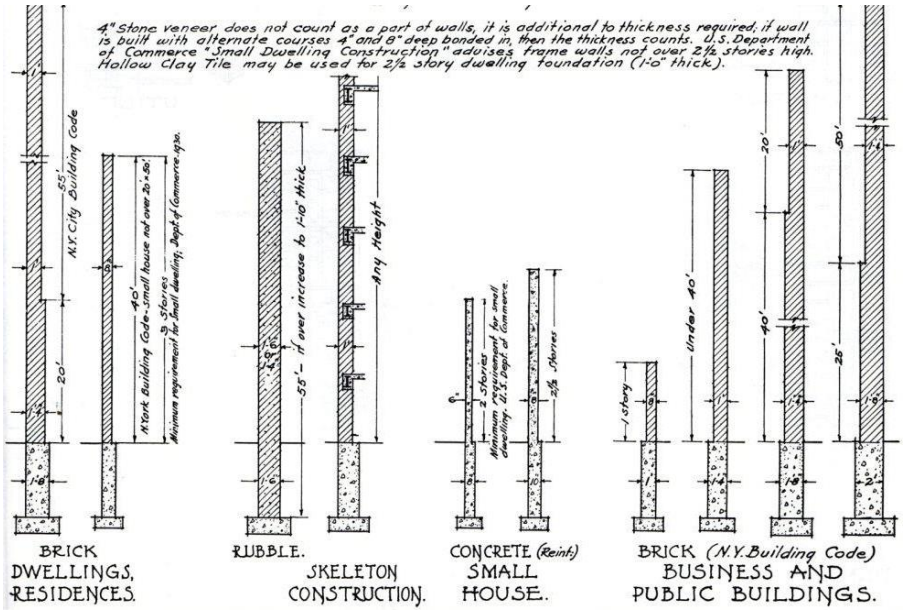

Figure 3-8 Minimum thickness recommended for NYC (Friedman 1995)

3.3.5 Masonry Walls

Masonry walls were fully characterized by defining the average masonry unit type, shape and size, masonry unit bonding and coursing as presented in Table 3-1. The stretcher and header bonding are illustrated in Figure 3-9. It is important to highlight that at the beginning of the nineteenth century; almost all houses in NYC were designed and constructed by ordinary bricklayers and carpenters (Friedman 1995). Thus, the skillfulness and masonry construction practices are highly unknown. Because of the significant variability on masonry brick and mortar construction qualities, it was required to define these properties by experimental testing of samples obtained from demolished buildings. More information on these experiments can be found in Section 6.

Table 3-1 Masonry wall properties

Material property data	Parameter
Masonry unit type	Clay brick from natural materials
Unit shape and size	Solid bricks 4x6x8
Masonry unit bonding and coursing	American bond-Stretcher and header
Masonry grout requirements	No space between wythes but the inner wythes are of lesser quality construction
Type of masonry wall	Multi-wythe, approximately 16 in. to 24 in. at the base and 8 in. to 12 in. at the top floor
Quality of construction	The outer wythes are of good construction and the inner wythes are of fair construction. The mortar can be friable

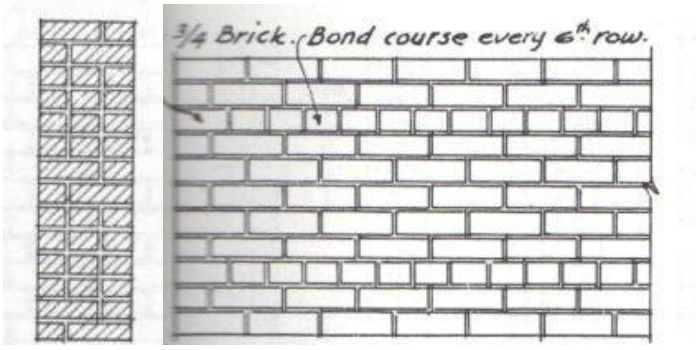

Figure 3-9 Type of bonding on masonry walls (Friedman 1995

)

3.3.6 Floor Diaphragms

Structural characteristics of floor diaphragms in URM buildings constructed between the 1800s and 1930s in NYC were mainly prescribed by Fire Building Codes. By the 1840s, it was common that horizontal floors in ordinary construction of URM buildings in NYC were made of wood boards and joists as shown in Figure 3-10. Wood boards were nailed directly to joist which in turn were supported on masonry walls (Friedman 1995). Plywood was not implemented until 1930; therefore it is believed that very few buildings will have it.

Because of the grid law of 1811, most wood floors in URM buildings had plan dimensions of 20 to 26 feet wide and between 60 to 80 feet long. In general, lumber sheathing of one-inch thickness was used in straight-sheathed or diagonally-sheathed diaphragms. The thickness was usually controlled by consideration of the gravity loads. Wood boards had dimensions of 1”x6” and 1”x8” inches and were placed straight or diagonally across the joist.

Wood joists were mostly sized by rules of thumb based in experience of previous constructions. The 1860 code already specified a minimum size of 3”x10”. Also by this time, some engineering analysis was available and allowable stress was used to size the joist. Nonetheless, floors constructed at this time tended to be bouncy because joist tended to be wider and shallower than modern joist. Later, the 1892 rules required maximum beam or joist spans of 26 feet. Figure 3-11 illustrates parameters recommended in the literature (Ramsey 1998).

The connection between square-cut joist ends and masonry walls was particularly critical during joist failure in fires, where the embedded segment induced the partial or total collapse of the brick walls, as depicted in Figure 3-10. By the 1860s, this problem was already addressed in the code by specifying “fire cuts”. A fire-cut joist had both ends cut at a small angle from vertical, so that in case of failure during a fire, it would freely rotate without damaging the bricks above.

Table 3-2 lists the mean dimensions and mechanical properties assumed in defining the wood floor that will be used in the archetype building of NYC and Figure 3-12 illustrates the plan dimensions and main structural components.

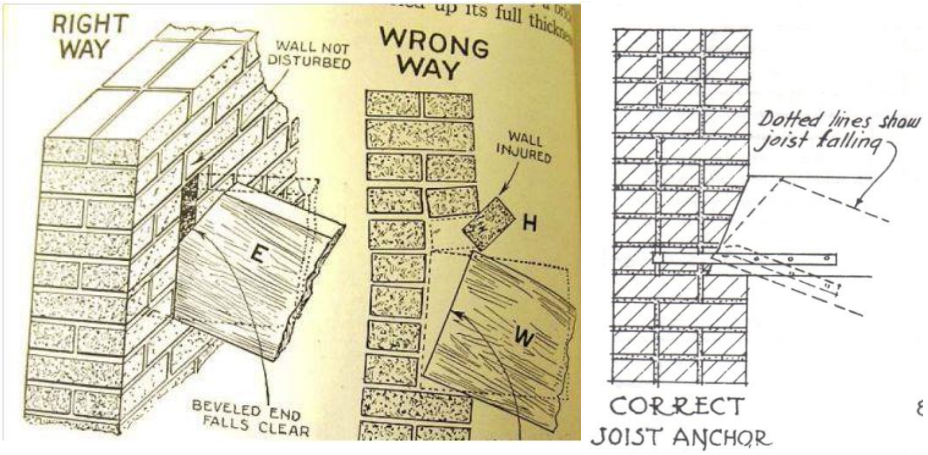

Figure 3-10 Old illustrations on the connections between walls and wood floors (Ramsey 1998)

MAXIMUM SPANS FOR FLOOR JOISTS № 1 COMMON

LIVE LOAD FOR RESIDENTIAL USE OF 40# PER SQ. FOOT UNIFORMLY DISTRIBUTED WITH & WITHOUT PLASTERED CEILING

AMERICAN STANDARD LUMBER SIZES		DIST. ON CENTER	MAXIMUM CLEAR SPAN BETWEEN SUPPORTS					
			SO. PINE & DOUGLAS FIR		WESTERN HEMLOCK		SPRUCE	
NOMINAL	NET		UNPLAST'D	PLASTERED*	UNPLAST'D	PLASTERED*	UNPLAST'D	PLASTERED*
2" x 6"	1-5/8" x 5-5/8"	12"	12'-0"	10'-0"	11'-6"	9'-6"	10'-11"	9'-1"
		16"	10'-6"	9'-1"	10'-0"	8'-8"	9'-6"	8'-3"
3" x 6"	2-5/8" x 5-5/8"	12"	15'-0"	11'-8"	14'-4"	11'-2"	13'-8"	10'-6"
		16"	13'-1"	10'-8"	12'-6"	10'-2"	12'-0"	9'-8"
2" x 8"	1-5/8" x 7-1/2"	12"	15'-11"	13'-3"	15'-3"	12'-8"	14'-6"	12'-0"
		16"	13'-11"	12'-1"	13'-4"	11'-7"	12'-8"	11'-0"
3" x 8"	2-5/8" x 7-1/2"	12"	19'-8"	15'-4"	18'-10"	14'-8"	17'-11"	13'-11"
		16"	17'-4"	14'-0"	16'-7"	13'-5"	15'-9"	12'-9"
2" x 10"	1-5/8" x 9-1/2"	12"	19'-11"	16'-8"	19'-1"	16'-0"	18'-3"	15'-2"
		16"	17'-4"	15'-3"	16'-8"	14'-7"	15'-11"	13'-10"
3" x 10"	2-5/8" x 9-1/2"	12"	24'-7"	19'-3"	23'-6"	18'-5"	22'-5"	17'-6"
		16"	21'-8"	17'-8"	20'-9"	16'-11"	19'-9"	16'-1"
2" x 12"	1-5/8" x 11-1/2"	12"	23'-11"	20'-1"	22'-11"	19'-3"	21'-10"	18'-3"
		16"	20'-11"	18'-5"	20'-1"	17'-7"	19'-3"	16'-9"
3" x 12"	2-5/8" x 11-1/2"	12"	29'-4"	23'-1"	28'-1"	22'-1"	25'-5"	20'-11"
		16"	25'-11"	21'-3"	24'-10"	20'-4"	22'-8"	19'-4"
2" x 14"	1-5/8" x 13-1/2"	12"	27'-8"	23'-5"	26'-6"	22'-6"	25'-3"	21'-2"
		16"	24'-4"	21'-5"	23'-4"	20'-6"	22'-3"	19'-6"
3" x 14"	2-5/8" x 13-1/2"	12"		26'-11"		25'-9"	30'-0"	24'-5"
		16"		24'-10"		23'-9"	27'-6"	22'-6"

*Note:- Deflection limited to 1/360 th. of the span. Dead load figured to include weight of joists, lath and plaster ceiling (10lbs.) and sub-floor and finish floor.

Figure 3-11 Maximum spans for floor joist (Ramsey 1998)

Table 3-2 Wood floor properties

Material property data	Parameter
Young Modulus of Wood	E=1798 ksi
Wood Boards Dimensions	Solid board 1"x6" in
Wood Joist Dimensions	Solid joist 2"X10" in
Nails Type and Spacing	8d @ 16" o.c.

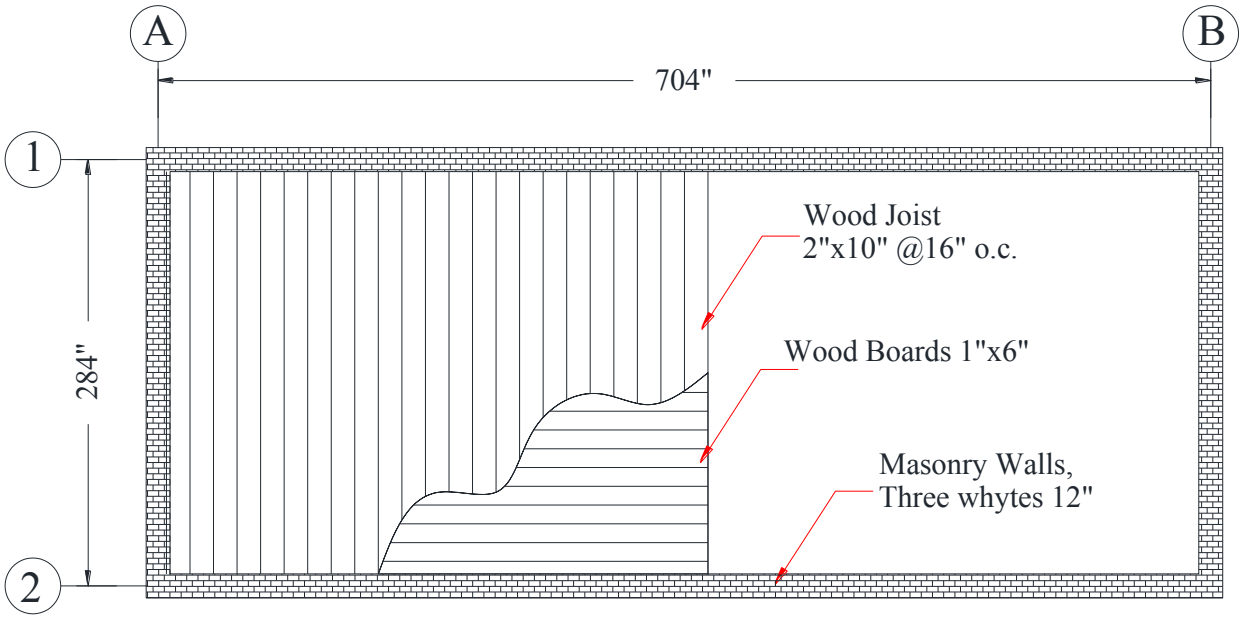

Figure 3-12 Typical architectural plan of wood floor in the archetype building

3.4 Structural Vulnerabilities of the URM Building Archetype

Given the structural characteristics highlighted in previous sections, the most important structural issues that could have a significant impact in the seismic behavior of the URM building stock in NYC could be identified. Identifying these vulnerabilities was a key component in defining, in subsequent sections, which structural elements or components needed to be further investigated to understand their seismic behavior. URM buildings are analyzed here considering loading in the direction perpendicular to the longer walls such that the out-of-plane effects including diaphragm flexibility will be more severe. Note that the seismic building codes were not implemented in New York City until 1996, so it is impractical to apply new concepts and definitions to these particular types of buildings.

3.4.1 Large Openings at In-plane Walls

Significant large openings can be seen in most of the in-plane walls of URM Row-Houses. Therefore, substantial dynamic filtering of the input seismic force along the height of the building can be expected, which is against the common assumption that in-plane walls in masonry buildings are rigid enough to prevent any increase or decrease in the seismic demands

transferred to the diaphragm and out-of-plane walls. This issue has been previously discussed by Bruneau (1994a) and Menon and Magenes (2011), as a significant shortcoming in earlier research studies of URM buildings and needs to be further investigated.

3.4.2 Flexible Diaphragms with Rotted Components

Due to the presence of flexible wood diaphragms, large amplification of accelerations and displacements in upper floors could be expected. In addition, the global stiffness of the structural system can be significantly reduced due to precarious structural condition of wood boards, nails and wood joists (Eschenasy 2011). Also, existing large openings in the diaphragm may have a significant impact in the demands delivered by the diaphragm to the out-of-plane walls. Sample wood diaphragms are depicted in Figure 3-11. Developing three-dimensional nonlinear computer models of wood diaphragms is a daunting task for structural engineers and significant additional research is still required, particularly when considering the aged material properties.

Figure 3-13 Flexible Diaphragms in NYC (Eschenasy 2011)

3.4.3 Missing Joist Anchorage and Rotted Wood Joists

As discussed in Section 2.3, the lack or failure of anchorage between wall and floors has been identified as a major causes of collapse in masonry buildings. Recommendations for tying the walls to floor were also given by the NYC old codes, which suggested using iron anchors to connect the end of the beam to brick walls (Ramsey 1998). Also, the lack of joist fire-cuts has been recently reported as major cause of failures in URM buildings in NYC (Eschenasy 2011). A recent example is the building at 222 East 62nd Street, where the whole floor collapsed on June 29, 2012.

Nonetheless, very little information can be found in the literature regarding the modeling and analysis of this type of connection. Even less information can be found regarding the seismic behavior either during past seismic events or in the laboratory.

Figure 3-14 Rotten connections and wall anchorage (Eschenasy 2011)

3.4.4 Potential Out-of-plane Collapse of Old Masonry Walls

The combination of large openings in in-plane walls, flexible diaphragms, and lack of joist anchorage, increases the potential out-of-plane collapse of the masonry walls. Most of these walls span over the complete large dimension of the building without any intermediate support or party wall. Yet, there are no experimental studies on the seismic behavior of out-of-plane walls attached to flexible diaphragms through bearing wood joists.

3.5 Summary

This section characterizes the building stock in New York City and in particular, the URM buildings commonly called Row-Houses. The conclusions of these studies are summarized below:

- Key architectural and structural characteristics of these buildings were determined and used to define a representative archetype building. The typical archetype URM building in NYC is five-story high, with wood diaphragms spanning over long horizontal transverse multi-wythe walls, and many openings at the façade. The floor plan dimension of the building is 25'x 60' and typical story height is about 12'.
- Current structural vulnerabilities of these buildings include: (1) In-plane walls with large openings; (2) Flexible wood diaphragms with rotted components; (3) Missing joist anchorage and rotted wood joists and (4) Potential out-of-plane collapse of URM masonry walls.

The archetype building and its current vulnerabilities provide a basic framework for this report. Studies on this type of building model will be expanded through the development of simulation capabilities supported by experimental testing to evaluate the seismic performance of typical NYC masonry buildings. Moreover, the overall geometric and mechanical characteristics of the structural components requiring further research were identified.

SECTION 4
NUMERICAL MODELING OF FLEXIBLE WOOD DIAPHRAGMS IN URM BUILDINGS

4.1 Introduction

The numerical modeling of flexible wood diaphragms is a key component in the seismic assessment of pre-1950's unreinforced masonry (URM) buildings in regions of moderate to high seismicity. As discussed in Section 2, the dynamic characteristics of wood floors play a fundamental role in controlling the final response of out-of-plane masonry walls and the strength demands in the connection between diaphragm and walls (Bruneau 1994b; Costley and Abrams 1996; Tomaževič et al. 1990).

In this section, suitable numerical models of wood diaphragms with similar structural characteristics to those found in older URM buildings in NYC are identified and evaluated for performance-based seismic design applications. As one of the goals is to provide well-validated, accessible analytical tools to practicing engineers and design community; two analyses codes, namely, OpenSees (2012) and SAP2000 (CSI 2009) were used to model the behavior of relevant diaphragm specimens found in the literature. OpenSees is an open-source software framework for simulating the seismic response of structural systems. It has been designed for parallel computing, and includes advanced capabilities, wide range of materials, elements and solution algorithms. Although simple problems can be tackled using this platform, it is more suitable for research and specialized applications. On the other hand, SAP2000 is a practical general purpose structural program which includes advanced analytical techniques and several integrated design codes (CSI 2012) .

After reviewing the literature on wood diaphragms, a comprehensive evaluation of the more relevant detailed and simplified models is performed. The in-plane response of a wood diaphragm is simulated and compared to test results from Peralta et al. (2004). Herein, the intention is not to match the experimental results but rather to determine key parameters that may significantly impact the predicted response. First, a benchmark numerical simulation using a refined finite element model (FEM) in OpenSees is presented. Then, a similar model more

appropriate for practicing engineers using SAP2000 is examined. Next, a simplified single degree of freedom (SDOF) model was also developed, analyzed and compared to the OpenSees benchmark model. Monotonic and cyclic quasi-static, modal and nonlinear time history analyses were completed in these numerical models. Comparison of the results indicates that finite element models can fully characterize the dynamic response of wood diaphragms, but at a very high computational cost. On the other hand, simplified models can only reasonable estimate few dynamic parameters and engineering demands at key locations of the diaphragm. Hence, a reduced multi-degree of freedom (MDOF) model of the diaphragm, able to capture the full dynamic characteristic while significantly reducing analysis time is proposed.

4.2 Previous Related Research on Straight-Sheathed Wood Diaphragms.

The purpose of this section is to identify and select suitable analytical tools for the seismic assessment of horizontal wood diaphragms. The focus is on wood floors similar to those existing in older URM buildings (i.e. floors constructed with straight boards as sheathing material and wood joist as framing members). To this end, the experimental behavior and numerical models of diaphragms subjected to in-plane monotonic static loads are first discussed. Then, numerical models suitable for diaphragms subjected to in-plane cyclic quasi-static and dynamic loads are presented. Few other models, which are more related to wood shear wall but relevant to this research are also briefly discussed. Finally, the state-of-the-art of numerical simulation of wood diaphragms in URM buildings is reviewed.

4.2.1 Diaphragms Subjected to Static Monotonic Load

An extensive literature review prepared by Carney (1975) and then updated by Peterson (1983) reveals that research related to wood diaphragms started as early as 1930's. However, until 1970's, most of this research focused on determining experimental values of maximum strength, stiffness or deflections of diaphragms with different sheathing pattern and materials. Horizontal plywood-sheathed diaphragms were tested by Countryman et al. (1955), Tissell (1966) and Johnson (1971); diagonally sheathed diaphragms were investigated by Doyle et al. (1957), and straight sheathed diaphragms were studied by Green and Horner (1934); Green et al. (1935), Stillinger et al. (1952), Stillinger (1953), and Johnson (1954). These tests were usually conducted under monotonic static load applied in several points along the longer dimension to simulate distributed loads. Typical results obtained included load versus deflection of the diaphragms and

modes of failure. Most test results concluded that, in general, the behavior of wood diaphragms was highly nonlinear and that nonlinearity was mainly due to the connection between boards and joists. Figure 4-1 shows the force-deformation relationship of a 20 x 60 feet plywood diaphragms tested by Doyle et al. (1957). Note that large displacements were obtained for relatively small in-plane shear forces.

With such a complex nonlinear behavior, mathematical models of wood diaphragms could be developed only through the finite element method (FEM). Between the 1970's and the 1980's, several numerical models of different levels of complexity were produced and implemented in non-commercial software specifically oriented to solve research problems.

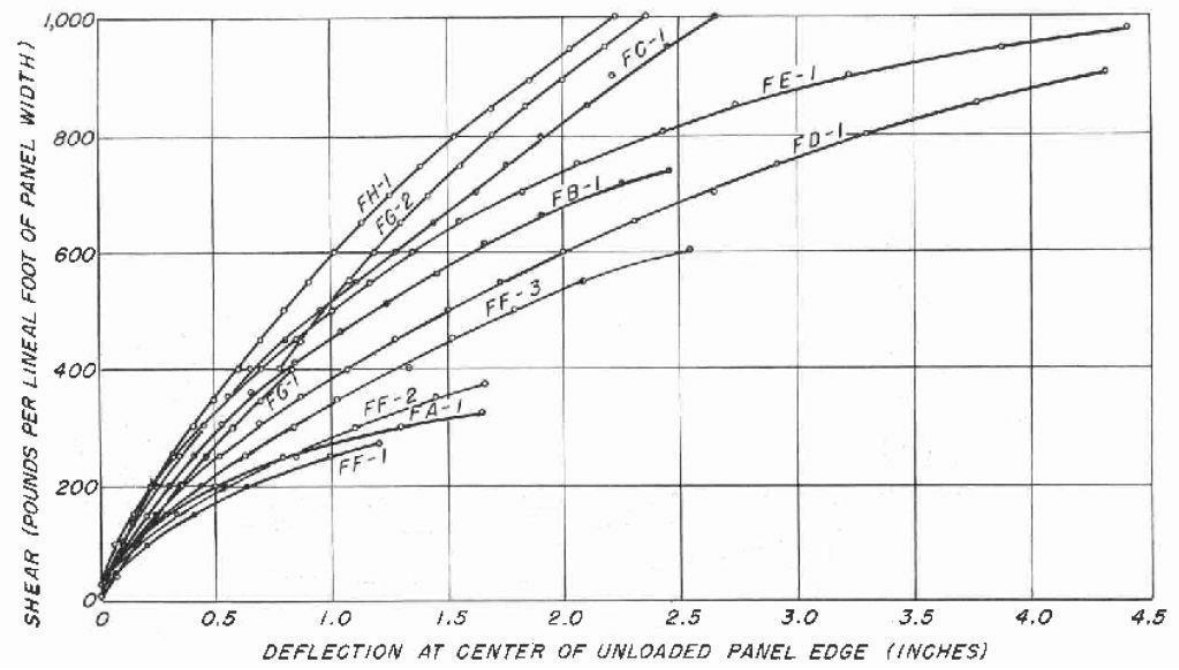

Figure 4-1 Shear-deflection relationship for diagonally sheathed panels tested by Doyle et al. (1957)

For instance, Foschi (1977) developed a general FEM that considered the cover sheathing material as plane-stress cubic isoparametric element, the framing system as a Bernoulli beam element, and the sheathing to frame connection as nonlinear springs. The force-deflection relationship of a 20 ft by 60 ft wood diaphragm previously tested by Johnson (1971) was predicted with reasonable accuracy (see Figure 4-2). A similar model was proposed by Itani and Cheung (1984) but this model did not require a particular sheathing arrangement and diaphragm

geometry. Instead of modeling nail by nail, an element representing a line of nails was developed. With this model, good agreement between analytical predictions and six diaphragms previously tested was obtained (see Figure 4-3). Nonetheless, the simulation still required a significant number of degrees of freedom if larger diaphragms needed to be modeled. A model requiring fewer DOF was then proposed by Falk and Itani (1989). In this model, a new finite element that represents the stiffness and distribution of multiple nails between the sheathing and the framing system was proposed. Since this new element accounted for all the nails connecting the sheathing panels to the framing, the number of DOF was significantly reduced. The numerical model was compared with ten diaphragms tested for ultimate load capacity. The results indicated that the model can predict the diaphragm response fairly well (see Figure 4-4).

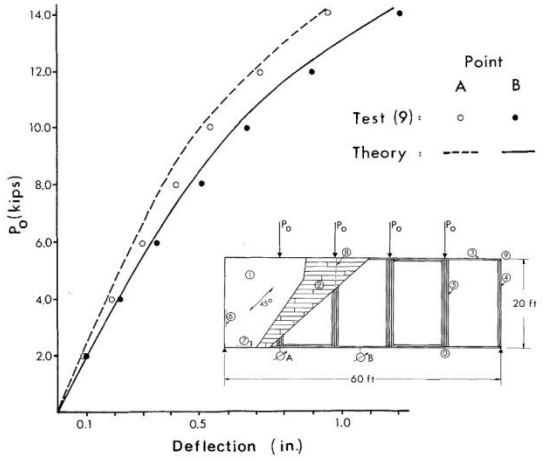

Figure 4-2 Sample numerical force-displacement relationship predicted by Foschi (1977)

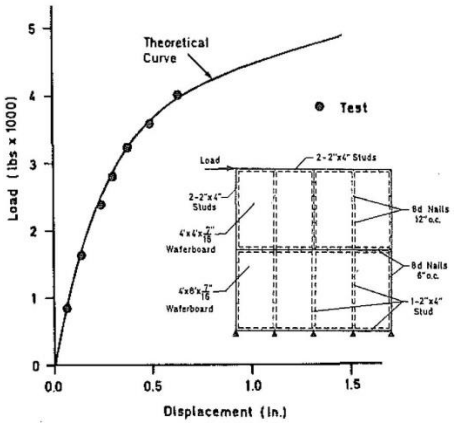

Figure 4-3 Sample numerical force-displacement relationship predicted by Itani and Cheung (1984)

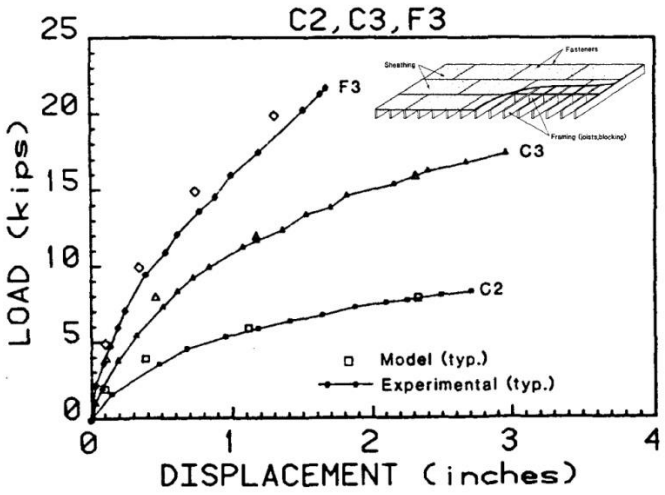

Figure 4-4 Sample numerical force-displacement relationship predicted by Falk and Itani (1989)

Note that most of the previous mentioned models were developed for static analysis of plywood sheathed diaphragms. Explicit modeling of straight and diagonally sheathed diaphragms has only been reported by the ABK program (Ewing and Johnson 1981) and Peralta et al. (2004). Those models are discussed in the next section.

4.2.2 Diaphragms Subjected to Cyclic Quasi-static and Dynamic Loads

Dynamic tests on horizontal wood diaphragms were first carried out by the ABK program (Ewing and Johnson 1981). As explained in Section 2, these tests were part of a larger research program with the main goal to mitigate the seismic hazards in existing URM buildings. Fourteen 20 ft by 60 ft diaphragms were subjected to quasi-static, cyclic in-plane displacement and dynamic, in-plane earthquake shaking. Three specimens were constructed with 1"x6" straight-sheathed boards on a wood framing system fabricated with 2" x 12" members. All lumber was Douglas Fir, Construction Grade. Common 8d nails were used at the boards to joist connections.

Dynamics loads were applied at the two ends by hydraulic actuators programmed to produce the displacement history of selected ground motions. Since the dynamic seismic input was obtained from numerical models of multi-story buildings, the tests indirectly accounted for the nonlinear dynamic interaction between URM walls and diaphragm. In addition, fifteen 1-ton lead weights that simulate the inertial forces of URM side walls were attached at each diaphragm.

Sample test results shown in Figure 4-5 and Figure 4-6 confirmed the highly nonlinear behavior of wood diaphragm. Yet, the specimens exhibit moderate damage after the last test sequence,

which subjected the diaphragm to about 3 inches of maximum displacement. No correlation was made between the cyclic quasi-static and the dynamic test, as the interpretation of the test results was never published by the ABK program.

A simplified lumped parameter model was developed for the analysis of the models. The diaphragm was discretized in a small number of segments with an associated tributary mass. Masses were connected to each other with a system of nonlinear springs and viscous damper in parallel, as shown in Figure 4-7. The nonlinear hysteretic model for the springs was developed based on the test results. The force-displacement envelope and cyclic load are also shown in Figure 4-7. Unloading stiffness and maximum residual force were specified to match experimental data. The simplified model gave good estimates of the quasi-static response and the cyclic dynamic behavior was properly captured.

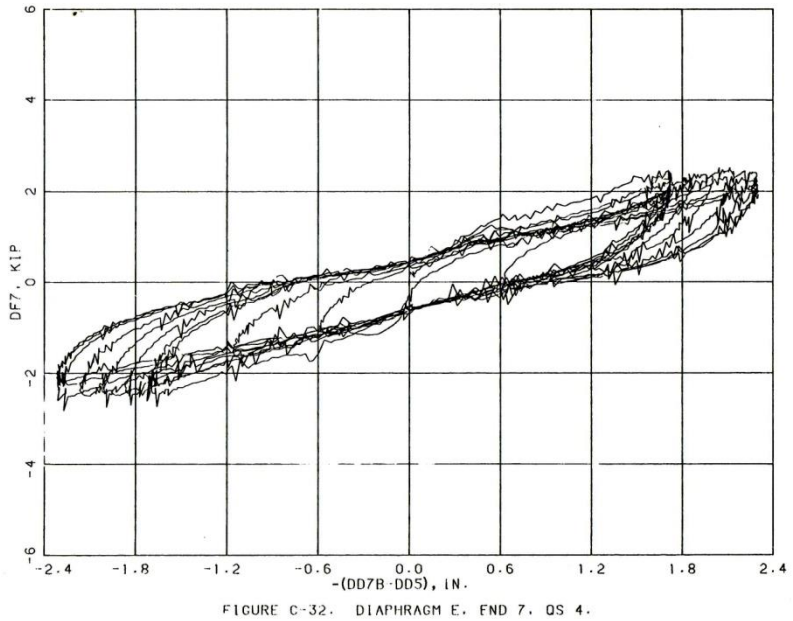

Figure 4-5 Sample test result of wood diaphragms under cyclic quasi-static load (Ewing and Johnson 1981)

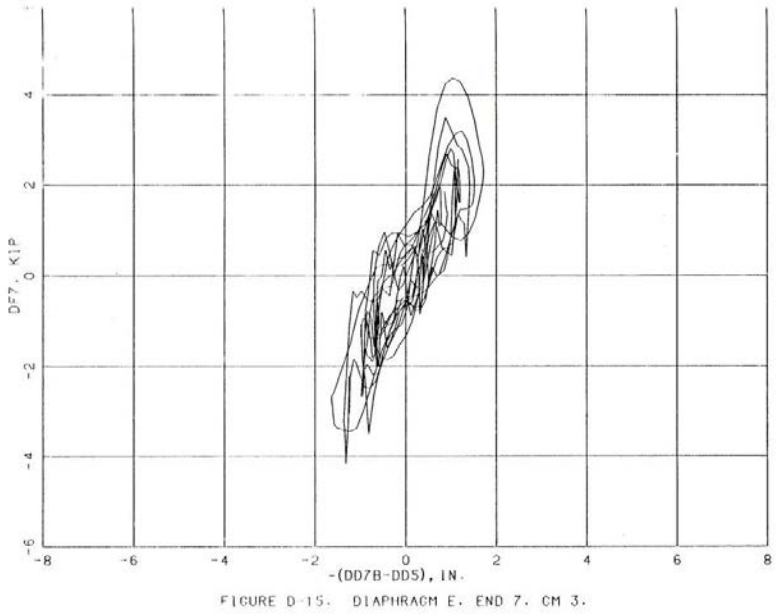

Figure 4-6 Sample results of wood diaphragms under dynamic loads (Ewing and Johnson 1981)

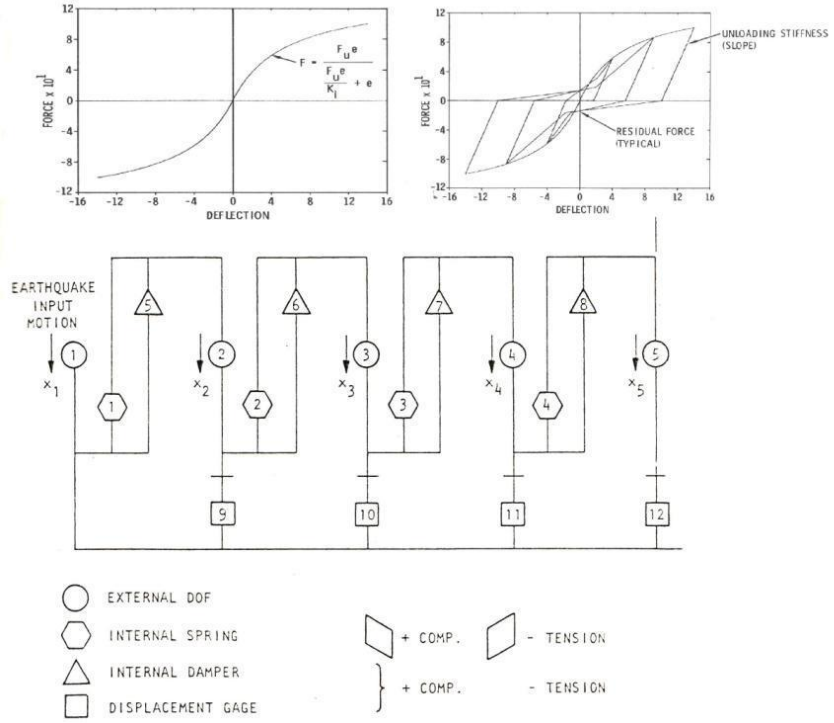

Figure 4-7 Lumped parameter and hysteretic model proposed by ABK (Ewing and Johnson 1981)

Between the 1980's and the 1990's, several other dynamic tests were conducted by Falk and Itani (1987) on wood diaphragms. These tests, however, were mainly oriented to investigate the dynamics characteristics of plywood sheathed diaphragms most common in modern wood houses.

In 2003, Peralta et al. (2004) investigated the experimental and analytical in-plane behavior of wood diaphragms with similar characteristic to those existing in pre-1950s unreinforced masonry buildings in Central and Eastern areas of United States. In this research, three wood diaphragms composed of Southern pine were constructed and tested under cyclic quasi-static loads. Loads were applied to the third of the length of the diaphragms. The plan dimensions of the diaphragm were 3.66 m wide by 7.32 m long. Wood boards and beam joist were of pine lumber and standard 10d finishing head type nails were used.

Sample test results are shown in Figure 4-8. Again, the nonlinear behavior of the diaphragm is evident. Also, note the characteristic pinching behavior due to nail tearing and slippage. As in the ABK program, limited damage was observed in the specimens at the end of the experiments.

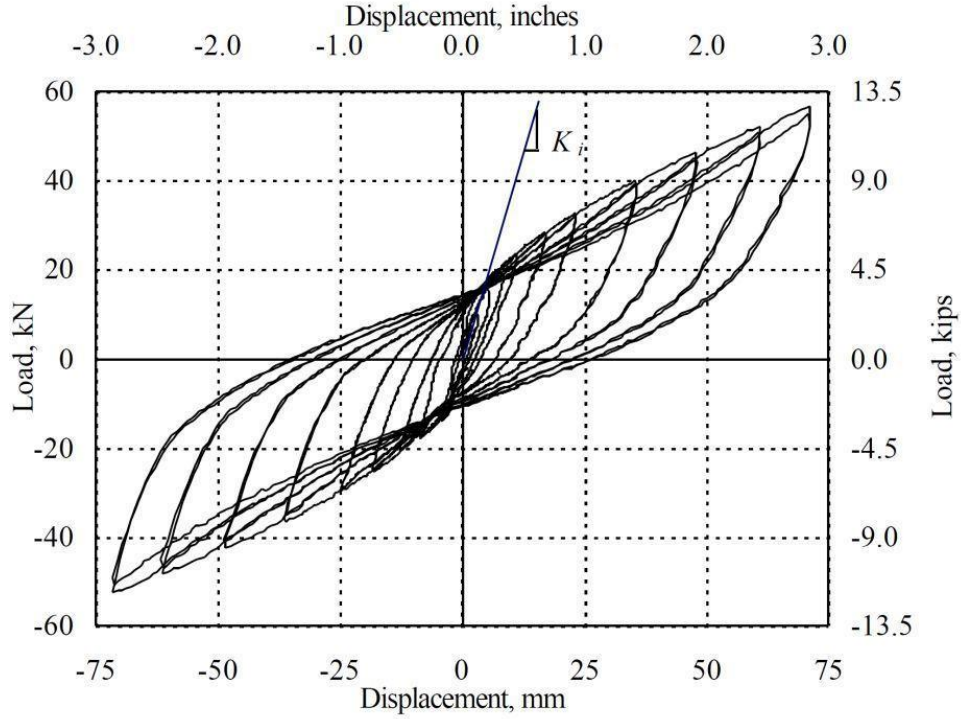

Figure 4-8 Sample results from experiments by (Peralta et al. 2004)

Numerical analyses were also carried out to predict strength, stiffness and hysteretic behavior of the diaphragms. Finite element analyses were conducted in ABAQUS. Wood boards were modeled using 8-node rectangular plane-stress elements, framing members were simulated using 2-node linear Timoshenko beams elements and nails were idealized as two zero-length spring perpendicular to each other. The monotonic and cyclic lateral load-nail slip relationships were taken from previous analytical and experimental research program conducted by McLain (1975) and then expanded by Pellicane et al. (1991). McLain (1975) proposed the following equation to predict the lateral force-displacement relationship of nailed joints:

$$V_n = A \log_{10} (1 + B\, e_n)$$

Where $\mathbf{V_n}$ is the lateral load, $\mathbf{e_n}$ is the relative displacement between joint members, **A** and **B** are constants derived from coupon testing or from using the specific gravity of the members. Parameters A and B as estimated by Peralta et al. (2004) are shown in Figure 4-9. A sample numerical result of the ABAQUS simulation of the diaphragm is also shown in Figure 4-10

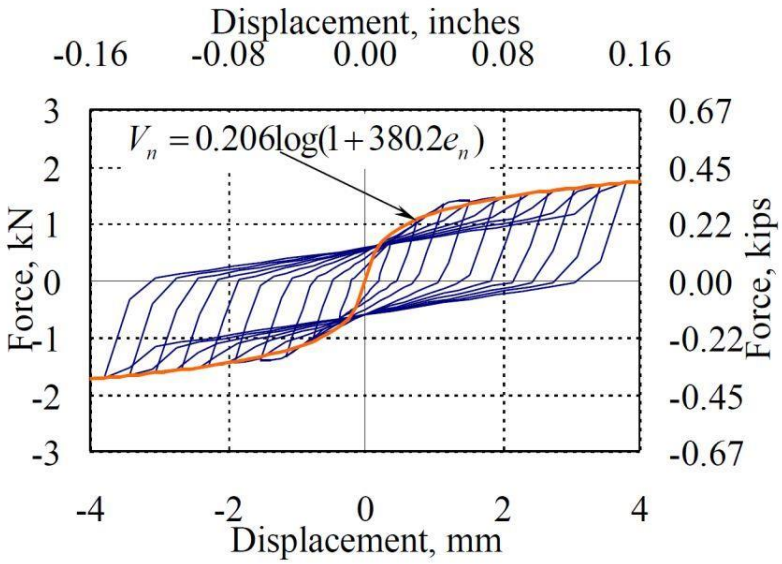

Figure 4-9 Monotonic and cyclic nail-slip model used by Peralta et al. (2004).

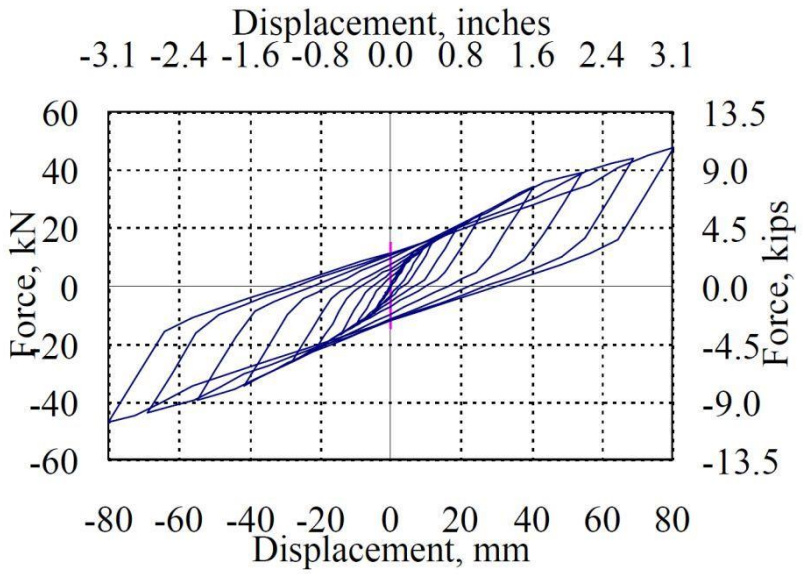

Figure 4-10 Sample result simulation from (Peralta et al. 2004)

Recently, Wilson et al. (2011), conducted experiments to assess the timber wood diaphragms typical of historical URM buildings in New Zealand. Four diaphragms of 18 ft by 34 ft plan dimensions were constructed with 1"x 6" straight-sheathed boards nailed on 2"x 12" wood joists spaced at 16" centers. Diaphragms were subjected to increasing cyclic quasi-static load. For comparison purposes, two diaphragms were tested with load parallel to wood joists and two were tested in the perpendicular direction. Test results confirmed the highly nonlinear behavior of this type of diaphragms and its high dissipation of energy (See Figure 4-11 and Figure 4-12). Damage observed after the test was minimum, even at 6" of maximum displacements. Diaphragms tested perpendicularly to wood joist presented a higher stiffness and strength, but smaller dissipation of energy. Although, no numerical attempts were made to simulate the diaphragm behavior, a comparative assessment was completed using the equations for stiffness and strength specified by the NZSEE and the ASCE 41-06 guidelines. It was found that the equations poorly predicted the diaphragm performance obtained from the tests.

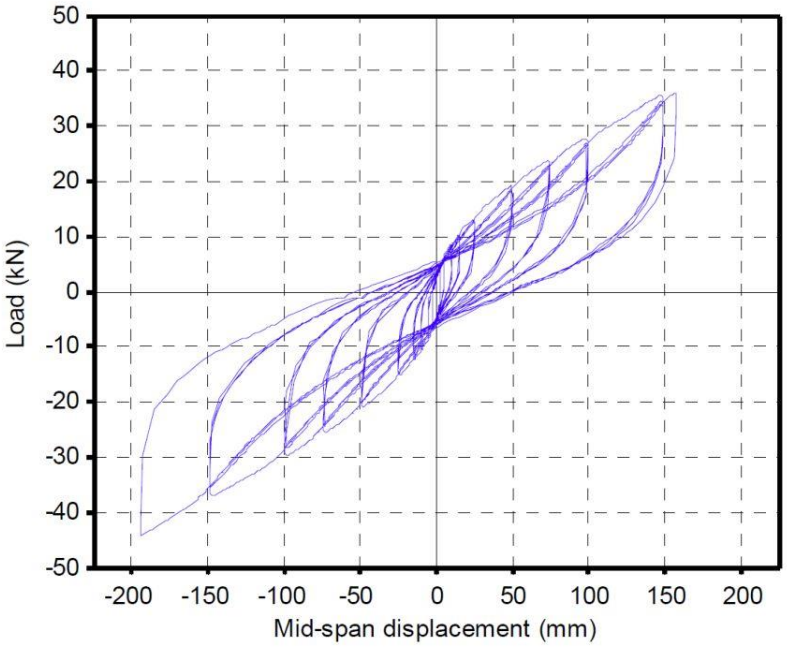

(a) Diaphragm FS1a

Figure 4-11 Testing result of wood diaphragm tested under cyclic load perpendicular to wood joist (Wilson et al. 2011)

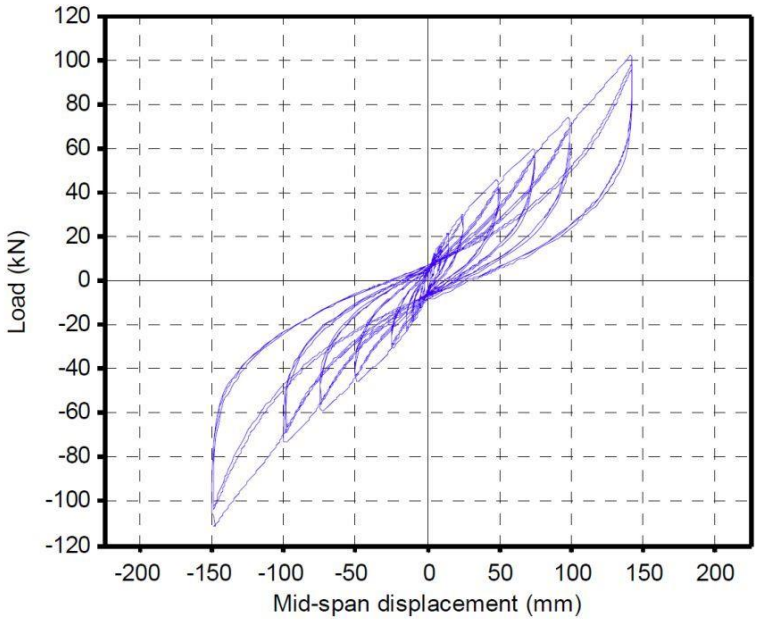

(c) Diaphragm FS3a

Figure 4-12 Testing result of wood diaphragm tested under cyclic load parallel to wood joist (Wilson et al. 2011)

4.2.3 Related Numerical Models of Wood Shear Walls and Sheathing to Framing Connections

A likely larger number of numerical models have been developed for wood shear walls. Simplified models that only account for the nonlinear behavior of the connection between sheathing and framing to predict the seismic response of the wall were proposed by Gupta and Kuo (1985) and Filiatrault (1990). The dynamic behavior of wood shear walls was also studied by Foliente (1995) who proposed a general hysteresis model for dynamic analysis of SDOF and MDOF systems. These hysteretic models were versatile and good simulation of different failure modes for wood panels was achieved when appropriate model parameters were used. However, as noted by Folz and Filiatrault (2001) a significant limitation exists in this models because they need to be calibrated to full scale data. Refined finite element that accounted for the interaction between sheathing, framing and connectors were also developed by Dolan and Foschi (1991) and White and Dolan (1995).

Because previous numerical models were excessively complex or too simple, Folz and Filiatrault (2001) developed a numerical model with reduced degree of freedom to capture the cyclic dynamic response of wood shear walls. As usual, the structural systems consisted of sheathing elements, framing elements and nonlinear springs to model the sheathing-framing connection. Two uncoupled orthogonally oriented springs with nonlinear behavior originally proposed by Foschi (1977) and then modified by Dolan (1989) (see Figure 4-13) were utilized.

The hysteretic features of the model developed by Stewart (1987) were incorporated in this model. Because using two uncoupled springs will usually overestimate the force and stiffness in the connector element, a novel solution strategy was implemented. In short, the energy absorbed by the wall was adjusted until it matched the energy absorbed for an equivalent SDOF wall. Also, this model was used to calibrate a SDOF system which predicts with reasonable accuracy the nonlinear behavior. The shear wall model validated against full-scale test of shear walls was implemented into the CASHEW (Cyclic Analysis of SHEar Walls) software.

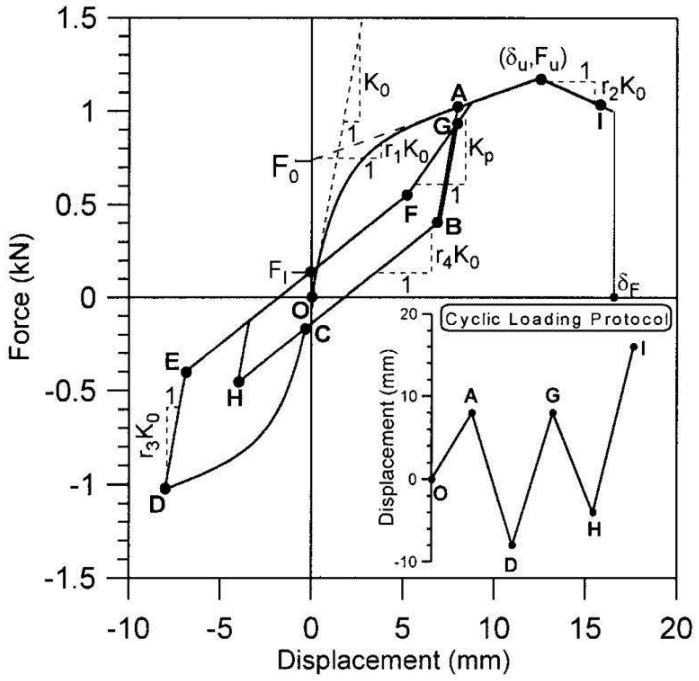

Figure 4-13 Force-displacement relationship of nails implemented by Folz and Filiatrault (2001)

This numerical model was later modified by Judd and Fonseca (2005), introducing an oriented spring model that does not need to be scaled or adjusted. In this model, the two orthogonal nonlinear springs, which simulates the sheathing to framing connection, are oriented using the initial displacement trajectory. As a result, the orthogonal springs are coupled through the initial orientation angle specified. Note that no significant improvement was achieved in capturing the nonlinear behavior of wood shear walls.

Judd (2005) also prepared an extensive survey regarding the sheathing-to-framing connections testing (see Table 4-1), parameters influencing the response of this connection (see Table 4-2), and idealization of the monotonic load-displacement response (Table 4-3). A detailed discussion on hysteresis models for this type of connections has also been discussed by Foliente (1995) and summarized in Table 4-4.

Table 4-1 Survey summary of sheathing-to-framing connection testing[a] (Judd 2005)

Reference	Monotonic	Cyclic	Dynamic	Primary components
Cruz (1993)	✓	✓		plywood, nails
Kent, Gupta, Miller (1996)	✓	✓	✓	plywood, nails
Ni, Chui (1994)	✓	✓	✓	plywood, nails
Gutshall (1994)	✓	✓	✓	plywood, nails, bolts
Dolan, Gutshall, McLain (1994)	✓	✓	✓	plywood, nails, bolts
Winistorfer, Soltis (1993)		✓		floor-wall-foundation
Dolan, Madsen (1992)	✓	✓		plywood, nails
Gavrilovic, Gramatikov (1991)	✓	✓		metal plate
Dolan (1989)	✓	✓		plywood, nails
Dean (1988)		✓		plywood, nails
Girhammar, Anderson (1988)	✓			plywood, nails, bolts
Chui, Ni, Jiang (1998)		✓		plywood, nails
Polensek, Schimel (1988)			✓	floor-wall-foundation
Polensek, Bastendorff (1987)		✓		various
Soltis, Mtenga (1985)			✓	floor-wall-foundation
Jacobsen (1960)		✓		plywood, nails, bolts
Kaneta (1958)		✓		plywood, nails
Countryman (1952)	✓			plywood, nails

[a] *See Judd (2005) for the complete list of references*

Table 4-2 Survey summary of parameters influencing the sheathing-to-framing connection response[a] (Judd 2005)

Connection Component	Parameter	Reference
Wood member	Wood specie	Fonseca et al. (2002), Hunt and Bryant (1990), Ehlbeck (1979)
	Moisture content	Fonseca et al. (2002), Hunt and Bryant (1990), Leach (1964)
	Thickness	Fonseca et al. (2002), Leach (1964), Mack (1960)
	Edge distance	Fonseca et al. (2002)
Fastener	Type, Diameter	Albert and Johnson (1967)
	Material	Fonseca et al. (2002), Hunt and Bryant (1990)
	Surface texture	Hunt and Bryant (1990)
	Wood penetration	Fonseca et al. (2002), Hunt and Bryant (1990)
	Head depth	Fonseca et al. (2002)
Configuration	Type	Fonseca et al. (2002), Hunt and Bryant (1990)
	Fastener pattern	Hunt and Bryant (1990)
	Grain direction	Hunt and Bryant (1990)
	Friction	Hunt and Bryant (1990)
Loading	Direction	Dolan et al. (1994), Hunt and Bryant (1990)
	Duration	Hunt and Bryant (1990)

[a] *See Judd (2005) for the complete list of references*

Table 4-3 Idealization of monotonic load-displacement response of sheathing-to-framing connections (After Judd 2005)

Type of Curve	Equation	Reference	Comments
Power	$P = C_1 d^{a_1} D\delta^{a_2}$	Mack (1977)	Appealing for design applications
	$P = C\delta^{1/a}$	Countryman (1952)	Mostly used by The American Plywood Association (APA)
Logarithmic	$P = A\log(1+B\delta)$	McLain (1975)	Later expanded by Pellicane et al. (1991)
Exponential	$P = C_1(B+A\delta)[1-e^{C_2\delta}]^a$	Mack (1966)	
	$P = C_1(1-e^{-C_2\delta})$	Easley et al. (1982)	
	$P = (P_0 + K_2\delta)[1-e^{-K_1\delta/P_0}]$	Foschi (1977)	Later expanded by Dolan (1989) and modified by Folz and Filiatrault (2001)
	$F = sgn(\delta) * (F_0 + r_1 K_0\lvert\delta\rvert) * \left[1 - \exp\left(-\frac{K_0\lvert\delta\rvert}{F_0}\right)\right], \lvert\delta\rvert \leq \lvert\delta_u\rvert$ $F = sgn(\delta) * F_u + r_2 K_0[\delta - sgn(\delta) * \delta_u, \lvert\delta_u\rvert \leq \lvert\delta\rvert \leq \lvert\delta_f\rvert$ $F = 0, \quad \lvert\delta\rvert > \lvert\delta_f\rvert$	Folz and Filiatrault (2001)	
	$P = A\delta/(B+\delta)$	Mc Cutcheon (1985)	
Asymptotic	$P = \frac{P_{yield}\delta}{\delta_{yield}}\left[\frac{K_2}{K_1} + \frac{(1-K_2/K_1)}{\left(1+(\delta/\delta_{yield})^R\right)^{1/R}}\right]$	Fonseca (1997) and Dugan (1995)	

As seen in Section 4.2.3, a number of analytical models can effectively reproduce the sheathing-to-framing connection. Thus, in selecting the most amenable model for this study, the following criteria were considered: a) the curve should have easily identifiable parameters which are readily available b) it should be easy to implement in commercial and research software and c) it should be a smooth hysteretic model. Smooth models produce a continuous change of stiffness due to yielding but sharp changes due to unloading and deteriorating behavior (Sivaselvan and Reinhorn 1999).

Table 4-4 Hysteresis models f sheathing-to-framing connections (After Foliente 1995)

Hysteretic curve	Reference	Comments
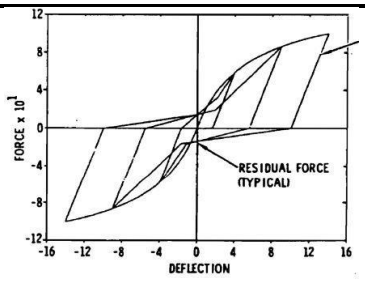	Ewing et al. (1980)	Smooth nonlinear backbone curve. Trilinear path for unloading and reloading calibrated to match experimental data.
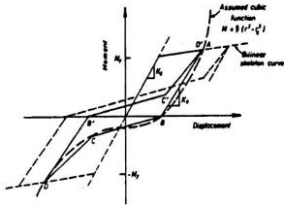	Kivell et al. (1981)	Bilinear backbone curve based on Takeda Model. Smooth trilinear path for unloading and reloading.
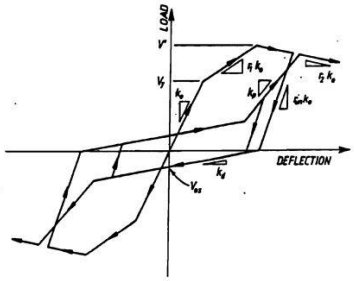	Stewart (1987)	A initial slackness to simulate shrinkage at bolt holes can be incorporated.
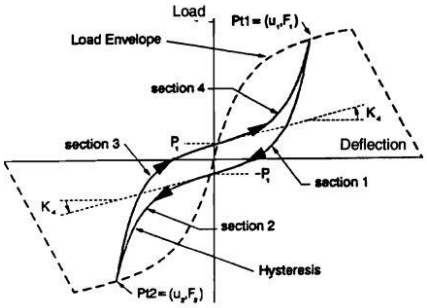	Dolan (1989)	Four segments defined by an exponential equation with four boundary conditions.
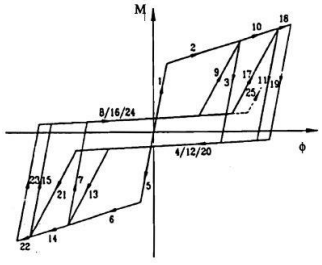	Ceccotti and Vignoli (1990)	Used to simulate moment-resisting wood joints. Pinching and stiffness degradation can be modeled.

4.2.4 Numerical Simulation of Wood Diaphragms in URM Buildings

Previous sections described numerical models that were typically developed without considering the interaction of the wood diaphragm with other building components or systems. To date, few numerical studies reported in the literature have been performed on horizontal wood diaphragms that are part of a URM building. In particular, the explicit modeling of older straight and diagonally-sheathed diaphragms and its interaction with URM buildings has not been published.

As discussed in section 2, Tena-Colunga and Abrams (1992) used a discrete linear elastic MDOF system to replicate the seismic response of a two-story URM building, which survived the 1989 Loma Prieta earthquake. In modeling the flexible diaphragm, an elastic shear springs and lumped mass was considered at the center of the diaphragm (see Figure 4-14). Also, an ABAQUS model with linear shell elements was developed to investigate the diaphragms flexibility in the torsional response of the building. To obtain good correlation with the measured response, the flexibility of the foundation had to be included in MDOF the model, although the soil was identified as stiff and the building was supported on spread foundations. With slight variations, the MDOF modeling approach using elastic springs has been recently used by Craig et al. (2002), Cohen et al. (2004) and Park et al. (2009).

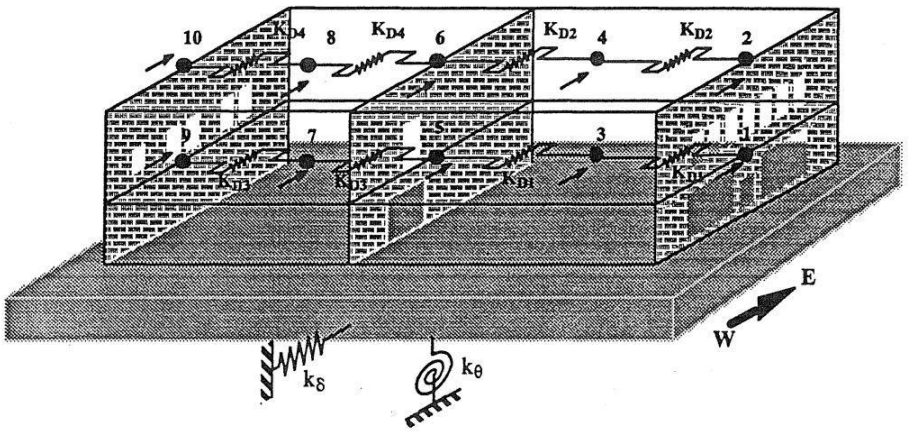

Figure 4-14 Analytical model used by Tena-Colunga and Abrams (1992)

Costley and Abrams (1996) also simulated the dynamic behavior of the shake table experiment discussed in section 2. They developed three analytical models for response spectrum, pushover and time history analysis. The wood diaphragm was simulated using elastic beam elements. In

particular, the displacement histories predictions using the 3-DOF model were in good agreement with the measured response (see Figure 4-15).

The idea of using a linear beams with reduced DOF has been also implemented by Kim and White (2004a) to carry out linear static analysis of low rise masonry buildings. The model was later extended for nonlinear analysis of 3D low rise URM buildings, where the beam element was replaced by a six DOF diaphragm element (see Figure 4-16). The proposed MDOF predicted with good accuracy the dynamic behavior of the diaphragm tested by Cohen et al. (2004).

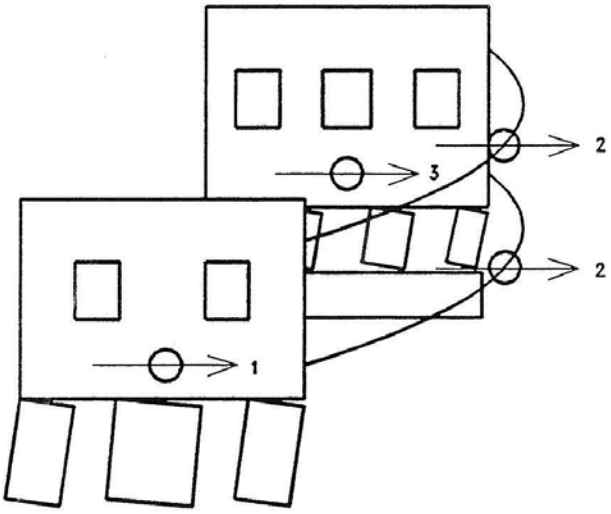

Figure 4-15 Three-DOF model implemented by Costley and Abrams (1996)

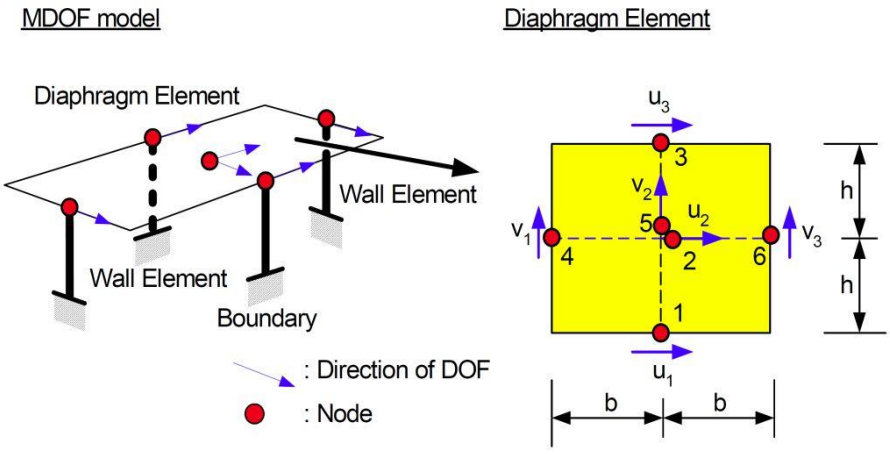

Figure 4-16 Six-DOF model proposed by Kim and White (2004b)

More recently, an experimental program on URM buildings was conducted at the Mid-American Earthquake Center (MAEC). In this program, several numerical models to represent the URM building and flexible diaphragm were implemented. Yi et al. (2006a) built a 3D elastic FEM of the two story URM building and an isotropic material was employed for the flexible diaphragm. Because the external forces were applied at the in-plane walls of the building, the analysis results showed that the presence of a flexible diaphragm had negligible effect on the behavior of the test structure.

Numerical analysis of a multi-story URM building with flexible diaphragms were carried out by Mendes and Lourenço (2009). In modeling the wood floor, shell elements combined with beam elements were used to capture the in-plane flexibility. The model, however, was only used to perform pushover analysis which did not properly capture the failure mode of the structure (See Figure 4-17).

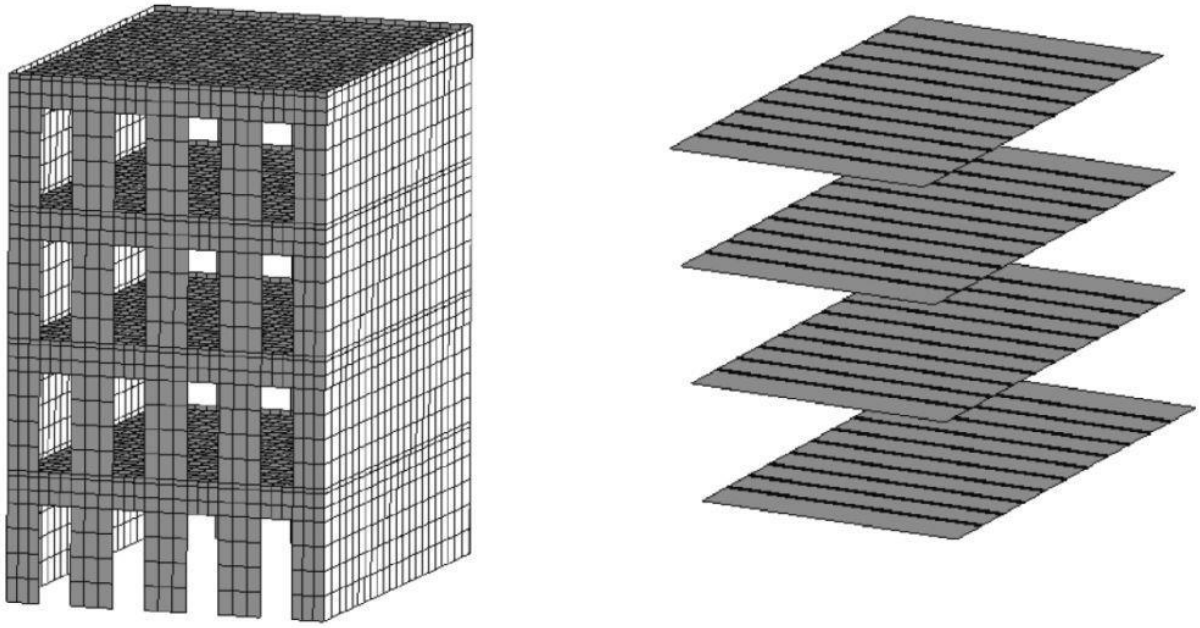

Figure 4-17 Finite element model proposed by Mendes and Lourenço (2009)

Other commercial programs specifically developed to analyze URM buildings, such as SAM and TRIMURI currently do not account for flexible diaphragms and its interaction with masonry walls.

4.3 Evaluation of Current Numerical Tools

In this section, the capabilities of a detailed FEM and a simplified SDOF modeling techniques of wood diaphragms are evaluated by simulating the in-plane response of a wood diaphragm tested by Peralta et al. (2004). As it will be shown in Section 4.3.1, this experiment was selected due to its similar characteristic in construction with wood diaphragms existing in older URM buildings located in NYC.

In Section 4.3.2 a refined finite element model is built in OpenSees. This model uses the specialized material model SAWS (Folz and Filiatrault 2001) for the sheathing-to-framing nailed connection. Then, in Section 4.3.3 it is demonstrated that a similar model in SAP2000 can reproduce the global behavior of the diaphragm, when appropriate parameters are used in the Pivot hysteretic model of the sheathing-to-framing connection. The development of a SDOF model of the wood floor implemented in OpenSees and SAP2000 is discussed in Section 4.3.4.

The comparison of the experimental and numerical results indicates that the refined FEM models can effectively capture the nonlinear behavior of the specimens and accurately forecast their strength and initial stiffness. Nonetheless, the computer time required to carry out every analysis is significant, making it unfeasible to analyze the larger diaphragms present in the building prototypes, and to complete parametric or sensitivity analysis. On the other hand, the SDOF is highly computer efficient, yet it underestimates the maximum response and requires precise calibration against numerical or experimental data. To overcome this issue, in Section 4.4 a dynamic model with reduced degree of freedom is introduced and validated against previous numerical and experimental results.

4.3.1 Selected Experimental Model -MAE-2 Peralta et al. (2004)

Two criteria were used in selecting experimental models from the literature, namely 1) its type of construction, which should be similar to that existing in NYC (i.e. 1x6 in. straight-sheathed boards, 2x10 in. joist and 10d nails) and 2) its plan dimensions, which should have a length to width ratio between 2 and 3, similar to those found in the prototype.

Under these conditions, one specimen was selected from the experiments conducted by Peralta et al. (2004). This specimen, MAE-2, is a 24 ft. by 12 ft. diaphragm with 1 x 6 in. square edge straight boards and 2 x 10 in. pine lumber joist each spaced at 16 in.. Typical 8d common nails were used to connect the boards to joists. As described in Section 4.2.2, cyclic quasi-statics loads were applied at the third points along the length of the diaphragms. This diaphragm was rehabilitated after testing and then tested again. However, in this research only the first test is considered. In this diaphragm, boards are perpendicular to the joists which are in turn supported by a steel frame, which was not considered in the numerical model. Figure 4-18, shows dimensions and components considered in this model, and Table 4-5 presents the material and section properties considered for numerical simulation. Because Peralta et al. (2004) did not carry out material identification tests, the material properties were directly taken from AF&PA-97 and APA-86 documents.

Figure 4-19 presents the experimental force-displacement relationship of the diaphragm, measured at the loading points. The response of the diaphragm is basically dominated by yielding and slippage of the nails connecting boards to joists. Maximum shear strength of about 13 kip was attained at 3.1 inches and high dissipation of energy can be observed.

Table 4-5 Material properties for MAE-2 diaphragm

Structural component	Material and section properties
Beam joist	A=20 in^2, Iz=167 in^4, E=1798 ksi, Nu=0.2
Boards sheathing	A=6 in^2, Ix=18 in4, E=1798 ksi, Nu=0.2, Rho=5.15x10^{-8}

A, Cross section area
Iz, Moment of inertia around z axis
Ix, Moment of inertia around x axis
E, Young's Modulus
Nu, Poisson ratio
Rho, Mass density

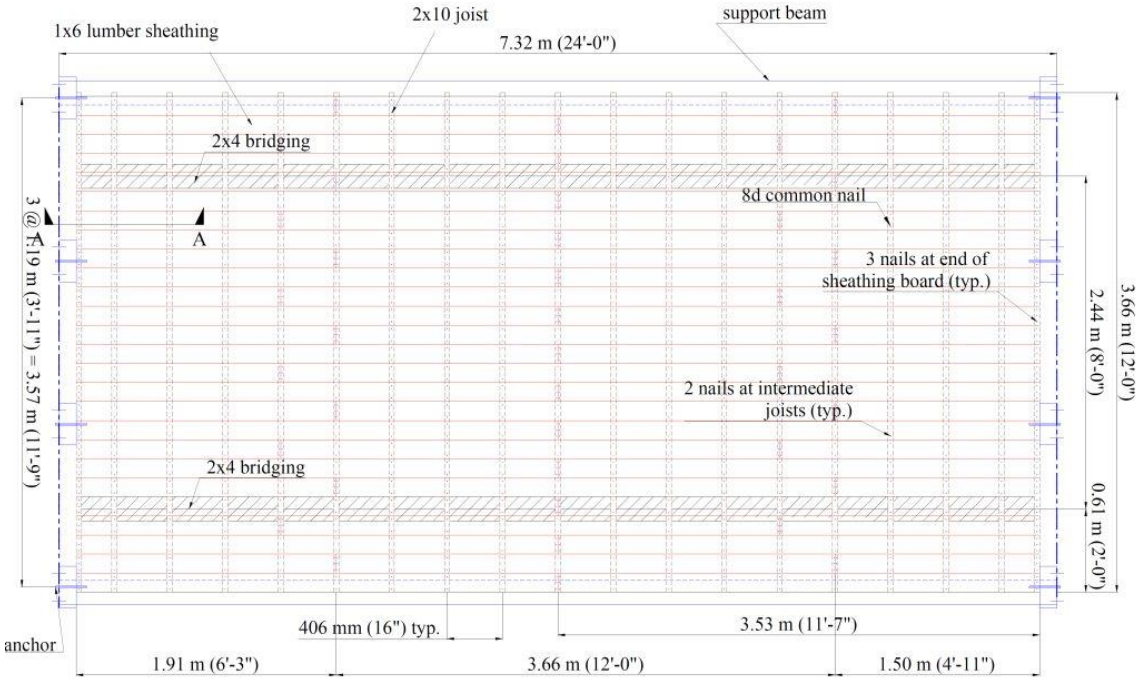

Figure 4-18 Typical components on wood diaphragms MAE-2 (Peralta et al. 2004)

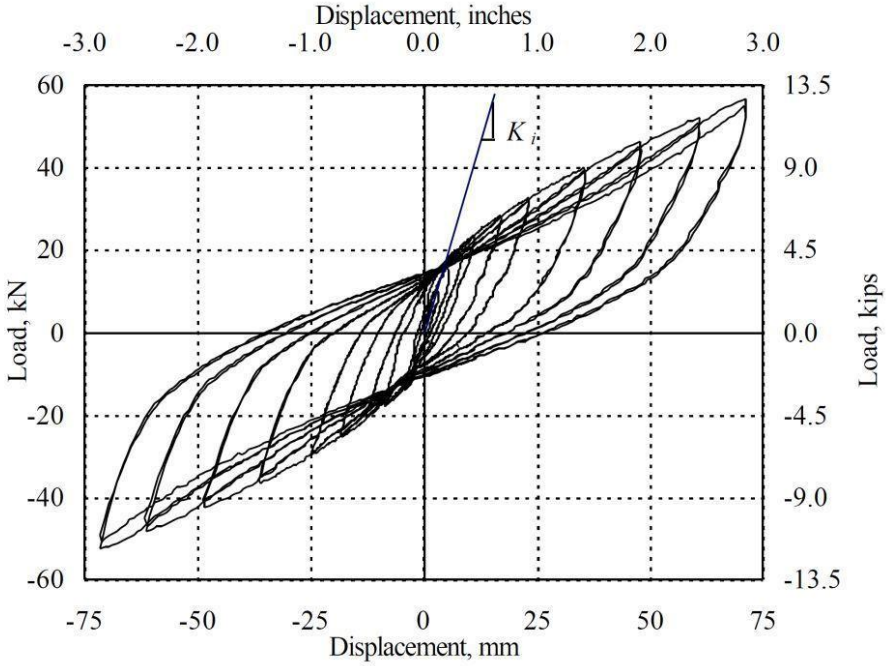

Figure 4-19 Experimental force-displacement relationship of MAE-2 diaphragm (Peralta et al. 2004)

4.3.2 Numerical Model in OpenSees

A two dimensional finite element model of MAE-2 diaphragm was built in OpenSees. Specific information on the geometry, material properties and experimental response was presented in the previous section. Figure 4-20 illustrates the structural components and OpenSees elements used in modeling the diaphragm. Herein, the modeling approach is similar to that followed by Foschi (1977) and Peralta et al. (2004) using different software.

Since OpenSees does not have a graphical user interface (GUI), the model definition was partially carried out in SAP2000. Node coordinates, boundary conditions, element connectivity and loadings were initially defined in SAP2000. Then, the model was exported to MS Excel format, where additional modifications were needed to finally produce a file in OpenSees format. This file was then completed with information regarding material properties and analysis commands.

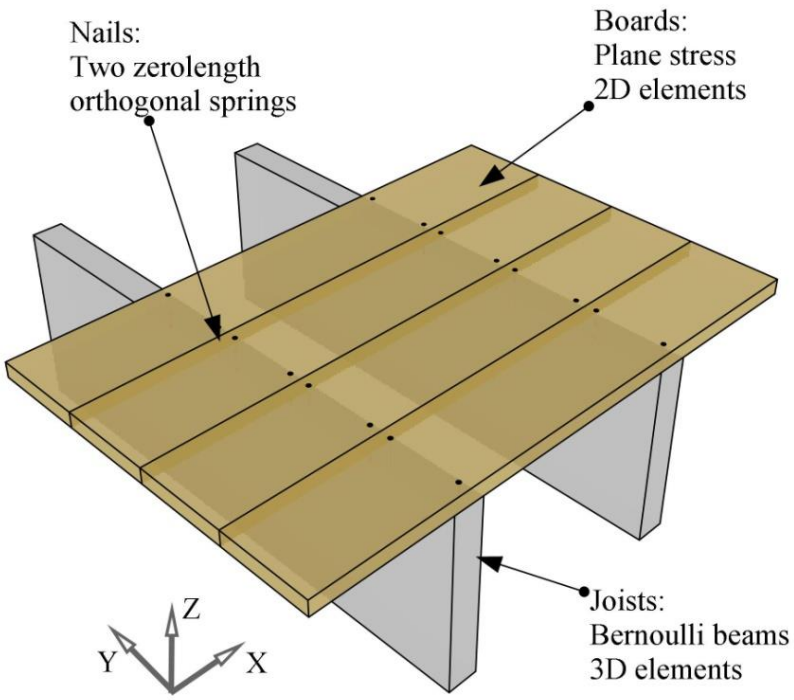

Figure 4-20 Structural components and equivalent OpenSees elements

Boards were modeled using *quad* elastic isotropic elements, which have only two translational DOF at each node. This type of element is suitable to model two-dimensional solids of uniform thickness in a state of plane-stress or plane-strain. No variation of stresses and strains in the thickness direction are assumed. A state of plane-stress was assumed for the boards, as its thickness is small compared to its planar dimensions.

Joists were simulated using *elasticBeamColumn* elements with three DOF at each node, two translations (x and y) and one rotation (around z). Herein, it is assumed that all properties are constant along the full length of each element.

Nails were replicated using *zeroLength* springs in two perpendicular directions. The *uniaxialMaterial* SAWS, developed by Folz and Filiatrault (2001) was utilized to simulate the nonlinear force-displacement relationship of the springs. Calibration of the SAWS material was performed using the load-displacement response proposed by Mclain (1975); with parameters A and B as calculated by Peralta et al. (2004). Note that these values were estimated based on lower bound properties of the nails. A minimization procedure similar to that described by Folz and Filiatrault (2001) was used to fit the SAWS model. A comparison between force-deformation relationships of both models can be seen in Figure 4-21 and the material parameters required for SAWS to match McLain (1975) model are presented in Table 4-6. The model reaches a maximum shear force of 0.35 kip at 0.16 in. displacement. This is consistent with previous nails models used by Folz and Filiatrault (2001), and Judd (2005). Also, the cyclic behavior is presented in Figure 4-22.

Table 4-6 SAWS material parameters fitted to McLain (1975) model

F0 (kip)	F1 (kip)	DU (in)	S0 (kip/in)	R1	R2	R3	R4	alpha	beta
0.27	0.12	0.30	18.0	0.033	-0.050	1.0	0.060	0.080	1.10

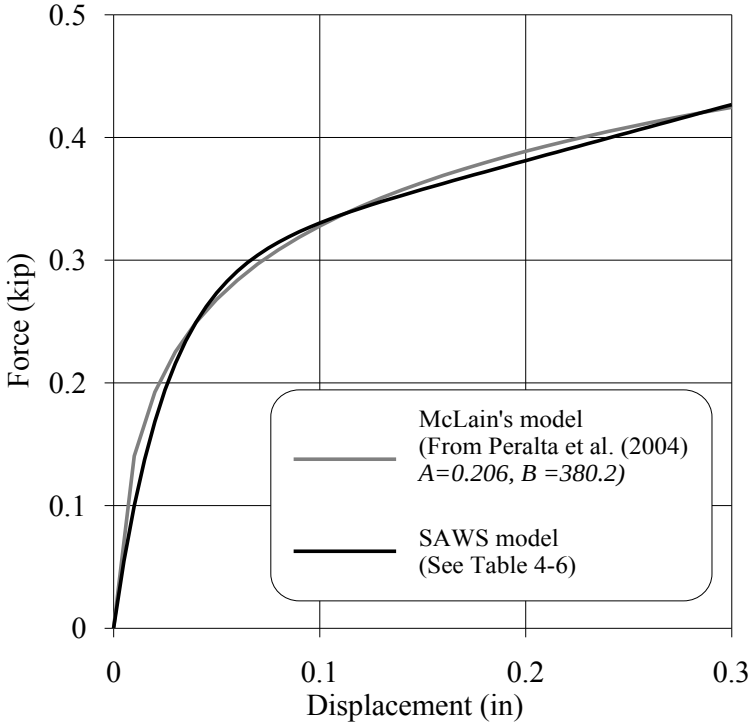

Figure 4-21 Comparison between McLain's model and SAWS material

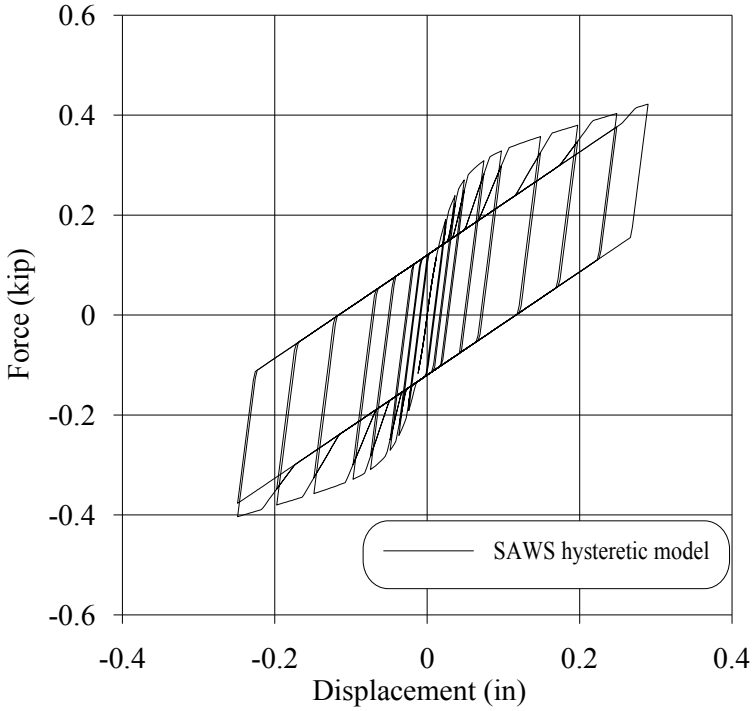

Figure 4-22 Cyclic force-displacement behavior of SAWS model of one nail

Fonseca (1997) demonstrated that no appreciable difference was found between coarse and fine mesh elements in modeling a shear wall sheathing component. Thus, in this study a coarse mesh was implemented. The characteristic length of the elements was kept close to 1, to avoid hourglass modes or numerical errors. About 17,000 quad elements, 500 beam elements and 2000 springs were defined.

Since *quad* elements work only for two-dimensions, and *elasticBeamcolumns* are defined in three-dimensions, the OpenSees TCL file should be defined in two domains. Those domains must be connected through the *EqualDof* command. Figure 4-23 shows a detailed view of the connectivity between quad, springs and beam elements. The 2d-quad elements are connected to the *zeroLength* springs in x and y directions which in turns are connected to the 3D-beam element. Observe that concurrent edge nodes of *quad* elements that represent individual wood boards do not have to be connected to properly simulate the independence between boards.

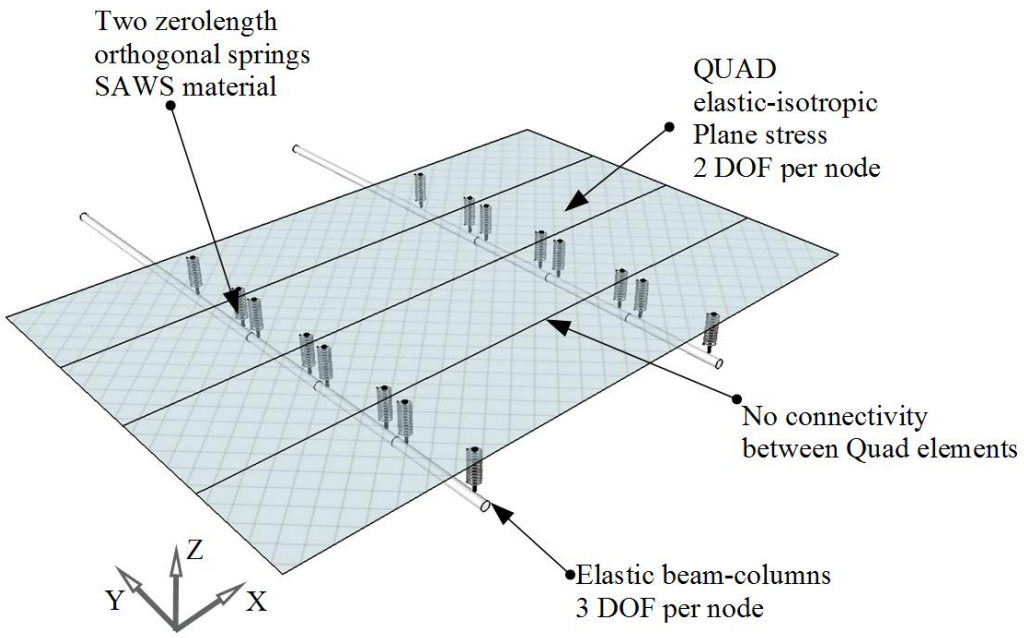

Figure 4-23 Connectivity between quad, springs and beam elements in OpenSees

The model was subjected to cyclic quasi-static loads applied at one third along the diaphragm length. The loading protocol is the same as in Peralta et al. (2004) and it can be seen in Figure Figure 4-24 .This loading profile applies two cycles for each lateral displacement amplitude. The displacement amplitude effectively induces elastic and inelastic lateral response in the

diaphragm. A maximum actuator stroke of 3.0 in. is the maximum amplitude of the loading protocol.

The analysis commands used are summarized in Table 4-7. Although OpenSees includes a significant number of analysis options, no special considerations were made in defining the type of analysis performed on this model. More information regarding default OpenSees commands can be found elsewhere (OpenSees 2012). Note that the analysis time of this model took about 130 hours, using a PC running windows XP S3 on an Intel Core 2 duo processor.

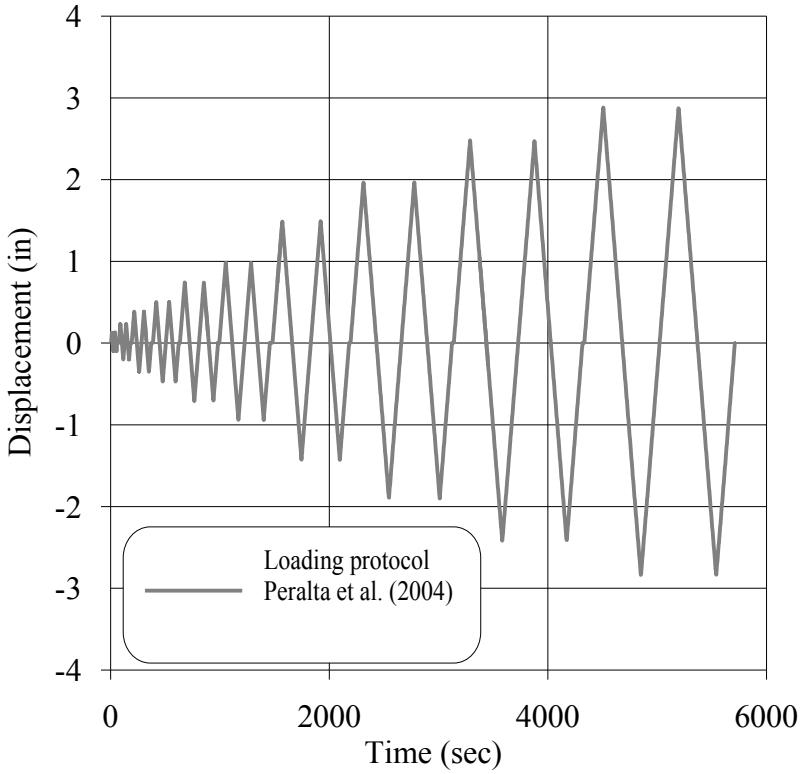

Figure 4-24 Loading protocol as defined by Peralta et al. (2004)

Table 4-7 OpenSees analysis parameters

Component class	OpenSees command	Parameter value
Constraint handler	constraints	Penalty $alphaS= 1.0e12, $alphaM= 1.0e12
DOF Numberer	numbered	RCM
System of eqn. solver	system	BandGeneral
Convergence test	test	NormDispIncr $tol=1.0e-8, $iter=6
Soultion algorithm	algorithm	Newton
Integrator	integrator	LoadControl $lambda=1
Analysis type	analysis	Static

Figure 4-25 presents the load-displacement relationships for MAE-2 diaphragm obtained using OpenSees with SAWS material. The response obtained closely reproduces the experimental behavior. The major difference between the experiment and OpenSees predictions is the maximum strength attained. The experimentally measured maximum strength is overestimated by the numerical model in 5%. The unloading and pinching responses are accurately predicted but the reloading degrading stiffness is also overestimated. This discrepancy at large displacement is attributed to the assumed force-displacement relationship of the connectors, which was taken without adjustments or modifications from Mclain's and Peralta's studies.

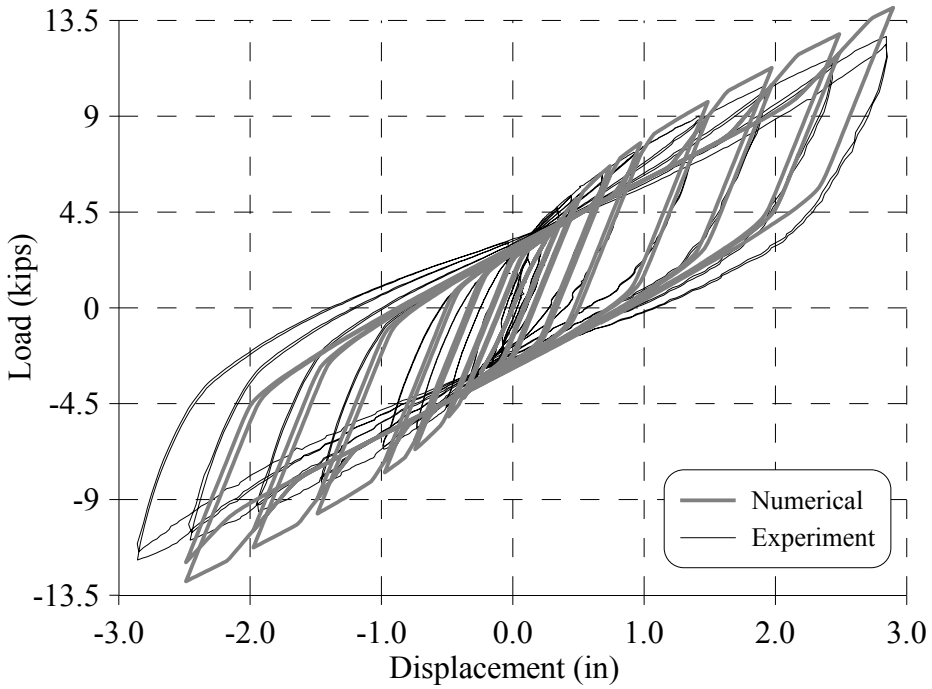

Figure 4-25 Predicted load-displacement relationship for MAE-2 diaphragm a) Experiment b) OpenSees SAWS model

Also, for completeness, modal, pushover and time history analysis were carried out using this model. The results are shown in Section 4.4, where a comparison between different models developed in this section is completed. In estimating the seismic mass, only the self-weight of the diaphragm was included.

4.3.3 Numerical Model in SAP2000

The MAE-2 experiment is also simulated using SAP2000. The same geometry built to generate the OpenSees model was used. Specific information on this geometry was presented in Section 4.3.1. A three-dimension view of the model is shown in Figure 4-26. Four pinned joint restraints were used at each side of the diaphragm. The material parameters for wood are presented in Table 4-8. These values were specified as defined in Section 4.3.1.

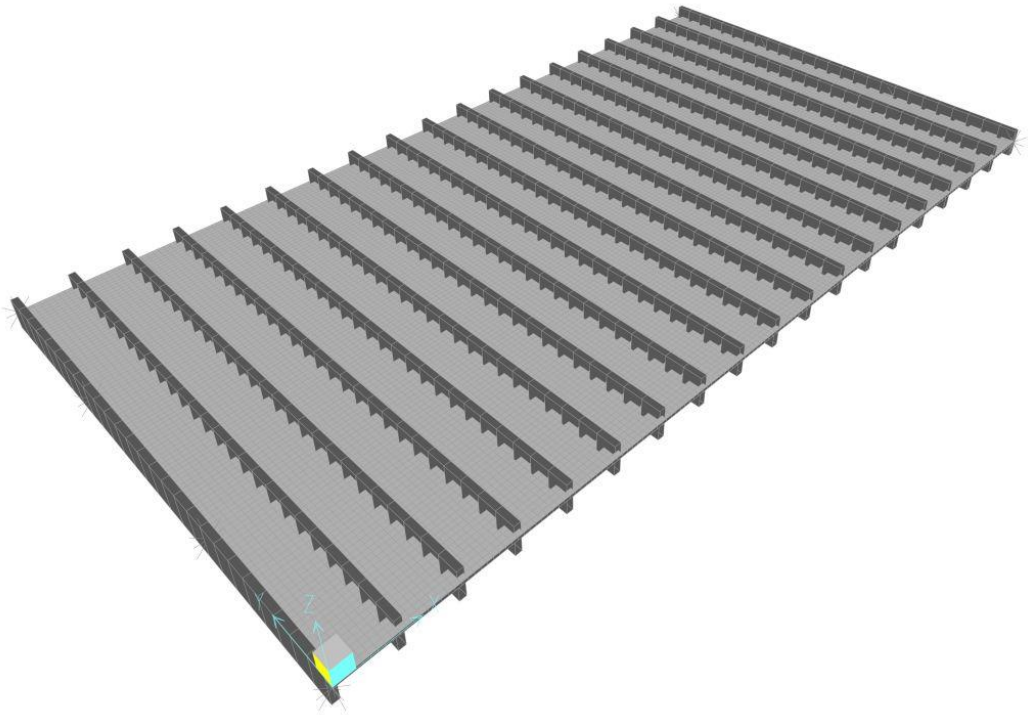

Figure 4-26 Three-dimensional view of the model built in SAP2000

Table 4-8 Material parameters defined in SAP2000

Material property data	Parameter	Parameter value
General data	Material type	Other
Weight and mass	Weight per unit volume	1.987E-05
	Mass per unit volume	5.147E-08
Isotropic property data	Modulus of Elasticity, E	1800
	Poisson's Ratio, U	0.2
	Coefficient of Thermal Expansion, A	6.50e-06
	Shear Modulus, G	750

Wood boards were simulated using the *Plane* element available in SAP2000. As assumed in OpenSees, a state of plane-stress is considered for the boards, since the thickness is small compared with its planar dimensions. Specifically, a one inch thickness section is used for each *Plane* element. All other section parameters were the default values specified in the software. Incompatible bending modes option was used, since it allows models with coarser meshes to achieve acceptable results. For the Plane element, only three translational degree of freedom are activated at each of its connected joints, resulting in a faster computer time when compared to shell elements, which activate six degree of freedom (CSI 2010).

Joists were modeled as *Frame* elements. In SAP2000, these elements use a three-dimensional beam-column formulation which includes axial, torsion and biaxial bending and shear deformations (CSI 2010). Frame element activates all six degree of freedom at each of its connected joints. However, only two translational (x and y) DOF and one rotational (z) DOF were set available for this simulation. A 2 in x10 in. cross section was created in the *Section Designer* modulus available in SAP2000.

Nails were modeled as *zero-length* nonlinear spring elements. Two springs were used to simulate the behavior of each nails in two perpendicular directions. Uni-axial behavior was assumed for each spring and the Advanced Local Coordinate system feature was used to orient each spring in the direction of the longitudinal axis 1.

As shown in Section 4.2, the cyclic behavior of the sheathing-to-framing connection is characterized by pinching, stiffness and strength degradation. These characteristics are only partially captured by the *multi-linear plastic Pivot* hysteretic property in SAP2000. This hysteretic model was originally proposed by Dowell et al. (1998) to model nonlinear behavior of reinforced concrete members. It assumes that unloading and reverse loading are directed toward specific points, "pivot" points, in the force-displacement plane. Three parameters define the cyclic behavior namely, 1) alpha, which locates the pivot point for unloading to zero from positive or negative force, 2) beta, which locates the pivot point for reverse loading from zero toward positive or negative force and 3) nu, which determines the amount of degradation of the elastic slopes after plastic deformation (CSI 2010). Those parameters are shown in Figure 4-27.

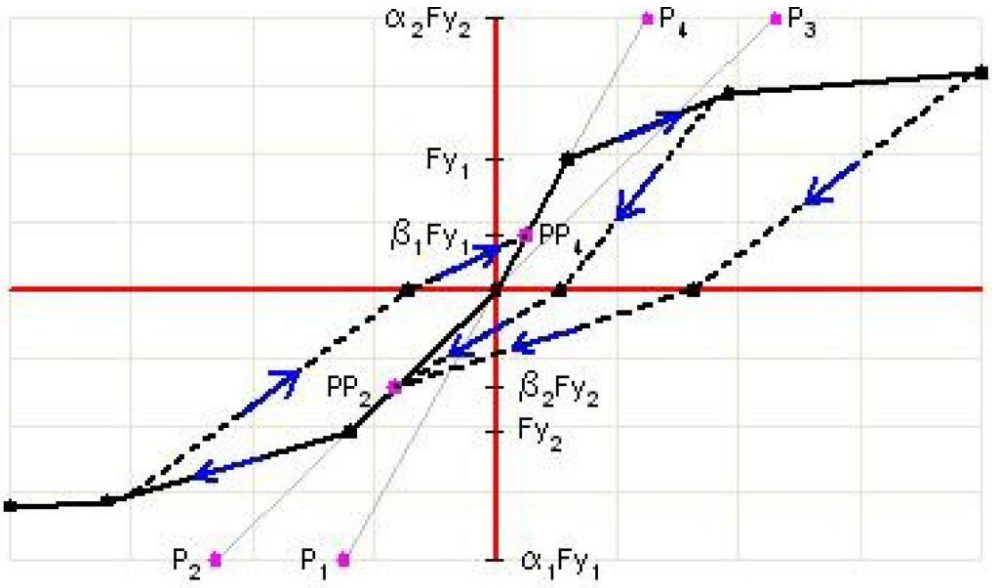

Figure 4-27 Multi-linear Pivot plasticity property for uniaxial deformation (CSI 2010)

In defining the nonlinear *Link* properties, a multi-linear force-deformation curve and hysteresis parameters must be specified. The nonlinear force-deformation relationship properties were copied from the smooth multi-linear curve defined by the SAWS material. After several trials, the hysteretic parameters were defined as alpha=1000, Beta=0.9 and nu=100. Note that the pivot point of the model has to be defined far enough from the origin so that the unloading stiffness at large displacements is equal to the unloading stiffness at small displacements.

Figure 4-28 presents the cyclic force-displacement relationship for one nail obtained using the SAWS and Pivot models, respectively. The loading protocol proposed by Peralta et al. (2004) was used to complete this quasi-static simulation, but its amplitude was scaled down by one tenth. The Pivot model exactly follows the backbone curve copied from the SAWS model. Yet, the unloading stiffness and pinching effect are completely different. This was expected, since the Pivot model requires the unloading goes back to zero force from any displacement level, before heading to the pivot point. The total dissipated energy[1] is overestimated by the Pivot model in 6%.

[1] The total dissipated energy is calculated using the trapezoid rule

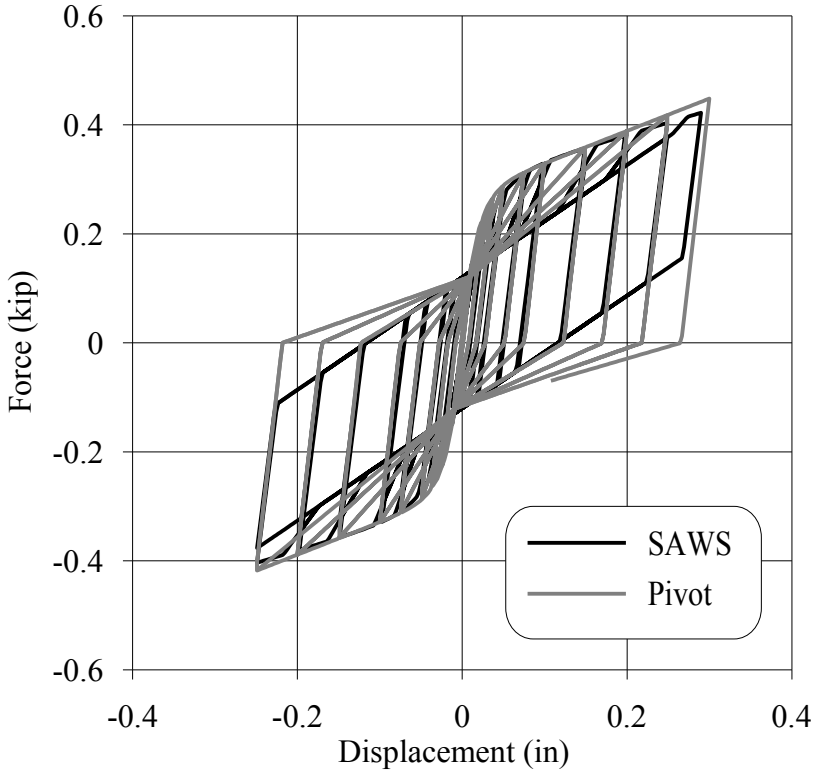

Figure 4-28 Analytical force-displacement relationship for one nail obtained using the SAWS and Pivot models

The two-dimensional cyclic quasi-static analysis was completed using a Multi-threaded solver with only three DOF's available, namely UX, UY and RZ. No inertial or damping forces were considered. The kinetic energy was monitored after the analysis to guarantee that inertial effects were negligible. Herein, the same loading function used to complete the quasi-static analysis in OpenSees was implemented. Note that, however, the load case defined in SAP2000 is a nonlinear time history analysis. The numerical simulation is conducted using *Newmark Direct Integration* method with default nonlinear parameters.

Figure 4-29 shows the deformed shape of the diaphragm at maximum displacement. Note that area elements close to the boundaries overlap considerably, which is clearly an unrealistic behavior. The effect of considering mechanical contact between area elements is investigated later in this section.

Figure 4-30 presents the load-displacement relationships for MAE-2 diaphragm obtained using SAP2000 with Pivot hysteretic rule. The response obtained closely reproduces the experimental behavior. Again, the major difference between the experiment and SAP2000 predictions is in the

maximum strength obtained. The experimentally measured maximum strength is overestimated 7% by the numerical model.

To further understand the kinematic behavior of the diaphragm, shear and bending stress values at maximum deformation are depicted in Figure 4-31 and Figure 4-32. Bending stresses are significantly higher than shear stresses, which imply a predominant bending behavior of the system. This is confirmed in Figure 4-32, where almost zero shear stress can be observed at the middle of the diaphragm. This finding is contrary to what is usually assumed for other types of flexible diaphragms (e.g. plywood shear walls, steel decks), which can experience large shear deformations [Gupta and Kuo (1985), Reinhorn et al. (1988)].

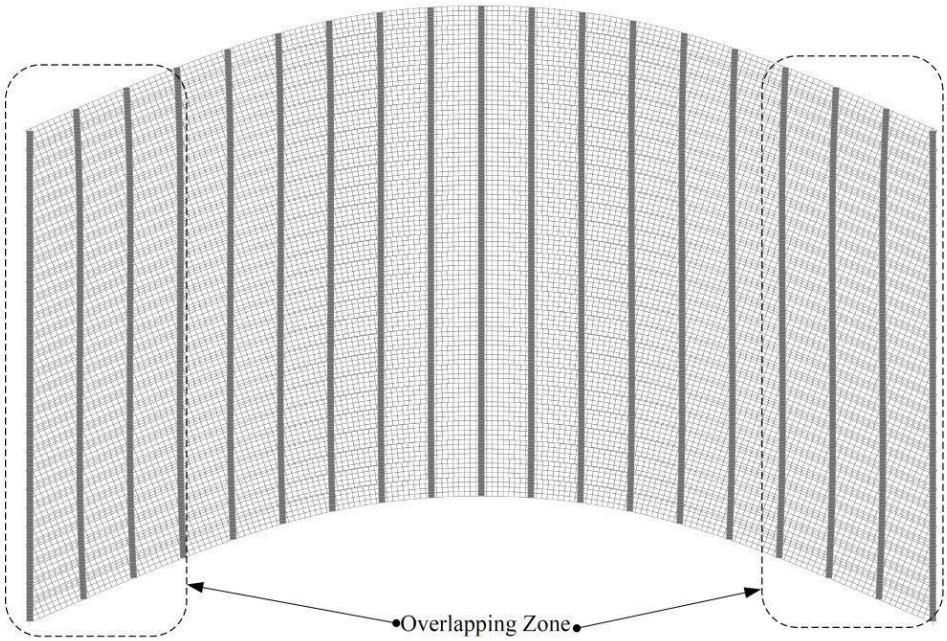

Figure 4-29 Deformed shape of MAE-2 at maximum displacement obtained in SAP2000

To investigate the influence of mechanical contact between wood boards, a gap (i.e. compression-only) element with contact stiffness **Kc** was introduced between individual plane stress elements. These elements were introduced only in the overlapping zone illustrated in Figure 4-29. Since no experimental data were available to quantify **Kc**, an initial value of 0.5 kip/in was used, as suggested by Dolan and Foschi (1991). Then, pushover analysis was repeated using increasing values of **Kc**, as shown in Figure 4-33. The results indicate that for displacements of up to 30% of the maximum, the system was not significantly affected by the

contact stiffness. At the maximum displacement of three inches, an increase in load capacity between 5 to 30 percent can be observed.

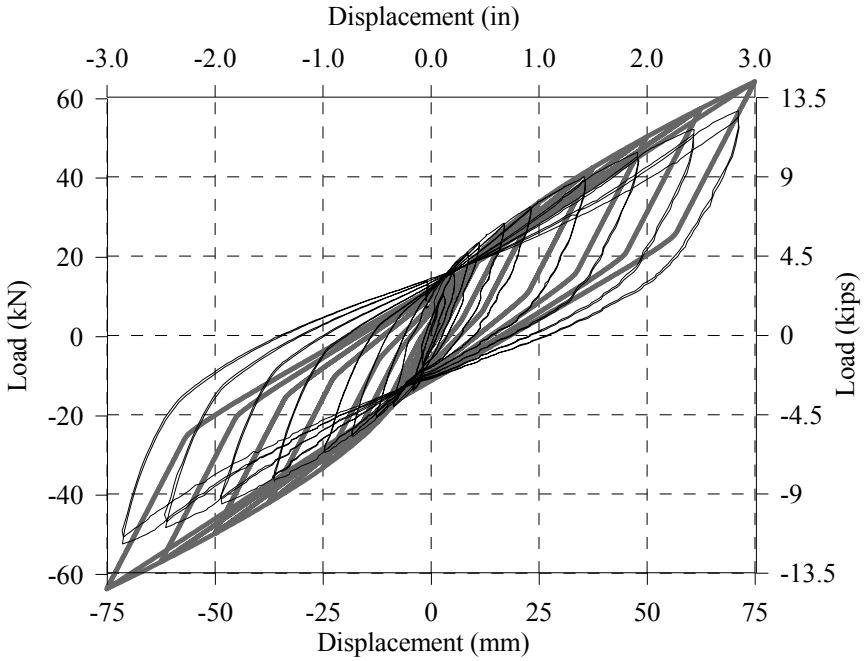

Figure 4-30 Predicted load-displacement relationship for MAE-2 diaphragm a) Experiment b) SAP2000 Pivot model

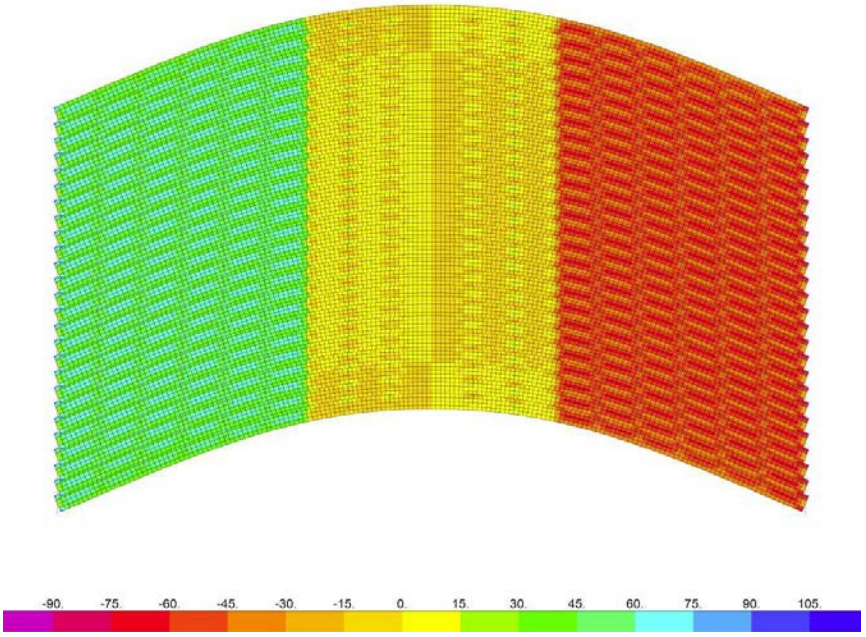

Figure 4-31 Shear stress distribution at maximum displacement for MAE-2 diaphragm obtained using SAP2000

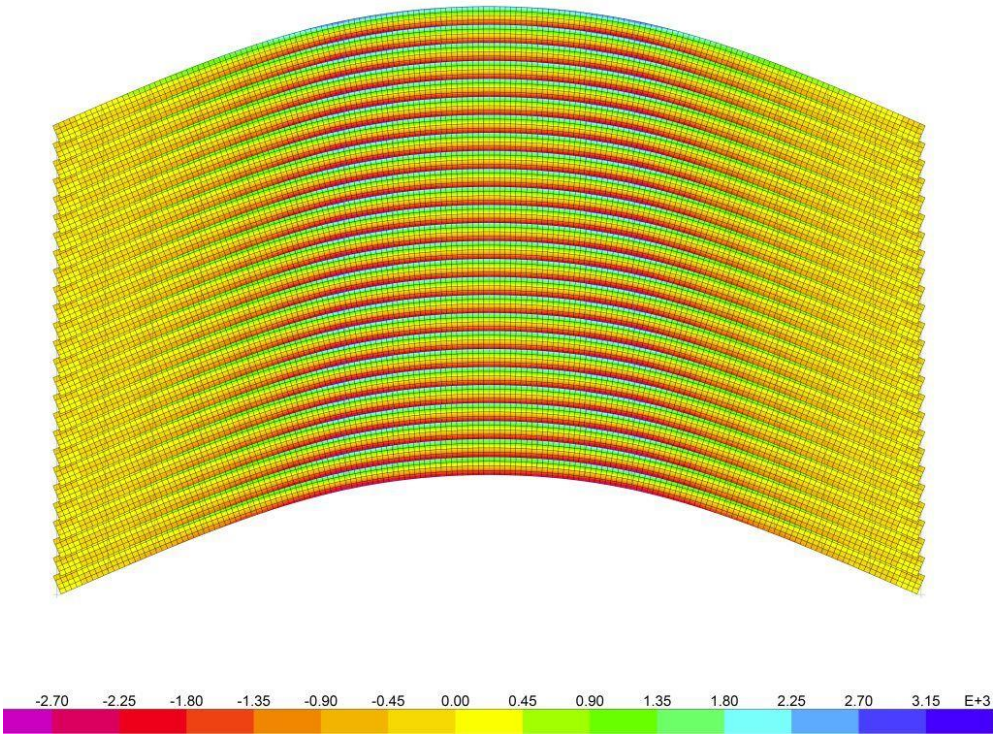

Figure 4-32 Bending stress distribution at maximum displacement for MAE-2 diaphragm obtained using SAP2000

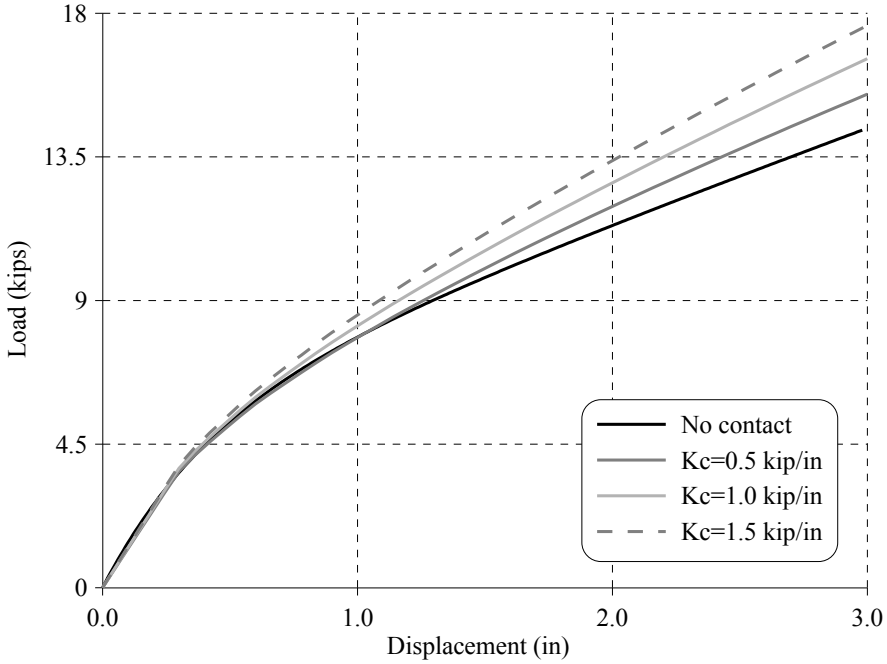

Figure 4-33 Pushover curves obtained for different values of contact stiffness, Kc

4.3.4 SDOF Model

It has been demonstrated that refined finite element models are capable of simulating the force-displacement response of wood diaphragms under cyclic loading. In completing this analysis, only Young's modulus of the wood diaphragm and information regarding the cyclic behavior of the sheathing-to-framing connection are needed as input data. However, the analysis time to complete each simulation is burdensome.

As discussed in Section 4.2.4, previous studies have simulated the dynamic behavior of wood diaphragms using a linear SDOF lumped parameter models. The same approach has been applied for modeling wood shear walls. In these studies, the SDOF hysteretic model was fitted to experimental or simulated data of full scale specimens (Foliente 1995); (Folz and Filiatrault 2001). The same approach is adopted in this study, the full scale simulation performed in OpenSees and SAP2000 will be used to calibrate the SDOF hysteretic properties of a nonlinear spring. The idealization of the diaphragm as SDOF can be seen in Figure 4-34. In this model, the displacement at the center of the diaphragm is the only DOF available. Also, half of the available seismic mass is considered in the model.

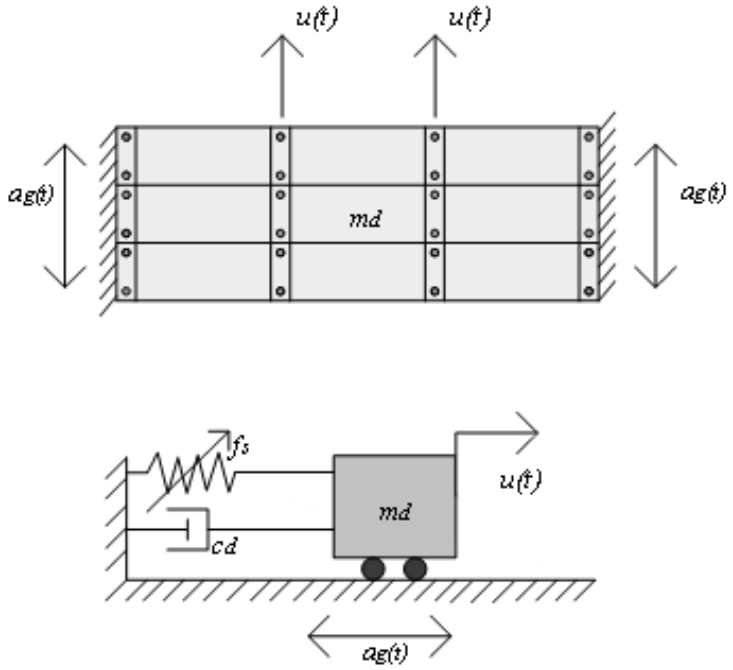

Figure 4-34 Idealization of diaphragm as SDOF

The equation of motion of the SDOF system is given by

$$m_d\ddot{u}(t) + c_d\dot{u}(t) + f_s[u(t)] = -m_d a_g(t) \quad (4.1)$$

Where m_d= Tributary mass of the diaphragm; c_d= viscous damping coefficient, $f_s[u(t)]$= nonlinear force- displacement relationship of the spring; a_g= ground acceleration ; ü(t), u (t) and u (t) are the acceleration, velocity and displacement at the center of the diaphragm. This equation will be solved in both, OpenSees and SAP2000 using Newmark constant average-acceleration time integration scheme.

It has been previously noted that the characteristics of the global response of wood shear walls and diaphragm is similar to those of individual connections. Therefore, the nonlinear force-displacement relationship of the spring in Equation 4.1, which will use SAWS material, can be determined using the global force-displacement response predicted by OpenSees. The parameters of the SAWS model were obtained by a fitting procedure to match the monotonic and cyclic global response of the diaphragm. Three parameters, namely k_0, $r1_{ko}$, and $r2_{k0}$, were obtained using the pushover curve of the diaphragm and by the linear regression method available in Excel MS software. The other two parameters, $r3_{k0}$ and $r4_{k0}$ were estimated from the hysteretic curve by minimizing the dissipated energy in each cycle.

Figure 4-35, presents a comparison between the monotonic force-deformation relationships obtained using the detailed FEM in OpenSees and the monotonic curve of the SDOF with calibrated SAWS model. The SAWS parameters are summarized in Table 4-10. Also, the cyclic behavior is presented in Figure 4-36, where a good match can be seen between both models.

Table 4-9 SAWS material parameters fitted to full diaphragm

F0 (kip)	F1 (kip)	DU (in)	S0 (kip/in)	R1	R2	R3	R4	alpha	beta
5.60	2.70	5.0	12.50	0.22	-0.050	1.00	0.26	0.55	1.10

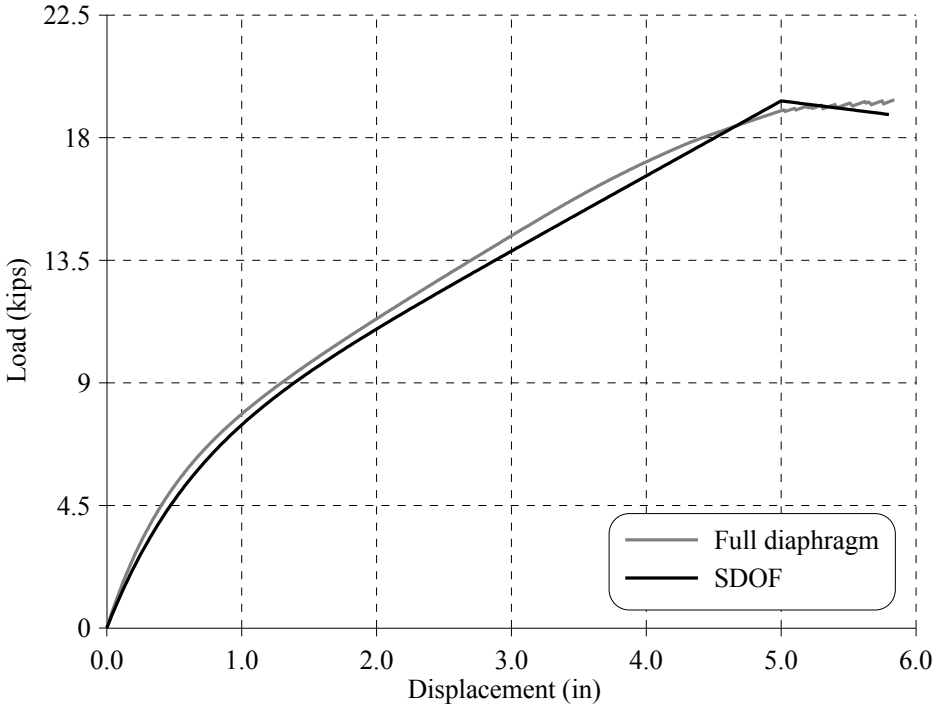

Figure 4-35 Predicted monotonic force-deformation using detailed FEM and SDOF models in OpenSees

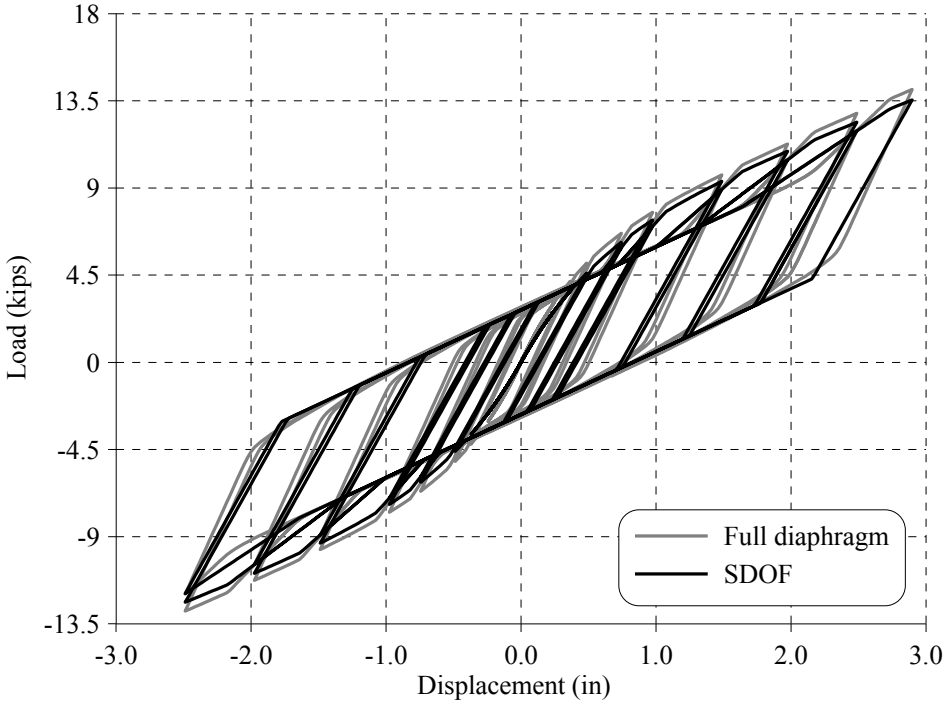

Figure 4-36 Predicted force-deformation relationship obtained using detailed FEM and SDOF in OpenSees

4.4 Simplified MDOF Model for Flexible Diaphragms

In this section, a reduced MDOF model of the straight-sheathed wood diaphragm studied in previous sections is proposed and implemented in OpenSees and SAP2000. The model is suitable for monotonic, increasing cyclic quasi-static and time history analysis in two and three dimensions. It also requires significantly less computational time while fully capturing the nonlinear seismic behavior of the diaphragm.

The model is based on the nail-couple method suggested by the ATC-7 (ATC-7 1981) and ATC-7-1 (ATC 7-1 1979) to estimate the in-plane shear strength of straight-sheathed diaphragms. These documents suggested that this type of diaphragm behaves like a series of individual beams which interact only through the connection with the supporting joists. The total strength of the diaphragm is then estimated considering only the nail-couple required to resist forces perpendicular to the sheathing boards.

4.4.1 Structural Configuration

Figure 4-37(a) presents a typical wood horizontal diaphragm in URM buildings. It is usually composed of four basic structural components, namely sheathing boards, framing members, sheathing-to-framing connectors, and connections to the URM buildings. A detailed explanation of every component related to older URM buildings was provided in Section 3. In existing wood diaphragm, the arrangement of wood boards can have different configurations, yet it has been proved that this variable does not affect the stiffness of the diaphragm (Brignola et al. 2009). Thus, herein it is assumed that wood boards are arranged as shown in Figure 4-37. Also, for simplicity nails and joist are considered to be constructed equally spaced, although this can be adjusted to accommodate more complex configurations.

4.4.2 Kinematic Assumptions

Figure 4-37 shows the undeformed and deformed structural configuration of a typical straight sheathed diaphragm under seismic load applied perpendicularly to the joist. Under this load, the boards distort as bending beams while the joists remain essentially vertical. It is assumed herein that the lateral supports are sufficiently anchored so that additional deformation from the connectors can be effectively eliminated.

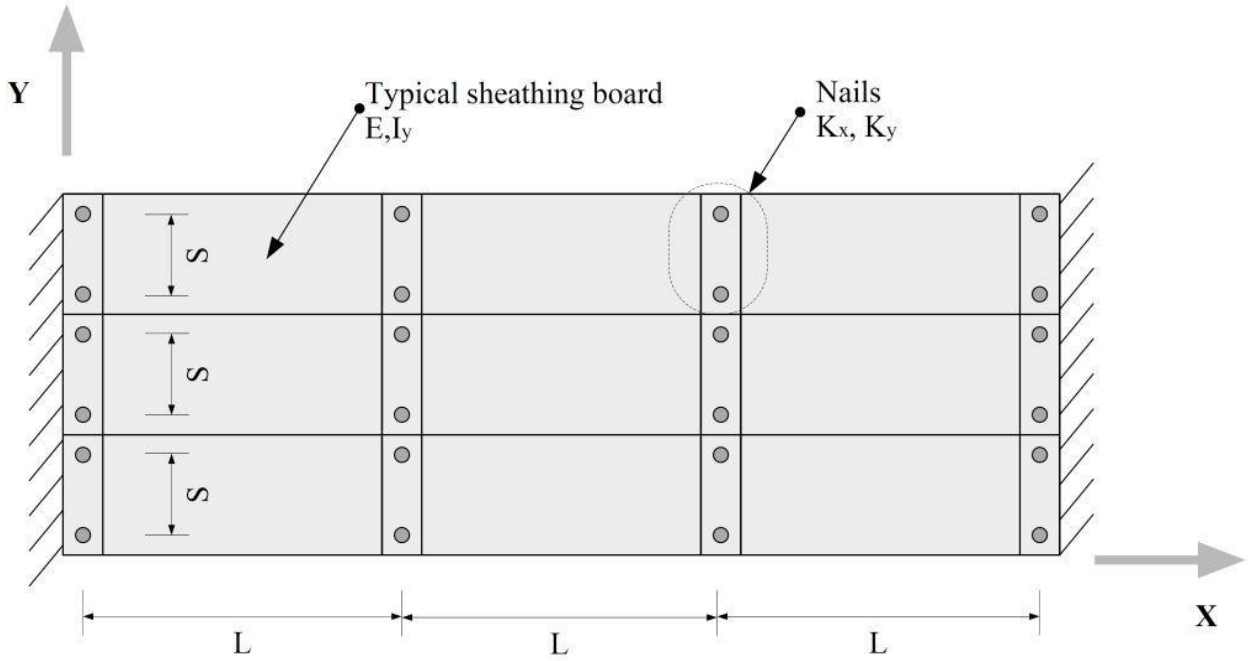

(a)

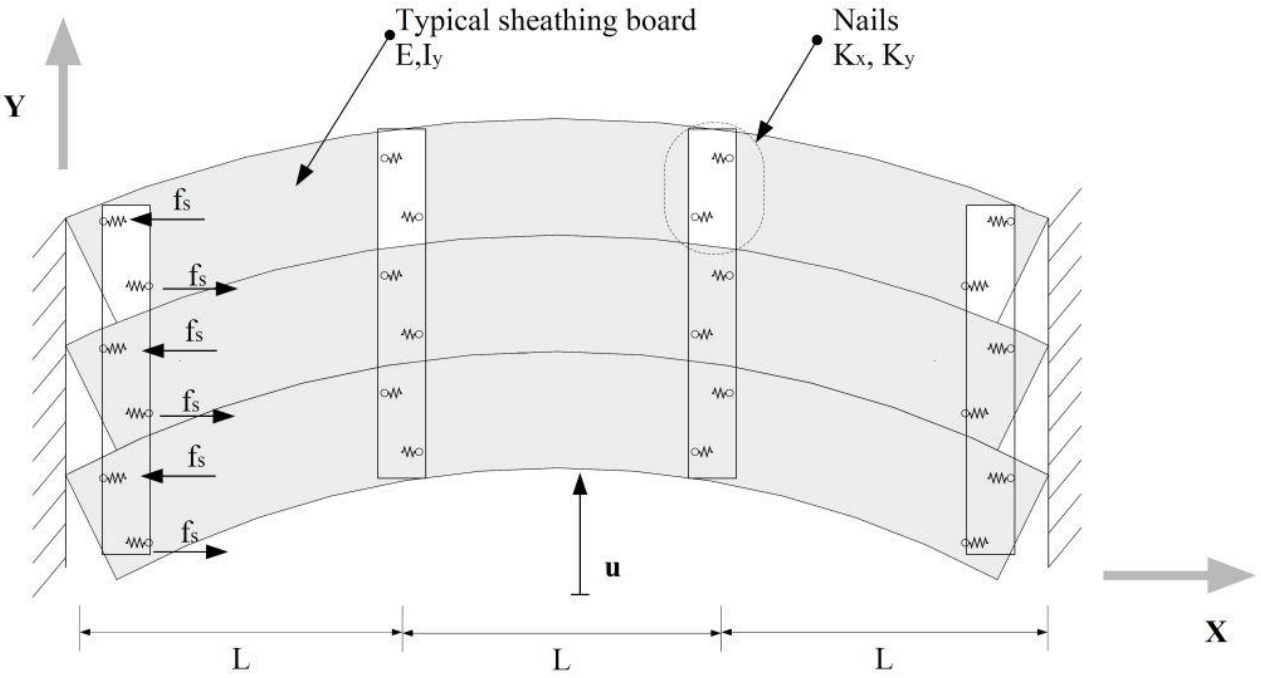

(b)

Figure 4-37 Typical configuration of wood diaphragms in older URM buildings: (a) Undeformed shape; (b) Deformed shape

It has also been shown in Section 4.3.3 that shear stresses and strains in the wood boards remain well below the maximum capacity of the wood material so that shear deformations can be neglected. Therefore, the plane-stress area elements of dimensions **h**, **w** and **L,** and Young's modulus **E** used in Section 4.3.2 and Section 4.3.3 can be effectively replaced by Bernoulli beam elements with Young's modulus $\mathbf{E_b=E}$ and inertia $\mathbf{I_y=(hw^3/12).}$ Because the beam elements are located at the geometric centroid of each area element, and the springs are located at a distance **S/2** from the centroid, a rigid link element which connects the beam element to zerolength springs is required, as shown in Figure 4-38.

In this new formulation the total lateral displacement $\mathbf{U_d}$ is only affected by the bending properties of the boards, and the stiffness of individual nails. Moreover, as demonstrated in Section 4.3.3, mechanical contact between boards have a minimum effect in the seismic response of this type of diaphragms. Hence, in this study the individual boards are assumed to deform independently of each other. Due to this assumption, the total number of boards $\mathbf{N_b}$, in the wood floor can be reduced to only one beam element with equivalent Young's Modulus, $\mathbf{E_{eq}=N_bE_b}$, where $\mathbf{E_b}$ is the Young's modulus of one individual board. Likewise, zerolength springs with equivalent stiffness $\mathbf{K_{eqx}= N_bK_x}$ and $\mathbf{K_{eqy}=N_bK_y}$ can be adopted at each connection in the **X** and **Y** direction, respectively. When using this equivalent structural configuration, the properties of the wood joists are not modified, yet any motion in **X** direction must be constrained so that out-of-plane bending is properly prevented.

The system shown in Figure 4-38 can be further reduced by replacing the rigid link element and translational springs with a rotational spring with equivalent force-displacement relationship, as depicted in Figure 4-39. For this change to be valid, it is assumed that rigid body translation in **X** and **Y** direction is negligible. When the diaphragms deforms, the equivalent beam introduce only rotations θ, at each connection with the framing system. This rotation is measured with respect to the center of each nail-couple.

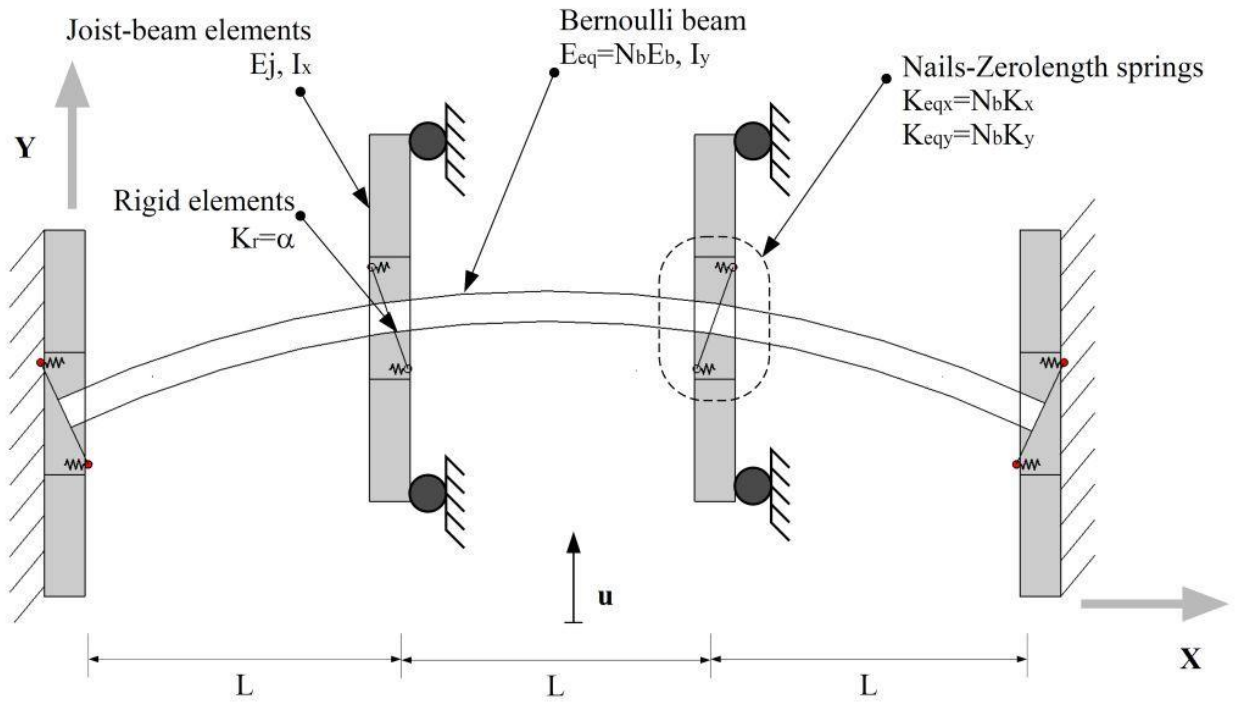

Figure 4-38 Equivalent wood diaphragm model: Bernoulli beam and rigid links

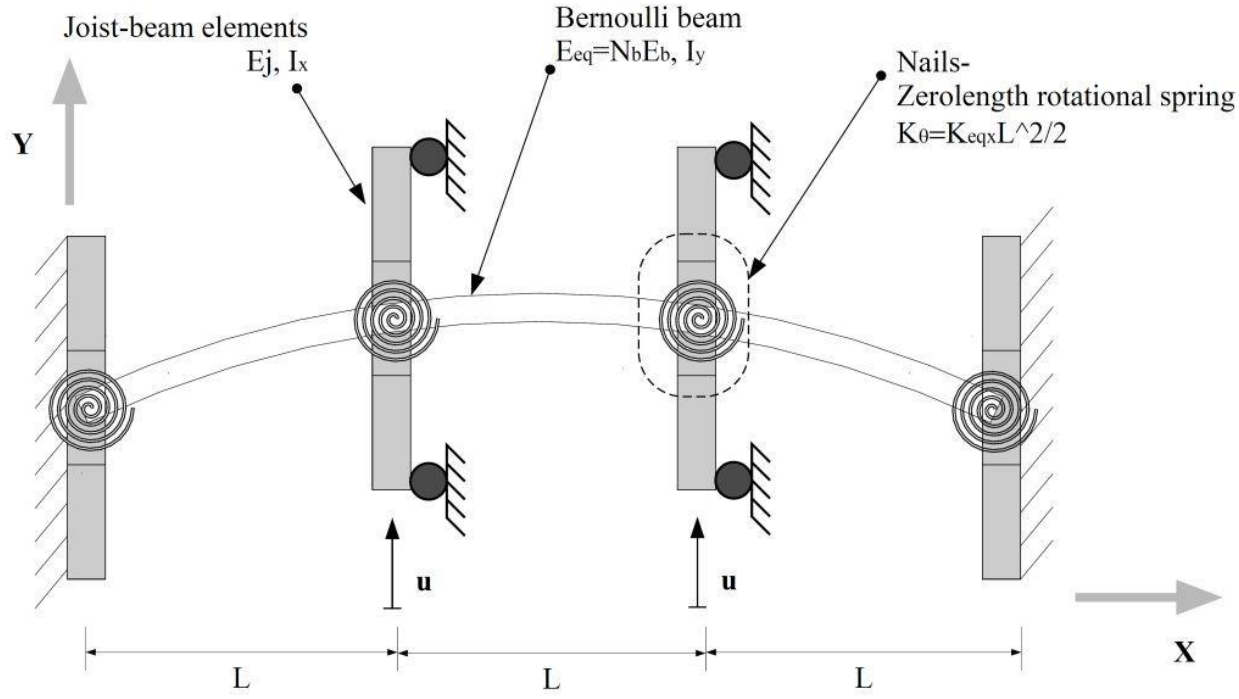

Figure 4-39 Reduced equivalent system with rotational springs

Figure 4-40 present the basic structural element formulation of the reduced system and its associate DOFs. Nine DOFs are required to fully characterize the in-plane behavior of the diaphragm. Figure 4-41 shows the equivalent system further reduced if we neglect rigid body translation in **X** and **Y** direction. The 9-DOFs system was reduced to 3-DOFs. Under this assumption , the original and equivalent stiffness matrixes are given by,

$$K_o = \begin{pmatrix} 4EI_y / Ls^2 + k_x & -6EI_y / L^2 s \\ -6EI_y / L^2 s & 12EI_y / L^3 + k_y \end{pmatrix} \tag{4.2}$$

$$K_{eq} = \begin{pmatrix} 4EI_y / L + k_\theta & -6EI_y / L^2 \\ -6EI_y / L^2 & 12EI_y / L^3 + k_y \end{pmatrix} \tag{4.3}$$

Where ***E*** is Young's Modulus, I_y is the moment of inertia around *y* axis, **L** is separation between joists, and **S** is the distance between nails. Global displacement $\mathbf{U_d}$ is not included in this formulation. Note that the only difference is the rotational stiffness, which is given by

$$K_\theta = K_x s^2 / 2 \tag{4.4}$$

Note that out-of-plane deformation is not considered in this formulation, as each board is usually designed to sustain gravitational forces. Extension of this work to diaphragms with $\mathbf{N_b}$ boards is straightforward. In the general case, the number of DOF required is $\mathbf{nDOF=3N_b}$.

The nonlinear relationship of the rotational spring is obtained by converting the SAWS force-displacement values previously implemented into moment-rotation using Equation 4.4 previously calculated.

Using orthogonal springs in **X** and **Y** directions, the stiffness of the system is usually overestimated, as demonstrated by Judd and Fonseca (2005). An attractive feature of the RMDOF is that it does not need to be oriented nor calibrated or adjusted. As demonstrated in the next section, the model gives good results at a significant reduced computational time. Also, diaphragms can be analyzed for any orientation of seismic force.

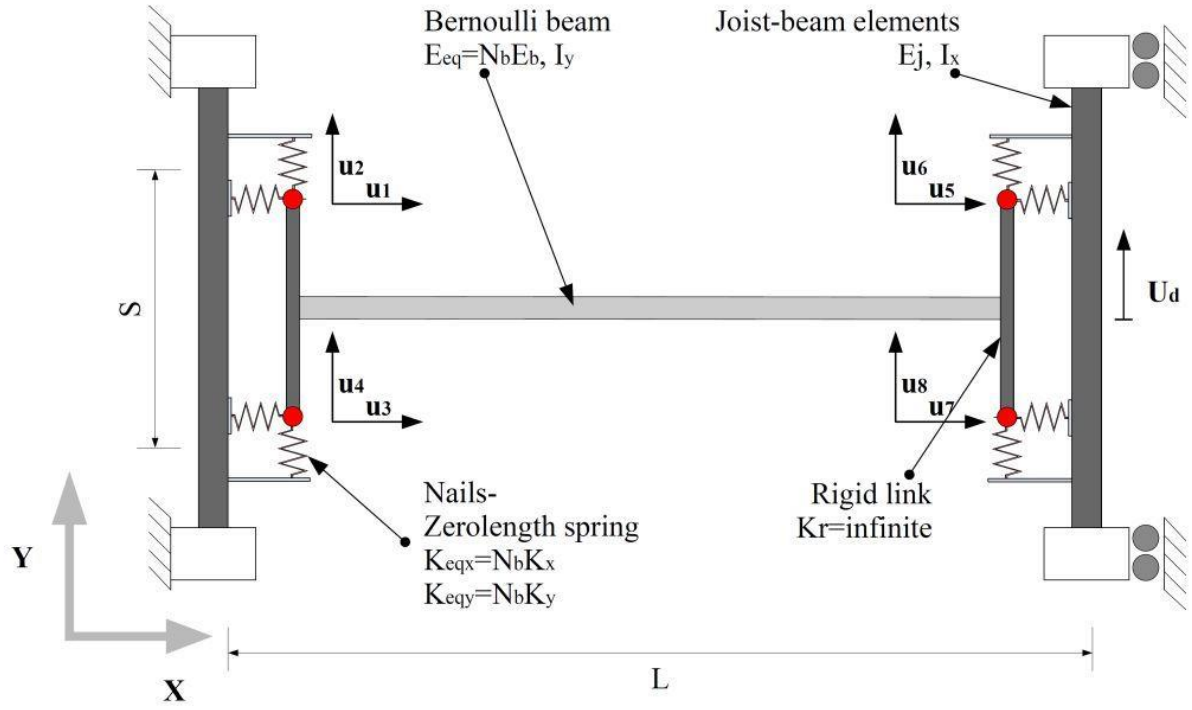

Figure 4-40 Basic structural element formulation.

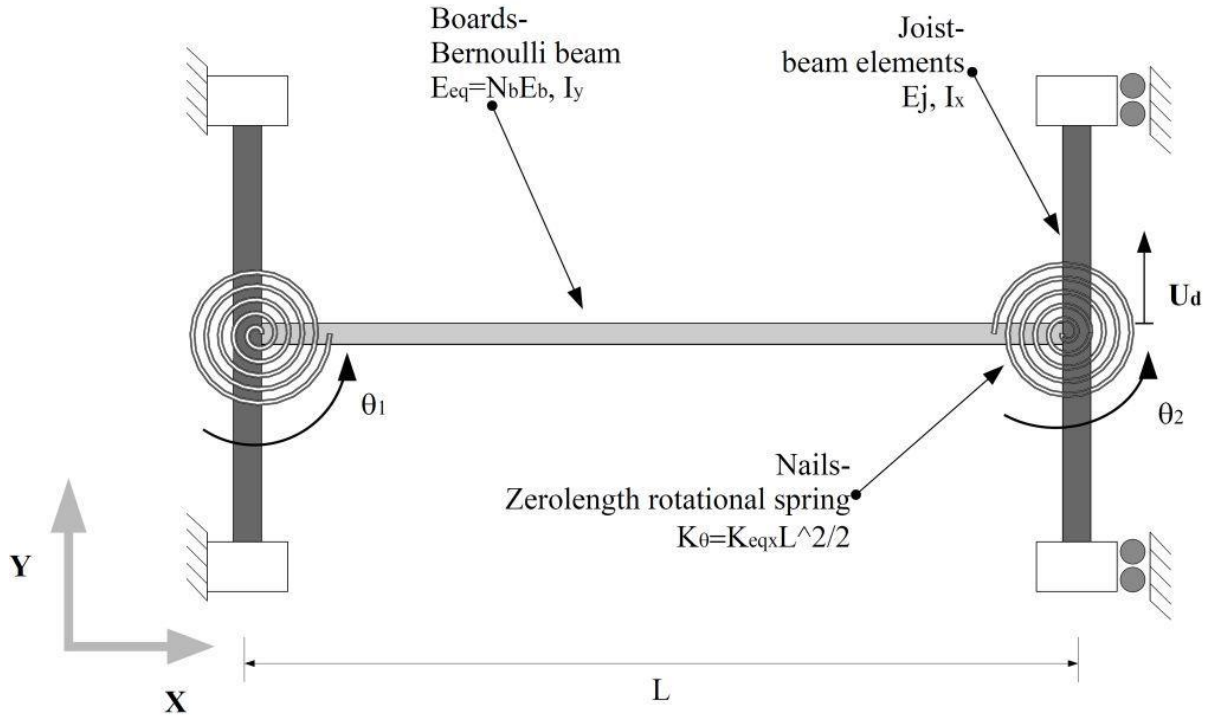

Figure 4-41 Beam and translational degree of freedom, beam with rotational springs

4.4.3 Model Verification

The reduced MDOF model was implemented in both, OpenSees and SAP2000 programs. It predictive capabilities were compared with those of finite element models and experiments described in Section 4.3.2, Section 4.3.3 and Section 4.3.1, respectively. Figure 4-42 presents a three dimensional view of the model in SAP2000. The model was validated through cyclic quasi-static, pushover, modal and nonlinear response history analysis.

Figure 4-42 3D view of the reduced MDOF model in SAP2000

4.4.3.1 Cyclic quasi-static behavior

Figure 4-43 presents a comparison between the RMDOF in SAP2000 and the FEM in OpenSees. Major differences arise in the reloading and downloading stiffness, yet the energy dissipated by the RMDOF model is only 5% higher that refined model in OpenSees. Another important difference is the computational time required to complete this simulation. The RMDOF model completed the full loading protocol in about 3 hours whereas the FEM model took about 130 hours.

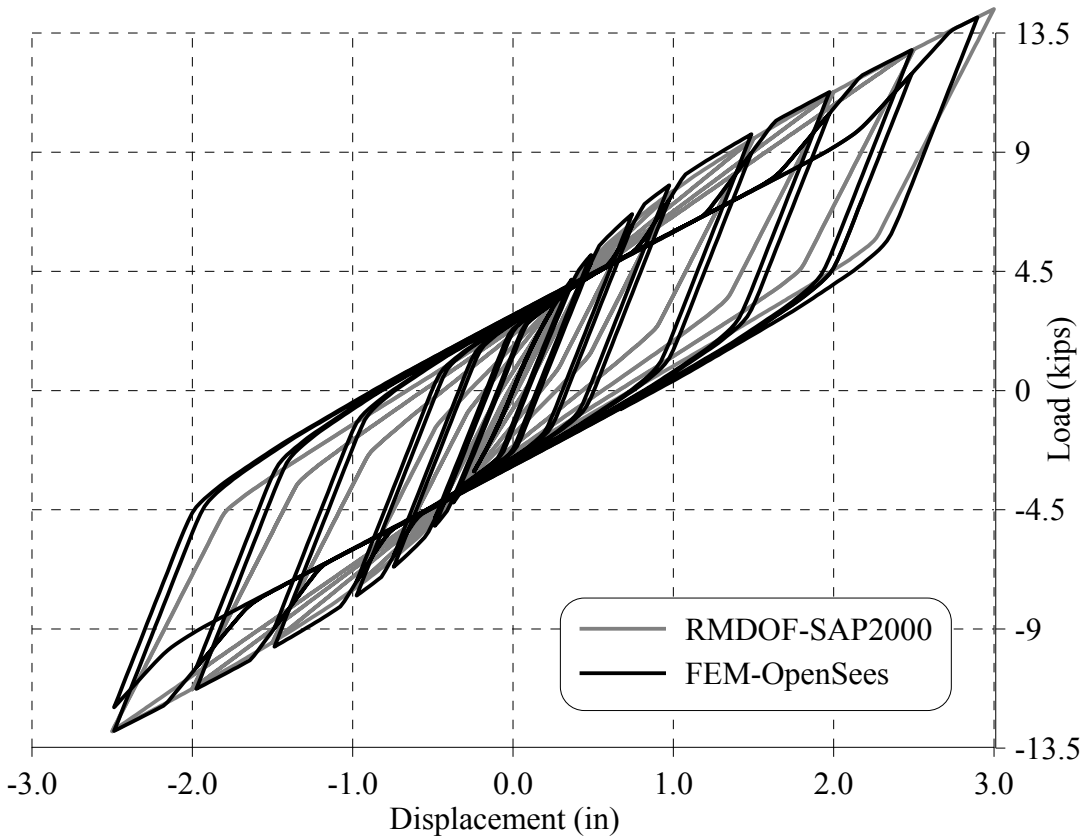

Figure 4-43 Cyclic quasi static behavior of MAE-2 simulated by RMDOF in SAP2000 and FEM in OpenSees

Figure 4-44 shows a comparison between the experiment results and the SAP2000 RMDOF model. The numerical model effectively predicts the load-displacement relationship of the diaphragm.

Pushover analysis was completed using the RMDOF model in SAP2000. A comparison result can be seen in Figure 4-45. The pushover curves of the RMDOF model and refined FEM are identical. Initial stiffness, nonlinear behavior and maximum capacity are accurately predicted by the model as seen in Table 4-10.

Table 4-10 Summary of model predictions under monotonic load

Software	Modeling Technique	Initial stiffness (kip/in)	In-plane force at max. displ.	Analysis time (sec)
SAP2000	SDOF	11.75	13.83	6
	Refined FEM	11.87	14.09	282

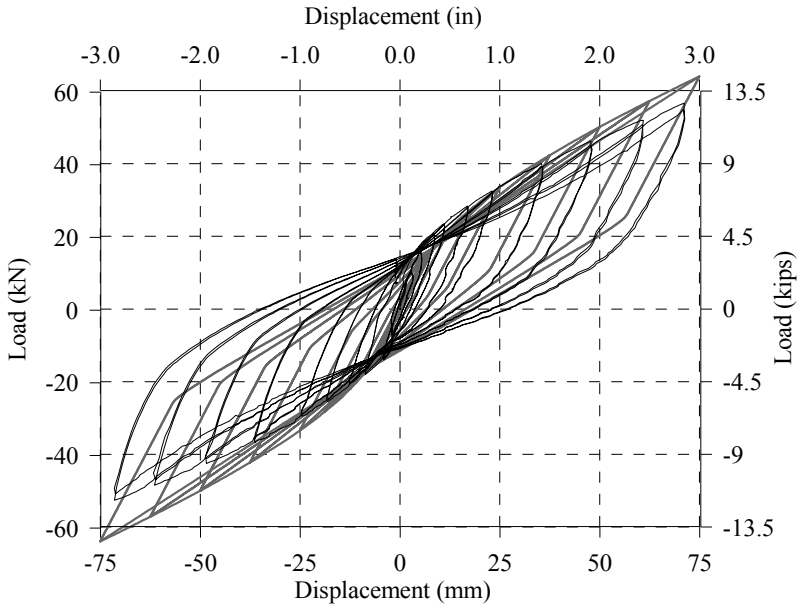

Figure 4-44 Predicted cyclic load-displacement relationship for MAE-2 diaphragm a) Experiment b) SAP2000 RMDOF model

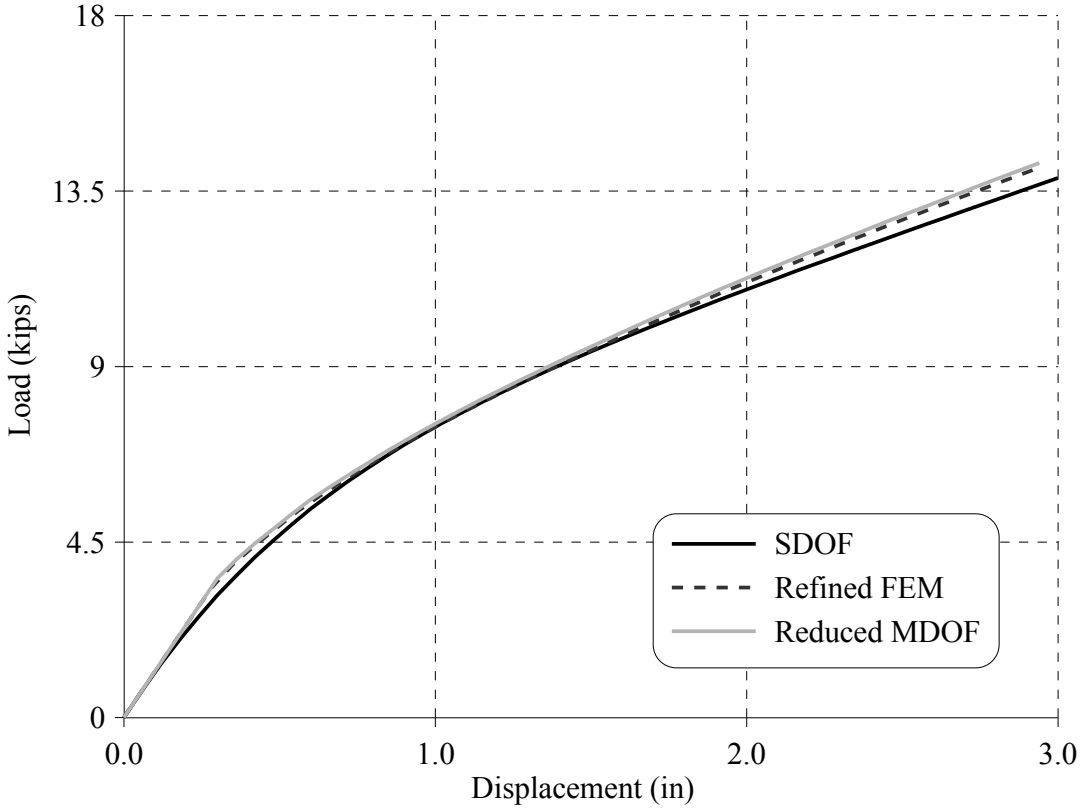

Figure 4-45 Comparison between Pushover curve obtained with different modeling techniques SAP2000

4.4.3.2 Modal Analysis

For completeness, modal analysis was carried out using the RMDOF model and compared with previous models in OpenSees and SAP2000. In SAP2000, the *Eigen Vectors* option was used with default properties. In OpenSees the *eigen* command was used. Two modes were computed. Table 4-11 presents comparative results of the first and second mode frequencies estimated with different modeling techniques. The number of DOF required in each model and its total analysis time is also presented.

Figure 4-46 and Figure 4-47 shows the first mode shapes of the MAE-2 diaphragm modeled using a refined FEM and the RMDOF model, respectively. Good agreement in the first mode shape is obtained. Note that, because this is a very large system, only the 83% percent of mass participation is captured in the first mode of the refined FEM.

Figure 4-48 and Figure 4-49 also shows good agreement between the second mode shapes of the MAE-2 diaphragm modeled using a refined FEM and the RMDOF model, respectively.

Table 4-11 Modal analysis- comparative results

Software	Modeling Technique	Number of DOF	First mode frequency (hz)	Second mode frequency (hz)	Analysis time (sec)
OpenSees	Refined FEM	44273	11.01	26.51	0
	SDOF	1	10.86	n/a	0
	RMDOF	1113	10.63	25.38	0
SAP2000	Refined FEM	44273	11.05	26.56	16
	SDOF	1	10.19	n/a	0
	RMDOF	1113	9.36	23.24	0

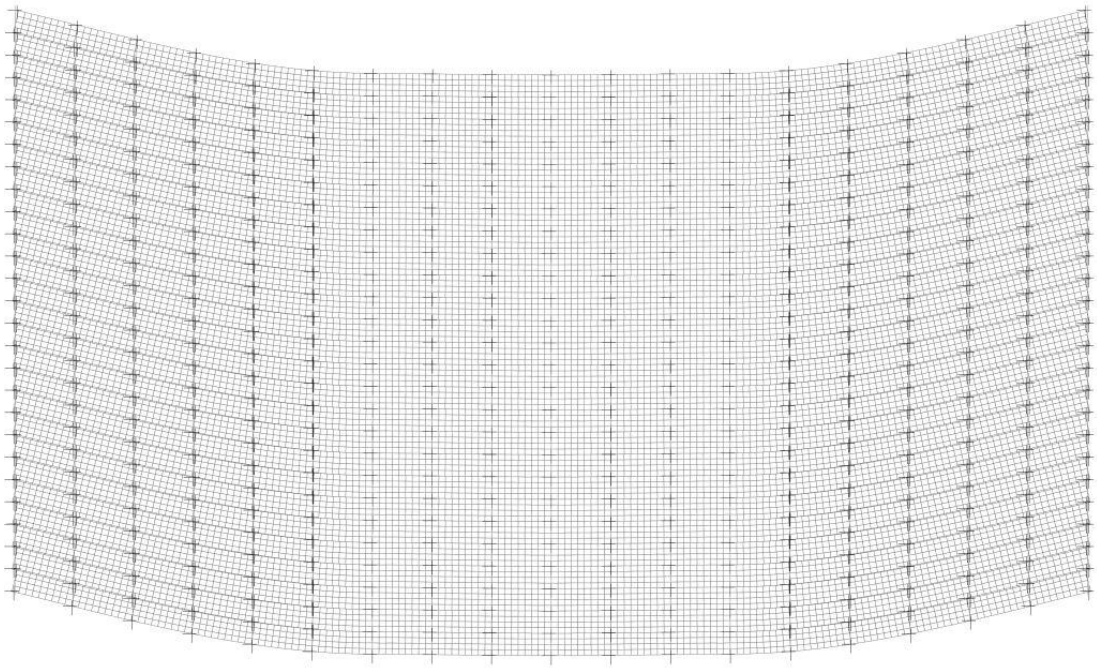

Figure 4-46 First mode shape of the refined FEM MAE-2 model in SAP2000

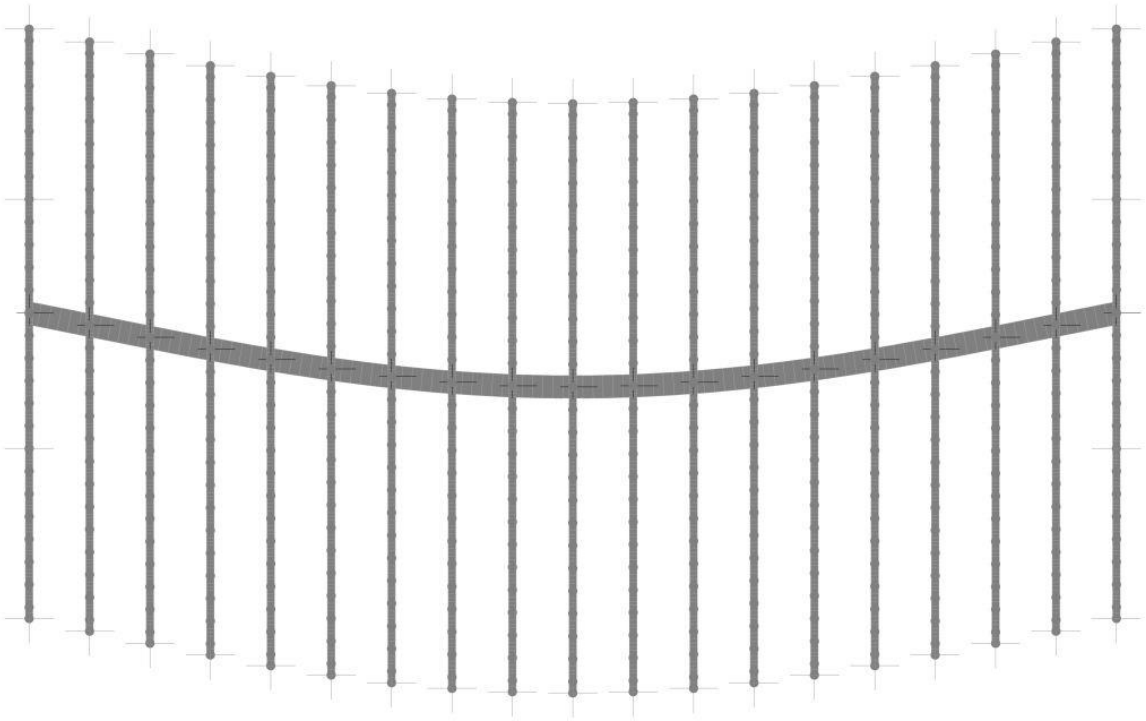

Figure 4-47 First mode shape of the RMDOF MAE-2 model in SAP2000

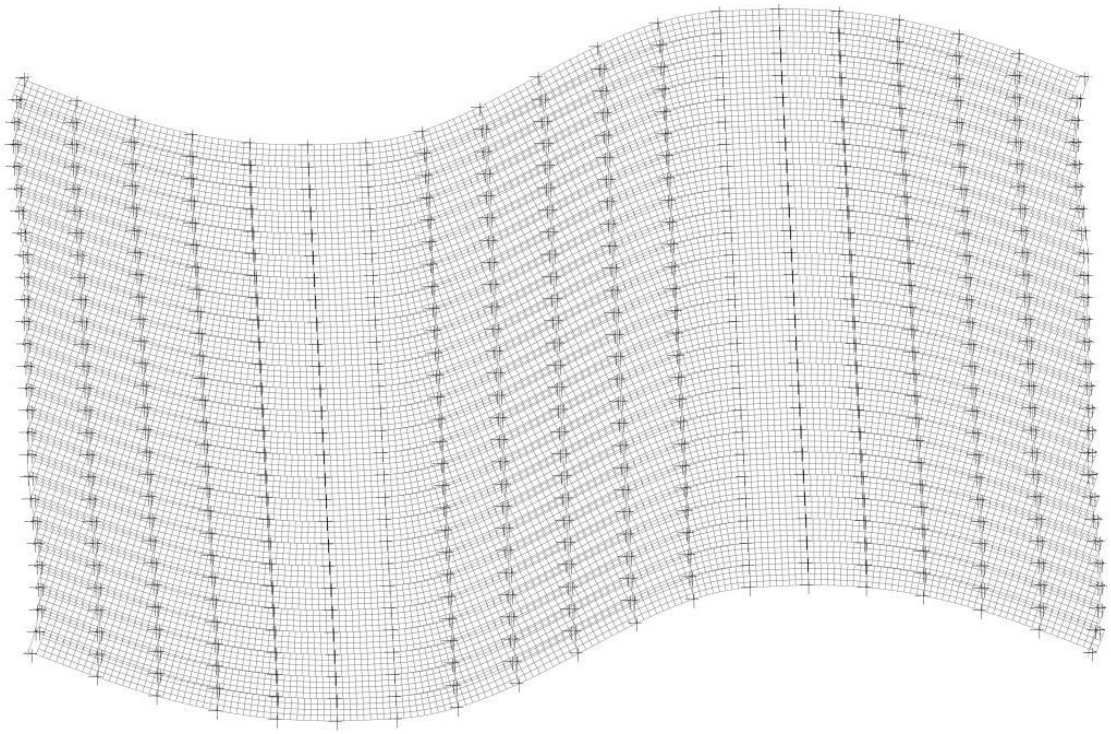

Figure 4-48 Second mode shape of the refined FEM MAE-2 model in SAP2000

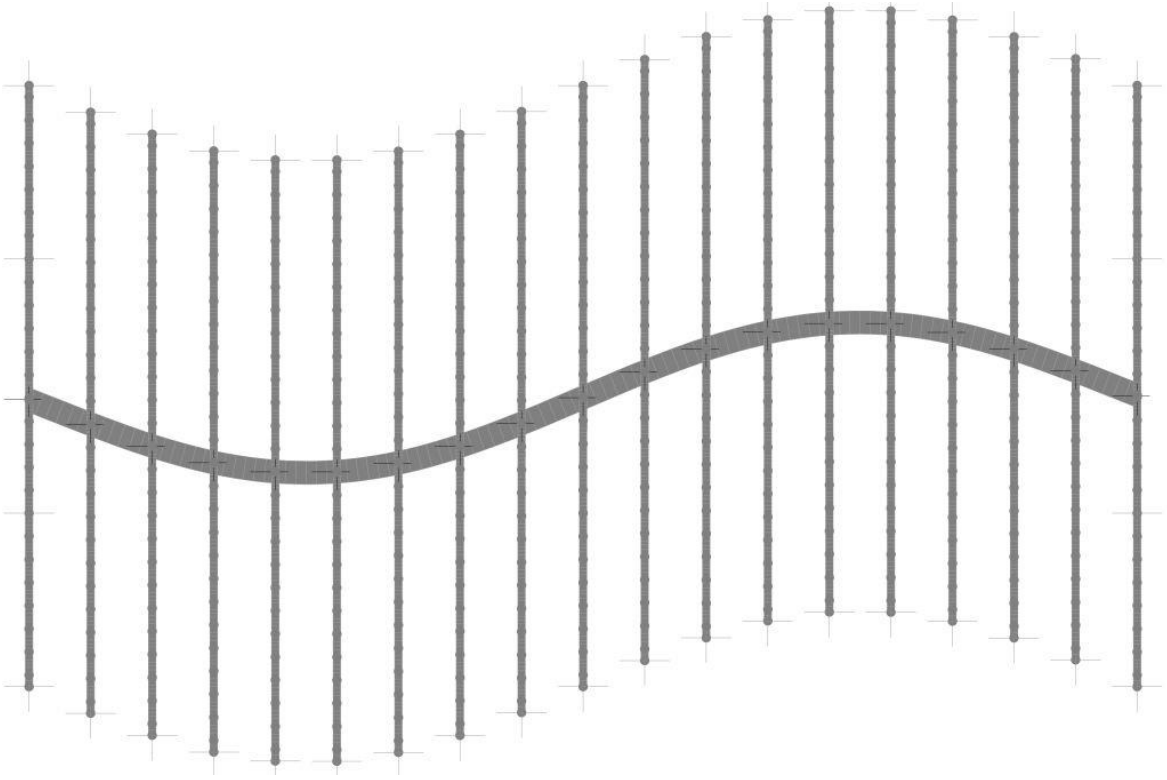

Figure 4-49 Second mode shape of the RMDOF MAE-2 model in SAP2000

4.4.3.3 Response History Analysis

To fully explore the capabilities of the RMDOF model, nonlinear response history analysis was conducted using the El Centro record. For comparison purposes, nonlinear analysis was also completed in all other modeling techniques described in this section. Table 4-12 summarizes the displacement and acceleration predictions obtained with each model and the analysis time required.

Because of the small size of the MAE-2 diaphragm, the maximum displacement obtained is only about 1% of the maximum displacement capacity of the diaphragm which is about 3 in., as seen in Figure 4-45. In all models, the displacement is measured at the third length of the diaphragm.

A comparison of the response obtained with different OpenSees models, shows that the RMDOF model under-predict the maximum response obtained with the refined FEM model by about 6%. This is confirmed in Figure 4-50, which shows that the response displacement history obtained with the RMDOF model is, in general, in good agreement with the response obtained with the refined FEM. On the other hand, the SDOF model significantly under-predict the response by 47%. Using half of the mass in the model is most likely the reason for this result. Another significant difference is the computer time required to complete each analysis. While the analysis using the SDOF model is highly efficient, the RMDOF analysis is still computationally cheap when compared with the analysis time required for the refined FEM.

Figure 4-51 presents a comparison between displacement time histories of the diaphragm subjected to El Centro Earthquake in SAP2000.

In terms of accelerations, the RMDOF in OpenSees slightly under-predict the peak response whereas the SDOF peak response is about 17% less than the refined FEM response. On the other hand, there is a good match between the RMDOF and the FEM in SAP2000, yet the SDOF under-predict the response by 48%. Figure 4-52 and Figure 4-53 present a comparison between acceleration time-histories of the diaphragm modeled in OpenSees and in SAP2000, respectively.

Table 4-12 Summary of model predictions under dynamic loading

Software	Modeling Technique	Dmax (+) [in]	Dmax (-) [in]	Amax (+) [g]	Amax (-) [g]	Analysis time (sec)
OpenSees	Refined FEM	0.049	-0.074	0.56	-0.54	510
	SDOF	0.032	-0.053	0.41	-0.36	1
	RMDOF	0.046	-0.073	0.53	-0.51	43
SAP2000	Refined FEM	0.064	-0.102	0.66	-0.60	14400
	SDOF	0.033	-0.054	0.41	-0.36	145
	RMDOF	0.065	-0.103	0.66	-0.60	540

The RMDOF was also validated for dynamic loads using the ABK experiments described in section 4.2.2. Figure 4-54 presents the Diaphragm E as modeled in SAP2000. The diaphragm was subjected to 10 seconds of the 1971 San Fernando Earthquake. A comparison between the numerical prediction and the experimental results can be seen in Figure 4-55. Peak force and deformations obtained in SAP2000 are in good agreement with the experimental results. In conducting this simulation, the nail properties were neither calibrated nor adjusted. The same properties used to model MAE-2 diaphragm were used, yet the results are still satisfactory.

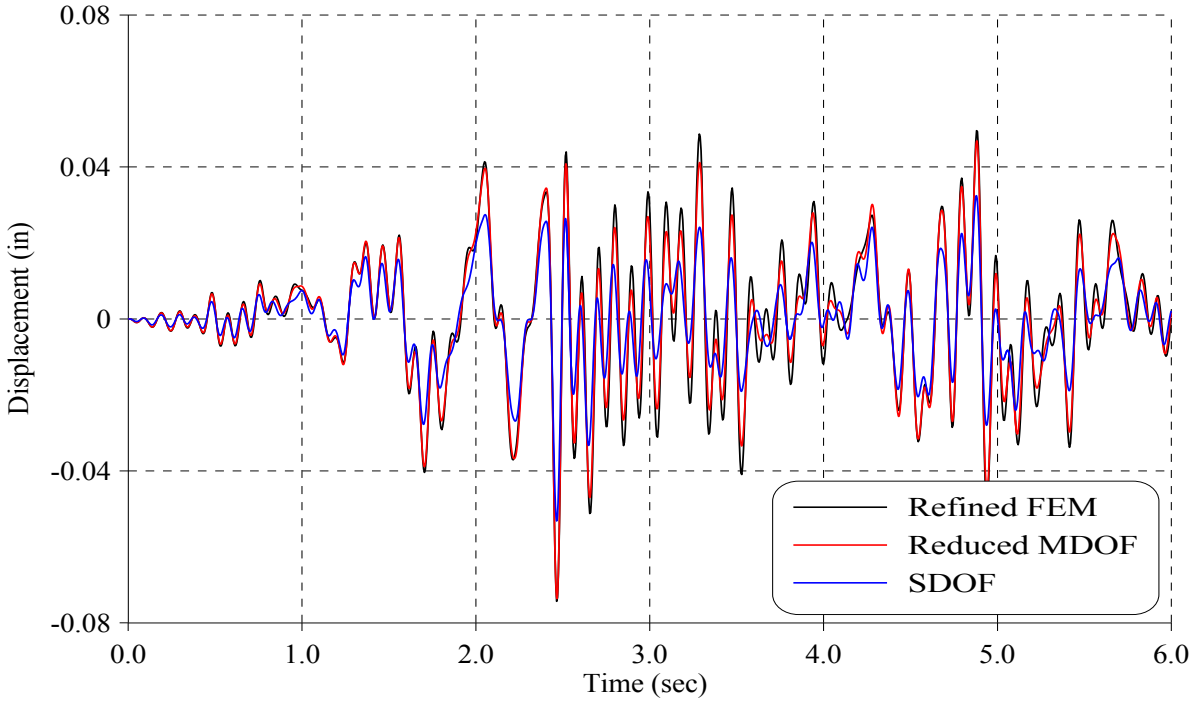

Figure 4-50 Displacement time history in OpenSees

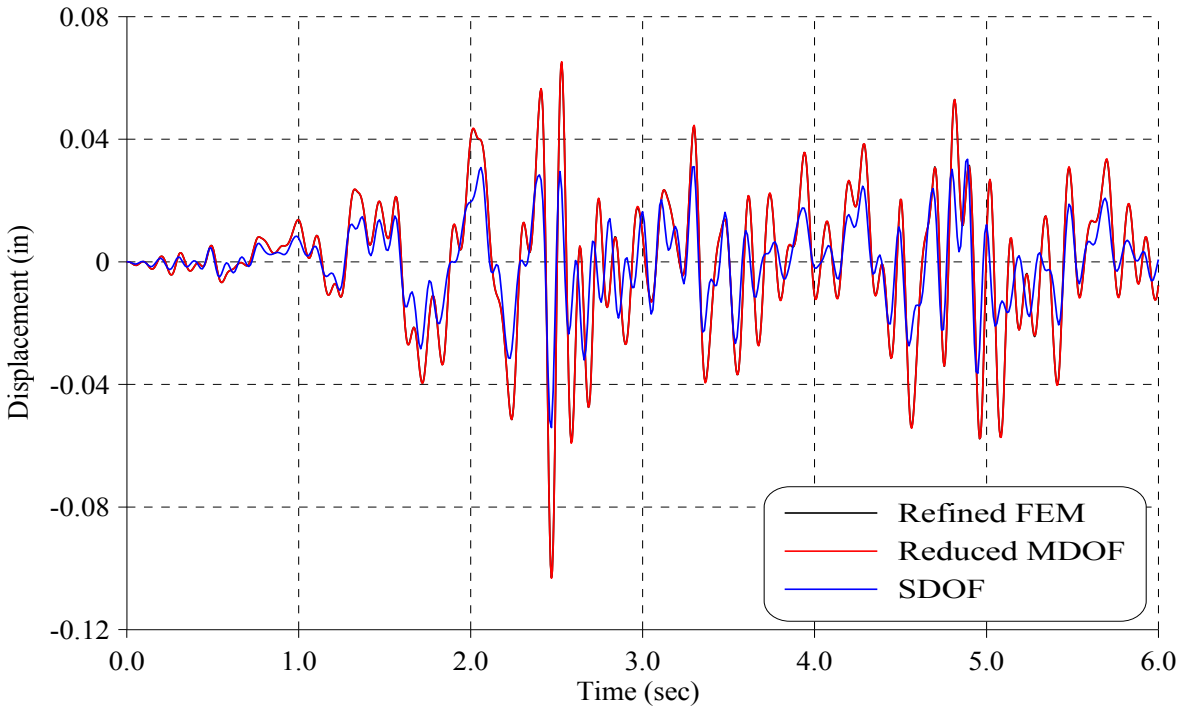

Figure 4-51 Displacement time history in SAP2000

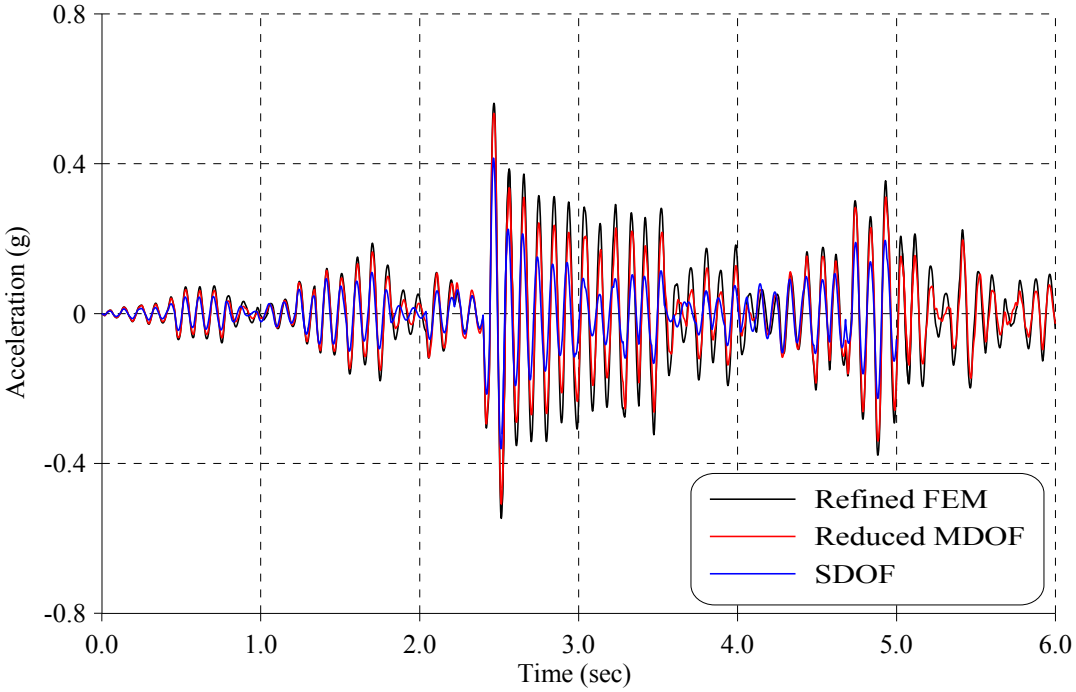

Figure 4-52 Acceleration time history in OpenSees

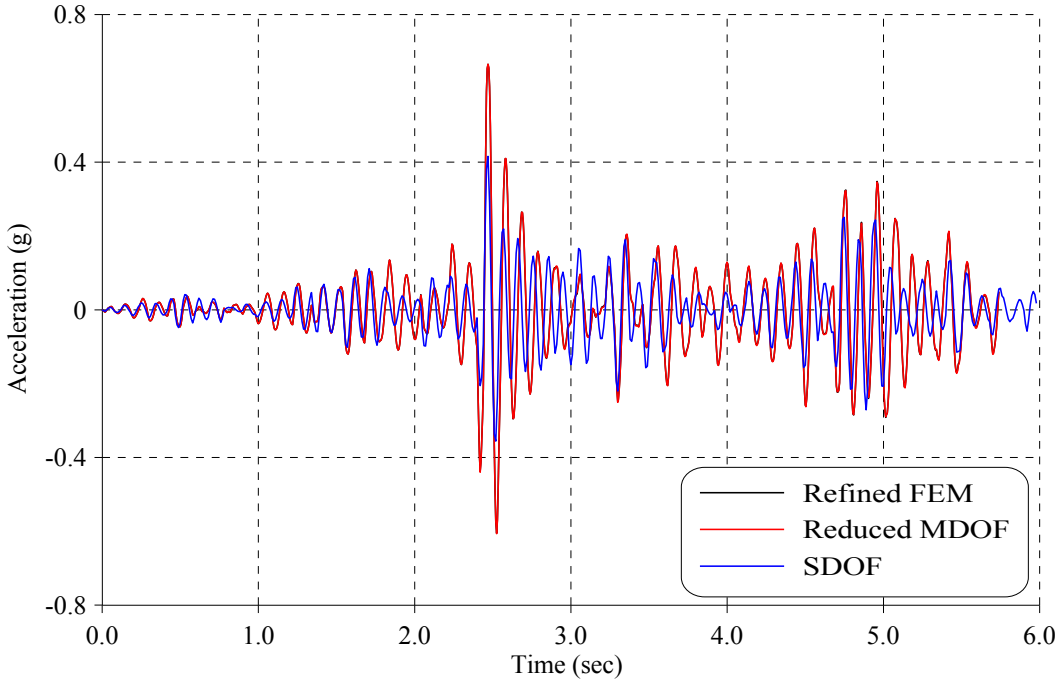

Figure 4-53 Acceleration time history in SAP2000

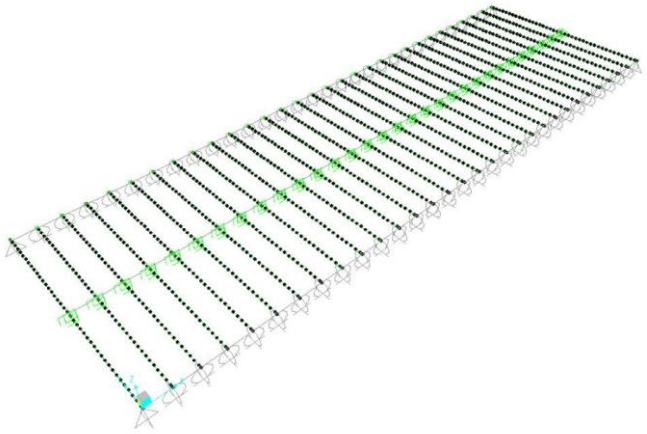

Figure 4-54 Diaphragm E tested by the ABK program (Ewing and Jhonson 1981) modeled in SAP2000

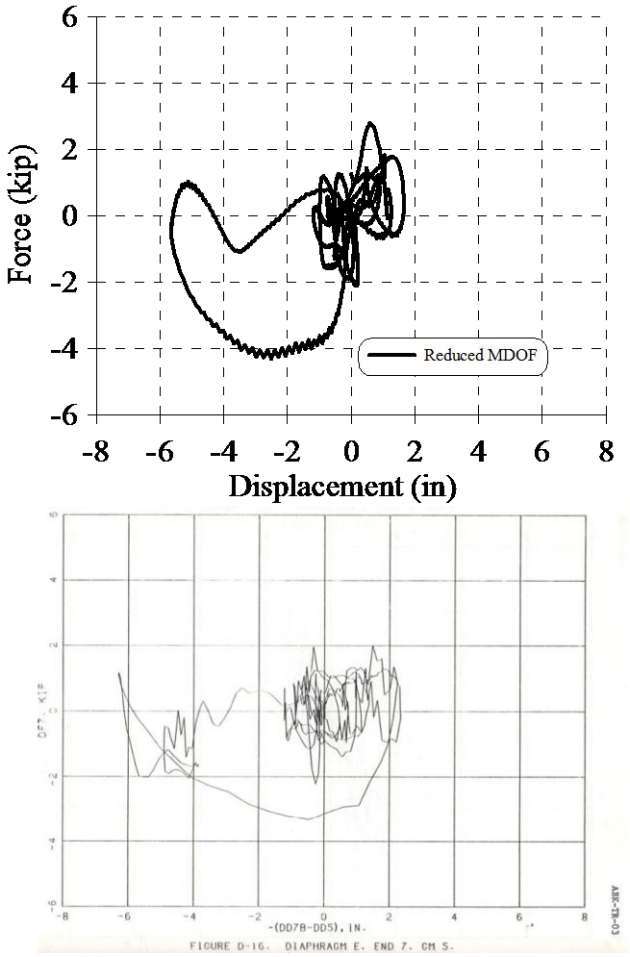

Figure 4-55 Numerical prediction and experimental force-displacement response of Diaphragm E (Ewing and Johnson 1981)

4.4.4 Numerical Example

The purpose of this exercise is to evaluate the computer efficiency and the accuracy of the RMDOF when implemented in a more complex structural system. To this end, the first story of the archetype URM building was analyzed using both the refined FE modeling approach and the reduced MDOF model. Note that the SDOF model cannot be applied here since it cannot fully connect to the joist-supporting walls.

The building model and dimensions are shown in Figure 4-56 along with the refined FE model and the reduced MDOF model of the structure. Masonry walls were modeled using the equivalent frame methodology, as discussed in Section 8 and the diaphragms were modeled as described in previous sections. The model was built in SAP2000 v14.0.0. Modal and nonlinear time history analyses were conducted using six seconds of El Centro earthquake as input excitation.

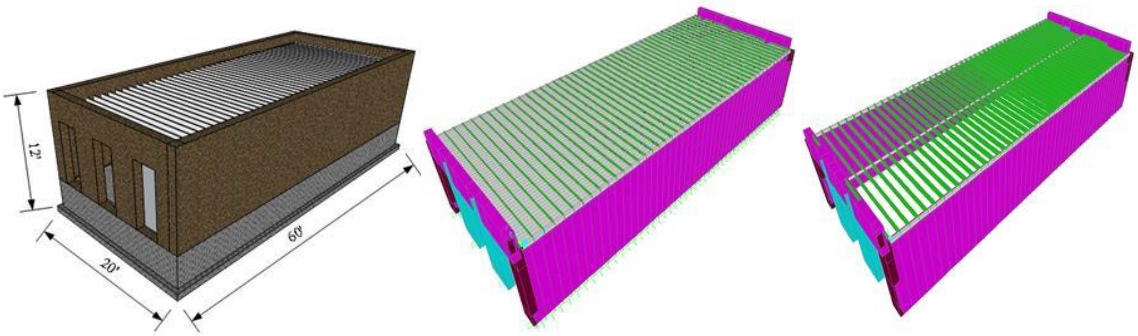

a) b) c)

Figure 4-56 First story of the URM building archetype :a) SketchUp Model b) Refined FE model c) Reduced MDOF

The first, second and third mode of vibration along with the associated periods are presented in Figure 4-57, Figure 4-58 and Figure 4-59, respectively. A good agreement between the refined FE model and the reduced MDOF was obtained for the mode shapes and the periods. The comparison between time history displacements and accelerations, presented in Figure 4-60 and Figure 4-61, reveals a close agreement between both numerical models.

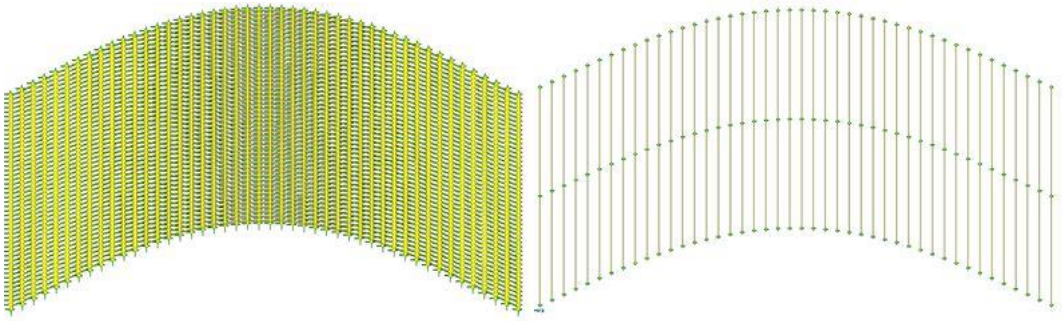

a) b)

Figure 4-57 Comparison of the first mode of vibration a) Refined FEM, Tn=0.58sec b) RMDOF, Tn=0.62 sec

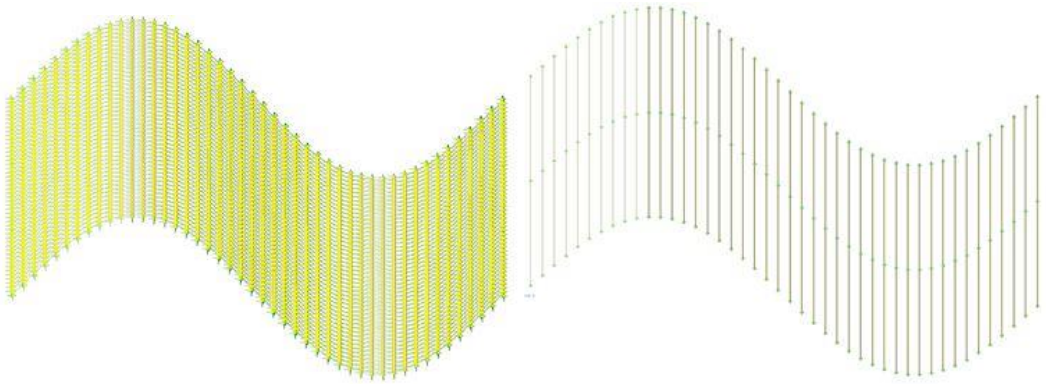

a) b)

Figure 4-58 Comparison of the first mode of vibration a) Refined FEM, Tn=0.28sec b) RMDOF, Tn=0.30 sec

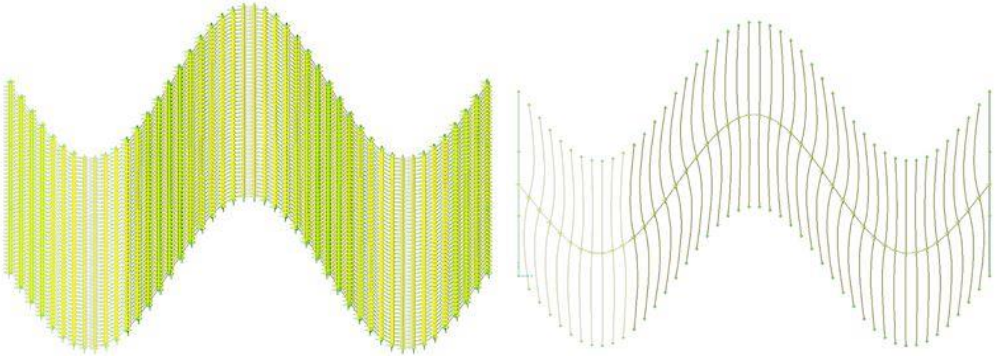

a) b)

Figure 4-59 Comparison of the first mode of vibration a) Refined FEM, Tn=0.17sec b) RMDOF, Tn=0.20 sec

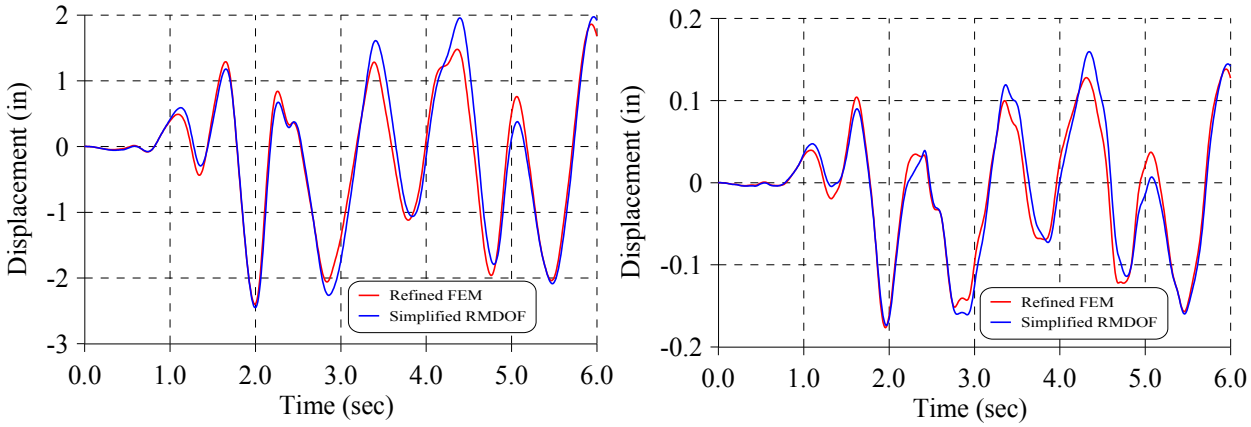

Figure 4-60 Comparison of displacement time-histories at the diaphragm a) at center b) at the right edge

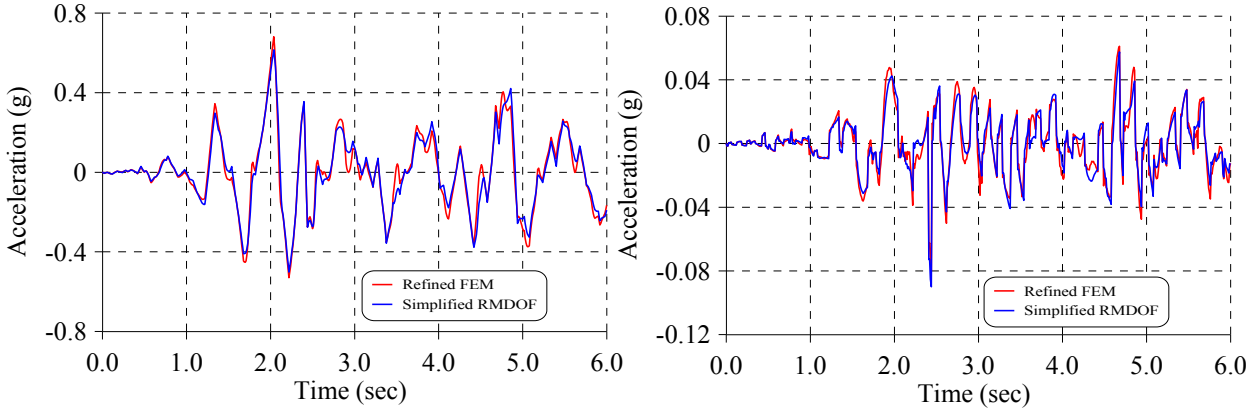

Figure 4-61 Comparison of acceleration time-histories at the diaphragm a) at center b) at the right edge

4.5 Summary and Conclusions

In this section, numerical models of wood diaphragms available in the literature were identified and evaluated for performance based seismic design applications. Diaphragms subjected to static monotonic, cyclic quasi-static and dynamic loads were discussed. Also, related numerical models for wood shear walls and sheathing to framing connections were briefly described. Then, some common numerical models for simulation of wood diaphragms in URM buildings were identified.

A thorough evaluation of current numerical tools indicated that finite element models can fully characterize the dynamic response of wood diaphragms, but at a very high computational cost. On the other hand, simplified SDOF models could reasonable estimate only few dynamic

parameters and engineering demands at key locations of the diaphragm. Hence, a reduced MDOF model of the diaphragm, able to capture the full dynamic characteristic while significantly reducing analysis time has been proposed, verified and validated.

Upon demonstration that the horizontal mechanical contact and friction between wood boards are negligible, the straight sheathing system was replaced with an equivalent Bernoulli beam element located at the center of the diaphragm. Then, nonlinear rotational springs were proposed to simulate the nail coupling at the connection between wood boards and joists. Modal, cyclic quasi-static and nonlinear response history analysis of the reduced MDOF model were carried out in OpenSees and SAP2000. Comparison with previous numerical models and key experimental results from the literature indicates that the reduced MDOF model accurately predict the seismic response of this type of diaphragms with computational efficiency.

SECTION 5
NUMERICAL MODELING OF CONNECTIONS BETWEEN WOOD DIAPHRAGMS AND MASONRY WALLS

5.1 Introduction

It is widely recognized that existing unreinforced masonry (URM) buildings are one of the most seismically vulnerable type of structures. As noted by Bruneau (1994a), among different failure modes, the out-of-plane collapse of walls and parapets is perhaps the most hazardous to human life. This failure mode is usually aggravated by lack or failure of anchorage between walls and floors and excessive flexibility of diaphragms. Experimental programs have shown that the seismic response of URM buildings is strongly dependent of the connection between floor diaphragms and masonry walls (Paquette and Bruneau 2006; Tomazevic 1993).

Current seismic evaluation and rehabilitation codes consider the lack of anchorage as a primary deficiency in URM buildings and specify a minimum strength and spacing of anchors that must be installed to achieve different performance levels (ASCE/SEI 31-03 2003; ASCE/SEI 41-06 2007). The effectiveness of those retrofit measures have been qualitatively verified after the 1994 Northridge earthquake, where unretrofitted URM buildings performed worse than both, reinforced masonry and retrofitted URM buildings (FEMA P774 2009).

Nonetheless, existing information regarding the explicit seismic evaluation of the connection between masonry walls and wood diaphragms and its effects in the global response of URM buildings is scarce. Experimental and analytical research addressing this issue is quite limited. Cross and Jones (1993) proposed a two-dimensional friction-impact model for this type of connection. Very recently, Lin and LaFave (2012a) carried out an experimental program on this subject and a phenomenological model was proposed. Practicing engineers have commonly assumed that the connection between wood diaphragms and masonry walls can be modeled as a pin-connection.

In this section, a three-dimensional nonlinear macro-model of a floor-to-wall connection with structural configuration as shown in Figure 5-1, is proposed. The model accounts for friction, impact and potential nonlinear behavior of anchors or nails. Additional gravity loads, lateral

displacement in any direction, and static or dynamic lateral loads can be applied. The user friendly commercial software SAP2000 is used so that the model can be easily replicated by other structural engineers.

The friction slider element available in SAP2000 accounts for the inherent friction between wood joist and masonry walls. In addition, a gap element combined with a spring-dashpot system simulates the potential impact between the end of the joist and the masonry walls. Also, a nonlinear spring element is used to simulate steel anchors, which were occasionally used in older masonry buildings and are a common retrofit solution recommended by the current rehabilitation codes. The friction-impact-nailed element was validated with previous experiments available in the literature. As a result, the cyclic behavior was characterized and key parameters were determined.

This model will be further validated in Section 8, in which shake table tests of full scale masonry walls, including realistic floor-to wall connections, are examined.

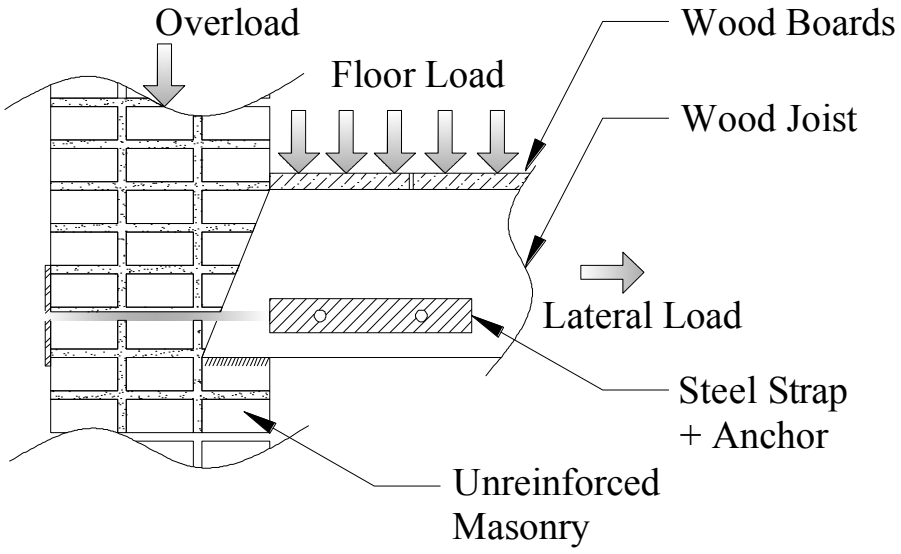

Figure 5-1 Structural configuration of URM wall-wood connection

5.2 Background

Cross and Jones (1993) proposed the first connection model for wood joist on brick masonry. They considered the connection essentially as an impact-with-friction phenomenon and proposed a finite element model that accounts for both effects at the diaphragm-to-wall interface. Figure 5-2 illustrates this numerical model. The friction model is based on the well-known Coulomb friction model. The model was formulated so that the vertical reaction will be turned off if there is tension or if the joist has fallen off the bearing wall. Also, the models accounts for forces due to sliding, sticking and contact between the joist and the wall. In the case of impact, the formulation developed is based on a coefficient-of-restitution approach, using a linear spring-damper located at the point of impact. Also, modifying the properties of the stiffness and damping matrices, the model accounts for three states of the structure, namely 1) immediately prior to impact; 2) during impact; and 3) after impact. The model also assumes a finite time for impact duration, which is needed so that the structure will respond as a flexible body.

The 2D impact-friction model was verified using numerical examples, yet an experimental validation was not conducted. Also, no information regarding the cyclic behavior of the connection was provided. In a companion paper, also by Cross and Jones, they demonstrated that significant movement can occur in an un-retrofitted masonry structure. Thus, the joist is most likely to fall out the wall. Also, a key finding was that the additional force induced in the wall due to impact was significant, modifying the global response of the building.

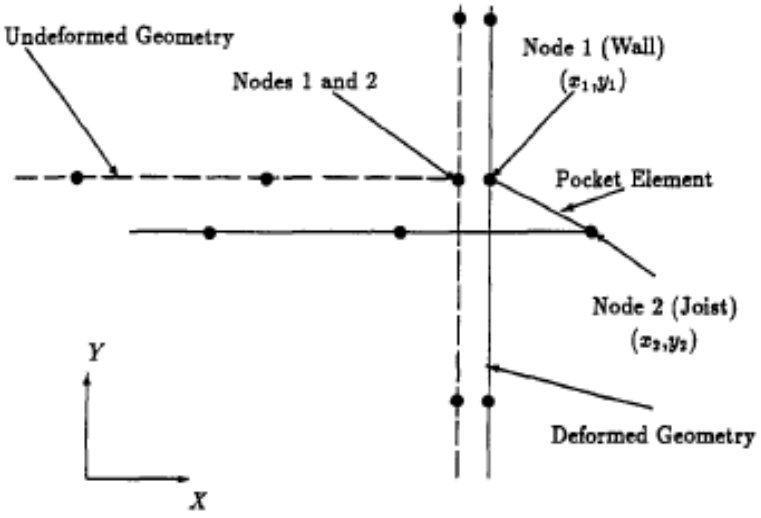

Figure 5-2 Joist pocket element proposed by Cross and Jones (1993)

Lin and LaFave (2012a) carried out experiments on the behavior of the connection between brick walls and wood diaphragms. Nineteen specimens were tested under monotonic, quasi-static and dynamic axial load. Each specimen consisted of a small section of brick wall with a pocket were a wood joist was resting, as shown in Figure 5-3. Three different set of connections between wood joist and masonry walls were considered. The first set had nine specimens using traditional wall-joist anchors. Each anchor was made of a steel trap welded to a threaded rod. In addition, a compressive force was applied at the top of each wall to simulate gravity forces and activate the friction between wood joists and the brick pockets. This type of connection is perhaps the most common in older masonry buildings. A second set had six specimens with the steel anchor described before, but no gravity force was applied. This case may be representative of buildings were the vertical acceleration acts downwards and therefore gravity forces cancel out. The final set had three specimens with no steel anchors but gravity force applied at the top. These are representative of building were the wood joist are resting on the walls without any additional connection. Force-displacement backbone curves were generated for each set of connections.

They found that the type of connection and number of nails was a key factor in determining the maximum strength and final failure mode of the connection. Frictional force was equally important and a lower bound value for the friction coefficient of 0.2, average value of 0.5, and an upper bound value of 0.8 was determined.

Figure 5-3 Small specimens tested by Lin and LaFave (2012a)

Additional experimental work has been recently conducted by Moreira et al. (2012) and Karim et al. (2011) but the characteristic of the connections are not similar to those found in Eastern North America masonry constructions.

Simplified rules that describe the hysteretic behavior of the connection were also proposed by Lin and LaFave (2012b). These rules were based on the experimental data of testing specimens and described the cyclic tensile and compressive behavior of the connection. Also, a simple numerical model including nails, friction and contact was proposed. Again, the friction, nail and contact models were calibrated to match the experiments previously conducted. The lack of robustness in this formulation prevents the application of these models to other load states, boundary conditions and different mechanical properties of the structural materials.

ASCE 31-03 provides a three-tiered process for seismic evaluation of existing buildings. Procedures for connections are specified in the Evaluation Phase or Tier 2 of the process. In general, floor-to-wall connections should be assessed as force-controlled actions. In the case of unreinforced masonry buildings, codes specify a minimum force for out-of-plane anchorage to flexible diaphragms defined by,

$$F = 2.1 S_{D1} W \tag{5.1}$$

Where S_{D1} is the seismic design category based on short period response, and W is the tributary weight of the wall. This force shall not be less than 200lb/ft and the maximum spacing between anchors should be 6 ft. on center. No other specifications are provided.

5.3 Simplified Model for Response History Analysis

After reviewing the literature on floor-to-wall connections in URM buildings it is clear that little research has been conducted on this subject. In this study, the behavior of this connection is modeled through an impact-friction-nail macro-model, as illustrated in Figure 5-4. The commercial software SAP2000 has been used so that the model can be easily replicated by practicing structural engineers.

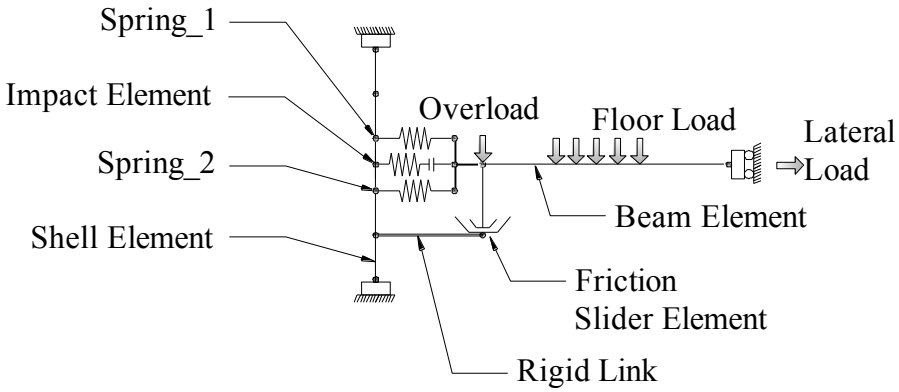

Figure 5-4 Numerical model of the URM wall-wood connections

A friction slider element which accounts for the inherent friction between wood joist and masonry walls is combined with a gap-spring-dashpot system which simulates the potential impact between the end of the wood joist and the masonry walls. In addition, a nonlinear spring element is used to simulate steel anchors which are commonly nailed to the joist and go through the walls.

The model accounts for any vertical overload due to upper masonry walls and also dead or live loads. A beam element models the joist and a rigid link is used to support the friction slider element. Each component is described in the following sections.

5.3.1 Numerical Model of Friction-Slider Element

Simulating the frictional behavior of wood joists simply supported on masonry walls is achieved through a flat slider bearing element. In SAP2000, this element includes a gap behavior in the axial direction, linear effective-stiffness properties for moment deformations and coupled friction properties for the shear deformations (Nagarajaiah et al. 1991). A flat surface was specified by setting the pendulum radii of the slipping surfaces equals to zero.

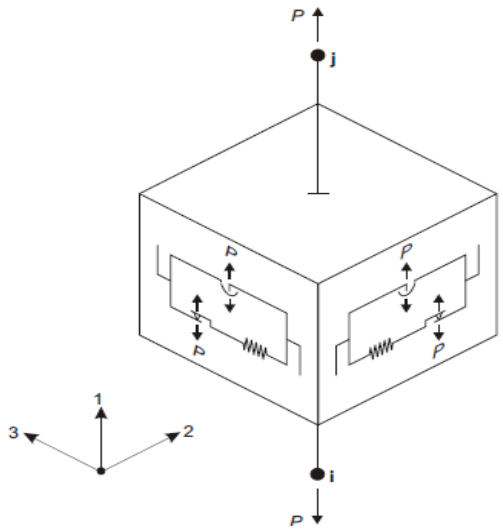

Figure 5-5 Friction-slider element in SAP2000 (CSI 2010)

A friction coefficient for the wood-brick interface between 0.3 and 0.8 has been recommended by Cross and Jones (1993) and Lin and LaFave (2012a). Herein, the average friction coefficient equal to 0.5 is assumed.

The equation for the axial stiffness is given by

$$K_{U1} = A_J E_w / H_J \tag{5.2}$$

The axial stiffness was calculated as the axial stiffness of a column having the height H_J of the wood joist, area A_J equals to the joist thickness times the length of the pocket and modulus of elasticity E_W of wood materials. No vertical damping was specified.

The shear stiffness was computed from the elastic equation given below as recommended by Sarlis and Constantinou (2010). This equation was developed to model triple friction pendulum isolators in SAP2000.

$$K_1 = \mu W / 2y \tag{5.3}$$

The axial compression force W or vertical reaction that will be delivered by the joist to the masonry wall can be computed from simple static equations if minimum parameters such as joist span, separation between joists and dead and live loads are known.

The shear deformation location is set equal to zero, so that the moment transferred by the wood joist to the bricks below will be maximum. The height of the element was assumed as the half of the joist height. The rotational and torsional stiffness of the element is currently assumed equals to zero, since fire cuts are assumed to be presented in every joist. The link element mass will be the lumped mass of the beam element simulating the joist. The rotational mass moment of inertia is currently assumed to be zero. The rate parameter does not have any influence in the element, since the friction coefficient is defined to be independent of velocity.

5.3.2 Numerical Model of Impact Element

The impact element is a contact-based model which accounts for the impact energy loss and can be easily implemented in any commercial structural software. The model is based on the Hertz damped contact model proposed by Muthukumar and DesRoches (2006). In this element the energy dissipated during impact is given by

$$\Delta E = k_h \delta_m^{n+1}(1-e^2)/(n+1) \tag{5.4}$$

Where k_h is the impact stiffness parameter, δ_m is the maximum penetration during impact, e is the coefficient of restitution, and n is the Hertz coefficient, typically taken as 3/2. The effective stiffness of the element, K_{eff}, can be computed as:

$$K_{eff} = K_h \sqrt{\delta_m} \tag{5.5}$$

The yield deformation, δy can be obtained from

$$\delta_y = a\delta_m \tag{5.6}$$

where a is the yield parameter which must satisfy the following relation:

$$a < 1 - 2/5(1-e^2) \tag{5.7}$$

Herein, a is assumed equal to 0.1, so that the yield displacement will be very small. This model is different from Cross and Jones (1993) because it includes dissipation of energy during impact, so that the displacement and accelerations are not overestimated. The stiffness parameters of the truss element can be obtained as follows:

$$K_{t1} = K_{eff} + \Delta E / (a\delta_m^2) \tag{5.8}$$

$$K_{t2} = K_{eff} - \Delta E / (1-a)\delta_m^2 \tag{5.9}$$

The parameters of the impact model are illustrated in Figure 5-6. In defining this element in SAP2000, two springs in parallel must be created: 1) A Multi-linear Elastic element with force-deformation as defined in Figure 5-6b and a Multi-linear Plastic element with Takeda hysteresis type and force-deformation as illustrated in Figure 5-6c.

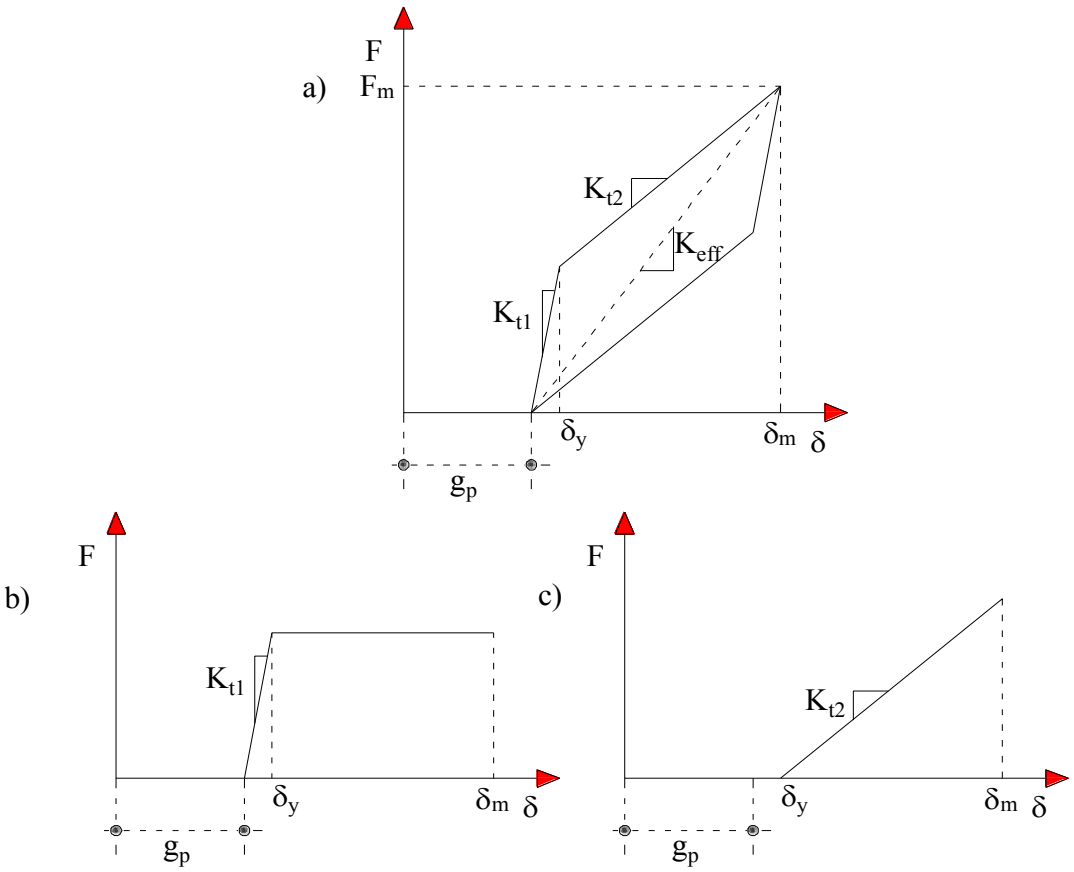

Figure 5-6 Parameters of the inelastic truss model (After Muthukumar and DesRoches 2006) for definition of impact element in SAP2000

5.3.3 Numerical Model of Nails

If the connection between wood floors and masonry walls include through bolts and steel angles or straps nailed to joists rods, additional springs are required to capture the dynamic behavior of the system. Previous experimental research indicates that the damage was concentrated in the nails. Therefore, it is assumed that the steel rod or angle will remain rigid and that the nonlinear behavior will come from the nail-slip deformation. The nonlinear force-deformation behavior of nails was discussed in Section 4. It was demonstrated that the SAWS material model (Folz and Filiatrault 2001) can be used to capture the behavior of the nail. It was also demonstrated that for 8d typical nails, the SAWS material properties can be obtained from simple equations proposed by Mclain (1975).

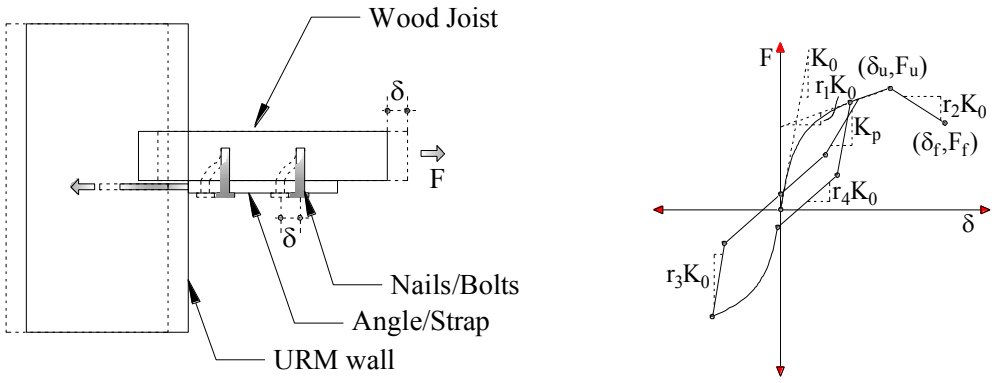

Figure 5-7 Force-deformation relationship assumed for nailed connections

5.3.4 Numerical Implementation and Validation

In this section, the friction-impact-nail model implemented in SAP2000 is examined and compared against experiments conducted by Lin and LaFave (2012a). Figure 5-8 illustrates the size and characteristic of the specimens considered. In this joist-to-wall attachment configuration, the nails are considered the weakest link whereas the bricks walls, steel anchors and straps are expected to remain elastic and almost rigid during loading. Some deformation is expected for the wood joist, therefore a Young Modulus for the wood of 1800 ksi has been considered. The three critical zones in which impact, friction and nail deformation occurs are also illustrated along with the location of axial and lateral loading applied during the experiments.

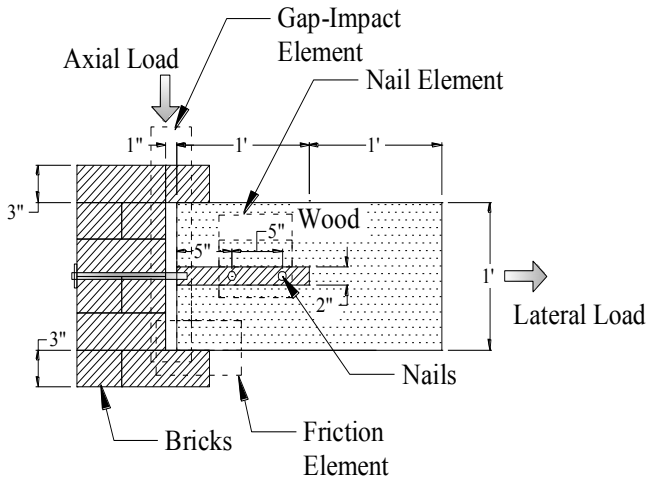

Figure 5-8 Size of the specimen tested by Lin and Lafave (2012a)

Critical parameters of the friction-slider element, K_1 and K_{U1} were calculated using Equation 5.2 and Equation 5.3, respectively. These are presented in Table 5-1 along with other parameters required to define the element. As mentioned before, the Friction Isolator element is used to define the link element. All degrees of freedom will be activated, but nonlinear behavior is considered only to the U1, U2 and U3 directions.

Table 5-1 Summary of friction-slider properties in SAP2000

Parameter	Value
Supported Weight, W	Variable
Elastic Stiffness, K1	25
Friction Coefficient, u1	0.5
Rate Parameter, r	1
Radius of Curvature, r1	0
Element Height	6
Shear Deformation Location	0
Axial Stiffness, (KU1)	100
Effective Axial Damping, bu1	3.1E-03
Rotational Stiffnes, (R2,R3)	1E-09
Torsional Stiffness (R1)	0
Link Element Mass	1E-05
Rotational Mass Moment of Inertia	1E-09

Defining the impact element requires an appropriate selection of the impact stiffness, maximum penetration during impact and the coefficient of restitution. The impact stiffness and the maximum penetration parameters were estimated based on the experimental results obtained by Lin and LaFave (2012b), since no other experimental evidence of collision between wood joist and masonry walls was found. The coefficient of restitution was assumed to be 0.5, a value in the range recommended by Cross and Jones. All other parameters can be calculated using the equations presented before. These parameters are summarized in Table 5-2. Figure 5-9 presents the force-displacement definition obtained for the multi-linear plastic and multi-linear elastic spring as implemented in SAP2000.

Table 5-2 Summary of Impact element properties

Parameter	Value
Maximum penetration during impact, δm	0.8
Gap distance, gp	0.0
Impact stiffness, K_h	25
Coefficient of restitution, e	0.5
Hertz coefficient, n	1.5
Energy dissipated during impact, ΔE	4.293
Effective stiffness, Keff	22.36
Yield deformation, δy	0.08
Stiffness, K_{t1}	89.44
Stiffness, K_{t2}	14.907

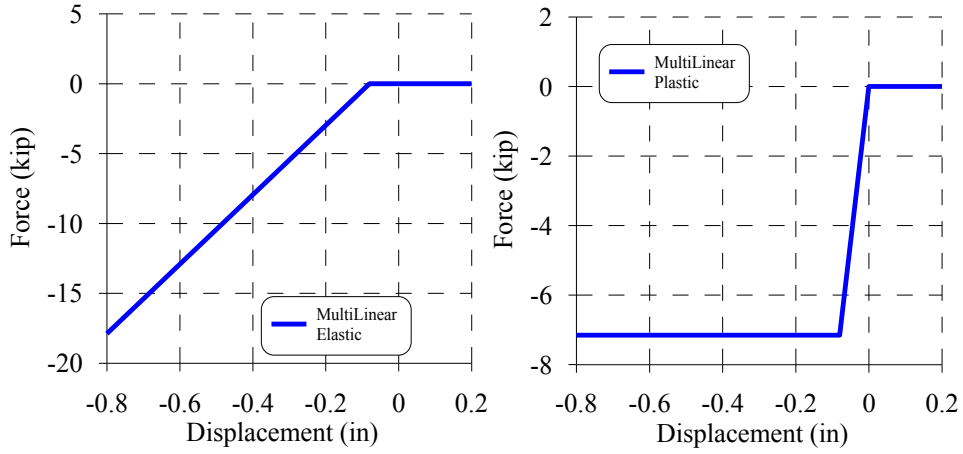

Figure 5-9 Force deformation definition of Multi-Linear Elastic and Plastic springs

Table 5-3 presents all parameters required to define the force-deformation relationship of 8d nails. These parameters were computed as in Section 4. Figure 5-10 presents the actual hysteretic behavior implemented in SAP2000.

Table 5-3 Summary of Nail Spring element properties

Parameter	Value
Effective Stiffness, K_{eff}	19 kip/in
Effective Damping, β	0.002
Pivot Hysteresis α_1, α_2	1000
Pivot Hysteresis β_1, β_2	0.1
Pivot Hysteresis η	100

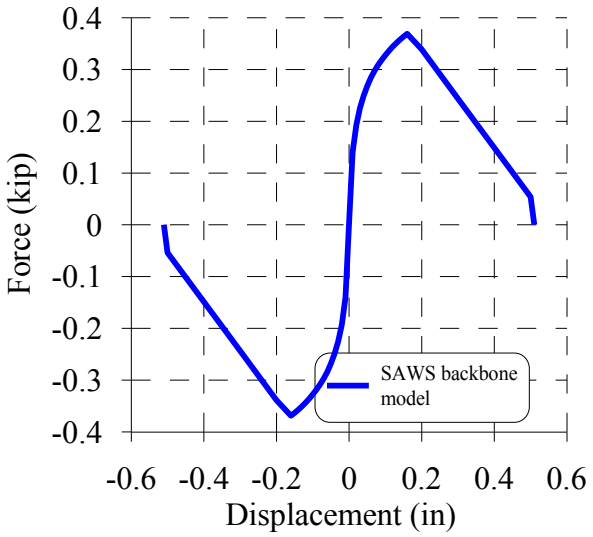

Figure 5-10 Force-displacement backbone model of nail-springs

The friction-impact-nail element as implemented in SAP2000 is illustrated in Figure 5-11. Fix supports were used at the base of the impact and friction elements. A pin connection was used at one end of the beam element. Axial loads were applied using ramp functions shown in Figure 5-12. The load was applied on top of the friction element. Nonlinear static analyses were conducted before each time-history analysis. Two lateral loading protocols were used, namely 1) a cyclic loading protocol with increasing displacements (see Figure 5-13) and 2) a loading protocol with constant amplitude designed to estimate the friction coefficient (see Figure 5-14). Both protocols were applied using nonlinear direct integration history analysis. Damping in the system was assumed to be 2% of critical damping. Note that this may overestimate the

accelerations and the maximum displacement of the friction element as described by Sarlis and Constantinou (2010).

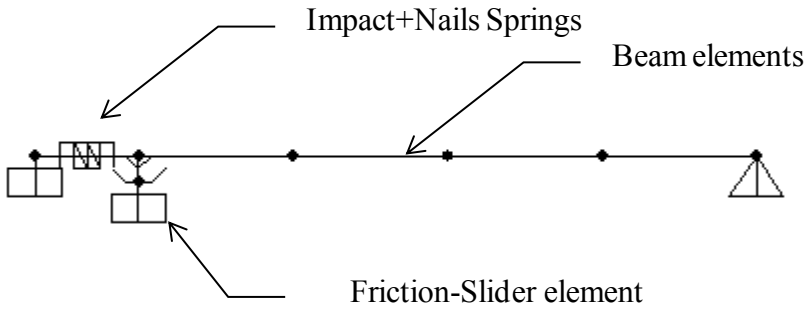

Figure 5-11 Friction-impact-nailed element as implemented in SAP2000.

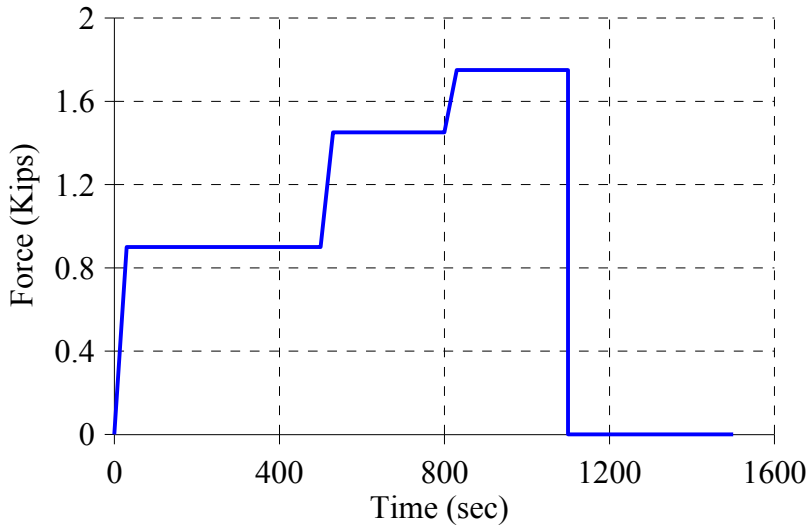

Figure 5-12 Axial load protocol applied for estimating the friction coefficient

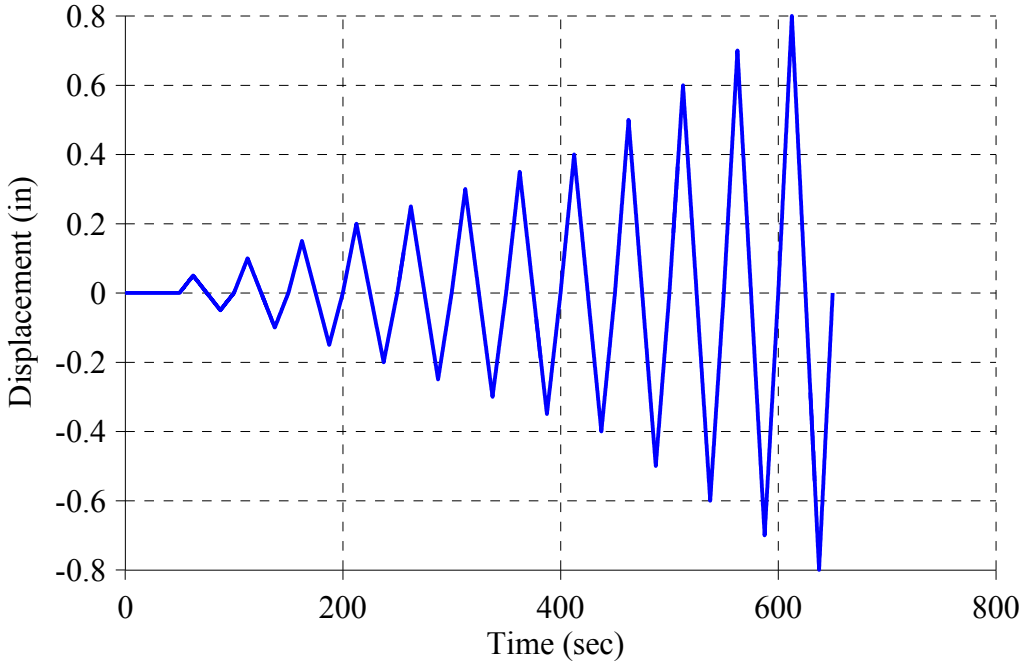

Figure 5-13 Loading protocol for static cyclic load

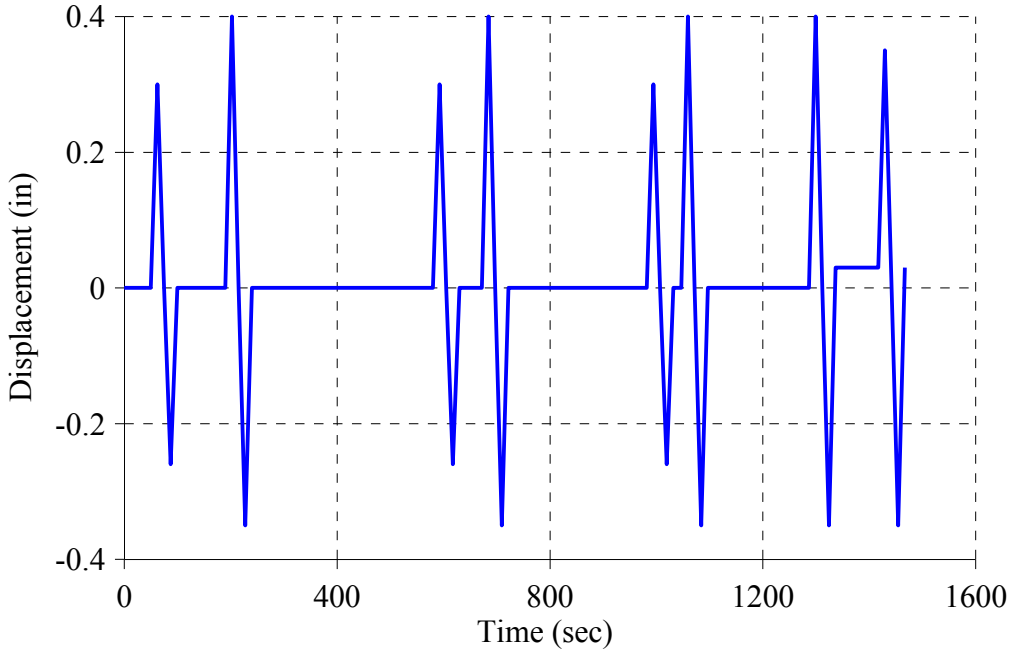

Figure 5-14 Loading Protocol used to estimate the friction coefficient

Figure 5-15 presents a comparison between the numerical model and the experimental results for friction only behavior. The model captures the maximum force fairly well including the hysteretic behavior for different axial loads.

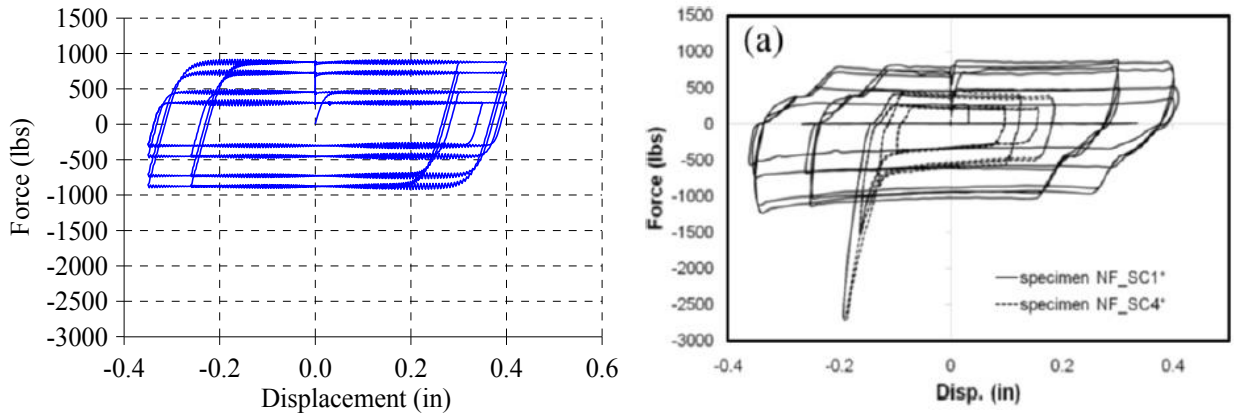

Figure 5-15 Force Displacement relationship for Friction Only Model: a) Numerical model; b) Experimental (Lin and LaFave 2012b)

An increasing monotonic analysis was also conducted in the model to evaluate the behavior of friction and nails combined. Figure 5-16 presents a comparison between the numerical model and the experimental results for combined friction and nail behavior. The nail model under predicts the maximum force obtained in the experiment for specimen NF_SM1 and specimen NF_SM2 by 20% and 40% respectively. The displacement in which the 1st nail is sheared off is well predicted, yet the model does not capture the moment when the 2nd nail is sheared off since both nails are defined with the same ductile capacity. Because of this, it is understood that the failure mode predicted by the model is different from that obtained during the experiment, where very large displacements were observed before the nails were sheared off.

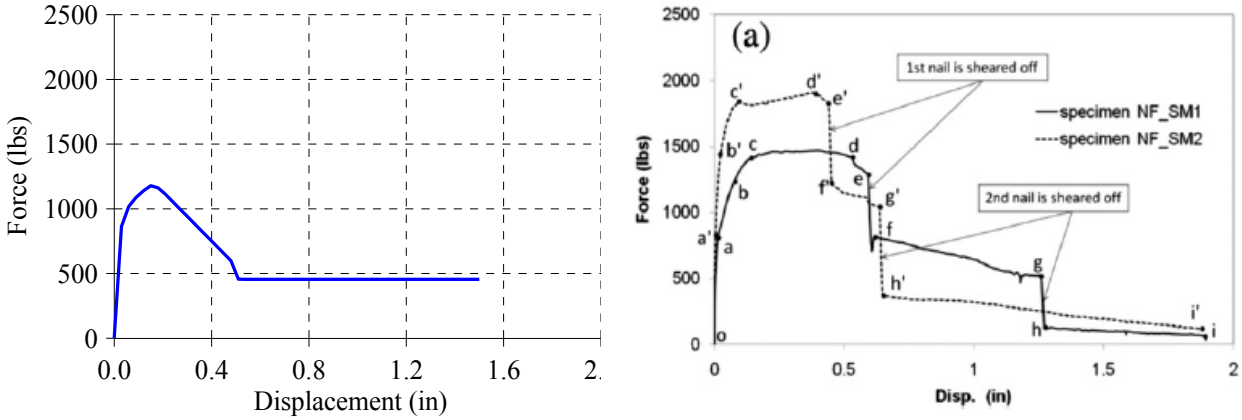

Figure 5-16 Force-displacement curves for monotonic loading a) Numerical model b) Experimental (Lin and LaFave 2012b)

The numerical model was then subjected to the cyclic quasi-static loading protocol previously described in Figure 5-13. Comparison results are shown in Figure 5-17. The model captured the maximum compression and tension forces fairly well. Yet, it is unable to capture the large displacements obtained in the tension side. As discussed before, such a large displacements may not be strictly related to the failure of the nails in shear but a combination of slippage and shear.

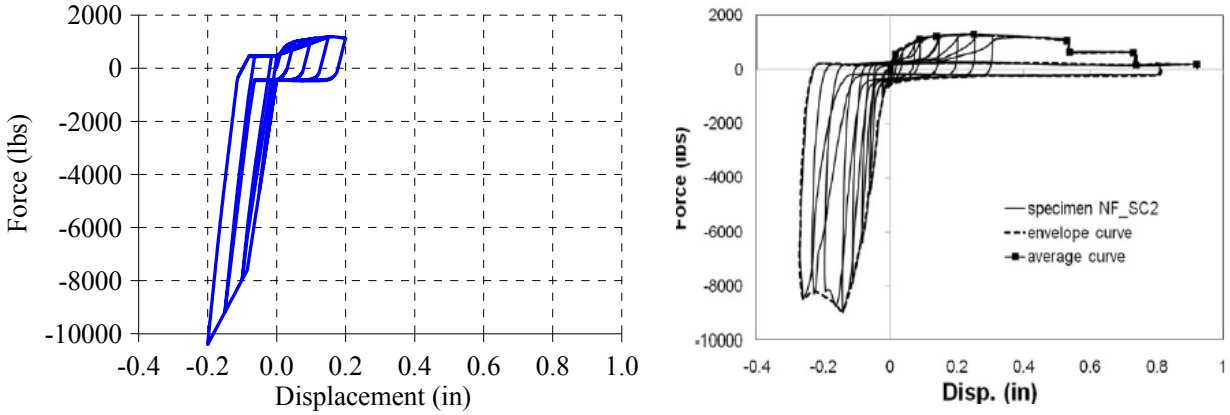

Figure 5-17 Force-displacement curves for cyclic quasi-static loading a) Numerical Model b) Experimental (Lin and LaFave 2012b)

5.4 Summary and Conclusions

The connection between wood floors and URM walls play a fundamental role in the seismic behavior of unreinforced masonry buildings. Yet, currently there is little information on the modeling and performance of this critical component under seismic loads. This section summarized the implementation and validation of a friction-impact-nailed model that simulates the connection between wood joist and unreinforced masonry walls. The numerical model was implemented in SAP2000 and validated against previous experiments conducted by other researchers on this type of connections.

The friction, impact and nail numerical models were developed by other researchers to analyze different phenomena and can be easily implemented in any commercial software. Herein, these models were combined so that it could accurately simulate the potential friction, impact and nailed behavior of the joist-to-wall connection. It was demonstrated that the combined friction-impact-nail model captured fairly well the cyclic behavior in tension and compression of a

typical joist-to-wall connection. Also, because the model does not require calibrations or adjustments, it can be suitable for different boundary and loading conditions.

Further studies are required to investigate the impact of key variables, such as the coefficient of friction, gravity loads and coefficient of restitution in the global seismic response of a multi-story URM building. Also, current ASCE 31-03 recommendations regarding the strength, minimum number and separation of required steel anchors can be explicitly evaluated.

SECTION 6
COMPUTER SIMULATION OF URM WALLS IN MULTI-STORY BUILDINGS

6.1 Introduction

Conducting reliable seismic analysis of multi-story URM buildings remains a challenging task within the earthquake and structural engineering field. Although several numerical methods have been proposed, the combination of highly nonlinear material and structural component behavior, complex geometric configurations and lack of experimental data make the problem difficult to solve. Even more, as of today there are no reported attempts to capture the nonlinear seismic response of multi-story URM buildings with flexible diaphragms.

In this section, simplified and robust non-linear numerical macro-models for in-plane and out-of-plane walls were developed and validated using previous experiments found in the literature. The models can be easily combined to analyze a full multi-story URM building subjected to seismic loads. The numerical models are suitable for pushover or nonlinear response history analysis. Peak accelerations and displacements can be obtained with minimal computational time. Moreover, the models were implemented and verified in SAP2000, so that they could be used by practicing engineers.

The first section of this section presents previous research on methods that simulate out-of-plane and in-plane behavior of URM walls. It can be seen in Table 6-1 that numerous computer methods exist in URM modeling. However, in this report, emphasis is made on macro-scale and analytical models appropriate for nonlinear time history analysis. Hence, “smeared crack” models, homogenized methods and “discrete crack” models common in finite element simulations were not considered.

In the second section, a nonlinear simplified model combining elastic shell elements and nonlinear rotational springs is proposed, implemented and validated in SAP2000. A nonlinear response history comparison with previous experiments is also provided.

As mentioned before, one of the primary goals of this study has been to assess the seismic behavior of URM walls subjected to out-of-plane loading in multi-story buildings. Thus, for

completeness a suitable numerical model for in-plane walls is also required. An attractive solution was found through a modified equivalent frame method for URM walls. This is a suitable methodology which balances complexity, efficiency and accuracy for performance based assessment. The model was also developed and implemented in SAP2000.

Finally, other simplified methodologies for modeling in-plane and out-of-plane walls were investigated. Key results are summarized in appendices.

Table 6-1 Summary of computer methods in structural masonry

Numerical Simulation	Micro-scale models	• Discrete element • Rigid body spring • Interface elements • Homogenization
	Macro-Scale models	• Equivalent frame • Fiber elements • Zero-length springs • Rigid body models
	Analytical models	• Limit analysis • Code based equations • Empirical equations

6.2 Previous Research on Out-of-Plane Macro-models of Unreinforced Masonry

Current numerical models to analyze out-of-plane URM walls can generally be classified as stiffness-based models and rigid body rocking models. Stiffness-based models are usually SDOF models that capture the main dynamic parameters of the wall and are suitable for nonlinear static and dynamic analysis. Also, these models can be easily implemented in most commercial computer software. On the other hand, rigid-body rocking models tend to offer a more accurate simulation of the actual behavior of the wall, but can be only implemented in specialized computer software. Recent research regarding these two methodologies is briefly discussed next.

6.2.1 Oscillator-based Models

One of the most relevant studies on out-of-plane behavior of URM walls has been conducted by Blaikie and Davey (2000) who developed equations that describe the behavior of URM walls under out-of-plane static loading. This research later became the main reference to develop

guidelines for seismic evaluation of URM walls in New Zealand. Derivation of the equations, as presented by Blaikie and Davey (2000) is summarized below.

The maximum force and cracking displacement of the walls were obtained by equating overturning and resistant forces acting in the wall just before instability. The walls were assumed to crack at the middle, with remaining portions remaining virtually rigid as shown in Figure 6-1. This figure also shows the forces assumed to act on a cracked wall element subjected to a static lateral load **V**. The total weight of the wall is **W**, and effective thickness, **t**. The bending moments developed in the wall when subjected to a point load **V**, acting at the mid-height are also depicted.

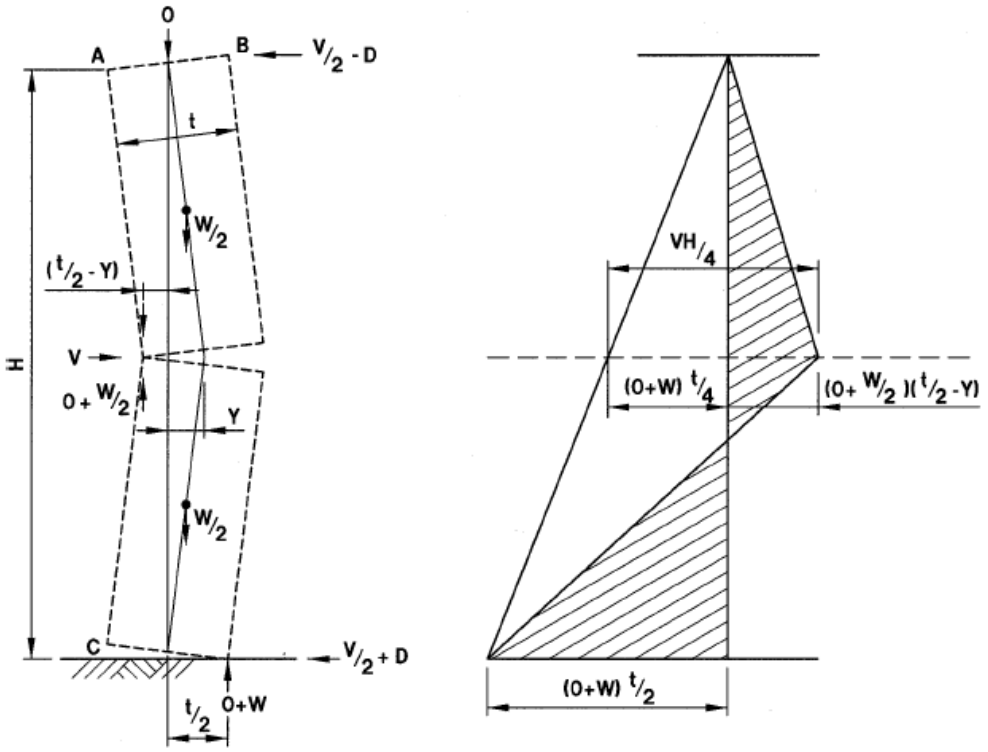

Figure 6-1 Behavior of face loaded single-story wall element under static loading (Blaikie and Davey 2000)

Under this configuration, equating the simply supported bending moment to the wall moment at the mid-height crack, yields:

$$\frac{VH}{4} = \frac{(O+W)t}{4} + (O + W/2)(\frac{t}{2} - Y) \quad (6.1)$$

V will have a maximum value, $\mathbf{V_{max}}$ when **Y=0.0:**

$$V_{max} = (2W + 3O)\frac{t}{H} \tag{6.2}$$

Moreover, the wall will become unstable when the applied load, **V**, reduces to zero and the wall displacement, **Y**, will then have its maximum static value, Y_{max}. Rearranging Equation 6.1and substituting **V=0.0**:

$$Y_{max} = \left(\frac{W+1.5O}{W+2O}\right)t \tag{6.3}$$

Equations 6.2 and 6.3 can be used to replace **O** and **W** in Equation 6.1, showing that:

$$V = V_{max}(1 - \frac{Y}{Y_{max}}) \tag{6.4}$$

The graphic form of this equation is shown in Figure 6-2:

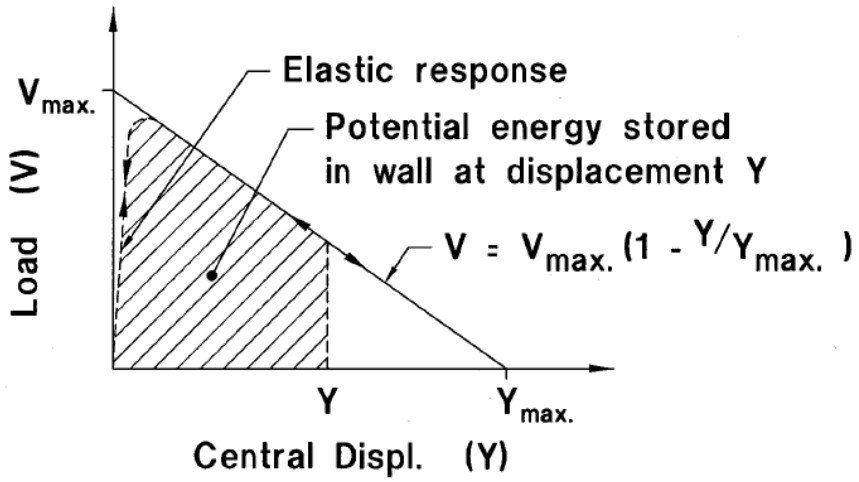

Figure 6-2 Load deformation relationship for point load acting at mid height crack (from Blaikie and Davey 2000)

In case that a uniform load **F,** replaces the point load **V,** the simply supported bending moment will be **$FH^2/8$.** Thus, the load **V,** would need to be replaced by **FH/2** in Equations 6.1 to 6.4. Blaikie and Davey (2005) also proposed the following generalized equations, for different boundary conditions and axial load eccentricities. The maximum displacement at which the wall becomes unstable is given by,

$$Y_{max} = t * \frac{\left(1+K_1\frac{O}{W}\right)}{\left(1+\frac{2O}{W}\right)} * fixity \tag{6.5}$$

Where **O** is the overburden, **W** is the weight of the wall, **t** and **fixity** are given by,

$$t = t_{nom}(0.975 - 0.025\frac{O}{W}) \tag{6.6}$$

$$fixity = \frac{\left((K_2+B_b)+(K_3+B_b+B_t)\frac{O}{W}\right)}{K_4\left(1+K_1\frac{O}{W}\right)} \tag{6.7}$$

$\mathbf{T_{nom}}$ is the nominal thickness of the wall, and the parameters $\mathbf{B_t}$ and $\mathbf{B_b}$ are eccentricities of the overburden at the top and bottom of the wall, as seen in Figure 6-1. The maximum force occurs when the wall crack starts to open and is given by:

$$F = \frac{4tW}{K_5}\left(1 + K_1\frac{O}{W}\right) * fixity \tag{6.8}$$

The parameters K_n are given in

Table 6-2 and cover different boundary conditions for the wall.

Table 6-2 Equation constants for the two wall element types (Blaikie and Davey 2005)

Type of wall Element	K1	K2	K3	K4	K5
Single story wall	1.5	1.0	2.0	2.0	1.0
Parapet of free standing wall	1.0	0.0	0.0	1.0	4.0

At the same time, in the University of Adelaide in Australia, Doherty et al. (2002) addressed the problem of assessing the seismic behavior of out-of-plane URM using a simplified linearized displacement–based procedure. The displacement profile of a rocking wall and its equation of motion was used to develop an equivalent lumped mass SDOF model. A tri-linear relationship was used to characterize the nonlinear force-displacement behavior of masonry as shown in Figure 6-3.

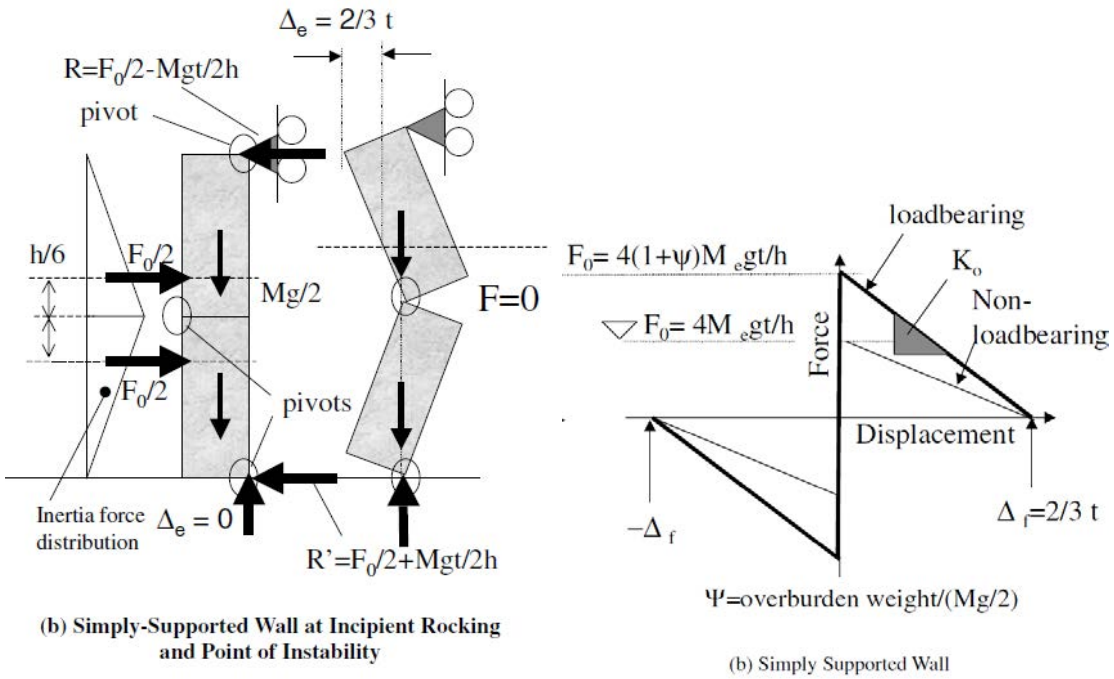

Figure 6-3 Inertia forces and reaction of rigid URM walls and force-displacement relationship (from Doherty et al. (2002))

Similarly, Simsir et al. (2004) developed a SDOF, a MDOF and a two-degree-of-freedom model to evaluate the dynamic stability behavior of URM walls. The models were calibrated to match the experiments discussed in Section 2 by Simsir et al. (2004). The same methodology was followed by Derakhshan et al. (2009) who used a SDOF system to simulate the out-of-plane behavior of masonry walls. Using experimental results obtained through monotonic loading with airbags, they developed a tri-linear force-displacement relationship. More recently, a similar methodology was implemented by Vaculik and Griffith (2008) to conduct time history analyses of masonry walls subjected to two-way bending.

6.2.2 Simplified FE and Rigid Body Models

Using a different approach, Lu et al. (2004) developed a finite element model to perform material and geometric nonlinear analysis of slender URM walls. The model had the capability to capture post-cracking and post-buckling behavior while allowing for different loading and boundary conditions. Similarly, Hamed and Rabinovitch (2008) developed an analytical model for the nonlinear dynamic behavior of URM walls subjected to one-way bending. This methodology was based on variational principles, dynamic equilibrium conditions, and nonlinear

constitutive equations of the masonry and mortar. In particular, the model was used to quantify the non-periodicity nature of URM walls, and the degradation of the natural frequency with the increase of the amplitude of the dynamic response. More recently, Okail et al. (2010) modeled a veneer masonry walls with wood studs subjected to out-of-plane loading using beam-column elements. The wood studs were assumed to remain elastic while the veneer was modeled using nonlinear fiber elements. A concrete material was used to simulate the behavior of the masonry. The model included a linear spring at the top to capture the additional deformation provided for the diaphragm. The model was implemented in OpenSees.

Rigid body formulations have also been recently implemented. For instance, Sharif et al. (2007) used a rigid-body approach to analyze the out-of-plane response of URM walls. Time history analyses was carried out in Working Model 2D and compared with shake table tests conducted by Meisl et al. (2007). Shawa et al. (2012) carried out the dynamic modelling of masonry walls rocking using the Discrete Element Method (commonly used for analysis of assemblages of blocks) and a SDOF system derived from the rocking motion of the walls. The first method captures the loss of contacts between adjacent blocks, whereas the second one included dissipation of energy through impact. More recently, Costa et al. (2013) investigated the free rocking response of regular masonry walls using an equivalent rigid body block approach. The loss of energy due to impact was investigated using a calibrated coefficient of restitution.

Overall, rigid body formulations provide a deeper insight in the nonlinear dynamic behavior of URM walls subjected to out-of-plane bending. However, more complex boundary conditions have not been investigated and as in the SDOF formulations, a predefined crack location is required to analyze the wall. Ongoing research at the University of British Columbia is partially addressing the problem of URM walls subjected to out-of-plane loading accounting for diaphragm flexibility (Penner and Elwood 2012).

6.3 Previous Research on Analytical In-Plane Macro-models of Unreinforced Masonry

Previous research on analytical macro-models for analysis of in-plane URM is summarized in this section. As mentioned before, preference was given to very simplified models which enable

the properly implementation of performance based design procedures. When available, practical applications of these macro-models have been described.

6.3.1 Macro-model of URM Pier Elements

Gambarota and Lagomarsino (1997) proposed a non-linear macro-element model representative of a whole masonry panel (pier or spandrel). Few degrees of freedom were used to represent the two main in-plane masonry failure modes, bending-rocking and shear-sliding mechanisms including friction. In addition, the macro-element took into account the effect of the limited compressive strength of masonry by means of nonlinear constitutive laws with stiffness deterioration in compression. Shear-sliding damage evolution which controls the stiffness degradation and the strength deterioration of the masonry panel in shear were also considered.

Figure 6-4 show the three substructures that define the macro-element panel. Axial effects and bending were concentrated in the outer layers whereas shear deformation was defined within the central substructure. Six material parameters define this macro-element: axial stiffness, shear strength and modulus of masonry, coefficient of friction, a non-dimensional coefficient that controls the inelastic deformation and a factor that control the softening phase.

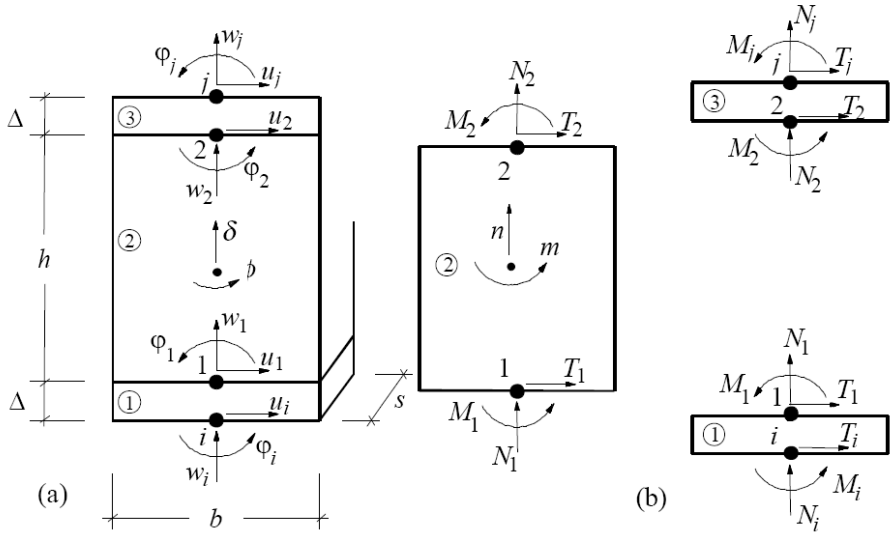

Figure 6-4. Kinematic macromodel proposed by Gambarota and Lagomarsino (1997)

This model was implemented in the program TREMURI which allows an accurate modelling of masonry buildings at a reasonable computational cost. Moreover, the software allows performing

nonlinear seismic analyses of unreinforced masonry buildings using a relatively complete set of analysis procedures: incremental static analysis both with force or displacement control and 3D pushover and time history dynamic analysis using the Newmark integration method and Rayleigh viscous damping. Recent studies [Rota et al. (2010), (Gallonelli 2007), (Rush 2007), (Galasco et al. 2004)], on seismic assessment and performance based design have been successfully carried out using TREMURI software.

Out-of-plane failure and flexible diaphragms are not currently addressed since this macro-model is based on the hypothesis that the seismic response of the building is governed by global box-type behavior, assuming that local mechanisms (mainly out-of-plane) are prevented by appropriate structural details and connecting devices (Rota et al. 2010).

6.3.2 Frame Equivalent Modelling

Calvi and Magenes (1997) implemented a frame equivalent model to analyze the nonlinear behavior of unreinforced masonry multi-story buildings with openings. This study was mainly based on previous simplified methods proposed by Tomazevic and Weiss (1990) and Paulay and Priestley (1992). In this method, piers and spandrels elements were defined as elements which can crack and dissipate energy whereas the joint elements were assumed infinitely rigid.

The force-deformation of piers and spandrels was modeled as a bilinear elastic-perfectly plastic shear- displacement relationship, as shown in Figure 6-5. The method gave a fair prediction of the wall capacity at collapse, failure mechanisms, and forces distribution at ultimate state. However, lower accuracy in the residual drift and deformed shape were obtained.

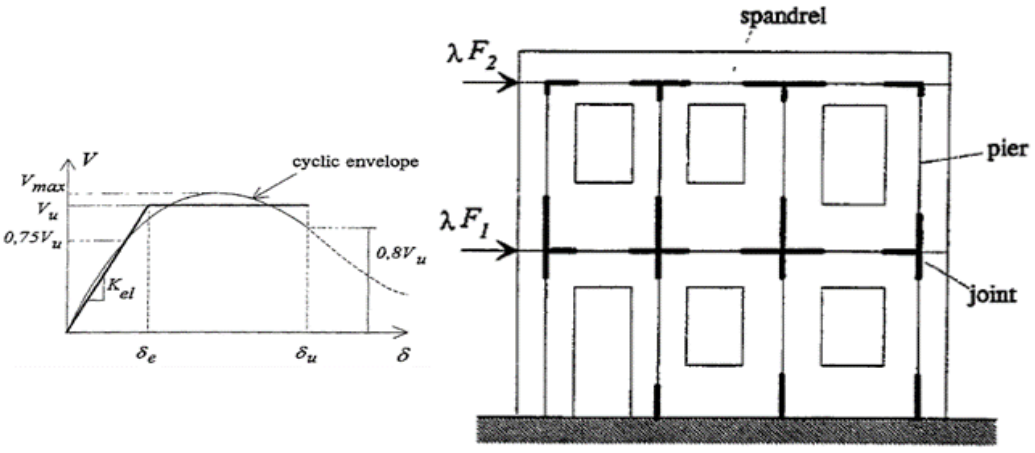

Figure 6-5 Equivalent Frame Modelling by Calvi and Magenes (1997)

Similar formulations have been proposed by Salonikios (2003), Roca et al. (2005), Belmouden and Lestuzzi (2007). The reliability of the simplified hypothesis adopted in the Equivalent Frame modelling approaches, in particular for masonry walls with regular opening patterns has been recently verified by Calderini and Lagomarsino (2009). Current implementation of this technique in a SAP2000 (CSI 2009) software can be found in Pasticier (2008) and Knox (2012).

6.3.3 Applied Element Model for Masonry Structures

Mayorca and Meguro (2003) proposed a simplified micro model approach based on the Applied Element Method (Meguro and Tagel-Din 2002). This technique is especially suitable for URM since it can model the beginning and propagation of cracks along the system without any initial presumption. The system behavior was fully captured from early stages of loading until collapse.

In this study, two types of spring were incorporated in the AEM formulation to model the connection brick-to-brick and the brick-mortar interface. Figure 6-6 shows the AEM principle and the corresponding brick-mortar spring.

Herein, tension and shear sliding were considered the dominant behavior of URM buildings subjected to seismic excitations. Four failure modes were captured with this model: (1) joint debonding, (2) joint bed sliding, (3) units cracking under compression and (4) units cracking due to shear. The first and second failure mode were reflected in the brick-mortar spring whereas the third and fourth were included in the brick springs.

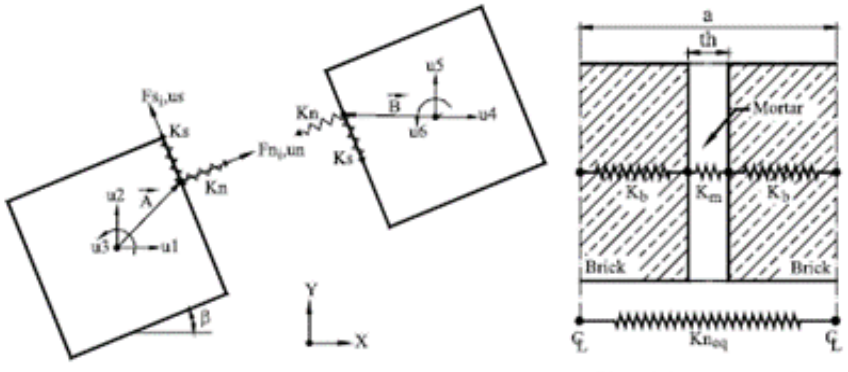

Figure 6-6 Masonry modelling in the Applied Element method by Mayorca and Meguro (2003)

The model was validated with experimental data obtained from wall subjected to shear loading. A good agreement was found in the force-deformation curve and crack pattern. Moreover, the failure mechanism was fairly well captured.

This modelling technique has been recently implemented by the Applied Science International Company on the Extreme Loading for Structures Software (Applied Science International (2009)). Examples applications can be found in Worakanchana and Meguro (2008), Tagel- Din and Rahman (2006), Karbass (2009), and Lupoae and Bucur (2009).

6.3.4 Discrete Crack Macro-models

A Rigid Body Spring Model (RBSM) was proposed by Casolo (2004) for the in-plane dynamical analysis of masonry walls. As shown in Figure 6-7 the RBSM consists of a set of plane quadrilateral rigid elements connected to each other by two normal springs and one shear spring at each side. Each spring describes rocking, shear cracking and sliding failure mechanism, respectively. Using previous experimental descriptions of the cyclic response of masonry and the mechanical degradation of mortar, a material model was proposed and specific separate hysteretic rules were assigned for the shear and axial deformation between elements. A Coulomb-like law was incorporated to relate the shear springs strengths to the vertical axial loading.

The RBSM accuracy and effectiveness were demonstrated by comparisons with previous experimental tests on URM. Results were in reasonable agreement with experimental data of pier walls and full scale walls previously tested. It was established that the key point of this macro-model was the mechanical description of the three springs that bond the elements at each side.

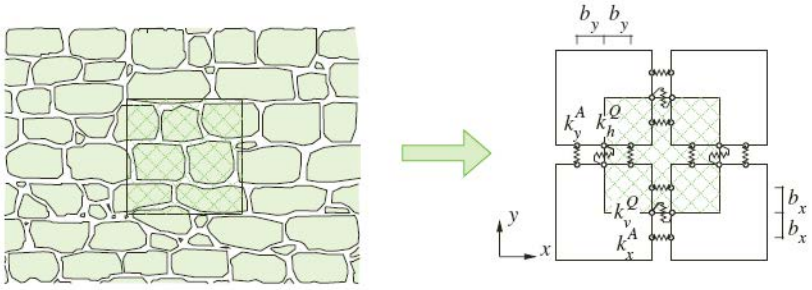

Figure 6-7 Macromodel proposed by Casolo (2004)

The seismic analysis and the strengthening design of some old very important masonry monuments have been recently approached by integrating the RBSM with traditional FE commercial software (Casolo and Sanjust 2009).

6.3.5 Nonlinear Discrete Springs Macro-models

Chen et al (2008) proposed a macroelement that involves placing nonlinear shear springs in series with rotational springs to simulate both shear and flexure response. The macroelement explicitly address the in-plane failure modes unique to URM by including an axial spring, three shear springs, and two rotational springs to simulate axial, bed joint sliding, diagonal tension, and rocking/toe crushing failure modes, respectively. Figure 6-8 shows the basic configuration of this macroelement. The macroelement was validated comparing ultimate strengths and failure modes obtained through Nonlinear Static (Pushover) Analysis against 21 experiments by previous researchers. The validation study concluded that 70% of failure modes were properly simulated and provided strength estimates with an average error of 20%.

Park et al. (2009) proposed a structural modeling method appropriate for two story- URM low-rise buildings located in the central and southern US (CSUS) region. In this study, a simple nonlinear spring element with limited degrees of freedom was used to model components of URM buildings such as foundations, walls (in-plane and out-of-plane) and diaphragms. Further simplification was achieved by lumping wall and floor diaphragm masses at each story level. Figure 6-9 shows the macromodel and the building prototype. In addition, masonry was considered as a homogeneous material and individual mortar and bricks were ignored. The failure modes, failure strengths, and the hysteretic behavior for each wall component were determined based on the provisions in FEMA-356. The model was effectively used on DRAIN-2DX to perform nonlinear dynamic analysis and develop fragility curves without significant increasing in computational time, and maintaining an acceptable level of accuracy.

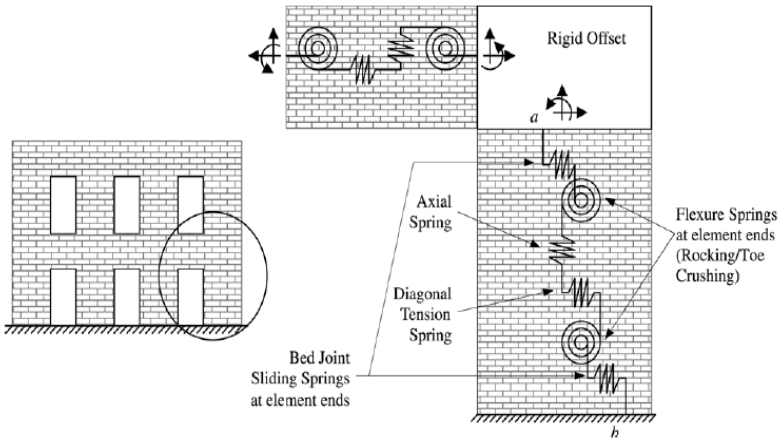

Figure 6-8 Macroelement proposed by Chen et al. (2008)

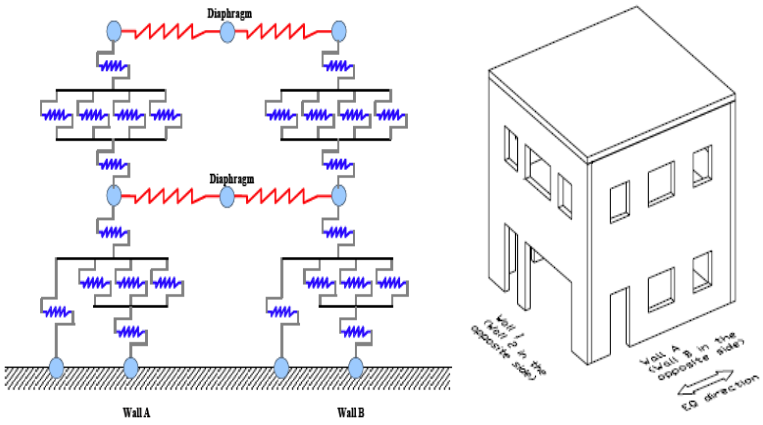

Figure 6-9 Building prototype and macromodel (Park et al. 2009)

6.4 Nonlinear Rotational Spring for Quasi-static Monotonic, Cyclic and Dynamic Analysis of Out-of-plane URM Walls

In this section, a reduced MDOF model of out-of-plane URM walls in one-way bending is proposed and implemented in SAP2000. The model is suitable for monotonic, increasing cyclic quasi-static and time history analysis in two dimensions. It also requires significantly less computational time than current finite element models and is easier to implement in commercial software while fully capturing the seismic behavior of the wall.

The model is based in the equations derived by Blaikie (1999) for face loaded walls in URM buildings and the methodology developed by Doherty et al. (2002). The first study suggested that, when subjected to strong lateral loads, multi-story URM walls can be expected to crack at the level of the supports and near the mid-height of the wall, if the supports do not fail before.

The maximum force and cracking displacement can then be obtained by equating overturning and resistant forces acting in the wall just before instability. The second study demonstrated that it is possible to represent the dynamic rocking behavior of masonry walls using a SDOF equivalent model. This approach is also followed in this study, but using the more simplified equations developed by Blaikie and Davey (2005).

6.4.1 Structural Configuration

Figure 4-37(a) presents a typical out-of-plane wall in URM buildings. Relevant variables include the floor load, the overload from upper floors, the inertia of the wall itself, and the height and thickness of the wall. In existing old URM multi-story buildings, the thickness of multi-wythe walls usually varies from 12 to 16 inches. Hence, the relative stiffness of the walls is usually low compared to the in-plane walls. Also, the connection between wood joist and masonry walls are not always adequate to resist seismic forces, as seen in Section 3. Nonetheless, for the sake of simplicity, herein is assumed that the walls are sufficiently anchored and the connections prevent slippage and global rotation of the masonry wall.

6.4.2 Kinematic Assumptions

Figure 4-37 shows the undeformed and deformed structural configuration of a typical URM wall under seismic inertial load applied perpendicularly to the wall. Under this load, the wall will likely develop one crack near the mid-height, and cracks at the support while the element in between remain essentially rigid. This behavior has been demonstrated by previous experimental research (Meisl et al. 2007; Penner and Elwood 2012). Therefore, the masonry wall can be effectively replaced by relatively rigid plane-stress area elements of dimensions **H/2**, **t**, and **L**, and Young's modulus of the masonry **Em.** This can also be achieved with beam elements, but the distribution of inertia loads and gravity support would be less accurate.

It has also been shown that the out-of-plane wall system can be replaced by a single DOF oscillator for which dynamic behavior only depends on the overload, the wall geometry and boundary conditions. Therefore, it is possible to concentrate the nonlinear behavior of the wall in a zero-length rotational spring located at its mid-height. For this change to be valid, it is necessary to transform the force-displacement relationship proposed by Blaikie and Davey (2005) into moment-rotation. The rotation is measured with respect to the boundaries of the wall. The maximum moment is given by

$$M_c = w * H^2/8 \tag{6.9}$$

Where *w* is obtained as

$$w = F/H \tag{6.10}$$

F is calculated using Equation 6.4 and the maximum rotation is calculated as

$$\theta = 2 * \frac{Y_{max}}{H} \tag{6.11}$$

It is also assumed that the in-plane wall deformations are negligible. Thus, in-plane translation of the wall is constrained. The simplified final configuration is illustrated in Figure 6-11.

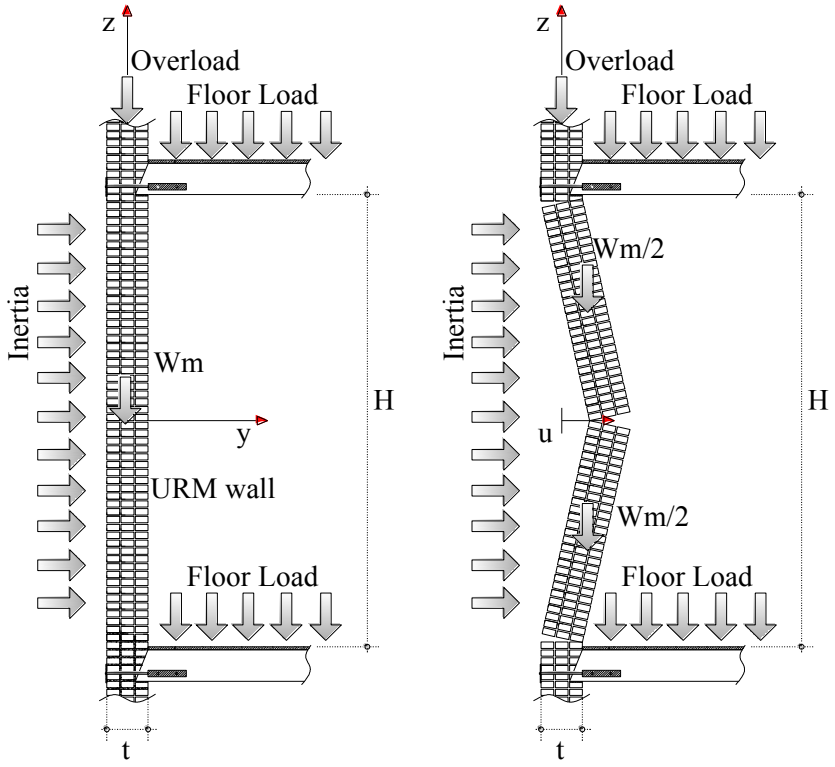

Figure 6-10 Typical configuration of URM walls in multi-story buildings : a) Undeformed shape; b) Deformed shape

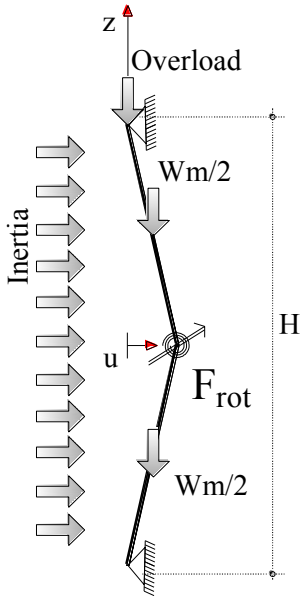

Figure 6-11 Reduced equivalent system with rotational spring

In this new formulation the shell elements have disconnected joints at the location of the zero-length springs. The number of springs connecting both shell elements should be adjusted to the mesh of the wall. Since a rigid body motion is expected for the wall, the mesh does not need to be fine.

It has been previously demonstrated by Makris and Konstantinidis (2003) that this oscillator-based methodology to model rocking out-of-plane walls is not appropriate to capture all fundamental properties of the system. However, as demonstrated in the next section, the model gives reasonably accurate results at a significantly reduced computational time. Also, in Section 8 it is shown that this modeling approach can be easily implemented in commercial engineering software to simulate the behavior of masonry panels in multi-story buildings. Another attractive feature of this formulation is that it does not need to be calibrated or adjusted. Yet, for higher axial loads, the maximum capacity of the wall will be generally overestimated. This is because the model does not include variables to account for crushing of the mortar or the brick or explicit axial-moment interaction.

6.4.3 Model Verification

The reduced MDOF model implemented in SAP2000 was compared with experiments conducted by Derakhshan et al. (2009), and by Meisl et al. (2007). Figure 6-12 presents a three dimensional view of the model in SAP2000. The model was validated through pushover and nonlinear response history analysis. The wall dimensions and material properties of both experimental specimens used in this study are provided in Table 6-3. In modeling the wall, pinned joint restraints were used at the base, whereas only a translation support in Y direction was provided at the top of the wall.

Masonry walls were simulated using the *Shell thick* element available in SAP2000. A state of plane-strain is considered for the walls, since the thickness is big compared with its planar dimensions. All other section parameters were the default values specified in the software. For the shell element, all six DOF are activated at each of its connected joints, allowing for full interaction with a potential frame at the boundaries (CSI 2010).

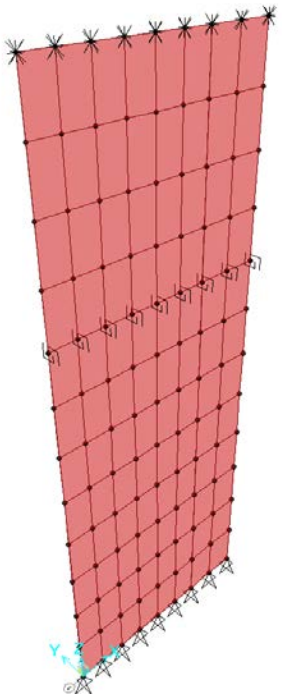

Figure 6-12 3D model of the wall in SAP2000

Table 6-3 Wall dimensions and material properties required for SAP2000 models

Wall	H (mm)	L (mm)	T (mm)	G (kN/m^3)	E kN/m^2	W kN	O kN	k1	k5	fix	F (kN)	Δ (mm)	M (kN-m)	θ (rad)
1	4100	1150	220	22.37	580	18.6	19	1.5	1.0	1.0	10.12	208	5.18	0.204
2	4133	1500	353	18.37	580	39.45	0	1.5	1.0	1.0	13.48	344	6.96	0.333

Discrete cracks were modeled as *zero-length* nonlinear spring elements. The cyclic behavior of cracking in out-of-plane is characterized by pinching, stiffness and strength degradation. These characteristics are partially captured by the *multi-linear plastic Pivot* hysteretic property in SAP2000. The features of this hysteretic rule were already discussed in Section 4. Note that cracks are located in the numerical model where they actually occurred during the experiment.

In defining the nonlinear *Link* properties, a multi-linear force-deformation curve and hysteresis parameters must be specified. The nonlinear moment-rotation relationship properties were obtained from the bilinear curve defined by the Blaikie equations. After several trials in trying to reproduce the global hysteretic behavior, the hysteretic parameters were defined as alpha=0.45, Beta=0.2 and nu=0.80. The multi-linear force-deformation definition in SAP2000 is illustrated in Figure 6-13.

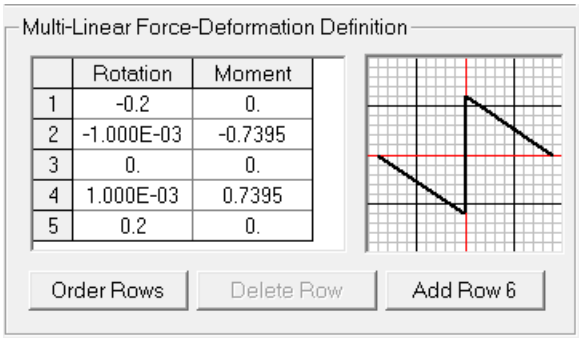

Figure 6-13 Moment-Rotation in SAP2000

6.4.3.1 Pushover analysis

To validate the numerical model for pushover analysis, the experiment carried out by Derakhshan et al. (2009) was replicated in SAP2000. A constant pressure of 1kN was applied over the area of the wall and increased until reaching the instability displacement at the center of the wall (i.e. almost equal to the thickness of the wall).

A comparison between numerical and experimental forced-displacement curve can be seen in Figure 6-14. As expected, the numerical model over predicts the maximum force of the wall, but captured the maximum deformation, the initial stiffness, and overall nonlinear behavior. The final deformation of the model and the experiment are also illustrated in Figure 6-15.

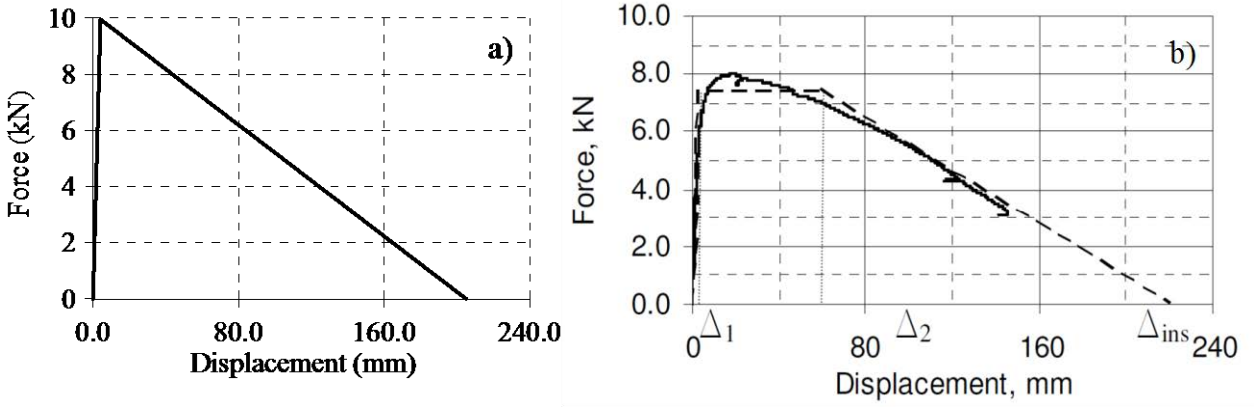

Figure 6-14 Force-displacement relationship of wall 3-B: a) Numerical and b) Experimental

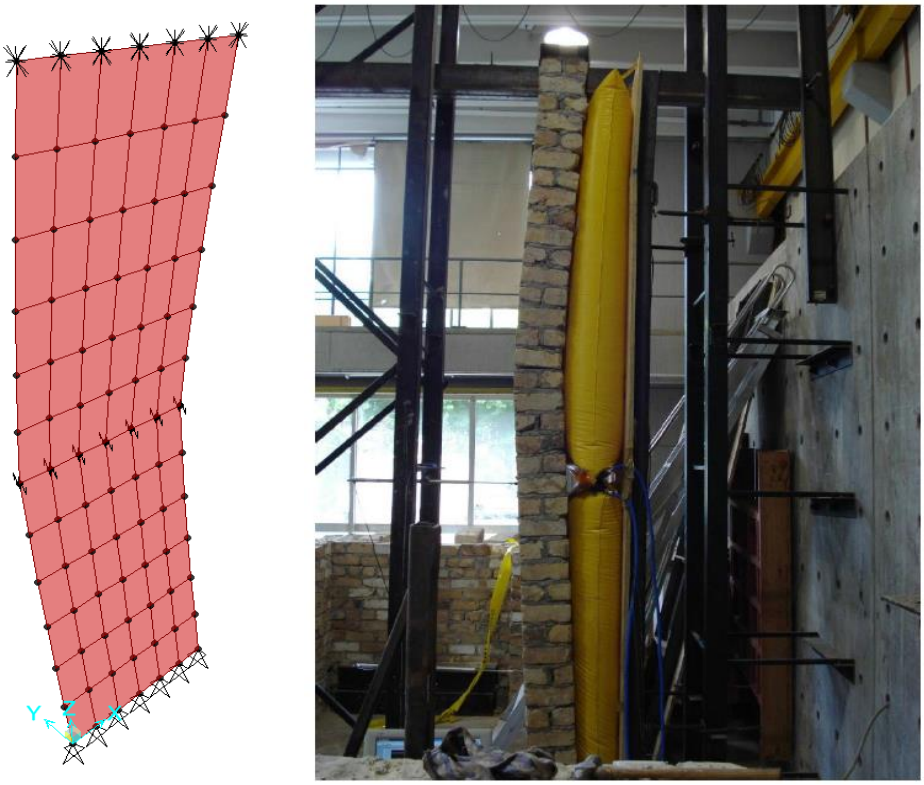

Figure 6-15 Deformed shape of Wall 1: a) Numerical and b) Experimental

6.4.3.2 Response History Analysis

To fully explore the capabilities of the MDOF model, nonlinear response history analyses were conducted and compared to the results of shake table test conducted by Meisl et al. (2007). The 1989 Loma Prieta earthquake recorded at Gilroy array #3 was used to perform nonlinear response history analysis. Note that the actual Gilroy record used by Meisl et al. (2007) was not used, since the actual array used in the experiment was not specified.

Table 4-12 lists the peak displacement, acceleration and force obtained with the numerical model and the actual experiment. The error in the peak displacement obtained is only about 3%, whereas for the acceleration and maximum force is about 25% and 15%, respectively. The displacement and acceleration are measured at the crack location. The maximum force is taken directly from the reactions of the system. As a reference, the experimental setup and damage in the wall at the end of the shake table test are reported in Figure 6-16.

Figure 6-17 shows that the response displacement history obtained with the numerical model which is, in general, in good agreement with the response obtained during the experiment. Given the uncertainties in the boundary conditions and the input excitation, these results are deemed acceptable.

The model also captured the hysteretic behavior at the crack location, as shown in Figure 6-18. Nonetheless, the peak acceleration was overestimated by about 20% of the experimental result. This is probably due to a higher initial stiffness of the numerical model. Note that during the experiment, the initial stiffness of the un-cracked wall dropped from 40kN/cm to about 12kN/cm for a cracked condition. This reduction in the initial stiffness due to progressive damage was not accounted for in the numerical model. This could also be a reason for obtaining a less accurate simulation in terms of the maximum hysteretic force, as illustrated in Figure 6-19. Nonetheless, the stiffness and strength degradation were properly simulated, while still under- predicting the maximum force.

As highlighted before, an appealing feature of this model is that it does not need to be calibrated nor adjusted. Even so, the numerical simulations are in good agreement with the experimental behavior observed in the laboratory.

Table 6-4 Summary of model predictions under dynamic loading

Methodology	Peak relative displacement [cm]	Peak absolute acceleration (g)	Maximum Force (kN)
Experiment	7.70	1.25	28
SAP2000	7.44	1.55	23.7

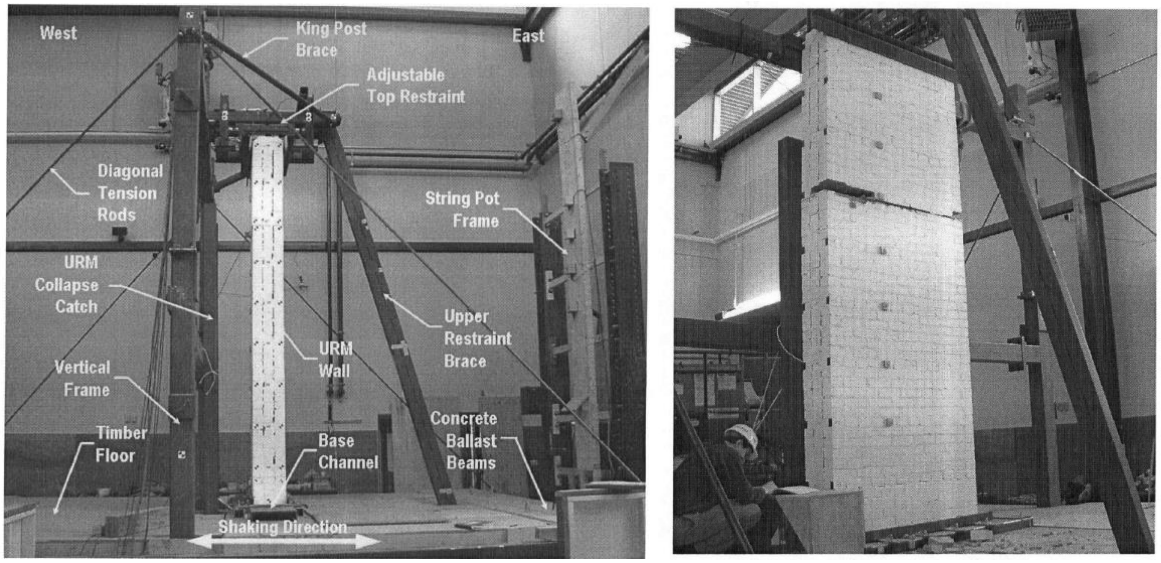

Figure 6-16 Experimental setup and damage in the wall after shake test GC4-1.21

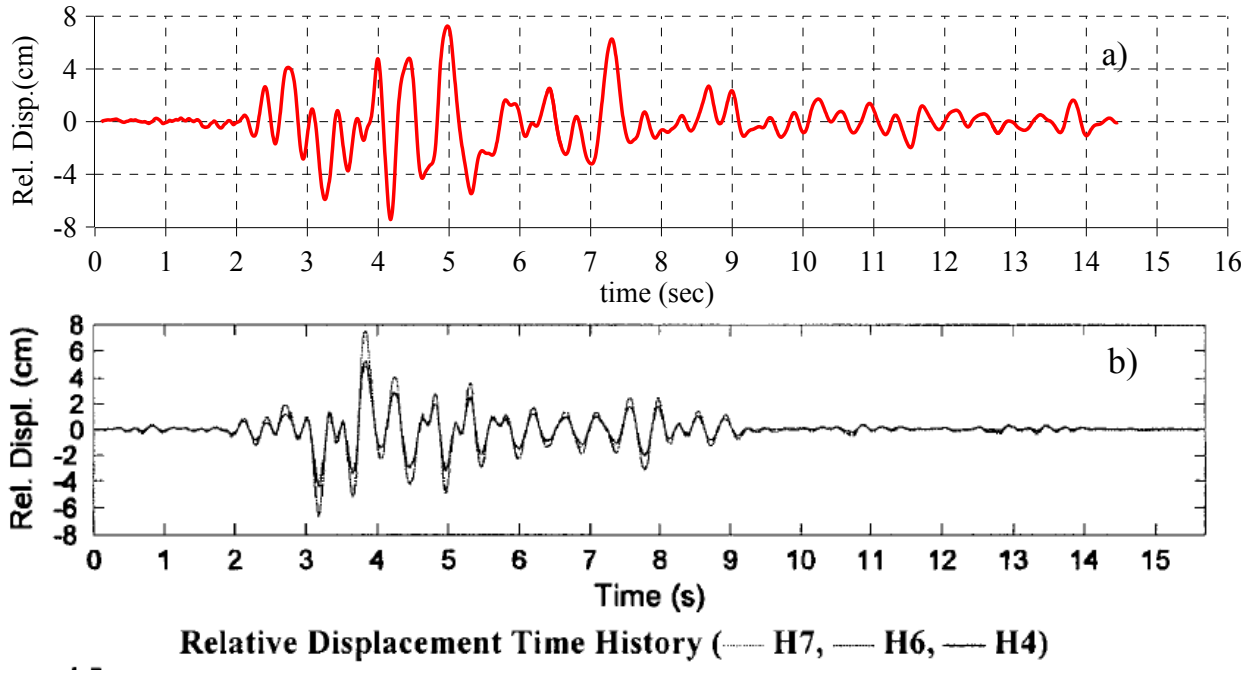

Figure 6-17 Comparison of relative displacement obtained: a) Numerical and b) Experimental (from Meisl et al. 2007)

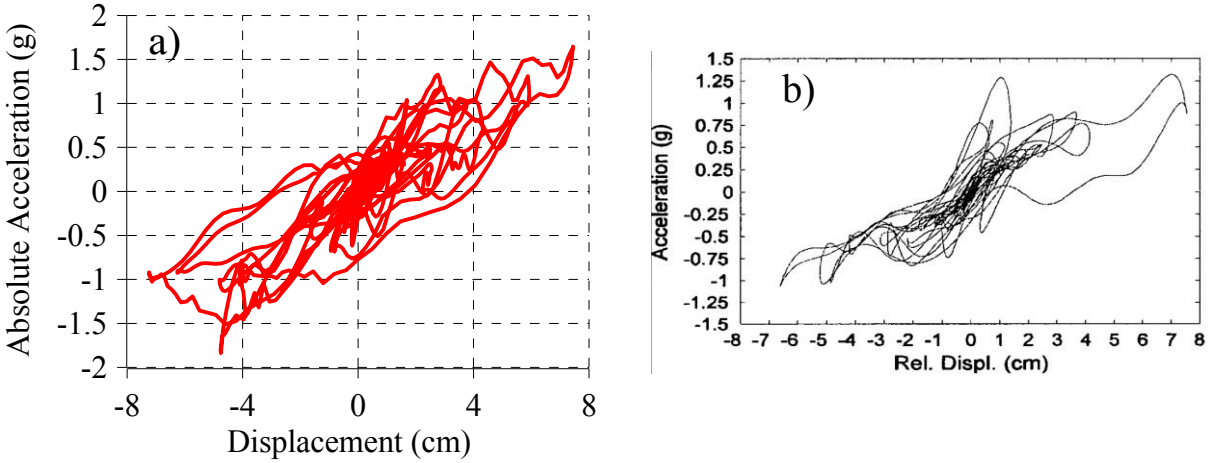

Figure 6-18 Comparison of absolute acceleration vs. relative displacement at crack location: a) numerical and b) experimental (taken from Meisl et al. 2007)

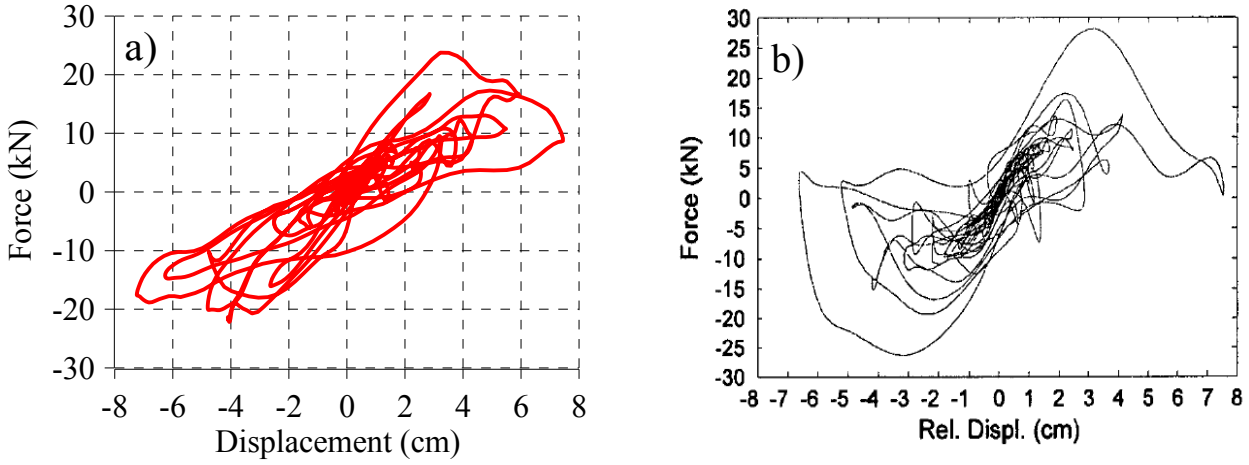

Figure 6-19 Comparison of total force vs relative displacement at crack location: a) Numerical and b) Experimental (taken from Meisl et al. 2007)

6.5 Modified Equivalent Frame Method for Nonlinear Analysis of In-plane Walls

In this section, a concentrated plasticity model of URM walls piers subjected to in-plane loading is proposed and implemented in SAP2000. This approach is similar to the Equivalent Frame method discussed before. However, the model is suitable for pushover, cyclic pushover and time history analysis in two dimensions. It requires less computational time than current finite element models and is easier to implement in the SAP2000 software. This model, combined with the out-of-plane wall, the diaphragm and connections models developed in Section 4 and 5, makes it feasible to conduct 3D nonlinear analysis of URM buildings.

It has been extensively demonstrated by previous experiments that given the geometry of the wall, material properties and seismic demands; the wall pier will likely have a kinematic response dominated by: a) rocking or b) sliding or c) diagonal shear failure or d) toe-crushing. Combinations of those failure modes can occur, but for the sake of simplicity it has been commonly assumed an uncoupled behavior.

Those failure modes are currently addressed by ASCE 41-06 and will also be in the upcoming ASCE 41-13. This new national consensus standard was developed from ASCE 41-06, FEMA 356 and FEMA 273. Those guidelines on the seismic behavior of URM wall piers are mainly based on experimental observations of research programs summarized in Table 6-5. The in-plane

behavior of URM walls and equations to estimate its stiffness, strength, and force-deformation curves as outlined in ASCE 41-06 will be discussed below.

Table 6-5 Research programs used to develop ASCE 41-06 guidelines on URM walls

Behavior mode	Researcher
Rocking	Abrams and Shah (1992) Anthoine et al. (1995) Costley and Abrams (1996b) Magenes and Calvi (1995) Epperson and Abrams (1989)
All others	ABK (1981) Manzouri et. al. (1996) Tomasevic and Weiss (1996)

6.5.1 Seismic Behavior, Stiffness and Strength of URM Wall Piers

Typically, URM walls show elastic behavior during the initial stage of in-plane seismic loading. This behavior can be described effectively using plane-stress models. Then, as the seismic loading increases, flexural or shear cracking (or both simultaneously) will take place and the behavior become highly nonlinear as large deformations occur in comparison with the applied forces. Small components of the wall such as piers will behave similarly and, therefore, can be modeled under the same principles (Craig et al. 2002).

ASCE 41-06 considers three kinds of in-plane failure modes for URM walls which can be classified either as ductile (displacement-controlled) or brittle (force-controlled). Those failures mechanisms are summarized as follows:

- Rocking failure: This deformation-controlled failure has the ability to absorb relatively high amount of energy after initial cracking at the base of the wall or pier. As the seismic load increases, rocking about the vertical axis of the element is produced and the final failure is obtained by overturning of the wall.

- Toe crushing: This happens when the base of the wall crushes under the combined action of shear force and overturning moment. This failure mode, which is considered force-controlled, tends to be brittle in nature and typically the wall undergoes a sudden failure.
- Bed-joint sliding: this failure mode is more frequent in walls with low aspect ratio, low compressive force and high shear loads. Potential sliding planes will form along the cracked bed joints when subjected to reverse seismic actions.

Since ASCE 41-06 assessment methods are mainly based on allowable drifts, it is necessary to calculate the initial in-plane stiffness of the wall. Conventional principles of mechanics for homogeneous materials are used, and both, flexural and shear deformations are taken into account. The standard recommends two equations to calculate the stiffness depending on boundary conditions (cantilevered or fully restrained against rotation at its top and bottom).

For cantilever shear wall

$$k=\frac{1}{\frac{h_{eff}^3}{3E_m I_g}+\frac{h_{eff}}{A_V G_m}} \tag{6.12}$$

For fixed-fixed shear wall

$$k=\frac{1}{\frac{h_{eff}^3}{12E_m I_g}+\frac{h_{eff}}{A_V G_m}} \tag{6.13}$$

Where

h_{eff}=Effective Wall height

A_v=Shear Area

I_g=Uncracked moment of Inertia

E_m=masonry elastic modulus

G_m=masonry shear modulus

It is further stated that these boundary conditions are hardly found in practice. Values for the elastic and shear modulus can be found in the standard or obtained through experimental test. Figure 6-20 shows that depending on the wall and pier geometry, the effective height may vary in the same wall assembly.

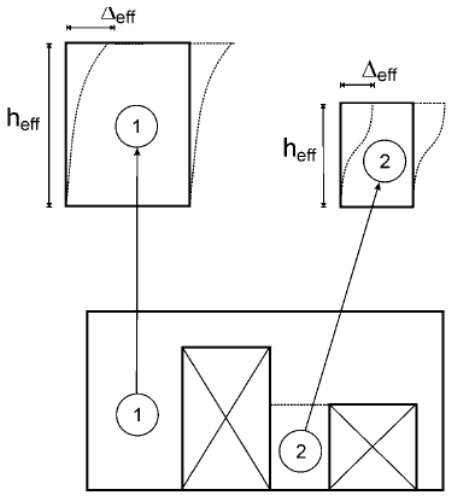

Figure 6-20 Effective stiffness for different wall configurations (ASCE/SEI 41-06 2007)

The strength is calculated according the mode of failure. Equations provided by ASCE 41-06 are given below. These formulas are for solid walls under an in-plane force applied along its top boundary.

Rocking Shear Strength

$$Q_{CE}=V_r=0.9\propto \mathbf{P_D}\left(\frac{\mathbf{L}}{\mathbf{h_{eff}}}\right) \quad (6.14)$$

Bed Joint Sliding

$$Q_{CL}=V_{CL}=v_{mL}A_n \quad (6.15)$$

Toe-Crushing

$$Q_{CL}=V_{tc}=\propto Q_G\left(\frac{\mathbf{L}}{\mathbf{h_{eff}}}\right)\left(\mathbf{1}-\frac{f_a}{\mathbf{0.7}f'_m}\right) \quad (6.16)$$

Where

Q_{CE} =Expected lateral strength

V_r =Rocking Strength of the wall

A =factor equal to 0.5 for fixed-free walls or equal to 1 for fixed-fixed walls

P_D =Superimposed dead load at the top of the wall

L =Length of wall or pier

h_{eff} =Effective Wall height

Q_{CL} =Lower bound lateral strength

V_{CL} =Lower bound shear strength

V_{ml} =lower bound masonry shear strength

A_n =area of net mortared/grouted section

Q_G =Lower bound axial compressive force

f_a =axial compressive stress

f'_m =lower bound masonry compressive strength

It is further specified that the compressive strength of existing masonry walls should be limited by the lower bound masonry compressive stress given below

$$Q_{CL}=P_{CL}=0.8(0.85\,\mathbf{f'_m}A_n) \quad (6.17)$$

Where

P_{CL}=lower bound compressive strength

Knowledge of the nonlinear force-deflection relations for individual wall, pier or spandrel members is needed to perform a nonlinear static and dynamic analysis. ASCE 41-06 prescribes a simplified force-deformation relation, as noted in Figure 6-21, based on rocking mechanisms. This backbone envelope is not valid for force-controlled elements as they experience brittle failure and do not show nonlinear behavior.

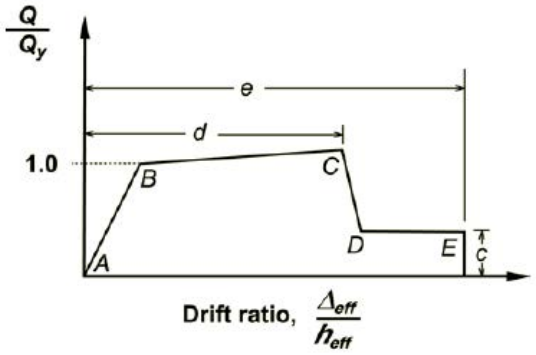

Figure 6-21 Idealized force-deflection backbone for walls and piers (ASCE/SEI 41-06 2007)

A bilinear curve defined by the elastic stiffness and the component strength is assumed for primary elements in the lateral-force resisting system. No strength degradation is allowed for these members. On the contrary, secondary elements (i.e. walls that do not form part of the main seismic resistant system) behavior can include strength deterioration. Acceptable drifts limits stated by ASCE 41-06 are shown in Table 6-6.

Table 6-6 Acceptable drift limits for URM walls and piers

Acceptance Criteria								
					Performance Level			
	Limiting Behavioral Mode				Primary		Secondary	
	c (%)	d (%)	e (%)	IO %	LS %	CP %	LS %	CP %
Rocking	0.6	0.4heff/L	0.8heff/L	0.1	0.3heff/L	0.4heff/L	0.6heff/L	0.8heff/L

In this research, the recommendation of Moon et al. (2006) were followed. The abrupt drops given in the ASCE 41-06 curve were eliminated and replaced with sloping lines to better estimate past experimental results as well as to avoid any numerical convergence problems during analysis. Also, the residual strength line was changed from 60% of the building yield strength to the toe crushing capacity of the pier. Table 6-7 gives the values that define the modified backbone curve for rocking failure mode. Expressions for those variables and derivations can be found in Moon (2004).

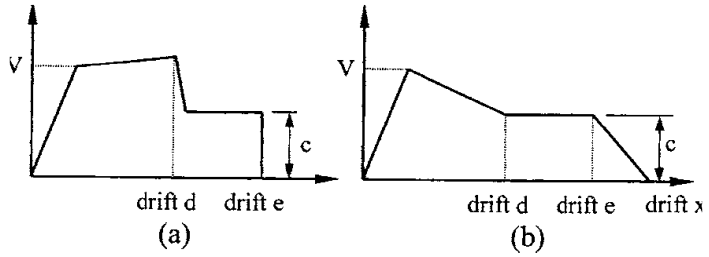

Figure 6-22 a) Generalized force-drift relationship provided by ASCE 41-06; b) Modified force-drift relationship

Table 6-7 Modified Force-Drift Relationships for URM Piers

Type	V	d	e	x	c
Rocking	V_r	0.004(H/L)	(Δ_{tc}/H)	$(\Delta_{tc}+\Delta_{elastic})/H$	V_{tc}

Another important recommendation adopted in this study is the effective height (h_{eff}) calculation proposed by Moon et al. (2006). As described before, ASCE 41-06 defines effective height as the vertical height of adjacent openings. The proposed calculation considers the diagonal distance

over which a compressive strut will likely develop between two openings to estimate the effective height.

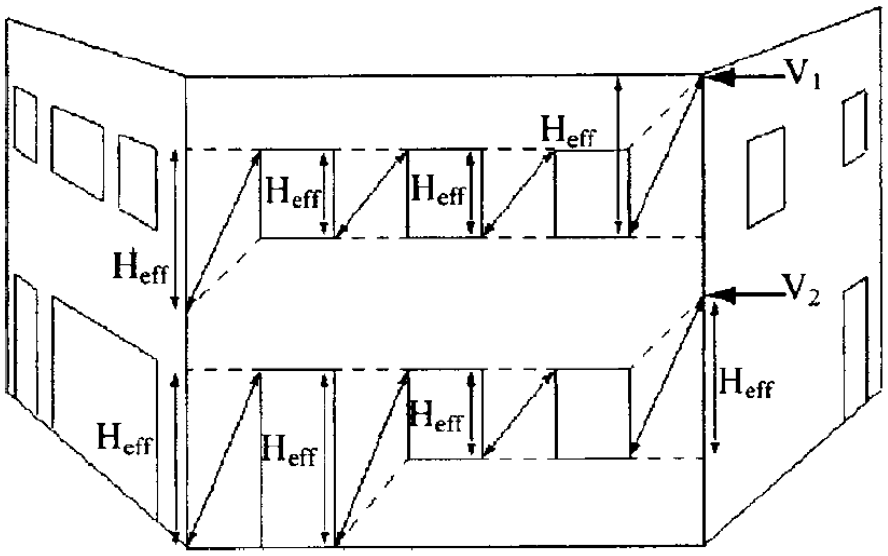

Figure 6-23 Modified effective height (H_{eff}) proposed by Moon et al. (2006)

6.5.2 Kinematic Assumptions

Masonry piers can be effectively replaced by a beam element with discrete non-linear springs representing a particular failure mode that is predicted in advance using equations given by ASCE 41-06. This approach is similar to that followed by Knox (2012). However, Knox used the equations in NZSEE (2006) standards to estimate the failure mode of the URM walls.

The beam element has dimensions **H**, **L** and **t**, and Young's modulus of the masonry **Em**. The rocking and toe-crushing behavior is modeled using a rotational spring located at the top and the base of the beam element, whereas the bed joint and diagonal shear is simulated by placing one spring in the middle of the element. Note that the force-displacement relationship needs to be converted to moment-rotation. As recommended by Knox (2012), spandrels can be modeled as beam elements with a shear spring at the middle, to somehow capture the maximum capacity. This is not quite accurate, since the spandrel capacity is in reality dependent on the interaction between axial and moment capacity. Nevertheless, most masonry walls are controlled by the behavior of the piers, rather than spandrels and this assumption gives acceptable approximations. The hysteretic behavior of piers and spandrels are characterized by stiffness degradation and pinching behavior. This behavior has been previously simulated using different hysteresis rules.

Pasticier et al. (2008) used a Takeda rule, whereas Craig et al. (2002) used a bilinear elastic rule to simulate the rocking mode of failure of piers whereas the spandrel members were defined by a bilinear Inelastic Hysteresis rule to represent the Bed Joint Shear Sliding collapse mode. Knox (2012) used a Pivot model for both piers and spandrels. In this study, the Pivot model discussed in Section 4was also selected to simulate the hysteretic behavior of piers and spandrels.

6.5.3 Model Verification and Validation

The equivalent frame model with nonlinear springs was implemented in SAP2000. The model was validated through pushover and cyclic pushover analysis. To this end, experiments conducted by Manzouri et al. (1996) on single pier elements and Yi et al. (2006b) on a full scale two-story URM building were used for comparison purposes.

6.5.3.1 Pushover analysis

To validate the numerical model at the component level (i.e. only for piers), the experiment carried out by Manzouri, Schuller et al. (1996) was replicated in SAP2000. The wall dimensions are shown in Figure 6-24. The thickness of this wall is approximately 13" and the modulus of elasticity is 1250 ksi. This wall was subjected to a compressive stress of 70 psi on each pier. Given this properties, the moment-rotation relationship of the piers was calculated. As mentioned before, two rotational springs were used, one at the top, one at the bottom of each pier. The wall was modeled in 2D with fixed joint restraints at the base. A unit load was applied on top of the wall to carry out the pushover analysis.

Following the equivalent frame methodology, piers and spandrels were simulated using beam elements connected by rigid link elements. All parameters of the multilinear plastic Pivot hysteresis rule were set equal to 0.45, as recommended by Pasticier et al. (2008).

The force-displacement relationship obtained from both the experiment and the analysis are plotted in Figure 6-25. The composite spring model provided a reasonable bilinear approximation to the in-plane behavior and closely reproduced the strength (about 40 kips).

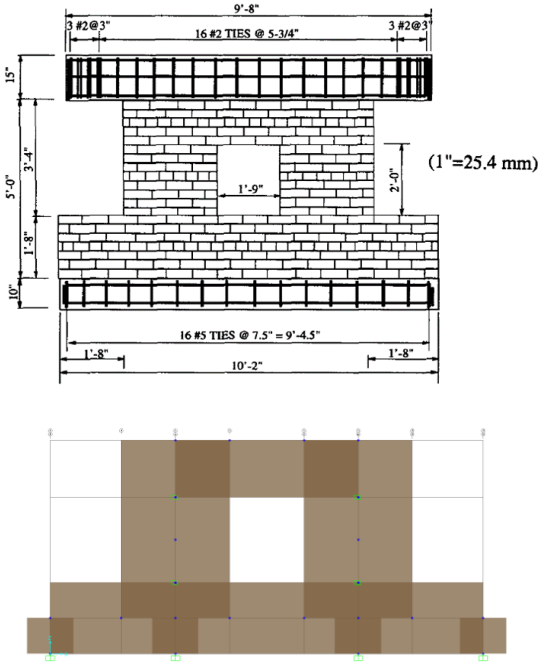

Figure 6-24 Experimental wall and its equivalent SAP2000 model

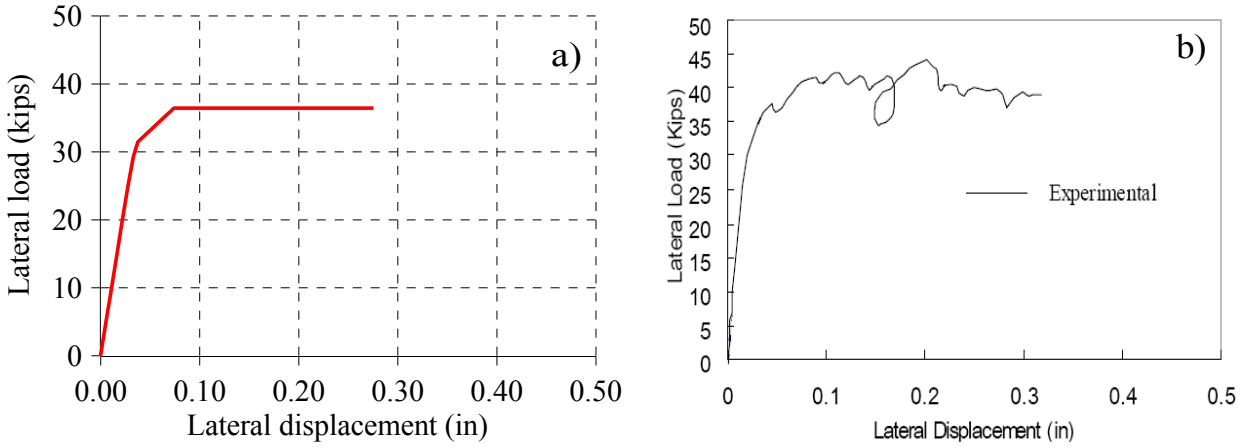

Figure 6-25 Force-displacement curve for the wall: a) Numerical and b) Experimental

6.5.3.2 Cyclic pushover analysis

The Mid-America Earthquake (MAE) Center conducted a research project in 2002 focused on evaluating the procedures specified in FEMA 356 on unreinforced masonry buildings. The research program included a full-scale quasi-static test of a two-story masonry building that will be used herein to further validate the proposed nonlinear macro-model at the global response level. Figure 6-26 shows detailed dimensions of the two-story masonry building. In this study, only Wall B, 1 and 2 results were considered for comparison purposes.

The moment-rotation relationship for piers and spandrels was calculated using the material properties and axial loads from walls and floor as described in Yi et al. (2006b). The cyclic loading protocol was applied at the floor and the roof of the model, as it was done in the real experiment. A displacement controlled simulation was conducted, therefore, the DOF associated to the point of loading were constrained in the same direction of the applied loading. The hysteretic behavior was also simulated using the Pivot rule available in SAP2000 with all parameters set equals to 0.45.

Figure 6-27, Figure 6-29 and Figure 6-31 show a comparison between the numerical and experimenta force displacement curve obtained for Wall A, Wall 1 and 2, respectively. Overall, a good agreement can be seen in terms of maximum force and cyclic behavior. Also, Figure 6-28, Figure 6-30 and Figure 6-32 illustrate the final damage state of both, the numerical model and experiments. Note that separated panels are observed for the spandrels, because of the number of output stations used for each element. Despite being a simplified model, good agreement was obtained with the experiments.

It must be highlighted that several major limitations are presented in this modeling approach. First of all, SAP2000 doe not account for axial-moment interaction when using Nlink elements. In a real building, the axial force distribution in the piers changes significantly as the walls enter in the nonlinear range and experience global overturning. This could affect the final failure mode of the pier and final response of the building.

Another shortocoming comes from neglecting the contribution of flanges in the force-displacement curve of the piers. It has been previously demonstrated that flanges or return wall have a major impact in the initial dominant failure mode of the piers, shifting it from rocking to shear sliding depending of the location of the flange. Moreover, the model does not account for axial-bending interaction in spandrels, which could lead to over conservative estimates of the response.

Moreover, as disscussed in Section 2.3.2, the bidirectional simultaneous behavior of URM wall piers under seismic loads could have major impact in stiffness and strength degradation, and should be incorporated in the model.

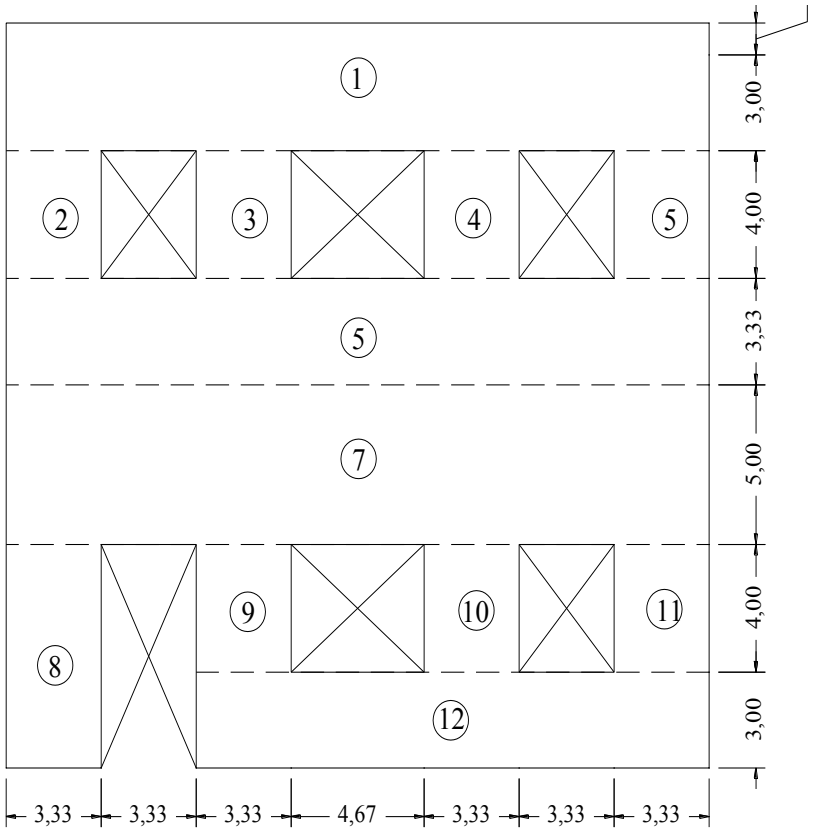

Figure 6-26 Dimensions of Wall B of MAE project (Craig et al. 2002)

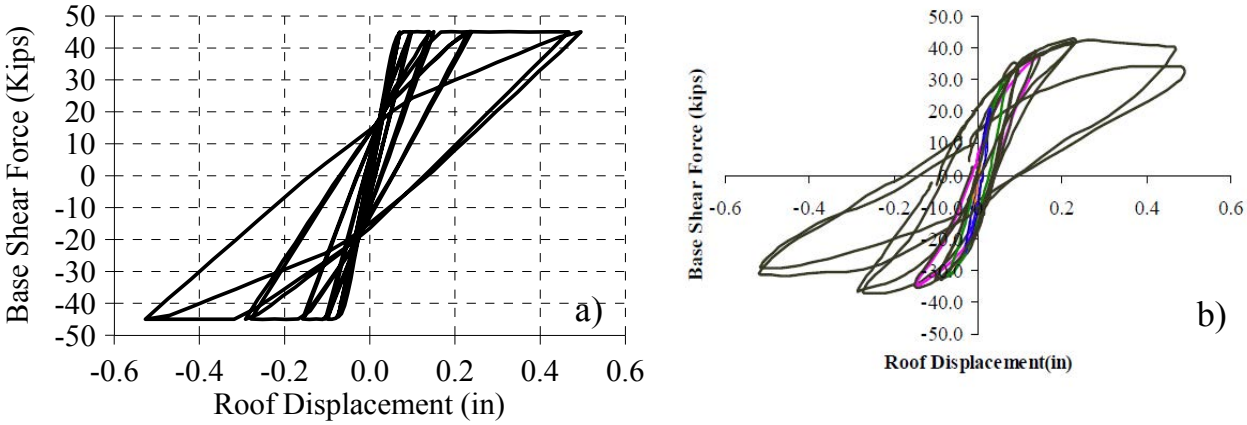

Figure 6-27 Force displacement relationship of Wall A: a) Numerical and b) Experimental (Yi et al. 2006b)

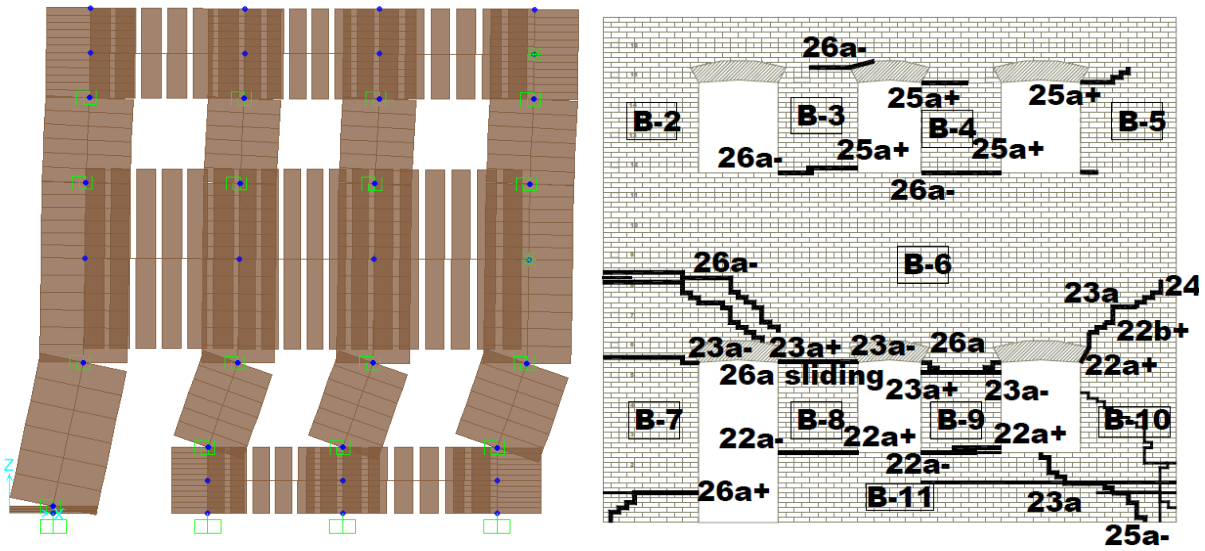

Figure 6-28 Damage state of Wall A at the end of cyclic loading protocol: a) Numerical and b) Experimental

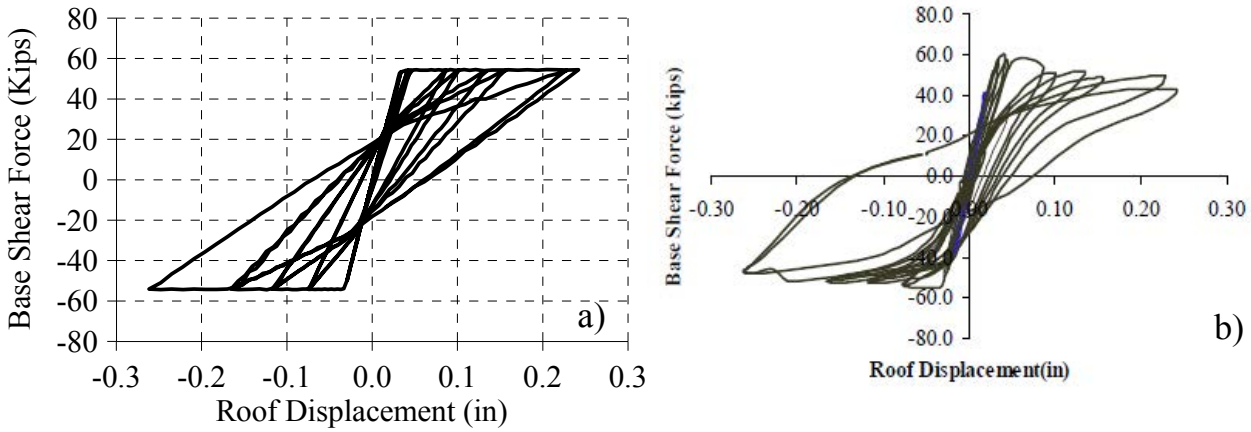

Figure 6-29 Force displacement relationship of Wall 1: a) Numerical and b) Experimental (Yi et al. 2006b)

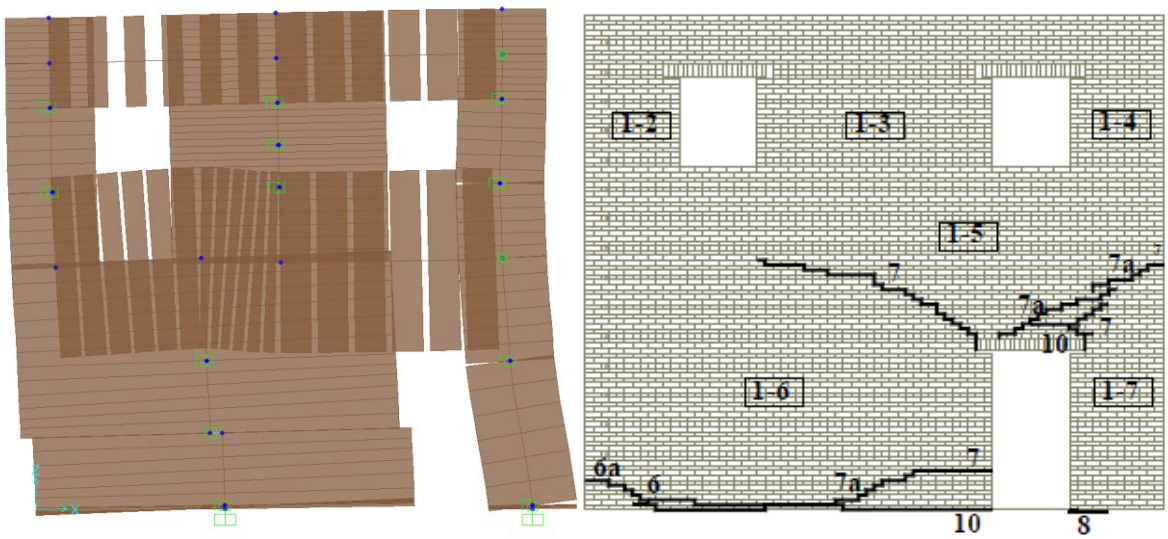

Figure 6-30 Damage state of Wall 1 at the end of cyclic loading protocol: a) Numerical and b) Experimental

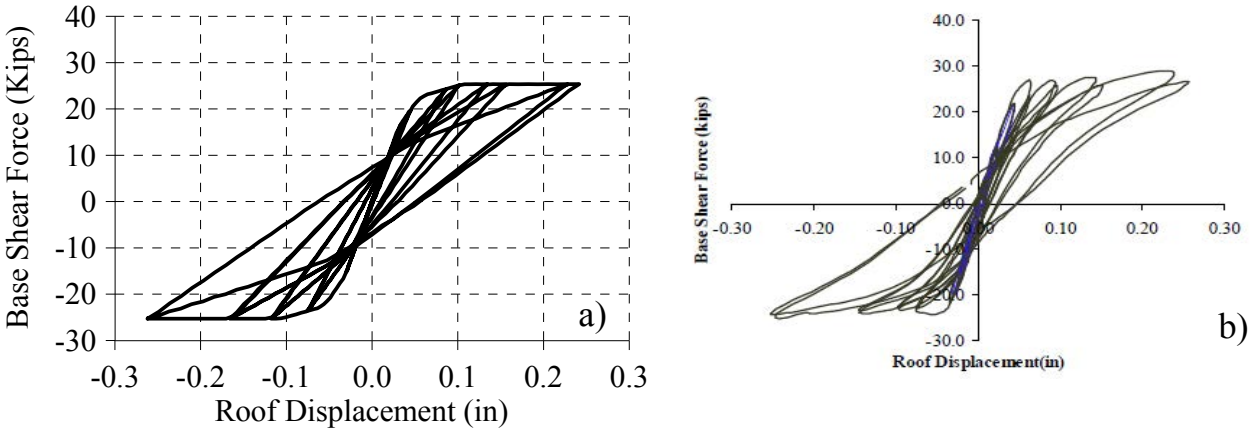

Figure 6-31 Force displacement relationship of Wall 2: a) Numerical and b) Experimental (Yi et al. 2006b)

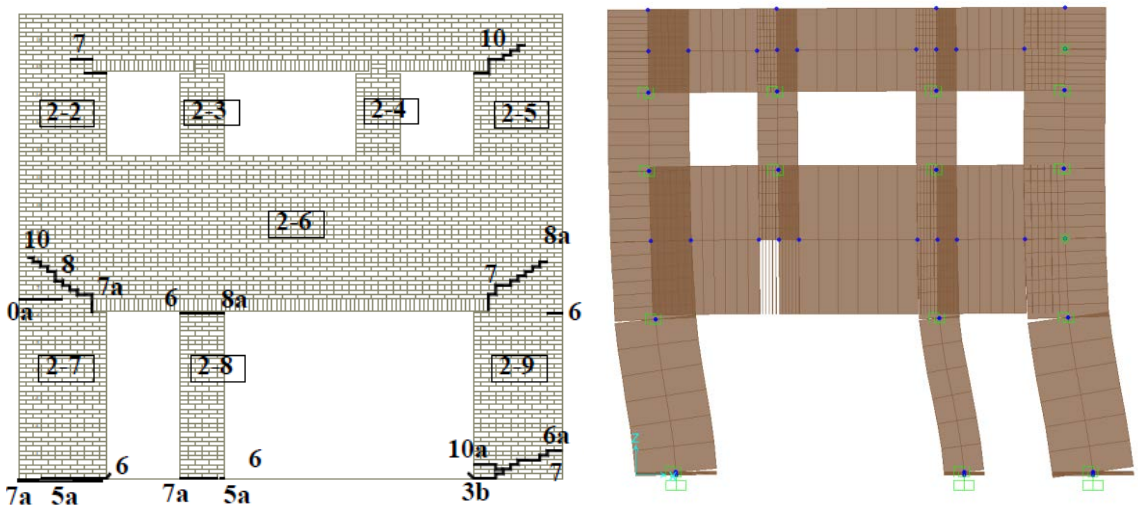

Figure 6-32 Damage state of Wall 2 at the end of cyclic loading protocol: a) Numerical and b) Experimental

6.6 Summary and Conclusions

This section presents practical modeling techniques for nonlinear analysis of out-of-plane and in-plane walls, which could be developed and implemented in SAP2000 and potentially combined to simulate the seismic behavior of a multi-story URM building. A literature review of existing macro-models highlighted the need to develop code-based simplified numerical models which could be used to estimate the seismic response of complex URM buildings. In particular, the major contributions of this section are:

1. The out-of-plane behavior of URM walls subjected to one-way bending was simulated using a hybrid formulation based on equations derived from rigid body dynamics but implemented in a SDOF oscillator. Masonry walls could be effectively simulated using shell, rigid elements and nonlinear rotational springs at crack locations. A comparison between numerical models and experimental results for nonlinear response history analysis showed good agreement in terms of peak displacements and accelerations.
2. The rocking and shear sliding behavior of URM wall piers was simulated using the Equivalent Frame Method. The force displacement or moment-rotation relationships were taken from the equations provided in ASCE 41-06 and implemented in SAP2000, using rotational or shear nonlinear springs. Pushover and cyclic pushover analysis were in good agreement with previous experiments on in-plane walls.

SECTION 7
EXPERIMENTAL PROGRAM PART I: CHARACTERIZATION OF MATERIAL PROPERTIES FOR SEISMIC ASSESSMENT OF OLD URM WALLS

7.1 General Overview of Experimental Program

As presented in previous sections, a small number of laboratory experiments can be found in the literature on wood diaphragms, wood joist-to-wall connections, and in-plane and out-of-plane masonry walls subjected to dynamic loads. However, full scale experiments that combine these structural elements in a single structural model to capture subassembly or system level response under realistic seismic loads are more limited. Although it was shown that the numerical macro-models developed to simulate the behavior of each individual component were reliable, there is not sufficient data to evaluate the applicability and effectiveness of these models in capturing the system level seismic behavior of an URM building with flexible diaphragms.

In this experimental program, a full scale structural system composed of a flexible wood diaphragm, realistic wood-to-wall connections, and out-of-plane masonry walls was designed, constructed and tested until collapse for realistic seismic loads. The results of these tests were used to validate the computer models developed in previous sections. Also, these experiments provided new information regarding the seismic behavior and vulnerability of masonry walls, parapets, wood joist-to-wall connections and flexible diaphragms.

The experimental studies were conducted in two phases. First, material characterization tests were conducted to determine mechanical properties for brick units, mortar and masonry walls that better represent actual conditions of the building stock in the New York City region. Section 7 is devoted to this material characterization phase. Secondly, the data obtained in this first phase was used to build two full-scale masonry walls that represented the central portion of a first story URM building in NYC to examine the combined out-of-plane behavior of walls with flexible diaphragms and connectors. The walls were tested for out-of-plane dynamic loads using the earthquake simulator in the Structural Engineering and Earthquake Simulation Laboratory (SEESL) of the University at Buffalo. This phase of the project is discussed in Section 8.

7.2 Material Properties for Seismic Assessment of Old URM Walls

Due to the tremendous variety in the masonry materials and construction practices throughout various regions in the US, replication of older masonry construction in the laboratory is a difficult challenge. Further, aging and weathering effects are very difficult to capture and simulate. A small change in the constitutive materials properties can have a significant impact on the behavior of the entire masonry building. To characterize material properties, there is some disagreement among researchers regarding the material properties that should be measured in laboratory tests. Several researchers propose that aging and weathering primarily affects the properties of the mortar in URM walls. Hence, it is practical to assume that old URM walls have a strong brick-weak mortar interface and cracking will occur across the mortar bed joints. Therefore, when the seismic vulnerability of old URM walls is evaluated, shear testing on joints should be more relevant than tests on compressive strength of specimens. On the contrary, other researchers argue that both brick and mortar are equally affected by aging and weathering. As a result, a weak brick-weak mortar interface should be considered and the compressive strength in mortar and bricks must be thoroughly evaluated to predict potential crushing and brittle failures under seismic loads.

To address some of these concerns, material testing was conducted for mortar, bricks and masonry specimens in order to identify the masonry characteristics more appropriate to replicate the construction of old URM walls in the laboratory. Newly constructed specimens and old specimens extracted from demolished buildings were tested. No presumptions were made regarding the brick-mortar interface. Instead, focus is given to the material properties required by ASCE 41-06 to calculate the expected lateral strength of unreinforced masonry walls or piers (i.e. masonry compressive and shear strength).

A significant effort was made to collect representative data on the actual conditions of old URM walls in the NYC region. In collaboration with the International Masonry Institute, several wall, bricks and mortar specimens were obtained from a demolished building constructed in the 1920's in Syracuse, NY. Additionally, Atkinson-Noland & Associates provided in-situ flat-jack testing reports of URM buildings in NYC (Schuller 2011). Also, suggestions on the mortar-brick mechanical properties for masonry over 100 years old were given by Whitlock (2011) and Healy (2011) from Whitlock-Dalrymple-Poston & Associates and Ryan-Biggs Associates, respectively.

7.3 Scope and Objectives of Material Characterization Testing

The aim of this section is to identify appropriate properties of materials that can be used to construct URM in the laboratory representative of older construction in NYC. The objectives below were identified to achieve this goal with the total number of specimens for each type of test summarized in Table 7-1.

1) Determine and compare the compressive stress-strain curves of old and four different type of new mortars.
2) Determine and compare the compressive stress-strain curves of old and new brick units.
3) Determine and compare the compressive stress-strain curves of old and new masonry specimens.
4) Determine and compare the bed joint shear stress-displacement curves of old and new triplet masonry specimens.
5) Understand the influence of the mortar quality in the frictional properties of the brick unit interface.

Table 7-1 Properties of bricks, mortar and masonry specimens determined in the SEESL laboratory

Test Procedure	Mortar Type					Brick Type		No. of Specimens
	O	K	K*	L	Old	New	Old	
Compressive Strength of Mortar	x							3
		x						3
			x					3
				x				3
					x			6
Compressive Strength of Masonry	x					x		5
		x				x		5
					x		x	2
Compressive Strength of Bricks						x		20
							x	20
Bed joint shear strength	x					x		15
		x				x		15
					x		x	2

7.4 Background on Material Properties of URM Walls for Seismic Assessment

Although several laboratory tests have been conducted to understand the seismic behavior of old unreinforced masonry structures, very few have actually used old bricks and low quality mortars to replicate aging effects and long exposure to severe weather. As of today, the most consistent way to consider aging effect in the testing of full buildings and walls subjected to in-plane and out-of-plane loads has been to use new bricks and a weak type of mortar (i.e. Type O or K). Table 7-2 summarizes previous type of mortar used in URM research programs. Experimental tests on URM structures constructed with old bricks are briefly discussed below.

7.4.1 Testing of Full Buildings

Quasi-static or pseudo-dynamic testing on URM buildings constructed with old bricks has not been reported in the literature. A shake table test, however, has been recently conducted by Bothara et al. (2010). A two-story URM house designed to be representative of typical construction in New Zealand was subjected to earthquake loads. In constructing the half-scale model of the house, recycled bricks from 1930s were used. Experimental observations indicate that significant in-plane damage was concentrated in the bottom story whereas out-of-plane damage occurred at the top story. Out-of-plane failure was effectively reduced by increasing the bond strength between orthogonal walls and reducing the wood diaphragm flexibility. Note that the global behavior observed in this test was not different from tests in full buildings constructed with new bricks and old mortar.

7.4.2 Testing of Walls: In-plane Load

An experimental program on URM walls was carried out at the University of Illinois in the early 1990s. First, Epperson and Abrams (1989) tested five brick walls extracted from a 1917 building in Chicago. In-plane loads were applied at the top of the 4-wythes walls while axial load was maintained at a constant value. Significant in-plane loads were resisted after initial cracking although large reductions of the stiffness were observed. After this study, Abrams and Shah (1992) attempted to replicate the 1917 walls using reclaimed bricks and new mortar. Three similar walls were constructed and tested for in-plane loads. This study concluded it was impossible to replicate aging and severe weather effects that induced a significant lower flexural tensile strength in the old walls.

Yet, the global behavior of the walls was similar and predictable using numerical models. The results of these experimental studies were later incorporated in the FEMA 306/ATC-43 Evaluation of Earthquake Damage Concrete and Masonry Wall guidelines.

The efficacy of different retrofit techniques for URM structures was investigated by Manzouri et al. (1996). In this comprehensive study, four multi-wythes URM walls constructed with old clay bricks recycled from an old (1915) structure in Colorado were tested for in-plane loads. Again, the significant deformation capacity observed during the experiments was fully captured using numerical models.

More recently, Russell et al. (2007) conducted an in-plane static test on a single unreinforced masonry wall which was built with recycled bricks from a demolished buildings. The bricks were about 100 years old. Apparently, those bricks were used because the manufacturing process introduces significant difference in the mechanical properties of the bricks. Also, the difference in porosity between new bricks and old bricks makes a weaker interface in the bond between new bricks and mortars, when type O mortar is used. In addition, because buildings have a significant variability in the properties of bricks, using recycled old bricks seemed to be more realistic.

The issue of using old bricks and new mortar has been further discussed by Russell et al. (2007) They recognized that new bricks can be used but that the most realistic overall seismic behavior will be obtained if actual aged bricks are used. It is important to highlight that mortar brick bond is governed by the initial rate of absorption of the brick. Yet, no research has been reported comparing the absorption rate between new bricks and previously mortared bricks. As mentioned before, the only consistent way many researchers have found to replicate old masonry construction is using weaker mortar, type O or K.

7.4.3 Testing of Walls: Out-of-plane Loads

Out-of-plane quasi-static airbag testing and dynamic testing have been extensively conducted in URM walls. However, only few of them have used old bricks. Paquette et al. (2001) extracted three masonry walls with wood backing from an old three-story residential URM building. The specimens were tested for out-of-plane loading using an earthquake simulator. It was found that masonry walls were able to resist significant inertial accelerations without failure.

Another experiment in masonry components was conducted by Ehsani et al. (1999). This study tested six specimens to investigate the out-of-plane flexural behavior of URM retrofitted with fiber composites. Static load was applied to failure with two concentrated loads. One beam specimens was constructed with old reclaimed brick. Comparison between specimens reveals that the lower strength of reclaimed bricks resulted in a lower failure load of the specimen. This suggests that axial load plays a fundamental role in this type of test, where old bricks could fail prematurely significantly reducing the capacity of the wall.

In a recent study by Vaculik and Griffith (2007) the two-way out-of-plane bending behavior of URM wall was compared using cyclic airbag and shake table tests. Among other variables, the crack propagation pattern varied significantly in both tests. In the dynamic test, stepped cracks formed along mortar joints whereas line cracks were observed across the bricks in the airbag test. Apparently, the crack pattern is affected by the tensile strength of bricks and mortar used in the two different studies. From the comparison between hysteresis loops, it is observed that stepped cracks are more beneficial for seismic behavior due to the higher dissipation of energy.

In another study on the seismic evaluation of out-of-plane walls, Derakhshan (2011) points out that rounding of walls edges will theoretically reduce the wall out-of-plane strength by 15% to 25%.

Summing up, those studies suggest that using new bricks for the dynamic out-of-plane testing of URM walls will likely have three main effects, namely 1) The bond between bricks and mortars will be likely weaker, resulting in a lower initial stiffness, 2) fewer bricks will fail in compression, overestimating the rocking capacity and 3) stepped crack (if any) will prevail over line cracks, increasing the energy dissipated at each cycle. There remain the questions of which effect will have a more significant impact in the global response, whether or not this response will be conservative and if the failure mode will be other than a rigid body response at the crack location.

Other URM material properties obtained from previous researchers are summarized in Table 7-3. As discussed before, there is a significant variation in the range of values obtained. To reduce the uncertainty, it was decided to obtain more precise information about the material properties of URM buildings in NYC.

Table 7-2 Summary of previous type of mortar used in URM research

Researcher	Country	Mix	Type	Vintage/ Comments
Knox (2012)	NZ	1:2:9	O	
Stavridis (2009)	US	1:1:5	N	
Ahmad et al. (2010)	Pakistan	1:4:4		
Bothara et al. (2010)	NZ	1:1:6		1930
Russell et al. (2007)	NZ	1:2:9	O	Recycled bricks
Wijanto (2007)	Indonesia	1:4		Aged bricks
Meisl et al. (2007)	Canada	1:2:9	O	
Bean Popehn et al. (2007)	USA		S	
Paquette et al. (2004)	USA	1:2:9	O	
Simsir (2004)	USA		O	
Yi et al. (2006b)	USA	0.5:2:9	K'	Aged bricks
Griffith et al. (2004)	Australia	1:1:6		
Costley and Abrams (1996)	USA	1:2:9	O	Old building
Manzouri et al. (1996)	USA	1:2:9	O	
Atkinson et al. (1989)	USA	1:2:9	O	

Table 7-3 Summary of previous masonry properties used in URM research

Reference	**Mortar f'm (psi)**	**Brick f'm (psi)**	**Prism (psi)**						
			f'm	**E**	**Ft**	**Fdt**	**μ**	**τ**	**c**
ASCE 41-06 Table 7-1			300-900	165000-495000	0	13-27	0.70	100	
Abrams and Shah (1992)-Type N		3480	801			56			
Abrams and Shah (1992)-Type O			565			83	0.50		100
Abrams and Shah (1992)-Lime/ Mortar			472			0			
Manzouri et al. (1996) w1	555		2000					116-237	
Manzouri et al. (1996) w2	736	3140	2200						
Manzouri et al. (1996) w3	382		2600						
Manzouri et al. (1996) w4	0		1700						
Costley and Abrams (1996)		6730			41	46.5		361	
Paquette et al. (2004)	1340	15809	3219	2736150	26			61-76	
Yi et al. (2006b) Type O	350	5285	1458	1168000			1.10	60	
Yi et al. (2006b) Type K'	41	6030							
Atkinson et al. (1989)							0.67	25	
Meisl et al. (2007)	890	2233	1885		61				

7.5 Mortar Compression Test

A literature review on the material properties of masonry specimens, walls and full buildings tested under laboratory conditions revealed that most of them were fabricated using new construction materials. Very few specimens were actually tested in-situ or extracted from existent buildings [See for instance Epperson and Abrams (1989), Paquette et al. (2001), Russell (2010)] which is expected, given the technical and economic difficulties involved in those procedures.

Selecting the type of mortar is critical, since a slight change in its characteristics can completely change the failure mode and displacement capacity of the whole structure [Calvi et al. (1996)]. Nonetheless, most researches have arbitrarily used a weak type of mortar, especially Type O for construction of masonry specimens tested under seismic loads. The intention was to replicate the strong brick-weak mortar interface most likely to exist in old URM masonry buildings (Yi et al. 2006b). Schuller (2011) suggested to use Type K (1:3:12) or even a straight sand-lime mortar which can better replicate severe deteriorated mortar most typical of very old buildings. A good reference to select the type of mortar is also provided by ASTM C270, which summarizes different grade of masonry mortar used prior to 1950, as shown in Table 7-4.

Table 7-4 Type of masonry as specified by ASTM C270

Type	Ratio (cement:lime:sand)	Compressive Strength (psi)
M	1:0:3	2500
S	0.5-1:0.25-0.5:4.5	1800
N	1:0.5-1.25:6	750
O	1:2:9	350
K	0.5:2:7.5	75

In this research, the most appropriate type of mortar to simulate aging conditions in the laboratory is selected based on a comparative study between compressive stress-strain curves of old and new mortar specimens. The following sections discuss specimen characteristics, loading systems, instrumentations and comparative results.

7.5.1 Specimen Description, Loading System and Instrumentation

Compression test on new mortar specimens were conducted according to ASTM C109. Mortar cubes were tested after 28 days to obtain their compressive stress-strain curves. A similar approach was followed for smaller old mortar specimens, although the dimensions were not in full compliance with ASTM standard. Table 7-5 summarizes the dimensions and mortar type of each specimen. Figure 7-1 further illustrates several mortar samples obtained from demolished masonry walls.

Table 7-5 Dimensions and type of mortar for each specimen

Specimen	Dimensions (in)			Type of Mortar
	l	w	t	
1-3	2	2	2	O [1:2:9]
4-6	2	2	2	K[1:3:10]
7-9	2	2	2	K*[0.5:3:10]
10-12	2	2	2	L [0:1:4]
13-18	1.5	1.5	0.5	old

The uncapped specimens were placed on a flat circular metal steel plate and monotonically increasing displacements were applied using a Forney QC-400-C1 compression testing machine. A Linear Variable Differential Transformer (LVDT) with 1" stroke was placed in the machine to estimate global displacements during the test. The vertical force and displacement data were recorded using a data acquisition system. A better data resolution was obtaining by including an additional load cell for testing old mortar specimens, as seen in Figure 7-2. The type of failure was noted and photographs of each specimen were taken at the end of the tests.

Figure 7-1 Mortar samples taken from demolished masonry walls

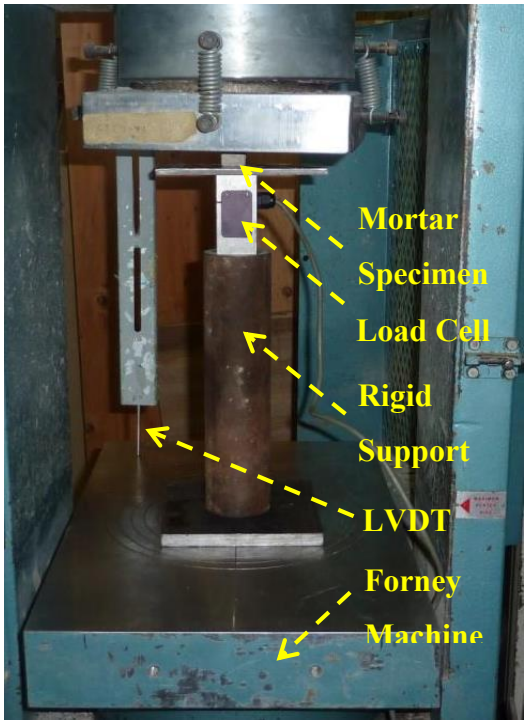

Figure 7-2 Test setup for testing of old mortar specimens

7.5.2 Test Results

Figure 7-3 presents the stress-strain curve for each type of mortar obtained by averaging the data from three specimens of each type. New mortar specimens behave linearly up to 75% of their maximum strength, followed by a nonlinear curve. Old mortar specimens were very soft, and behaved linearly during the test. For new mortars, the maximum compressive strength, $\mathbf{f_{bm}}$ occurred for an average strain of 0.4%. The compressive strain of old mortars computed at 0.4% strain is equal to 30 psi. Table 7-6 shows maximum strength and modulus of elasticity for each type of mortar. In average, the modulus of elasticity, $\mathbf{E_{bm}}$ of new mortar was found to be $270\mathbf{f_{bm}}$. Old mortar was found to have ¼ of the stiffness compared to new mortars.

Table 7-6 Summary of test results for new and old mortar specimens

Mortar Type	f_{bm} (psi)	E_{bm} (ksi)
O	237	35889
K	105	35536
K*	99	28686
L	76	22970
Old	30	7312

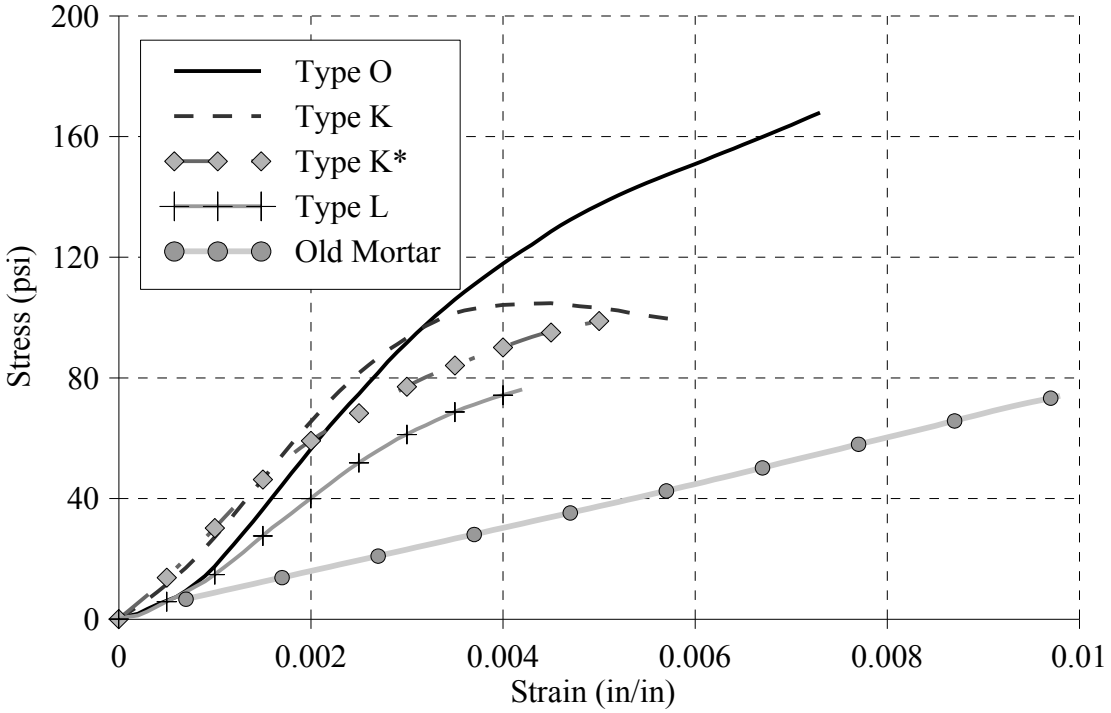

Figure 7-3 Average compressive stress-strain curves for different type of mortars

Figure 7-4 illustrates several failure modes of old mortars. Crushing and ductile failures were predominantly observed for all specimens.

Figure 7-4 Typical Failure modes observed for old mortar specimens.

7.6 Brick Compression Tests

These tests will provide useful information regarding the elastic modulus, maximum strength, non-linear behavior and limit states of new and old brick specimens. The compressive strength tests for half-brick specimens were performed in accordance to ASTM-C67 Standard Test Methods for Sampling and Testing Brick and Structural Clay Tile (ASTM 2011).

7.6.1 Specimen Description, Loading System and Instrumentation

Individual bricks were tested under uniaxial compression load according to the ASTM-C67 standard. Length, width, thickness and weight were measured in 20 new and old half-brick samples, as shown in Figure 7-5a. The average dimensions of new brick units were 3.55”x3.58”x2.29” (Wxlxt) whereas old bricks were slightly larger with dimensions 3.97”x3.63”x2.26”. Figure 7-5b also presents samples of old half-brick units. The core of old brick units show a black-carbon color , which according to experienced masons is an indication that these bricks were over fired and brittle or made of poor quality clay.

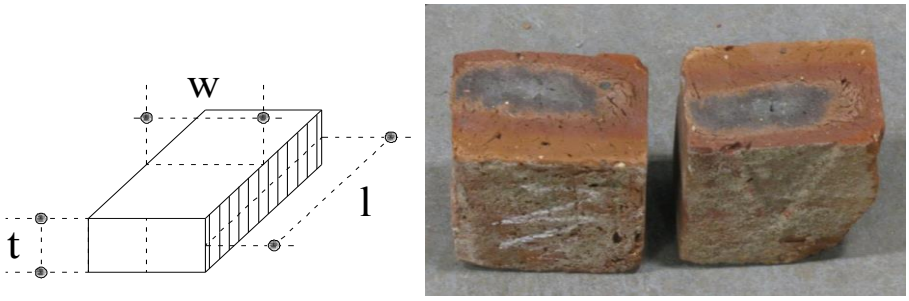

a) b)

Figure 7-5 a) Measuring of brick dimensions and b) old half-brick units

The uncapped specimens were placed on a flat circular metal steel plate and monotonically increasing displacements were applied using a Forney QC-400-C1 compression testing machine (see Figure 7-6). The data acquisition system was similar to that used in the mortar test. The type of failure was noted and photographs of each specimen were taken at the end of the tests.

Figure 7-6 Half-Brick specimen in testing machine

7.6.2 Test Results

Figure 7-7 shows the stress-strain curves for the new bricks and old brick specimens. New bricks exhibit linear behavior up to almost 80% of the maximum strength, after which the behavior is nonlinear. On the other hand, old bricks were found to be softer and highly nonlinear with no clear definition of the peak strength. Also, it is more difficult to define damage states of the old brick specimens. Average stress-strain curves for new and old bricks are also reported in Figure 7-7.

The summary of the test results for new bricks including the compressive strength, $\mathbf{F_b}$ and Elastic Modulus, $\mathbf{E_b}$ are presented in Table 7-7. Note that these values are the average of two halves of the same brick. The range of compressive strength of brick units is between 2995 to 4011 psi with a mean of 3400 psi and Coefficient of Variation (CV) of 0.11. This is consistent with the mean $\mathbf{F_b}$ obtained by previous researchers (See Table 7-7) of 4483 psi. Elastic modulus was found to vary between 992 and 1870 ksi, with a mean of 1420 ksi and CV of 0.26.

Old bricks presented a large variation of compressive strength, ranging from 392 to 1784 psi with mean of 981 psi and CV of 0.40. The elastic modulus ranges from 146 to 610 psi with a

mean of 346 ksi and also with a CV of 0.40. The large variation was expected, as these bricks were produced without following any standard procedure and could have aged differently. As a reference, the mean minus one standard deviation (μ-σ) compressive strength of bricks used in previous research programs presented in Table 7-8 is plotted in Figure 7-7.

New and old bricks Elastic Modulus can be estimated as 395Fb and 345Fb, respectively. These simplified relationships are similar to those obtained by Kaushik et al. (2007). Typical failure modes are shown in Figure 7-8 and Figure 7-9.

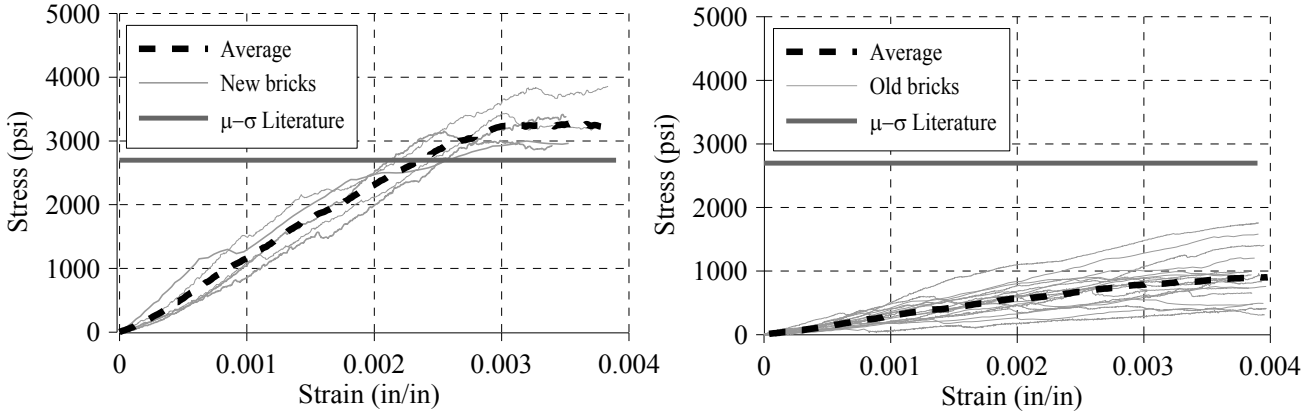

a) b)

Figure 7-7 a) Stress-strain curve of new half-brick specimens and b) Stress-strain curve of old half-brick specimens

Table 7-7 Summary of test results for new brick specimens

Specimen	f_b (psi)	E_b (ksi)
1[2]	3414	992
2[2]	3150	1274
3[2]	2995	1870
4[2]	4011	1755
5[2]	3431	1207
Mean	3400	1420
CV	0.11	0.26

Table 7-8 Summary of test results for old brick specimens

Specimen	f_b (psi)	E_b (ksi)
1	935	456
2	392	167
3	1186	283
4	726	222
5	1598	483
6	1214	480
7	1784	610
8	1113	282
9	1035	446
10	991	435
11	605	299
12	568	300
13	846	253
14	761	146
15	780	235
16	524	176
17	1613	417
18	989	542
Mean	981	346
CV	0.40	0.40

Figure 7-8 Typical failure mode of new half-brick specimens

Figure 7-9 Typical failure mode of old half-brick specimens

7.7 Compression Test of Masonry Specimens

Compression strength test on masonry specimens provides data regarding the elastic modulus, maximum strength, non-linear behavior and limit states on combined brick and mortar specimens.

7.7.1 Specimen Description, Loading System and Instrumentation

Five new masonry prisms constructed with type O mortar, five new masonry prisms constructed with type K mortar and two old masonry prisms were tested according to ASTM-C1314 Standard Test Method for Compressive Strength of Masonry Prisms (ASTM 2011). All new specimens were constructed with red bricks. Table 7-9 summarizes the dimensions and type of mortar of each masonry specimen. The prism height-to-thickness ratio, h_p/t_p was between 3.6 and 3.8. Also, Figure 7-10 illustrates the dimensions of old masonry specimens as extracted from the demolished building. Figure 7-11 shows one of the newer masonry specimens after 28 days ready to be tested.

The specimens were placed on a flat circular metal steel plate and monotonically increasing displacements were applied using a Forney QC-400-C1 compression testing machine. Similar to previous tests, the vertical force and displacement data were monitored and recorded. Analysis of the recorded data revealed that the stress-strain curves of all specimens with rubber pad caps presented anomalies and inconsistencies. Consequently, all data from these specimens were disregarded in this study. While there was little noise in the data, the unfiltered data is presented in the following sections.

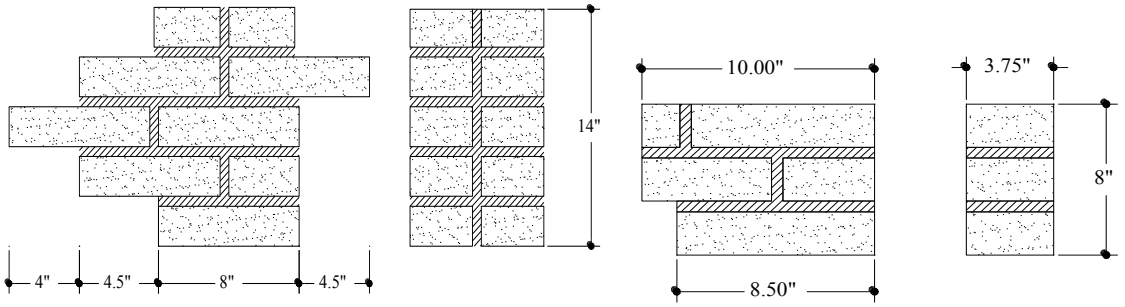

Figure 7-10 Dimensions of old masonry specimens

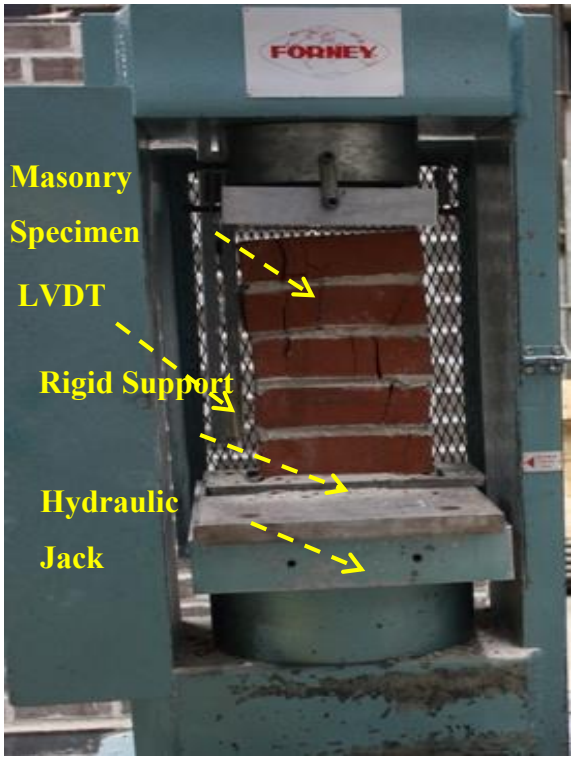

Figure 7-11 Masonry specimen in the Forney Machine

Table 7-9 Masonry Prism Specimens

ID	Mortar Type	Capping	New Bricks		
			l	w	h
2		Yes	7 1/2	3 9/16	13 1/4
3		No	7 9/16	3 5/8	13 1/2
4	O	No	7 1/2	3 1/2	13 9/16
5		Yes	7 1/2	3 5/8	13 1/4
6		No	7 5/8	3 1/2	13 5/8
7		Yes	7 9/16	3 1/2	12 3/4
8		No	7 9/16	3 9/16	12 15/16
9	K	Yes	7 5/8	3 5/8	13
10		No	7 1/2	3 9/16	13
1		No	7 9/16	3 5/8	13 1/4
μ			7 11/20	3 29/51	13 17/80
σ			0.049	0.055	0.29
CV			0.65	1.53	2.20

7.7.2 Test Results

The stress-strain curves of all masonry compression specimens are shown in Figure 7-12. The average stress-strain curves for Type O, Type K and Old masonry prisms are also included in this figure. A typical initial linear behavior followed by a nonlinear phase can be observed for the new prism, whereas a soft, nonlinear behavior was obtained for old specimens.

The summary of test results for new and old prisms including the peak compressive strength and elastic modulus are given in Table 7-10. For prisms with Type K mortar, the average compressive strength is 1317 psi with a CV of 0.14. As per Table 7-1 of ASCE 41-06, this masonry can be classified as in good conditions. However, the average elastic modulus is relatively lower for this type of masonry, with an average value of 116192 psi. Similar values for masonry properties were reported by Yi (2004). Masonry prisms constructed with Type O mortar had an elastic modulus about 2.5 times higher than Type K prisms and about 5 times higher than Old prisms. The average peak compressive strength of Type O, Type K and Old prisms was 1798 psi, 1317 psi and 535 psi, respectively.

Since both, Type K and Type O prisms were constructed with the same type of bricks, the large variation in stiffness and peak strength can be associated to the quality of the mortar. Yet, it is possible to observe some crushing in the upper bricks, probably due to absence of capping.

Figure 7-13 and Figure 7-14 illustrate typical failure modes in all specimens. Vertical splitting cracks along the height of the units were consistently observed during the experiment.

The lower and upper bound compressive strength and elastic modulus of in-situ flatjack test conducted by Atkinson and Noland Co in two NYC buildings are listed in Table 7-11. The tests were conducted according to ASTM C 1197 standard. The lower bound of the masonry compressive strength is in good agreement with the old specimens tested in the laboratory. Yet, there exist a significant variability in the masonry properties constructed with different type of bricks.

As a reference, ASCE 41-06 default lower-bound compressive strength for masonry in poor condition is 300 psi.

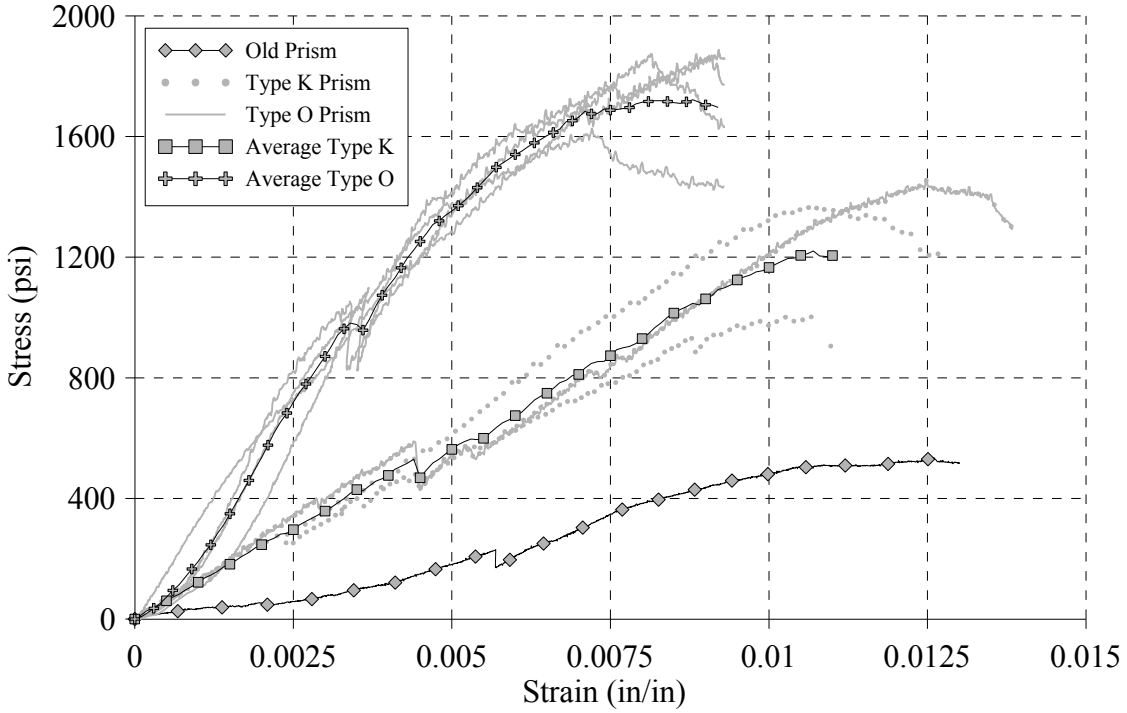

Figure 7-12 Stress-strain curve of masonry specimens

Figure 7-13 Typical failure mode of Mortar Type-K masonry prism

Figure 7-14 Typical failure mode of Mortar Type-O masonry prism

Table 7-10 Summary of test results for new brick specimens

Specimen	f_m (psi)	E_m (psi)
1K	1102	102661
8K	1396	135790
10K	1454	110126
Mean	1317	116192
CV	0.14	0.15
3O	1873	265146
4O	1887	274557
5O	1803	350052
6O	1627	250591
Mean	1798	285087
CV	0.07	0.16
Old	535	53561

Table 7-11 Summary of masonry properties of buildings in NYC

Building	Brick Type	Elastic Modulus (psi)		Compressive strength (psi)	
		E_m min	E_m max	f'_m min	f''_m max
Building 1, located on Greenwich St	Red Common brick	333,000	615,000	600	1100
Building 2, located on 90th Street	Crème brick	1,100,000	2,300,000	1570	5000
	Red face brick	700,000	1,500,000	1000	2140
	Red Common brick	400,000	600,000	570	1200

7.8 Bed Joint Shear Strength Test

In this section, the bed joint shear strength of new and old URM specimens was evaluated in order to compare their monotonic shear behavior. Initial shear stiffness, peak and residual strength values and the influence of the mortar quality in the frictional properties of the brick-mortar interface were also investigated.

The bed joint shear strength was obtained using triplet specimens, as illustrated in Figure 7-15. This test is usually conducted under a combination of direct shear stress and a constant normal stress. This method has been preferred for researchers to determine the shear strength of masonry bed joints because it gives a uniform distributed shear stress and lateral compressive stress and it is easy to build and execute (Yi 2004). It also provides enough information to estimate the cohesion and pre- and post-peak shear strength and stiffness. These parameters are required to develop reliable analytical models to describe the in-plane behavior of masonry walls. This test may also be relevant for cyclic two-way bending (Griffith et al, 2007) in which friction and cohesion of bed joints and tensile strength of bricks play an important role in the maximum force capacity and also on the post-cracking hysteretic behavior.

The triple test, however, does not provide a good simulation of the actual behavior under seismic forces, where the coupling between crack propagation along mortar beds due to flexural action and cyclic reversal of force direction may reduce significantly the shear strength (Paulay and Priestley 1992). Extensive information regarding this test can be found elsewhere [(Atkinson et al. 1989; Tisa and Kovári 1984).

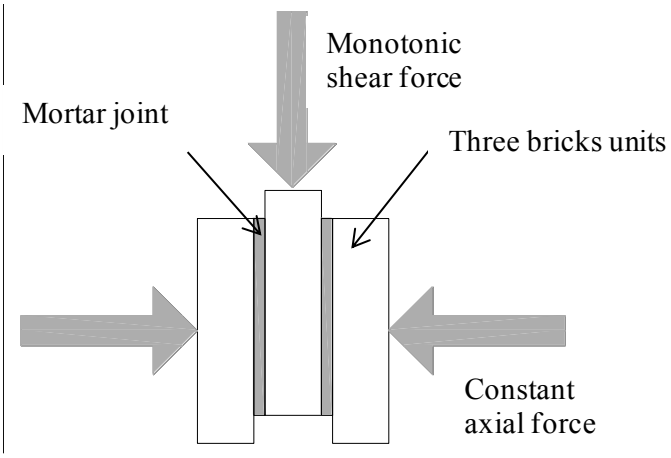

Figure 7-15 Concept of direct shear test on triplet specimens

There is consensus among researchers that the bed joint shear stress is strongly related to transverse compression stress. As a result, a Coulomb Law has been widely used to estimate the shear capacity. The linear equation of the shear strength is

$$\tau = \tau_0 + \mu * f_m 0 \tag{7.1}$$

This equation is an approximation of the actual shear-compression interaction, which is illustrated in Figure 7-16. It gives good results for the typical range of axial compression stresses presents in URM buildings (Paulay and Priestley 1992).

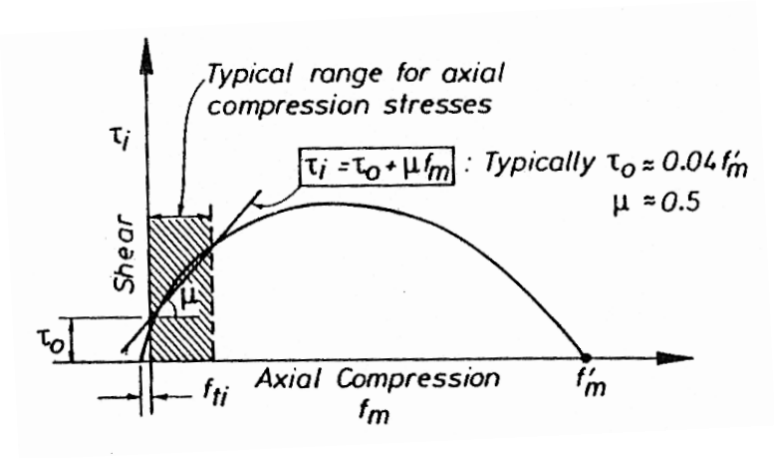

Figure 7-16 Shear-compression interaction (Paulay and Priestley 1992)

7.8.1 Specimen Description, Loading System and Instrumentation

In order to investigate the influence of mortar quality in the shear strength of URM, three groups of triplet specimens were tested with the loading system illustrated in Figure 7-17.

The first group consisted of 15 specimens constructed with new bricks and Type O mortar. The second group consisted of 15 specimens constructed with new bricks and Type K mortar. Finally, two experiments were conducted on intact specimens of brick and mortar collected from a demolished old URM building in Syracuse, NY. The dimensions of these specimens are illustrated in Figure 7-18. A range of axial loads between zero and 1.5 kips was pre-applied to each specimens, which was considered to be representative of actual compressive forces in medium-rise URM buildings. The area of each specimen is listed in Table 7-12. All new specimens were constructed by professional masons.

The test apparatus consists of three steel plates connected with four $^3/_8$ inch thick steel rods, as shown in Figure 7-17. This test fixture is similar to that used by Yi (2004). The three plates

provided a uniform, rigid contact area in which the triplet specimens are placed. A load cell was connected to one side to measure the normal stress. The load cell had a maximum capacity of 10 kips, but was calibrated to 3 kips. The lateral load of 0 to 1.5 kips was applied to the specimen by tightening bolts on one side of the apparatus.

The assembled test specimen was placed in the MTS Axial Torsion machine (SEESL 2010) and monotonic displacement was applied to induce direct shear stress. The recorded data presented little noise in the signal and was not further filtered.

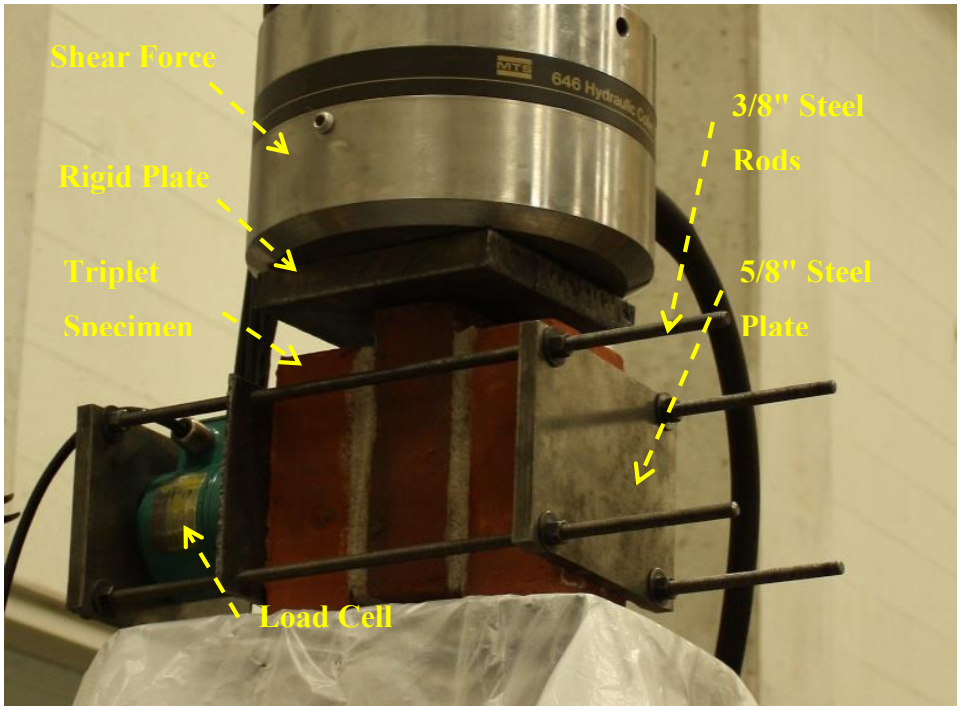

Figure 7-17 Shear test set up

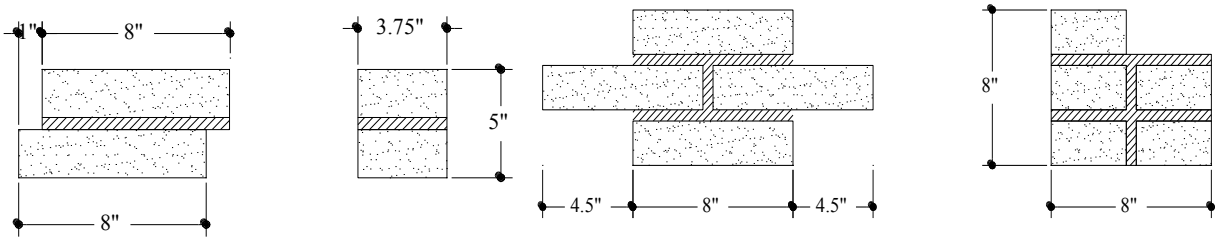

Figure 7-18 Dimensions of old triplet specimens

7.8.2 Test Results

The results of the direct shear test on type K, Type O and Old triplet specimens are summarized in Table 7-12, Table 7-13 and Table 7-14, respectively. The applied normal stress to these specimens ranged from zero to 65 psi. The initial maximum shear stress ranged from 11 to 72 psi for Type-K mortar and 38 to 138 psi for Type-O mortar. In the case of the two old specimens, the values were 38 psi and 45 psi.

The maximum shear stresses corresponding to different normal stresses are presented in Figure 7-19, Figure 7-20 and Figure 7-21. This data was used to estimate the internal friction coefficient, and the initial shear bond of the masonry. The initial shear bond for type K specimens was around 18 psi, for type O was around 43 psi and for old specimens was around 10 psi. The measured internal friction coefficient was around 0.68, 1.13 and 0.84 for type K, Type O and old triplet specimens.

The observed failure modes were always a mix between shear-sliding along the bed joint interface between brick and mortar and cracking inside the mortar, as shown in Figure 7-24. This is expected for low strength mortars (Alecci et al. 2013).

Figure 7-22 and Figure 7-23 show the variation of the lateral compressive confining force during the tests, for Type K and Type O respectively. This phenomenon was already observed by Yi (2004) and it is due to the intrinsic configuration of the test set up. The lateral normal stress remain constant until the shear sliding along the mortar bed starts. Then, mainly due to fracture in the mortar and mortar-brick interface, the lateral confining stress shows a large increase. Thereafter, the vertical force follows a path related to the type of mortar. In experiments by Yi, the behavior was similar to that observed in Type O mortar. The vertical force dropped off very quickly due to loss of the specimen stiffness and then due to dilatancy movement of the sliding interfaced the shear stress started increasing again. Herein, a different behavior can be observed for Type K specimens, in which the shear force linearly increases until failure, as depicted in Figure 7-23.

Table 7-12 Type K Triplet specimen results

Set	ID	Area (in2)	Shear Stress (psi)	Constant Normal Stress (psi)
1	20	22.31	27	11
	21	24.58	33	8
	26	22.29	25	12
2	4	23.06	35	35
	6	23.25	36	29
	10	22.97	50	45
	25	23.16	38	45
	27	22.34	60	47
3	28	23.20	72	56
	29	21.88	70	65
	30	22.31	40	60
	3	22.75	57	51
4	22	22.35	25	0
	23	21.81	11	0
	24	23.16	16	0

Table 7-13 Type O Triplet specimen results

Set	ID	Area (in2)	Shear Stress (psi)	Constant Normal Stress (psi)
1	7	22.87	127	28
	8	22.82	67	22
	18	21.59	83	24
2	15	22.42	108	53
	16	22.22	135	64
	17	22.53	138	58
3	5	23.06	77	56
	9	23.58	98	58
	11	22.22	81	44
	12	22.11	88	46
	14	22.31	65	46
4	2	22.42	38	8
	19	22.31	45	10

Table 7-14 Old Triplet specimen Results

Set	ID	Area (in2)	Shear Stress (psi)	Normal Stress (psi)
1	A	14.0	75	44
	B	24.5	30	23

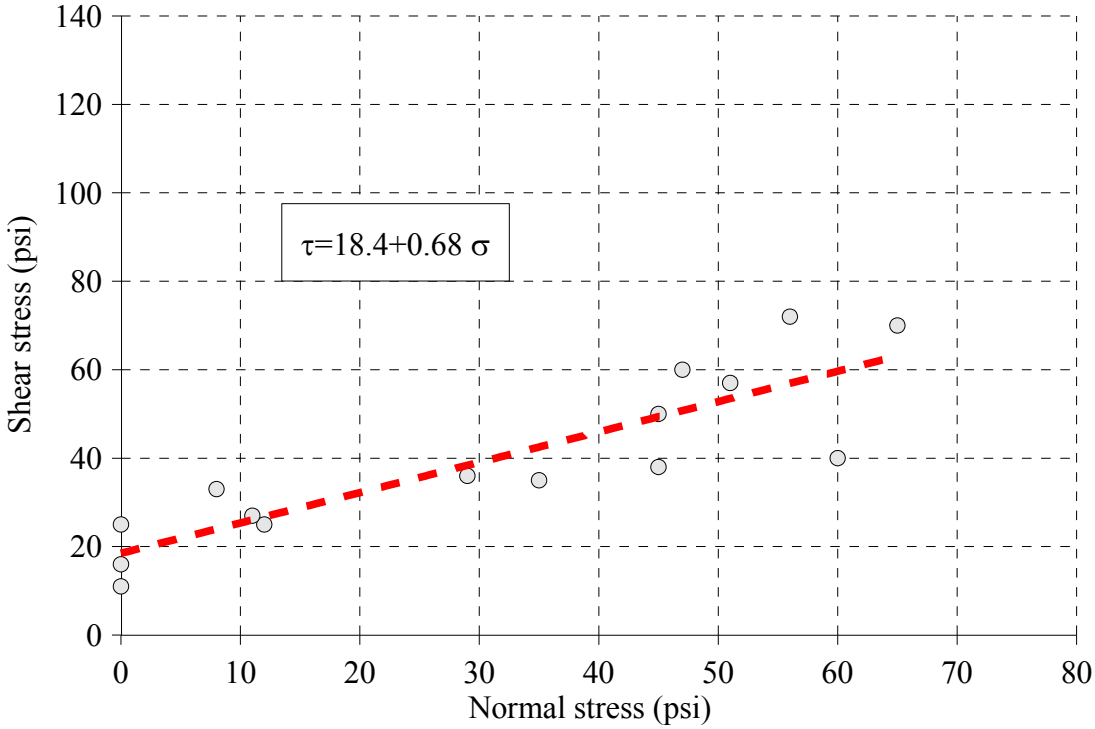

Figure 7-19 Initial shear stress vs constant normal stress for Type K specimens

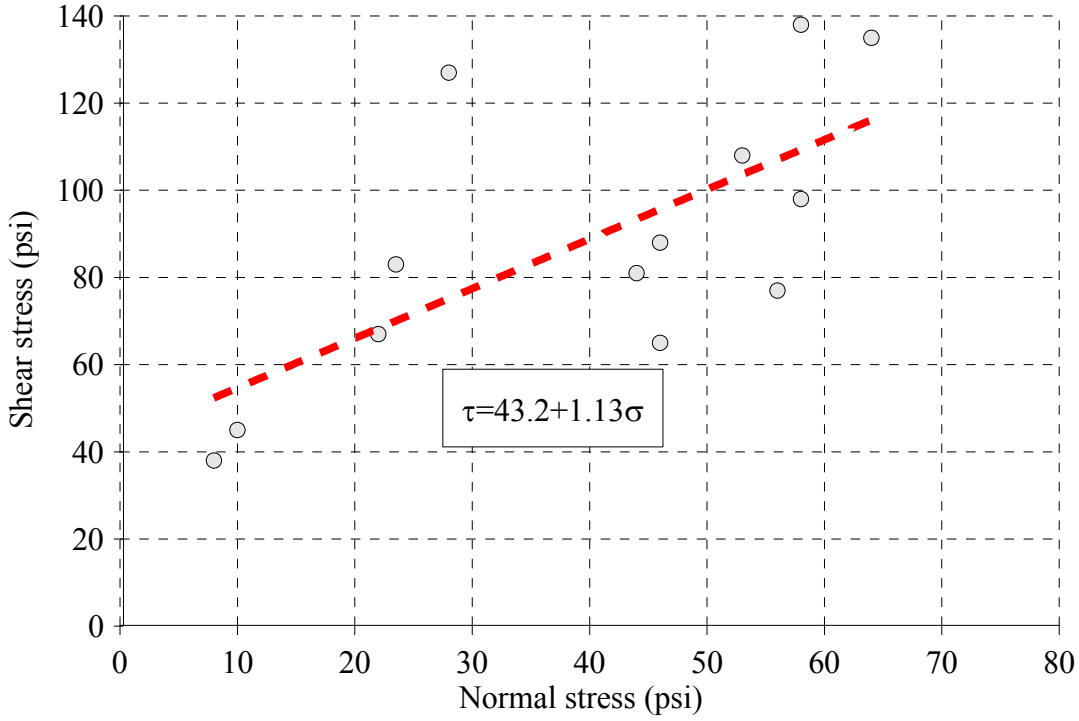

Figure 7-20 Initial shear stress vs constant normal stress for Type O specimens

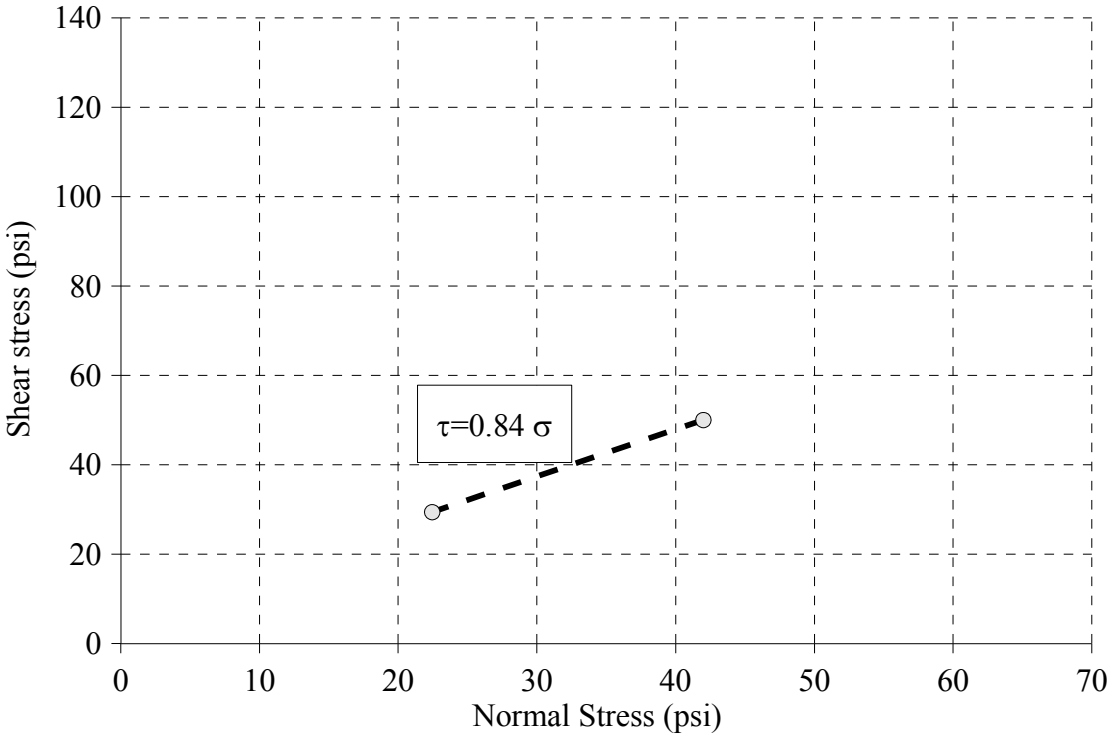

Figure 7-21 Initial shear stress vs constant normal stress for Old specimens

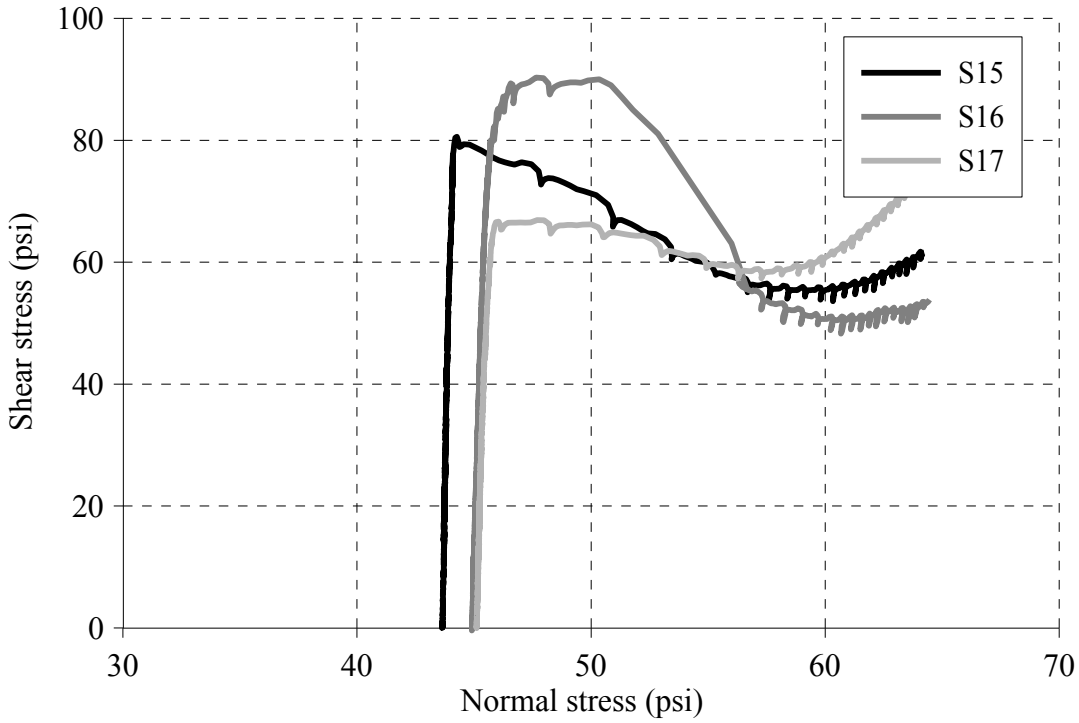

Figure 7-22 Variation of shear stress and normal stress for Type O specimens.

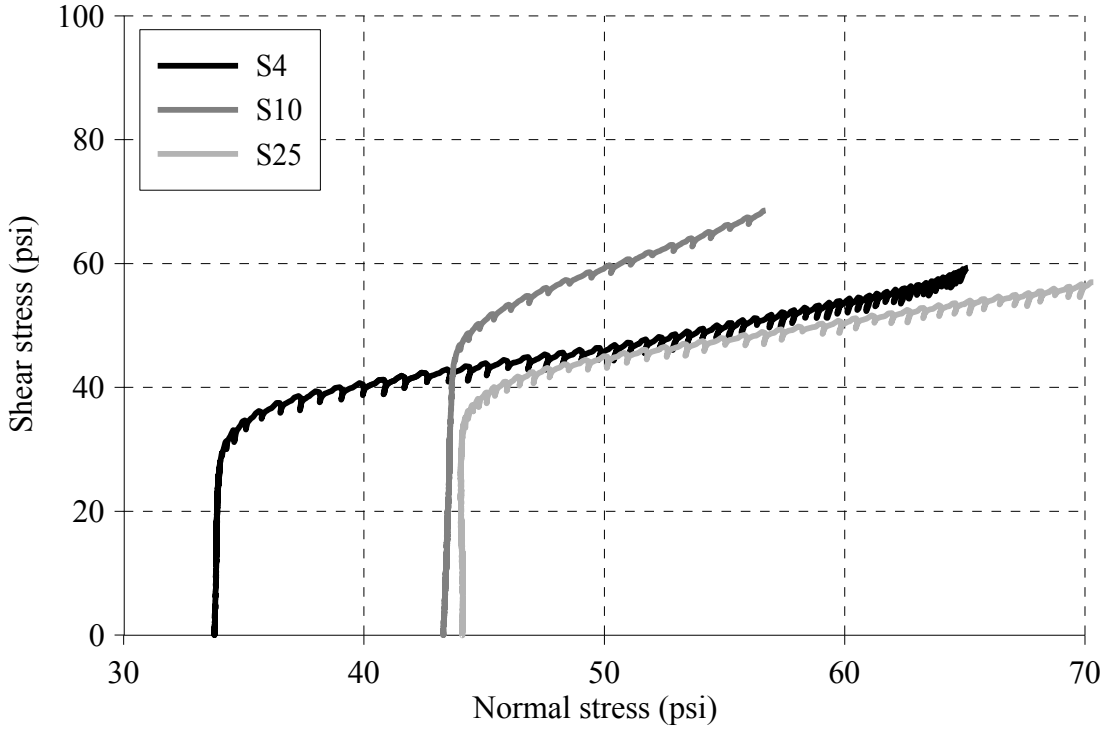

Figure 7-23 Variation of shear stress and normal stress for Type O specimens.

Figure 7-24 Typical failure mode of triplet specimens.

7.9 Summary and Findings

This section presented material characterization testing studies that focused on identifying the material and URM properties more appropriate to replicate actual conditions of URM in the laboratory. The major findings of the study presented in this section are listed below:

- A comparison between new mortar tested after 28-days and old mortar obtained from demolished buildings indicated that none of the newer mortar types tested could replicate the Elastic Modulus and Compressive Strength of old mortars. Old mortar was much

softer and behaved linearly during the tests. Type L or Type K* mortar were closest in term of maximum compressive strength.

- New bricks had significantly higher Elastic Modulus and Compressive Strength than old, reclaimed units. Old brick were found to be very soft and behaved nonlinearly during the tests.
- Masonry specimen samples constructed with type K and Type O mortar had significantly higher Elastic Modulus and Compressive Strength than Old masonry specimens extracted from demolished buildings. The maximum compressive strength of the old specimens was in good agreement with in-situ test conducted in URM building in NYC. However, the Elastic modulus was lower.
- The internal friction coefficient of Type K and Type O triplet specimen was found to be around 0.68 and 1.13, respectively. The friction coefficient was found to be insensitive to aging, since a value of 0.84 was estimated in old triplet specimens. Nonetheless, Type K mortar specimens had a closer initial maximum shear stress to the old specimens.

SECTION 8
EXPERIMENTAL PROGRAM PART II: SHAKE TABLE TESTING OF OUT-OF-PLANE URM WALLS WITH PARAPETS INCLUDING DIAPHRAGM FLEXIBILITY

8.1 Introduction

In this section, the second phase of the experimental program is presented. After obtaining data to characterize the material properties that better represent actual conditions of the building stock in New York City, shake table testing of two full-scale multi-wythe unreinforced masonry walls with parapets including diaphragm flexibility subjected to out-of-plane loading was carried out in the Structural Engineering and Earthquake Simulation Laboratory (SEESL) of the University at Buffalo.

After reviewing the literature, one of the first challenges in this study was to design a specimen that best replicates the seismic behavior of a central portion of an URM building. Therefore, a systematic procedure to define a simplified numerical model of out-of-plane URM walls in multi-story buildings was proposed to conduct nonlinear response history analysis. This numerical model was used to estimate the maximum response of the specimen and provided appropriate design parameters to define the test setup.

An effort was made to construct the walls with materials typical of late 19th-early 20th century construction in New York City. Moreover, the connections between masonry walls and wood diaphragms were designed according to construction practices in the NYC region. Also, rigid and flexible diaphragms were replicated by supporting a section of floor with reduced scale seismic isolation bearings of different stiffness characteristics. The effectiveness of common retrofitting techniques was also investigated by strengthening the parapet and wall-to-diaphragm connection of one of the walls with steel braces and steel rods, respectively.

Material properties were obtained through compressive strength tests of prims, bricks and mortars. The dynamic properties of the walls were first identified using white-noise tests. Then, damage progression and behavior of the walls was obtained by subjecting the walls to an

increasing intensity sequence of two sets of ground motions with different frequency content: The 2011 Virginia earthquake and the 2011 New Zealand earthquake.

Both masonry walls were able to sustain the Virginia earthquake record at 100% with minor damage. However, collapse of the parapet and the connection between masonry walls and wood joist was observed when the specimens were subjected to 100% amplitude of the New Zealand earthquake record. The results of these tests were used to validate computer models to be used for seismic vulnerability assessments. Also, it provided information regarding the seismic behavior and vulnerability of masonry walls with parapets and flexible diaphragms. In addition, new data about the wall-to-diaphragm connection has been collected and will be used to estimate the effectiveness of this type of retrofitting technique.

8.2 Scope and Objectives of Shake Table Testing

The main goal of the experiment described in this section is to obtain data to verify and validate simplified numerical models of URM walls with parapets, floor-to-wall connections and flexible wood diaphragms. In order to address this need, the following parameters were considered in this experiment:

1) *The frequency content of the ground motion inputs.* The wall was subjected to increasing intensities of two different ground motions, the 2011 Virginia and 2011 New Zealand earthquakes.
2) *The effect of common retrofitting techniques for parapets and floor-to-wall connections*. This was studied by strengthening one of the walls using steel braces and anchors.
3) *The effect of wood diaphragm stiffness*. The wood floor flexibility was simulated using lead rubber bearings and low damping rubbers, replicating a stiff and a flexible diaphragm, respectively.
4) *The aging effects in URM construction*. The walls were constructed using old reclaimed bricks and a weak Type K mortar.
5) *The filtering effects on the seismic input on top of out-of-plane walls*. The load path for seismic forces at the top of the walls traveled through stiff steel towers, which simulates the in-plane walls in a real URM building, and the elastomeric bearing isolators carrying the wood floors simulate diaphragm flexibility.

6) *The influence of gravity loads*. Concrete blocks were placed on top of the wood floors to simulate tributary dead loads from the prototype building.
7) *The behavior under low to medium seismic hazard*. The ground motions were scaled to match the DBE earthquake of a site in NYC, which is a medium seismic hazard area, and scaled up or down during the test.
8) *The modes of collapse of URM walls*. The walls were tested until collapse of any of their structural components.
9) *The seismic demands along the height of the wall*. Accelerations and displacements were obtained for each wall through an array of more than 60 measuring instruments.

8.3 Test Setup Overview

8.3.1 Simplified Numerical Model of URM Specimen

Previous research regarding out-of-plane testing of URM walls revealed that few specimens were designed to accurately represent a portion of a complete building prototype. The ABK program provided the first rational procedure to determine the specimen dimensions and seismic input for out-of-plane testing of URM walls. A procedure inspired by the ABK program is followed in this research.

In this work, a systematic procedure to define a simplified and reliable numerical model of vulnerable out-of-plane URM wall panels in multi-story buildings is proposed and later validated using experimental results. The model was primarily used to design the properties of the experimental specimen that will impose realistic seismic loads on a central portion of an URM building specimen.

As an interesting feature, the model can be also used by practicing engineers to investigate, with minimal computational cost, the dynamic stability of URM walls subjected to out-of-plane loading. Currently, ASCE 41-06 acceptance criteria for URM walls subjected to out-of-plane actions specifies that flexural cracking in URM walls shall be permitted provided that cracked walls segments will remain stable during dynamic excitations. This stability is checked using numerical models considering acceleration time histories at the top and base of the wall panel. Yet, no recommendations are provided regarding the methodology and tools available to develop these numerical models.

As in the ABK program, there are major assumptions in the procedure developed in this study. First, note that the ground motion is assumed to be transmitted unmodified to each floor by the end-walls which are in turn assumed to be infinitely rigid in-plane. For multi-story buildings with significant amount of openings this may not be appropriate. An extended discussion on this subject can be found in Bruneau (1994b). Second, a perfect tie between walls and diaphragms is considered so that an effective transfer of forces and accelerations is guaranteed and out-of-plane collapse due to failure in the connection is prevented during an earthquake.

The general procedure developed in this research to define the simplified model of the specimen is illustrated in Figure 8-1 and can be summarized as follows:

Step 1*: Define an archetype building and create a numerical model.* This step was completed in Section 3, in which a five-story URM building was selected as a representative archetype. Also, using the modeling techniques proposed in Section 4, 5 and 6, a numerical model was implemented in SAP2000.

Step2: *Replace the flexible diaphragm with a SDOF equivalent model.* The procedures used in Section 4 can be used to complete this task. Use the total mass of the diaphragm and a force-displacement relationship estimated from pushover analysis.

Step 3: *Replace the in-plane walls with equivalent infinite stiffness elements.* This step assumes that in-plane walls do not amplify the ground acceleration. The mass of the in-plane walls is neglected, since zero displacement is assumed.

Step 4: *Replace the out-of-plane walls below the upper story*. This step can be completed by conducting a pushover analysis of the bottom part of the building and using the force-displacement relationship in equivalent nonlinear springs located at the bottom of the URM walls.

The equivalent simplified model and the loading conditions used to generate all force displacement relationships are illustrated in Figure 8-2. Also, the actual numerical models developed in SAP2000 to complete the methodology are shown in Figure 8-3. The El Centro earthquake was used to run nonlinear time history analysis considering large displacements and P-Delta effects. To verify the infinite stiffness assumption regarding the in-plane walls, a comparison between the absolute accelerations along the height of in-plane walls of the prototype building subjected to El Centro earthquake was conducted. Figure 8-4 shows that a

35% maximum amplification of the peak input acceleration was obtained at the fifth floor. Since larger amplifications (between 200% to 300% of the input PGA) are expected in the accelerations at upper floors due to the presence of flexible diaphragm, 35% seems to be negligible. Nonetheless, further studies including different archetypes and a larger number of ground motions are required to obtain a better understanding of this assumption.

Figure 8-5 and Figure 8-6 show a comparison between the displacement response history of the prototype and simplified numerical models obtained for El Centro earthquake, at the top and bottom of the selected URM specimen (i.e. the central portion of the top story in the prototype structure) respectively. Although a good agreement can be seen in the history response and fundamental periods, a maximum error of 10% was obtained for the absolute peak displacement. On the other hand, the analysis time taken to solve the model in Step 5 is only 5% of the time required to solve the Full model in Step 1.

Figure 8-7 and Figure 8-8 show a comparison between the acceleration response history of the prototype and simplified numerical models obtained for El Centro earthquake, at the top and bottom of the selected URM specimen, respectively. Note that the higher mode effects and significant amplification of acceleration introduced by the full model of the diaphragm are filtered out by the reduced model and the error obtained in the response of Step 5 model is about 50%.

The fundamental period of each model, analysis time, peak absolute acceleration and peak displacement of the selected URM specimen are listed in Table 4-12.

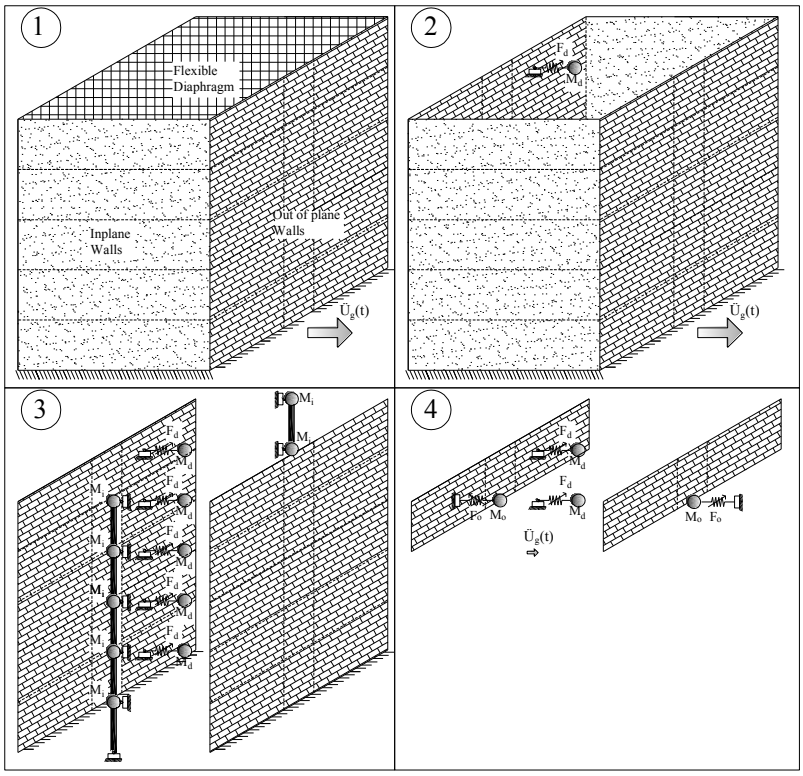

Figure 8-1 Simplified numerical model of OOP masonry walls in multi-story buildings

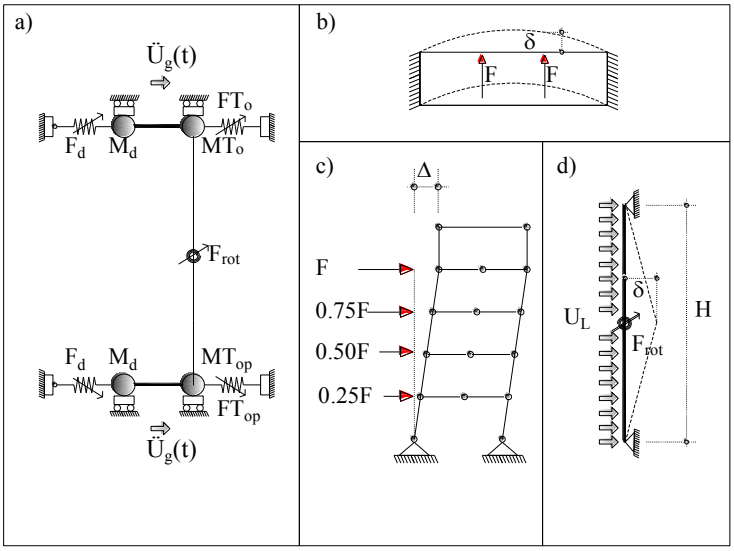

Figure 8-2 Final simplified numerical model of URM walls in multi-story buildings and loading conditions considered to obtain force-displacement relationships. a) Final model, b) Pushover of diaphragm, c) Pushover of lower stories and d) Pushover of the URM wall

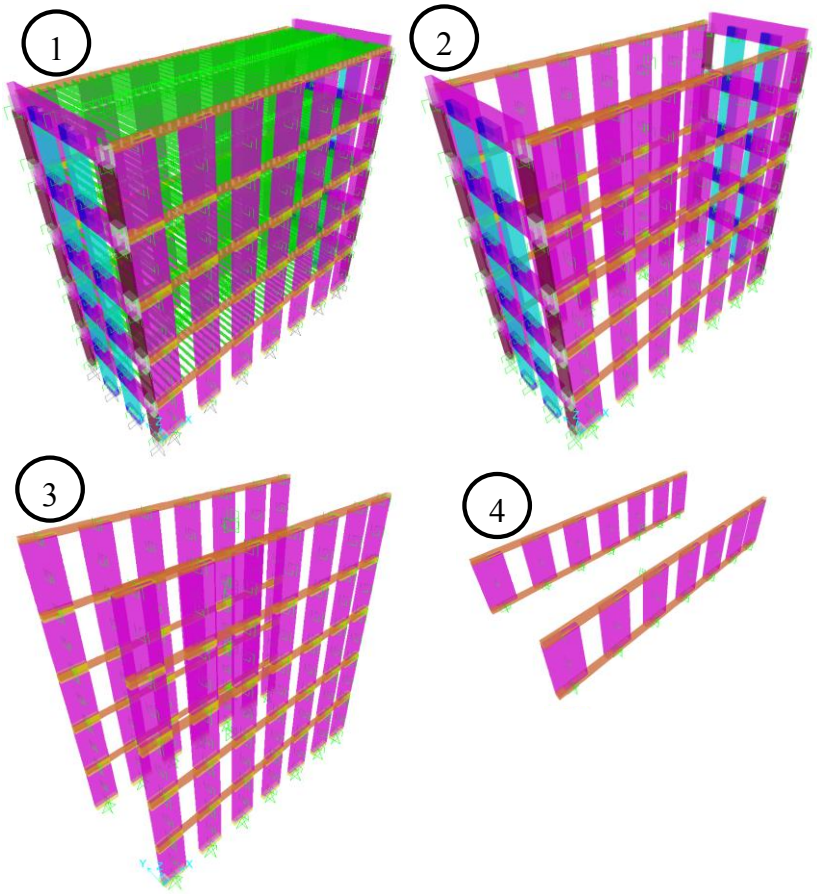

Figure 8-3 Actual numerical models developed in SAP2000 in each step of the methodology

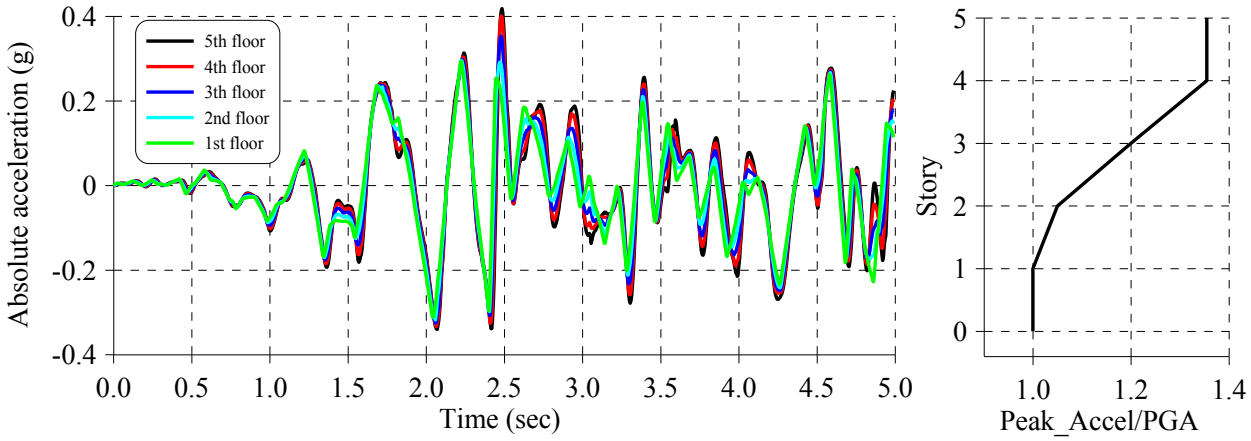

Figure 8-4 Absolute accelerations along the height of the in-plane walls of the prototype building and normalized acceleration amplification at each story (El Centro earthquake)

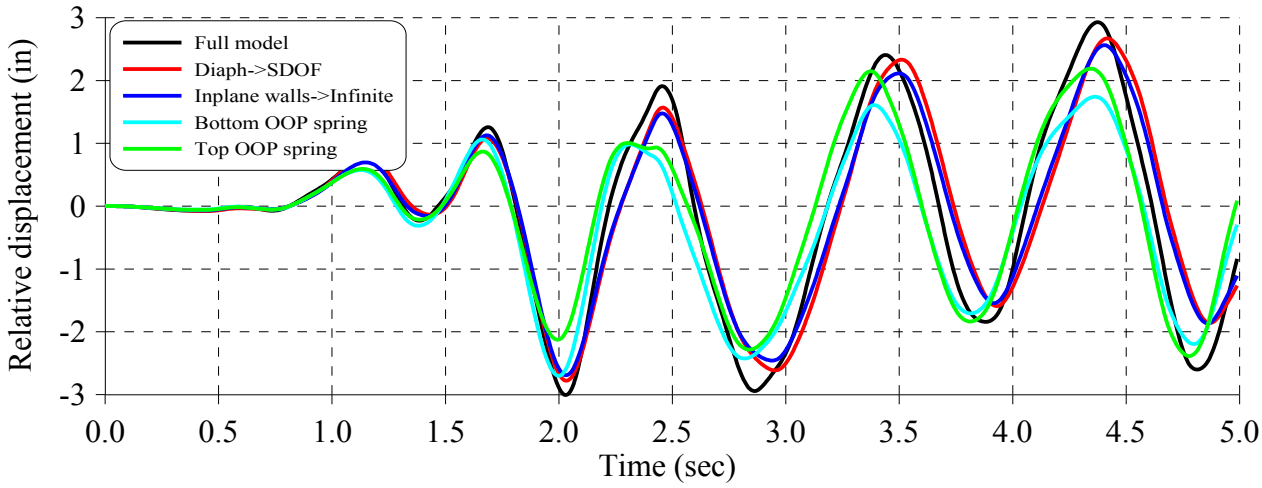

Figure 8-5 Relative displacement response at the top of central OOP walls for each step of the proposed methodology

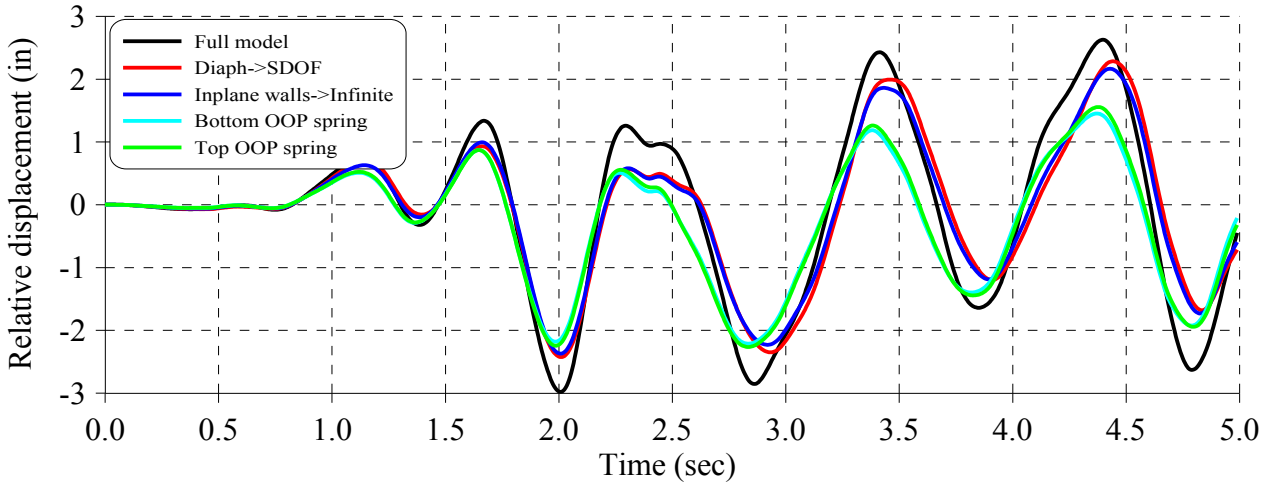

Figure 8-6 Relative displacement response at the bottom of central OOP walls for each step of the proposed methodology

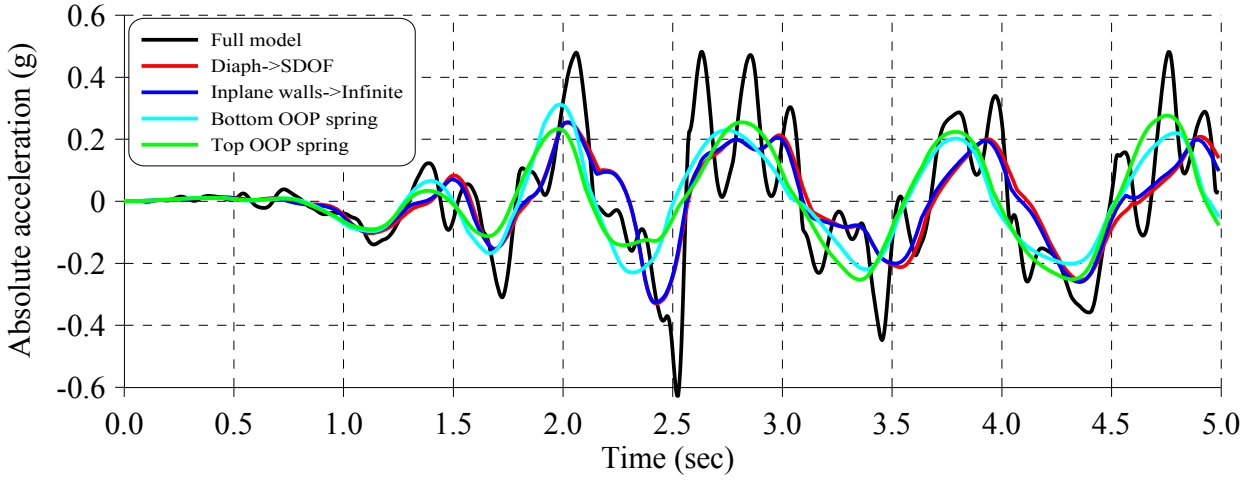

Figure 8-7 Absolute acceleration response at the top of OOP walls for each step of the proposed methodology

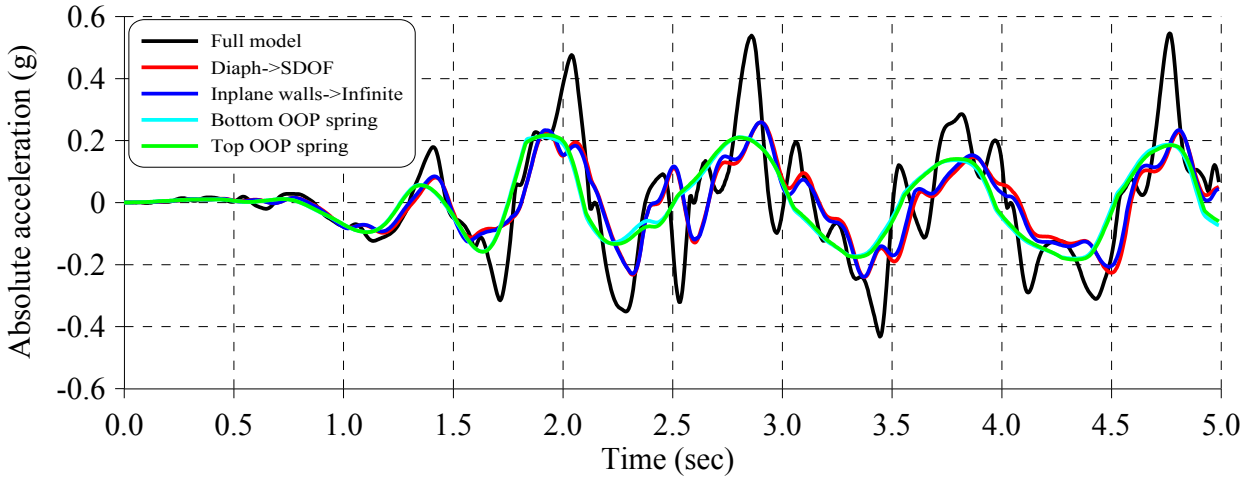

Figure 8-8 Absolute acceleration response at the bottom of OOP walls for each step of the proposed methodology

Table 8-1 Comparison of response parameters obtained using simplified and full model of URM building

Step	Modeling Technique	Period (sec)	At the top of central OPP wall		At the bottom of central OOP wall		Analysis time (sec)
			Peak displacement (in)	Peak absolute acceleration (g)	Peak displacement (in)	Peak absolute acceleration (g)	
1	Full model	0.73	3.01	0.62	2.98	0.54	7200
2	Replace diaphragm for a SDOF	0.81	2.78	0.32	2.43	0.25	1122
3	Assume infinite in-plane walls	0.76	2.69	0.32	2.37	0.26	970
4	Bottom equivalent OOP spring	0.73	2.70	0.31	2.21	0.21	350

8.3.2 Specimen Design

Although good agreement was found between the response history analysis of the five story prototype and the specimen at the upper floor of the building, there were some technical and financial constraints that prevented the full implementation of the specimen in the laboratory. First, an equivalent method to simulate the flexibility of the diaphragm at the top and bottom of the specimen was needed. The most obvious method to achieve this was using actual coil springs. However, the nonlinear nature of the equivalent spring required to simulate the diaphragm was difficult to simulate. Therefore, reduced scale elastomeric isolation bearings were considered. The bilinear force-displacement relationship of these isolators was deemed to be more appropriate, as demonstrated in Figure 8-10. However, the required number and appropriate type of isolators was not available in the SEESL laboratory. Secondly, the equivalent mass required to simulate the bottom portion of the five-story building (about 240 kips) was also out of the capabilities of the laboratory.

As a result, it was decided to reduce the prototype to one story building and take the central portion to be replicated in the laboratory. This way, isolators were only required at the top of the specimen. Also, the mass required to simulate the wood diaphragm was considerable less and feasible to be replicated. Figure 8-9 shows the new building prototype and the specimen design concept implemented in the laboratory. The methodology described in previous section was followed to develop a simplified numerical model, as illustrated in Figure 8-10.

Figure 8-11 shows a comparison between the displacement response history obtained for the one story prototype and the corresponding specimen for the 2011 New Zealand earthquake. Again, there is good agreement in the response but the peak displacement is underestimated in the specimen. A better agreement was obtained for the acceleration response history, as seen in Figure 8-12.

It is important to clarify that the actual numerical model of the specimen was improved after the experiments were completed, as was the corresponding building prototype. However, the results obtained in this section were used to estimate the maximum response of the specimen, and provide reasonable design parameters to define the structural components to be used for the shake table test of the specimen.

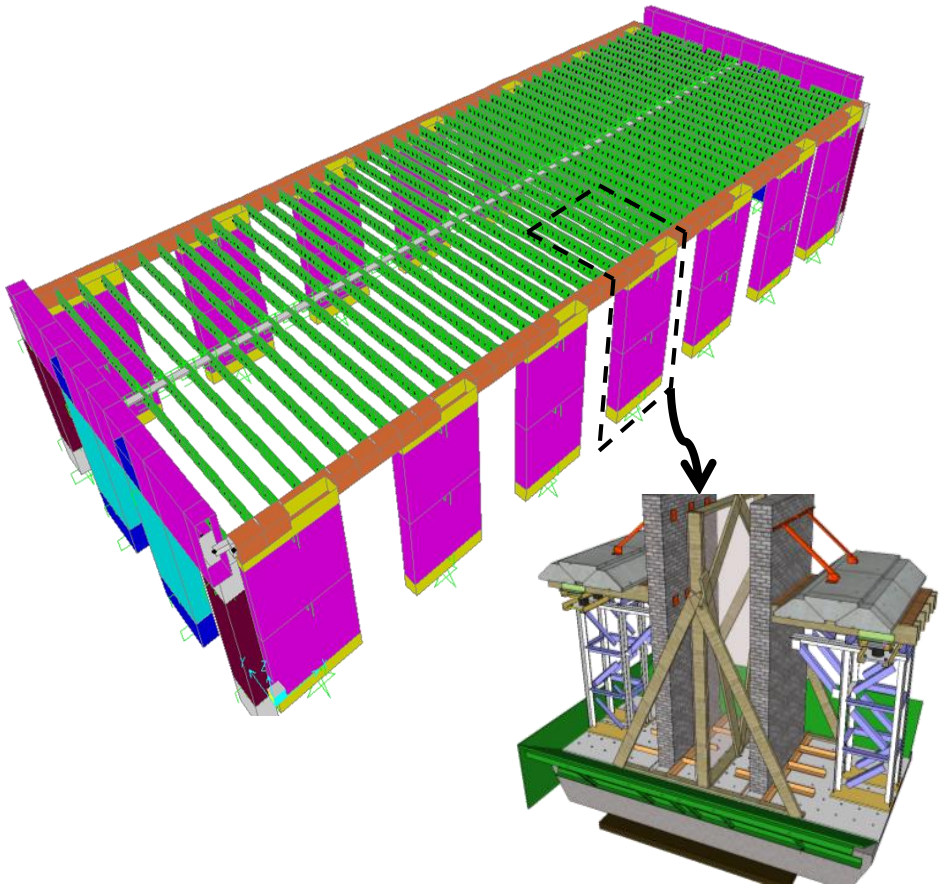

Figure 8-9 Prototype and specimen design concept

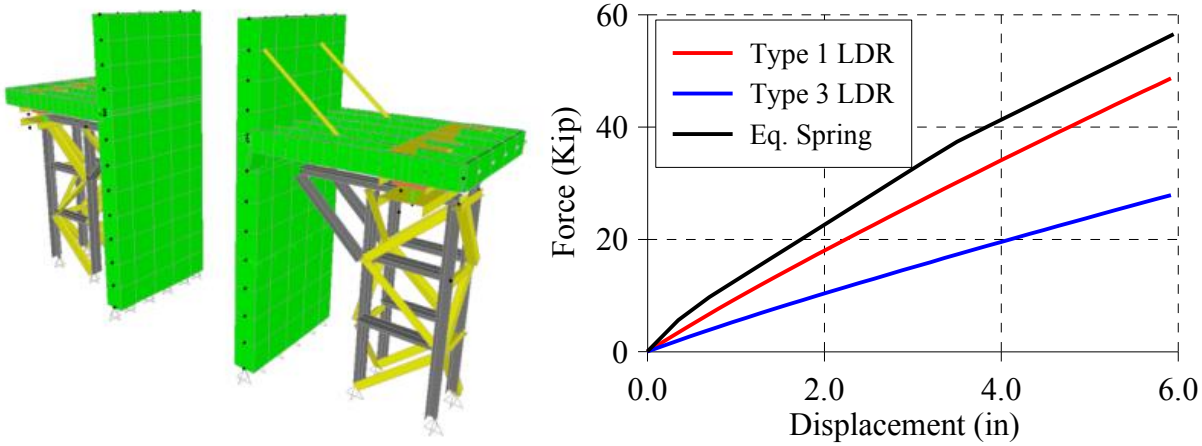

Figure 8-10 Actual numerical model of the laboratory specimen and force-displacement relationship required to simulate the diaphragm stiffness

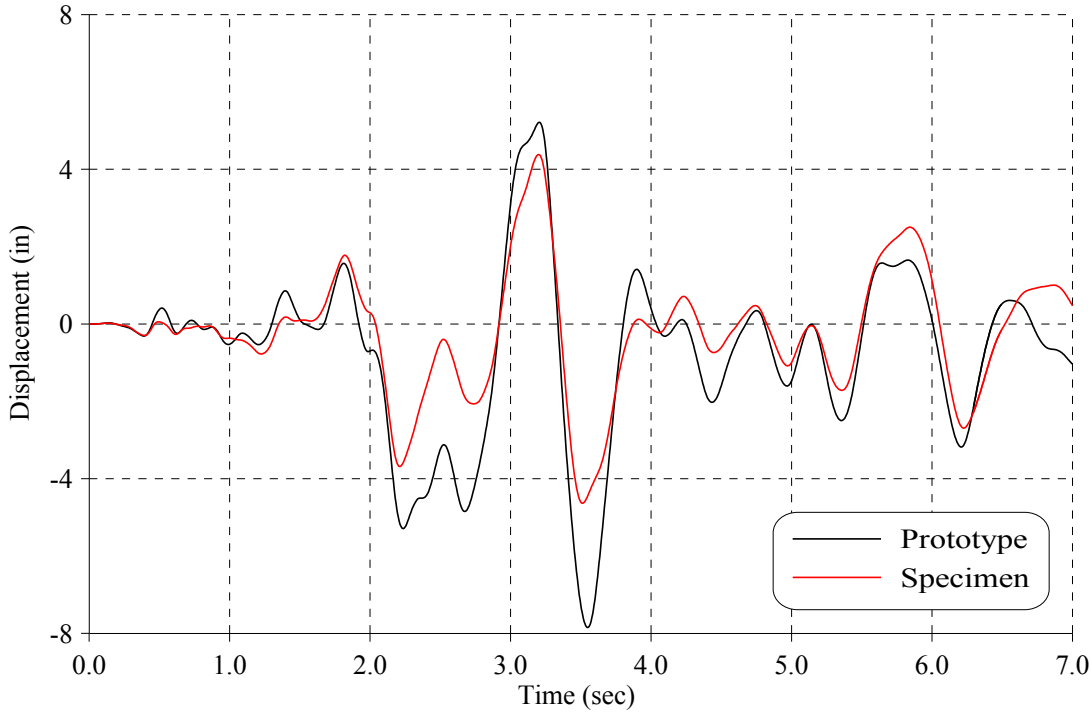

Figure 8-11 Response history displacement of one-story building prototype and specimen subjected to New Zealand earthquake

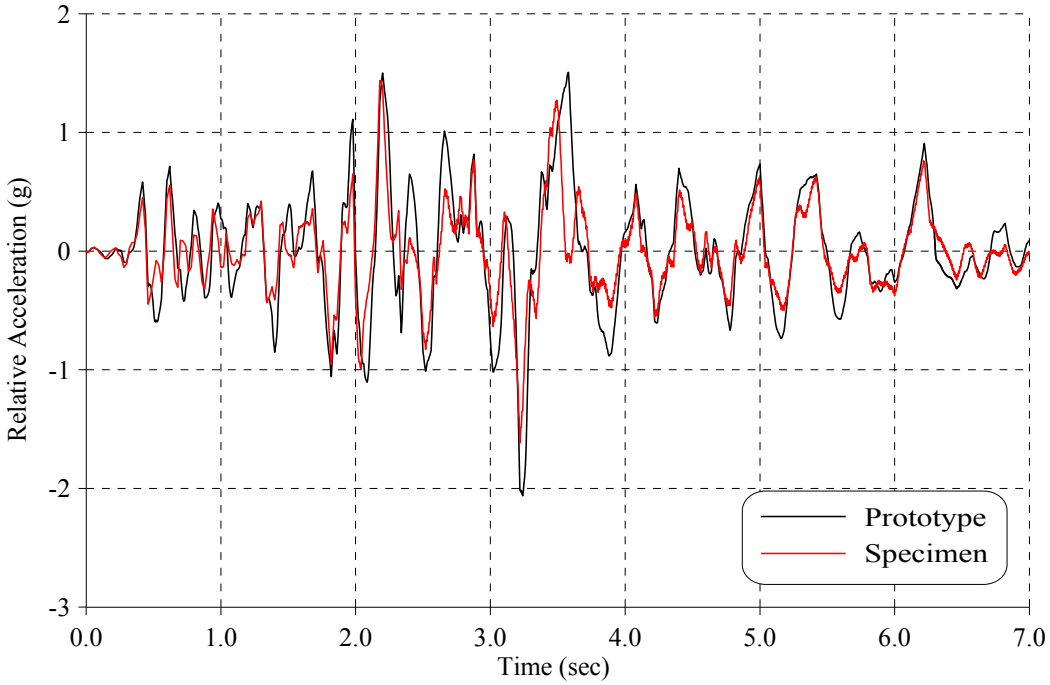

Figure 8-12 Response history acceleration of one-story building prototype and specimen subjected to New Zealand earthquake

8.3.3 Specimen Description

Wall specimens were selected to simulate a central portion of one-story URM buildings in NYC, as illustrated in in Figure 8-9. The two walls were tested simultaneously. The major difference between Wall 1 and Wall 2 is that retrofitted connections are implemented in Wall 2, where the parapet has been strengthened with steel braces and the wood joist-to-wall connection reinforced with steel anchors and plates, respectively. In both walls, the wood floor is supported by elastomeric bearings, which simulated the flexibility of the diaphragm. The rigid steel towers transferred the input acceleration from the base of the table to the top of the floor without significant amplification. This test was performed with additional mass placed on the diaphragm to provide a constant axial load on the walls, and with the application of a dynamic excitation in the shake table as described in the next section. Details of the wall configuration and structural components are provided below and illustrated in Figure 8-13 and Figure 8-14.

8.3.3.1 Steel towers

Two rigid steel towers were used to support the wood floors and transfer the input acceleration from the base of the table to the top of the diaphragm without significant amplification. The elastic stiffness of each frame was approximately 3000 kip/in as calculated using pushover analyses in SAP2000. Each frame had a total weight of 6 kips and a fundamental period of 0.1 seconds. Dimensions are illustrated in Figure 8-18.

8.3.3.2 Lead and low damping rubber bearings

Diaphragm flexibility was simulated using flexible low damping rubber (LDR) and stiff lead rubber bearings (LRB) isolators. Four LRB and four LDR were installed in Wall 1 and Wall 2, respectively. The isolators were bolted to the steel tower, as illustrated in Figure 8-19. The number and properties of the bearings were selected to match the initial stiffness of the wood diaphragm obtained through pushover analysis, as shown in Figure 8-10. The physical properties of the isolators were obtained from previous experimental studies (Sanchez-Ferreira 2011). Typical shear force versus displacement of the LDR and the LRB isolators are illustrated in Figure 8-15 and Figure 8-16, respectively. A photograph of the isolators is shown in Figure 8-17.

8.3.3.3 Wood floor

The wood floors were designed to support additional dead load and to provide a realistic connection between the masonry walls and the diaphragm. The dimensions were selected to match the width of the wall and to accommodate concrete blocks that provided additional floor mass. Each wood joist was placed at 16" inches, as typically specified in old URM buildings. All boards and joist were constructed of Douglas Fir material. Typical 8d nails were used to connect the wood boards and joists. "Fire cuts", as described in Section 3, were provided at each wood joist. Structural details of the wood floor are provided in Figure 8-19 and Figure 8-20. The wood diaphragms were constructed at the laboratory and then placed on top of each steel tower. The wood floors were bolted to steel angles, which in turn were welded to the base of each isolator.

8.3.3.4 Additional Concrete blocks

These pieces were intended to simulate the tributary dead load of the prototype. Three concrete blocks were placed on top of each wood floor. The average weight of each block was about 2 kip. The blocks were attached to the wood floors using standard 7/8" diameter bolts. The dimensions are illustrated in Figure 8-22 and the connection details between each block and the floor are shown in Figure 8-19.

8.3.3.5 Retrofitting options

Two standard retrofitting techniques were implemented in Wall 2. These techniques are recommended in FEMA P547 (2006) to prevent premature failure of parapets and URM walls subjected to out-of-plane loading. These procedures have a largely empirical base and have not been tested in a laboratory, to the knowledge of the authors.

The simplest way to prevent out-of-plane collapse of URM walls is to tie them to the floor using steel anchors, as recommended in Figure 8-19. A 6"x6"x1/4" steel plate is placed in one side of the anchors, whereas the other side is bolted to the wood joists. The next step to achieve Life Safety is to fix the parapets and the chimneys to the roof using steel braces, as shown in Figure 8-14. Structural details to incorporate those components in the specimen are presented in Figure 8-19, Figure 8-21 and Appendix D.

8.3.3.6 Masonry walls

Two identical full-scale masonry walls were constructed on a shake table. The dimensions of the walls were approximately 6 feet in width, 14 feet in height and 1 foot thick. Similar dimensions have been used by Meisl et al. (2007) and Penner and Elwood (2012) in testing of out-of-plane URM walls. Data obtained from material identification tests previously conducted has been considered in selecting the properties of brick and mortar for the walls. Reclaimed bricks were laid out using an American Bond pattern. The mortar proportions were target to match a Type K mortar (1:3:10), but to improve workability during construction, a slightly stronger mortar was used. An adjustable steel base restraint was placed at the bottom of each wall, to prevent sliding but to allow free rotation. Figure 8-23 shows a plan view and elevation of the masonry wall.

8.3.3.7 Safety frame and plates

A safety frame was built in the middle of the shake table to prevent one wall from damaging the other, in case of premature collapse. The frame was designed to resist the maximum impact load that could be generated by the mass of the wall if sliding out the joist pockets. Steel plates were placed around the shake table to prevent falling bricks from posing a hazard to the table actuators and pumping system. The dimensions of the safety frame and plate are specified in Figure 8-24.

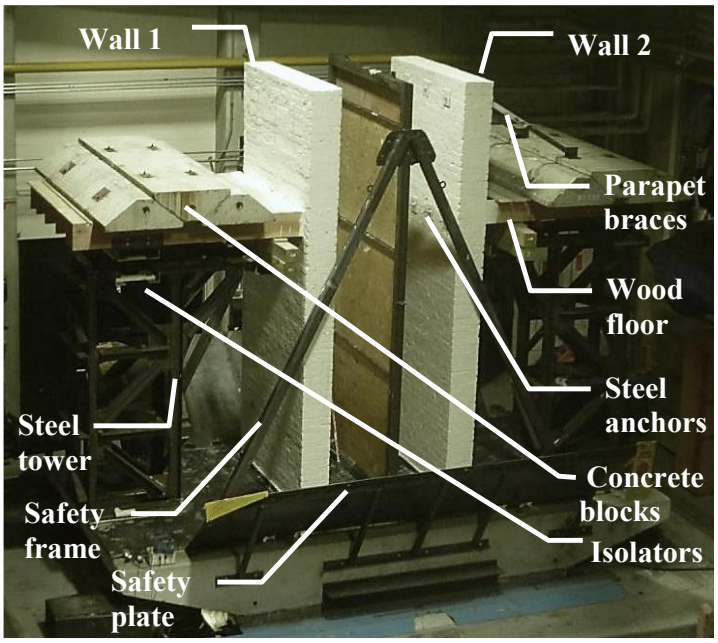

Figure 8-13 Actual test setup

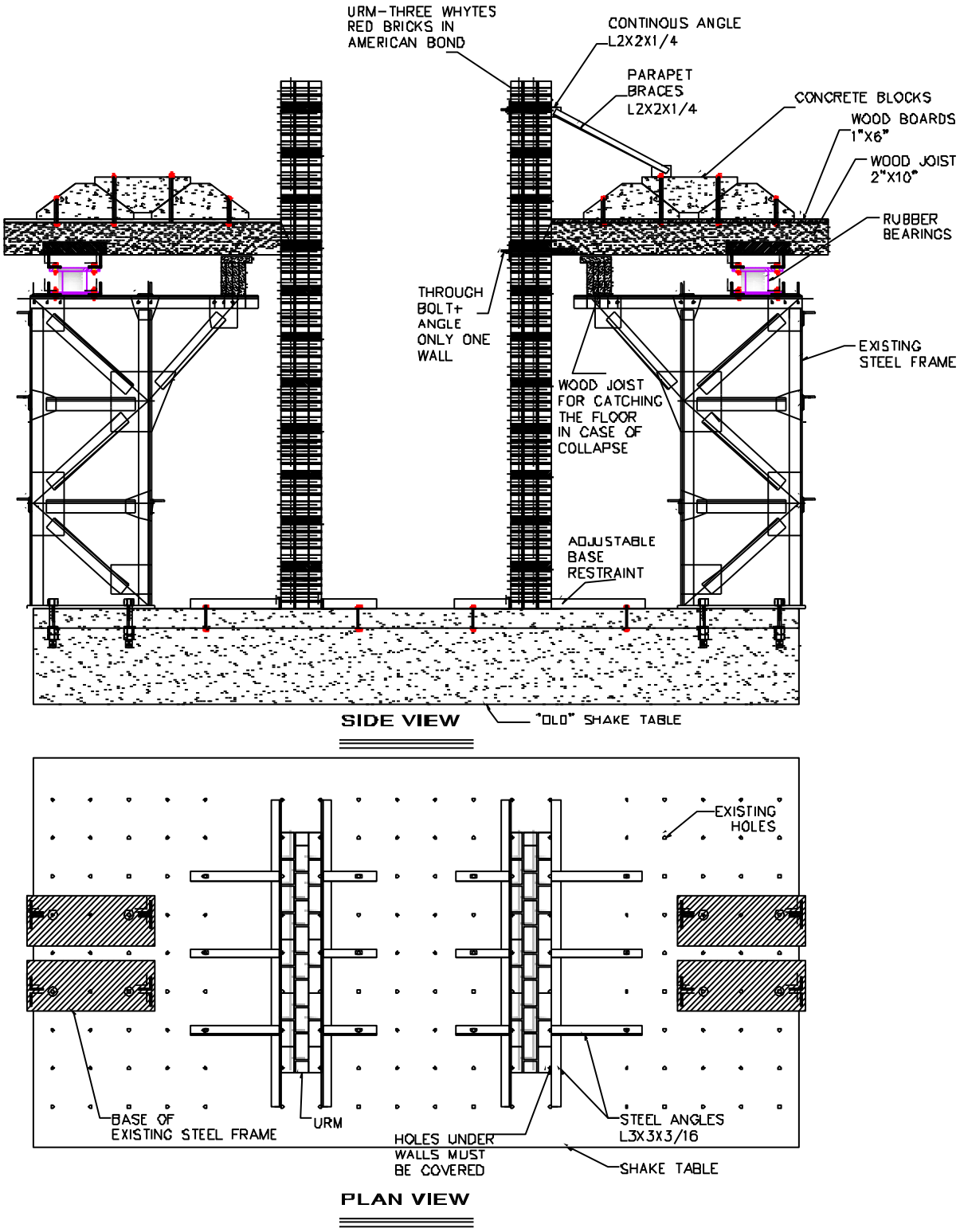

Figure 8-14 Structural plan view and elevation of test setup

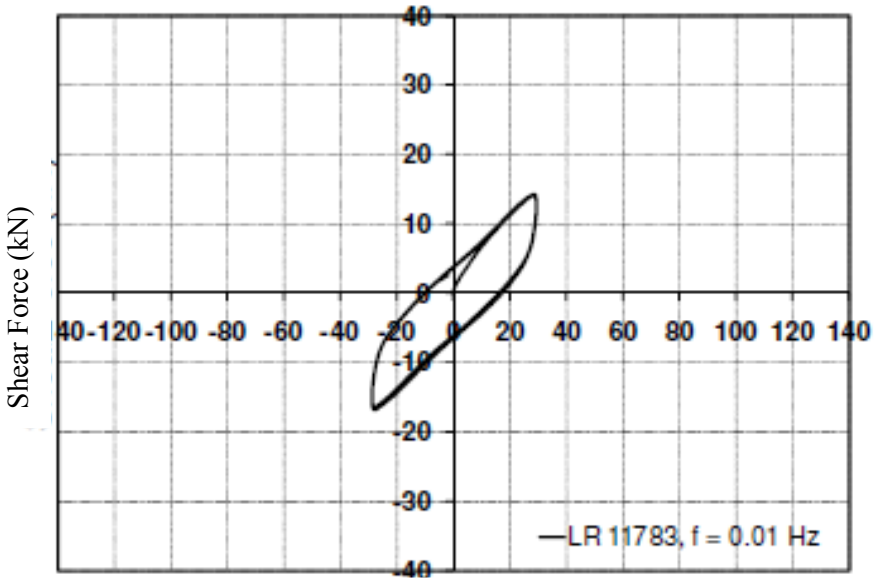

Test 2, f=0.01 Hz, γ=50%

Figure 8-15 Typical force-displacement curve of lead rubber bearings used in this study (Sanchez-Ferreira 2011)

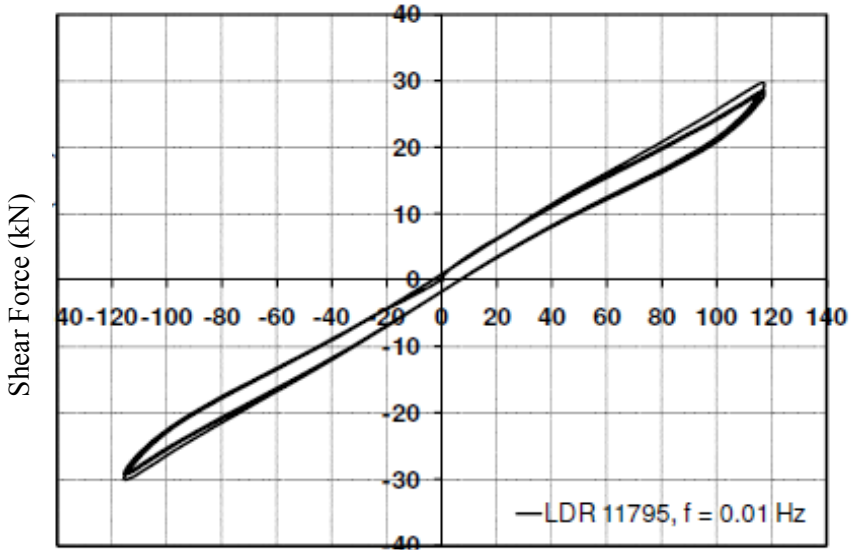

Figure 8-16 Typical force-displacement curve of low damping rubbers used in this study (Sanchez-Ferreira 2011)

Figure 8-17 Isolators used in the experiment

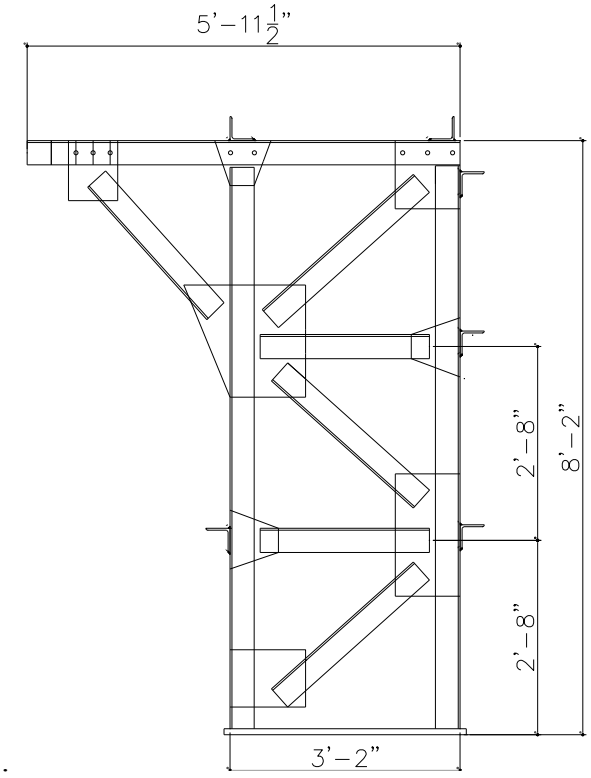

Figure 8-18 Structural elevation and dimensions of steel tower

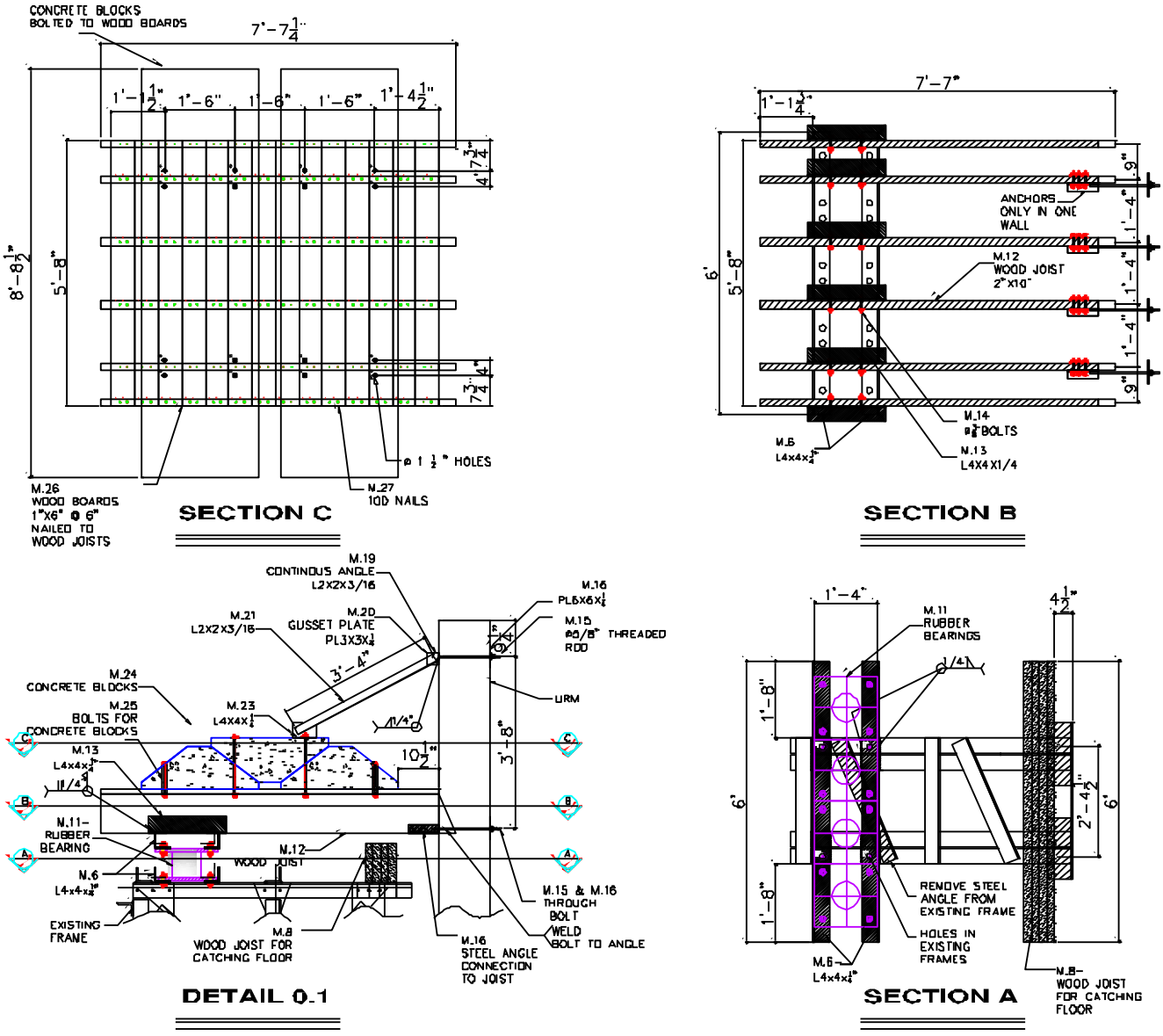

Figure 8-19 Structural plan view, elevation and dimensions of wood floor

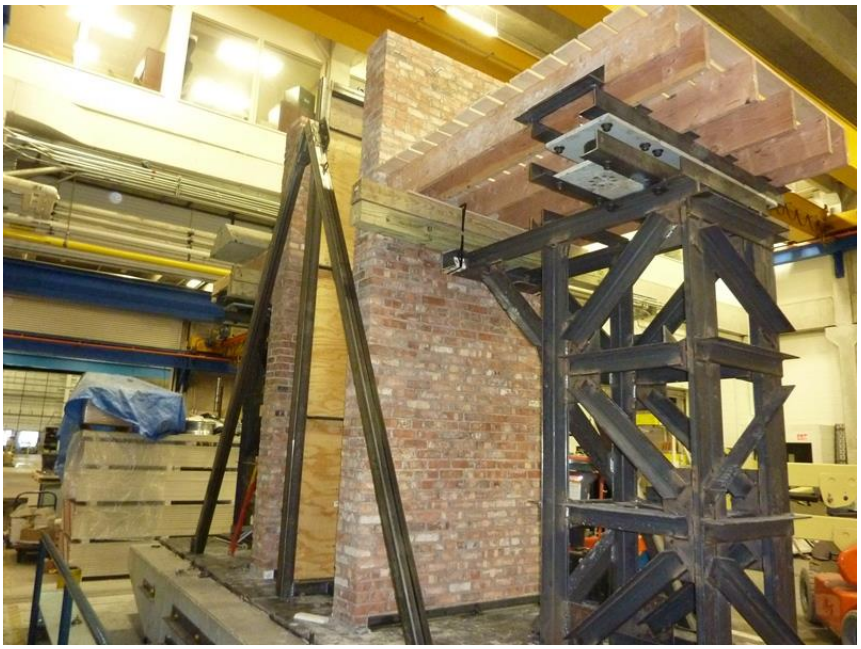

Figure 8-20 Steel tower, isolator and wood floors

Figure 8-21 Steel anchors installed in Wall 2

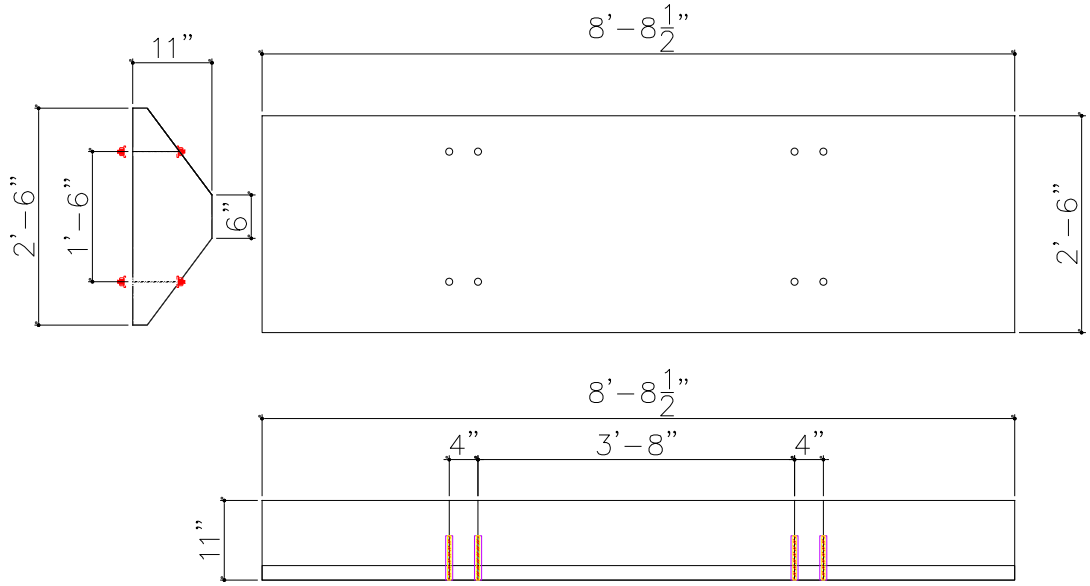

Figure 8-22 Structural plan view and elevation of concrete blocks

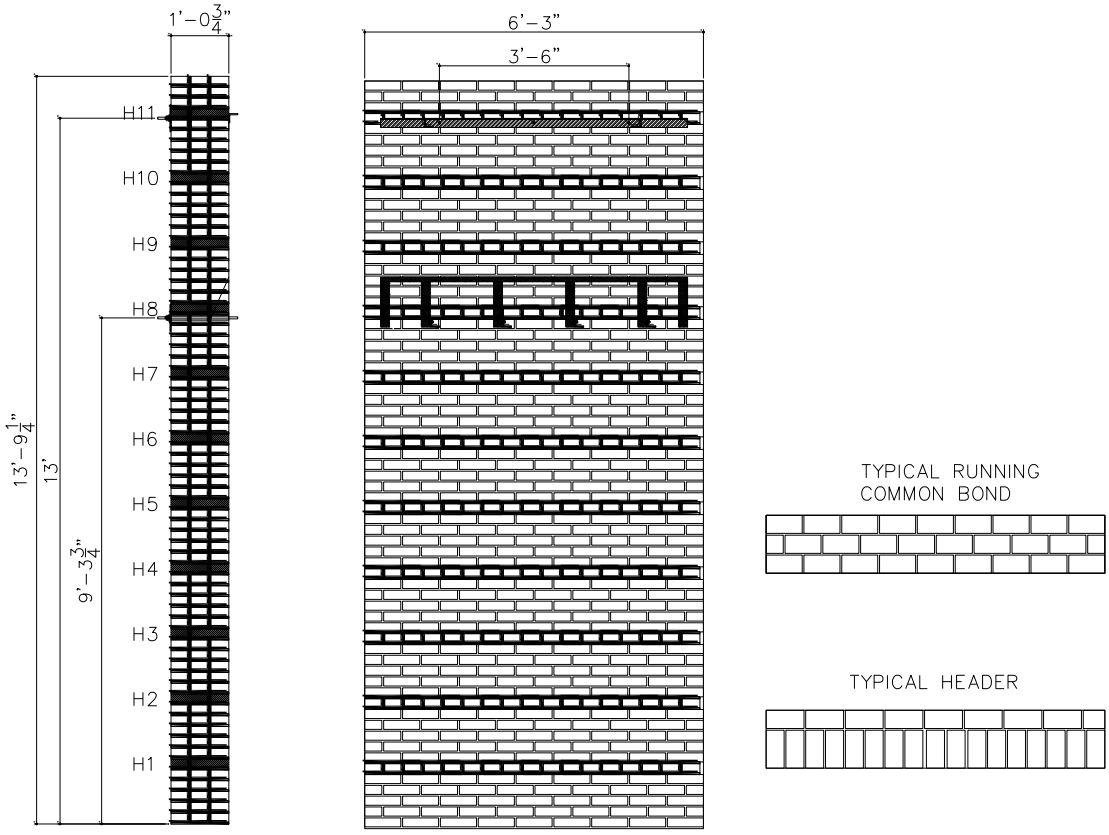

Figure 8-23 Structural plan view and elevation of masonry wall

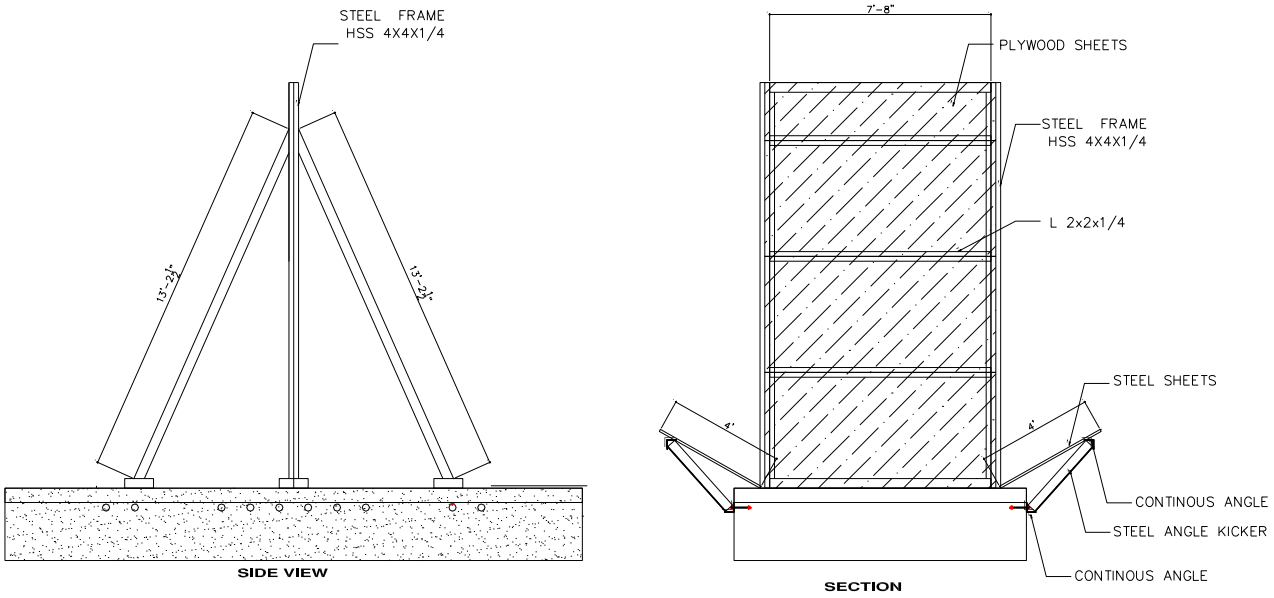

Figure 8-24 Structural elevation of safety frame and plates around the table

8.3.4 Specimen Construction

Professional masons constructed the masonry specimens on top of the shake table. Figure 8-25 illustrates the construction sequence of the test setup. The process started by placing the steel towers on the table. Then, several members were removed from the top of the tower to allow space for the base of the isolators. Once the isolator base was welded to the tower, lead rubber bearing were installed and bolted to one tower and low damping rubbers were installed on the other one. Steel angles were bolted on the top of the bearings to provide support for the wood floor. Then, masonry walls were constructed up to the level of the bearings. This was required so that the wood floors could be installed on the tower and properly placed on the walls. Afterwards, the masons continued the construction of the wall parapet. Wood boards were nailed thereafter.

After 28 days, the concrete blocks providing dead load were placed on the wood floors and steel anchors and braces were added to Wall 2 as a retrofit strategy. Also, at this time steel angles were bolted along the base both walls to limit sliding. Finally, safety frames and plates were constructed and placed on the table. The walls were tested after 69 days of the initial construction date. Several stages of the construction can be seen in Figure 8-26 to Figure 8-29.

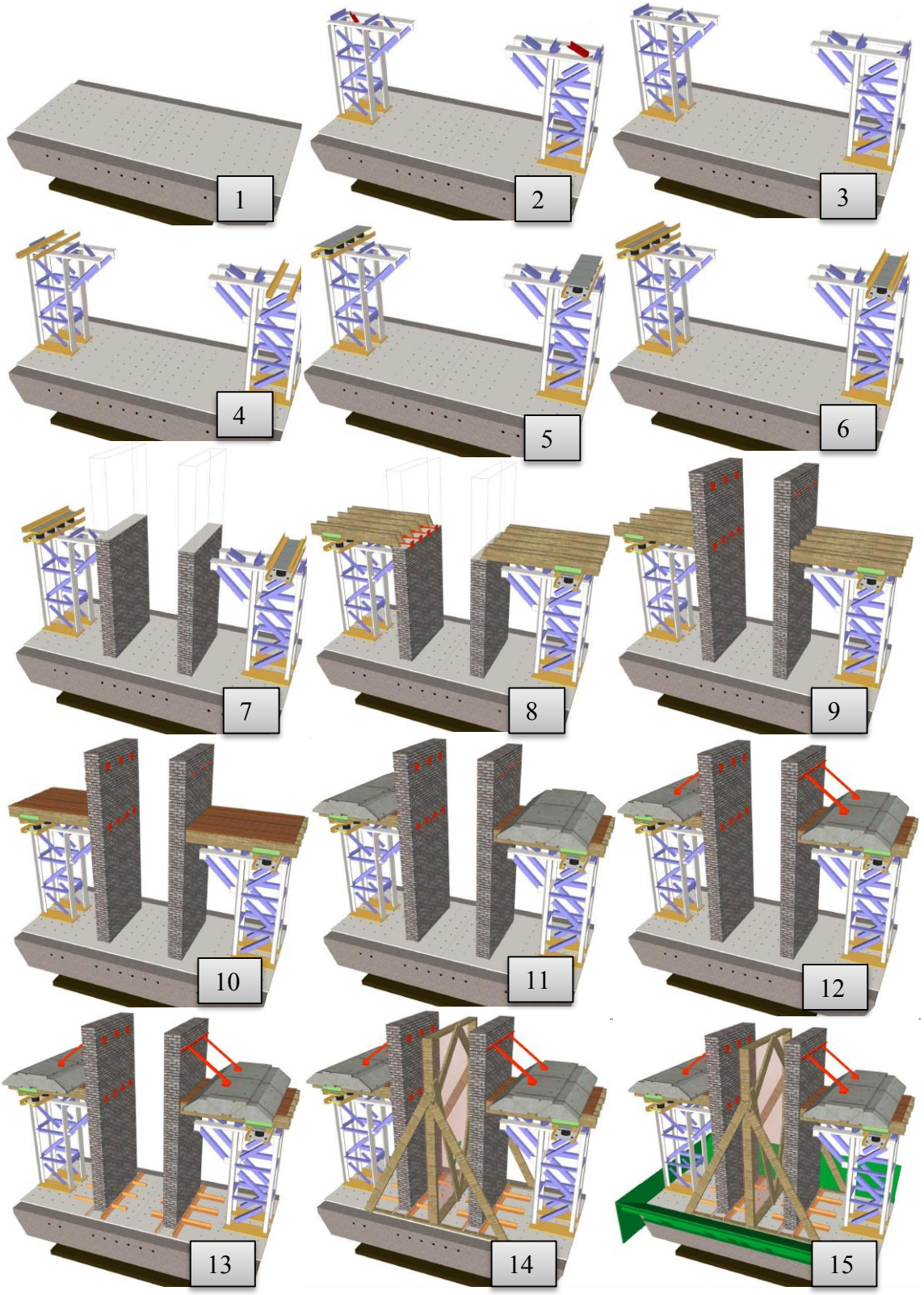

Figure 8-25 Construction sequence of the test set up

Figure 8-26 Construction of first header of Wall 1 (Beginning of stage 7)

Figure 8-27 Construction of parapet of Wall 1 (stage 8-9)

Figure 8-28 Wall 1 and Wall 2 specimens ready to support concrete blocks (stage 10)

Figure 8-29 Installation of concrete blocks

8.3.5 Material Properties

Typical compressive tests on five masonry prisms, five brick units and nine mortar cubes were conducted to obtain the material properties of the tested URM walls. All specimens were obtained during the construction of the walls and kept in a storage area until the material test would be conducted. All tests were conducted according to ASTM standards. Dimensions of prisms, brick units, mortar cubes and loading system and instrumentation were similar to that deployed for new specimens as described in Section 6. All tests were conducted after 150 days of casting.

Figure 8-30 and Figure 8-31 present the stress-strain curve for each type of specimen. The mortar strength was higher than recommended, closer to Type O mortar. However, the overall stiffness of the prisms remained closer to those specimens previously tested with Type K mortar. The shear strength was not tested, since previous tests showed that the friction coefficient is insensitive to mortar quality and aging.

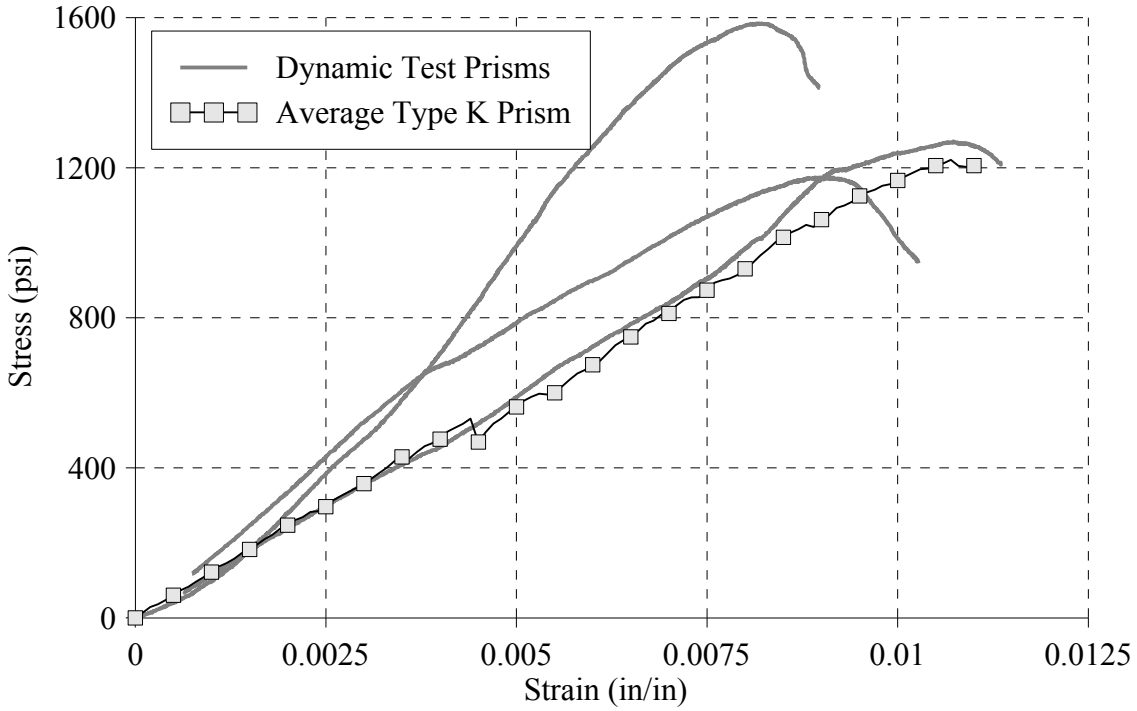

Figure 8-30 Average properties of masonry prisms

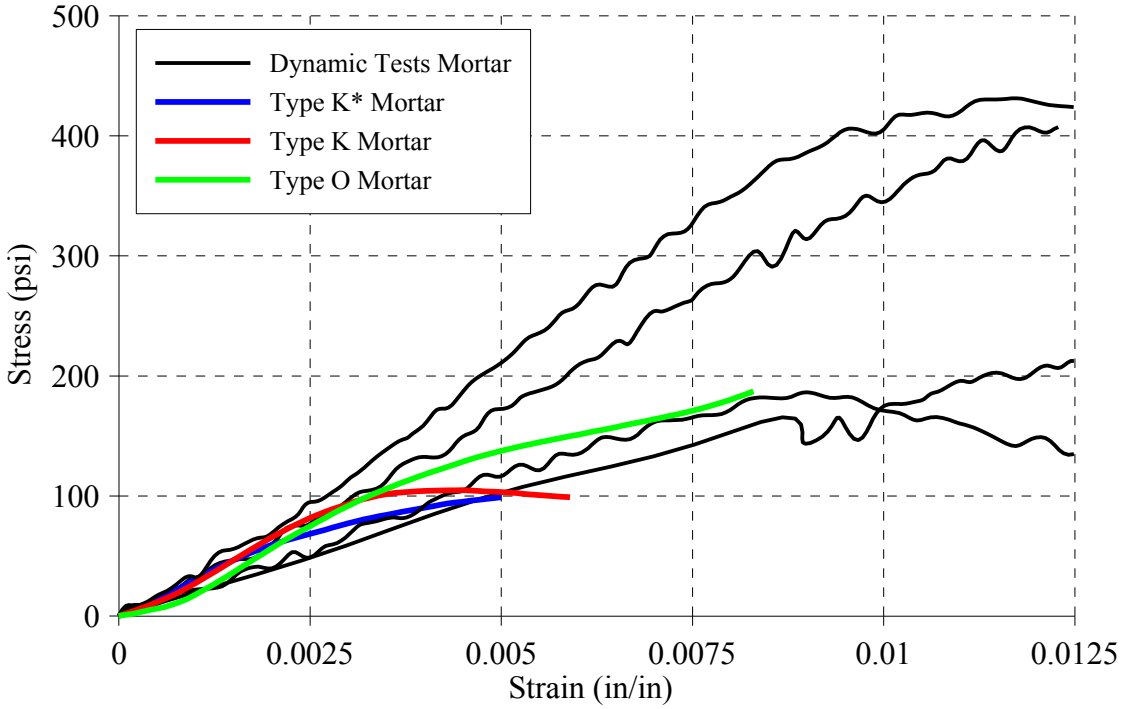

Figure 8-31 Average properties of masonry mortar

8.3.6 Instrumentation/Data Acquisition/Archiving

Loading to both walls specimen was applied simultaneously by the shake table at SEESL. This shake table has five-degree-of-freedom and a payload capacity of about 40 tons. The useful range of frequency is between 0 to 50 Hz. Dimensions of the table including its concrete testing platform are 12'x 20'. Additional technical information about the table can be found in the SEESL technical manual.

The instrumentation array deployed for the shake table testing consisted of 8 string potentiometers, 19 temposonics, 25 accelerometers, 6 strain gauges and 8 video cameras. All sensors were sampled at 256 readings per seconds. It was found that 6 displacement transducer and 5 accelerometers did not work properly during the test. Due to time constraints, it was not possible to fix or replace them. The location, direction and type of instrument are listed in Table 8-2 and also illustrated in Figure 8-32 through Figure 8-37**.**

Two types of instruments were used to measure displacements, namely string potentiometers and temposonics. String potentiometers were used to measure absolute displacement of the table, tower, isolators and concrete blocks in the shaking direction. Temposonics were used to measure

the relative displacement between the steel tower and the masonry walls, and to measure the absolute displacements of the parapets.

Accelerometers were installed in the shake table, steel tower, concrete blocks and along the height of the wall. The horizontal shaking acceleration was the main direction of measurements; however, two accelerometers were deployed in the extremes of the table to measure vertical excitation and record potential rocking. Strain gauges were used to measure the force in the steel anchors and steel braces. The location and number of strain gauges is illustrated in Figure 8-37.

Also, video cameras were installed in the steel towers, the shake table and at distance from the table to obtain a general view of the experiment.

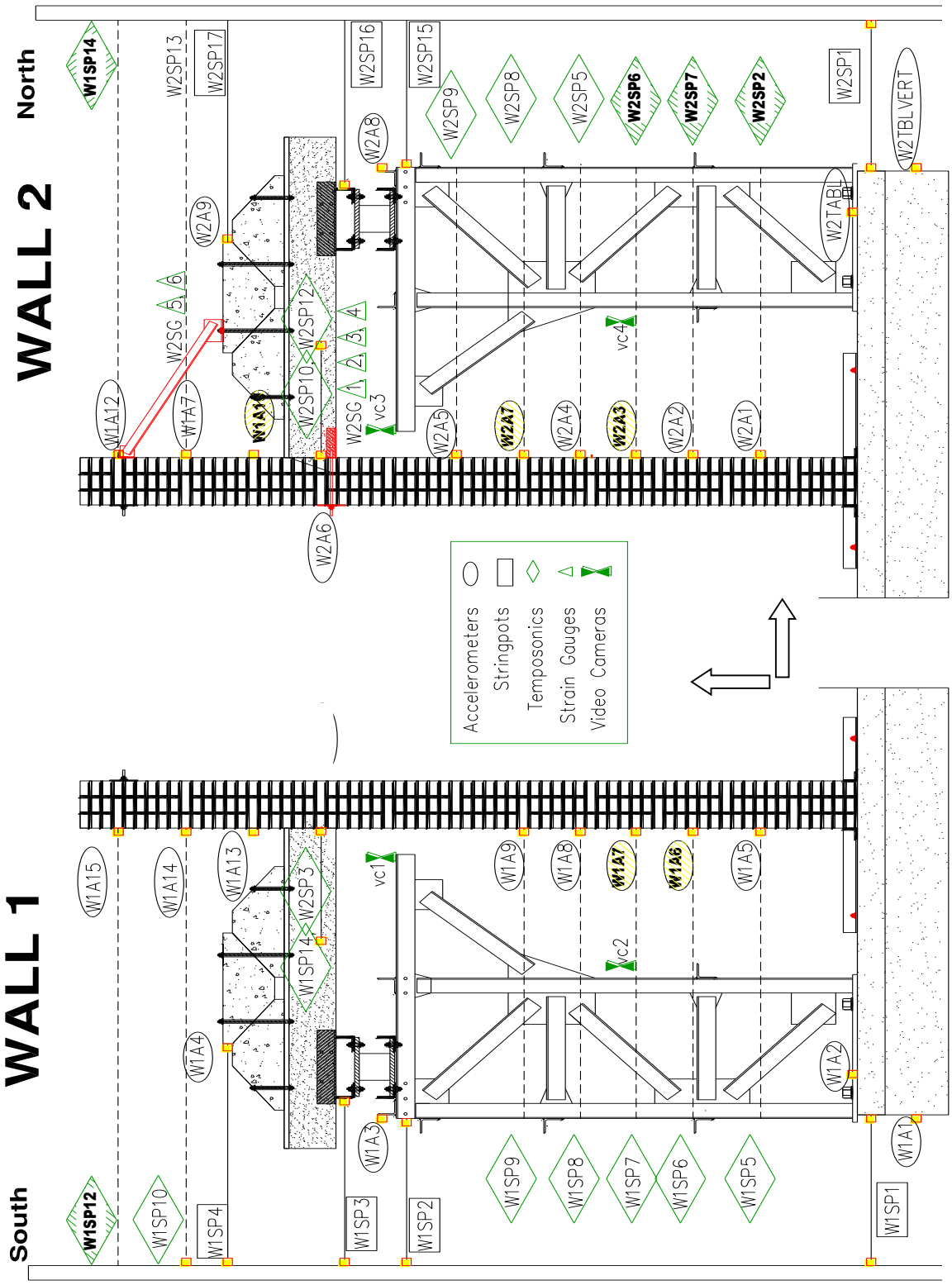

Figure 8-32 Location of instruments on the wall, steel tower and shake table

Figure 8-33 String potentiometers installed on a fixed reference frame off the shake table

Figure 8-34 Accelerometers installed at the top of the tower

Figure 8-35 Temposonics installed in the tower

Figure 8-36 Accelerometers, temposonics and video cameras

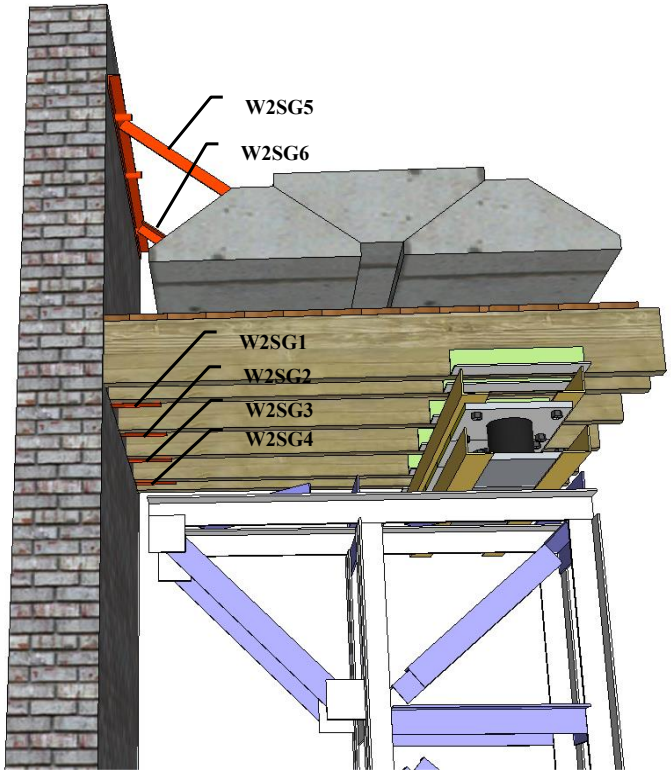

Figure 8-37 Location of strain gauges at WALL 2

Table 8-2 List of instruments installed in Wall 1 and Wall 2 to measure displacements and accelerations.

Location	Direction	Wall 1		Wall 2	
		Displacement Transducer	Accelerometer	Displacement Transducer	Accelerometer
Shake table	Z		W1A1		W2tblver
	X	W1SP1[a]	W1A2	W2SP1[a]	W2TAB
Top of tower	X	W1SP2[a]	W1A3	W2SP15[a]	W2A8
Isolator	X	W1SP3[a]		W2SP16[a]	
Wood floor	X	W1SP4[a]	W1A4	W2SP17[a]	W2A9
Wall	X	W1SP5	W1A5	W2SP2[b]	W2A1
	X	W1SP6	W1A6[b]	W2SP7[b]	W2A2
	X	W1SP7	W1A7[b]	W2SP6[b]	W2A3[b]
	X	W1SP8	W1A8	W2SP5	W2A4
	X	W1SP9	W1A9	W2SP8	W2A7[b]
	X			W2SP9	W2A5
Parapet	X		W1A13		W1A10[b]
	X	W1SP10	W1A14	W2SP13	W1A7
	X	W1SP12[b]	W1A15	W2SP14[b]	W1A12
Connection	X	W1SP14		W2SP10	
	X	W2SP3[b]		W2SP12	

[a] String potentiometers

[b] Instrument did not work during the experiment.

Table 8-3 List of strain gauges installed in Wall 2

Location	Direction	Strain Gauge
Steel anchors	X	W2SG1
	X	W2SG2
	X	W2SG3
	X	W2SG4
Steel braces	X	W2SG5
	X	W2SG6

8.4 Test Procedures

8.4.1 Ground Motion Inputs

Two ground motions were used as input to the shake table, with one motion selected for its high frequency content and the other for its low frequency content. The short-period motion selected was recorded during the 23 August 2011 earthquake in Virginia, USA. It was recorded at the Reston station. The long-period motion selected was recorded during the 21 February 2011 earthquake in Christchurch, New Zealand. It was recorded at the Hospital Station. Acceleration time series and response spectra of the two motions are shown in Figure 8-38, Figure 8-39 and Figure 8-40, respectively.

8.4.2 Seismic Hazard Levels

The ground motions were scaled up or down to match the MCE Response Spectrum for a site Class A located in New York City (coordinates 40.7724,-73.9670). The Design Spectrum was obtained using the Hazard Tool provided at the USGS website (USGS 2012). Figure 8-41 shows the resultant Design Response Spectrum and the MCE Response Spectrum.

8.4.3 Test Protocol

The specimens were subjected to an increasing intensity sequence of nine dynamic tests until collapse. The loading protocol was designed to gradually introduce damage in the specimens. Only one component of each ground motion was applied in the X-direction (i.e South-North direction). White-noise excitation with acceleration amplitude of 0.03g was applied first to the specimen to identify its dynamic properties. The testing sequence listed in Table 8-4 was followed thereafter. Note that for the Virginia Earthquake, the actual PGAs obtained during the tests were significant smaller than the target PGA.

Figure 8-42 shows the response spectrum of Virginia Earthquake scaled to match MCE in NYC. Figure 8-43 shows the response spectrum of New Zealand Earthquake also scaled to match MCE of NYC. Ground motions were amplitude scaled to match the spectral acceleration at the fundamental period of the specimen, T_1=0.22 seconds.

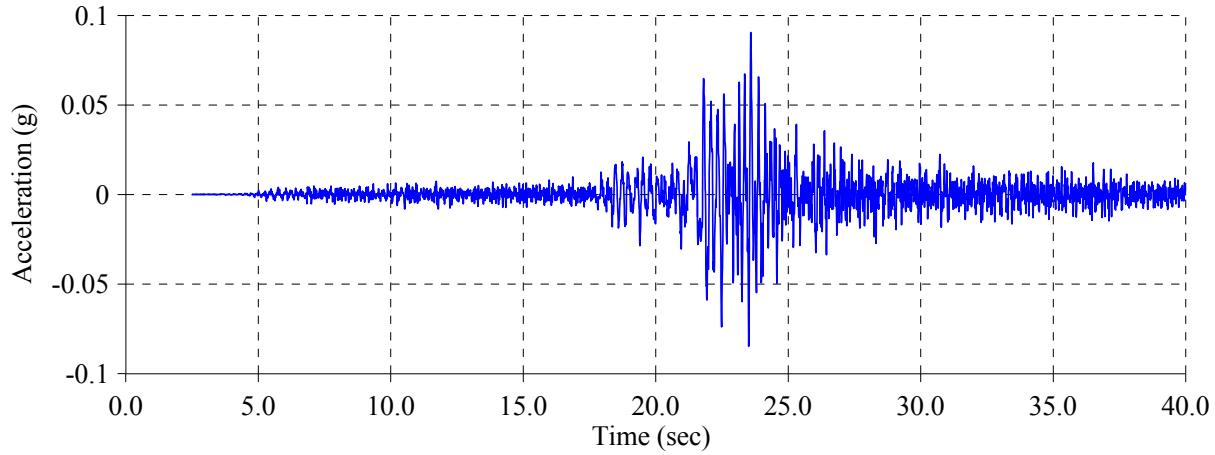

Figure 8-38 Acceleration-time series of Virginia Earthquake of 23 August 2011 recorded at Reston Station

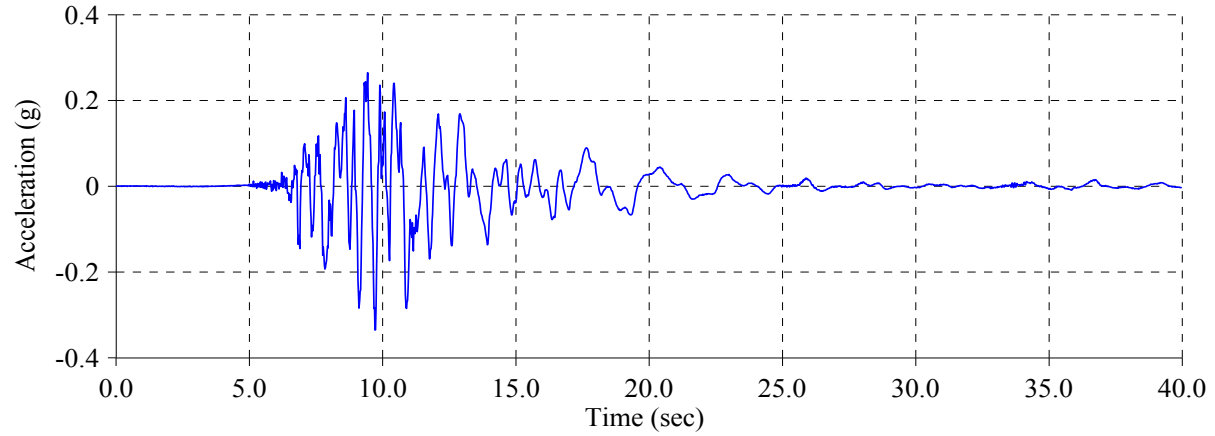

Figure 8-39 Acceleration-time series of New Zealand Earthquake of 23 August 2011 recorded at Hospital Station.

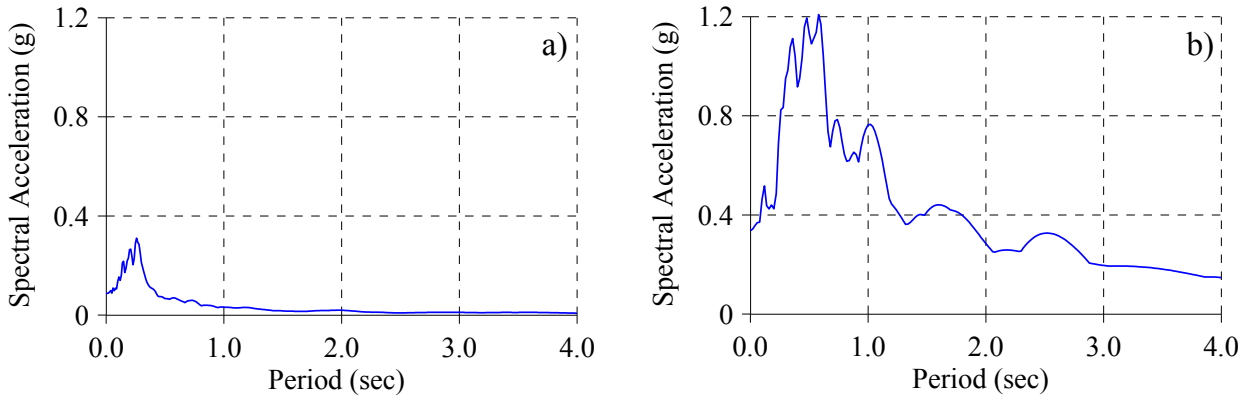

Figure 8-40 Response spectrum of a) Virginia and b) New Zealand earthquake, 5% damping

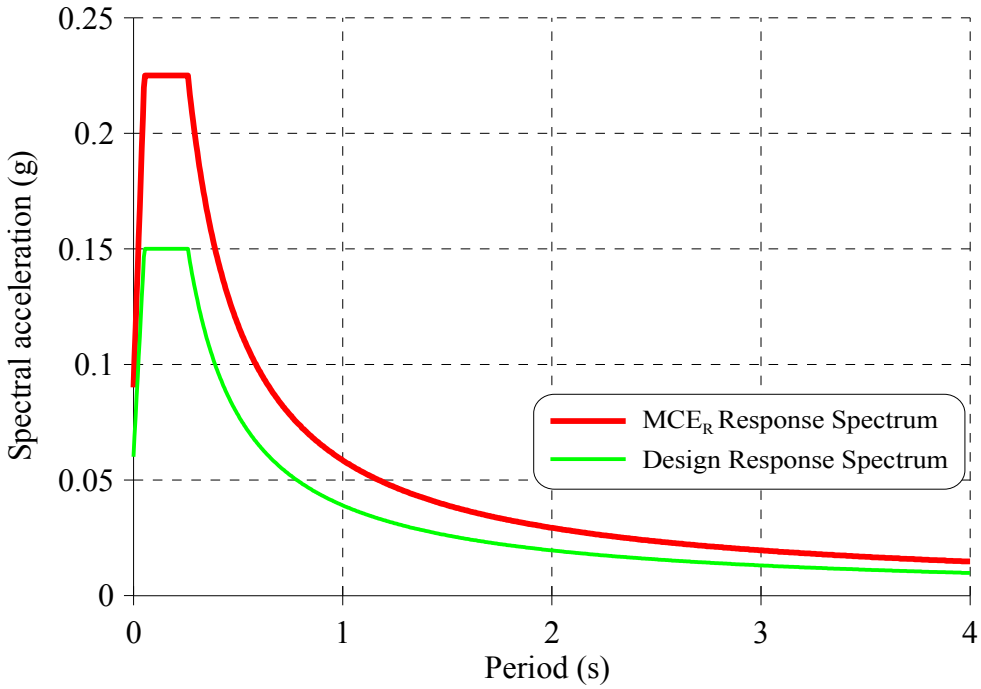

Figure 8-41 Target response spectrum

Table 8-4 Test Sequence followed for two-wall specimen

Earthquake/Input	Test No.	PGA (g)	Scale factor	Target hazard level
White noise	1	0.03	n/a	n/a
Virginia_Reston (Mw=5.8, R=124.1 km)	2	0.033	30%	Service Level
	3	0.11	100%	MCE Spectrum
	4	0.16	150%	1.5 MCE Spectrum
	5	0.22	200%	2 MCE Spectrum
	6	0.32	300%	3 MCE Spectrum
NZ_Hospital (Mw=6.3, R=10 km)	7	0.18	50%	MCE Spectrum
	8	0.27	75%	1.5 MCE Spectrum
	9	0.365	100%	2 MCE Spectrum

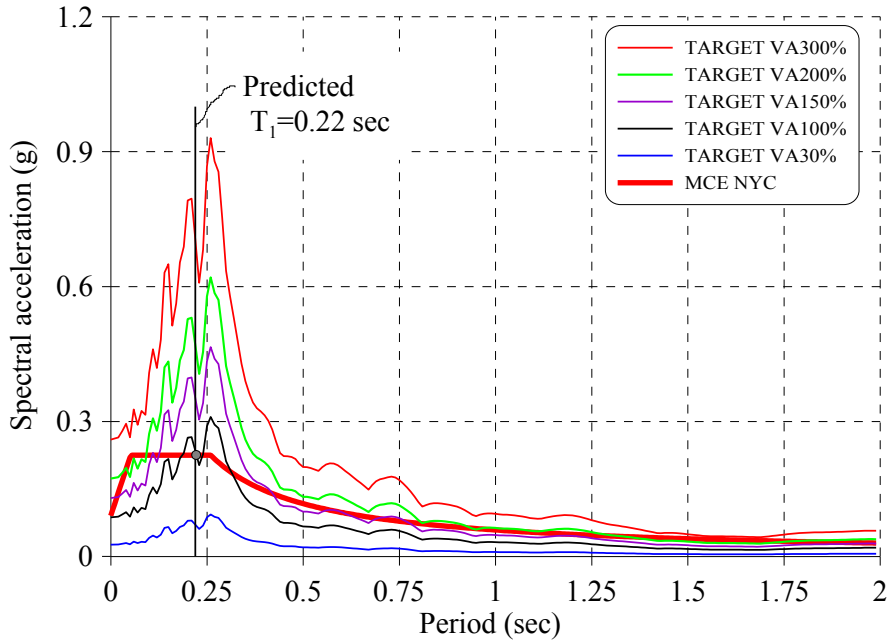

Figure 8-42 Response spectrum of Virginia Earthquake scaled to match MCE in New York City

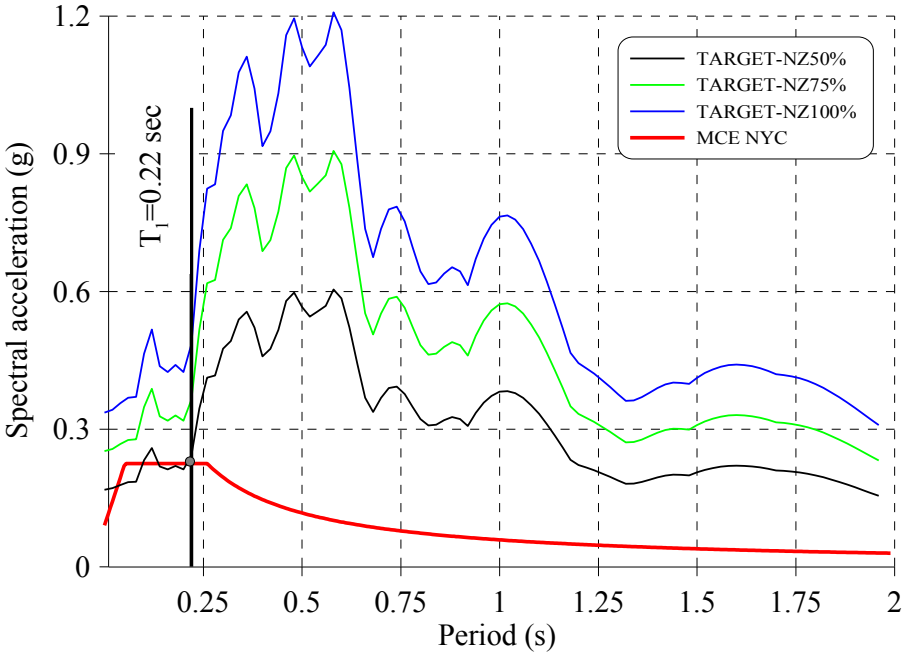

Figure 8-43 Response spectrum of New Zealand Earthquake scaled to match MCE of New York City

8.5 Test Results

Test results are presented and discussed in this this section. The fidelity of the shake table in reproducing the desired input motions and white-noise test results for system identification are first discussed. Then, the results of the shake table test of Wall 1 and Wall 2 for the Virginia earthquake are presented. Peak displacements and accelerations are included, as well as the hysteretic behavior of isolators, parapets and masonry walls. A comparison of the response of both walls is also studied. The last section presents results of the shake table test of Wall1 and Wall 2 for the New Zealand earthquake. Again, peak responses and hysteretic behavior of main components are discussed. Finally a comparison of the response of the walls for the same PGA but different input motion is investigated.

8.5.1 Shake Table Fidelity

Typically for a shake table test, the table is initially calibrated for the approximate payload expected during testing. Due to time constraints, it was not possible to properly calibrate the shake table before testing nor was it possible to implement low level calibrations once the specimens were constructed to the sensitivity of the masonry. As a result, the target spectrum was not achieved for the Virginia Earthquake, as seen in Figure 8-44. These test results were used to recalibrate the table and in the case of New Zealand earthquake, the table performed appropriately and no adjusted scale factors were needed. Table 8-5 lists the nominal and actual spectral acceleration at the fundamental period of the specimens achieved during the test. For convenience, all subsequent results of the testing program are referred using the nominal scale factor presented in Table 8-4.

Note that these mismatches do not affect the test results, as the main goal is to use them to validate numerical models. The acceleration recorded on the table was used in subsequent analysis and simulations.

Table 8-5 Target and actual spectral acceleration at the fundamental period obtained during shake table tests

Earthquake/Input	Test No.	Target Sa_{T1} (g)	Actual Sa_{T1} (g)
White noise	1	0.03	0.03
Virginia_Reston (Mw=5.8, R=124.1 km)	2	0.09	0.03
	3	0.31	0.14
	4	0.46	0.24
	5	0.62	0.40
	6	0.93	0.91
NZ_Hospital (Mw=6.3, R=10 km)	7	0.18	0.20
	8	0.27	0.26
	9	0.36	0.36

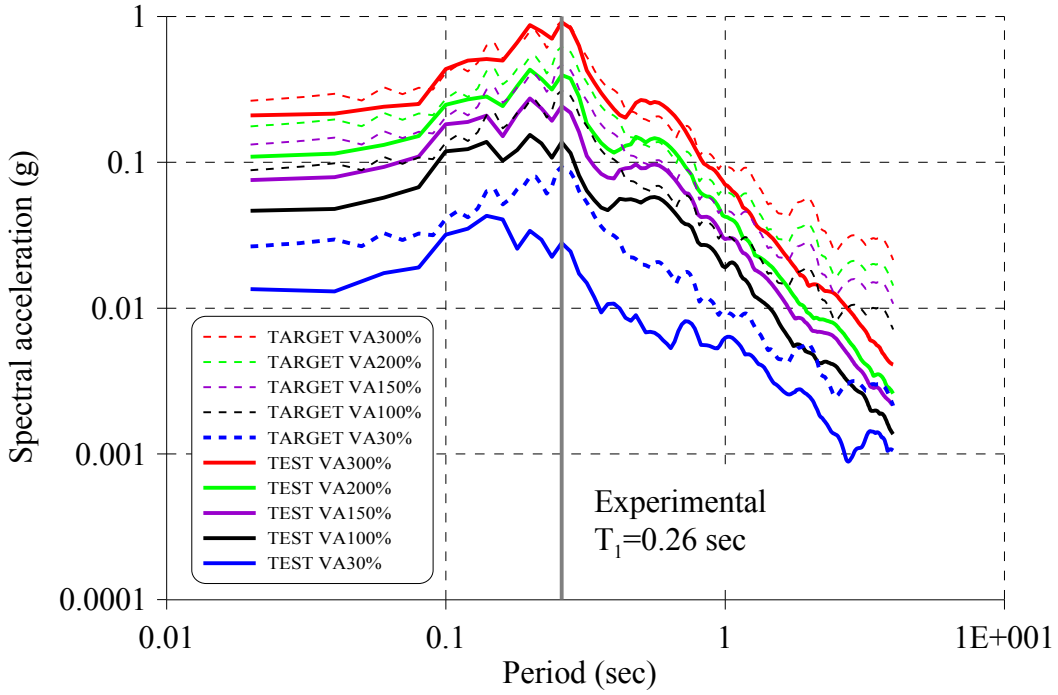

Figure 8-44 Target vs. actual response spectrum of Virginia earthquake

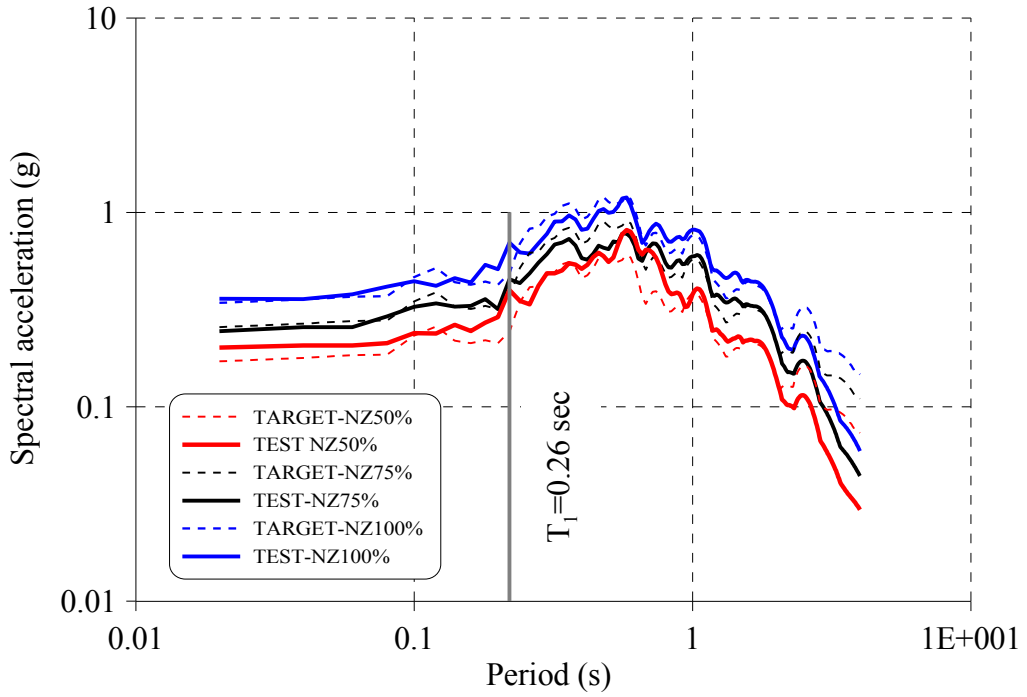

Figure 8-45 Target vs. actual response spectrum of New Zealand earthquake

8.5.2 White Noise Test Results

The main goal of the white noise test was to determine the undamaged modal properties of the wall specimens at the beginning of the seismic test program. The modal properties of interests included the natural frequencies and mode shapes. No additional white noise tests were conducted since a highly nonlinear behavior was anticipated for the selected levels of seismic excitation (e.g. the walls were expected to suffer significant damage or even collapse at very early stages of the testing program).

The process of identifying modal shapes and frequencies is conducted by obtaining the transfer function in frequency domain of acceleration time histories recorded during the white-noise test at locations indicated in Figure 8-46, over acceleration signals recorded on the shake table. The transfer function of output accelerations over input acceleration is calculated using the equations defined by Bracci et al. (1992).

All signals recorded during the white noise experiments were filtered by a zero-phase low-pass filter with a cutoff frequency of 40 Hz.

These fundamental frequencies are for the entire system, including the steel towers, wood floors and masonry walls. Other variables that could affect the results, such as oil column resonance effects in the shake table actuators, noise in the accelerometers due to electric current were not considered in this study. Also, it was assumed that the inputs are pure white noise and no table-structure interaction was considered during the test.

Figure 8-48, Figure 8-49, Figure 8-50 and Figure 8-51 show the transfer function amplitude for tower, wood floor and masonry of Wall 2 and Wall 1. The first mode was found to be around 3.80 Hz, related to the flexibility of the isolator, as shown in Figure 8-46. The second mode was approximately 19 Hz and it is mainly due to the rigid body rotation of the tower. A summary of the frequencies is listed in Table 8-6.

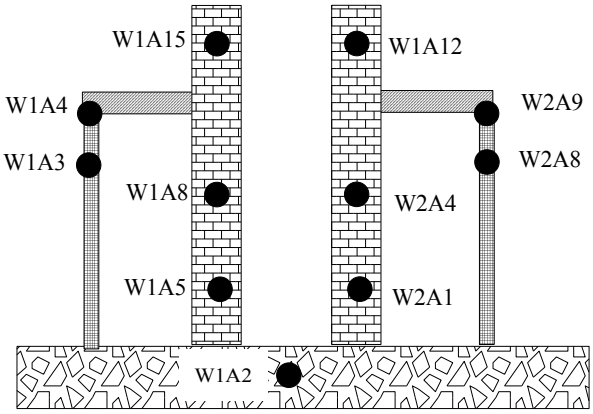

Figure 8-46 Location of accelerometers used for system identification and first mode shape

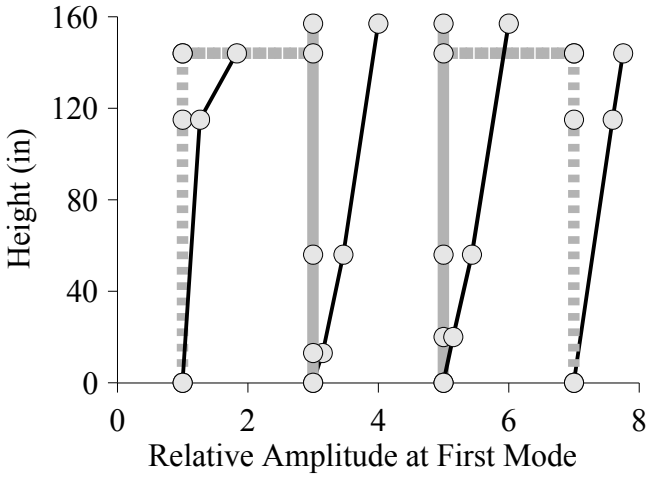

Figure 8-47 First mode shape of the walls

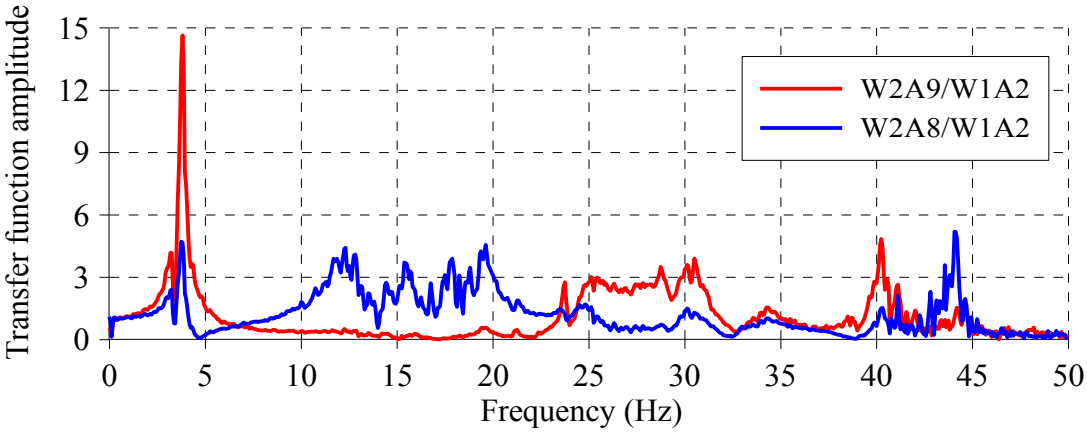

Figure 8-48 Amplitude of transfer functions for tower and wood floor of Wall 2

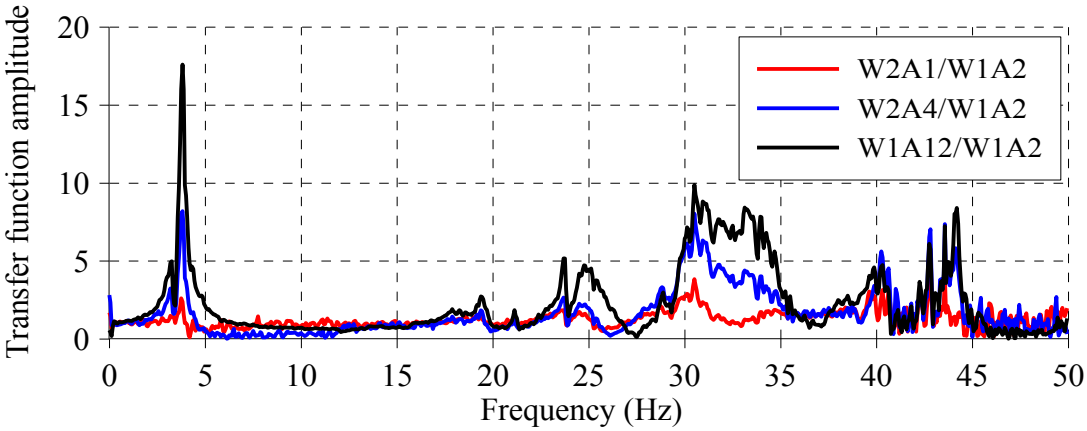

Figure 8-49 Amplitude of transfer functions for masonry bricks of Wall 2

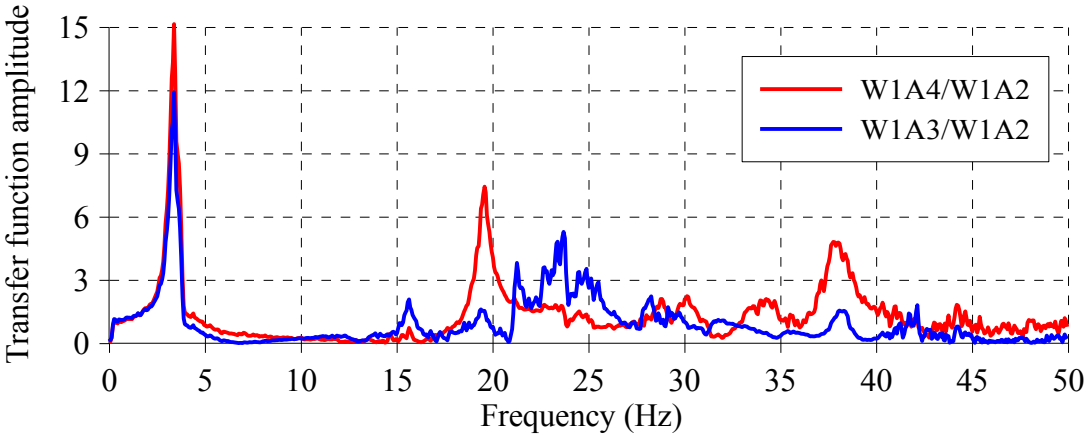

Figure 8-50 Amplitude of transfer functions for tower and wood floor of Wall 1

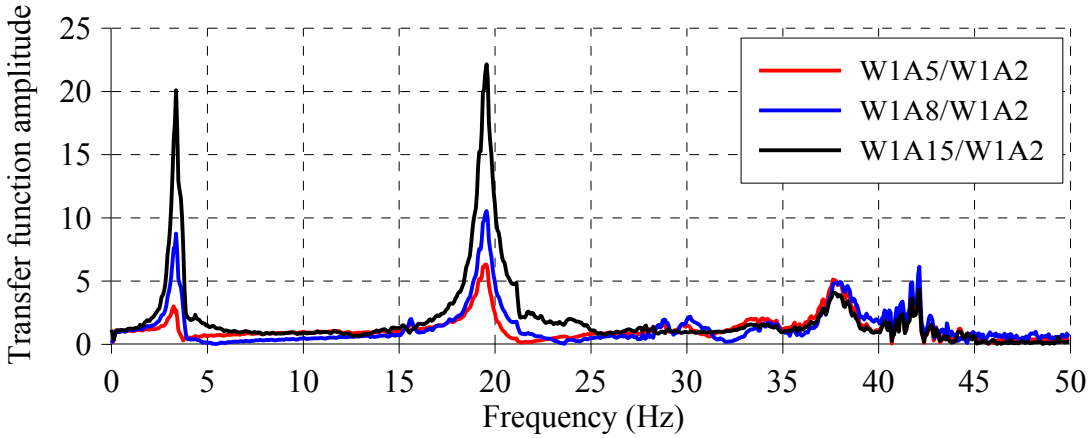

Figure 8-51 Amplitude of transfer functions for masonry bricks of Wall 1

Table 8-6 Identified modal parameters for Wall 1 and Wall 2

Specimen	Transfer Function Location	1st Mode		2nd Mode		3rd Mode	
		Frequency Hz	Amplitude -	Frequency Hz	Amplitude -	Frequency Hz	Amplitude -
Wall 2	W2A9	3.81	14.63	19.56	0.55	23.75	2.75
	W2A8	3.75	4.70	12.31	4.41	15.38	3.705
	W2A1	3.75	2.60	-	-	-	-
	W2A4	3.81	8.18	19.44	1.78	23.69	2.66
	W1A12	3.81	17.60	19.38	2.73	23.69	5.17
Wall 1	W1A4	3.38	15.15	15.63	0.75	19.56	7.44
	W1A3	3.38	11.92	15.63	2.01	19.50	1.55
	W1A5	3.25	3.00	15.63	1.68	19.50	6.3
	W1A8	3.38	8.75	15.63	2.01	19.56	10.53
	W1A15	3.38	20.09	-	-	19.56	22.13

8.5.3 Virginia Earthquake Results for Wall 1

Peak values of relative displacement response at several locations in Wall 1 are shown in Figure 8-52. A linear distribution of relative displacement over the height can be observed for all tests. Since the wall was free to rotate at the base, rigid body rocking at the base was the predominant behavior. A maximum peak displacement of 0.45 inch at the parapet was obtained for a maximum acceleration of 0.20 g generated at the base of the wall for VA300%. The inertia generated in the masonry wall was insufficient to cracks the walls. Moreover, no relative displacement was observed at the connection between the wood joist and the masonry wall.

Peak values of absolute acceleration response at several locations in Wall 1 are shown in Figure 8-53. Constant acceleration profiles along the height of uncracked walls are expected when the wall is rigidly connected at the top and bottom, as discussed in Meisl et al. (2007). Nonetheless, for intensities VA150%, VA200% and VA300% a parabolic profile can be observed, revealing a strong influence of the parapet and the frequency content of the seismic input in the distribution of inertial forces in the wall. The absolute acceleration was amplified from 0.2 g at the base to almost 0.4 g at the parapet, but little amplification was observed at the diaphragm level (see W1A13).

Large relative displacements were observed at the top of the steel tower, as shown in Figure 8-54. This was due to a rigid body rotation at the base of the steel tower, which was connected to the most flexible part of the shake table that cantilevered out and underwent significant vertical deformations during testing. The flexibility of this part of the table, combined with the frequency content of the input motion affected the seismic response of the tower, as can also be seen in Figure 8-55, in which absolute accelerations decreased at the top. A maximum relative displacement of the isolators of 0.1 in was obtained for VA300%, as shown in Figure 8-54. Figure 8-54 also shows a small relative displacement between the concrete blocks and the wood floor connected to the isolators, suggesting that the number of bolts used to fix the blocks were not enough to keep it fully in place during the tests.

Although a stiff diaphragm was provided, the absolute acceleration between the steel tower and the blocks was slightly amplified for all tests, as illustrated in Figure 8-55. A summary of the peak displacements and peak acceleration results are also listed in Table 8-7, and Table 8-8 respectively.

Table 8-7 Peak values of relative displacement response at Wall 1

Location	Instrument ID	Peak relative displacement (in)				
		VA30%	VA100%	VA150%	VA200%	VA300%
Shake table[1]	W1SP1	0.033	0.119	0.189	0.254	0.426
Top of tower	W1SP2	0.016	0.048	0.081	0.130	0.272
Isolator	W1SP3	0.020	0.071	0.108	0.174	0.377
Wood floor	W1SP4	0.022	0.089	0.141	0.205	0.395
Wall	W1SP5	0.005	0.013	0.022	0.036	0.089
	W1SP6	0.008	0.020	0.033	0.056	0.128
	W1SP7	0.010	0.027	0.048	0.080	0.176
	W1SP8	0.012	0.035	0.059	0.096	0.213
	W1SP9	0.016	0.042	0.077	0.124	0.262
Parapet	W1SP10	0.046	0.082	0.134	0.221	0.455
Connection	W1SP14	0.034	0.003	0.005	0.006	0.004

[1] W1SP1 sensor measured absolute displacement.

Table 8-8 Peak values of absolute acceleration response at Wall 1

Location	Instrument ID	Peak absolute acceleration response (g)				
		VA30%	VA100%	VA150%	VA200%	VA300%
Shake table-Vertical	W1A1	0.008	0.027	0.042	0.068	0.126
Shake table-Horizontal	W1A2	0.012	0.045	0.072	0.106	0.200
Tower	W1A3	0.017	0.048	0.059	0.096	0.141
Blocks	W1A4	0.021	0.064	0.096	0.150	0.226
Wall	W1A5	0.010	0.035	0.060	0.084	0.156
	W1A8	0.021	0.041	0.056	0.072	0.134
	W1A9	0.023	0.047	0.062	0.087	0.157
	W1A13	0.022	0.066	0.099	0.160	0.230
	W1A14	0.024	0.082	0.110	0.167	0.303
	W1A15	0.032	0.101	0.152	0.244	0.387

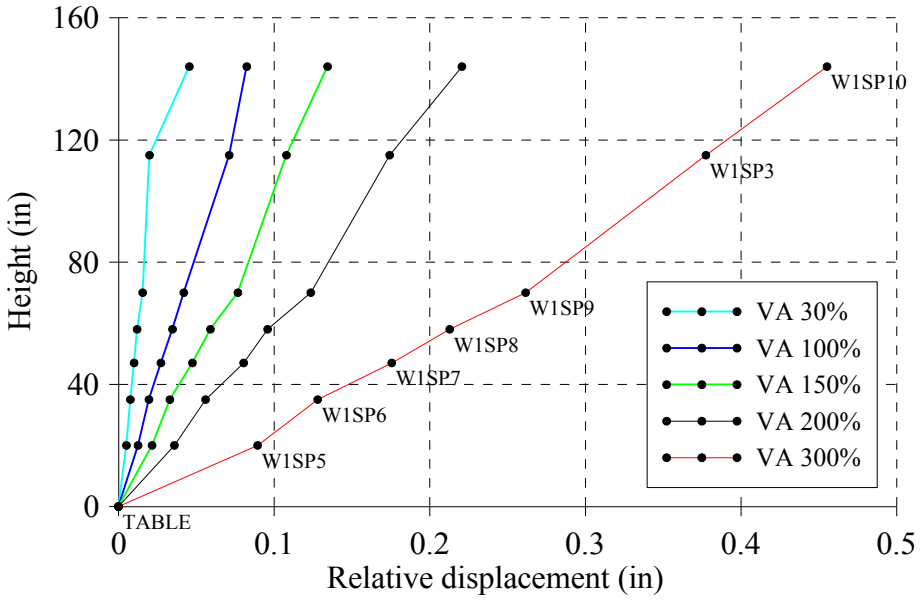

Figure 8-52 Profile of maximum displacements along the height of Wall 1

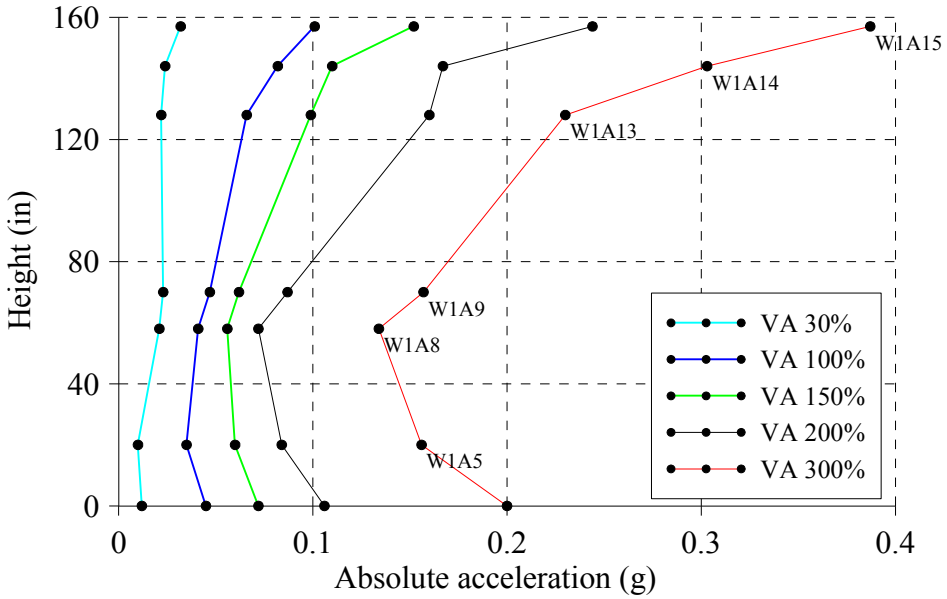

Figure 8-53 Profile of maximum accelerations along the height of Wall 1

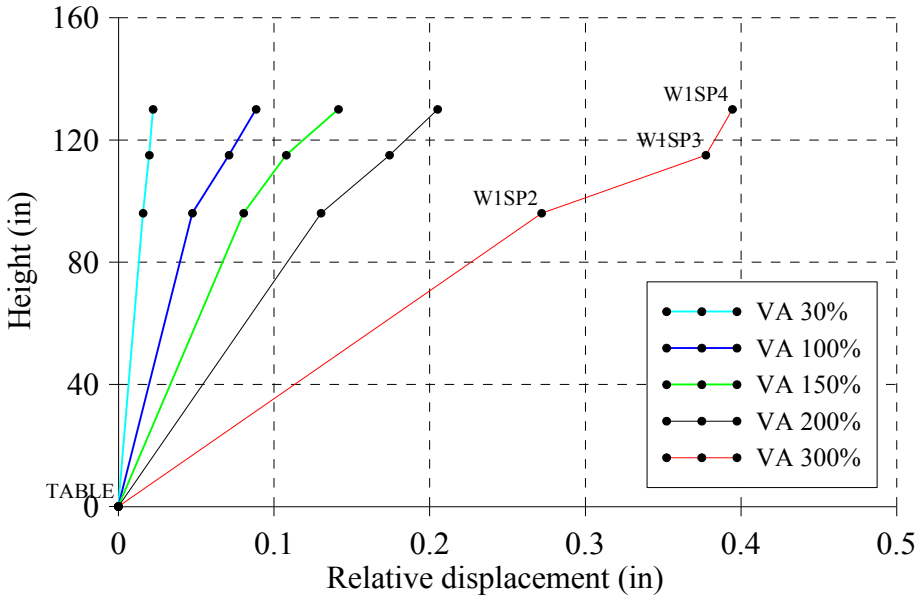

Figure 8-54 Profile of maximum displacements of the tower, isolator and concrete blocks at Wall 1

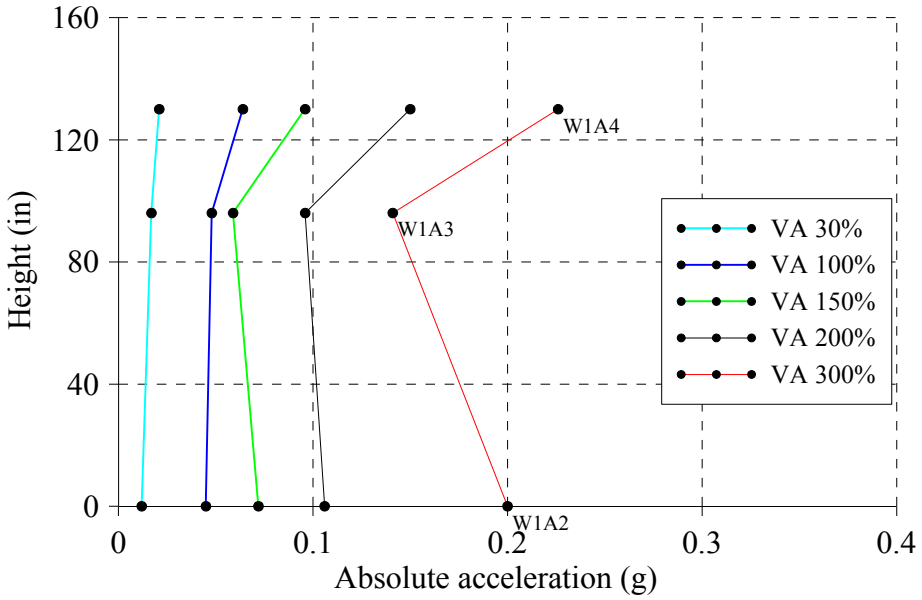

Figure 8-55 Profile of maximum accelerations of the tower, isolator and concrete blocks at Wall 1

8.5.3.1 Hysteretic behavior of isolator, parapet and wall

The hysteretic behavior of isolators, parapet and walls were extracted from the test data and used to validate simplified numerical models for low level seismic excitations. Other relevant parameters that can be obtained include the energy dissipated and critical damping ratio. Data obtained from shake table test conducted for low level intensities (from 0.05 g to 0.20 g) was used to generate force vs displacement hysteresis loops for isolators, parapet and masonry wall in key locations.

The behavior of lead rubber bearing can be observed in Figure 8-56. A maximum displacement of 0.1 inch and a corresponding force of 0.65 kips were obtained for VA300% intensity level.

The parapet response was also in the linear range, as shown in Figure 8-57. However, for the VA300% level of intensity, a slight change in the initial effective stiffness can be observed from Figure 8-57, indicating initial cracking and nonlinear behavior. The input acceleration was significantly amplified at the parapet, as observed from comparing Figure 8-57 and Figure 8-58.

Figure 8-58 illustrates the hysteretic behavior of different portions of the wall below the wood diaphragm level. A linear behavior between header courses can be observed for VA300%. The hysteretic response of the first header course of the wall illustrates the nonlinear rocking behavior of the wall at the base. No significant damage can be inferred from this data.

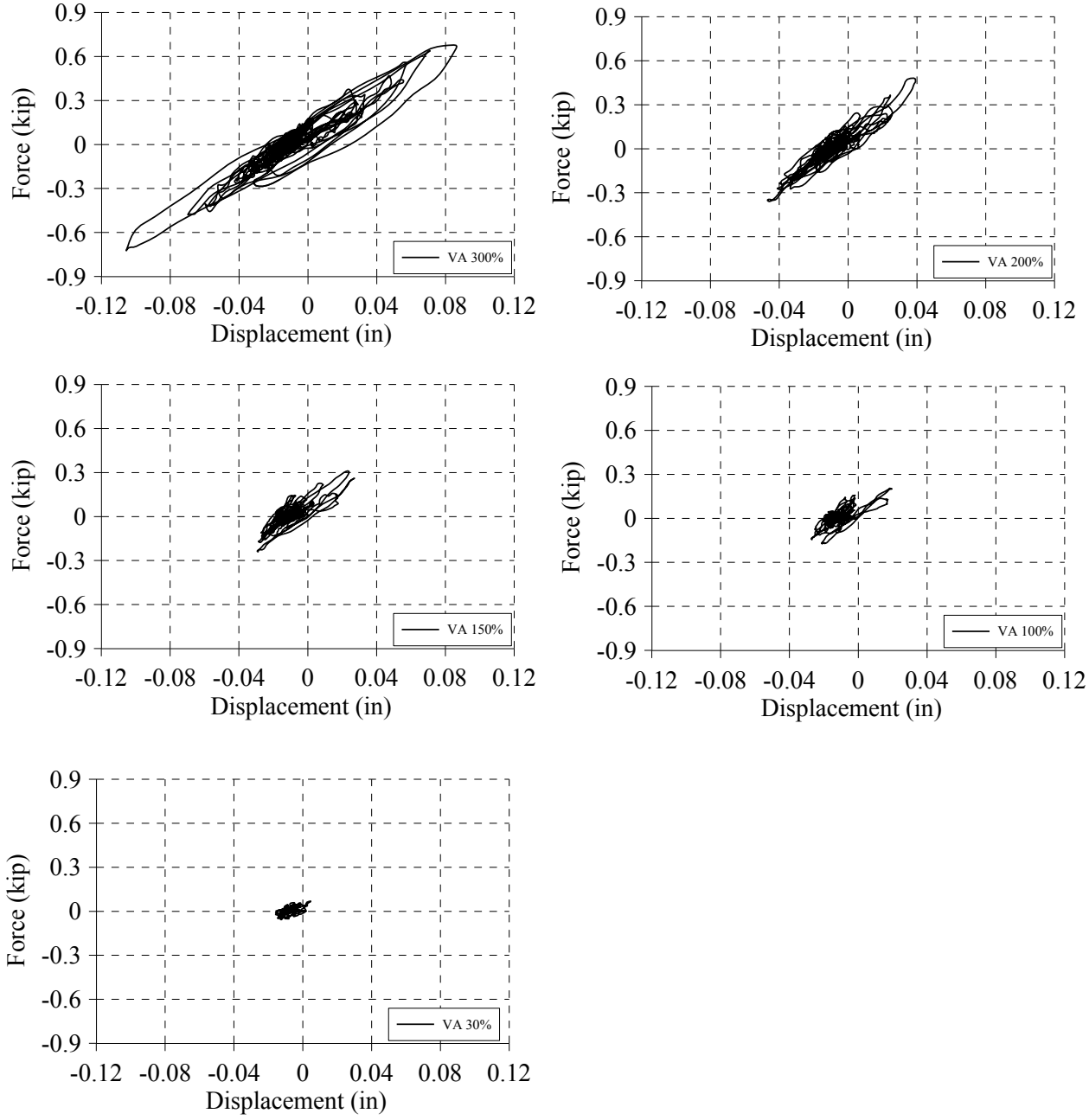

Figure 8-56 Force versus relative displacement of isolators at Wall 1 (W1A4 vs W1SP4-WISP3)

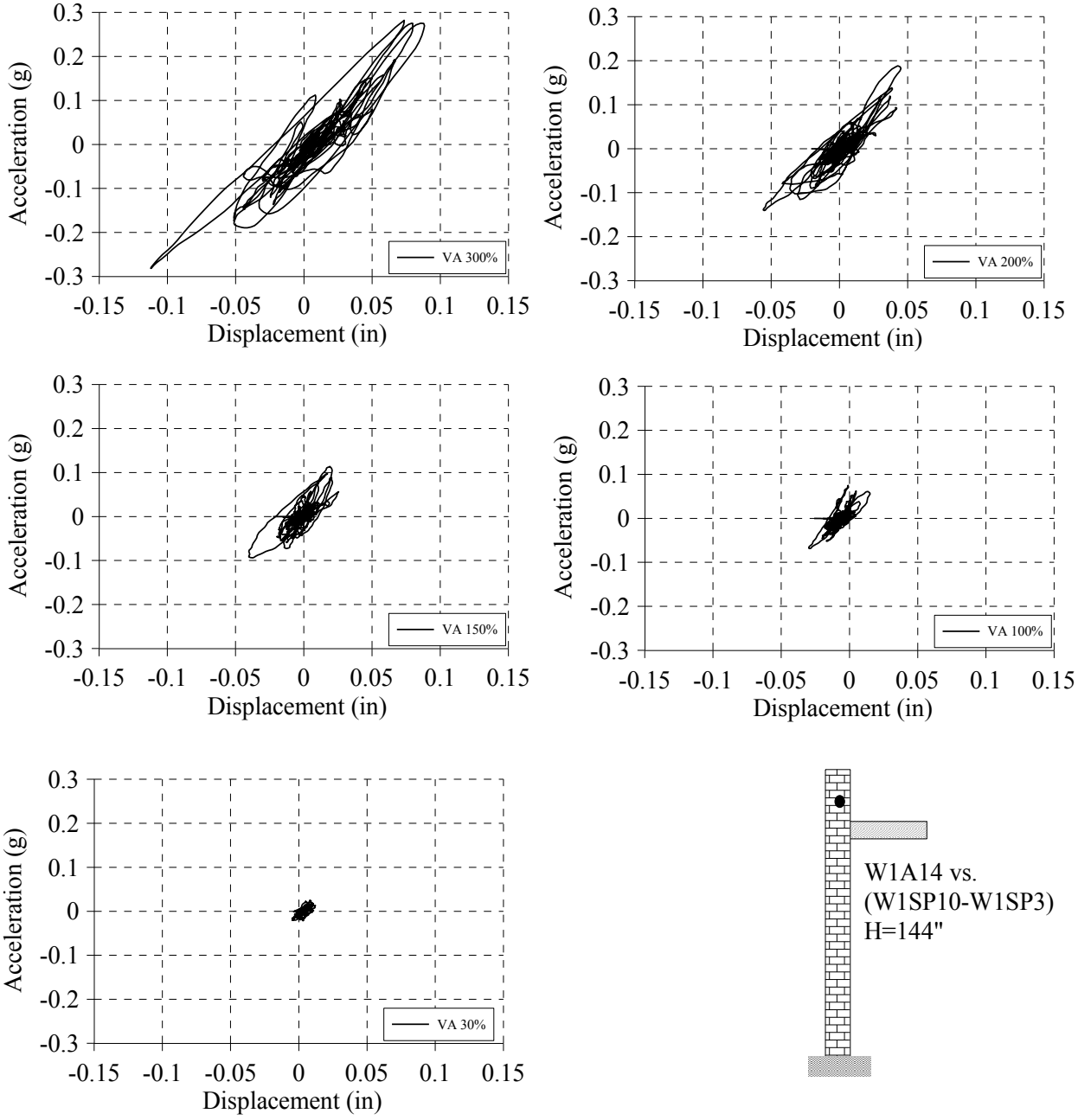

Figure 8-57 Acceleration versus relative displacement of parapet at Wall 1

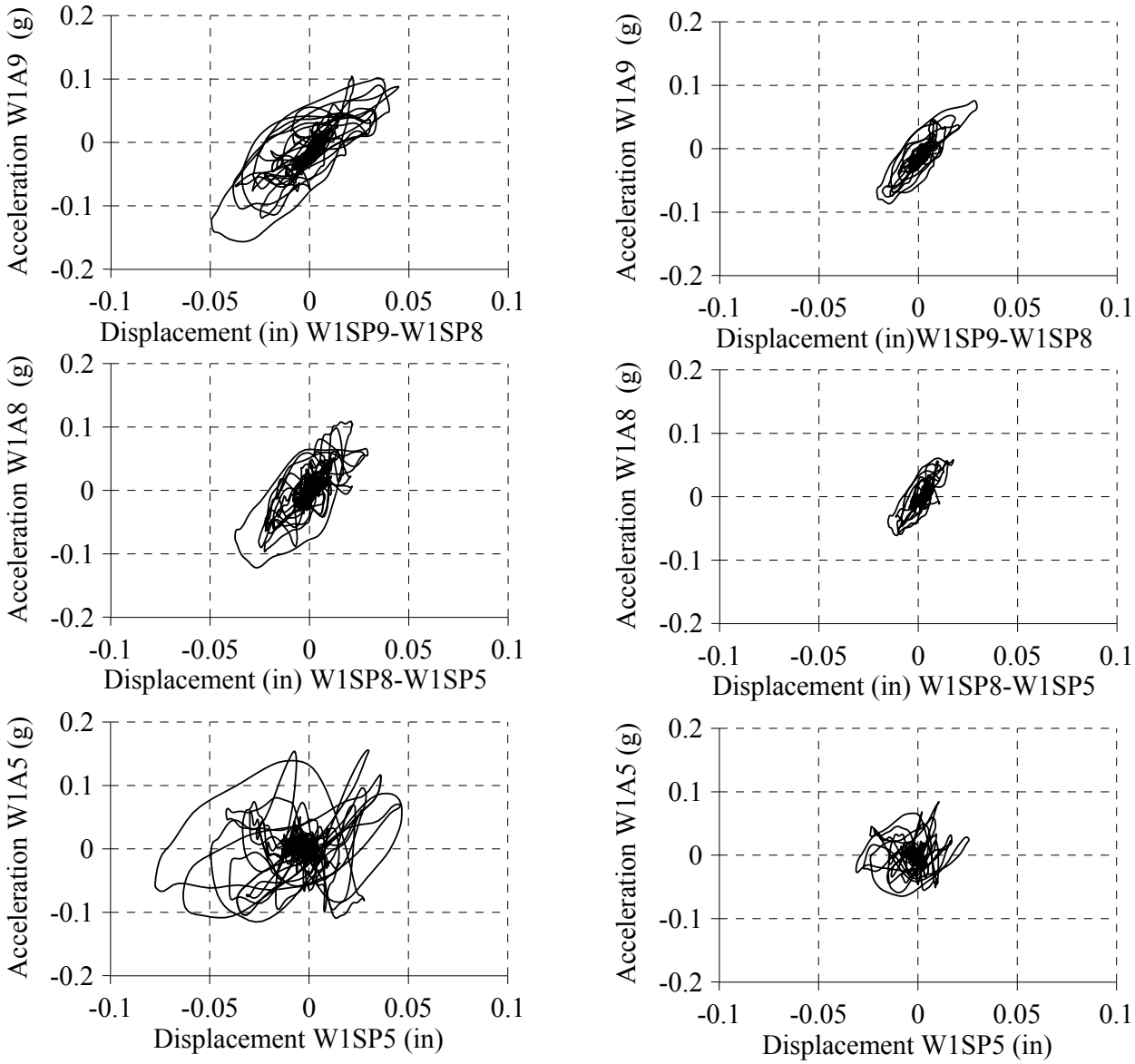

a) b)

Figure 8-58 Acceleration versus relative displacement along the height of Wall 1: a) Test VA300% and b) Test VA200%

8.5.4 Virginia Earthquake Results for Wall 2

Peak values of relative displacement response at several locations of Wall 2 are shown in Figure 8-59. A linear distribution along the height of the specimen can be observed for all intensity level tests, except VA300%. This linear distribution is attributed to the rigid body rocking motion at the base of the wall, as explained in the previous section. A maximum peak displacement of 0.44 inch at the diaphragm was obtained for a maximum acceleration of 0.20 g generated at the base of the wall for VA300% intensity level. The smaller peak relative displacement observed for the parapet (at W2SP13) for VA300% is an indication of cracking at its base. Nonetheless, as in Wall 1, the inertia generated in the masonry wall for all tests was not sufficient to generate cracks in the portion of the wall below the wood diaphragm. Also, no relative displacement was observed at the connection between the wood joist and the masonry wall.

Peak values of absolute acceleration response at several locations in Wall 2 are shown in Figure 8-60. Similar to Wall 1, a profile of parabolic absolute accelerations can be seen for all intensity levels. Again, the flexibility of the low damping rubbers and the parapet modified the distribution of inertial forces in the wall. The absolute acceleration was amplified from 0.2 g at the base to 0.23 g at the wood diaphragm level and to 0.29 g at the parapet level.

A relative displacement of 0.15 inches was observed at the top of the steel tower, as shown in Figure 8-61. Similar to Wall 1, this was due to a rigid body rotation at the base of the steel tower. The acceleration at the top of the tower decreased as can also be seen in Figure 8-62. A maximum relative displacement of the isolators of 0.3 in. was obtained for VA300%, as shown in Figure 8-61. Like in Wall 1, Figure 8-61 also shows a small relative displacement between the concrete blocks and the wood floor connected to the isolators, indicating a slippage between the concrete blocks and the wood diaphragm.

Because of the flexibility of the bearings, the absolute acceleration between the steel tower and the blocks was amplified for all tests, as illustrated in Figure 8-62. A summary of the peak displacements and peak acceleration results are also listed in Table 8-9 and Table 8-10, respectively.

Table 8-9 Peak values of relative displacement response at Wall 2

Location	Instrument ID	Peak relative displacement (in)				
		VA30%	VA100%	VA150%	VA200%	VA300%
Shake table	W2SP1	0.03	0.12	0.19	0.25	0.43
Top of tower	W2SP15	0.03	0.04	0.05	0.07	0.15
Isolator	W2SP16	0.04	0.07	0.13	0.19	0.44
Wood floor	W2SP17	0.05	0.11	0.16	0.25	0.53
Wall	W2SP5	0.02	0.05	0.06	0.10	0.24
	W2SP8	0.03	0.05	0.07	0.12	0.29
	W2SP9	0.04	0.06	0.09	0.15	0.34
Parapet	W2SP13	0.03	0.12	0.19	0.25	0.41
Connection	W2SP10	0.00	0.00	0.00	0.00	0.00
	W2SP12	0.00	0.00	0.00	0.00	0.01

[1] W2SP1 sensor measured absolute displacement.

Table 8-10 Peak values of absolute acceleration response at Wall 2

Location	Instrument ID	Peak absolute acceleration (g)				
		VA30%	VA100%	VA150%	VA200%	VA300%
Shake table-Vertical	W2tblver	0.01	0.02	0.04	0.05	0.09
Shake table-Horizontal	W2TAB	0.01	0.05	0.07	0.11	0.21
Tower	W2A8	0.01	0.04	0.06	0.08	0.15
Blocks	W2A9	0.03	0.07	0.11	0.16	0.25
Wall	W2A1	0.01	0.03	0.05	0.07	0.15
	W2A2	0.01	0.03	0.04	0.06	0.14
	W2A4	0.01	0.04	0.06	0.08	0.13
	W2A5	0.02	0.05	0.08	0.10	0.15
	W2A6	0.03	0.07	0.10	0.15	0.23
	W1A7	0.03	0.08	0.13	0.18	0.26
	W1A12	0.03	0.09	0.14	0.19	0.29

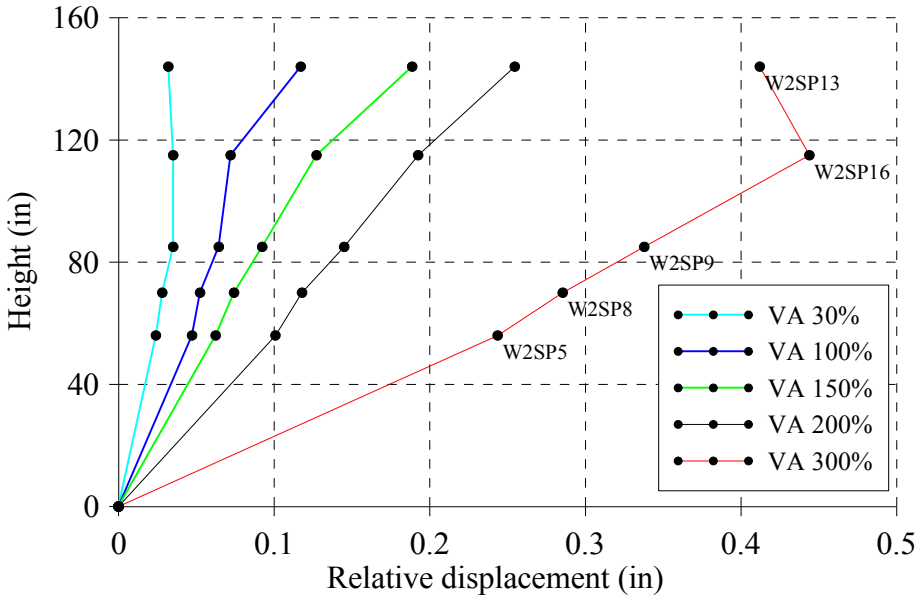

Figure 8-59 Profile of maximum displacements along the height of Wall 2

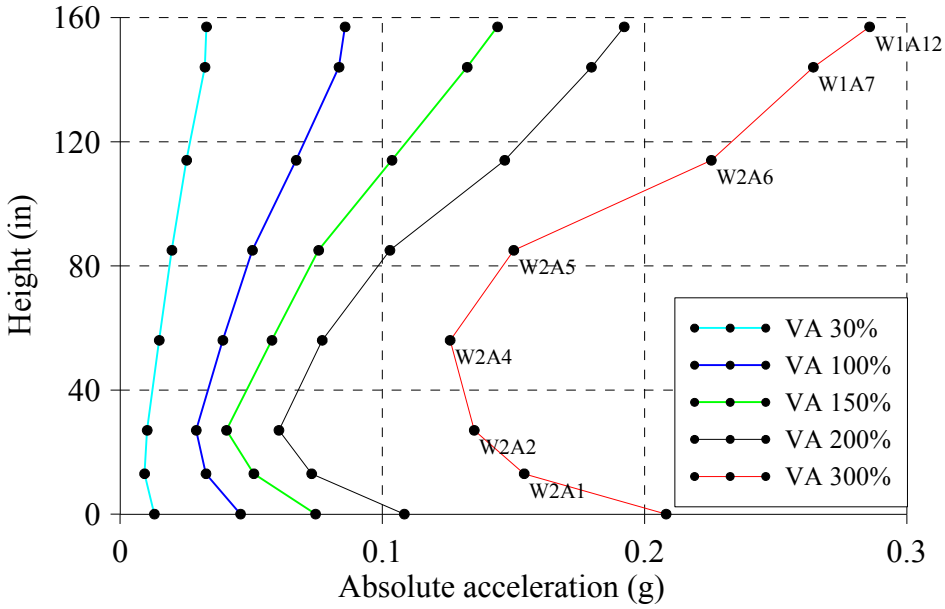

Figure 8-60 Profile of maximum accelerations along the height of Wall 2

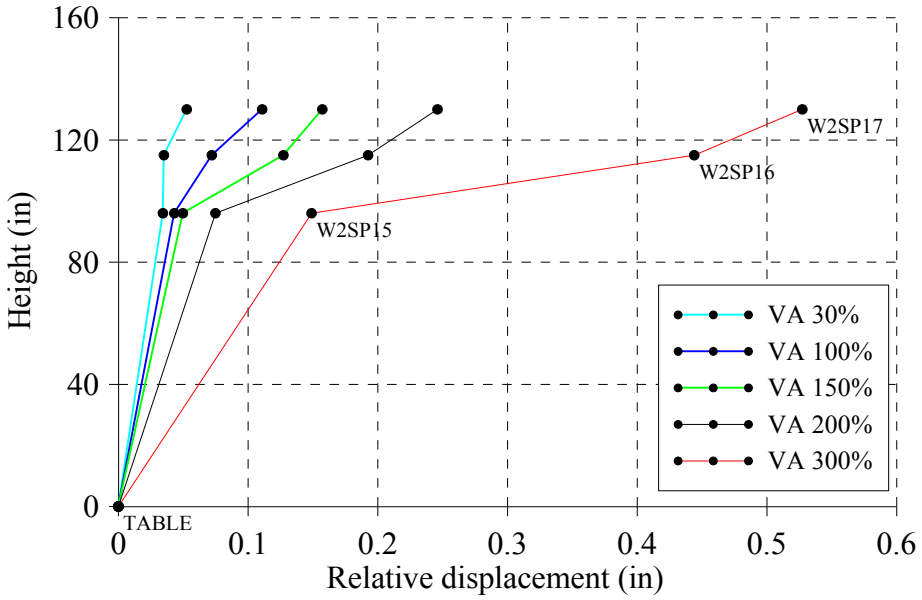

Figure 8-61 Profile of maximum displacements of the tower, isolator and concrete blocks at Wall 2

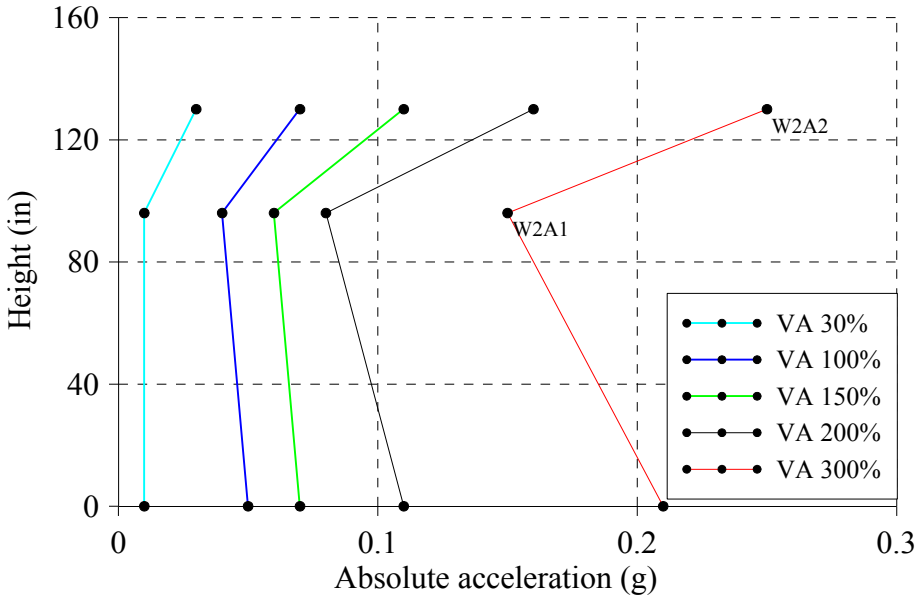

Figure 8-62 Profile of maximum accelerations of the tower, isolator and concrete blocks at Wall 2

Peak axial stresses in the steel anchors obtained for all intensity levels are shown in Figure 8-63. As expected, the maximum stress increases with an increase in the intensity of the motion. The

axial stress demanded in the central anchors was almost 2.5 higher than the axial stress in the edge anchors. This is because the tributary seismic mass is higher at the center of the wall.

Figure 8-64 shows peak axial stresses in steel braces of Wall 2 for all intensity levels. The non-uniform distribution of stresses indicates that one brace was attracting more seismic forces than the other. This was due to a loose connection between the wall and one of the braces, probably due to bad workmanship. In any case, the axial stress was well below the yielding limit. Table 8-10 lists all peak axial stresses at each location.

Table 8-11 Peak values of axial stress of steel anchors and braces at Wall 2

Location	Instrument ID	Peak axial stress (psi)				
		VA30%	VA100%	VA150%	VA200%	VA300%
Floor to wall Connection	W2SG1	1	2	4	6	8
	W2SG2	10	24	36	42	104
	W2SG3	13	40	55	79	104
	W2SG4	14	25	34	41	45
Braces	W2SG5	9	24	34	49	62
	W2SG6	83	89	139	126	181

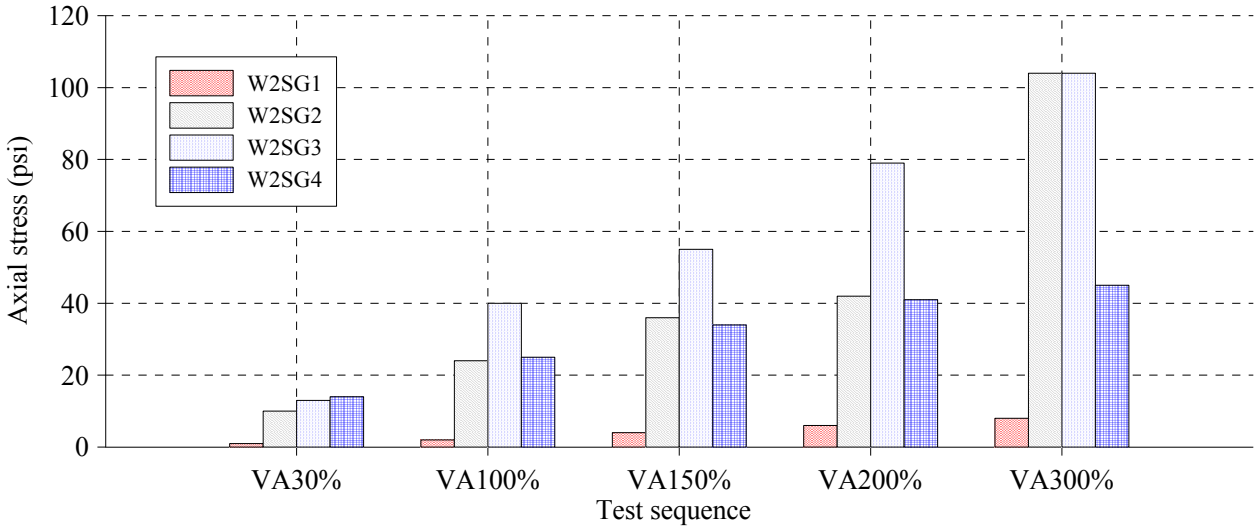

Figure 8-63 Peak axial stresses in steel anchors of Wall 2

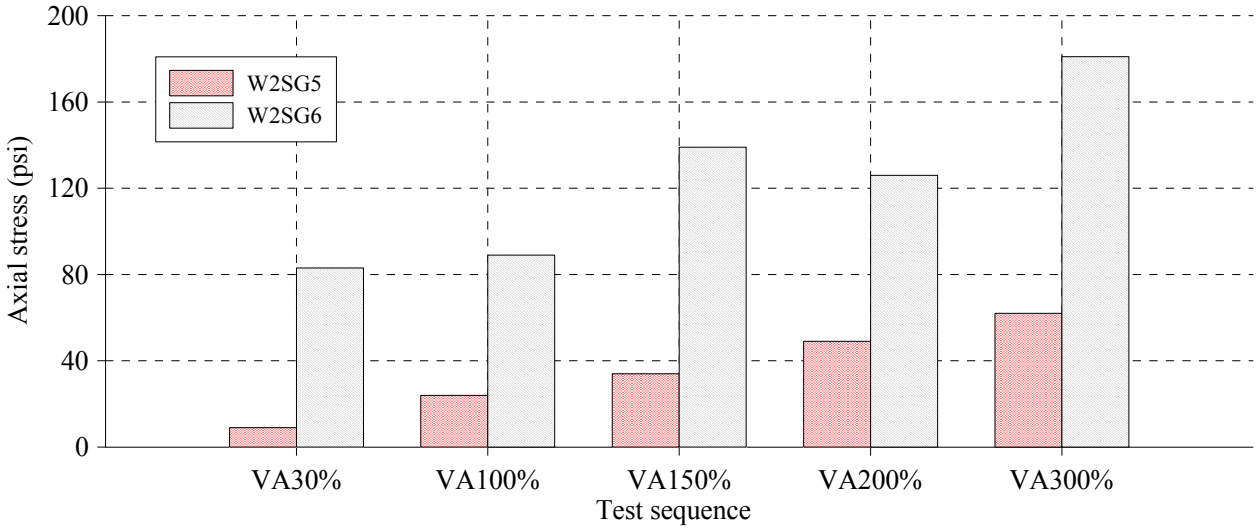

Figure 8-64 Peak axial stresses in steel braces of Wall 2

8.5.4.1 Hysteretic behavior of isolator, parapet and wall

Data obtained from shake table test conducted for low level intensities (from 0.05 g to 0.20 g) was used to generate force vs. displacement hysteresis loops for Wall 2 specimens in key locations.

Low damping rubbers hysteretic behavior is shown in Figure 8-65. A maximum displacement of 0.3 inches and a corresponding force of 0.65 kips were obtained for VA300% intensity level.

The parapet response was in the linear range, as shown in Figure 8-66. However, for the VA300% level of intensity, a slightly change in the initial effective stiffness can be deduced from Figure 8-66, indicating initial cracking and nonlinear behavior. The acceleration at the base of the wall was significantly amplified at the parapet, as observed from comparing Figure 8-66 and Figure 8-67.

Figure 8-67 illustrates the hysteretic behavior of different portions of the wall below the wood diaphragm level. A linear behavior between header courses can be observed for VA300%. The hysteretic response of the first header course of the wall illustrates the nonlinear rocking behavior of the wall at the base. No significant damage in the wall can be inferred from this data.

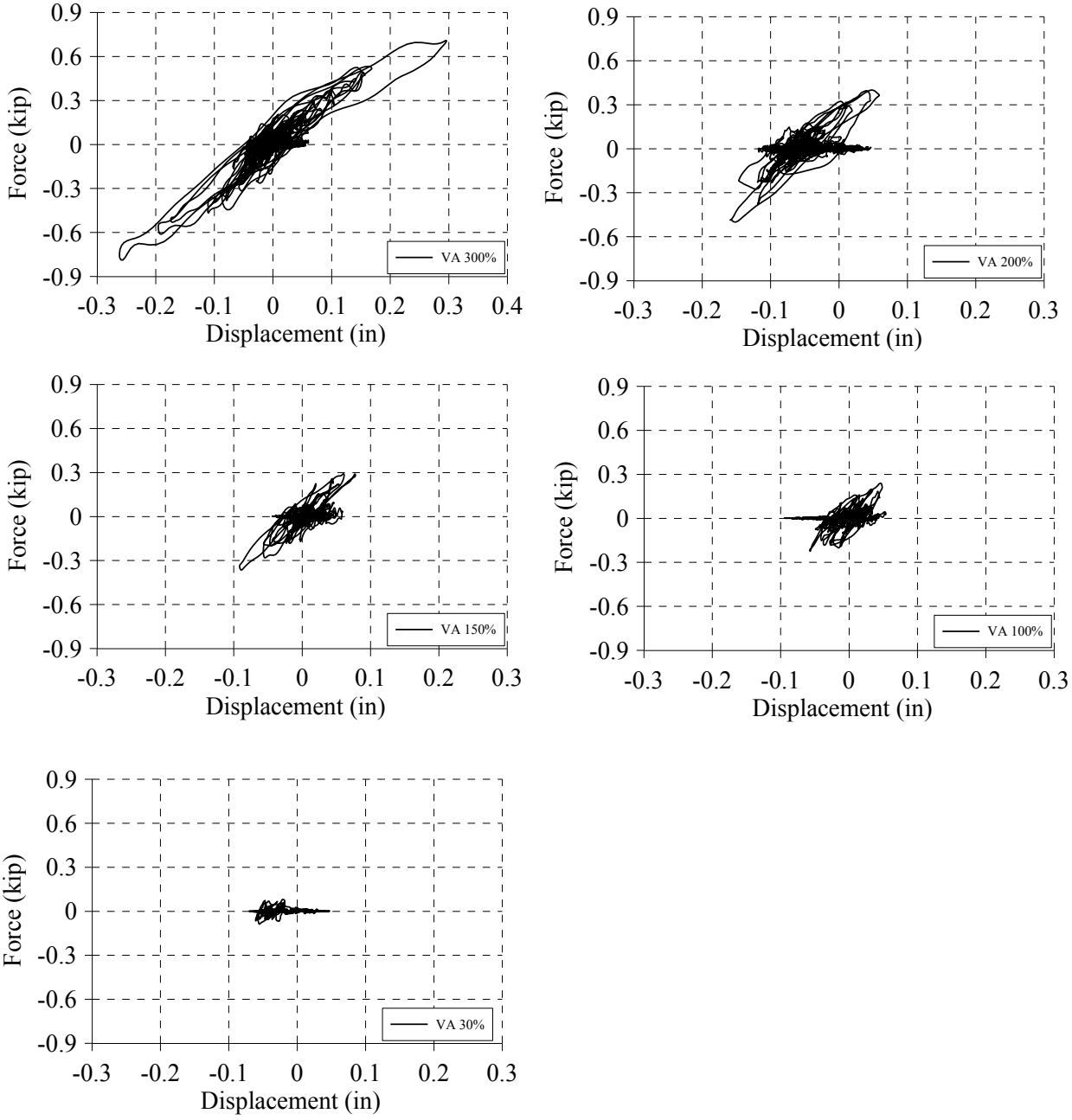

Figure 8-65 Force versus relative displacement of isolators at Wall 2 (W2A9 vs W2SP16-W2SP15)

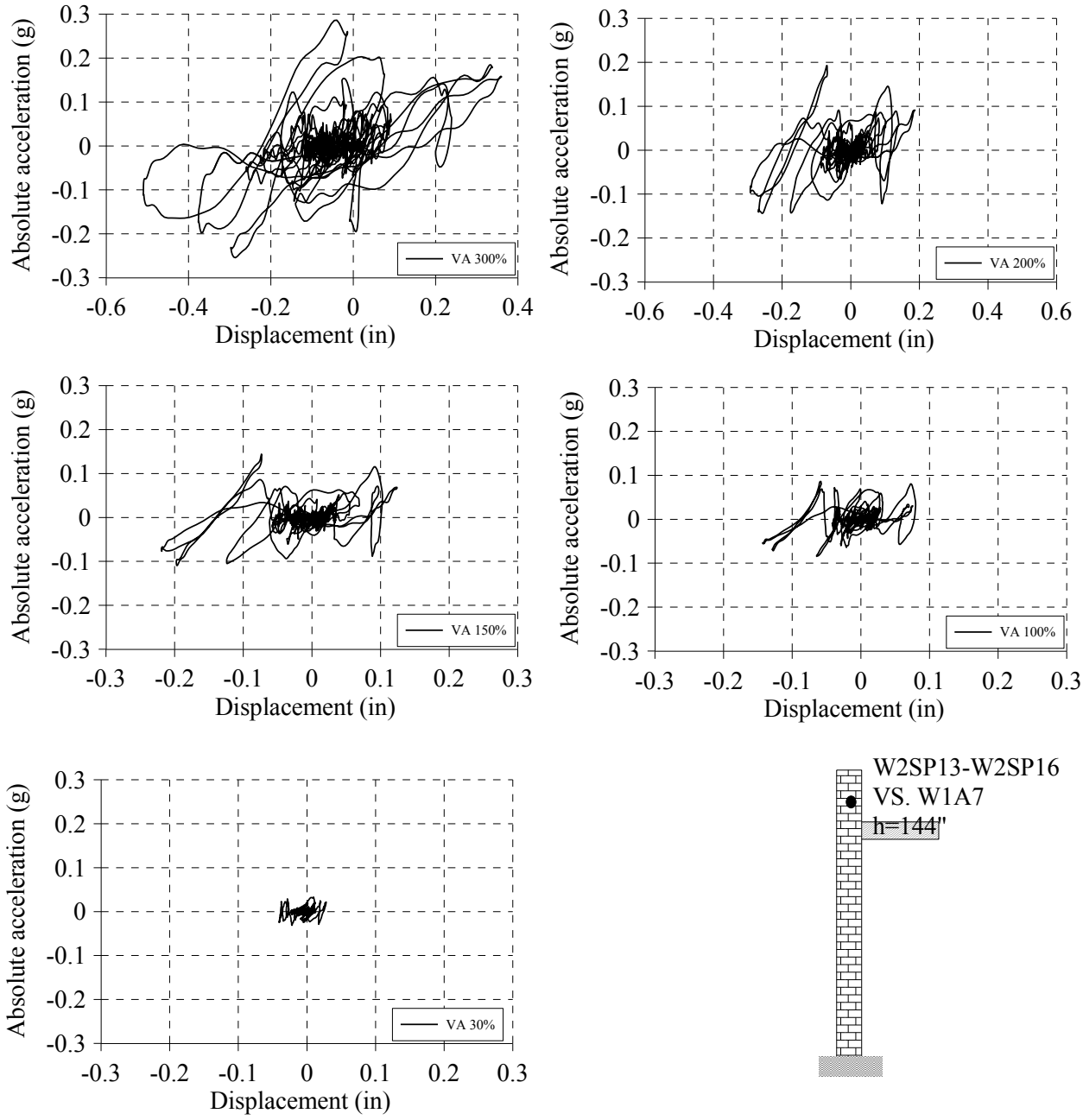

Figure 8-66 Acceleration versus relative displacement of parapet at Wall 2

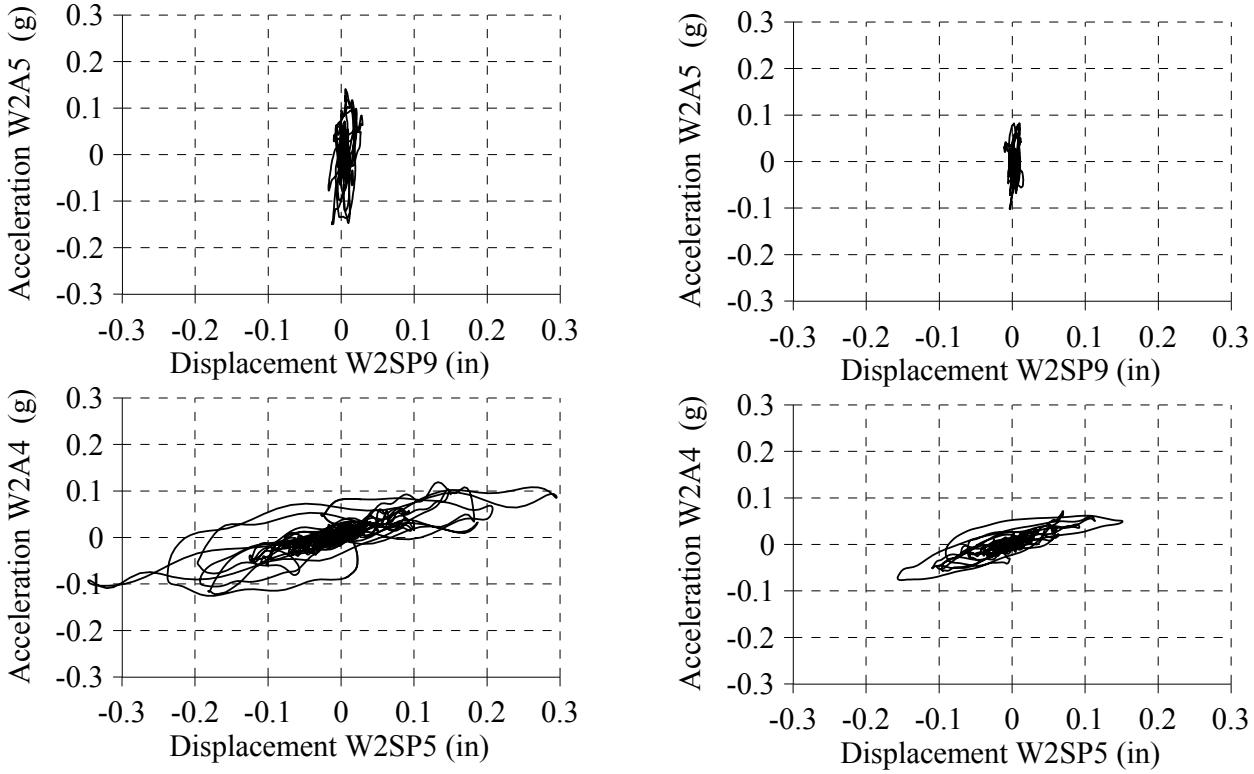

a) b)

Figure 8-67 Acceleration versus relative displacement along the height of Wall 2: a) Test VA300% and b) Test VA200%

8.5.5 Comparison Between the Response of Wall 1 and Wall 2 for Virginia Earthquake

Figure 8-68 shows the vertical absolute acceleration response of the shake table recorded under the towers of Wall 1 and Wall 2 for VA300% intensity level. The peak vertical acceleration was about 0.12g, almost 50% of the peak horizontal acceleration, which could be interpreted as rocking of the table during testing.

As previously noted, stiff and flexible diaphragms were simulated for Wall 1 and Wall 2, respectively. Comparison between peak relative displacements at mid-height of the wall and parapets in Figure 8-70 shows a similar behavior for both specimens, despite Wall 2 having relatively more flexible bearings. This can also be seen in Figure 8-71, despite of more evident relative displacement of Wall 2 at the diaphragm level. Figure 8-69b shows that providing steel braces in Wall 2 reduced the maximum displacement of the parapet to similar levels than for Wall 1.

The peak relative displacements obtained at the top of the isolators were similar in both specimens, as shown in Figure 8-70a. However, as seen in Figure 8-70b, a larger relative displacement was obtained at the top of the tower of Wall 1, which in turn introduced a larger relative displacement for the wall.

A comparison of peak values of relative displacement response at several locations in Wall 1 and Wall 2 are shown Figure 8-71a. A linear distribution of relative displacement over the height can be observed for all tests. As discussed before, since the walls were free to rotate at the base, rigid body rocking around the base was the predominant behavior. The inertia generated in the masonry walls was insufficient to cracks the walls. Moreover no relative displacements were observed at the connection between the wood joist and the masonry wall.

Peak values of absolute acceleration response at several locations in Wall 1 and Wall 2 are shown in Figure 8-72a. Although a linear profile of accelerations was expected, a parabolic profile of inertia forces was observed, revealing a significant influence of the frequency content of the seismic input in the distribution of inertial forces in the wall. In next sections, it will be demonstrated that the New Zealand earthquake did not modify the expected linear distribution of accelerations in the wall.

Large relative displacement was observed at the top of both steel towers, as shown in Figure 8-71b.

The influence of diaphragm stiffness can be seen in Figure 8-71b and Figure 8-72b. As expected, larger peak relative displacements of the isolators were observed in Wall 2. However, the absolute acceleration was slightly amplified at the diaphragm level (height=115 in), regardless the type of isolator implemented and the rigid body rotation of the towers. The peak absolute accelerations are about the same in both walls for a given simulation, demonstrating the effectiveness of using steel braces as a retrofitting technique to reduce seismic demands.

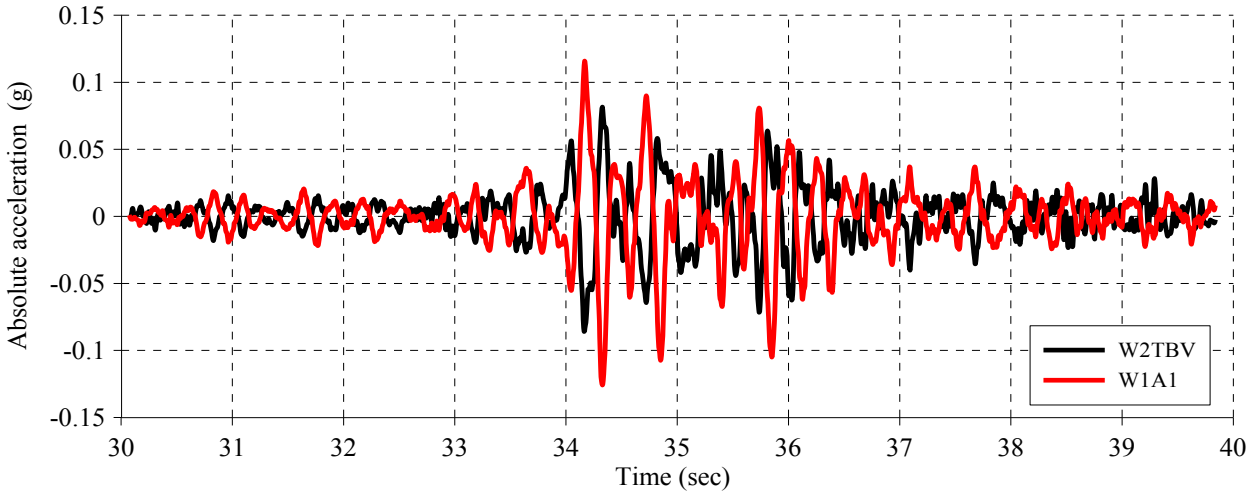

Figure 8-68 Vertical absolute acceleration response of the shake table at Wall 1 and Wall 2

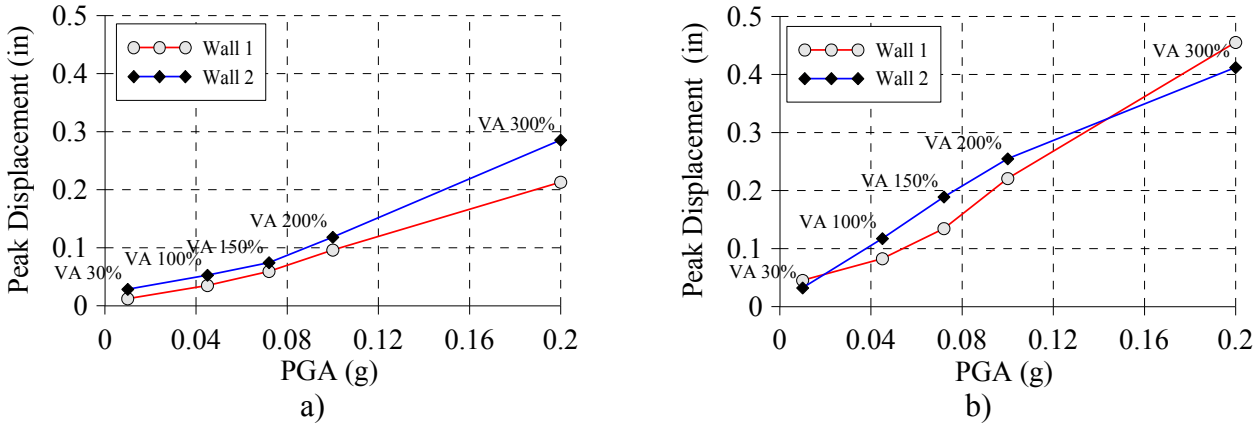

Figure 8-69 Peak relative displacement vs PGA at a) Mid-height of the walls b) Parapets

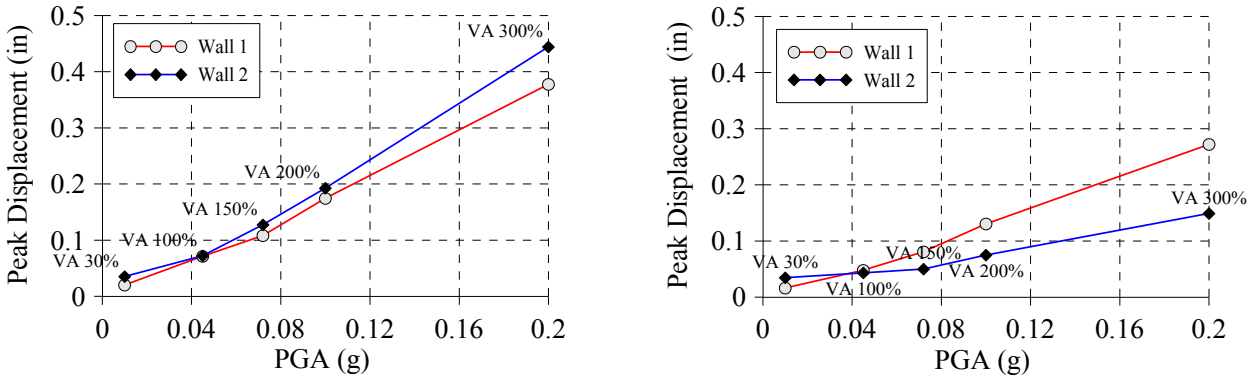

Figure 8-70 Peak relative displacement vs PGA at a) Isolators b) Steel tower

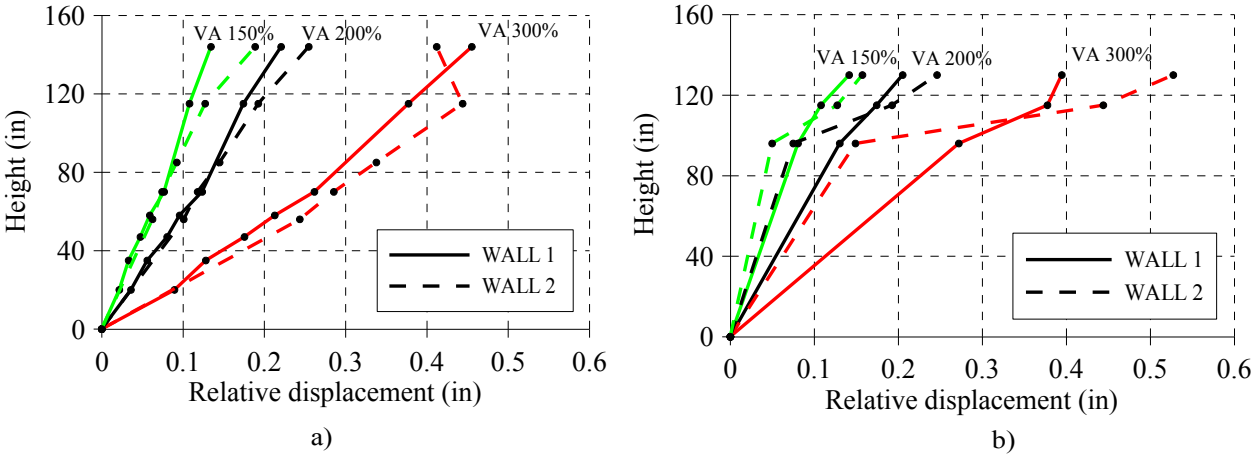

Figure 8-71 Comparison of peak relative displacement profile of Wall 1 and Wall 2 at a) masonry wall and b) steel tower and isolators

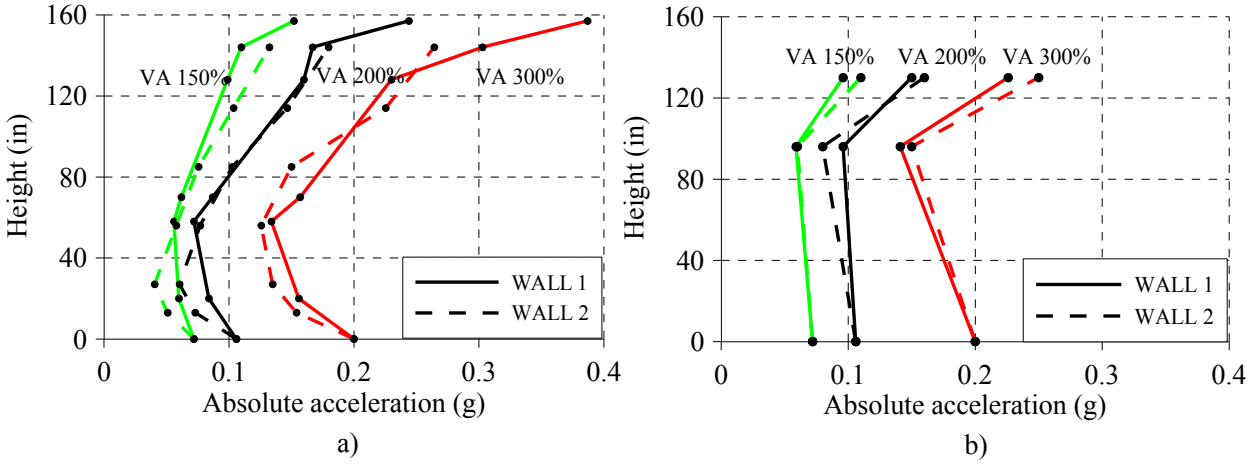

Figure 8-72 Comparison of peak absolute acceleration profile of Wall 1 and Wall 2 at a) Masonry wall and b) Steel tower and isolators

8.5.6 New Zealand Earthquake Results for Wall 1

Peak values of relative displacement response at several locations in Wall 1 are shown in Figure 8-73. A linear distribution along the height of the wall, up to the wood diaphragm level can be observed for intensity levels NZ50% and NZ75%. Again, this linear distribution is attributed to the rigid body rocking motion at the base of the wall. A maximum peak displacement of 1.35 inch at the diaphragm was obtained for a maximum acceleration of 0.25 g generated at the base of the wall for NZ75% intensity level. The large peak relative displacement observed at the base of the parapet, with respect to the diaphragm level, it is due to cracking in this zone. From this figure, it is implied that the inertia generated in the masonry wall for these tests was enough to generate small cracks in the portion of the wall below the wood diaphragm.

Also, it can be seen in Figure 8-73 that large displacements were obtained in the parapet at intensity level NZ75%. Because of this severe damage, intensity level NZ100% collapsed the parapet at early stage of the test. Also, a small displacement was observed at the connection between the wood joist and the masonry wall.

Peak values of absolute acceleration response at several locations in Wall 1 are shown in Figure 8-74. A profile of linear absolute accelerations can be seen for intensity levels NZ50% and NZ75%. For NZ100%, higher amplification can be seen at the parapet, due rocking behavior at the base. The absolute acceleration was amplified from 0.38 g at the base to 0.85 g at the wood diaphragm level and to 2.32 g at the parapet level.

As in the Virginia earthquake tests, a large relative displacement was observed at the top of the steel tower, as shown in Figure 8-75. The absolute acceleration was amplified at this level, as can also be seen in Figure 8-76. Note that the frequency content of the earthquake had less effect in the distribution of accelerations along the height of the wall. A maximum relative displacement of the isolators of 0.57 inches was obtained for NZ100%. Figure 8-75 also shows a significant sliding between the concrete blocks and the wood floor.

Since a stiff diaphragm was provided, the absolute acceleration between the steel tower and the blocks was not significantly amplified for all tests, as illustrated in Figure 8-76. A summary of the peak displacements and peak acceleration results are also listed in Table 8-12, and Table 8-13 respectively.

Table 8-12 Peak values of absolute acceleration response at Wall 1

Location	Instrument ID	Peak absolute acceleration (g)		
		NZ50%	NZ75%	NZ100%
Shake table-Vertical	W1A1	0.16	0.17	0.16
Shake table-Horizontal	W1A2	0.22	0.25	0.38
Tower	W1A3	0.46	0.47	0.60
Blocks	W1A4	0.55	0.65	0.76
Wall	W1A5	0.27	0.26	0.42
	W1A8	0.40	0.43	0.56
	W1A9	0.43	0.48	0.61
	W1A13	0.58	0.65	0.85
	W1A14	0.64	0.69	1.32
	W1A15	0.75	0.79	2.32

Table 8-13 Peak values of relative displacement response at Wall 1

Location	Instrument ID	Peak relative displacement (in)		
		NZ50%	NZ75%	NZ100%
Shake table	W1SP1	2.486	3.607	4.913
Top of tower	W1SP2	0.908	0.910	1.050
Isolator	W1SP3	1.325	1.346	0.578
Wood floor	W1SP4	1.154	1.910	2.482
Wall	W1SP5	0.247	0.316	0.194
	W1SP6	0.424	0.511	0.270
	W1SP7	0.642	0.659	0.337
	W1SP8	0.776	0.828	0.400
	W1SP9	0.946	1.017	0.498
Parapet	W1SP10	2.067	5.744	4.816
Connection	W1SP14	0.034	0.057	0.074

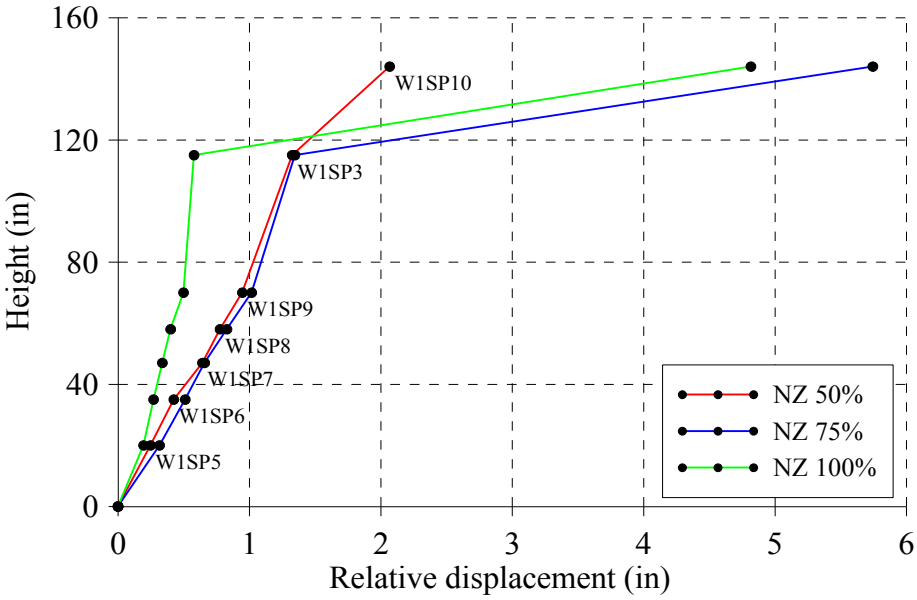

Figure 8-73 Profile of maximum displacements along the height of Wall 1

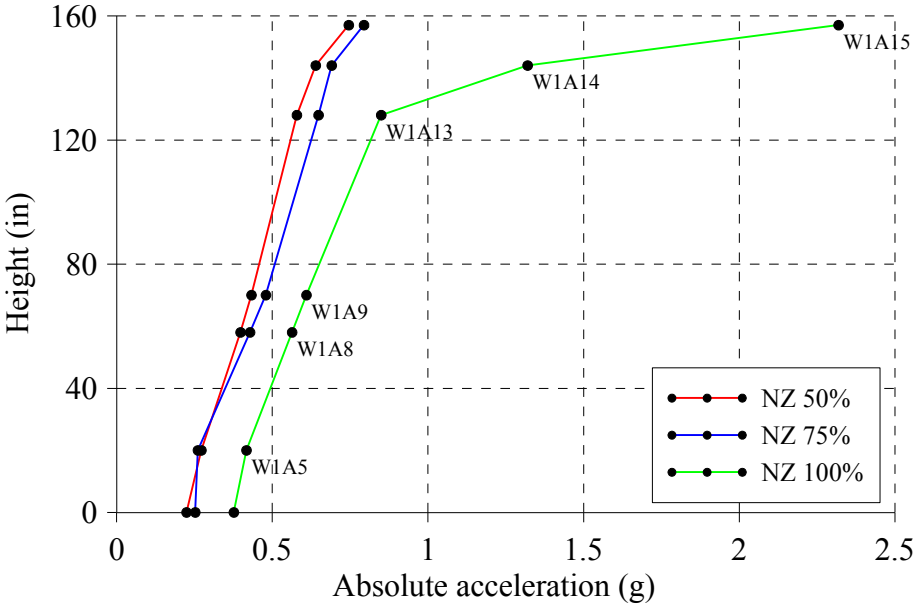

Figure 8-74 Profile of maximum absolute accelerations along the height of Wall 1

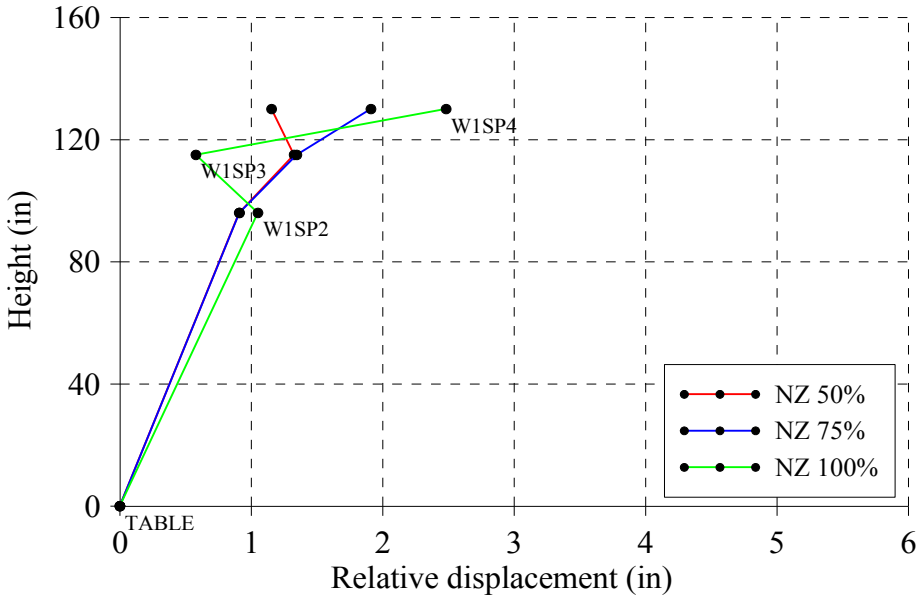

Figure 8-75 Profile of maximum displacements of the tower, isolator and concrete blocks at Wall 1

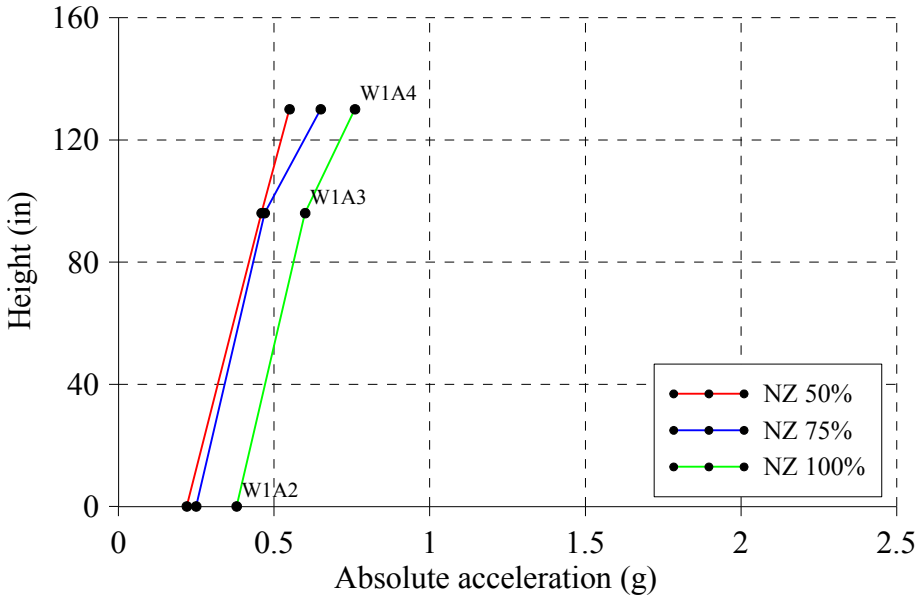

Figure 8-76 Profile of maximum accelerations of the tower, isolator and concrete blocks at Wall 1

8.5.6.1 Hysteretic behavior of isolator, parapet and wall

Data obtained from shake table tests conducted for high level intensities (from 0.22 g to 0.38 g PGA) was used to generate force vs displacement hysteresis loops for Wall 1 specimens in key locations. Lead rubber bearings hysteretic behavior can be observed in Figure 8-77. A maximum displacement of 0.58 inches and a corresponding force of 2 kips were obtained for NZ100% intensity level.

The parapet response is shown in Figure 8-78 for all intensity levels. Significant rocking can be observed for intensity levels NZ50% and NZ 75%. The parapet collapsed for NZ100% after 2.5 seconds of the ground motion. Figure 8-80 illustrates the hysteretic behavior of different portions of the wall below the wood diaphragm level. A linear behavior between header courses can be observed for NZ100%. The hysteretic response of the first header course of the wall illustrates the nonlinear rocking behavior of the wall at the base. No significant damage can be inferred from this data and visual observations.

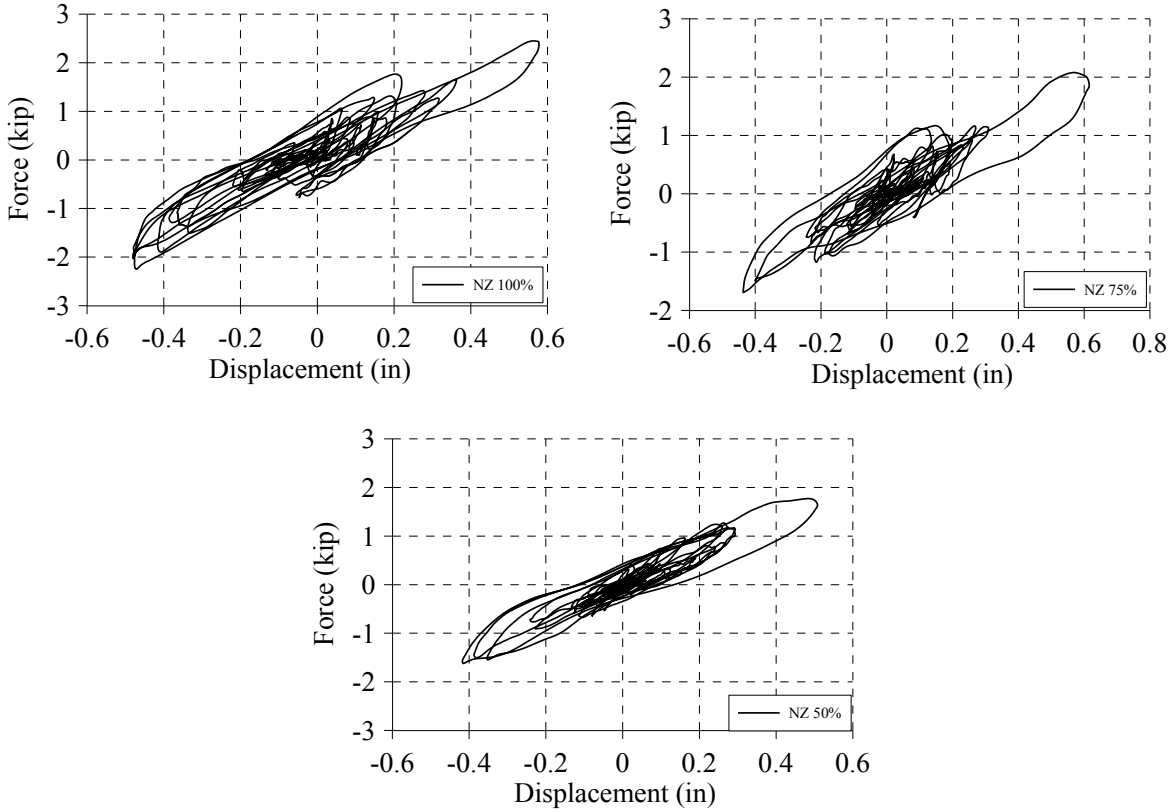

Figure 8-77 Force versus relative displacement of isolators at Wall 1 (W2A9 vs W2SP16-W2SP15)

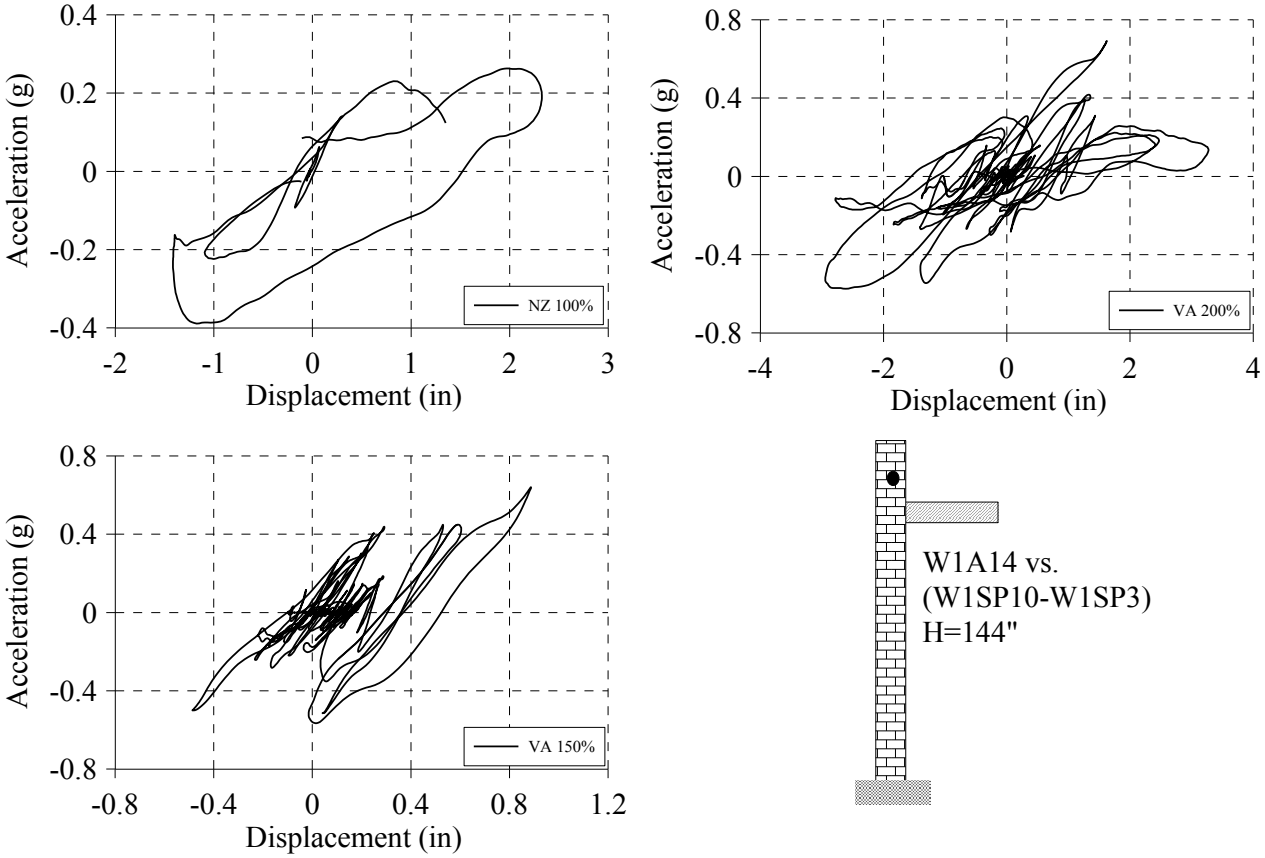

Figure 8-78 Acceleration versus relative displacement of parapet at Wall 1

Figure 8-79 Final damage state of parapet in Wall 1

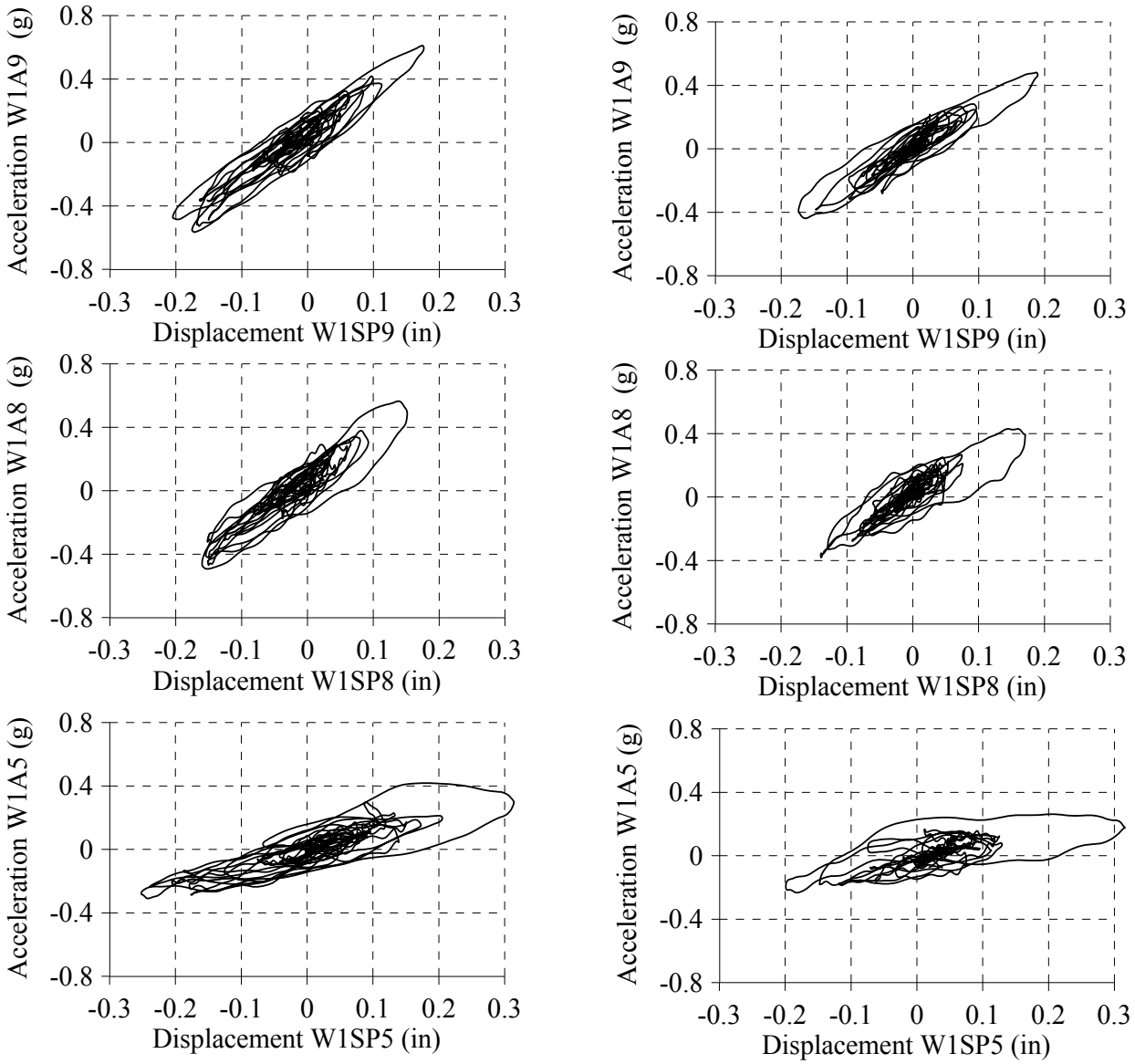

Figure 8-80 Acceleration versus relative displacement along the height of Wall 1: a) Test NZ100% and b) Test NZ75%

8.5.7 New Zealand Earthquake Results for Wall 2

Peak values of relative displacement response at several locations in Wall 2 are shown in Figure 8-81. Different from Wall 1, a nonlinear distribution along the height of the specimen up to the wood diaphragm level can be observed for all intensity levels. This nonlinear distribution is attributed to the cracking in the wall below the wood diaphragm. A maximum peak displacement of 4.51 inch at the diaphragm was obtained for a maximum acceleration of 0.38 g generated at the base of the wall for NZ100% intensity level. The large relative displacement observed for the parapet is also an indication of cracking. Also, Figure 8-81 shows that the peak displacement at the wood diaphragm is reduced after cracking of the portion of the wall beneath the parapet.

Peak values of absolute acceleration response along the height of Wall 2 are shown in Figure 8-82. A nonlinear profile of absolute accelerations was obtained for all intensity levels due to cracking at the mid-height of the wall between the wood floor and the base. The absolute acceleration was amplified from 0.38 g at the base to 1.05 g at the wood diaphragm level and to 1.95 g at the parapet level.

A relative displacement of 1.45 inches was observed at the top of the steel tower, as shown in Figure 8-84. The absolute acceleration was doubled at the top of the tower as can also be seen in Figure 8-83. A maximum relative displacement of the isolators of 4.35 inches was obtained for NZ100%, as shown in Figure 8-83.

Because of the relative large flexibility of the diaphragm, the absolute input acceleration was amplified at the wood diaphragm, steel tower, concrete blocks and parapet levels, as illustrated in Figure 8-84. A summary of the peak displacements and peak acceleration results are also listed in Table 8-14, and Table 8-15 respectively.

Table 8-14 Peak values of absolute acceleration response

Location	Instrument ID	Peak absolute acceleration (g)		
		NZ50%	NZ75%	NZ100%
Shake table-Vertical	W2tblver	0.22	0.20	0.20
Shake table-Horizontal	W2TAB	0.20	0.24	0.36
Tower	W2A8	0.42	0.44	0.55
Blocks	W2A9	0.83	1.02	1.17
Wall	W2A1	0.26	0.28	0.38
	W2A2	0.36	0.38	0.52
	W2A4	0.58	0.62	0.79
	W2A5	0.69	0.73	0.92
	W2A6	0.83	0.88	1.05
	W1A7	0.97	1.32	1.53
	W1A12	1.23	1.68	1.97

Table 8-15 Peak values of relative displacement response

Location	Instrument ID	Peak relative displacement (in)		
		NZ50%	NZ75%	NZ100%
Shake table	W2SP1	2.486	3.607	4.913
Top of tower	W2SP15	1.147	1.115	1.456
Isolator	W2SP16	3.262	3.544	4.354
Wood floor	W2SP17	3.493	3.551	4.514
Wall	W2SP5	1.972	2.064	2.898
	W2SP8	2.056	2.129	3.215
	W2SP9	2.221	2.343	3.118
Parapet	W2SP13	3.566	4.041	5.109
Connection	W2SP10	0.024	0.029	0.045
	W2SP12	0.014	0.018	0.042

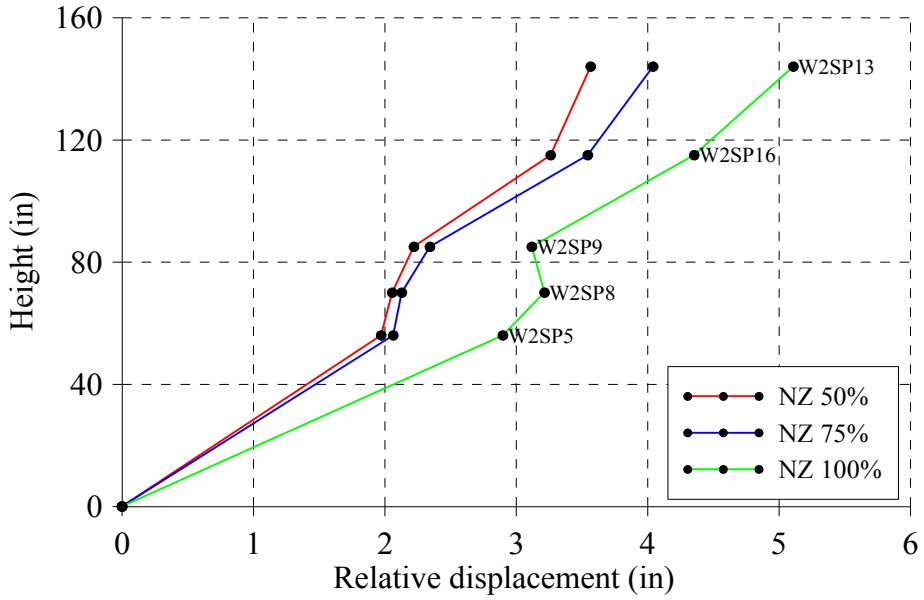

Figure 8-81 Profile of maximum displacements along the height of Wall 2

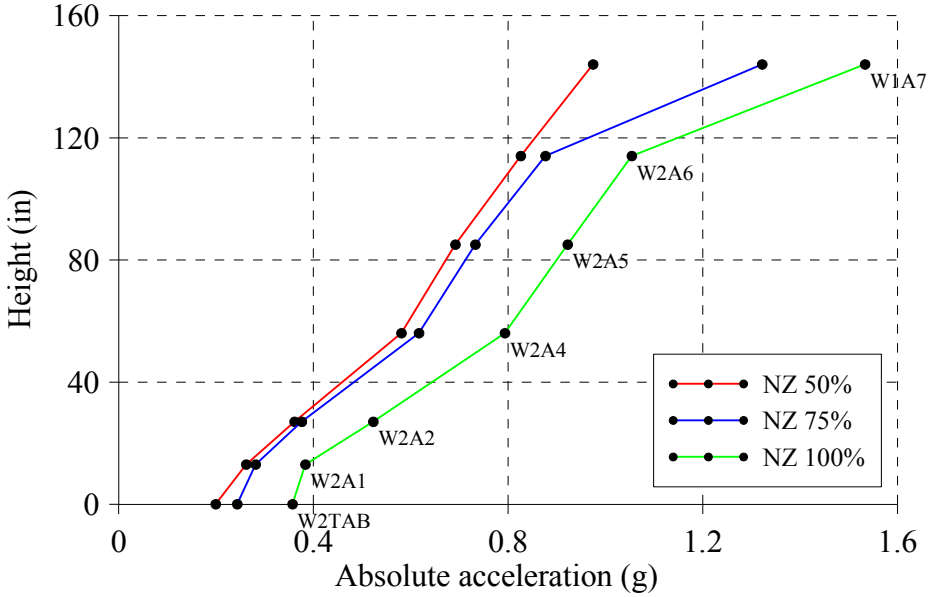

Figure 8-82 Profile of maximum accelerations along the height of Wall 2

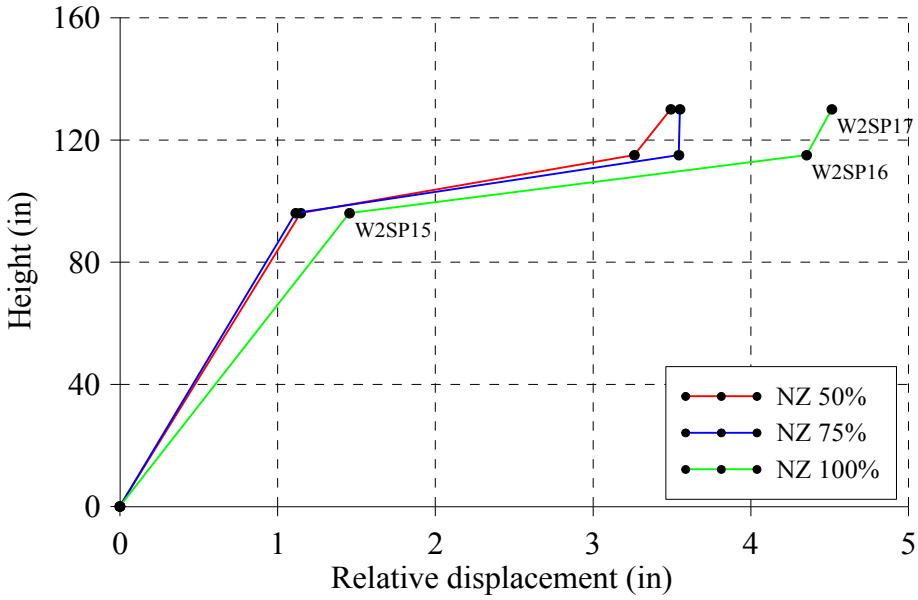

Figure 8-83 Profile of maximum displacements of the tower, isolator and concrete blocks at Wall 2

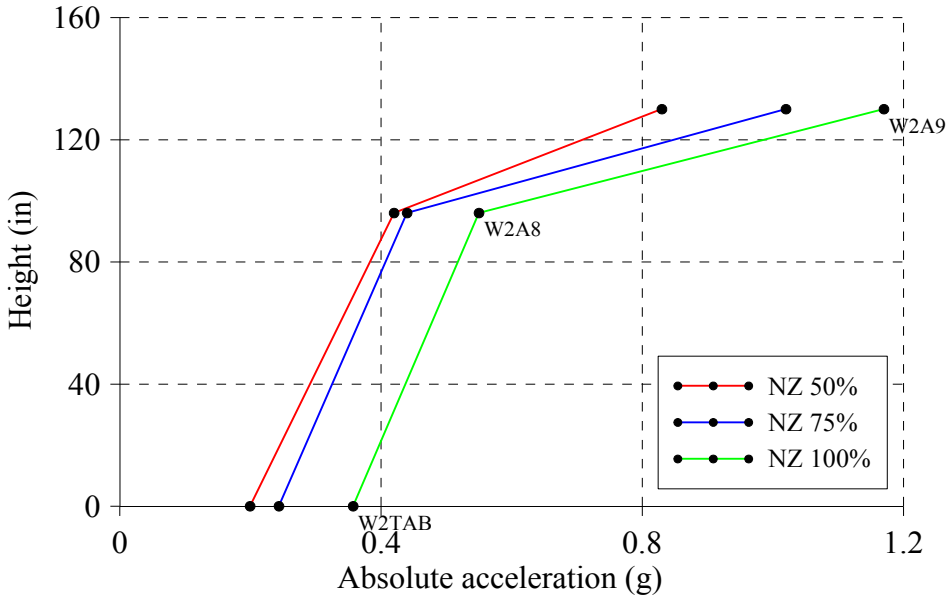

Figure 8-84 Profile of maximum accelerations of the tower, isolator and concrete blocks at Wall 2

Peak axial stresses in the steel anchors between wood joists for all intensity levels of NZ earthquake are shown in Figure 8-85. As expected, the maximum stress increases with an increase in the intensity of the motion and the effect of wall failure. The axial stress in the central

anchors was almost 2.5 higher than the axial stress in the edge anchors, since the tributary seismic mass is higher at the center of the wall.

Figure 8-86 shows peak axial stresses in steel braces in Wall 2 for all shaking intensities involving the NZ earthquake. Again, the non-uniform distribution of stresses indicates that one brace was attracting more seismic force than the other. This was due to a loose connection between the wall and one of the braces. As expected, the axial stress was well below the yielding limit.

Table 8-16 Peak values of axial stress of steel anchors and braces at Wall 2

Location	Instrument ID	Peak axial stress (psi)		
		NZ50%	NZ75%	NZ100%
Floor to wall Connection	W2SG1	36	49	57
	W2SG2	341	204	408
	W2SG3	325	166	187
	W2SG4	165	148	259
Braces	W2SG5	265	257	359
	W2SG6	1389	2154	2261

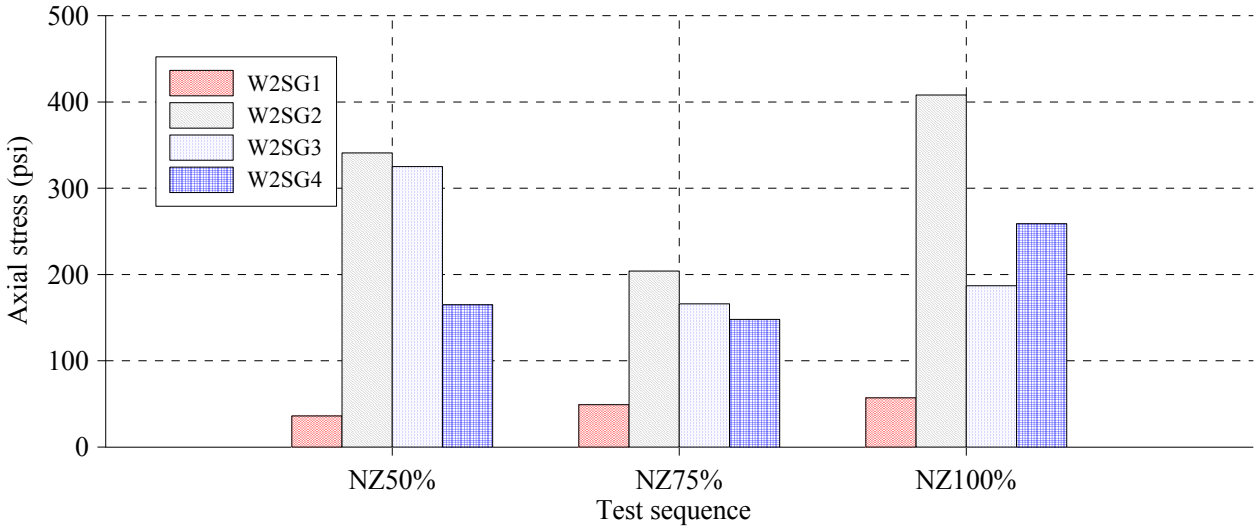

Figure 8-85 Peak axial stresses in steel anchors of Wall 2

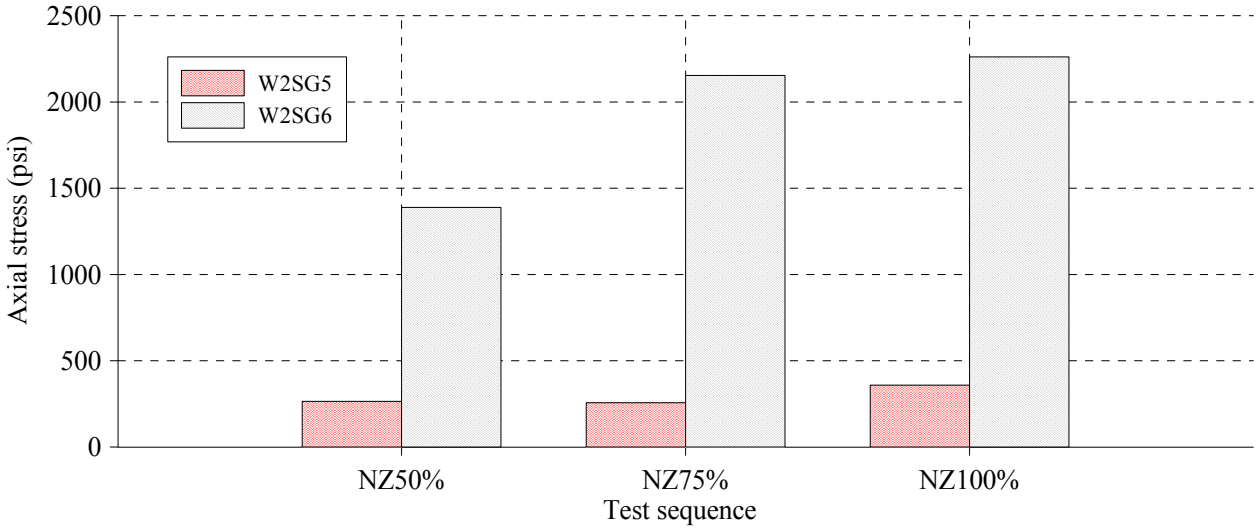

Figure 8-86 Peak axial stresses in steel braces of Wall 2

8.5.7.1 Hysteretic behavior of isolator, parapet and wall

The hysteretic behavior of low damping rubbers is shown in Figure 8-87. A maximum displacement of 2.5 inches and a corresponding force of 3000 lb. were obtained for N100% intensity level.

The nonlinear behavior of the portion of the wall above the wood floor is shown in Figure 8-88. After cracking, a predominant frictional and self-centering behavior can be observed. Note that residual deformation occurred for higher shaking intensities, making the wall as unrepairable, despite having implemented two standard retrofitting techniques. The peak absolute acceleration remained almost constant for all NZ intensity levels.

Figure 8-90 illustrates the hysteretic behavior of different portions of the wall below the wood diaphragm level. A nonlinear behavior between header courses can be observed for NZ100%. The hysteretic response of the first header course of the wall illustrates the nonlinear rocking behavior of the wall at the base, which is very similar to the hysteretic behavior of the isolator.

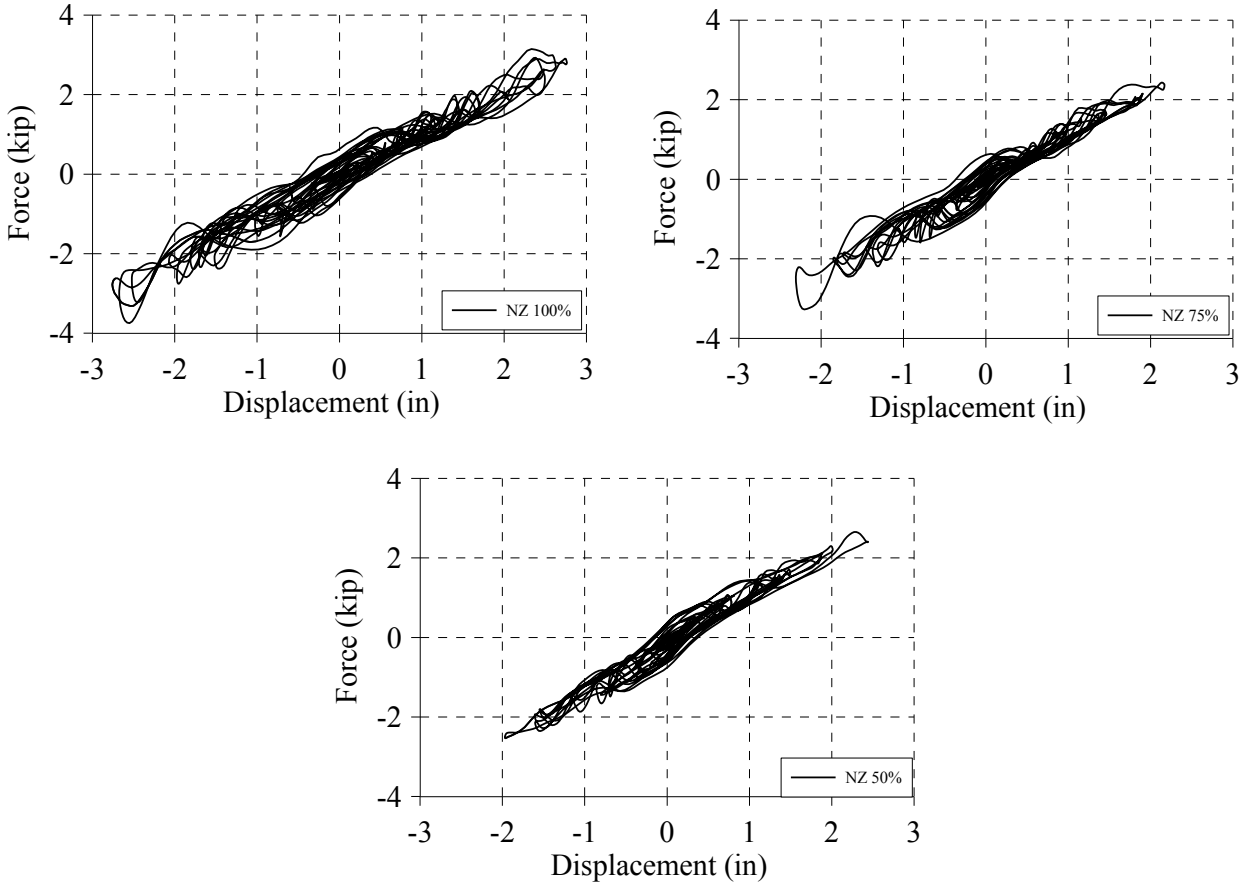

Figure 8-87 Force versus relative displacement of isolators at Wall 2

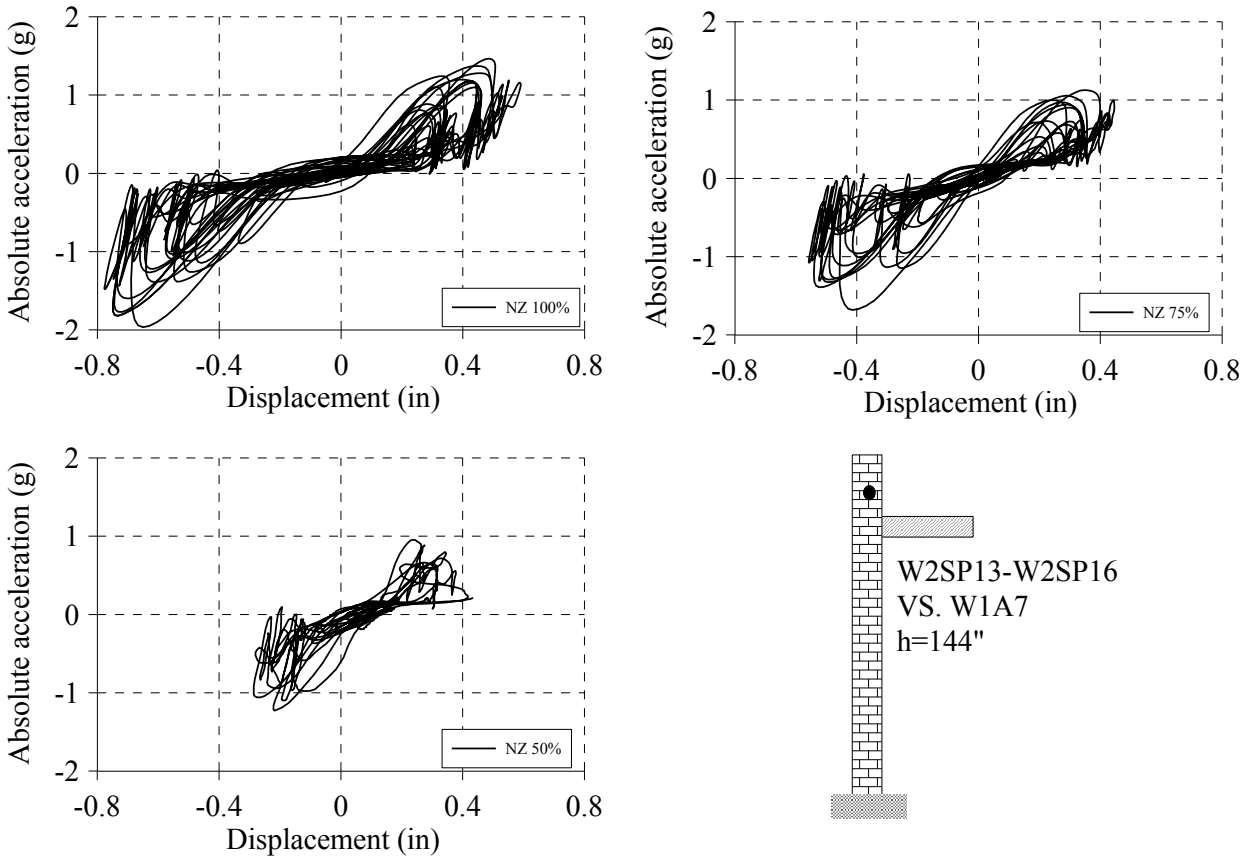

Figure 8-88 Acceleration versus relative displacement of parapet at Wall 2

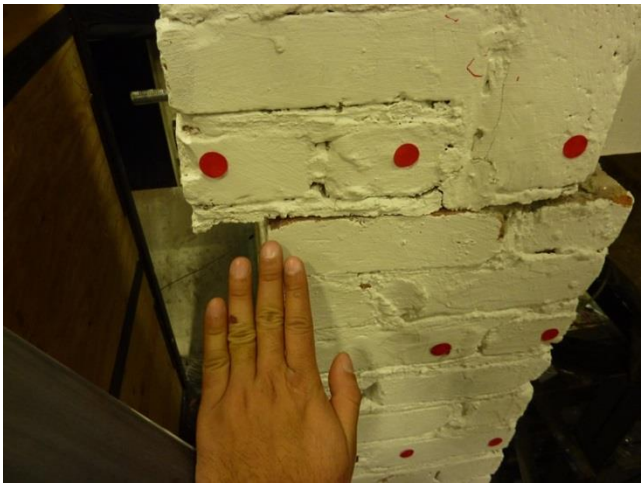

Figure 8-89 Final residual drift of Wall 2, after NZ 100%

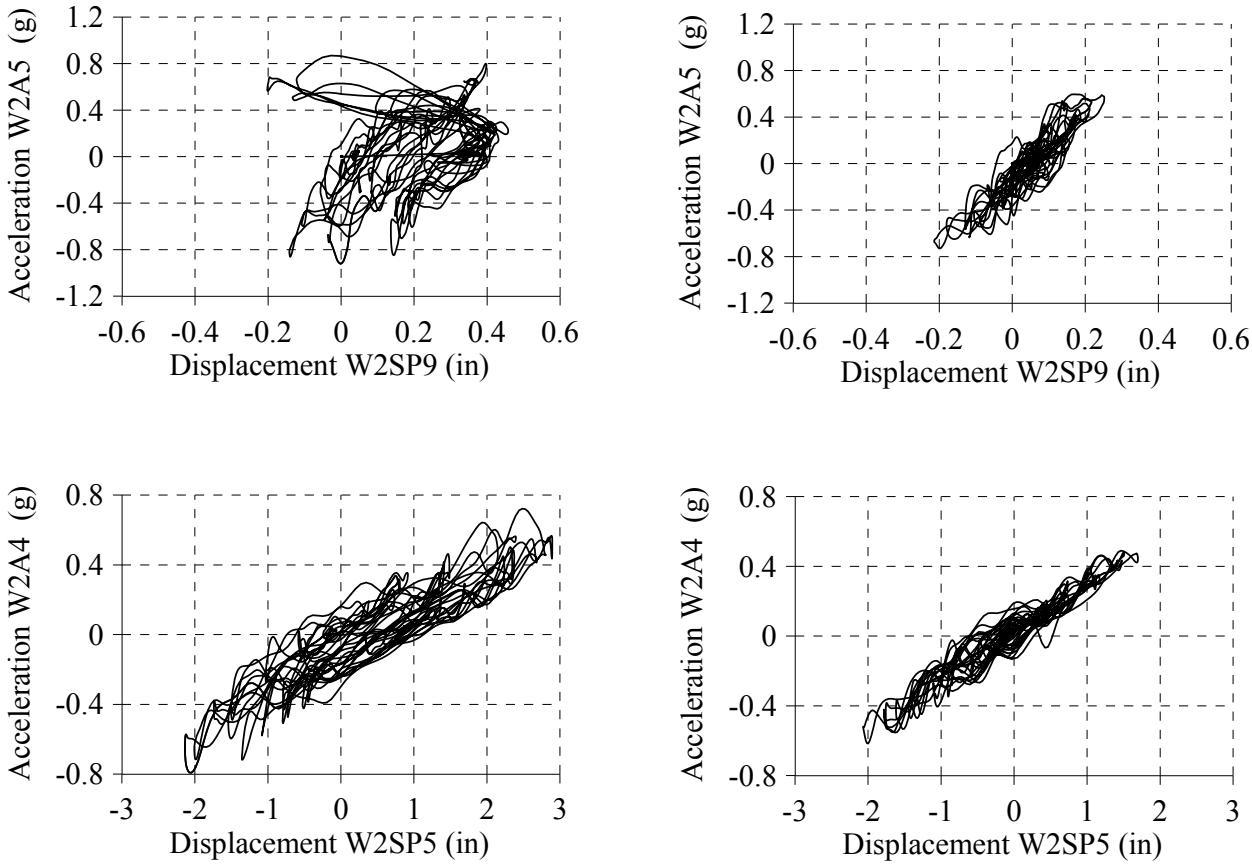

a) b)

Figure 8-90 Acceleration versus relative displacement along the height of Wall 2: a) Test NZ100% and b) Test NZ75%

8.5.8 Comparative Response of Wall 1 and Wall 2 for New Zealand Earthquake

Figure 8-91 shows a comparison between peak relative displacements at mid-height of the walls and parapets. A different behavior for both specimens can be seen, mainly due to Wall 2 having more flexible bearings. As in low level intensity tests, steel braces and steel rods in Wall 2 reduced the maximum displacement in the parapet for similar PGA levels, as illustrated in Figure 8-91. Note that the parapet of Wall 1 collapsed for NZ100%, whereas Wall 2 did not collapse but experienced irreparable damage.

Again, the peak relative displacements obtained at the top of the isolators were also different in both specimens, as shown in Figure 8-92 (a). However, as seen in Figure 8-92 (b), similar peaks displacements were obtained at the top of the tower of both walls.

Peak values of relative displacement response at several locations of Wall 1 and Wall 2 are shown in Figure 8-93. A linear distribution is dominant for Wall 1 whereas a nonlinear behavior is observed for Wall 2.

Peak values of absolute acceleration response at several locations in Wall 1 and Wall 2 are shown in Figure 8-94. A profile of linear absolute accelerations can be seen for both specimens. Both walls had a large relative displacement of the steel tower, as shown in Figure 8-93(b). The absolute acceleration was amplified at this level, as can also be seen in Figure 8-94(b).

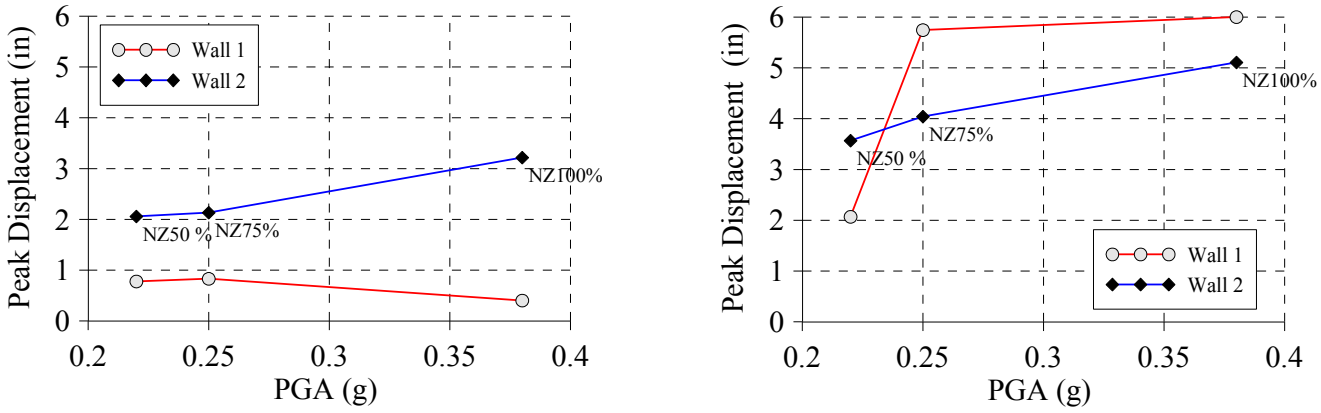

Figure 8-91 Peak relative displacement vs. PGA at a) Mid-height of the walls b) Parapets

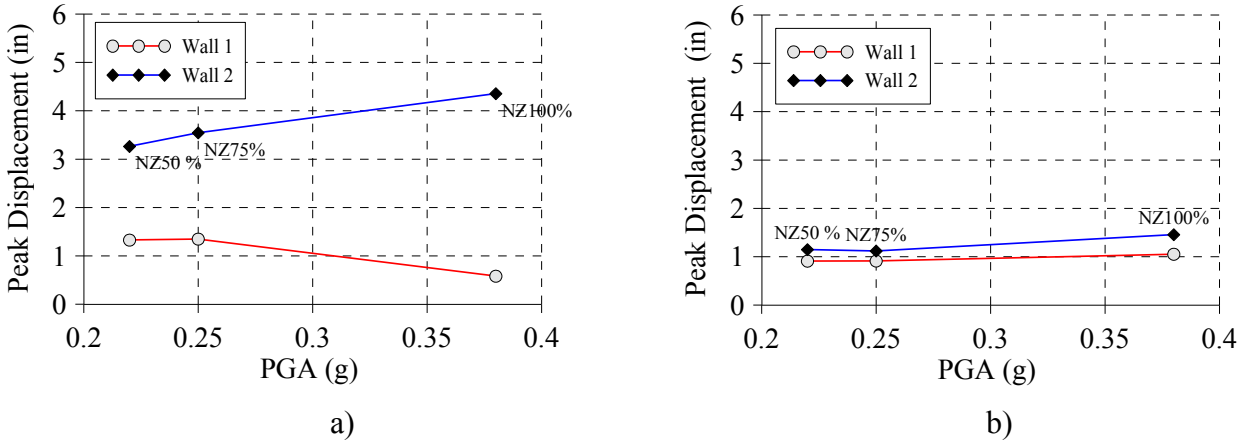

Figure 8-92 Peak relative displacement vs PGA at a) Isolators b) Steel tower

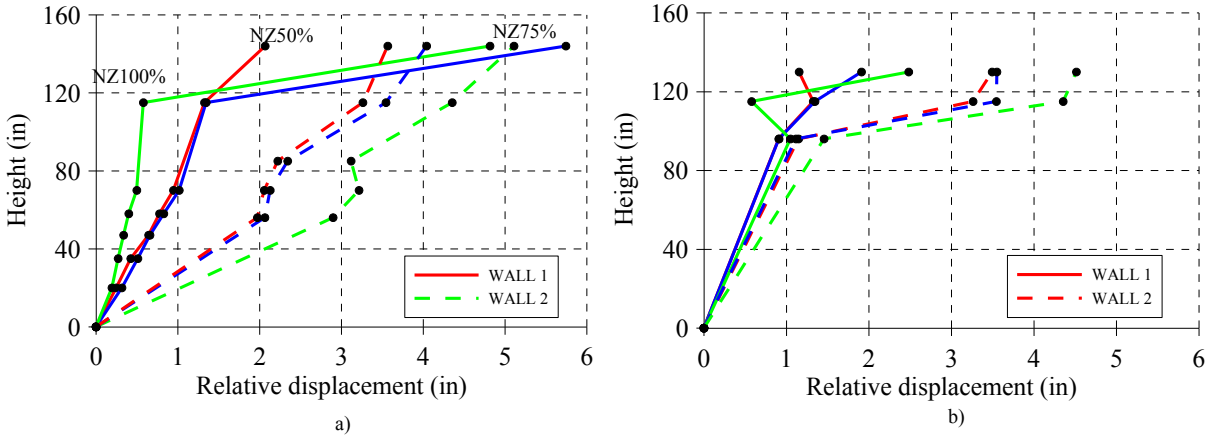

Figure 8-93 Comparison of peak relative displacement profile of Wall 1 and Wall 2 at a) Masonry wall and b) Steel tower and isolators

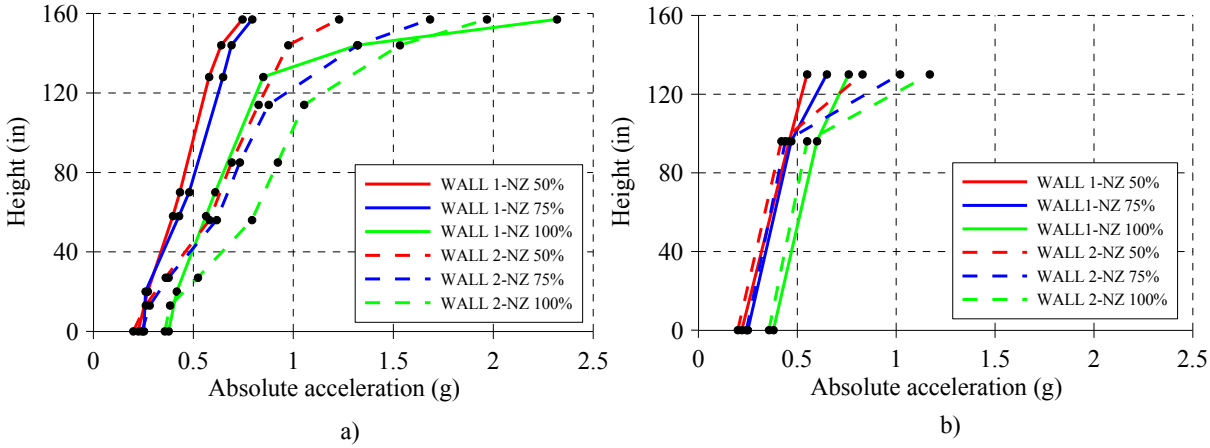

Figure 8-94 Comparison of peak absolute acceleration profile of Wall 1 and Wall 2 at a) Masonry wall and b) Steel tower and isolators

8.5.9 Effect of Frequency Content in the Response of Wall 1 And Wall 2

The effect of the frequency content on the seismic response of both walls was observed by subjecting the specimens to the same PGA but different ground motions. Figure 8-95 presents the absolute acceleration obtained at the shake table for VA300% and NZ50%. Note that the peak acceleration in both cases is about 0.20g. On the other hand, the absolute displacement response obtained in the table is significantly different, as shown in Figure 8-96. As discussed before, out-of-plane masonry walls are more sensitive to displacements than accelerations.

The response of the walls in terms of peak displacements can be seen in Figure 8-97. Note the larger deformations for NZ50%, at the tower, isolators and the masonry walls. A comparison of the absolute acceleration response is shown in Figure 8-98. The parabolic distribution of accelerations in the masonry wall indicates a strong influence of the frequency content of the input motion. This influence can also be observed in the steel tower and isolators. Note that resonance issues between the natural frequency of the table and the input motions could also explain this unexpected behavior. This issue, however, was not further investigated.

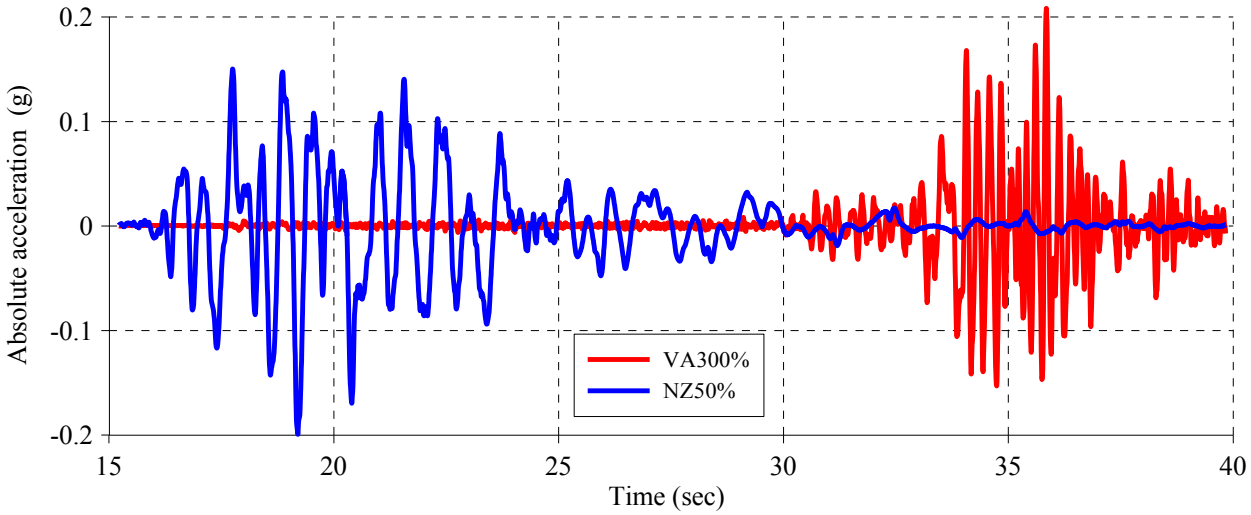

Figure 8-95 Absolute acceleration of the shake table for VA300% and NZ50%

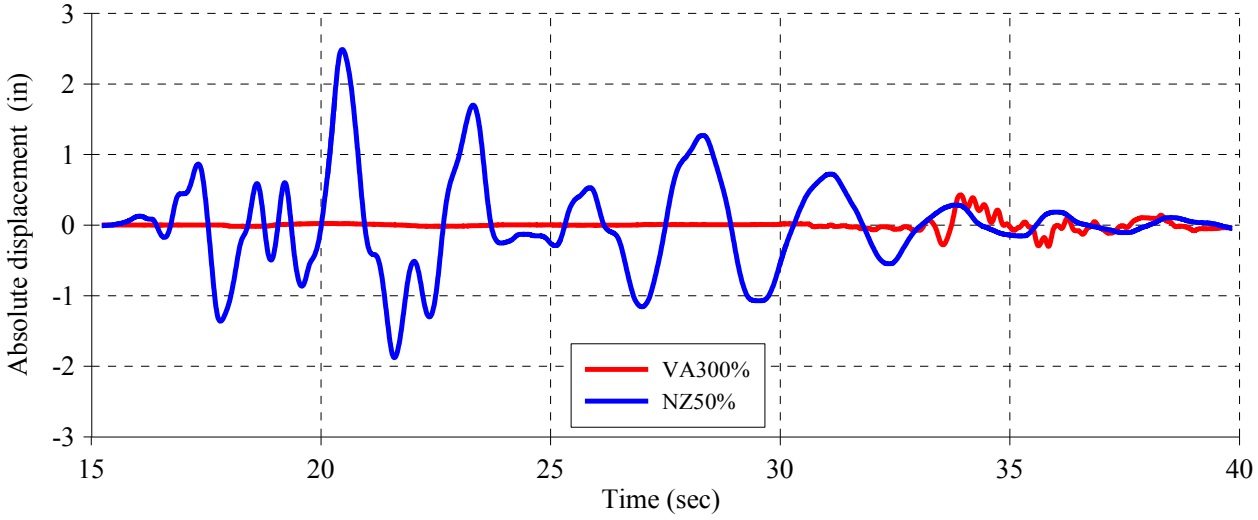

Figure 8-96 Absolute displacement of the shake table for VA300% and NZ50%

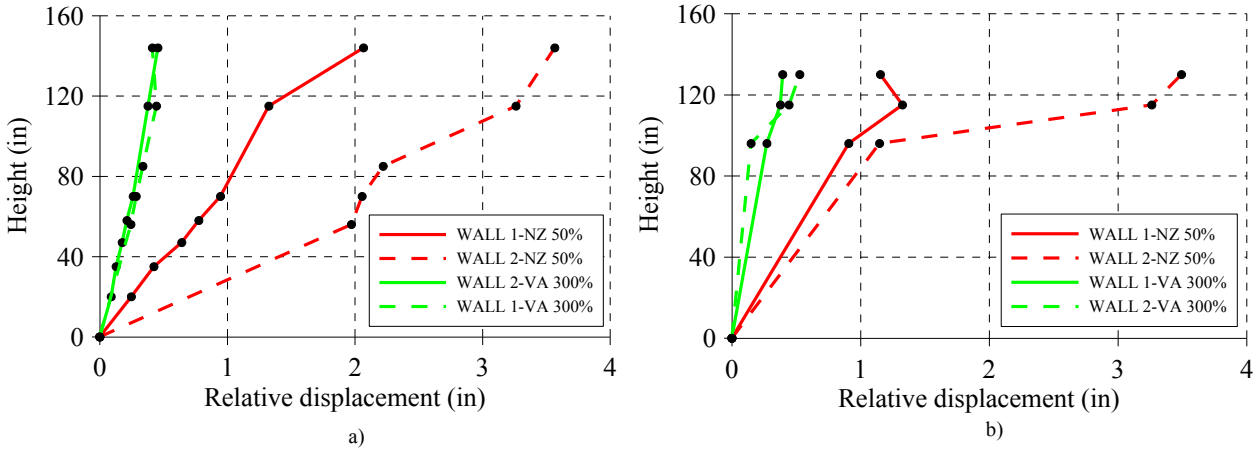

Figure 8-97 Comparison of peak relative displacement profile of Wall 1 and Wall 2 for VA300% and NZ50% intensity levels at a) Masonry wall and b) Steel tower and isolators

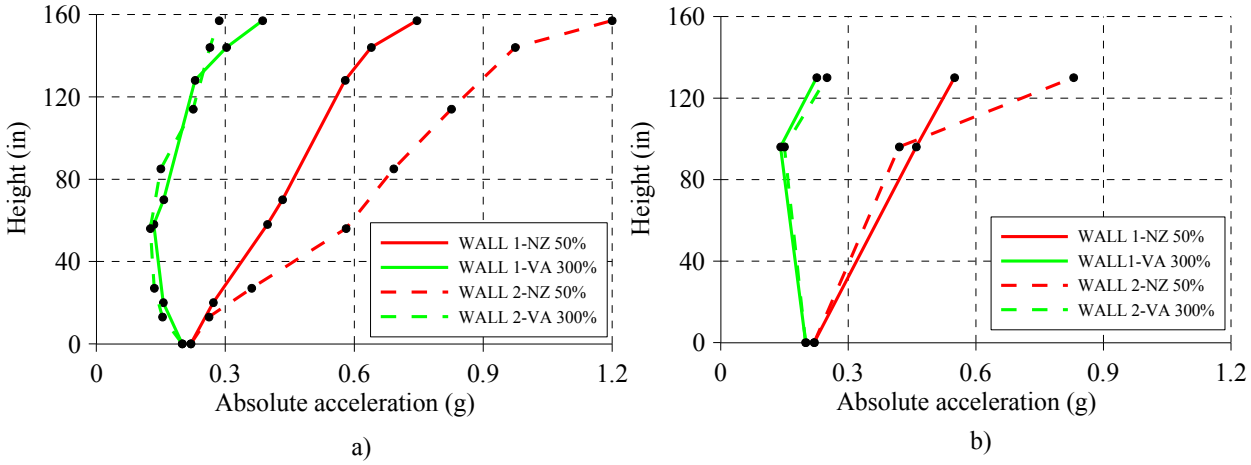

Figure 8-98 Comparison of peak absolute acceleration profile of Wall 1 and Wall 2 for VA300% and NZ50% intensity levels at a) Masonry wall and b) Steel tower and isolators

8.6 Comparison of the Walls and Diaphragm Response with ASCE 41-06 Standard and ABK Methodology

In this section, a comparison of the walls and flexible diaphragm shake table response with ASCE 41-06 standard and the ABK methodology is presented. This comparison will provide more insight regarding the level of conservatism existing in these current methodologies. However, it is important to clarify that a larger number of shake table testing and specimens are required to define a trend in the response of the walls, and reduce the uncertainty in current seismic assessment methodologies.

Code based evaluation of out-of-plane walls is currently addressed by ASCE 41 (2006), NZSEE (2006) and EUROCODE 8. Current stability limits (h/t ratios) for out-of-plane unreinforced masonry (URM) walls, as described in ASCE/SEI 41-06 (2007), are based on recommendations provided by the ABK experimental program (ABK 1984). As discussed in Section 3, the concept of defining an h/t ratio for URM out-of-plane walls has been suggested many years ago through the empirical design of URM walls in the United States.

Recent research conducted on out-of-plane URM walls to evaluate the ASCE 41-06 h/t limits showed contradictory results. In one hand, Simsir et al. (2004), Sharif et al. (2007) and Penner and Elwood (2012) suggested that the allowable h/t ratios in the current seismic design guidelines are somewhat conservative and can be increased from 20 to as much as 31 for low

intensity ground accelerations, as shown in Figure 8-99. In contrast, research programs conducted in New Zealand by Derakhshan (2011) on out-of-plane walls subjected to near field ground motions and shallow soils concluded that the ASCE 41-06 h/t limits are significantly unconservative, as illustrated in Figure 8-100.

Recommendations provided in NZSEE (2006) for evaluation of one-way spanning walls are based on the work by Blaikie (1999) and Blaikie and Spurr (1992). They formulated an analytical model of the walls based on stability concepts. Similar to ASCE 41-06, if the walls are not properly restrained to the diaphragms, then this methodology cannot be used. Since the methodology was validated using the ABK experimental results, its shares the same shortcomings and range of validity. Moreover, the method does not include details that show whether the effects of diaphragm flexibility have been included in the methodology (Derakhshan, 2011).

EUROCODE 8 provides some constraints regarding the minimum thickness and maximum slenderness of URM walls. However, it is recognized that the proposed approach for seismic evaluation of URM buildings is inappropriate or incomplete (Magenes and Penna 2011). Regarding the out-of-plane evaluation of masonry buildings, a recent methodology has been implemented in the Italian code for the seismic analysis of this local collapse mechanism based on equilibrium limit analysis. This methodology is based on the analytical and experimental work conducted by several researchers [D'ayala and Speranza (2003), De Felice and Giannini (2001), Doherty et al. (2002), Griffith et al. (2007), Vélez and Magenes (2009)].

Although the proposed methodology is useful to evaluate the assessment of out-of-plane walls, further research is required to verify the results in low seismicity areas in which the limit states might never be reached, and account for slender walls with non-negligible initial elastic deformability (Magenes and Penna, 2011).

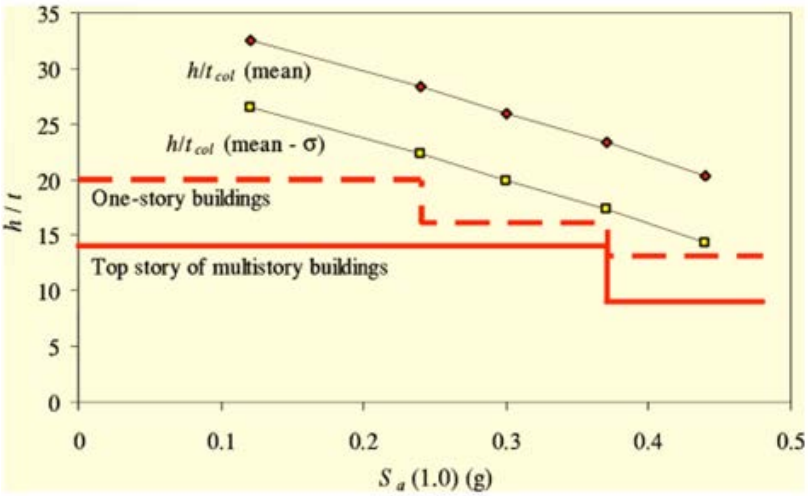

Figure 8-99 Results of the evaluation of ASCE 41-06 h/t limits conducted by Penner and Elwood (2012)

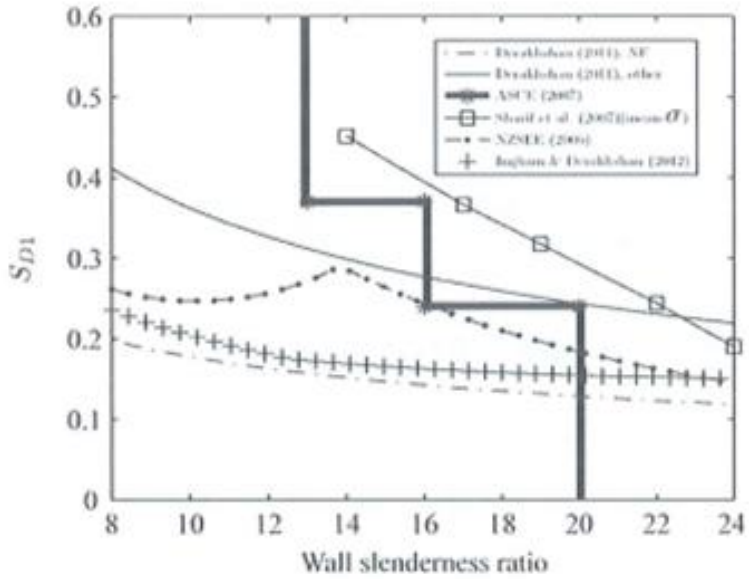

Figure 8-100 Results of the evaluation of ASCE 41-06 h/t limits conducted by (Derakhshan 2011)

Figure 8-101 shows the experimentally obtained spectral acceleration at 1 second, **Sa (1.0)** for the specimens at NZ75% intensity level (Walls exhibited severe damaged at this intensity level) overlaid on the permissible h/t ratios for URM out-of-plane walls recommended in ASCE 41-06 standard. This standard stated that for the wall specimens (h/t=10), stability need not to be checked since the slenderness is less than 20, which is the limit for walls of one-story buildings.

Also, spectral accelerations which would cause damage to the walls are expected to be higher than 0.37g. From Figure 8-101, it can be seen that these recommendation are unconservative, since severe damage was observed in the walls at **Sa(1.0)** equals to 0.24g. Even the permissible limits for walls at the top story of multi-story buildings appear to be unconservative, as also highlighted in Figure 8-101.

As indicated in Section 8.1.1, current stability limits (h/t ratios) for URM out-of-plane walls, as described in ASCE/SEI 41-06 (2007), are based on recommendations provided by the ABK experimental program (ABK 1984). However, these stability limits (h/t) were first recommended by ABK in terms of velocities, rather than accelerations. As indicated by Bruneau (1994b), input velocities are directly related to the seismic energy delivered to the system and can be a convenient demand parameter, for both, the walls and flexible diaphragms. Figure 8-102 shows the experimentally obtained peak velocities at diaphragm levels of Wall 1 and 2. It can be seen that the ABK methodology is also unconservative, since both walls were damaged at peak diaphragm velocities lower than expected.

Regarding the seismic behavior of existing buildings with flexible diaphragms, the ABK methodology specifies boundary limits (See Figure 8-103), in which the existent structure must fall in order to prevent excessive inter-story drifts and velocity amplifications. In Region 1, crosswalls are required to keep the velocity (V) less than 21 in/sec and the velocity amplifications (**Av**) less than 1.75. For Region 2, crosswalls are not needed, since the demand-capacity ratio (DCR) is sufficient to keep **Av** less than 1.75 and V less than 21 in/sec. For Region 3, the DCR is not sufficient to prevent **Av** and V to be less than 1.75 and 21 in/sec, respectively.

The corresponding DCR for the prototype and the wall specimens were computed to assess their expected performance, as per ABK methodology. The DCR was computed as the ratio between the peak shear and the ultimate capacity of the diaphragm. For the prototype, the peak shear was obtained through nonlinear response history analysis under the NZ75% intensity level, and the capacity through pushover analysis of the diaphragm. For Wall 1 and Wall 2 the peak shear was obtained from the response of the isolators during the NZ75% intensity level, as seen in Figure 8-77 and Figure 8-87, respectively. The capacity was obtained from the force-displacement relationship of each isolator, which was taken from Sanchez-Ferreira (2011). The prototype building, and Wall 1 and 2 fall in Region 3, as seen in Figure 8-103.

Figure 8-104a and Figure 8-104b presents the peak velocities obtained for all intensity levels in Wall 1, tower and isolators, respectively. Little amplification was obtained for all intensities of the Virginia earthquake. However, the input velocity was amplified up to three times at the diaphragm level, for all New Zealand earthquake intensities. Note that the velocities were obtained by integrating the recorded accelerations. Velocities at the parapet for NZ100% could not be estimated due to numerical errors introduced by the recorded accelerations at that level due to rocking behavior.

Figure 8-105a and Figure 8-105b presents the peak velocities obtained for all intensity levels in Wall 2, tower and isolators, respectively. Similar to Wall 1, the input velocity remained almost constant for all intensity levels of the Virginia earthquake. Larger amplifications of the input velocity (up to 4 times) at the diaphragm level were obtained for all intensities of the New Zealand earthquake.

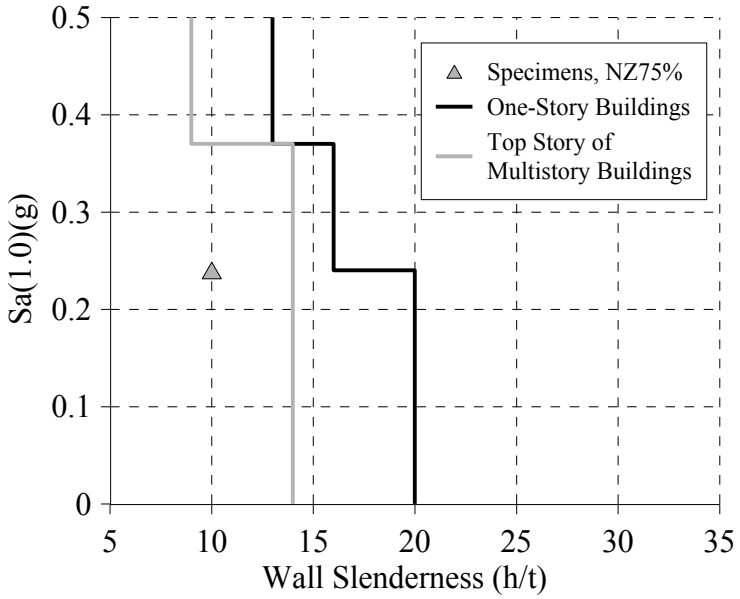

Figure 8-101 Experimentally obtained Sa (1.0) superposed on figure of permissible h/t ratios for URM out-of-plane walls (ASCE 41-06)

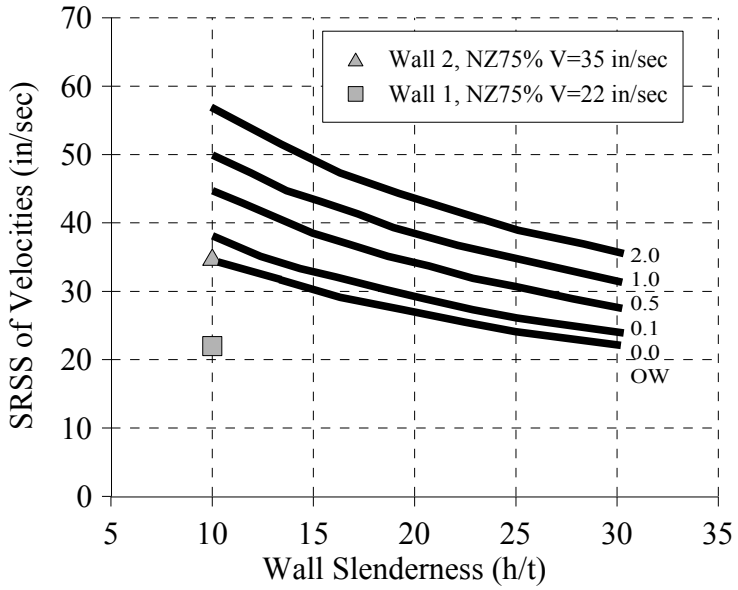

Figure 8-102 Experimentally obtained peak velocities superposed on ABK's regression analysis curves for 98% probability of survival for out-of-plane dynamic stability response of URM walls (calculation of permissible limits: SRSS denotes the square root of the sum of the squares). [Adapted from Bruneau (1994b)]

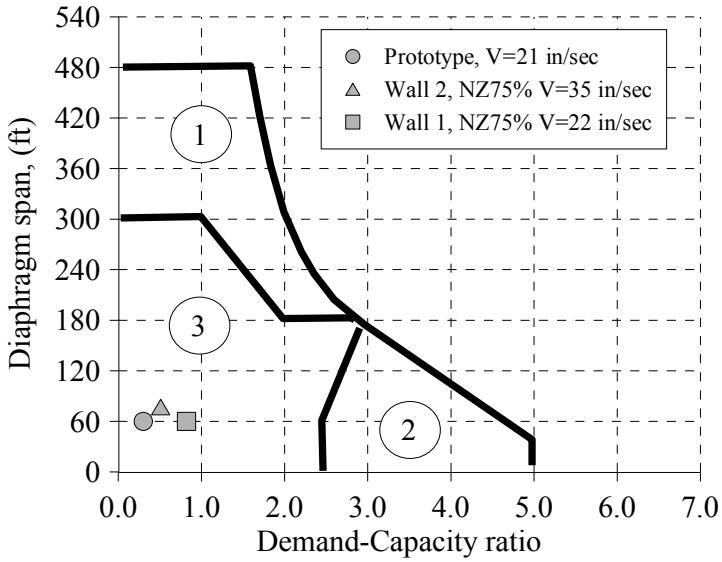

Figure 8-103 DCR of the building prototype, Wall 1 and Wall 2, superposed on figure of acceptable diaphragm span versus demand-capacity ratio [Adapted from Bruneau (1994b)]

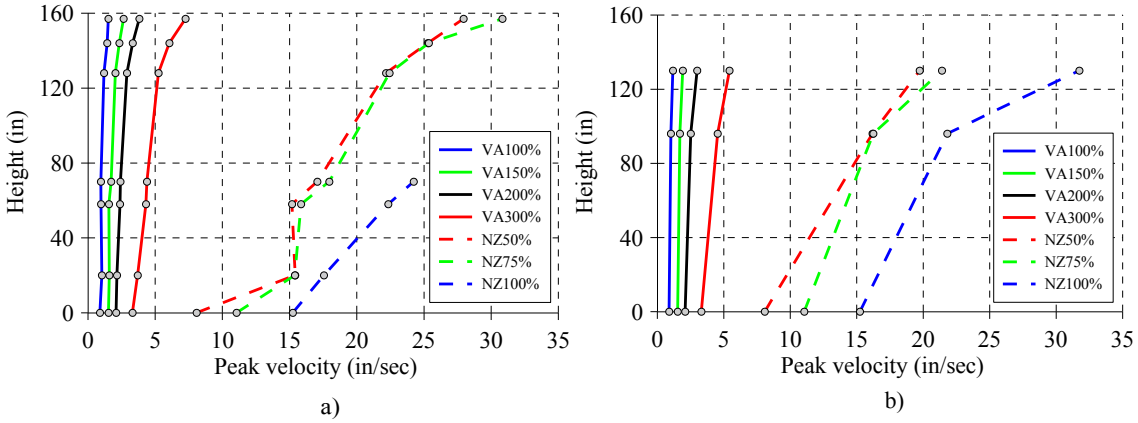

Figure 8-104 Peak velocity profile of Wall 1 at a) Masonry wall and b) Steel tower and isolators

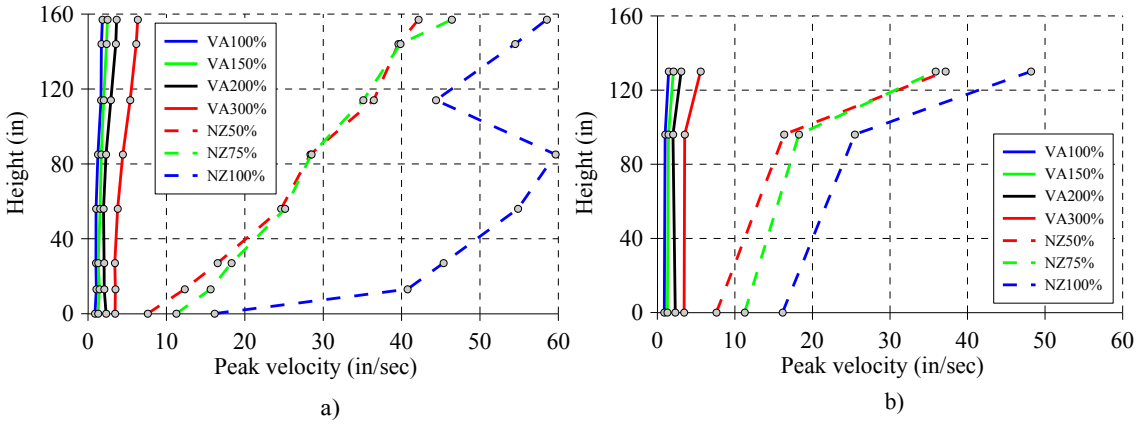

Figure 8-105 Peak velocity profile of Wall 2 at a) Masonry wall and b) Steel tower and isolators

8.7 Comparison Between Numerical and Experimental Results

In this section, predictions of the seismic response and dynamic characteristics for the experimental structure were performed on a numerical model developed in SAP2000. The modelling techniques developed in Section 4, 5 and 6 were used to develop a simplified numerical model of the experiment conducted in Section 8. The numerical model includes the masonry wall, connections and diaphragm flexibility.

Herein, the intention was not to calibrate the main structural elements of the model to match the experimental results. Instead, an effort was made to validate previous numerical models, which

are based on simple equations and understand its overall performance in capturing the nonlinear seismic response of the system.

8.7.1 Numerical Model in SAP2000

The numerical model of the masonry walls was developed following the approach described in Section 6. Figure 8-106 illustrates a 3D view of the final model in SAP2000 and its main structural components.

A 12”x72”x167” shell thick element with Modulus of Elasticity of 500 ksi and unit weight of 6.944e-05 kip/in^3 was created in SAP2000. Two cracks were connecting three independent shell elements. One crack was located at mid-height of the wall while the other one was placed at the base of the parapet. Moment-rotation relationships were also defined using equations proposed in Section 6.

Elastic beam elements were used to model 2”x10”wood joists. Elastic modulus and unit weight were set equals to 1800 ksi, and 1.98E-05 kip/in^3, which are values used in Section 4. Note that wood boards were not modeled, but an **x-y** constraint between intermediate joints was applied. The concrete block was simulated by applying a distributed load on certain joists elements, as illustrated in Figure 8-107.

An impact-friction-nail model, as recommended in Section 5, was defined to connect the masonry wall to the wood joist element. A close-up view of the model can be seen in Figure 8-108. Note that the nail model was modeled only in Wall 2, which had steel anchors to prevent relative sliding. Also, elastic beam elements were used in Wall 2, to model the steel braces used to reinforce the parapet.

As discussed before, diaphragm flexibility was accounted for using elastomeric bearings. Numerical model of this type of bearing are incorporated in SAP2000. A Rubber Isolator Nlink type was used for this purpose. The properties of lead rubber bearings and low damping rubbers were obtained from previous experimental studies (Sanchez-Ferreira 2011), calibrated and then implemented in the model of the wall, as shown in Figure 8-109 and Figure 8-110.

Elastic beam elements were used to model the steel tower. The cross section properties and dimensions were also obtained from previous research (Alzeni 2014). To capture the global rotation of the tower, due to flexibility of the concrete extension of the shake table, gap and

elastic spring elements were introduced at the base of the tower and the masonry wall. The properties of these elements were calibrated to match the rotational movement of the tower.

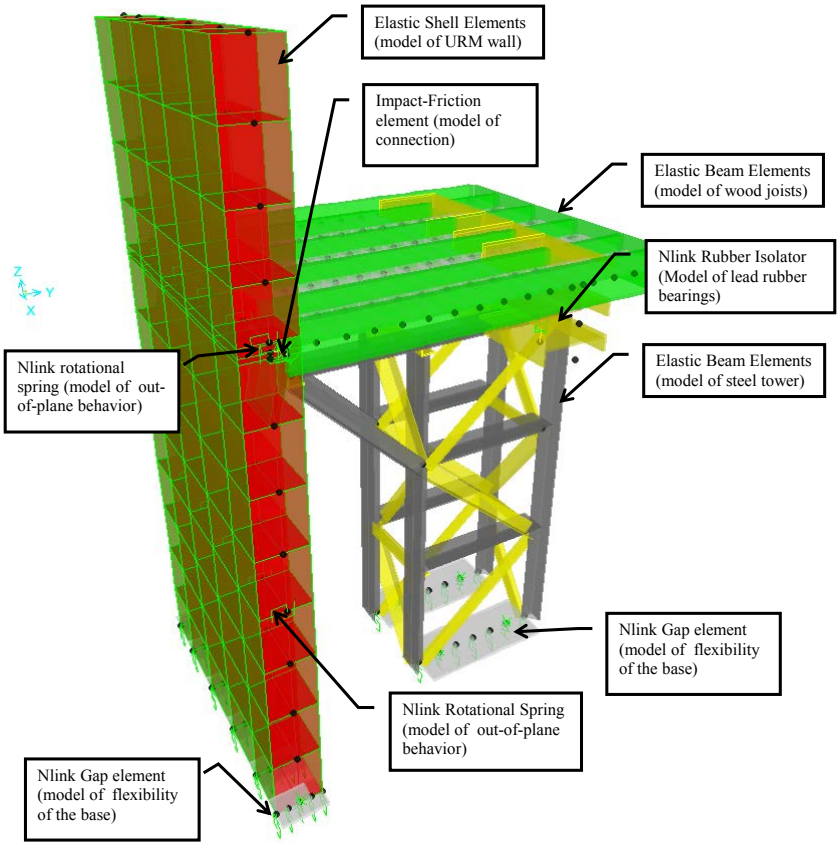

Figure 8-106 3D model of the URM wall specimen using SAP2000

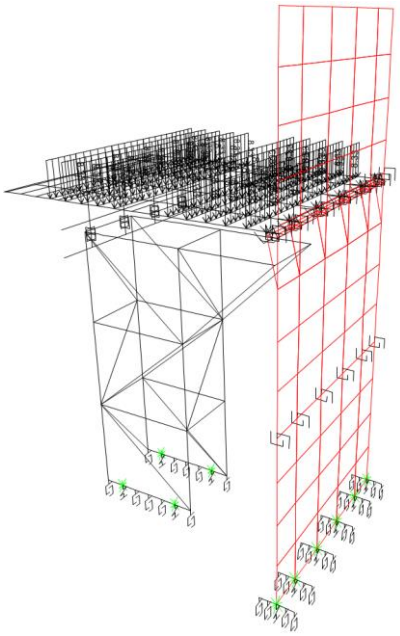

Figure 8-107 Superdead loads applied to the numerical model to simulate concrete blocks

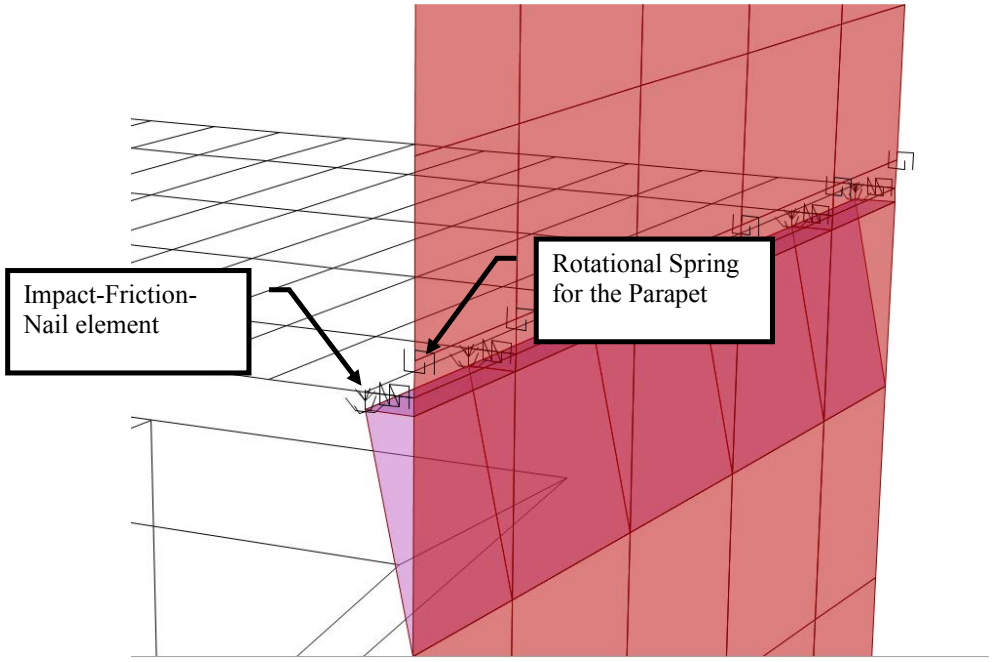

Figure 8-108 Modeling of the connection between wood joist and masonry walls

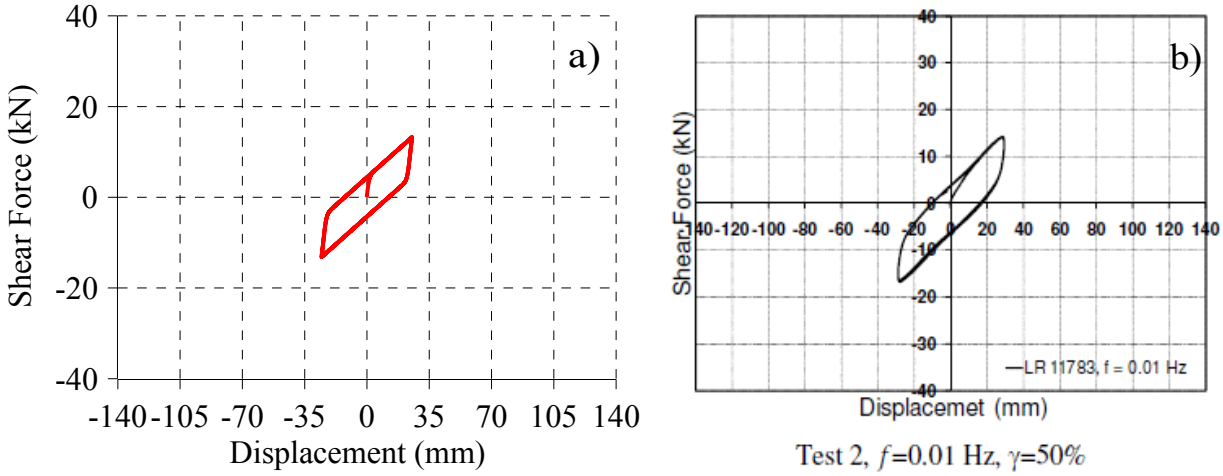

Figure 8-109 Calibration of isolator properties used in Wall 1: a) Numerical and b) Experimental

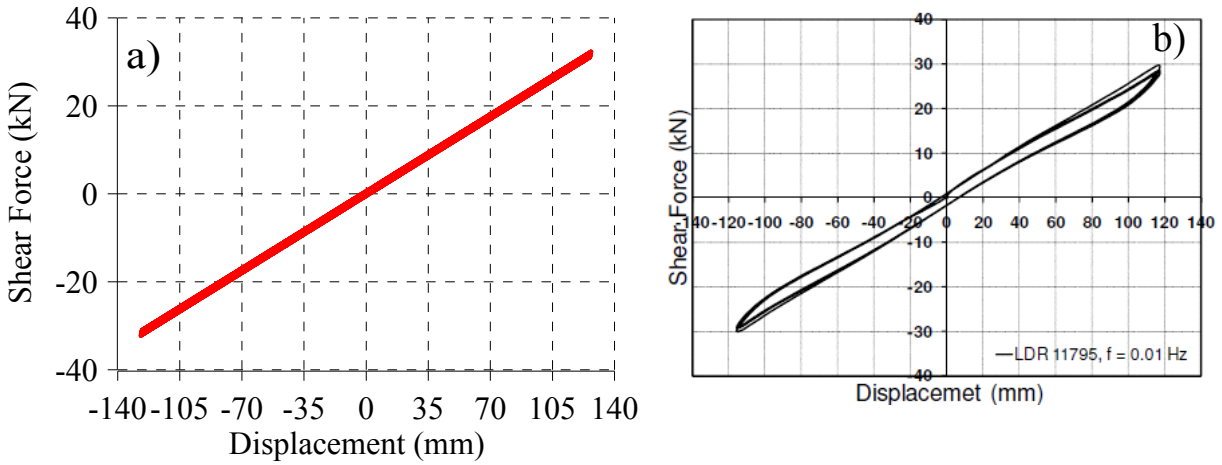

Figure 8-110 Calibration of isolator properties used in Wall 2: a) Numerical and b) Experimental (Sanchez-Ferreira 2011)

Actual absolute accelerations recorded at the base of the table during the test were used as an input to analyze this structure. Gravity loads were first applied to the structure using a nonlinear static case. Then nonlinear response history was conducted using Hilber Hughes-Taylor direct integration scheme available in SAP2000. Mass and stiffness proportional damping were used, with 2% damping applied to the first mode, and 5% to the second. Lower damping values can be considered since most energy dissipation is expecting to come from the Nlink elements included

in the model. The P-delta plus large displacement option was selected for all time-history analysis.

8.7.2 Comparison of Numerical and Experimental Results for Wall 1 and Wall 2

A comparison of numerical and experimental peak relative displacements and absolute accelerations obtained for NZ75% ground motion intensity is presented in this section. This run was considered more appropriate to compare the nonlinear response of the wall, since the final run caused collapse in both specimens and the VA300% intensity barely caused damage in the wall.

Overall, the numerical model underestimated the accelerations of Wall 1 and Wall 2, as observed in Figure 8-111 and Figure 8-112. A very good agreement was obtained for accelerometers located close to the bottom part of the walls. In particular, the accelerations obtained for Wall 1 at the parapet and for Wall 2 right underneath the wood joist were underestimated by almost 100%. This is mainly because the numerical model for the cracks in the parapet cannot capture impact due to rocking.

A better prediction was obtained for peak relative displacements. Figure 8-113 and Figure 8-114 present a comparison between peak relative displacements obtained for Wall 1 and Wall 2 respectively. The numerical model overestimated most peak displacements, in particular for Wall 2. Nonetheless, a good prediction was obtained for the displacement at the top of the steel tower and isolators.

Response history comparison of relative displacements and absolute accelerations are presented in Figure 8-115 through Figure 8-120 and from Figure 8-121 to Figure 8-124, respectively, for Wall 1. In general, the dynamic characteristics of the wall are well simulated along the height of the wall. However, the highly nonlinear behavior of the parapet (See Figure 8-115) was poorly captured by the model since cumulative damage from previous runs are not accounted for in this simulation.

For Wall 2, the response history displacements are presented from Figure 8-126 to Figure 8-133. A very good agreement was found during transient response of the system, while a minor lengthening of the period can be seen during free response. Absolute accelerations are shown from Figure 8-134 to Figure 8-140. Again, good agreement was found between the numerical

model and the experiment. The most notable disagreement occurred at the steel braces and anchors, in which the numerical model significantly overestimated the peak axial responses.

A comparison of peak displacements at the top of wall 1, between one-story building prototype, specimen and numerical model is presented in Figure 8-125. A good agreement can be observed between the numerical model of the experiment and the prototype. However, the peak response is overestimated in both models.

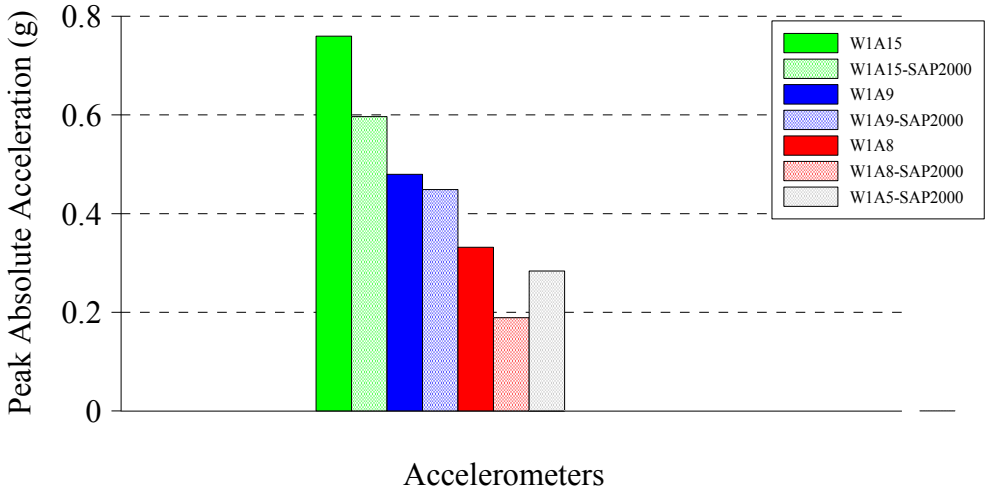

Figure 8-111 Numerical and experimental comparison of peak absolute accelerations of Wall 1

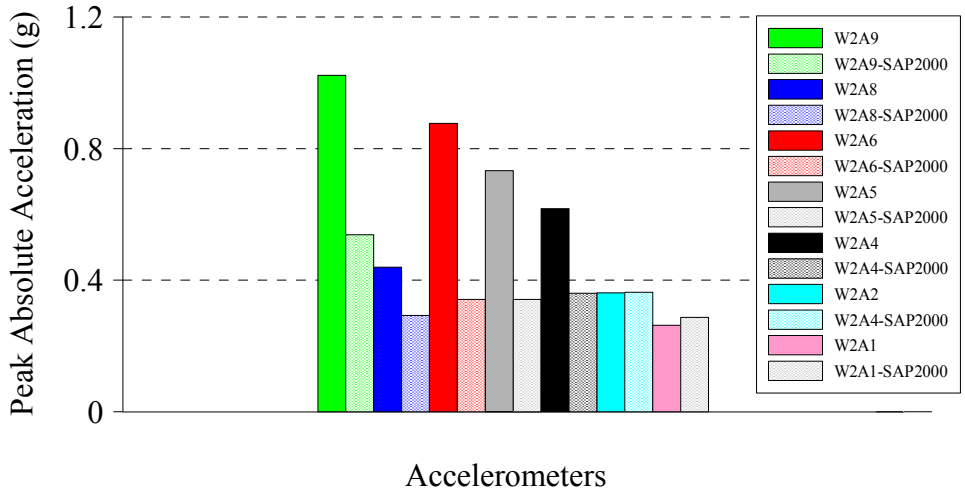

Figure 8-112 Numerical and experimental comparison of peak absolute accelerations of Wall 2

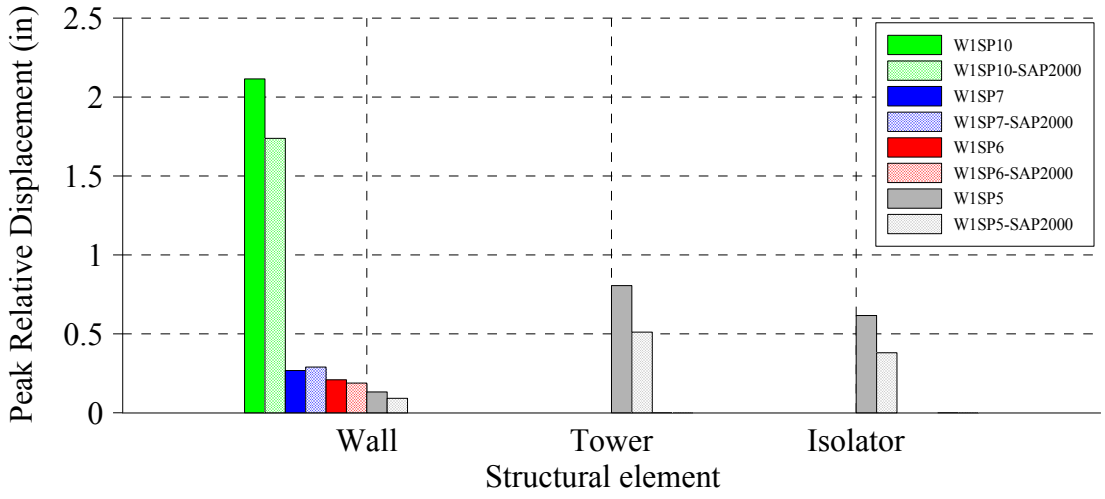

Figure 8-113 Numerical and experimental comparison of peak relative displacement of Wall 1

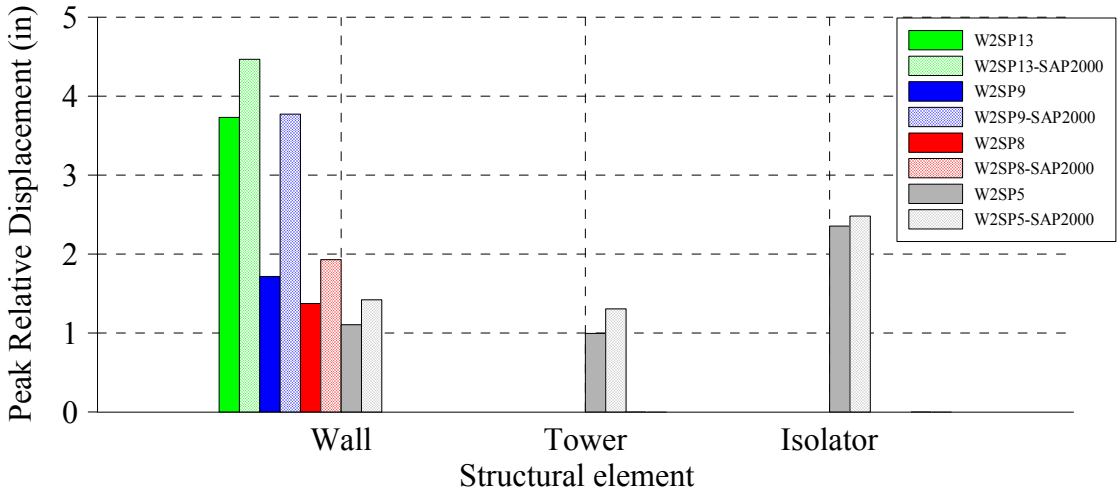

Figure 8-114 Numerical and experimental comparison of peak relative displacement of Wall 2

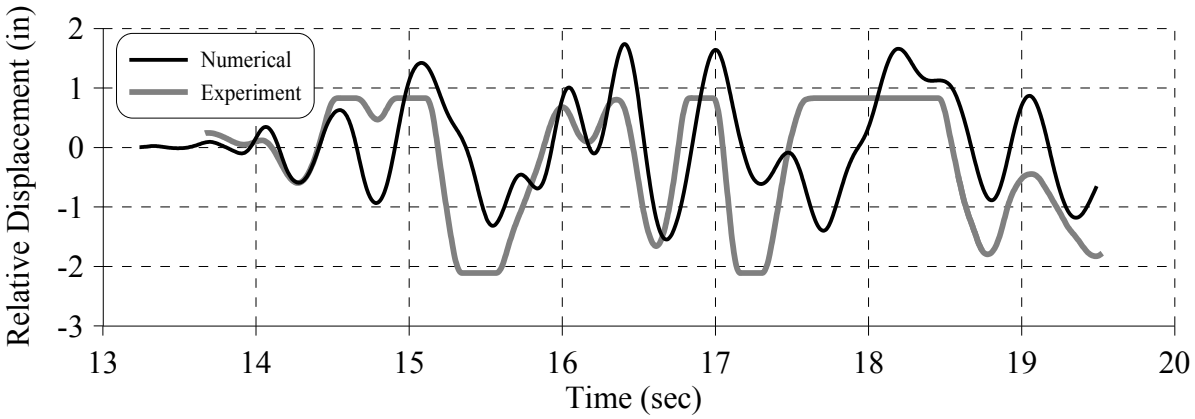

Figure 8-115 Comparison of relative displacement W1SP10

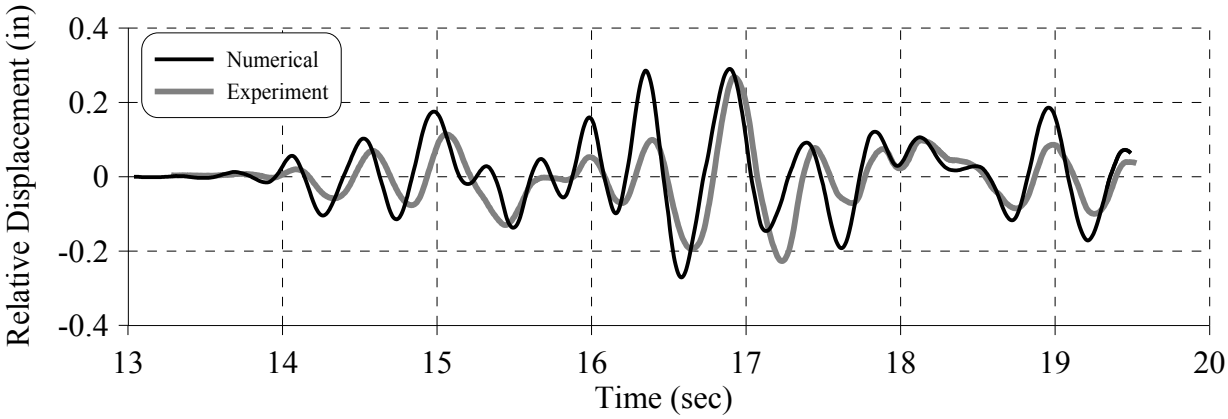

Figure 8-116 Comparison of relative displacement W1SP7

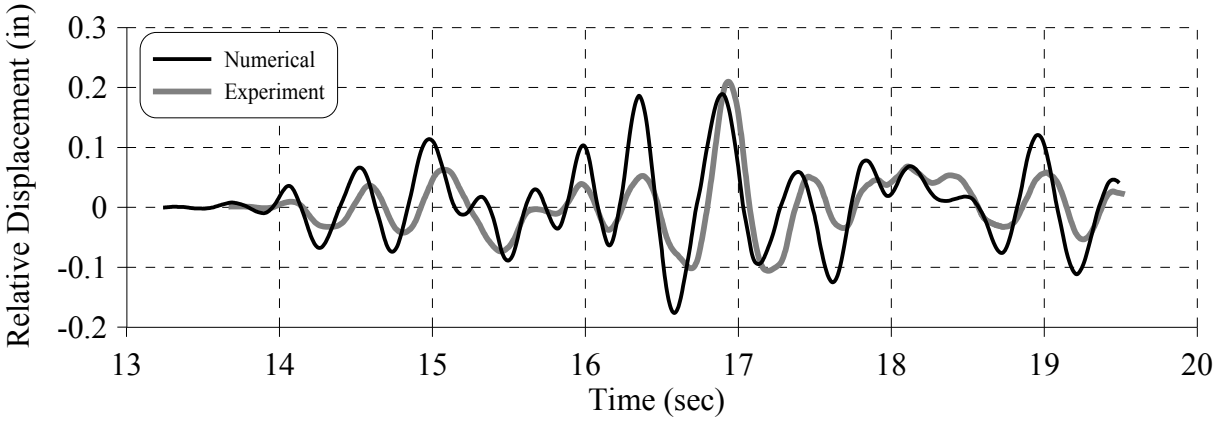

Figure 8-117 Comparison of relative displacement W1SP6

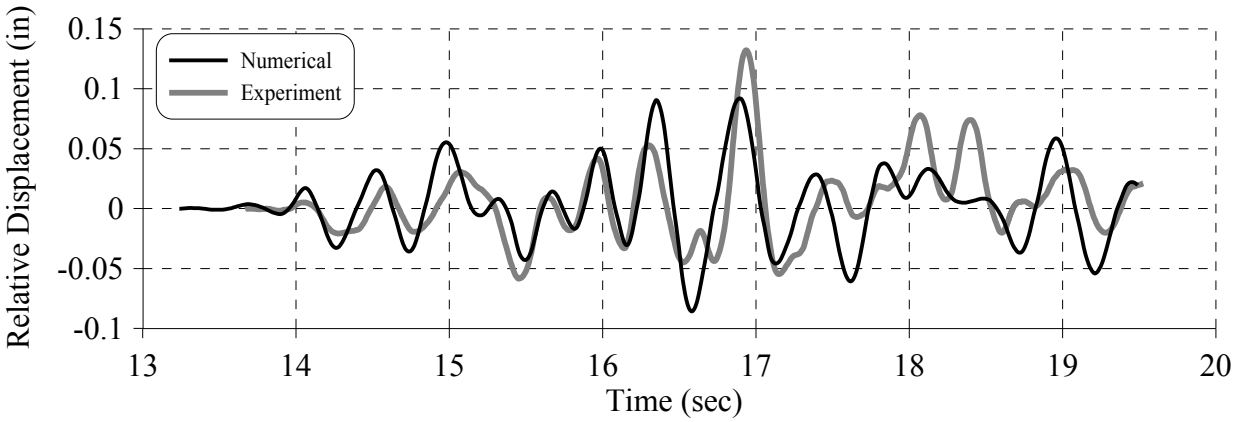

Figure 8-118 Comparison of relative displacement W1SP5

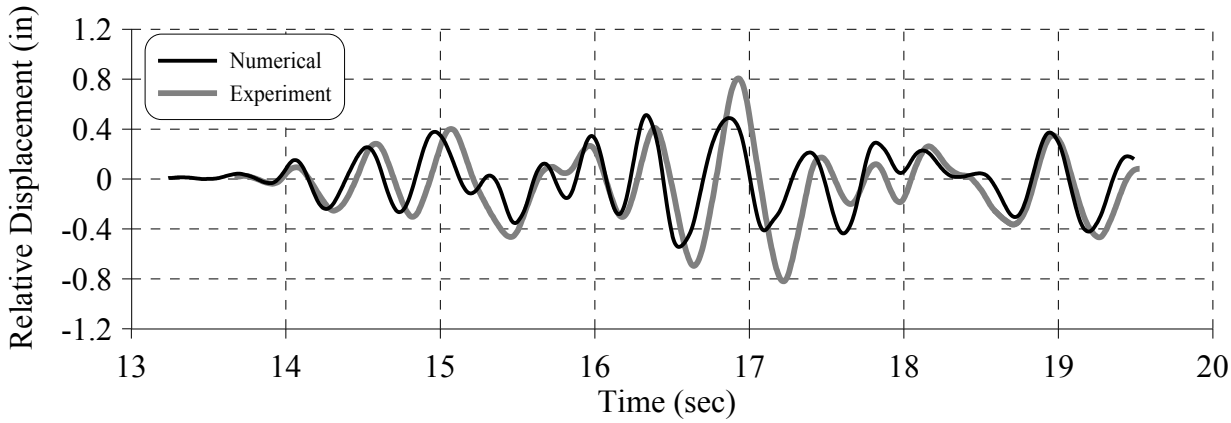

Figure 8-119 Comparison of relative displacement of tower W1SP3

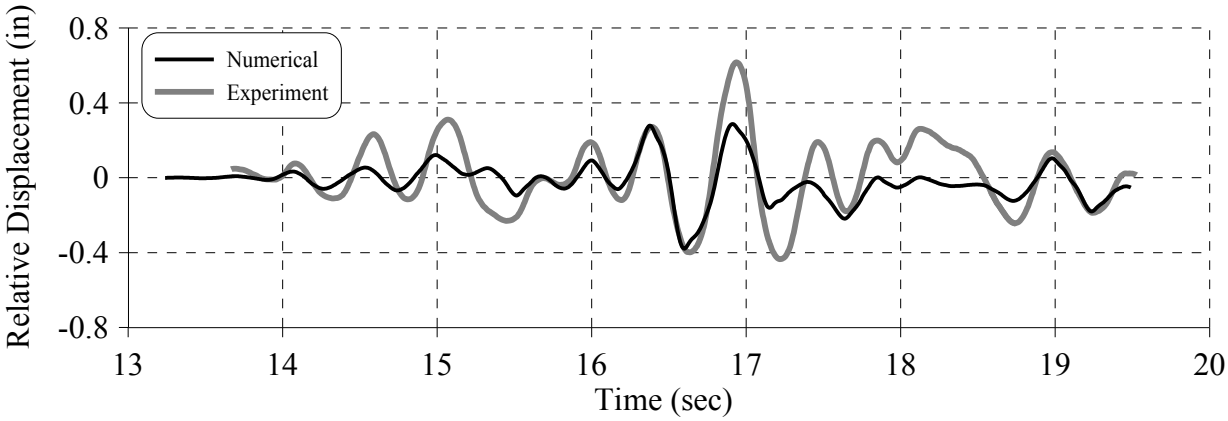

Figure 8-120 Comparison of relative displacement of Isolators W1SP3-W1SP2

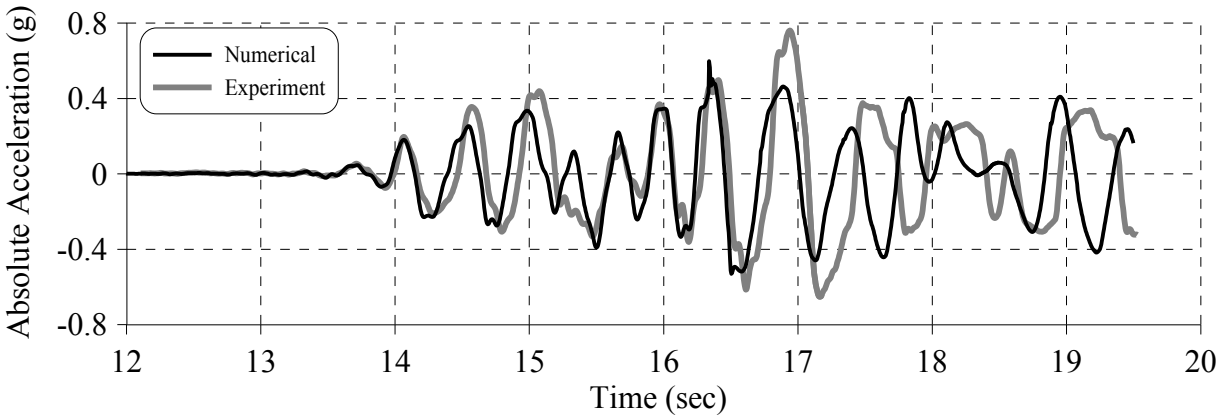

Figure 8-121 Comparison of absolute acceleration W1A15

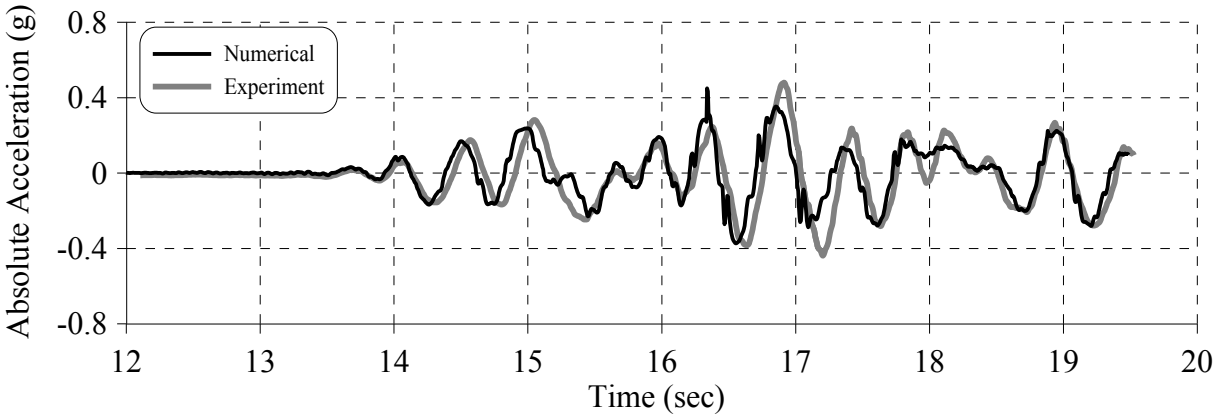

Figure 8-122 Comparison of absolute acceleration W1A9

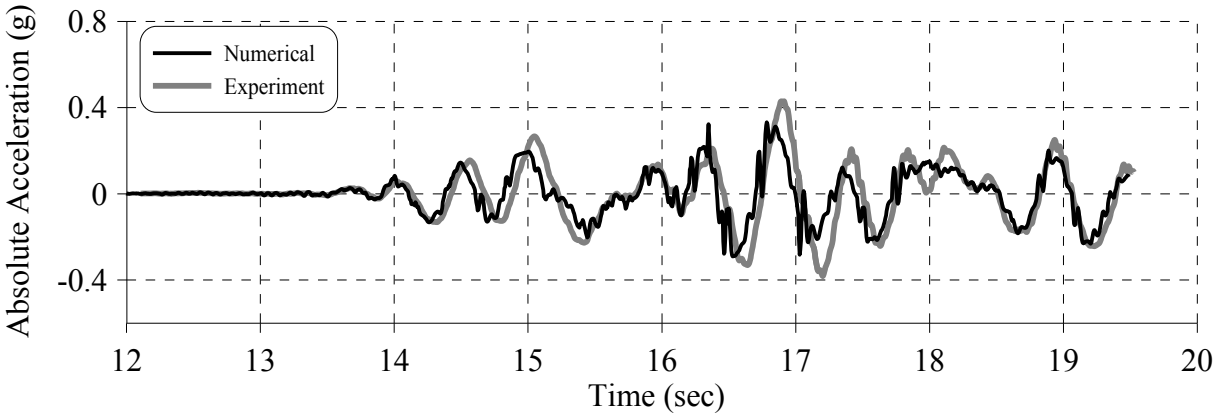

Figure 8-123 Comparison of absolute acceleration W1A8

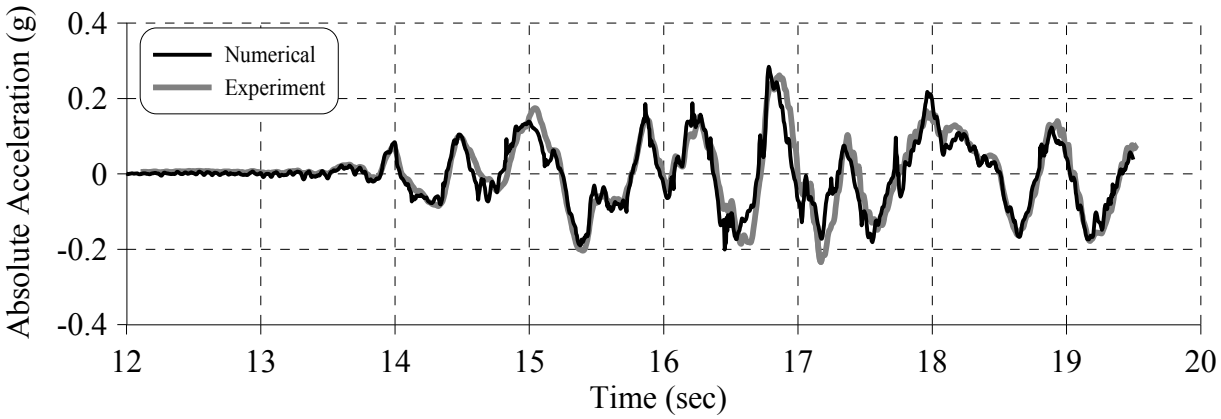

Figure 8-124 Comparison of absolute acceleration W1A5

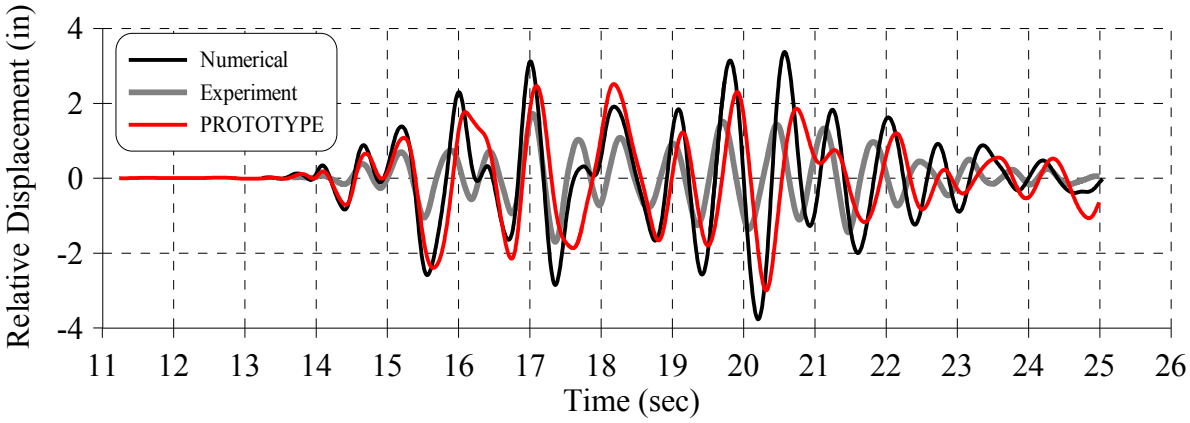

Figure 8-125 Peak displacement at the center of the diaphragm obtained with prototype, experiment and numerical model of the experiment

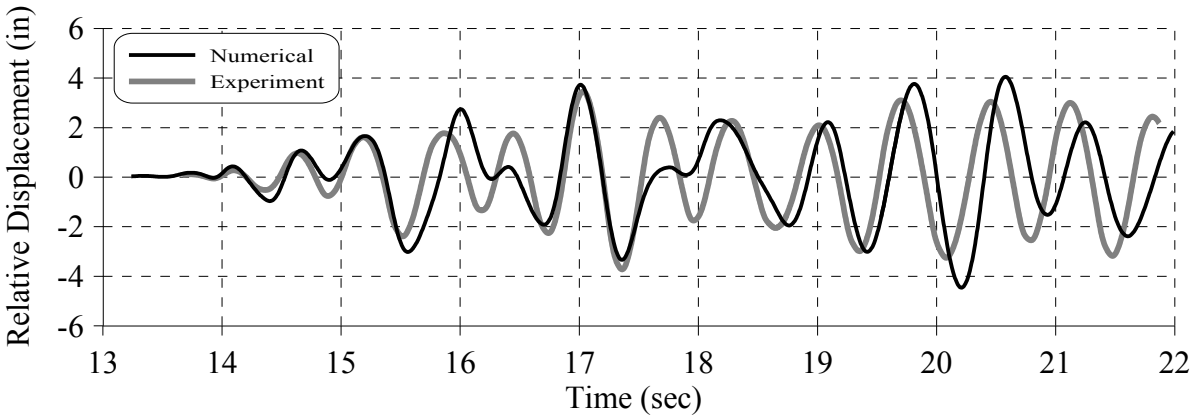

Figure 8-126 Comparison of relative displacement W2SP13

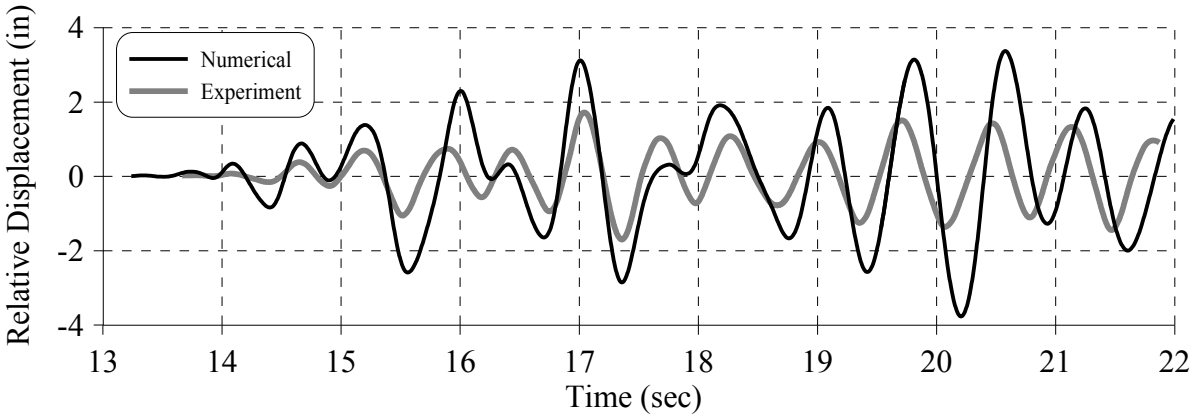

Figure 8-127 Comparison of relative displacement W2SP9

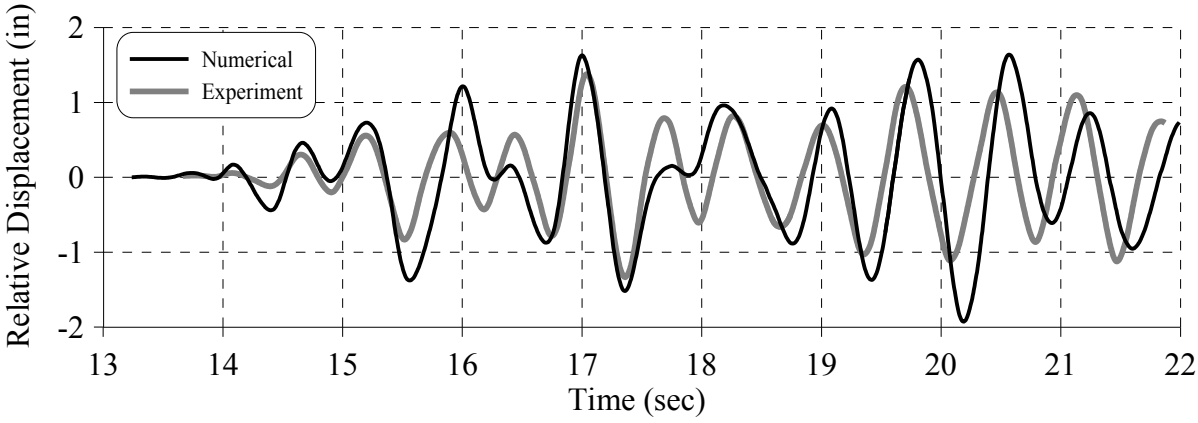

Figure 8-128 Comparison of relative displacement W2SP8

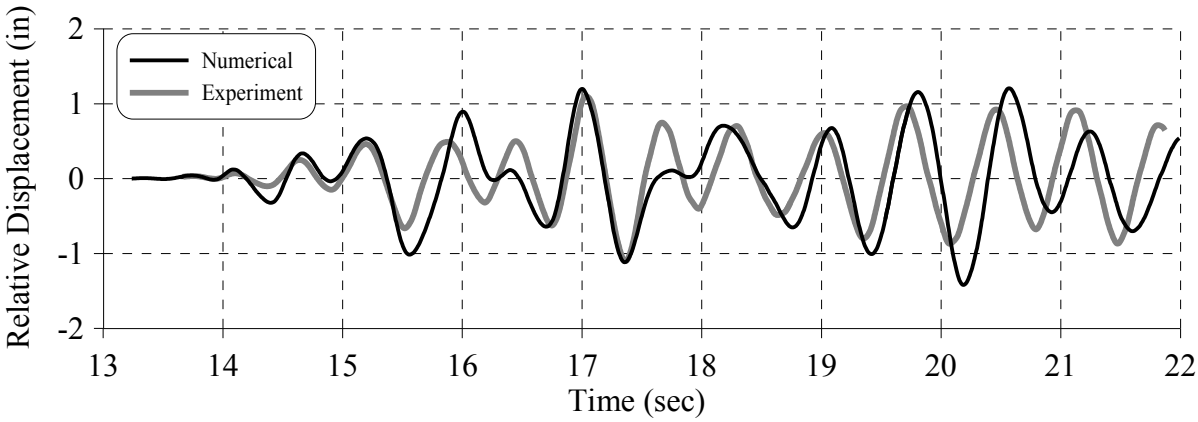

Figure 8-129 Comparison of relative displacement W2SP5

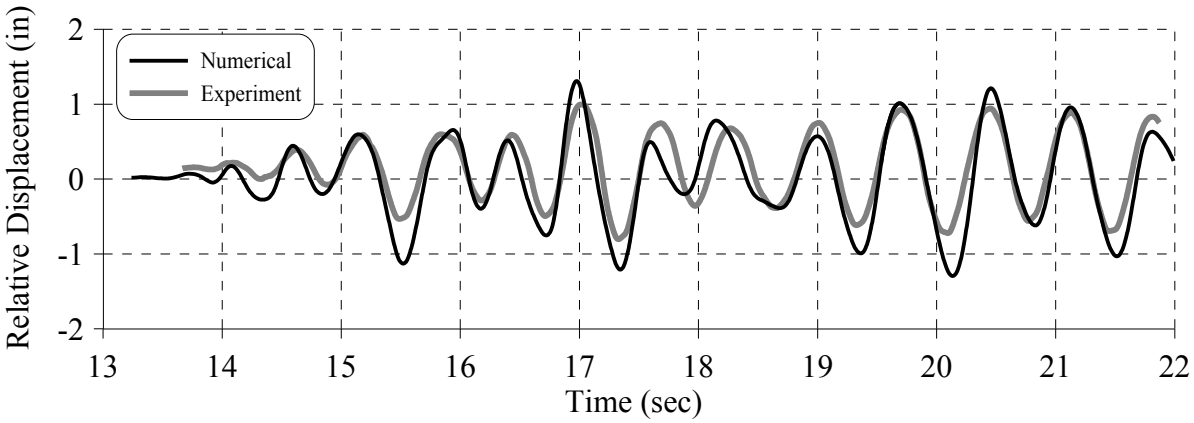

Figure 8-130 Comparison of relative displacement at the tower W2SP16

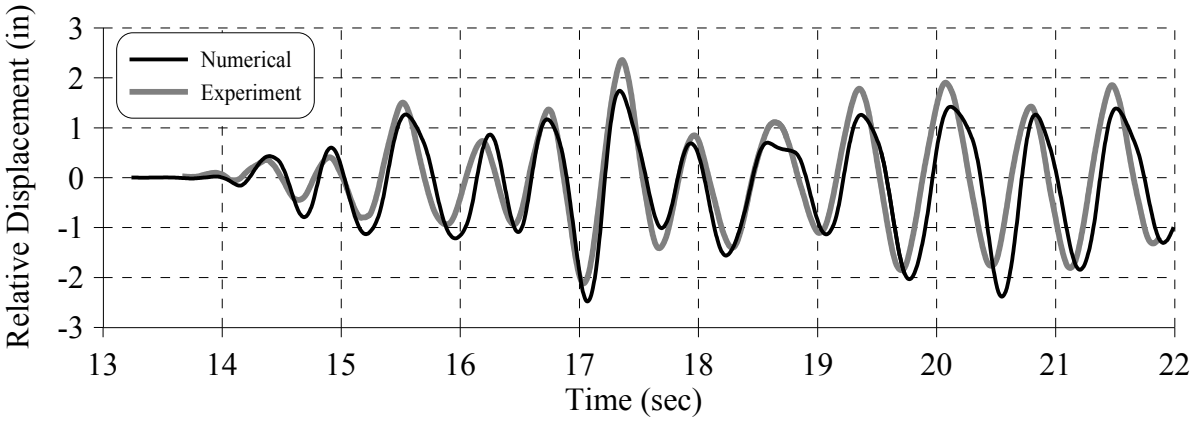

Figure 8-131 Comparison of relative displacement of Isolators W2SP16-W2SP15

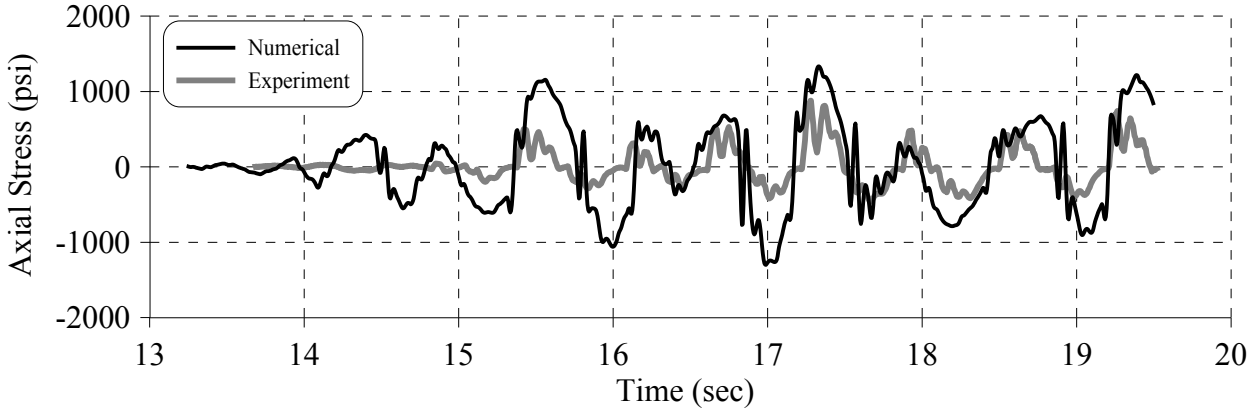

Figure 8-132 Comparison of axial stresses in the braces W2SG6

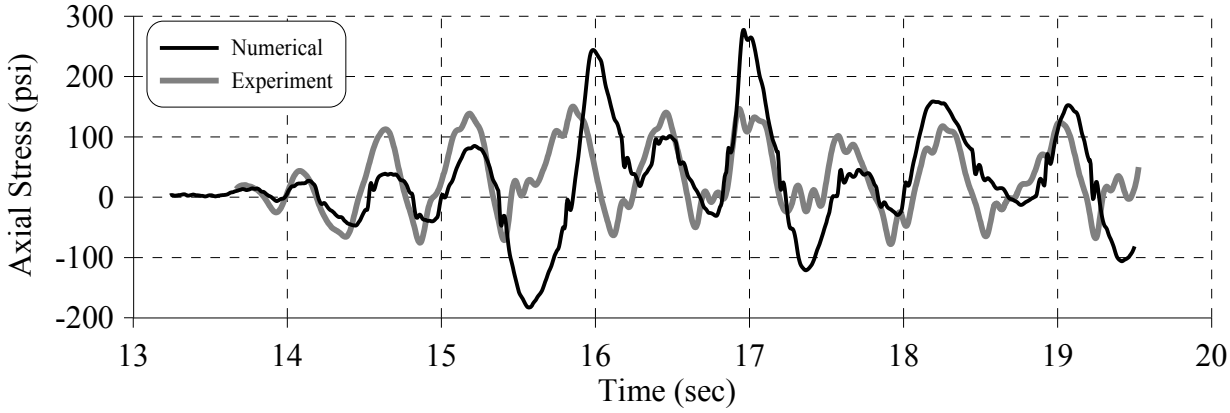

Figure 8-133 Comparison of axial stresses in the steel anchors W2SG2

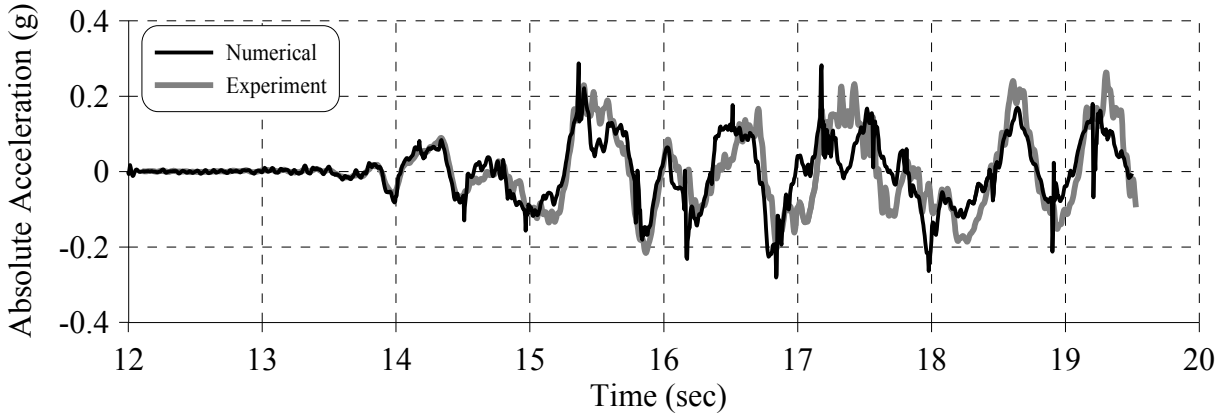

Figure 8-134 Comparison of absolute acceleration W2A1

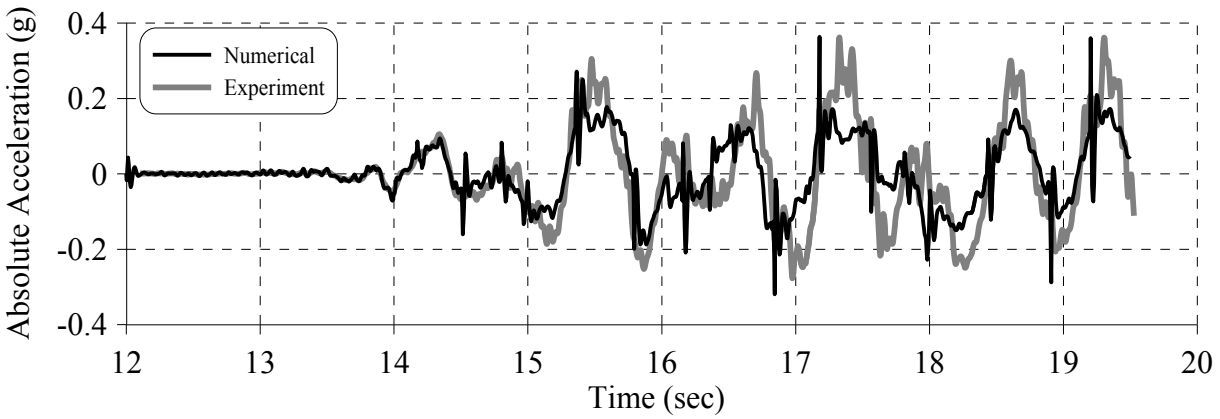

Figure 8-135 Comparison of absolute acceleration W2A2

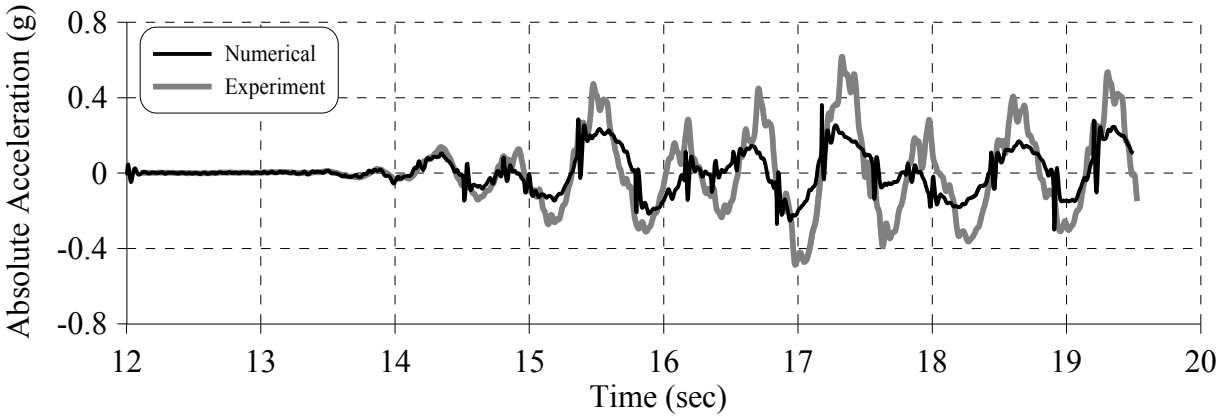

Figure 8-136 Comparison of absolute acceleration W2A4

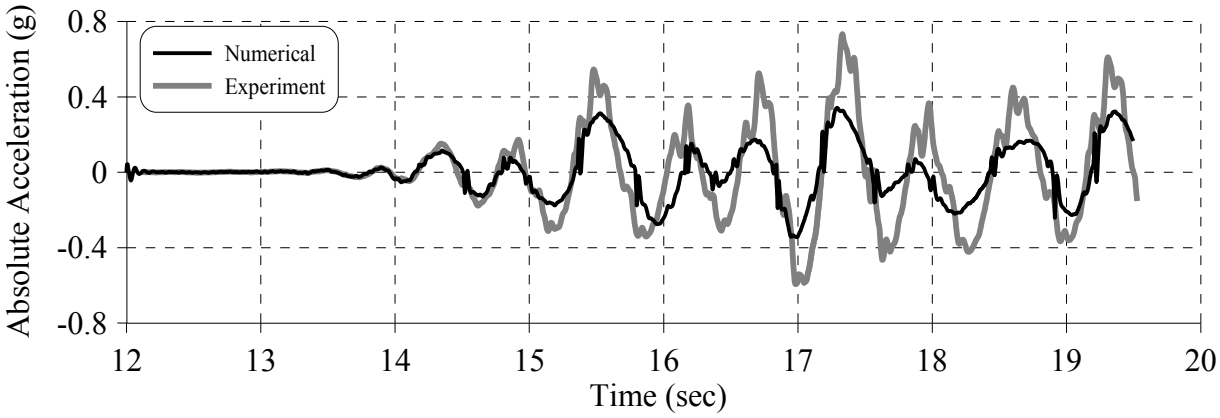

Figure 8-137 Comparison of absolute acceleration W2A5

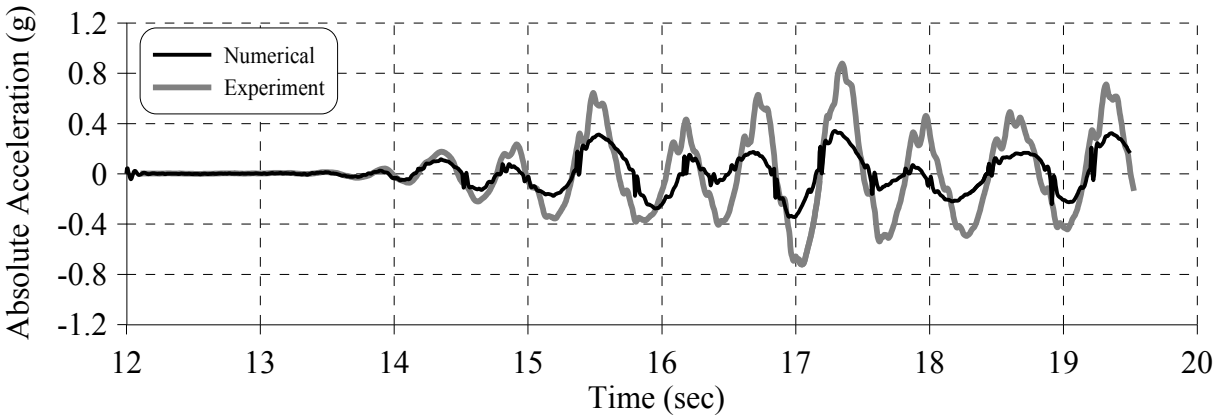

Figure 8-138 Comparison of absolute acceleration W2A6

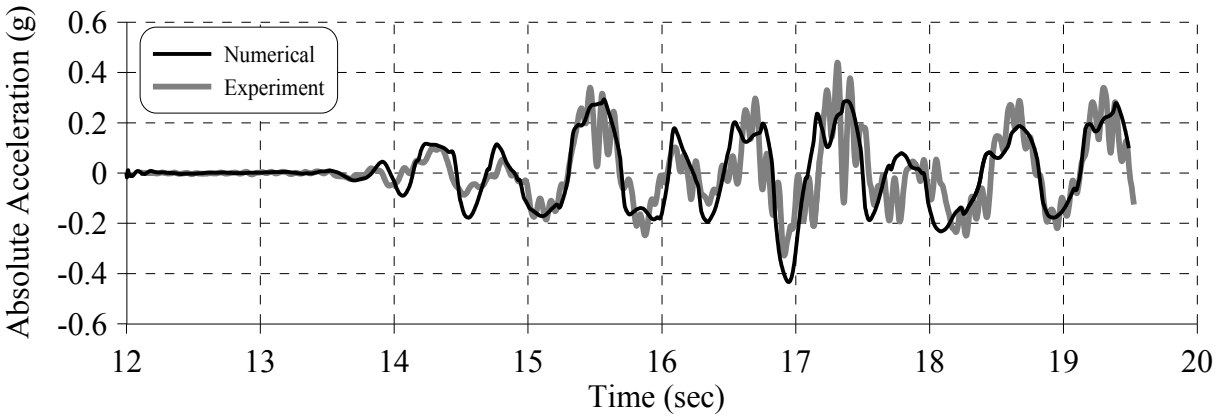

Figure 8-139 Comparison of absolute acceleration W2A8

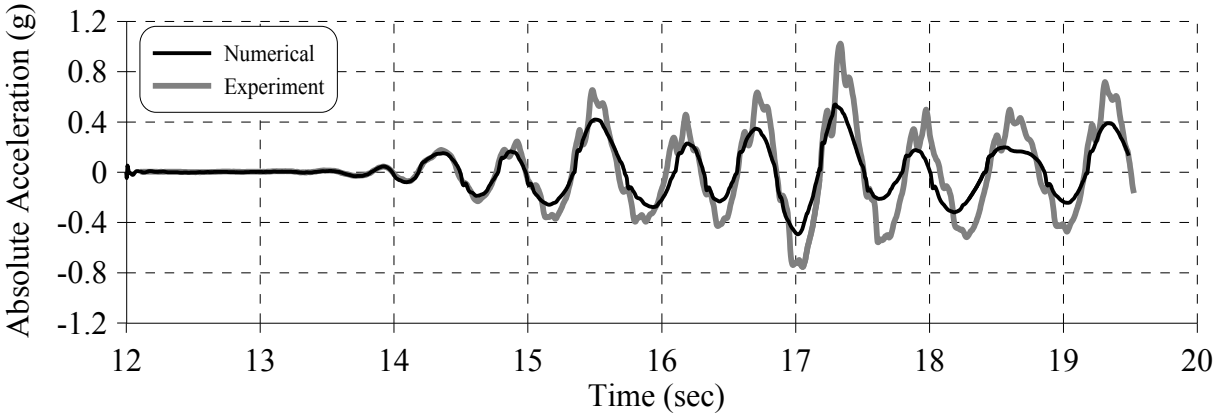

Figure 8-140 Comparison of absolute acceleration W2A9

8.8 Summary and Findings

The main goal of the experiment described in this section was to obtain data to verify and validate simplified numerical models of URM walls with parapets, floor-to-wall connections and flexible wood diaphragms. A summary and main findings, considering each parameter considered in this study are summarized below:

- *A systematic procedure to define a simplified, reliable numerical model of out-of-plane URM walls in multi-story buildings was proposed*. The models were validated through nonlinear response history analysis. Peak responses of URM walls subjected to out-of-plane loading in multi-story buildings can be estimated with the new methodology developed in this study.
- *Effect of the frequency content of the seismic input*: During the test, the walls were subjected to two ground motions having the same PGA but different frequency content, namely VA300% and NZ50%. Comparison of acceleration and peak displacement profile of the wall suggests that distribution of accelerations in the walls and dynamic amplification over the height are affected by the frequency content of the input motion. Thus, this variable should be incorporated in future revisions of the ASCE 41-06 standard. Expressing the stability limits in terms of velocities rather than spectral accelerations can provide a better understanding of the input seismic energy. Note that resonance issues between the natural frequency of the table and the input motions could also explain this unexpected behavior. This issue, however, needs to be further investigated.
- *Effect of common retrofitting techniques for parapets and floor-to-wall connections*: For the low intensity levels of the Virginia Earthquake, no significant differences were observed in the seismic response of retrofitted and unretrofitted walls. Although the specimens were able to sustain the Virginia Earthquake with minor damage, the actual vulnerability of full URM buildings in low to medium seismic hazard areas needs to be further investigated. For the strong seismic intensities of the New Zealand Earthquake, common retrofitting techniques were effective in reducing accelerations at the diaphragm and preventing out-of-plane collapse of parapets. However, unexpected collapse modes were triggered, thus reducing the overall benefit of the strengthening methods. A

comparative study of the experimental walls and diaphragm response with the ASCE 41-06 standard suggested that current ASCE 41-06 stability limits may not be conservative, regarding the assessment of URM walls with strengthened and as built parapets and flexible diaphragms.

- *The effect of wood diaphragm stiffness*: For low seismic intensity levels, no significant differences were observed in the seismic response of walls with flexible and stiff diaphragms. For strong motion shaking, larger accelerations and displacements were observed at mid-height and floor level of Wall 2 with flexible bearings (However, the flexibility of the diaphragm appears less relevant at the parapet level, as suggested by the collapse of parapets in Wall 1 which had a stiff diaphragm simulated.)
- *The aging effects in URM construction*: Although the walls were constructed using old reclaimed bricks and a weak type of mortar, no compression cracks were observed in the units and mortar-units interfaces. Parametric analyses are required to analyze different mortar and unit strengths, and their effect in the final failure mode of the specimens.
- *The filtering effects on the seismic input of out-of-plane walls*: Rigid body motion was the dominant kinematic behavior of the steel towers transferring the ground shaking to the flexible floor diaphragms. Thus, although the seismic excitation, (e.g. input acceleration to the floor) was modified, it is unclear if this effect could be representative of the actual behavior of in-plane walls in URM buildings. Nevertheless, experimental results can still be used to validate analytical models, if rotational springs are introduced at the base to capture this effect.
- *The influence of gravity loads*: Observed failure modes in both specimens were likely affected by additional dead loads from the parapet and diaphragm, which enhanced wall out-of-plane stabilities, preventing the formation of cracks at mid-height of the walls, but shifted the concentration of stresses to the shear capacity of the mortar-brick interface.
- *The seismic demands along the height of the wall*: the distribution of the inertial forces, displacements and accelerations in the walls were significantly affected by the presence of parapets and realistic connections in the test setup. Despite the limitations in producing the input excitation at the diaphragm level due to the rocking steel frame, no previous tests had accounted for the effects of parapets and connections to diaphagms.

- *The numerical models generated in SAP2000 for wood diaphragms, floor-to-wall connections and masonry walls provided satisfactory results at the system level response.* Peak displacement response was better predicted than peak accelerations, since the model for masonry walls does not account for impact effects generated by rigid body rocking.

SECTION 9
PRELIMINARY PERFORMANCE-BASED ASSESSMENT OF URM BUILDINGS IN NEW YORK CITY

9.1 Introduction

The experimental program and numerical studies conducted in this report were motivated by the need for efficient and reliable models of masonry buildings at the system level for use in performance-based seismic assessment. Here, a preliminary study is presented for an archetype unreinforced masonry (URM) building in New York City (NYC) with an emphasis on out-of-plane behavior. The main objective is to demonstrate the feasibility of such a study with proposed model. A fully detailed analysis of URM buildings considering other potential failure modes is beyond the scope of this report.

The probabilistic framework and new performance definitions provided by the FEMA-P58 project (FEMA P58-1 2012) were used to conduct the assessment. The macro-models for in-plane walls, wood diaphragms and out-of-plane walls developed in previous sections were used to generate out-of-plane URM fragility curves, a building-specific collapse fragility function, and estimate the seismic response of the building when subjected to intensity ground shaking similar to the 2011 Virginia earthquake. Sample results are presented from the performance calculations that illustrate the probable loss and repair time for the archetype building.

As discussed in Section 2 and 8, the high vulnerability of URM buildings to out-of-plane damage and collapse has been observed in past earthquakes. Since the URM building stock in NYC shows evidence of missing joist anchorage and rotted wood joists (Eschenasy 2011), the first stage of this study focused on estimating the performance of the buildings considering this failure mode. This section describes the implementation of this methodology including the numerical models, and presents preliminary results of the seismic performance of the archetype building.

9.2 Performance Based Assessment Framework

The FEMA P58 framework explicitly accounts for all uncertainties involved in the process of estimating the seismic performance of a building. Uncertainties in the seismic hazard, construction materials, modelling and response of the building, damage states and their consequences are considered. The seismic performance is expressed in terms of deaths and serious injuries, repair and replacement costs, and business interruption time. It can be implemented in five steps, namely, 1) assemble a building performance model, 2) define earthquake hazards, 3) analyze the building response, 4) estimate collapse fragility functions, and 5) performance calculations. Figure 9-1 illustrates the FEMA P58 methodology with each step briefly described below.

Step 1: A building performance model is an organized description of building assets (i.e., structural system, non-structural components and occupancy); vulnerability of each of these assets; relevant demand parameters they will be subjected to during ground shaking; all potential damage they will experience due to these demands and the consequences of this damage.

Step 2: Earthquake hazard is defined according to the assessment type considered. The methodology enables intensity-, scenario- and time-based assessments. An intensity-based assessment estimates the probable losses in a building subjected to a particular ground shaking intensity. Scenario-based assessment provides estimated losses for an earthquake of specific magnitude and location. Lastly, time-based assessment estimates probable annual losses considering all possible earthquakes and seismic sources.

Step 3 and 4: Analyzing the building response involves computing demand parameters such as drift, floor accelerations, floor velocity, and residual drift. Nonlinear response-history analysis is used for calculating demand parameters and developing building-specific collapse fragility functions, which are required to determine potential casualties. Because the seismic response of the building is obtained with a limited suite of ground motions, additional performance calculations require generating simulated demands. This process is completed using Monte-Carlo analysis. An extended discussion on this procedure can be found in the FEMA P58 guidelines.

Step 5: The simulated demands are used to determine whether collapse occurs, estimate damage, and compute casualties, repair costs and repair time. This process is usually completed using the Performance Assessment Calculation Tool (PACT), developed as part of the FEMA P58 project.

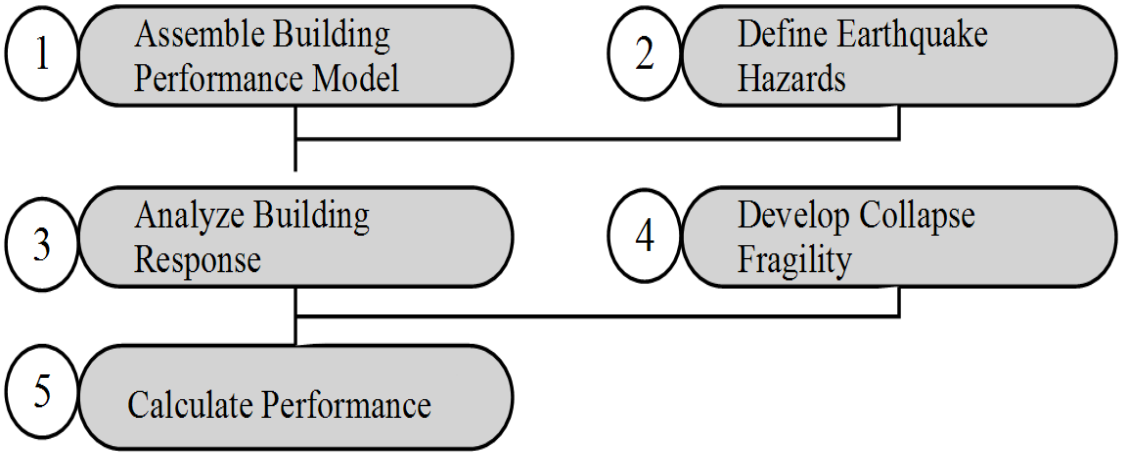

Figure 9-1 Performance-based assessment methodology (after FEMA P58)

9.3 Building Performance Model

A building performance model is an organized description of building assets (i.e., structural system, non-structural components and occupancy); vulnerability of each of these assets; relevant demand parameters they will be subjected to during ground shaking; all potential damage they will experience due to these demands and the consequences of this damage.

A complete characterization of the building includes: 1) A general geometric description of the building 2) list of structural and nonstructural components relevant to the archetype building evaluated 3) a thorough description of the performance groups associated to the building 4) the best estimation of occupancies and population models.

9.3.1 Building Geometry

Characteristics of the archetype building in NYC were identified in Section 3. The archetype URM building in NYC is five-stories, with wood diaphragms consisting of 2”x6”straight sheathing and 2”x10” wood joist spanning over long horizontal transverse 12” multi-wythe URM walls, and many openings at the façade. The floor plan dimension of the building is 25’x 60’ and

typical story height is about 12'. Typical nonstructural components, such as interior walls, mechanical and electrical equipment were taken from PACT, for commercial and residential buildings. This was deemed appropriate, since the main goal of this section was to illustrate the relative performance of out-of-plane walls as compared to other nonstructural components. An illustration of the building is provided in Figure 9-2 and assumed building information is listed in Table 9-1.

The total replacement cost of the building performance model was calculated to be about US $750,000. This value is similar to that estimated for URM buildings in Los Angeles (USGS 2008) but it should be considered as a rough estimate only. The main purpose is to have a reasonable value to estimate loses. Considering only the core and shell replacement cost was estimated to be $450,000. A replacement time of 180 days was assumed.

Table 9-1 Building information for assessment

Building Information	
Number of Stories	5
Occupancy	Commercial office Residential
Floor Area	1,500 ft^2
Story Height	12 ft
Total Replacement Cost	$ 750,000
Core and Shell Replacement Cost	$ 450,000
Replacement Time	180 days
Structural System	Wood floors 12"URM walls
Non-structural Components (PACT)	Wall partitions of gypsum Prefabricated steel stairs Suspended ceilings Piping, HVAC

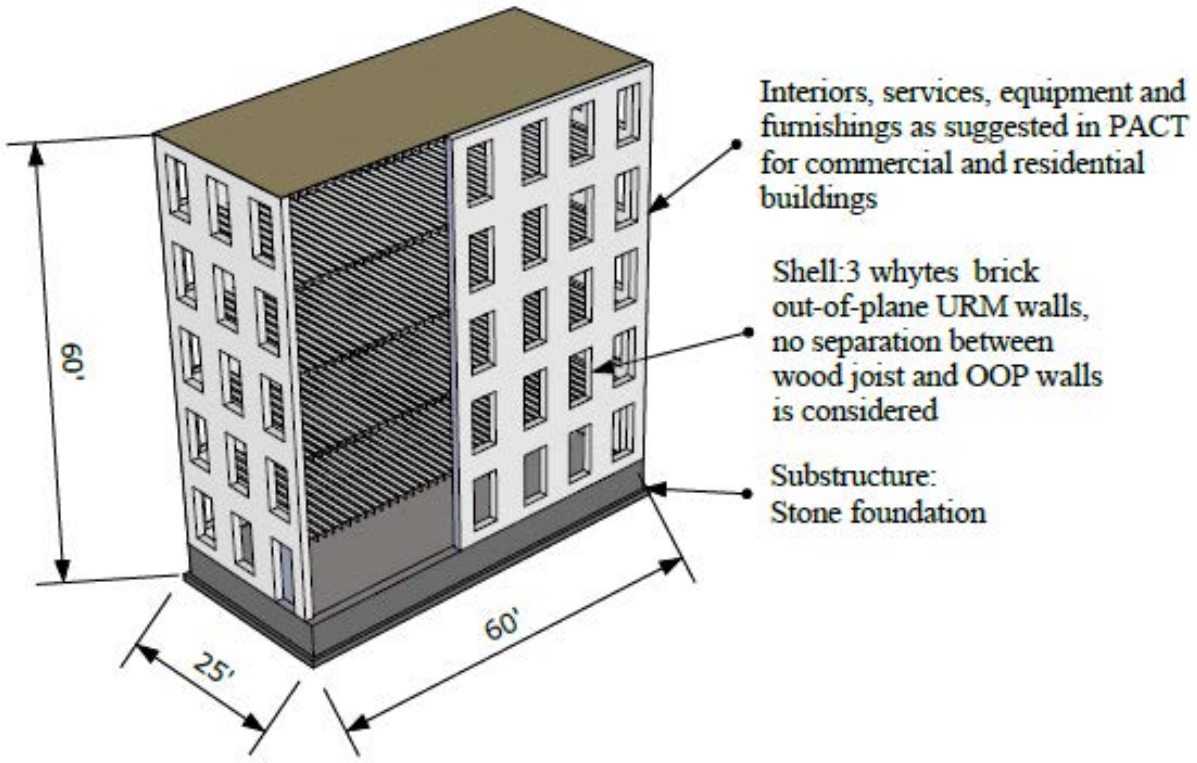

Figure 9-2 Building performance model for NYC

9.3.2 Structural Components

The Normative Quantity Estimation tool provided by ATC-58 was utilized to define typical quantities, vulnerability and distribution of damageable components and contents for commercial and residential buildings.

A user defined fragility function for out-of-plane URM walls was constructed using incremental dynamic analysis. In defining this function, two damage states were considered, namely, 1) onset of flexural cracking requiring cosmetic repairs (DS1) and 2) significant cracking along the height of the wall that may lead to partial or total collapse of the wall (DS2).

Also, a repair cost and repair time consequence function were defined. These consequence functions were estimated from (McMonies 2010) where the cost of implementing several retrofit techniques is provided.

In defining the gravity load due to residential and commercial occupancy, the default values provided in ASCE 7-10 were used. No special distribution of loads or reductions of live loads were considered. Limited information exists on the population models of the buildings and the default functions provided in the PACT software for residential and commercial buildings were

utilized. The building population model is illustrated in Figure 9-3. These building population models express the number of people in the building during the day per 100 square feet of building floor space. Population patterns fluctuate during the day, since many buildings have specific hours of operation and also lunch time variations. For commercial buildings, a higher number of people are expected during the day, whereas for residential occupancy, this number is expected to be lower, as illustrated in Figure 9-3.

Figure 9-4 shows the 3D numerical model used to develop the out-of-plane fragility functions. This model is based on the experiments pictured in Figure 9-4b and described in Section 8. The proposed fragility and consequence functions based on this model are also shown in the figure. The experimental setup that was used to validate the numerical model is also shown.

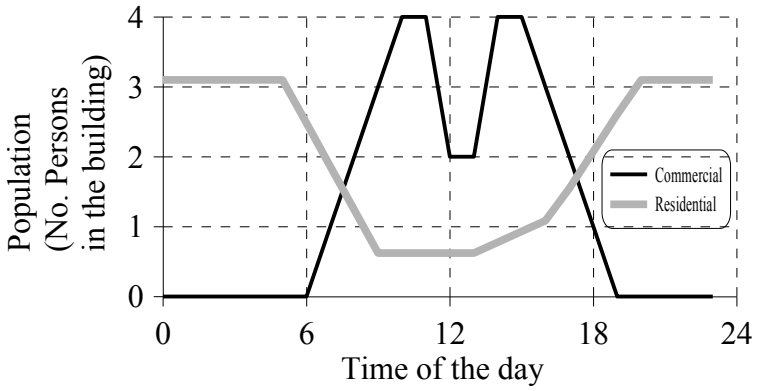

Figure 9-3 Population model (From PACT software)

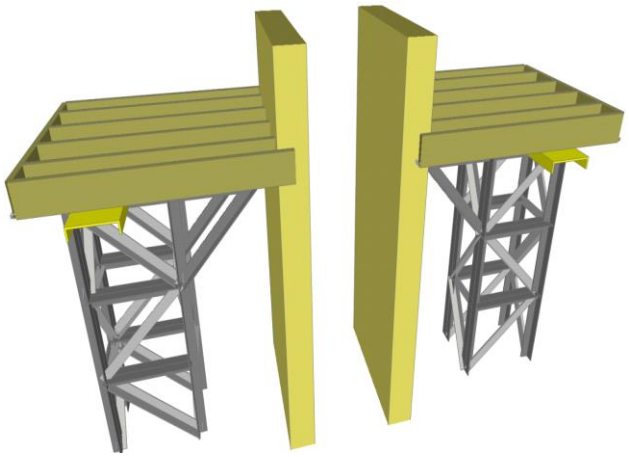

a) 3D Numerical Model

b) Experimental Model

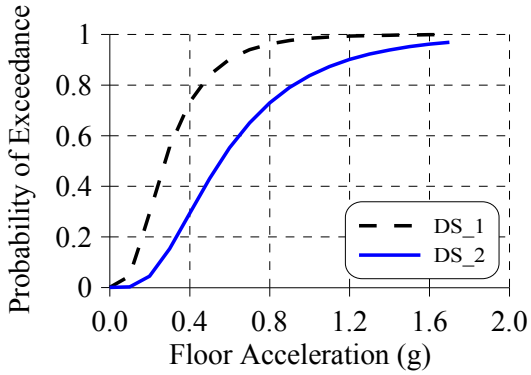

c) Out-of-plane Fragility Function

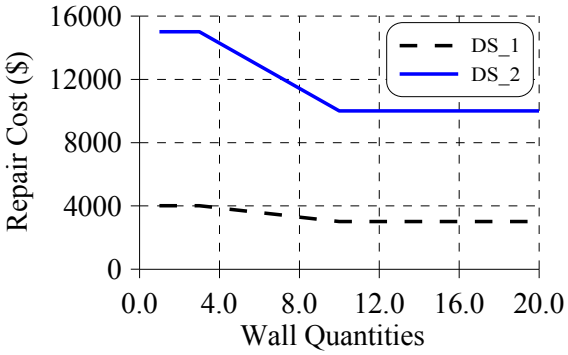

d) Repair Cost Consequence Function

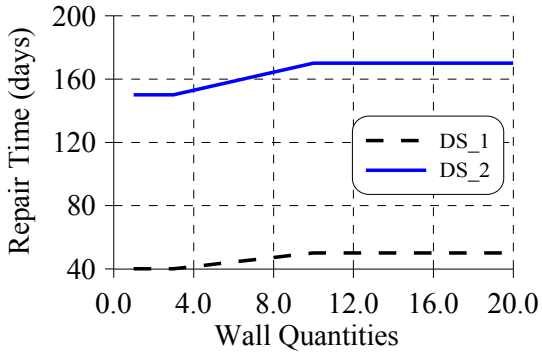

e) Repair Time Consequence Function

Figure 9-4 a) Numerical model, b) Experimental model, c) Preliminary out-of-plane fragility function, d) Repair cost function, and e) Repair time function (From McMonies 2010)

9.4 Seismic Hazard

For intensity-based assessment, ground shaking was represented by the 2% probability of exceedance in 50 years Uniform Hazard Response Spectrum (UHRS) for a site Class A located in New York City. The UHRS was obtained from the hazard tool provided by the USGS (USGS 2012).

Table 9-2 presents a set of 10 ground motions that were selected and amplitude-scaled to match the UHRS. The spectral shape of this set is intended to be consistent with geologic characteristic of the Central and Eastern United States region, as shown in Figure 9-5. The geomean spectrum of each ground motion pair was constructed over the period range of 0.17 seconds to 1.7 seconds, since the fundamental period T, of the performance building model was estimated equal to 0.85 seconds. The amplitude of each pair of ground motion was scaled by the ratio of Sa(T) obtained from the target spectrum to that of the geomean spectrum for the pair.

Table 9-2 Selected ground motions for intensity-based assessment

Earthquake	Station Name	Mw	R (km)	PGA (g)
Gaza (US)	Ball Mountain Dam	4.3	103.2	0.01
Gaza (US)	North Hartland Dam	4.3	82.4	0.04
Gaza (US)	North Springfield Dam	4.3	74.6	0.03
Gaza (US)	Union Village Dam	4.3	60.8	0.04
Nahanni (CA)	6098 Site 2	6.8	6.5	0.49
Nahanni (CA)	6099 Site 3	6.8	22.4	0.15
Val-Des-Bois (CA)	Orio	5.0	49.9	0.434
Virginia (US)	Corbin	5.8	57.5	0.135
Virginia (US)	Charlottesville	5.8	53.5	0.121
Virginia (US)	Reston Fire Station 25	5.8	124.1	0.109

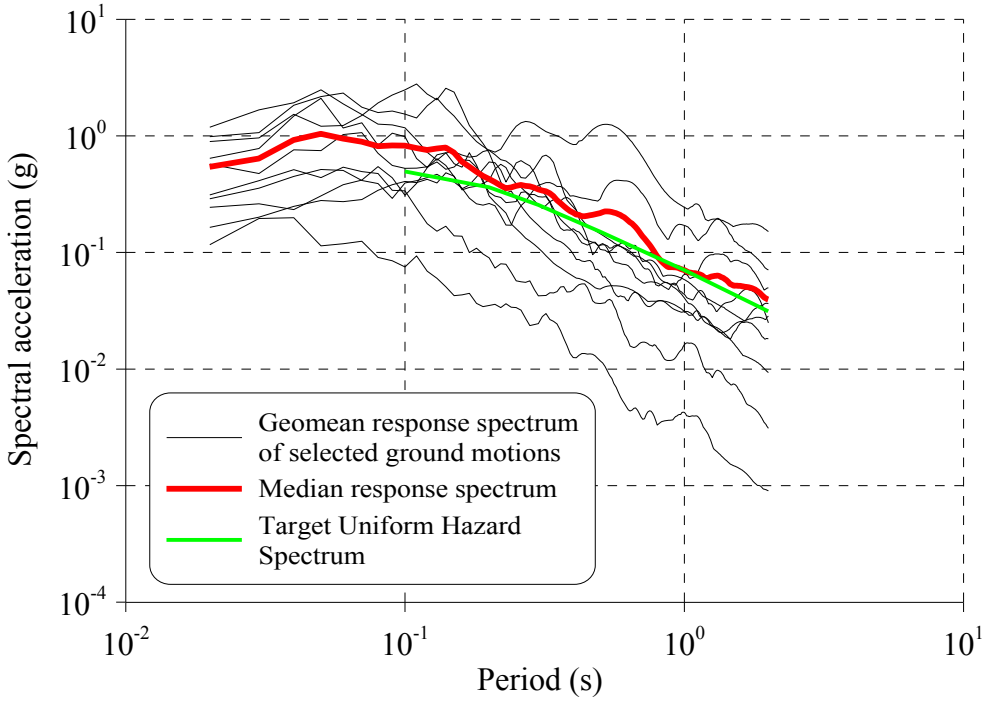

Figure 9-5 Target and median response spectrum of selected ground motions

9.5 Building Analytical Model

An analytical model of the building is required to predict the response of the structure subjected to seismic loads. However, modeling older multi-story URM buildings poses a significant challenge due to the highly nonlinear behavior of bricks, mortars and their interaction with other structural components. In this section, a macromodel for multi-story masonry buildings suitable for nonlinear dynamic analysis was developed. This model accounts for the complex interaction between in-plane walls, wood diaphragms and out-of-plane walls. More details about modeling of components and their interaction can be found in Sections 4, 5 and 6.

It is important to mention that soil-structure interaction was not considered in this preliminary study. Dead and live loads were calculated for this structure as suggested by the ASCE-7 (ASCE/SEI 7-10 2010) for commercial buildings. Mean values of the material properties were estimated from experimental results of small specimens, in-situ flat jack testing on masonry buildings and previous research on URM walls, as discussed in Section 7.

A numerical model of the walls and diaphragms was developed using SAP2000 (CSI 2009) as shown in Figure 9-6. Nonlinear response-history analyses using the set of 10 ground motions

were conducted using Newmark direct integration method. A damping ratio of 1% of critical damping was assumed for all modes of vibration, since most energy will be dissipated through the nonlinear spring elements in the walls and the wood diaphragm.

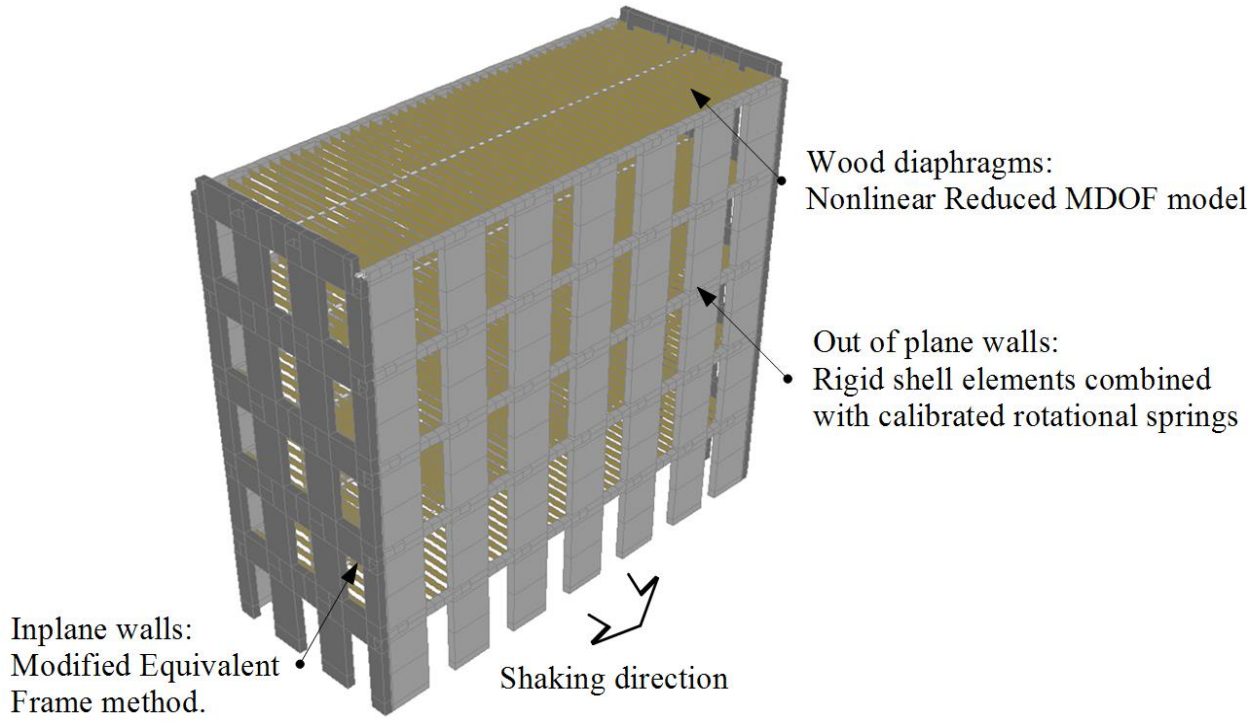

Figure 9-6 3D Analytical model of the URM building in SAP2000

9.6 Collapse Fragility Analysis

The URM analytical building model was used to establish a building-specific collapse fragility function. In developing the collapse fragility functions for the building, currently only the out-of-plane collapse of the walls was considered. Since the model does not explicitly captures the collapse of the walls, a collapse limit state is used to estimate this non-simulated collapse mode. For walls with aspect ratios h/t larger than 10, as in this case, the ABK methodology (ABK 1984) specifies maximum velocities of the diaphragm of 25 in/s. Herein, collapse is assumed to occur when the maximum velocity of the diaphragm has exceeded this threshold.

Following FEMA P58 guidelines to estimate collapse fragility functions, each ground motion of the set previously identified was scaled up or down to generate 10 intensity levels. Then, nonlinear response-history analyses were performed using each intensity level. The conditional probability of collapse can be obtained by dividing the number of analyses for which collapse is predicted by the total number of analyses performed at that intensity. The conditional probability of collapse is then plotted as a function of intensity and a lognormal distribution is fitted to this data.

The resultant incremental dynamic analysis curves, the collapse fragility function with the median value of the spectral acceleration at the building's effective first mode period, Sa(T) and dispersion β are shown in Figure 9-7.

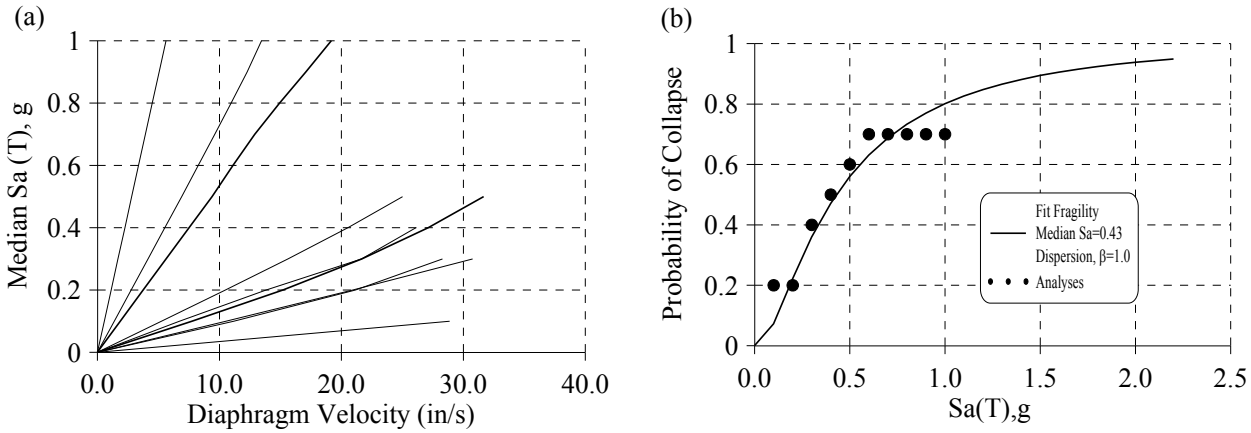

Figure 9-7 Preliminary collapse fragility analysis: a) IDA curves b) Building-specific fragility function for out-of-plane collapse

9.7 Building Response

Nonlinear response history analysis was used to obtain peak drifts, peak absolute accelerations and peak absolute velocities for 0.10g ground shaking intensity. Since the geomean spectral shape of the scaled motions matches reasonably well with that of the target spectrum in the period range Tmin, to Tmax, the set of 10 records was expected to provide a good prediction of median response (2012). The reliability of the nonlinear URM model was checked by first conducting response spectrum analysis, nonlinear static lateral and gravity analysis and nonlinear analysis with and without P-Delta effects. The hysteretic response was verified for selected in-plane, diaphragms and out-of-plane elements. To account for uncertainties in building definition

and construction quality, a dispersion factor βc of 0.40 was assumed. Likewise, a dispersion factor βq of 0.4 was also assumed for model quality and completeness. Residual drifts were not currently considered in this study.

The first mode shape of the building, peak transient drift ratios and peak floor accelerations are presented in Figure 9-8 and Figure 9-9, respectively. This results are also summarized in Table 9-3 and Table 9-4. Note that those parameters were estimated only for one direction of analysis. Two of the ground motions predicted collapse and therefore were removed from the simulation, as recommended in FEMA P58-1 (2012).

Table 9-3 Estimated values of peak floor accelerations (g)

Floor/Story	EQ1	EQ2	EQ3	EQ4	EQ5	EQ6	EQ7	EQ8
Roof (g)	0.111	0.028	0.11	0.028	0.143	0.008	0.044	0.056
Floor 5 (g)	0.106	0.025	0.115	0.028	0.201	0.008	0.071	0.185
Floor 4 (g)	0.122	0.021	0.116	0.018	0.192	0.008	0.071	0.236
Floor 3 (g)	0.083	0.024	0.107	0.025	0.188	0.009	0.075	0.21
Floor 2 (g)	0.065	0.029	0.116	0.028	0.179	0.009	0.079	0.231
Floor 1 (g)	0.065	0.029	0.116	0.028	0.179	0.009	0.079	0.231

Table 9-4 Estimated values of peak story drift ratios (rad)

Floor/Story	EQ1	EQ2	EQ3	EQ4	EQ5	EQ6	EQ7	EQ8
Floor5-Roof (rad)	0.00053	0.00013	0.00053	0.00015	0.00036	5.33E-05	0.000161	0.000247
Floor 4-5 (rad)	0.00025	0.00013	0.00079	2.35E-05	0.00015	2.55E-05	0.000251	0.000459
Floor 3-4 (rad)	0.0006	0.00013	0.00059	5.95E-05	0.00053	3.32E-05	0.00015	6.89E-05
Floor 2-3 (rad)	0.00102	0.0002	0.0011	8.64E-05	0.00101	6.25E-05	0.000405	0.000304
Floor 1-2 (rad)	0.00182	0.00037	0.00193	0.00034	0.00197	0.00013	0.000847	0.001579

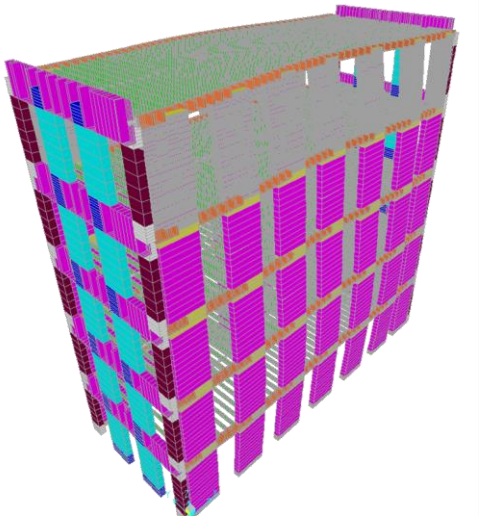

Figure 9-8 First mode shape of the building

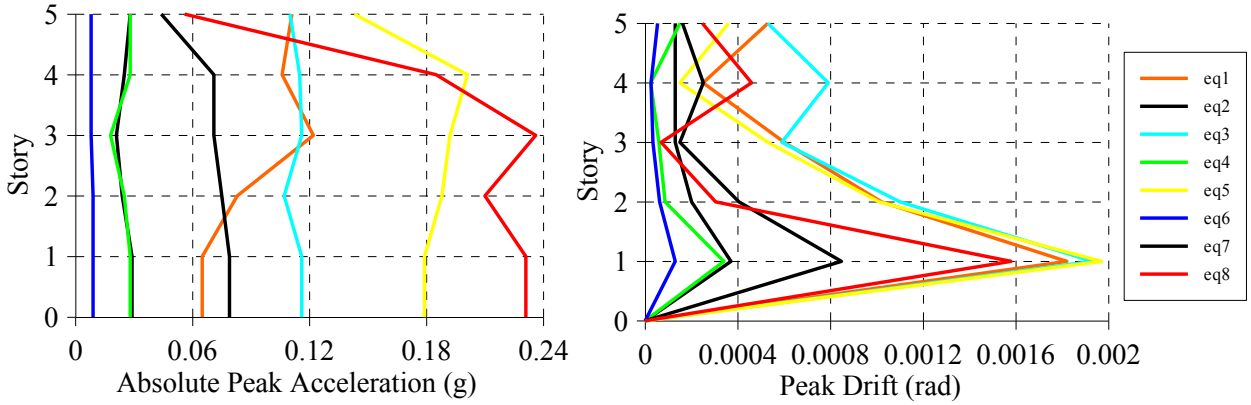

Figure 9-9 Peak accelerations and drift obtained for each ground motion

9.8 Performance Calculations

PACT uses the median drifts, accelerations and velocities to make damage state assessments for structural and non-structural components specified in the building performance model. This process requires fragility and consequence functions for each component considered in the building performance model.

Before conducting performance calculations, a large number of simulated demands or demand distributions are generated accounting for variability of each random parameters and its consequence on the seismic response. Each set of demands, associated damage and consequences is called a realization.

The performance assessment starts by determining the number of people present in the building when the earthquake occurs. This information is used to determine the number of casualties if

collapse occurs. PACT will then estimate for each realization if collapse has occurred. In this case, the collapse mode of the structure must also be determined. Herein, the collapse mode is out-of-plane wall failure at any story of the building. The number of casualties are then estimated based on the number of people present in the building and the fraction of floor area at each floor subjected to collapse, in this case 100%. Finally, repair cost and repair time are set equal to the building replacement values, namely $750,000 and 180 days.

If PACT determines that collapse has not occurred, simulated demands are used together with fragility functions to generate damages states for each structural and non-structural component in the building. Those damage states are then used together with consequence functions of repair cost, casualties and repair time to estimate the associated losses for each realization. This process is repeated for each realization.

Repair cost and repair time function are given in Figure 9-10 and Figure 9-11, respectively. These preliminary results indicate that if an earthquake of 0.1g intensity happens in NYC, the median repair cost for the archetype building will be US$75,000 which is mainly due to out-of-plane damage of the walls, as seen in Figure 9-10b. This is 10% of the building's total replacement cost. Likewise, the mean repair time will be 123 days, as most of the damage will occur in upper stories, as implied from Figure 9-11b. Note that for this earthquake intensity, PACT did not predict deaths or serious injuries.

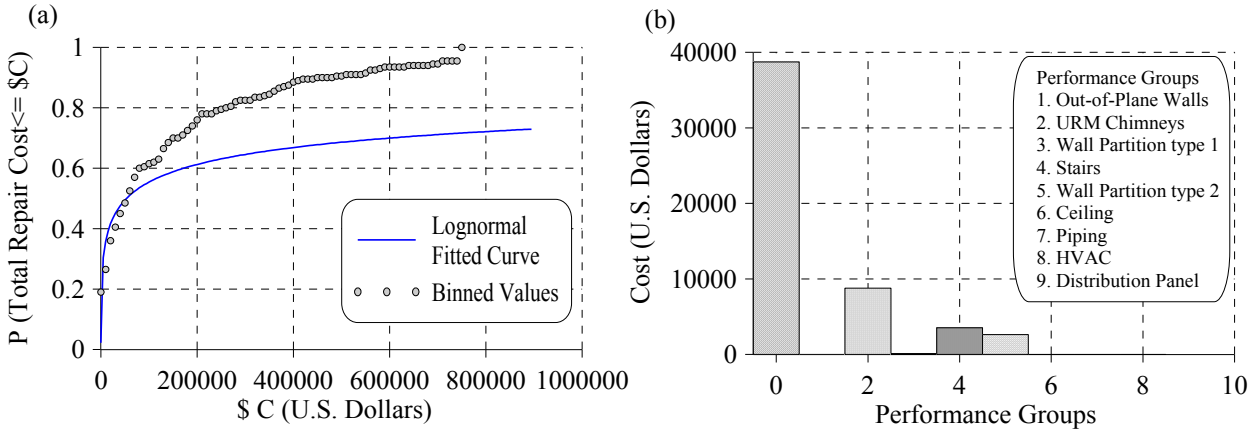

Figure 9-10 Repair cost results: a) Loss curve for cost associated with Sa=0.1g b) Disaggregation of losses among performance groups for a 50% of probability of exceedance of the total repair cost

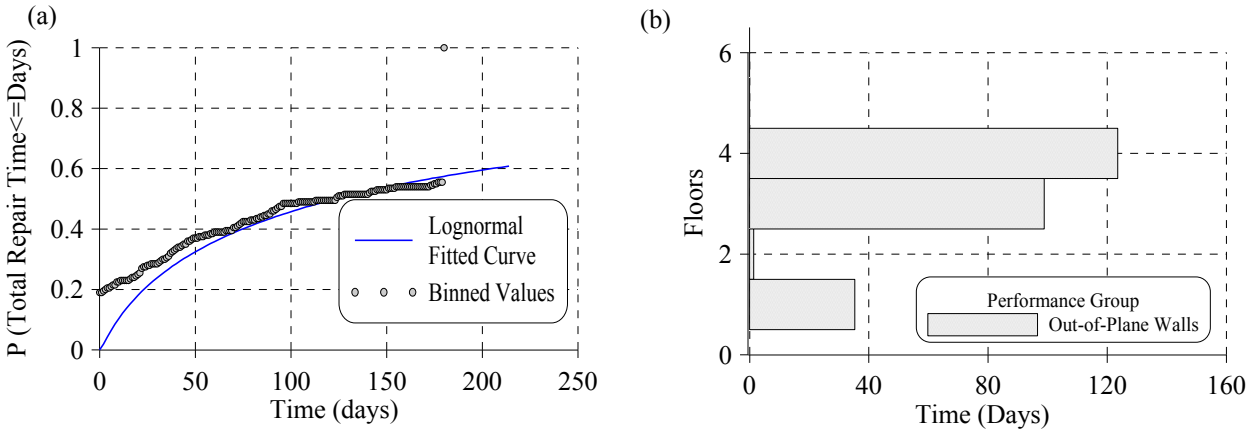

Figure 9-11 Repair time results: a) Repair time probability b) Contribution of each performance group to the total repair time for a 50% of probability of exceedance of the total repair cost

SECTION 10
SUMMARY AND CONCLUSIONS

10.1 Summary

The main goal of this report was to develop and validate numerical macro-models to evaluate the seismic performance of typical URM buildings located in New York City. Simplified numerical macro-models of wood diaphragms, masonry walls and floor-to-wall connections were developed and validated individually using data from past experiments. These models were also validated at the system level, through shake table testing of two full-scale specimens conducted as part of this study. The specimens were designed and constructed to represent the expected loading conditions of a central portion of a one-story URM building.

A characterization of the building stock in New York City was conducted and in particular, the URM buildings commonly called Row-Houses were examined. Key architectural and structural characteristics of these buildings were determined and used to define a representative archetype building. Current structural vulnerabilities were identified and discussed. The archetype building and its current vulnerabilities provided a basic framework to define the overall geometric and mechanical characteristics of wood diaphragms, floor-to-wall connections and masonry walls, which were further investigated in this research program.

Current numerical models available in the literature for simulation of wood diaphragms in URM buildings were identified and evaluated. A reduced 3D multi-degree of freedom (RMDOF) model of the diaphragm, able to capture the full dynamic characteristic while significantly reducing analysis time was proposed, verified and validated by comparison to detailed finite element models. Such models can be beneficial for use in performance based seismic design applications requiring numerous simulations.

The connections between wood floors and URM walls play a fundamental role in the seismic behavior of unreinforced masonry buildings. Yet, currently there is little information on the modeling and performance of this critical component under seismic loads. Hence, a friction-impact-nail model that simulated the connection between wood joist and unreinforced masonry walls was developed and validated. The numerical model was implemented in SAP2000 and

validated against previous experiments conducted by other researchers on this type of connections.

A literature review of existing macro-models highlighted the need to develop simplified numerical models which could be used to estimate the seismic response of multi-story URM buildings with flexible diaphragms. Thus, modeling techniques for nonlinear analysis of out-of-plane and in-plane walls were developed and validated using experiments from the literature. These models were implemented in SAP2000 and reproduced the dynamic behavior of the walls while significantly reducing the analysis time.

Full scale experiments that combine wood diaphragms, wood joist-to-wall connections, in-plane and out-of-plane masonry walls in a single structure to capture subassembly or system level response under realistic seismic loads are more limited. Although it was shown that the numerical macro-models developed to simulate the behavior of each individual component were reliable, there was not sufficient data to evaluate the applicability and effectiveness of these models in capturing the system level seismic behavior of an URM building with flexible diaphragms.

As a result, after obtaining data to characterize the material properties that better represent actual conditions of the building stock in New York City, shake table testing of two full-scale multi-wythe unreinforced masonry walls with parapets including diaphragm flexibility subjected to out-of-plane loading was carried out in the Structural Engineering and Earthquake Simulation Laboratory (SEESL) of the University at Buffalo. The results of these tests were used to validate the computer models previously developed. Also, these experiments provided new information regarding the seismic behavior and vulnerability of masonry walls, parapets, wood joist-to-wall connections and flexible diaphragms.

The validated macro-models were used to develop out-of-plane URM fragility curves, a building-specific collapse fragility function, and estimate the seismic response of the building when subjected to a intensity ground shaking similar to the 2011 Virginia earthquake. The probabilistic framework provided by the FEMA P58 project was used to conduct a performance-based seismic assessment for an archetype unreinforced masonry building in New York City with an emphasis on out-of-plane behavior. This preliminary study served to demonstrate the applicability of the proposed models for applications in performance-based design.

10.2 Conclusions

In this section, major findings of this research are summarized. Specific conclusions of different parts of this study are presented at the end of each corresponding section. Major conclusions of this report are summarized below:

- Current structural vulnerabilities of URM buildings in NYC include: (1) In-plane walls with large openings; (2) Flexible wood diaphragms with rotted components; (3) Missing joist anchorage and rotted wood joists and (4) Potential out-of-plane collapse of URM masonry walls from moderate earthquake shaking.
- Based on the numerical work conducted to develop reliable macro-models for wood diaphragms, floor-to-wall connections and masonry walls, the following finding were reached:
    - A comprehensive evaluation of current numerical tools for modeling wood diaphragms indicated that refined finite element models can fully characterize the dynamic response of wood diaphragms, but at a very high computational cost. On the other hand, simplified SDOF models could reasonably estimate only a few dynamic parameters and engineering demands at key locations of the diaphragm.
    - The proposed reduced MDOF model for wood diaphragms accurately estimated the seismic response of wood diaphragms at a fraction of the computational time.
    - The friction, impact and nail numerical models developed by other researchers can be combined to accurately simulate the behavior of typical joist-to-URM wall connection.
    - It was demonstrated that the combined friction-impact-nail model can capture the cyclic behavior in tension and compression of a typical joist-to-wall connection and can be implemented in commercial software.
    - The out-of-plane behavior of URM walls subjected to one-way bending was effectively simulated using a hybrid formulation based on equations derived from rigid body dynamics but implemented as a SDOF oscillator. Masonry walls can be effectively simulated using shell, rigid elements and nonlinear rotational springs at crack locations. A comparison between numerical models and

experimental results for nonlinear response history analysis showed good agreement in terms of peak displacements and accelerations.

  - The rocking and shear sliding behavior of URM wall piers was simulated using a modified Equivalent Frame Method. The force displacement or moment-rotation relationships were taken from the equations provided in ASCE 41-06 and implemented in SAP2000, using rotational or shear nonlinear springs. Pushover and cyclic pushover analysis were in good agreement with previous experiments of in-plane walls.

- The material testing conducted for mortar, bricks and masonry specimens in order to identify the masonry characteristics more appropriate to replicate the construction of old URM walls in the laboratory, led to the following conclusions:
  - Both brick and mortar are affected by aging and weathering. However, the friction coefficient was found to be insensitive to aging.
  - A weak brick-weak mortar interface should be assumed and the compressive strength in mortar and bricks must be considered to predict potential crushing and brittle failures under in-plane or out-of-plane loading.
  - A combination of old reclaimed bricks and Type L or Type K* mortar will better replicate the actual conditions of old URM buildings, at least in term of maximum compressive strength.
- The experimental studies executed to understand the seismic behavior and vulnerability of masonry walls with parapets and flexible diaphragms, estimate the effectiveness of common retrofitting techniques and validate the numerical models, led to the following conclusions:
  - Distribution of accelerations in the walls and dynamic amplification over the height are affected by the frequency content of the input motion. Hence, this parameter must be considered in the stability assessment of URM walls under out-of-plane loading.
  - The distribution of the inertial forces, displacements and accelerations in the walls were significantly affected by the presence of parapets and realistic connections in

the test setup. Hence, these parameters must be included in future out-of-plane shake table testing of URM walls and numerical models.

  - For all intensity levels of the Virginia Earthquake, no significant differences were observed in the seismic response of retrofitted and unretrofitted walls. Hence, strengthening the parapets and floor to wall connections might not be the most effective method to improve the seismic performance of URM walls in the NYC region.
  - For strong seismic intensities, retrofitting techniques were effective in reducing accelerations at the diaphragm and preventing out-of-plane collapse of parapets. However, unexpected collapse modes were triggered, thus reducing the overall benefit of the strengthening methods. This experimental result also suggests that ASCE 41-06 stability limits may be unconservative, regarding the assessment of URM walls with strengthened and as built parapets and flexible diaphragms.
  - The numerical models generated in SAP2000 for wood diaphragms, floor-to-wall connections and masonry walls provided satisfactory results at the system level response. Peak displacement response was better predicted than peak accelerations, since the model for masonry walls do not account for impact effects generated by rigid body rocking motion.
  - A systematic procedure to define a simplified numerical model of out-of-plane URM walls in multi-story buildings was proposed and validated through nonlinear response history analysis. Peak responses of URM walls subjected to out-of-plane loading in multi-story buildings can be estimated with the new methodology developed in this study.

- A preliminary probabilistic assessment of the archetype URM building in NYC subjected to small intensity ground motions, led to the following conclusion:
  - A small intensity earthquake can have significant cost and business impacts in NYC. Most damage is due to out-of-plane failure of URM walls in upper stories. The associated cost of this failure mode is higher than the cost related to damage in non-structural components.

10.3 Recommendations for Future Research

Recommendations for future research which could complement the studies presented in this report include the following:

- The numerical model for wood diaphragms can be used to investigate simultaneous in-plane and out-of-plane loading interaction, the effect of common stiffening techniques, and current equations in ASCE 41-06 to estimate the strength, stiffness and fundamental period.
- The numerical model developed for floor-to-wall connections can be used to investigate the impact of key variables, such as the coefficient of friction, gravity loads and coefficient of restitution in the global seismic response of a multi-story URM building. Also, current ASCE 31-03 recommendations regarding the strength, minimum number and separation of required steel anchors can be explicitly evaluated.
- The filtering effects on the seismic input of out-of-plane walls due to nonlinear behavior of in-plane walls and flexible diaphragms can be studied using the numerical models proposed for masonry walls. Interacting axial-moment (P-M) and axial-shear (P-V) elements should be incorporated in the model for in-plane walls. Impact should be accounted for in the out-of-plane model, and two-way bending as well.
- The numerical models can be further validated through shake table testing of multi-story URM wall specimens, which could be easily developed using the methodology and test setup proposed in this report.
- Conduct intensity-, scenario- and time-based assessment of a larger number of building archetypes or building aggregates for NYC. The numerical models developed in this research can be used to analyze larger multi-story buildings. Moreover, a larger number of archetypes can be developed if the database used in this study is complemented with information from key websites, such as the Open Accessible Space Information System (OASIS), the NYC Department of Housing and Google Maps.

SECTION 11
REFERENCES

ABK (1984). *Methodology for Mitigation of Seismic Hazards in Existing Unreinforced Masonry Buildings: The Methodology*, ABK, El Segundo, California.

Abrams, D. (1994). *Masonry in the Americas*, American Concrete Institute, Detroit, Michigan.

Abrams, D., and Shah, N. (1992). *Cyclic load testing of unreinforced masonry walls*, University of Illinois, at Urbana-Champaign, Advanced Construction Technology Center, Urbana, Illinois.

Ahmad, N., Crowley, H., Pinho, R., and Ali, Q. (2010). "Displacement-Based Earthquake Loss Assessment of Masonry Buildings in Mansehra City, Pakistan." *Journal of Earthquake Engineering*, 14(sup1), 1-37.

Alecci, V., Fagone, M., Rotunno, T., and De Stefano, M. (2013). "Shear strength of brick masonry walls assembled with different types of mortar." *Construction and Building Materials*, 40(0), 1038-1045.

Allen, D. (1958). "Annotated Bibliography on Lateral Loads on Unreinforced Masonry Walls." *Bibliography*, 10.

Alzeni, Y. (2014). "Cyclic Inelastic Behavior of Concrete Filled Sandwich Panel Walls Subjected to In-plane Flexure." Ph.D. Dissertation, University at Buffalo, SUNY, Buffalo, NY.

Angel, R., Abrams, D., Shapiro, D., Uzarski, J., and Webster, M. (1994). "Behavior of Reinforced Concrete Frames with Masonry Infills." *Structural Research Series*, University of Illinois at Urbana-Champaign, Urbana, Illinois, 238.

Anthoine, A., Magonette, G., and Magenes, G. (1995). "Shear-Compression Testing and Analysis of Brick Masonry Walls." *Proceedings of the 10th European Conference on Earthquake Engineering,* Rotterdam, The Netherlands.

Applied Science International. (2009). Extreme Loading for Structures, version 3, Durham, NC.

ASCE/SEI 7-10 (2010). *Minimum Design Loads for Buildings and Others Structures*, American Society of Civil Engineers, Reston, Virginia.

ASCE/SEI 31-03 (2003). *Seismic Evaluation of Existing Buildings*, American Society of Civil Engineers, Reston, Virginia.

ASCE/SEI 41-06 (2007). *Seismic Rehabilitation of Existing Buildings*, American Society of Civil Engineers, Reston, Virginia.

ASTM (2011). "Standard Test Method for Compressive Strength of Masonry Prisms." *ASTM C1314-11a*, ASTM International, West Conshohocken, PA, 10.

ASTM (2011). "Standard Test Methods for Sampling and Testing Brick and Structural Clay Tile." *ASTM C67-11*, ASTM International, West Conshohocken, PA, 12.

ATC-7 (1981). *Guidelines for the Design of Horizontal Wood Diaphragms*, Applied Technology Council, H.J. Brunnier Associates, Redwood City, CA.

ATC 7-1 (1979). *Proceedings of a Workshop on Design of Horizontal Wood Diaphragms*, ATC-7-1 Report, Applied Technology Council, Berkeley, CA.

Atkinson, R., Amadei, B., Saeb, S., and Sture, S. (1989). "Response of Masonry Bed Joints in Direct Shear." *Journal of Structural Engineering*, 115(9), 2276-2296.

Bala, S. (2007). "Tiebreak Contact in LS-DYNA." <http://www.d3view.com/tiebreak-contact-in-ls-dyna/>. (Access Year: 2012).

Bean Popehn, J., Schultz, A., and Drake, C. (2007). "Behavior of Slender, Posttensioned Masonry Walls under Transverse Loading." *Journal of Structural Engineering*, 133(11), 1541-1550.

Belmouden, Y., and Lestuzzi, P. (2007). "On the Seismic Vulnerability assessment of Unreinforced Masonry Existing Buildings in Switzerland. ." École Polytechnique Fédérale de Lausanne (EPFL), Lausanne, Switzerland.

Benedetti, D., Carydis, P., and Pezzoli, P. (1998). "Shaking table tests on 24 simple masonry buildings." *Earthquake Engineering & Structural Dynamics*, 27(1), 67-90.

Blaikie, E. (1999). "Methodology for the Assessment of Face Loaded Unreinforced Masonry Walls under Seismic Loading." Opus International Consultants, Wellington, New Zealand.

Blaikie, E., and Davey, R. (2000). "Seismic behavior of face loaded unreinforced masonry walls." *12 World Conference of Earthquake Engineering,* Auckland, New Zealand.

Blaikie, E., and Davey, R. (2005). "Methodology for the seismic assessment of face-loaded unreinforced masonry walls and parapets." *2005 New Zealand Society for Earthquake Engineering Conference,* Wellington, New Zealand.

Blaikie, E., and Spurr, D. (1992). *Earthquake Vulnerability of Existing Unreinforced Masonry Buildings*, Works Consultancy Services, New Zealand.

Bothara, J. K., Dhakal, R. P., and Mander, J. B. (2010). "Seismic performance of an unreinforced masonry building: An experimental investigation." *Earthquake Engineering & Structural Dynamics*, 39(1), 45-68.

Bracci, J. M., Reinhorn, A. M., Mander, J. B., and National Center for Earthquake Engineering Research (U.S.) (1992). *Seismic resistance of reinforced concrete frame structures designed only for gravity loads. Part I, Design and properties of a one-third scale model structure*, National Center for Earthquake Engineering Research, Buffalo, N.Y.

Brignola, A., Pampanin, S., and Podesta, S. (2009). "Evaluation and Control of the In-plane Stiffness of Timber Floors for the Performance-Based Retrofit of URM Buildings." *Bulletin of the New Zealand Society for Earthquake Engineering*, 42(3), 204-221.

Bruneau, M. (1994a). "State-of-the-Art Report on Seismic Performance of Unreinforced Masonry Buildings." *Journal of Structural Engineering*, 120(1), 230-251.

Bruneau, M. (1994b). "Seismic Evaluation of Unreinforced Masonry Buildings - a State-of-the-Art Report." *Canadian Journal of Civil Engineering*, 21(3), 512-539.

Bruneau, M., and Yoshimura, K. (1996). "Damage to masonry buildings caused by the 1995 Hyogo-ken Nanbu (Kobe, Japan) earthquake." *Canadian Journal of Civil Engineering*, 23(3), 797-807.

Calderini , C. S., and Lagomarsino, S. (2009). "In-Plane Seismic Response of Unreinforced Masonry Walls: Comparison between detailed and Equivalent Frame Models." *COMPDYN 2009-ECCOMAS Thematic Conference on Computational Methods in Structural Dynamics and Earthquake Engineering*, M. Papadrakakis, N.D. Lagaros, and M. Fragiadakis, eds.Rhodes, Greece.

Calvi, G., and Magenes, G. (1997). "Seismic evaluation and rehabilitation of masonry buildings." *Proceedings of the U.S. - Italian workshop on seismic evaluation and retrofit*,

D. P. Abrams, and G. M. Calvi, eds., National Center for Earthquake Engineering Research (Technical Report NCEER, 97-0003), Buffalo, New York, U.S., 123-142.

Calvi, G. M., Kingsley, G. R., and Magenes, G. (1996). "Testing of Masonry Structures for Seismic Assessment." *Earthquake Spectra*, 12(1), 145-162.

Carney, J. M. (1975). "Bibliography on Wood and Plywood Diaphragms." *J Struct Div-Asce*, 101(11), 2423-2436.

Carr, A. 2004. RUAUMOKO, version 2D, Canterbury, New Zealand.

Casolo, S. (2004). "Modelling in-plane micro-structure of masonry walls by rigid elements." *International Journal of Solids and Structures*, 41(13), 3625-3641.

Casolo, S., and Sanjust, C. A. (2009). "Seismic analysis and strengthening design of a masonry monument by a rigid body spring model: The "Maniace Castle" of Syracuse." *Engineering Structures*, 31(7), 1447-1459.

Chen, S. Y., Moon, F. L., and Yi, T. (2008). "A macroelement for the nonlinear analysis of in-plane unreinforced masonry piers." *Engineering Structures*, 30(8), 2242-2252.

Chopra, A. K. (2007). *Dynamics of Structures: Theory and Applications to Earthquake Engineering*, Pearson/Prentice Hall.

Christovasilis, I., and Sideris, P. (2007). "Independent Study on IDA." University at Buffalo, Buffalo, NY.

Cohen, G. L., Klingner, R. E., John R. Hayes, J., and Sweeney, S. C. (2004). "Seismic Evaluation of Low-Rise Reinforced Masonry Buildings with Flexible Diaphragms: II. Analytical Modeling." *Earthquake Spectra*, 20(3), 803-824.

Costa, A. A., Arêde, A., Penna, A., and Costa, A. (2013). "Free rocking response of a regular stone masonry wall with equivalent block approach: experimental and analytical evaluation." *Earthquake Engineering & Structural Dynamics*, 42(15), 2297-2319.

Costley, A. C., and Abrams, D. P. (1996). *Dynamic response of unreinforced masonry buildings with flexible diaphragms*, National Center for Earthquake Engineering Research, State University of New York at Buffalo, Buffalo, NY.

Countryman, D., Colbenson, P., and Association, D. F. P. (1955). *1954 horizontal plywood diaphragm tests: full report*, Technical Dept., Douglas Fir Plywood Association.

Craig, J. I., Goodno, B. J., Towashiraporn, P., and Park, J. (2002). "Response Modification Applications for Essential Facilities." Mid-America Earthquake Center, Atlanta, GA.

Cross, W., and Jones, N. (1993). "Seismic Performance of Joist - Pocket Connections. I: Modeling." *Journal of Structural Engineering*, 119(10), 2986-3007.

CSI. 2009. SAP2000, version 14, Computers & Structures Inc., Berkeley, CA.

CSI (2010). "CSI Analysis Reference Manual for SAP2000, ETABS, and SAFE." Computers & Structures Inc., Berkeley, CA.

CSI (2012). "SAP2000 Overview." <http://www.csiberkeley.com/sap2000>.

D'Ayala, D., and Speranza, E. (2003). "Definition of Collapse Mechanisms and Seismic Vulnerability of Historic Masonry Buildings." *Earthquake Spectra*, 19(3), 479-509.

Davis, R. (2010). "Seismic Evaluation, Parameterization, and Effect of Light-Frame Steel Studded Gypsum Partition Walls."Master Thesis, University at Buffalo, Buffalo, NY.

De Felice, G., and Giannini, R. (2001). "OUT-OF-PLANE SEISMIC RESISTANCE OF MASONRY WALLS." *Journal of Earthquake Engineering*, 5(2), 253 - 271.

Derakhshan, H. (2011). "Seismic Assessment of Out of Plane Loaded Unreinforced Masonry Walls."Ph.D. Dissertation, The University of Auckland.

Derakhshan, H., Ingham, J., and Griffith, M. (2009). "Tri-linear force-displacement models representative of out-of-plane unreinforced masonry wall behavior." *11th Canadian Masonry Symposium,* Toronto, Ontario.

Doherty, K., Griffith, M. C., Lam, N., and Wilson, J. (2002). "Displacement-based seismic analysis for out-of-plane bending of unreinforced masonry walls." *Earthquake Engineering & Structural Dynamics*, 31(4), 833-850.

Dolan, J. (1989). "The Dynamic Response of Timber Shear Walls." PhD Dissertation, University of British Columbia, Vancouver.

Dolan, J., and Foschi, R. (1991). "Structural Analysis Model for Static Loads on Timber Shear Walls." *Journal of Structural Engineering*, 117(3), 851-861.

Dolatshahi, K. M., Aref, A. J., and Yekrangnia, M. (2014). "Bidirectional behavior of unreinforced masonry walls." *Earthquake Engineering & Structural Dynamics*, n/a-n/a.

Dowell, R. K., Seible, F. S., and Wilson, E. L. (1998). "Pivot Hysteresis Model for Reinforced Concrete Members." *ACI Structural Journal*, 95(5), 607-617.

Doyle, D. V., Forest Products Laboratory, and University of Wisconsin (1957). *Diaphragm Action of Diagonally Sheathed Wood Panels*, U.S. Department of Agriculture, Forest Service, Forest Products Laboratory.

Duke, M. (1951). "Bibliography on Masonry Failure under Impulsive Loads." *Bibliography*, University of California, Los Angeles.

Ehsani, M. R., Saadatmanesh, H., and Velazquez-Dimas, J. I. (1999). "Behavior of Retrofitted URM Walls under Simulated Earthquake Loading." *Journal of Composites for Construction*, 3(3), 134-142.

Epperson, G. S., and Abrams, D. P. (1989). *Nondestructive evaluation of masonry buildings*, Advanced Construction Technology Center, Newmark Civil Engineering Laboratory, University of Illinois at Urbana-Champaign, Urbana, Ill.

Eschenasy, D. (2011). "Cases of Failure of Unreinforced Brick Walls Due to Out-Of-Plane Loads." *Structure Magazine,* , May 2011, 14-16.

Ewing, R. D., and Johnson, A. W. (1981). *Methodology for mitigation of seismic hazards in existing unreinforced masonry buildings : diaphragm testing*, ABK, El Segundo, CA.

Ewing, R. D., and Kariotis, J. C. (1981). *Methodology for mitigation of seismic hazards in existing unreinforced masonry buildings : wall testing, out-of-plane*, ABK, El Segundo, CA.

Ewing, R. D., Kariotis, J. C., and ABK A Joint Venture (El Segundo Calif.) (1981). *Methodology for mitigation of seismic hazards in existing unreinforced masonry buildings : wall testing, out-of-plane*, ABK, El Segundo, Ca.

Falk, R., and Itani, R. (1987). "Dynamic Characteristics of Wood and Gypsum Diaphragms." *Journal of Structural Engineering*, 113(6), 1357-1370.

Falk, R., and Itani, R. (1989). "Finite Element Modeling of Wood Diaphragms." *Journal of Structural Engineering*, 115(3), 543-559.

FEMA P58-1 (2012). "Seismic Performance Assessment of Buildings Volume 1-Methodology." FEMA P58-1, prepared by Applied Technology Council for the Federal Emergency Management Agency, Washington, D.C.

FEMA P547 (2006). "Techniques for the Seismic Rehabilitation of Existing Buildings." prepared by Rutherford & Chekene Consulting Engineers for Federal Emergency Management Agency, Washington, D.C.

FEMA P774 (2009). "Unreinforced Masonry Buildings and Earthquakes: Developing Successful Risk Reduction Programs." prepared by Applied Technology Council for Federal Emergency Management Agency, Washington, D.C.

Filiatrault, A. (1990). "Static and dynamic analysis of timber shear walls." *Canadian Journal of Civil Engineering*, 17(4), 643-651.

Flanagan, R. D., and Bennett, R. M. (1999). "Bidirectional Behavior of Structural Clay Tile Infilled Frames." *Journal of Structural Engineering*, 125(3), 236-244.

Foliente, G. C. (1995). "Hysteresis Modeling of Wood Joints and Structural Systems." *Journal of Structural Engineering-Asce*, 121(6), 1013-1022.

Folz, B., and Filiatrault, A. (2001). "Cyclic Analysis of Wood Shear Walls." *Journal of Structural Engineering*, 127(4), 433-441.

Fonseca, F. (1997). "Cyclic Loading Response of Reinforced Concrete Tilt-up structures with Plywood Diaphragms." PhD Dissertation, University of Illinois at Urbana-Champaign, Urbana, Ill.

Foschi, R. O. (1977). "Analysis of wood diaphragms and trusses. Part I: Diaphragms." *Canadian Journal of Civil Engineering*, 4(3), 345-352.

Friedman, D. (1995). *Historical Building Construction: Design, Materials, and Technology*, New York.

Galasco, A., Lagomarsino, S., Penna, A., and Resemini, S. (2004). "Nonlinear seismic analysis of masonry structures." *13th World Conference on Earthquake Engineering*, Vancouver, Canada

Gallonelli, M. (2007). "Dynamic Response of Masonry Buildings with Rigid or Flexible Floors." Master Thesis, Rose School.

Gambarotta, L., and Lagomarsino, S. (1997). "Damage Models for the Seismic Response of Brick Masonry Shear Walls. Part II: The Continuum Model and its Applications." *Earthquake Engineering & Structural Dynamics*, 26(4), 441-462.

Green, N. B., and Horner, A. C. (1934). "Earthquake Resistance of Timber Floors." *Engineering News Record*.

Green, N. B., Horner, A. C., and Combs, T. C. (1935). "Tests Indicate Design Methods for Earthquake-Proof Timber Floors." *Engineering News Record*.

Griffith, M., Lam, N., Wilson, J., and Doherty, K. (2004). "Experimental Investigation of Unreinforced Brick Masonry Walls in Flexure." *Journal of Structural Engineering*, 130(3), 423-432.

Griffith, M. C., Vaculik, J., Lam, N. T. K., Wilson, J., and Lumantarna, E. (2007). "Cyclic testing of unreinforced masonry walls in two-way bending." *Earthquake Engineering & Structural Dynamics*, 36(6), 801-821.

Gulkan, P., Clough, R. W., Mayes, R. L., and Manos, G. C. (1990). "Seismic Testing of Single-Story Masonry Houses: Part 1." *Journal of Structural Engineering*, 116(1), 235-256.

Gupta, A., and Kuo, G. (1985). "Behavior of Wood - Framed Shear Walls." *Journal of Structural Engineering*, 111(8), 1722-1733.

Hamed, E., and Rabinovitch, O. (2008). "Nonlinear dynamic behavior of unreinforced masonry walls subjected to out-of-plane loads." *Journal of structural engineering*, 134(11), 1743-1753.

Hamid, E. (1993). "Performance of Loadbearing Masonry Buildings During the October 1992 Earthquake in Cairo, Egypt." *Proceedings of the North American Masonry Conference*, Philadelphia, PA.

Healy, J. (2011). "Suggestions on the mortar-brick mechanical properties for masonry."Personal Communication.

Ingham, J. (2011). "The performance of masonry buildings in the Christchurch earthquake." <http://www.slideshare.net/xanocosta/ingham-keynote-8444435>.

Ingham, J., and Griffith, M. (2010). "Performance of unreinforced masonry buildings during the 2010 Dari eld (Christchurch, NZ) earthquake." *Australian Journal of Structural Engineering*, 11(3).

Itani, R., and Cheung, C. (1984). "Nonlinear Analysis of Sheathed Wood Diaphragms." *Journal of Structural Engineering*, 110(9), 2137-2147.

Jaiswal, K. S., and Wald, D. J. (2008). "Creating a global building inventory for earthquake loss assessment and risk management: U.S. Geological Survey Open-File Report 2008-1160." 103 p.

Johnson, J. W. (1954). *Lateral tests on full-scale lumber-sheathed roof diaphragms of various length-width ratios*, Oregon Forest Products Laboratory, State Board of Forestry and School of Forestry, Oregon State College, Corvallis, Or.

Johnson, J. W. (1971). *Lateral test of a 20- by 60-foot roof section sheathed with plywood overlaid on decking*, School of Forestry, Oregon State University, Corvallis, Or.

Judd, J., and Fonseca, F. (2005). "Analytical Model for Sheathing-to-Framing Connections in Wood Shear Walls and Diaphragms." *Journal of Structural Engineering*, 131(2), 345-352.

Judd, J. P. (2005). "Analytical Modeling of Wood-Frame Shear Walls and Diaphragms." Master Thesis, Brigham Young University, UT.

Karbass, A. (2009). "Development of Seismic Vulnerability Curves for Masonry Buildings Using the Applied Element Method." *Improving the Seismic Performance of Existing Buildings and Other Structures*, San Francisco, CA.

Karim, A., Quenneville, P., Don, N., and Ingham, J. (2011). "Wall-Diaphragm Connection Assessment Guidelines for URM Buildings." *Ninth Pacific Conference on Earthquake Engineering,* Auckland, New Zealand.

Kaushik, H. B., Rai, D. C., and Jain, S. K. (2007). "Stress-Strain Characteristics of Clay Brick Masonry under Uniaxial Compression." *Journal of Materials in Civil Engineering*, 19(9), 728-739.

Kim, S.-C., and White, D. W. (2004a). "Linear static analysis of low-rise buildings with flexible diaphragms using the structural separation method." *Engineering Structures*, 26(1), 83-93.

Kim, S.-C., and White, D. W. (2004b). "Nonlinear analysis of a one-story low-rise masonry building with a flexible diaphragm subjected to seismic excitation." *Engineering Structures*, 26(14), 2053-2067.

Knox, C. L. (2012). "Assessment of Perforated Unreinforced Masonry Walls Responding In-plane." Ph.D. Dissertation, University of Auckland.

Krawinkler, H., Osteraas, J. D., McDonald, B. M., and Hunt, J. P. (2012). "Development of Damage Fragility Functions for URM Chimneys and Parapets." *15 World Conference of Earthquake Engineering.* Lisboa, Portugal.

Lin, T., and LaFave, J. (2012a). "Experimental structural behavior of wall-diaphragm connections for older masonry buildings." *Construction and Building Materials*, 26(1), 180-189.

Lin, T., and LaFave, J. (2012b). "Experimental Behavior and Modeling of Wall-Diaphragm Connections for Older Masonry Buildings." *15th World Conference on Earthquake Engineering.* Lisbon, Portugal.

Lu, M., Schultz, A., and Stolarski, H. (2004). "Analysis of the Influence of Tensile Strength on the Stability of Eccentrically Compressed Slender Unreinforced Masonry Walls Under Lateral Loads." *Journal of Structural Engineering*, 130(6), 921-933.

Lupoae, M., and Bucur, C. (2009). "Use of Applied Element Method to Simulate the Collapse of a Building." *SISOM 2009 and Session of the Commission of Acoustics.* Bucharest, Romania.

Magenes, G., and Penna, A. (2011). "Seismic Design and Assessment of Masonry Buildings in Europe: Recent Research and Code Development Issues." *9th Australian Masonry Conference*, Queenstown, New Zealand, 583-603.

Makris, N., and Konstantinidis, D. (2003). "The rocking spectrum and the limitations of practical design methodologies." *Earthquake engineering & structural dynamics*, 32(2), 265-289.

Manzouri, T., Schuller, M. P., Shing, P. B., and Amadei, B. (1996). "Repair and Retrofit of Unreinforced Masonry Structures." *Earthquake Spectra*, 12(4), 903-922.

Mayorca, P., and Meguro, K. (2003). "Modeling Masonry Structures using the Applied Element Method." *SEISAN KENKYU*, 55(6), 581-584.

Mclain, T. E. (1975). "Curvilinear Load-Slip Relations in Laterally Loaded Nailed Joints." Ph.D. Dissertation, Colorado State University, Fort Collins, CO.

McMonies, W. (2010). "Portland's Unreinforced Masonry Apartment Buildings: A Threatened Species?" *Center for Real Estate Quarterly Journal*, 4(3), 31-44.

Meguro, K., and Tagel-Din, H. (2002). "Applied Element Method Used for Large Displacement Structural Analysis." *J Nat Disaster Sci*, 24(1), 25-34.

Meisl, C. S., Elwood, K. J., and Ventura, C. E. (2007). "Shake table tests on the out-of-plane response of unreinforced masonry walls." *Canadian Journal of Civil Engineering*, 34(11), 1381-1392.

Mendes, N., and Lourenço, P. B. (2009). "Seismic Assessment of Masonry "Gaioleiro" Buildings in Lisbon, Portugal." *Journal of Earthquake Engineering*, 14(1), 80-101.

Menon, A., and Magenes, G. (2011). "Definition of Seismic Input for Out-of-Plane Response of Masonry Walls: I. Parametric Study." *Journal of Earthquake Engineering*, 15(2), 165-194.

Minaie, E. (2009). "Behavior and Vulnerability of Reinforced Masonry Shear Walls." Ph.D. Dissertation, Drexel University.

Moon, F. L. (2004). "Seismic Strengthening of Low-Rise Unreinforced Masonry Structures with Flexible Diaphragms." Phd Dissertation, Georgia Institute of Technology.

Moon, F. L., Yi, T., Leon, R. T., and Kahn, L. F. (2006). "Recommendations for Seismic Evaluation and Retrofit of Low-Rise URM Structures." *Journal of Structural Engineering*, 132(5), 663-672.

Moreira, S., Oliveira, D., Ramos, L., Lourenco, P., Fernandes, R., and Guerreiro, J. (2012). "Experimental Study on the Seismic Behavior of Masonry Wall-to-Floor Connections." *15 World Conference of Earthquake Engineering*, Lisboa, Portugal.

MSJC (2008). *Building Code Requirements and Specifications for Masonry Structures*, Masonry Society, American Concrete Institute, Structural Engineering Institute, Boulder, Colorado.

Muthukumar, S., and DesRoches, R. (2006). "A Hertz contact model with non-linear damping for pounding simulation." *Earthquake Engineering & Structural Dynamics*, 35(7), 811-828.

Nagarajaiah, S., Reinhorn, A. M., Constantinou, M. C., and National Center for Earthquake Engineering Research (U.S.) (1991). *3D-BASIS nonlinear dynamic analysis of three-dimensional base isolated structures. Part II*, National Center for Earthquake Engineering Research, State University of New York at Buffalo, Buffalo, NY.

Najafgholipour, M. A., Maheri, M. R., and Lourenço, P. B. (2014). "Definition of interaction curves for the in-plane and out-of-plane capacity in brick masonry walls." *Construction and Building Materials*, 55(0), 168-182.

Naseer, A., Khan, A. N., Hussain, Z., and Ali, Q. (2010). "Observed Seismic Behavior of Buildings in Northern Pakistan During the 2005 Kashmir Earthquake." *Earthquake Spectra*, 26(2), 425-449.

NZSEE (2006). *Assessment and Improvement of the Structural Performance of Buildings in Earthquakes*, New Zealand Society for Earthquake Engineering, Wellington, New Zealand.

Okail, H. O., Shing, P. B., Klingner, R. E., and McGinley, W. M. (2010). "Performance of clay masonry veneer in wood-stud walls subjected to out-of-plane seismic loads." *Earthquake Engineering & Structural Dynamics*, 39(14), 1585-1609.

OpenSees. 2012. "Open System for Earthquake Engineering Simulation." Pacific Earthquake Engineering Research Center (PEER). Available from: http://opensees.berkeley.edu/.

Paquette, J., and Bruneau, M. (2006). "Pseudo-dynamic testing of unreinforced masonry building with flexible diaphragm and comparison with existing procedures." *Construction and Building Materials*, 20(4), 220-228.

Paquette, J., Bruneau, M., and Brzev, S. (2004). "Seismic Testing of Repaired Unreinforced Masonry Building having Flexible Diaphragm." *Journal of Structural Engineering*, 130(10), 1487-1496.

Paquette, J., Bruneau, M., and Filiatrault, A. (2001). "Out-of-Plane Seismic Evaluation and Retrofit of Turn-of-the-Century North American Masonry Walls." *Journal of Structural Engineering*, 127(5), 561-569.

Park, J., Towashiraporn, P., Craig, J. I., and Goodno, B. J. (2009). "Seismic fragility analysis of low-rise unreinforced masonry structures." *Engineering Structures*, 31(1), 125-137.

Pasticier, L., Amadio, C., and Fragiacomo, M. (2008). "Non-linear seismic analysis and vulnerability evaluation of a masonry building by means of the SAP2000 V.10 code." *Earthquake Engineering & Structural Dynamics*, 37(3), 467-485.

Paulay, T., and Priestley, M. J. N. (1992). *Seismic Design of Reinforced Concrete and Masonry Buildings*, John Wiley & Sons, Inc.

Pellicane, P., Stone, J., and Vanderbilt, M. (1991). "Generalized Model for Lateral Load Slip of Nailed Joints." *Journal of Materials in Civil Engineering*, 3(1), 60-77.

Penner, O., and Elwood, K. J. (2012). "Experimental Investigation on the Effect of Diaphragm Flexibility on Out-of-Plane Dynamic of Unreinforced Masonry Walls." *15 World Conference of Earthquake Engineering.* Lisboa, Portugal.

Peralta, D. F., Bracci, J. M., and Hueste, M. B. D. (2004). "Seismic behavior of wood diaphragms in pre-1950s unreinforced masonry buildings." *Journal of Structural Engineering*, 130(12), 2040-2050.

Peterson, J. (1983). "Bibliography on Lumber and Wood Panel Diaphragms." *Journal of Structural Engineering-Asce*, 109(12), 2838-2852.

Radford, W. A. (1983). *Old House Measured and Scaled Detail Drawings for Builders and Carpenters: An Early Twentieth-Century Pictorial Sourcebook with 183 Detailed Plates.*, Dover Publications, New York.

Ramsey, C. G. (1998). *Architectural Graphic Standards for Architects, Engineers, Decorators, Builders, and Draftsmen.*, J. Wiley, New York

Reinhorn, A. M., Kunnath, S. K., Panahshahi, N., and National Center for Earthquake Engineering Research (U.S.) (1988). *Modeling of R/C building structures with flexible floor diaphragms (IDARC2)*, National Center for Earthquake Engineering Research, State University of New York at Buffalo, Buffalo, NY.

Reynolds, D. M. (1994). *The architecture of New York City: Histories and Views of Important Structures, Sites, and Symbols.*, J. Wiley, New York

Roca, P., Molins, C., and Mari, A. R. (2005). "Strength Capacity of Masonry Wall Structures by the Equivalent Frame Method." *Journal of Structural Engineering*, 131(10), 1601-1610.

Rota, M., Penna, A., and Magenes, G. (2010). "A methodology for deriving analytical fragility curves for masonry buildings based on stochastic nonlinear analyses." *Engineering Structures*, In Press, Corrected Proof.

Rush, A. (2007). "Seismic Evaluation of Masonry Building Conglomerations of adjacent structures." Master Thesis, Istituto Universitario di Studi Superiori di Pavia, Pavia.

Russell, A. P. (2010). "Characterisation and Seismic Assessment of Unreinforced Masonry Buildings." Ph.D. Dissertation, University of Auckland.

Russell, A. P., Mahmood, H., and Ingham, J. (2007). "Assessment of the Material Properties of New Zealand's Unreinforced Masonry Building Stock." *The Third International Conference on Structural Engineering, Mechanics and Computation*, Cape Town, South Africa.

Russell, A. P., Mahmood, H., and Ingham, J. (2007). "Pseudo-static In-plane Testing of Typical New Zealand Unreinforced Masonry Walls." *8th Pacific Conference on Earthquake Engineering (14IBMAC)*, Sydney, Australia.

Salonikios, T., Karakostas, C., Lekidis, V., and Anthoine, A. (2003). "Comparative inelastic pushover analysis of masonry frames." *Engineering Structures*, 25(12), 1515-1523.

Sanchez-Ferreira, J. (2011). "Stability of Elastomeric Bearings for Seismic Applications."Master Thesis, State University of New York at Buffalo, Buffalo, NY.

Sarlis, A., and Constantinou, M. (2010). "Modeling Triple Friction Pendulum Isolator in Program SAP2000." University at Buffalo, Buffalo, NY, 55.

Schuller, M. P. (2011). "Recomendated mortar proportions for URM testing."Personal Communication.

Sharif, I., Meisl, C. S., and Elwood, K. J. (2007). "Assessment of ASCE 41 Height-to-Thickness Ratio Limits for URM Walls." *Earthquake Spectra*, 23(4), 893-908.

Shawa, O. A., de Felice, G., Mauro, A., and Sorrentino, L. (2012). "Out-of-plane seismic behaviour of rocking masonry walls." *Earthquake Engineering & Structural Dynamics*, 41(5), 949-968.

Simsir, C. (2004). "Influence of Diaphragm Flexibility on the Out-Of-Plane Dynamic Response of Unreinforced Masonry Walls." Ph.D. Dissertation, University of Illinois at Urbana-Champaign.

Simsir, C., Aschheim, M., and Abrams, D. (2004). "Out-of-plane dynamic response of unreinforced masonry bearing walls attached to flexible diaphragms." *13th World Conference on Earthquake Engineering*, Vancouver, Canada.

Sivaselvan, M. V., and Reinhorn, A. M. (1999). *Hysteretic models for cyclic behavior of deteriorating inelastic structures*, Multidisciplinary Center for Earthquake Engineering Research, Buffalo, NY.

Spence, R. (2007). "Saving lives in earthquakes: successes and failures in seismic protection since 1960." *Bulletin of Earthquake Engineering*, 5(2), 139-251.

Stavridis, A. (2009). "Analytical and Experimental Study of Seismic Performance of Reinforced Concrete Frames Infilled with Masonry Walls." Ph.D. Dissertation, University of California, San Diego.

Stewart, W. G. (1987). "The Seismic Design of Plywood Sheathed Shear Walls." PhD Dissertation, University of Canterbury, Christchurch, New Zealand.

Stillinger, J. R. (1953). *Lateral tests on full-scale lumber-sheathed roof diaphragms*, Oregon Forest Products Laboratory, Corvallis, Or.

Stillinger, J. R., Johnson, J. W., Overholser, J. L., and Oregon Forest Products Laboratory. (1952). *Lateral tests on full-scale lumber-sheathed diaphragms*, Oregon Forest Products Laboratory, State Board of Forestry and School of Forestry, Oregon State College, Corvallis, Or.

Tagel-Din, H., and Rahman, N. A. (2006). "Simulation of the Alfred P. Murrah Federal Building Collapse Due to Blast Loads." *Building Integration Solutions*, 1-15.

Tantala, M., Nordenson, G., Deodatis, G., and Jacob, K. (2003). "Earthquake Risks and Mitigation in the New York/New Jersey/ Connecticut Region." NYCEM Summary Report 1999-2003.

Tena-Colunga, A., and Abrams, D. P. (1992). *Response of an unreinforced masonry building during the Loma Prieta Earthquake*, Dept. of Civil Engineering, University of Illinois at Urbana-Champaign, Urbana, IL.

Tena-Colunga, A., and Abrams, D. P. (1996). "Seismic Behavior of Structures with Flexible Diaphragms." *Journal of Structural Engineering*, 122(4), 439-445.

Tisa, A., and Kovári, K. (1984). "Continuous failure state direct shear tests." *Rock Mechanics and Rock Engineering*, 17(2), 83-95.

Tissell, J. R. (1966). *1966 Horizontal Plywood Diaphragm Tests*, Applied Research Department, Technical Services Division, American Plywood Association.

Tomazevic, M. (1993). *Influence of floors and connection of walls on seismic resistance of old brick masonry houses*, Institute for Testing and Research in Materials and Structures, Ljubljana.

Tomazevic, M. (1999). *Earthquake-resistant design of masonry buildings*, Imperial College Press.

Tomazevic, M., and Weiss, P. (1990). "A Rational, Experimentally Based Method for the Verification of Earthquake Resistance of Masonry Buildings " *Proceedings of the Fourth U.S. National Conference on Earthquake Engineering*, EERI, ed., Oakland, California.

Tomaževič, M., Weiss, P., Velechovsky, T., and Zavod, R. (1990). *The influence of rigidity of floors on the seismic resistance of of old masonry buildings : shaking-table tests of model houses A and B*, Institute for Testing and Research in Materials and Structures, Ljubljana, Slovenia.

USGS (2008). "The Shake Out Scenario-Unreinforced Masonry (URM) Buildings." United States Geological Survey, Pasadena, CA

USGS (2009). "Hazard Curve Application." *(http://geohazards.usgs.gov/hazardtool/application.php)*.

USGS (2012). "Hazard Curve Application." *(http://geohazards.usgs.gov/hazardtool/application.php)*.

Vaculik, J., and Griffith, M. (2008). "Time History Analysis for Unreinforced Masonry Walls in Two-Way Bending." *The 14th World Conference on Earthquake Engineering,* Beijing, China.

Vaculik, J., and Griffith, M. C. "Shaketable Tests on Masonry Walls in Two-Way Beding." AEES.

Vamvatsikos, D., and Cornell, C. A. (2002). "Incremental dynamic analysis." *Earthquake Engineering & Structural Dynamics*, 31(3), 491-514.

Vélez, L. F. R., and Magenes, G. (2009). *Static Tests on Dry Stone Masonry and Evaluation of Static Collapse Multipliers*, Iuss Press.

Wanitkorkul, A., and Filiatrault, A. (2005). "Simulation of Strong Ground Motions for Seismic Fragility Evaluation of Nonstructural Components in Hospitals." University at Buffalo, Sate University of New York.

White, M., and Dolan, J. (1995). "Nonlinear Shear-Wall Analysis." *Journal of Structural Engineering*, 121(11), 1629-1635.

Whitlock, R. (2011). "Suggestions on mortar-brick mechanical properties." Personal Communication.

Wijanto, L. S. (2007). "Seismic Assessment of Unreinforced Masonry Walls."Ph.D. Dissertation, University of Canterbury, Christchurch, New Zealand.

Willis, C. R., Yang, Q., Seracino, R., and Griffith, M. C. (2009). "Damaged masonry walls in two-way bending retrofitted with vertical FRP strips." *Construction and Building Materials*, 23(4), 1591-1604.

Wilson, A., Quenneville, P., and Ingham, J. (2011). "Assessment of Timber Floor Diaphragms in Historic Unreinforced Masonry Buildings." *International Conference on Structural Health Assessment of Timber Structures*, Lisbon, Portugal.

Worakanchana, K., and Meguro, K. (2008). "Applied Element Method For Nonlinear Analysis of Reinforced Concrete Structures Under Fault Action." *SEISAN KENKYU*, 60(3), 208-211.

Yi, T. (2004). "Experimental Investigation and Numerical Simulation of an Unreinforced Masonry Structure with Flexible Diaphragms."PhD Dissertation, Georgia Institute of Technology, Atlanta, GA.

Yi, T., Moon, F., Leon, R., and Kahn, L. (2006). "Analyses of a Two-Story Unreinforced Masonry Building." *Journal of Structural Engineering*, 132(5), 653-662.

Yi, T., Moon, F. L., Leon, R. T., and Kahn, L. F. (2006b). "Lateral Load Tests on a Two-Story Unreinforced Masonry Building." *Journal of Structural Engineering*, 132(5), 643-652.

Appendix A Alternative Modeling Methodologies for In-plane URM Walls

A.1 Introduction

This appendix will discuss two modelling techniques for in-plane URM walls that were also investigated in this research. The first approach, based on nonlinear springs, was studied to model uncertainties in the seismic assessment in future research of URM buildings. Due to its simplicity, reliability and very efficient computer time, the model is suitable for Monte Carlo simulations/ Latin Hypercube, first order-second moment methods, which require a significant large number of analyses. This model is implemented in RUAMOKO 2D (Carr 2004) software. The second approach, based on nonlinear shell elements, was investigated to develop reliable damage states of URM walls subjected to in-plane loading. The model accounts for axial-moment interaction, in both, piers and spandrels and no assumptions are made regarding effective height, or potential failure mode of the walls. This model was implemented in SAP2000 (CSI 2009).

Assumptions and limitations of the proposed methodologies are described in the next section. Then, validation of the models at the pier and global response level is presented. Experimental studies widely documented in the literature were used for this validation exercise.

Table A-1 Summary of type of analysis implemented

Software Used	Modelling Technique Nonlinear Behavior	Type of Analysis	
		Nonlinear Static	Nonlinear Time History
RUAUMOKO	Multi-linear Hysteresis Rule	YES	YES
	Takeda Hysteresis Rule	NO	YES
	Bilinear Elastic & Bilinear Inelastic	NO	YES
SAP2000	Nonlinear Shell element	YES	NO

A.2 Nonlinear Spring Macro-Model for In-plane Walls

The proposed modelling of the masonry building is based on the macro-model approach proposed by Park et al. (2009). This model was selected due to its simplicity, accuracy, reliability and efficient computer time. Pier, spandrel and diaphragm masses were lumped at each story level. In addition, masonry piers, spandrels and diaphragm were modeled on each analysis direction using a single nonlinear spring with limited degrees of freedom. Each spring represents a particular failure mode that is predicted in advance using equations given by ASCE 41-06. Since there is no general agreement on the type of hysteresis rule that better represents those failure modes, three distinct rules were investigated in this study. First, the modified backbone curve proposed by Moon et al. (2006) was modeled using the *Multi-linear* hysteresis rule. Second, the modified *Takeda* hysteresis rule as proposed by Pasticier et al. (2008) was utilized to model both, piers and spandrel assuming that most of the damage will be due to shear behavior. Finally, the *Bi-linear Elastic* hysteresis rule was used to model rocking behavior on piers whereas the *Bi-linear Inelastic* hysteresis rule was used to simulated sliding and shear behavior. The first hysteresis model was considered to perform both, nonlinear static analysis and time history analysis in RUAUMOKO 2D, whereas the second and third were only considered to complete time history analysis. Table A-1 summarizes the analysis cases implemented in this report. Main findings will be discussed in the following sections.

RUAUMOKO 2D software was chosen to perform nonlinear static analysis and dynamic time history analysis. RUAUMOKO 2D has a large selection of modelling options to characterize the building and its supports. The mass representation is via lumped or kinematically consistent mass matrices. In addition to the commonly used Rayleigh damping model, several damping model options are available within the program. The program offers a wide variety of element types to represent the structural system such as frame type members, wall and quadrilateral members and special members to represent effects such as spring and contact. It is worth noting that the program offers various models to represent the formation of concentrated plastic hinges in a critical location within the member. Also, the capabilities of the program include many different hysteretic rules to represent the inelastic behavior of the members noted above.

Two major issues, the Overturning Moment and P-Delta effects were not addressed in this research due to inherent limitations in the composite spring macro-model. In particular,

overturning moment effect could have been incorporated in the analytical model by modifying the soil-structure interface with a global rotational spring but a vertical constraint must be placed somewhere to avoid evident instability of the system. Nonetheless, as demonstrated in the next sections the global building response is still captured with acceptable accuracy.

In RUAUMOKO, pushover analysis for a given lateral pattern is slowly increased until a point is reached where the lateral resistance is equal to the inertia of the structure (Carr 2004). In this study, a uniform equivalent static loading pattern is applied to the structure by using a slow ramp loading function, as shown in Figure A-1. The nonlinear behavior was simulated by using the multi-linear hysteresis rule discussed below.

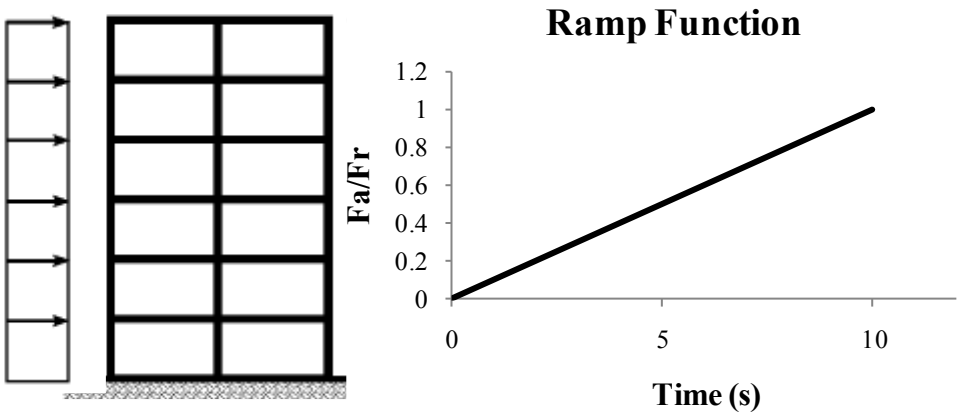

Figure A-1 Pushover loading patterns and ramp function

Multi-linear Hysteresis Rule

The force-drift curve implemented in RUAUMOKO is depicted in Figure A-2. It follows the recommendation proposed by Moon et al. (2006).

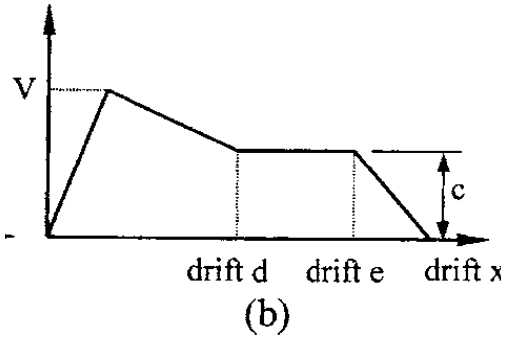

Figure A-2 Modified force-drift relationship (Moon et al. 2006)

Modelling of the modified ASCE 41-06 backbone curve in RUAUMOKO was achieved using a Multi-linear Elastic Hysteresis model depicted in Figure A-3.

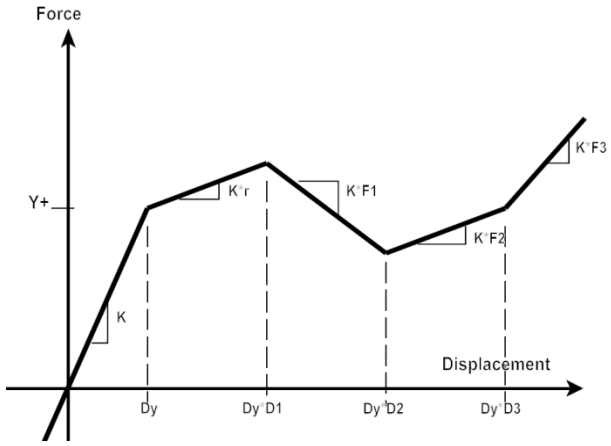

Figure A-3 Multi-Linear elastic hysteresis (Carr 2004)

Another important recommendation adopted in this study, it is the effective height (h_{eff}) calculation as proposed by Moon et al. (2006).

Takeda Hysteresis Rule

The nonlinear behavior of each spring for time history analysis was modeled using the Takeda hysteresis rule shown in Figure A-4. The Takeda model allows simulating the cyclic behavior of the pier or spandrel by defining the shape of the hysteresis loop and the stiffness degradation through a proper choice of the mechanical parameters.

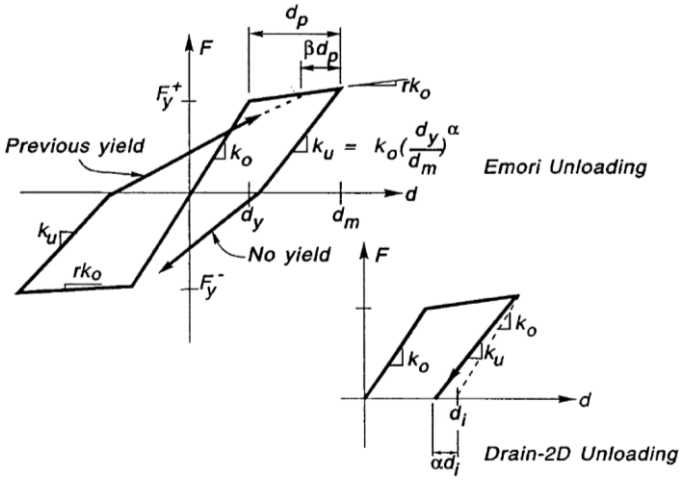

Figure A-4 Modified Takeda Hysteresis (Carr 2004)

The α and β factors were taken equal to 0.5 and 1 as recommended by Pasticier et al. (2008). Degrading strength parameters were not considered in this study, since is widely recognized that the URM walls subjected to in-plane lateral loads exhibits little strength degradation before failure.

Bilinear Elastic and Inelastic Hysteresis Rule

As recommended by Craig et al. (2002), the pier elements were modeled using a bilinear elastic rule to simulate the rocking mode of failure whereas the spandrel members were defined by a bilinear Inelastic Hysteresis rule to represent the Bed Joint Shear Sliding collapse mode. No strength or stiffness degradation was considered. Figure A-5 illustrates the hysteresis rules selected in RUAUMOKO software. The Ramberg-Osgood parameters was calculated in the same way that for the multilinear hysteresis case.

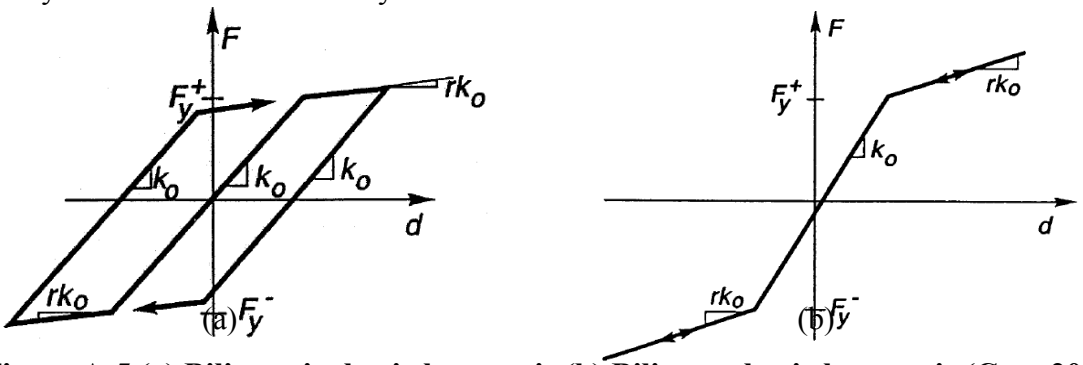

Figure A-5 (a) Bilinear inelastic hysteresis (b) Bilinear elastic hysteresis (Carr 2004)

A.3 Nonlinear Shell Element for In-plane Walls

In addition to the previous analysis, a SAP2000 (CSI 2009) nonlinear wall model was calibrated to match experimental results, both, at the pier/spandrel and global response level. This model is going to be used in next appendices to carry out a nonlinear static analysis (pushover) and verify the results obtained with the RUAUMOKO model when doing the seismic assessment of the five stories URM building representative of New York City.

The nonlinear behavior of unreinforced masonry walls was simulated in SAP2000 software by shell layers with calibrated nonlinear properties. The compressive stress-strain curve for 1:0:6 mortar mix shown in Figure A-6 was used as starting point to modify the Concrete material available in the software. Note that no tension was allowed for this material. An initial Elastic modulus of 500 psi was used and adjusted later to match the experimental data.

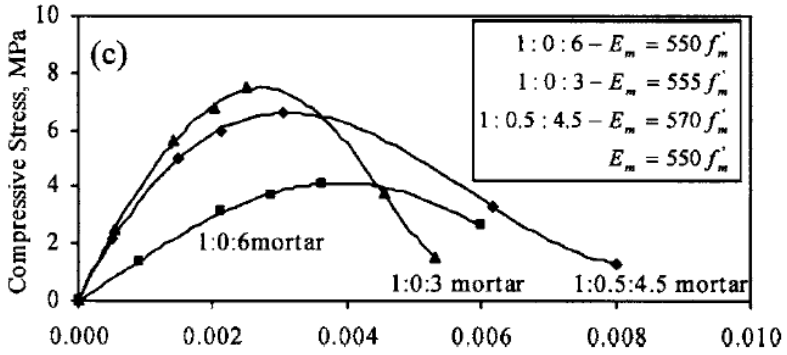

Figure A-6 Compressive stress-strain curve for masonry prisms (Kaushik et al. 2007).

One shell sections was defined to simulate both, piers and spandrels. Piers/Spandrel elements were assumed to present nonlinearity only as shears elements. This means that the flexural behavior remains elastic during the analysis. The out-of-plane behavior was assumed elastic for both sections and three integrations point along the thickness were considered. The static nonlinear analysis was performed under displacement control conditions using the Acceleration pattern load at the horizontal degrees of freedom. Geometric nonlinearity parameters were not considered in this study.

A.4 Macromodel Validation at Individual Pier Response

In order to verify the reliability of the proposed model at the individual pier response level, one wall previously tested by Manzouri et al. (1996) was modeled with RUAUMOKO software. A pushover analysis was carried out and a summary of the experimental test, the RUAUMOKO model and comparison of the results is provided below.

Experimental pushover curve obtained by Manzouri et al. (1996) was compared to the simplified RUAUMOKO spring model. Figure A-7 shows a particular wall with one opening at the center and its equivalent idealization. The force-displacement relationship obtained from both the experiment and the analysis are plotted in Figure A-8. The composite spring model provided a reasonable bilinear approximation to the in-plane behavior and closely reproduced the strength (40 kips).

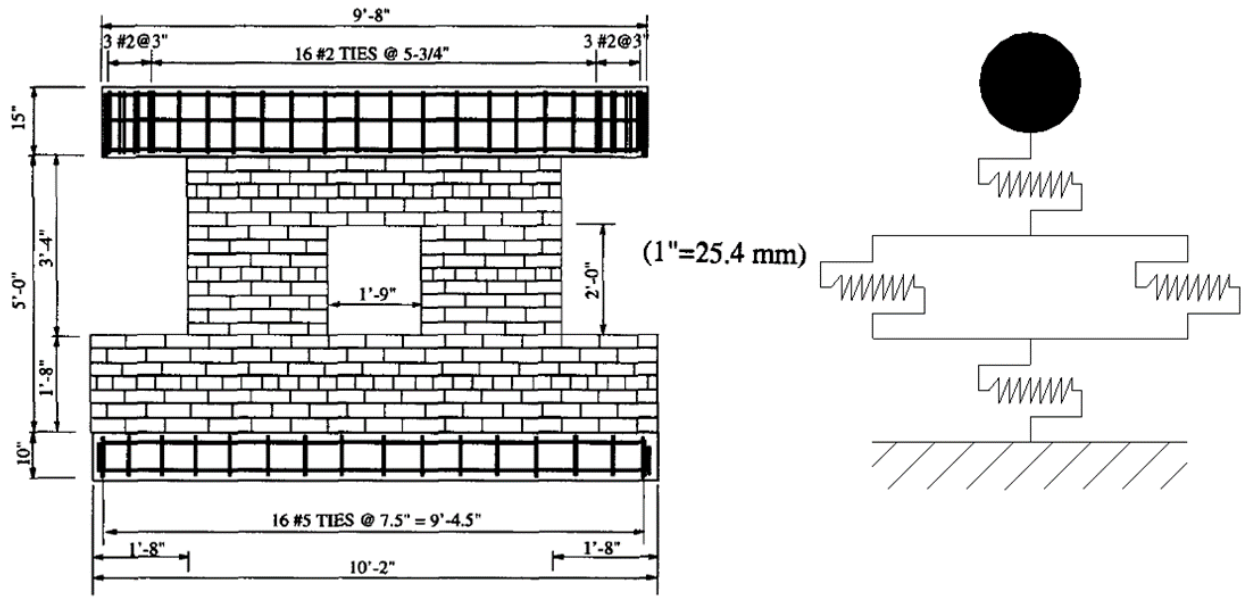

Figure A-7 Experimental wall and its equivalent RUAUMOKO model

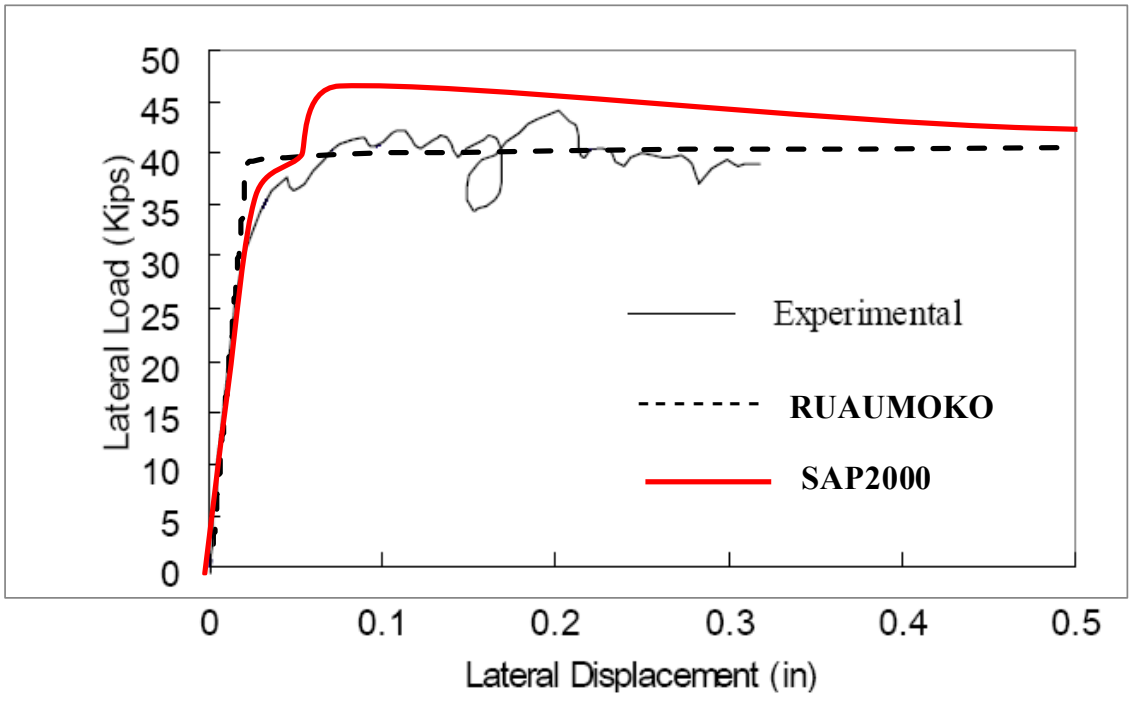

Figure A-8 SAP2000 and RUAUMOKO analytical pushover curve vs. experimental

The Manzouri experiment was used to calibrate a SAP2000 model as described in section A.4. Note that the top and bottom beams were physically modeled as elastic elements with

diaphragms constrains at the top joints. Pier and spandrels sections can be identified in Figure A-9, as well as boundary conditions, and initial axial loads applied to the wall.

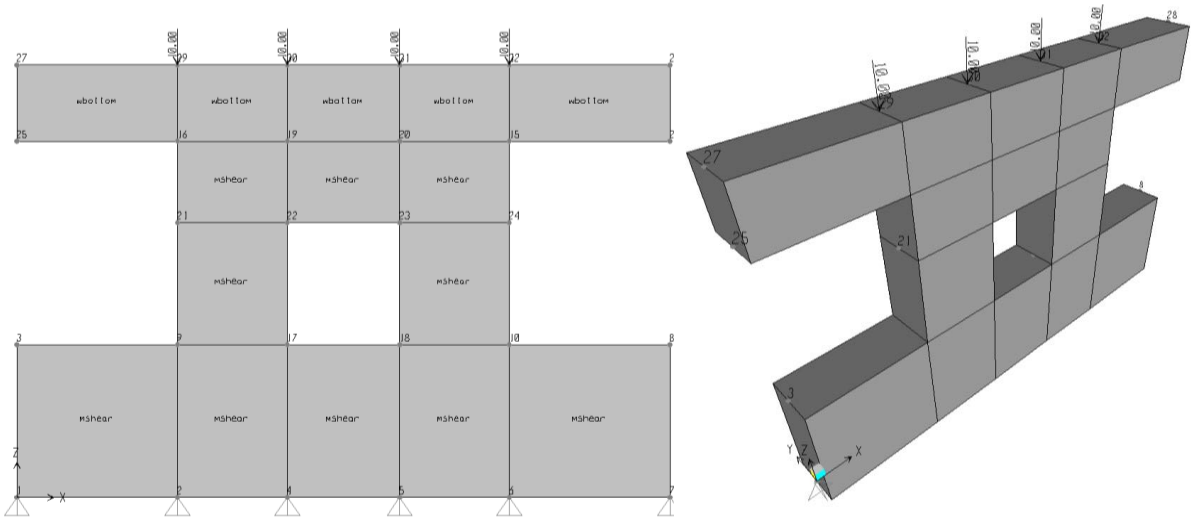

Figure A-9 SAP2000 analytical model developed

The material stress-strain curve obtained is shown in Figure A-10. Again, note that no tension was permitted for the URM material.

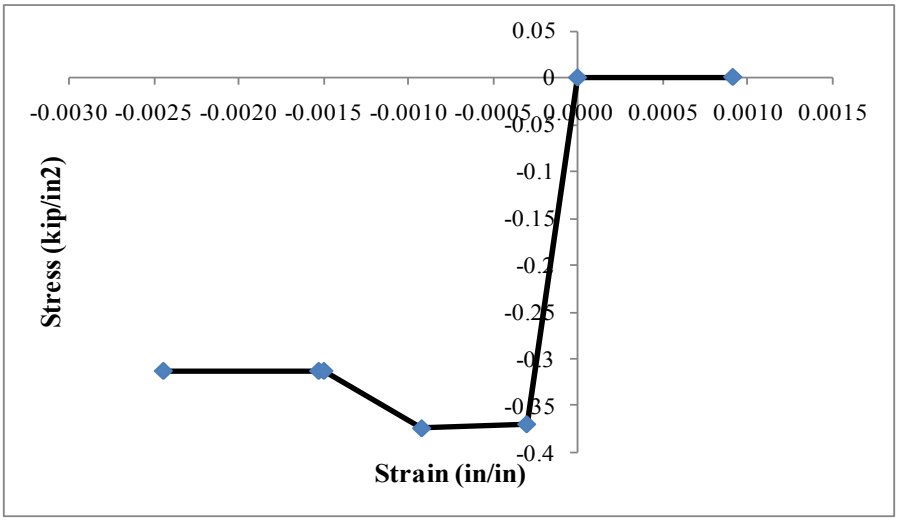

Figure A-10 Stress-strain curve for URM

As mentioned before, one section layer was defined for piers and spandrels. Table A-2 presents the Area Section Property Layers input utilized in the software. ConcP names correspond to the out-of-plane behavior which was considered elastic whereas the ConcM layer name is for In-plane behavior.

Table A-2 SAP2000 area section property layers

Section	LayerName	Thickness	Type	NumIntPts	Material	S11Opt	S22Opt	S12Opt
Text	Text	in	Text	Unitless	Text	Text	Text	Text
mshear	ConcM	13	Membrane	3	MAT	Nonlinear	Linear	Linear
mshear	ConcP	7.5	Plate	1	MAT	Linear	Linear	Linear

The Pushover Curve obtained in SAP2000 is shown in Figure A-8. Again, observe that the nonlinear shell element closely match the experimental pushover curve. Figure A-11 indicates the final stage of the structure during the analysis. Note that the main deformation occurs at the piers elements.

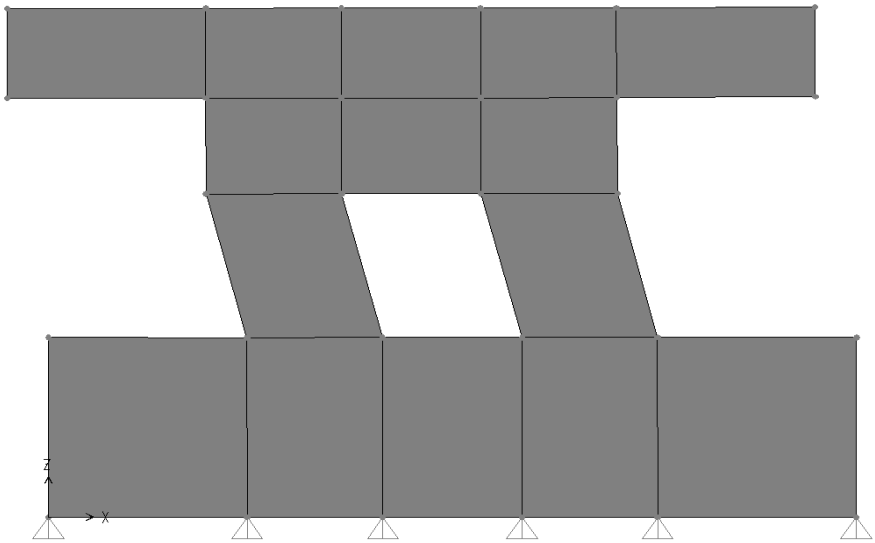

Figure A-11 SAP2000 final deformed shape of the model

A.5 Macromodel Validation: Global Response

The Mid-America Earthquake (MAE) Center conducted a research project in 2002 focused on evaluating the procedures specified in FEMA 356 on unreinforced masonry buildings. The research program included a full-scale quasi-static test of a two-story masonry building that will be used herein to further validate the proposed nonlinear macro-model at the global response level. Figure A-12 shows a 2D model and detailed dimensions of the two-story masonry building. In this study, only Wall A and B results were considered for comparison purposes.

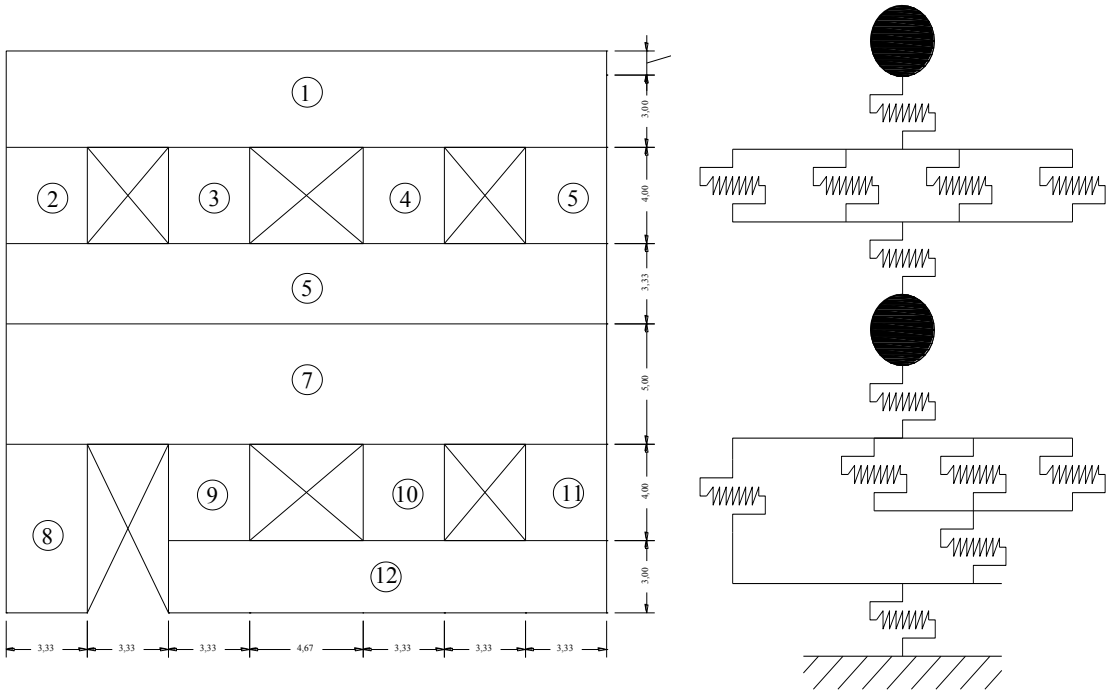

Figure A-12 2D model of MAE project (Craig et al. 2002), and spring equivalent model.

In addition, the SAP2000 nonlinear shell layers modelling technique for URM previously discussed was implemented to further validate the macro-model at the global response level. Figure A-13 and Figure A-14 show the MAE analytical model in SAP2000 and the pushover deformed shape, respectively. Observe that an additional element was introduced at the foundation level in order to capture the full shear deformation of pier No.8 (see Figure A-12).

As shown in Figure A-15, the analytical global pushover curve obtained with SAP2000 is in good agreement with the experiment, whereas the one obtained with RUAUMOKO is extremely conservative. Its prediction was approximately 20% below of the measured resistances for wall

A and B. This underestimation of the maximum wall capacity might be due to the fact that the RUAUMOKO model did not include a rotational spring at the base to capture the overturning moment effect.

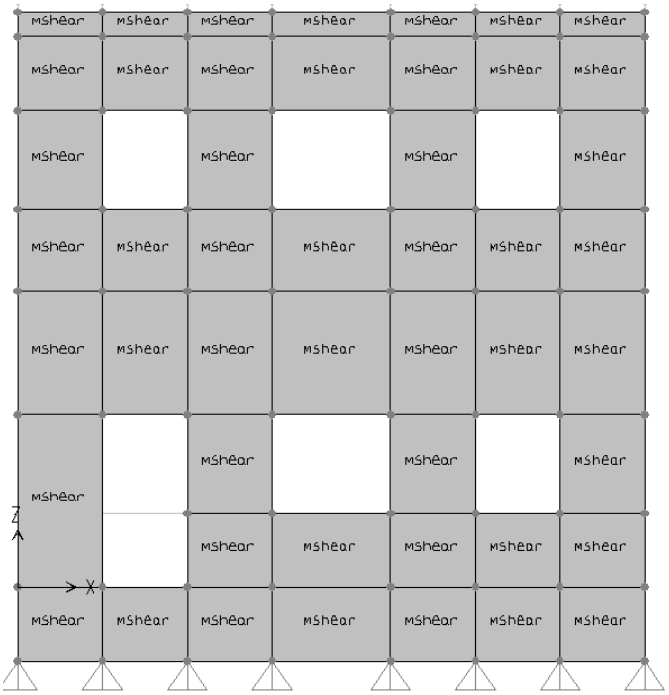

Figure A-13 SAP2000 Analytical model

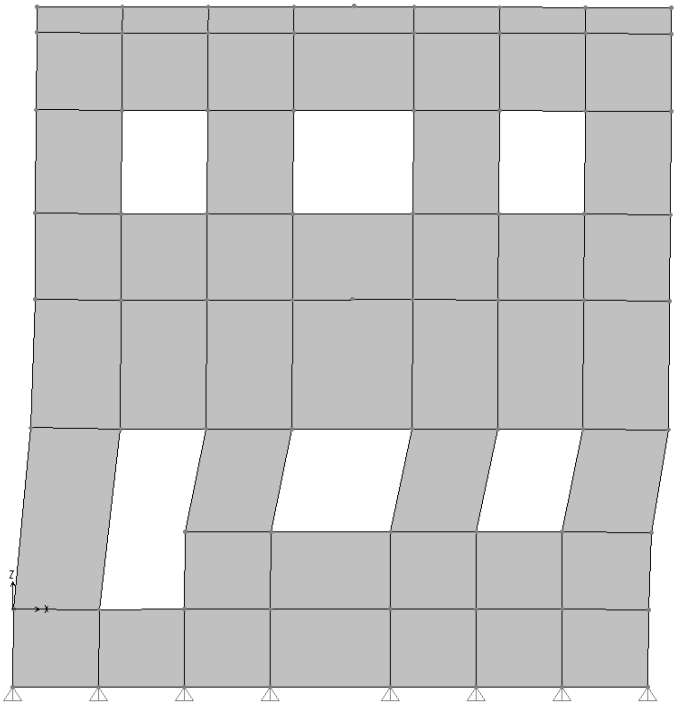

Figure A-14 SAP2000 pushover deformed shape

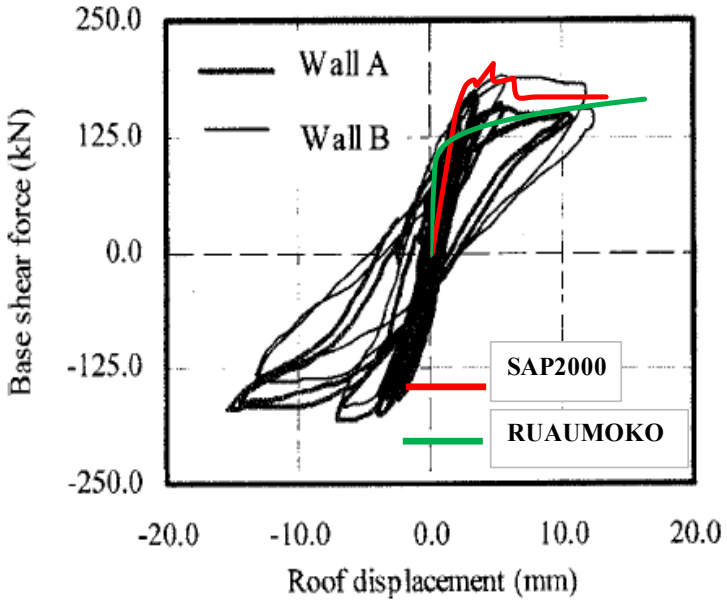

Figure A-1 Force-displacement comparison for Wall A and B (Yi et al. 2006b), RUAUMOKO and SAP2000

In general, the 2D pushover analysis produced good prediction for the maximum strengths of the test structure but the results should be considered as lower bound indicators when conducting performance based assessment since the response is highly dependent of the nonlinear parameters assumed. For example, considering the two strain-stress curves shown in Figure A-16 used to match the Manzouri Test and the MAE two story building in SAP2000. It is clear that a wide range of parameters can be considered when modelling masonry structures and extreme care should be exercised.

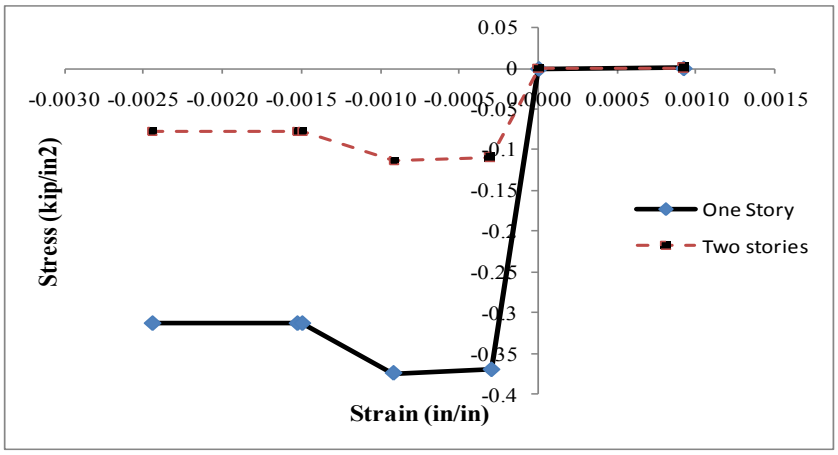

Figure A-16 Stress-strain curves used to model the Manzouri and MAE tests

Appendix B Development of Collapse Fragility Functions for In-plane Walls

B.1 In-Plane Collapse Fragility Functions

The Next Generation of Performance Based Design (NGPBD) requires a large number of response simulation to both, compute median values of demand parameters (inter-story drift, floor accelerations, etc) and to develop building-specific collapse fragility functions (FEMA P58-1 2012). Hence, it is important to have an analytical model that is easily applicable for both purposes. This section will demonstrate two applications of the model proposed in Appendix A, in the context of NGPBD. First, a nonlinear static analysis is carried out to estimate drift-threshold and damage states. The RUAUMOKO pushover curve is compared with the calibrated SAP2000 model. Secondly, an Incremental Dynamic Analysis (IDA) (Vamvatsikos and Cornell 2002) is performed in order to obtain in-plane collapse fragilities curves that will be used to estimate the probable performance of a building subjected to a ground motion intensity parameter.

B.1.1 Pushover Analysis and damages states

A pushover analysis was performed using the proposed RUAUMOKO model in order to estimate drift-threshold and damage states. As discussed in section A2, a uniform loading pattern was applied slowly with a ramp function. Figure B-1 shows both the RUAUMOKO and the SAP2000 analytical model being utilized. Good agreement was achieved between both models, as demonstrated in Figure B-2. Two damages states can be identified in the pushover curve obtained in SAP2000. The first damage state is defined where the wall displacement exceeds the elastic limit and the first crack appear in the system. This effect can be observed by the change in the slope of the elastic stiffness and correspond to a 0.1% drift value (4.3 mm). The second damage state occurs when the strength of the structure suddenly decreased. This behavior is observed at a 0.4% drift value. Note that similar values are recommended in the experimental work done by Moon et al.(2006). These damages states will be used to derive fragility functions in the next section.

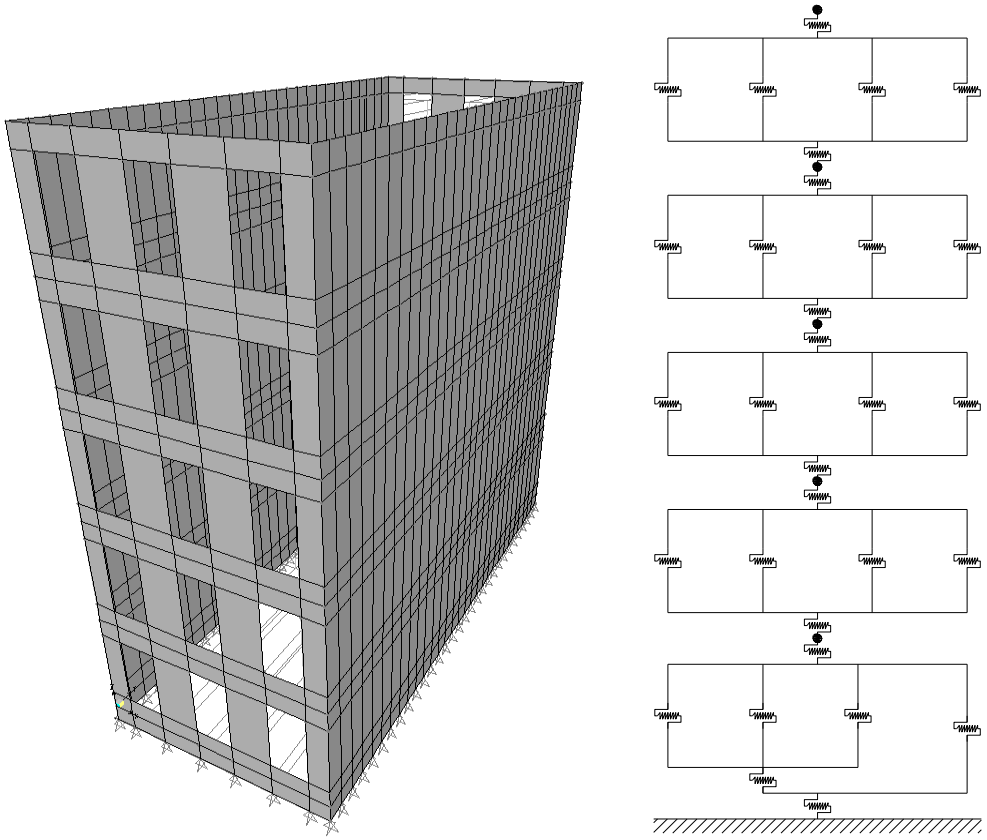

Figure B-1 SAP2000 and RUAUMOKO models of NYC masonry buildings

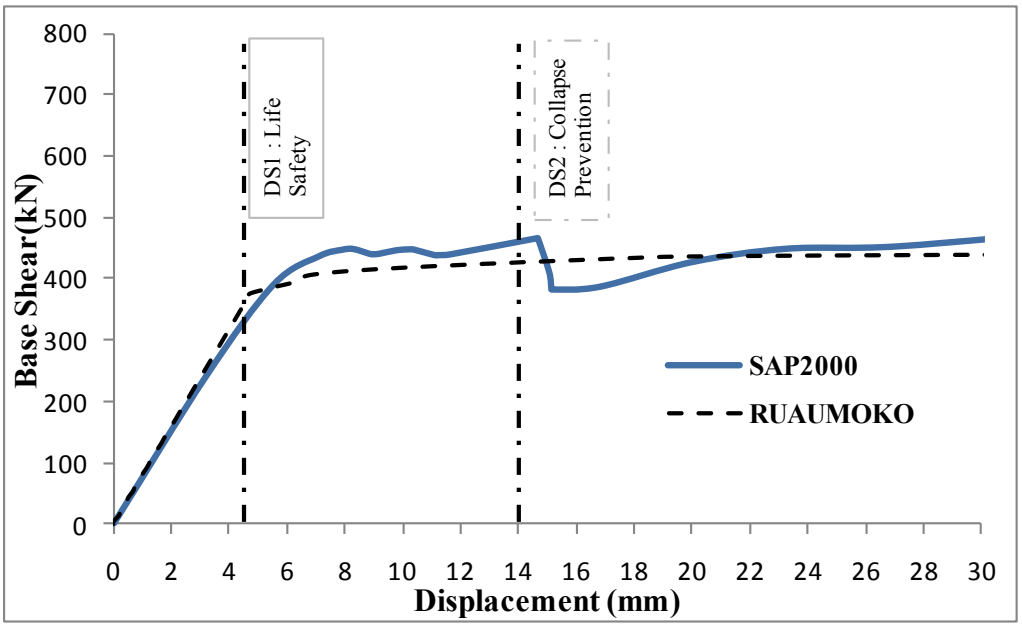

Figure B-2 SAP2000 and RUAUMOKO pushover curves and identified damage states

B.1.2 In-Plane Collapse Fragility Functions

Collapse fragility curves define the probability of collapse given a specific ground motion intensity parameter. In this research, the intensity parameter selected was the spectral acceleration at the fundamental period of the building.

The procedure for collapse assessment involves the following steps: (1) Define the collapse criteria (2) Define the best estimate model for collapse analysis (3) Characterization of the ground motion (4) Develop collapse fragility curves.

For the first step, although there are several recognized collapse modes of URM buildings (Bruneau 1994a; D'Ayala and Speranza 2003) only in-plane collapse was considered in this numerical study. This limit state occurs when a loss of lateral stiffness produce excessive buildings drifts. A drift threshold equal to 0.6% was used as recommended by Moon et al. (2006). Note that this mode of failure might not be the main source of probable damage on New York City buildings. The second step was already discussed in Section 3 and the remaining will be described in the following sections. Note that the collapse fragility functions were developed for three different hysteresis rules, as mentioned before.

Ground Motion Set

Since strong ground motion records for the Central and Eastern United States (CEUS) area are scarce, synthetic ground motions were used in this study. A minimum set of 11 ground motion pairs with 2% of probability of exceedance in 50 years were chosen from a strong ground motion database simulated by Wanitkorkul and Filiatrault (2005) specifically for New York City. Although the records were already scaled to match the USGS-Uniform Hazard Spectrum (UHS) at 1 sec, they were rescaled to match the spectral acceleration at the fundamental period of the building (0.27 seconds for the building considered).

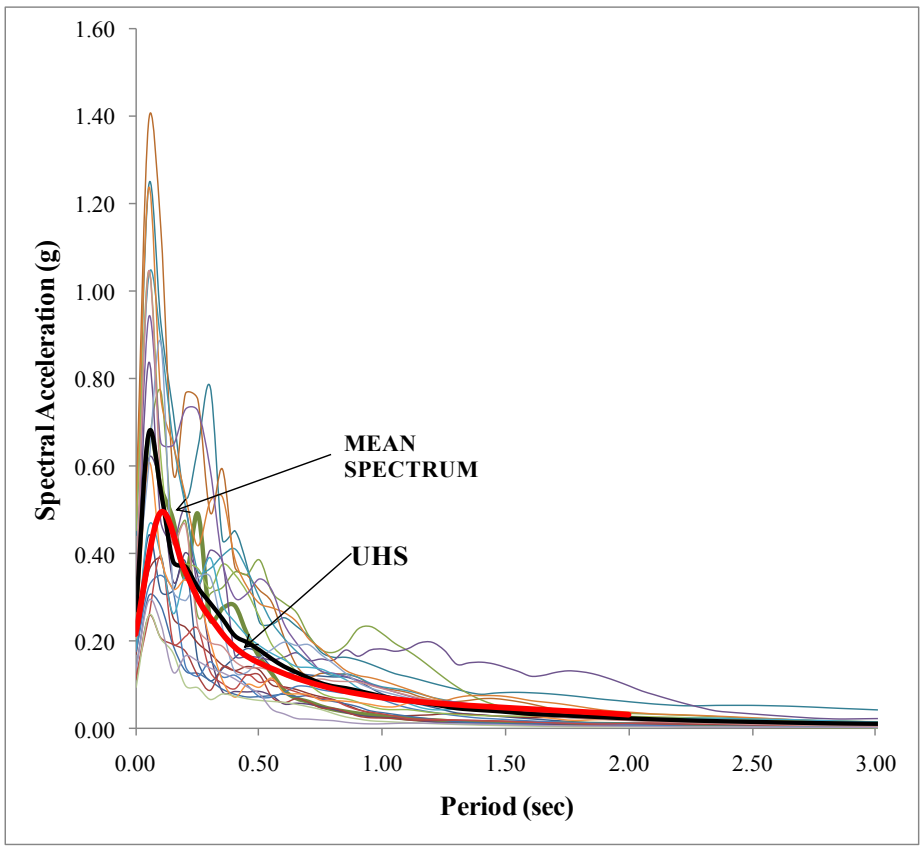

Figure B-3 Scaled ground motions and Uniform Hazard Spectrum

Table B-1 presents the scenario for each ground motions selected. Selecting the ground motions can be done following published guidelines (FEMA P58-1 2012). However, herein the selection of the ground motions was based in the USGS Deaggregation map shown in Figure B-4 for the site of interest.

Table B-1 Scenario list for 11 pairs of ground motions selected.

2% PE in 50 yrs @ 1.0 sec		
Scenario	R(km)	Mw
1	36.3	6.2
2	13.2	5.4
3	15.6	6.2
4	33.7	5.8
5	36.2	6.8
6	15.5	6.0

7	35.9	6.0
8	13.9	5.8
9	36.2	6.4
10	13.6	5.6
11	33.6	5.6

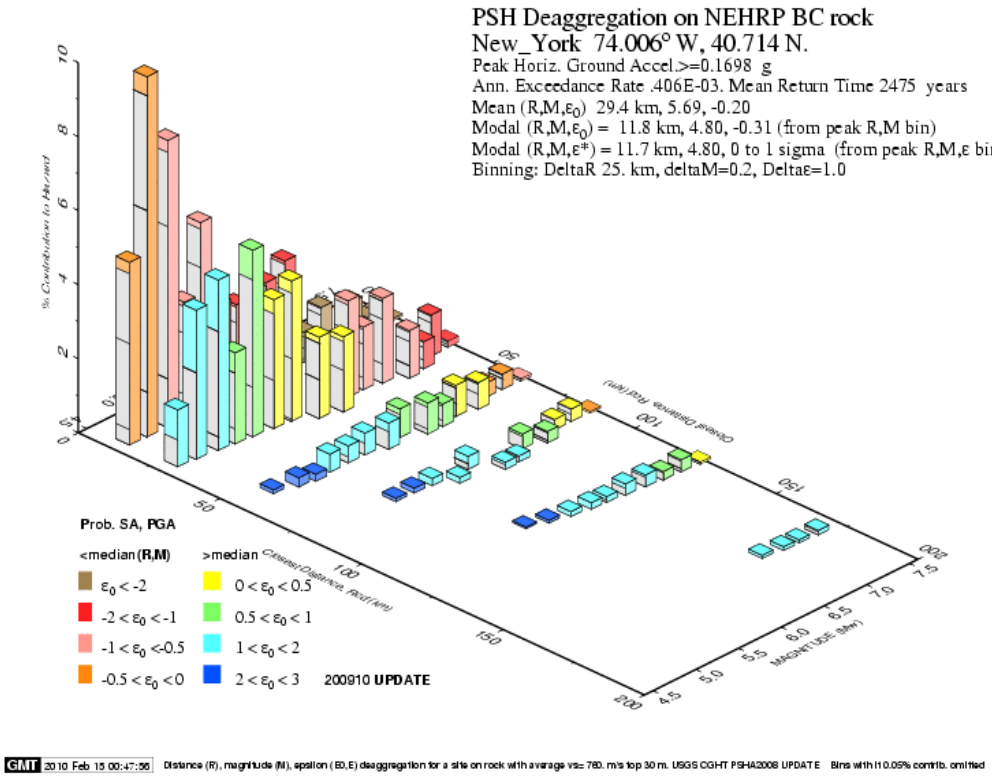

Figure B-4 USGS-Deaggregation map New York City (USGS)

Developing Collapse Fragility Functions

Collapse fragility curves were developed from the results of IDA using 11 pairs of synthetic ground motions previously described. A combination of modified MATLAB codes developed by Davis (2010) and Christovasilis and Sideris (2007) was used to perform automatic IDA in RUAUMOKO and to generate the associated fragility functions. Figure B-5 shows a plot of the maximum inter-story drift obtained versus spectral acceleration at the effective first mode period

of the building for each synthetic ground motion considered. Intensity of each ground motion was increased from 0.1g up to 2.0g in increments of 0.1g. It is worth to point out that 880 simulations were completed in about 20 minutes. As expected, the nonlinear spring macro-model is highly computationally efficient.

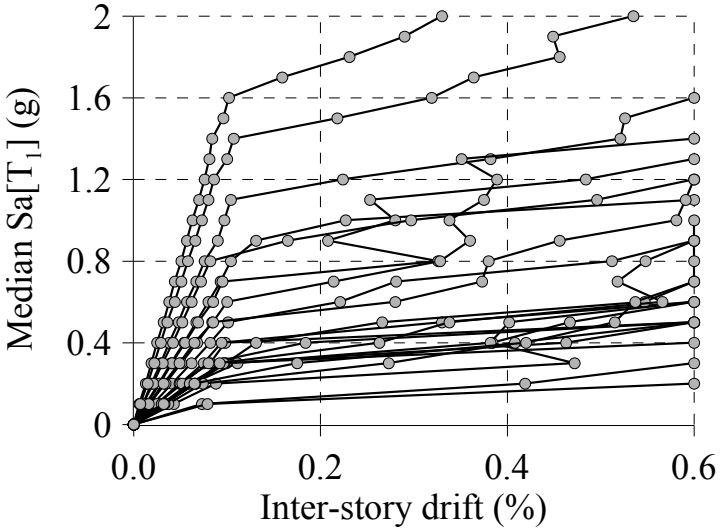

Figure B-5 Incremental dynamic analysis curves

Note that the only uncertainty parameter considered was the seismic record. The inherent variability of the mechanical properties of the analyzed masonry wall was not considered since it has been demonstrated by previous researchers that the uncertainty of the seismic record is more important than the scatter in the mechanical properties (Rota et al. 2010). Nonetheless, further studies are warranted to investigate this matter.

Adjusting the IDA curves to take into account non-simulated failures modes and components is possible but is beyond the scope of this study. The same applies to the collapse fragility curve shown in Figure B-6 which can be modified to include all sources of randomness and uncertainty (FEMA P58-1 2012).

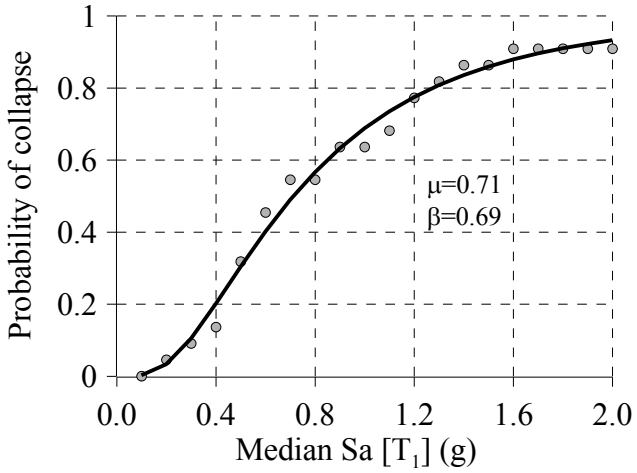

Figure B-6 Fragility curve for probability of collapse

Fragility curves were obtained by fitting the probability of the building exceeding the aforementioned limit state on each response simulation to a lognormal distribution. The fitting process was completed using the *logncdf* and the *lsqnonlin* MATLAB functions.

From the generated fragility functions, the probability of collapse for this particular type of building is about 10% which can have a significant economic impact considering that about 80% of total building stock in NYC has a similar profile. In fact, this percentage could be higher if others uncertainties are taken into account.

Probability of occurrence of others significant damages states can be derived from IDA. Figure B-7 shows fragility curves for three different discrete damages states associated to Life Safety, Immediate Occupancy and Collapse Prevention on URM buildings. Those damage states are recommended by Moon et al (2006) and verified in this study in section B.1.1.

.

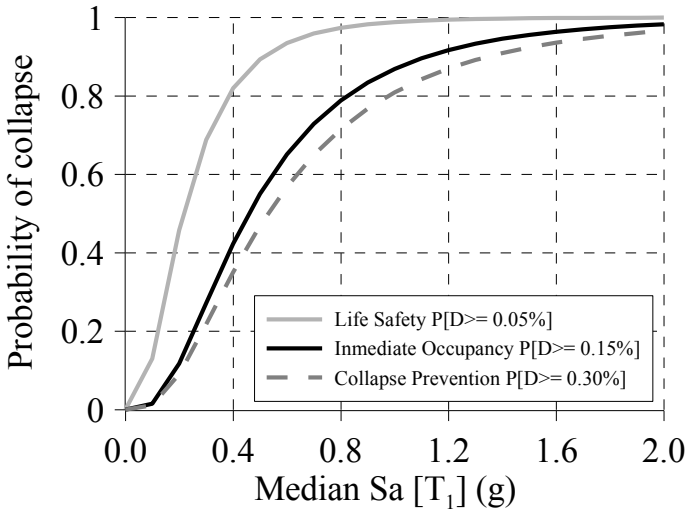

Figure B-7 Fragility Curves for three performance levels

Appendix C Modeling Two-way Bending of URM Walls in LS-DYNA and SAP2000

C.1 Modeling two-way bending in LS-DYNA and SAP2000

As of today, most research on out-of-plane numerical modeling and experimental behavior of URM walls has been conducted ignoring the effects of corners and realistic two-way bending behavior. Current ASCE 41-06 guidelines to estimate the dynamic stability of URM walls are based on the ABK program, which only tested one-way bending panels. It was observed in Section 2 of this report that URM walls rarely collapse in one-way bending. Thus, developing a new framework to test URM panel in two-way bending or incorporating the appropriate boundary conditions to account for this effect is highly desirable.

In this appendix, a finite element model of URM walls subjected to two-way bending is developed and validated. The experimental work conducted by Griffith et al. (2007) was used as a reference. The final goal of this exercise is to use this refined FE model to develop simplified macro-models that can be easily incorporated in SAP2000.

The strategy approach used in LS-DYNA is first described, and then comparison of the numerical models and previous experiments is presented.

C.1.1 Modeling Strategy in LS-DYNA

Figure C-1 presents the geometry of the walls was taken from Vaculik et al (2007).

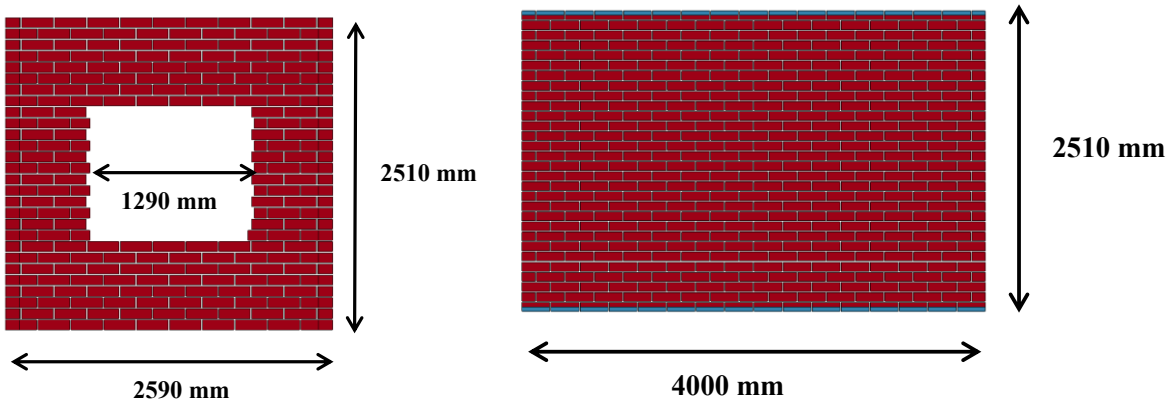

Figure C-1 Geometry of the walls considered in this study

Boundary conditions were provided at the top, bottom and sides of each wall. A full set of X, Y, and Z translational constraint were used at the bottom, while only Y was constrained at the top. A fix boundary was used on the sides of the wall.

Brick units were modeled using Solid elastic (MAT_ELASTIC) element with fully integrated S/R solid intended for elements with poor aspect ratio. Mass density, Young Modulus and Poisson ratio were estimated as 1.600e-010 Tonne/mm3, 3540 Mpa, 0.25 respectively.

Airbag loading was simulating using an increasing monotonic curve to applied uniform load over the brick elements.

Hourglass control was considered using Belytschko-Bindeman formulation, which assume strain co-rotational stiffness form for 2D and 3D solid elements only. This form is available for explicit and IMPLICIT solution methods.

LS-DYNA explicit solver with dynamic relaxation and artificial mass was considered to speed up the solution.

TIEBREAK contact connection was used to model the mortar. This approach is penalty based and allows for modeling the interface of two materials which transmits both compressive and tensile forces (Bala 2007). CONTACT_AUTOMATIC_SURFACE_TO_SURFACE_ TIEBREAK contact model is recommended to use in this formulation. OPTION 6, which allows damage by scaling the stress components after failure is met, was considered in this study. Damage will start when the stress reaches the failure criteria specified in Figure C-2. After damage is initiated, the stress decresases linearly until the crack depth reaches the crack width opening.

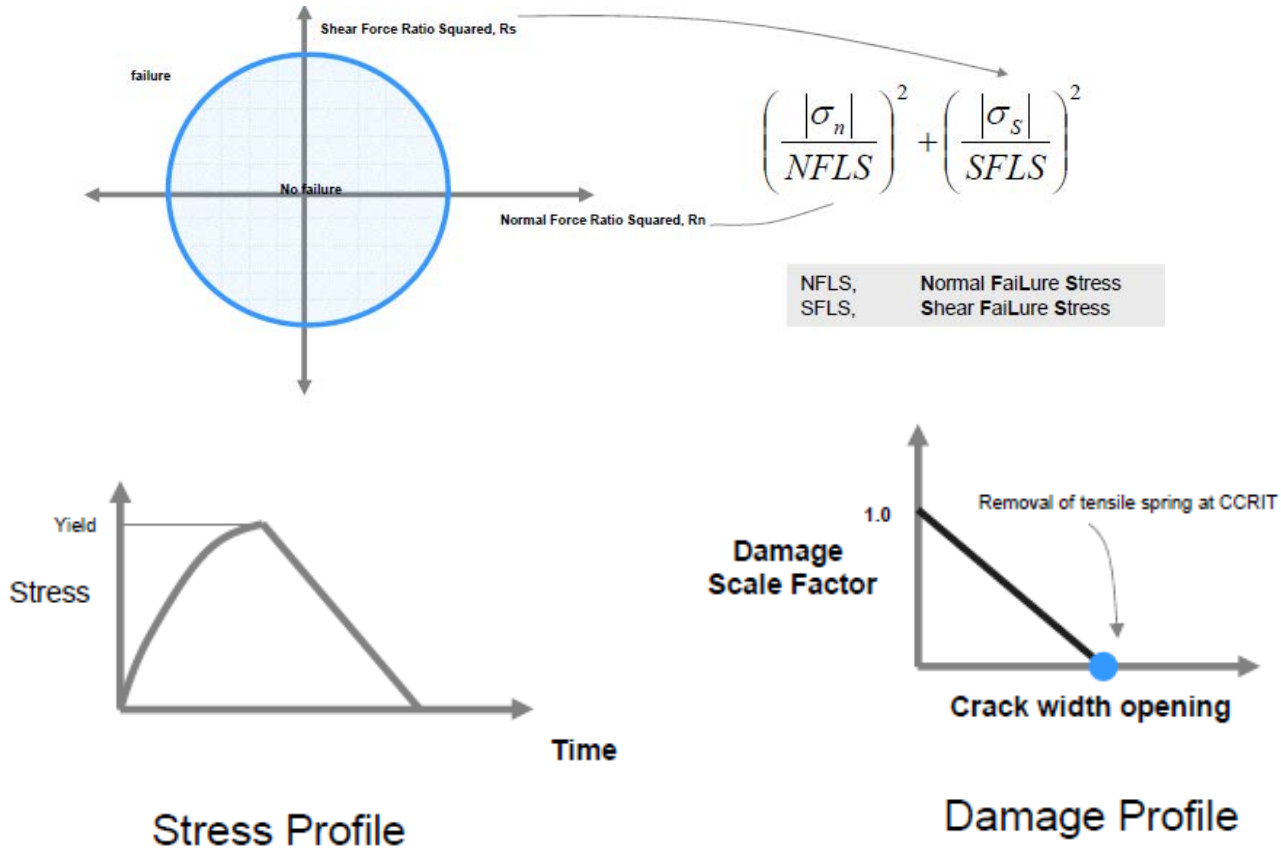

Figure C-2 Stress based failure criteria, stress and damage profile of OPTION 6 (Bala 2007)

C.1.2. Numerical Results

Two walls were modeled in LS-DYNA, as shown in Figure C-3. However, only the results for the solid wall are presented. Note that a numerical model was also developed in SAP2000. Preliminary results showing a comparison between the monotonic LS-DYNA response of the solid panel and the cyclic behavior in SAP2000 are presented in Figure C-5.

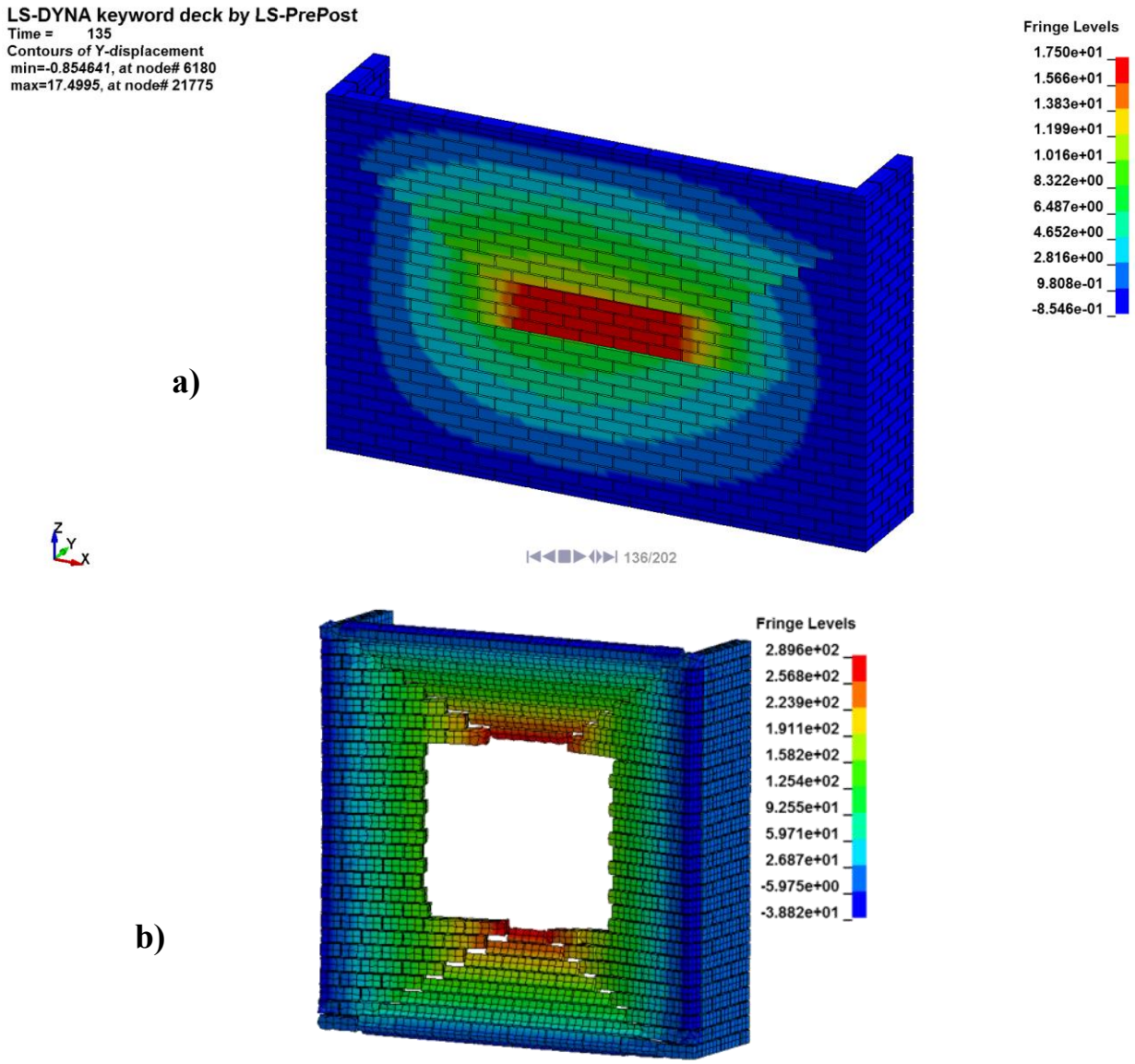

Figure C-3 Deformed shape of walls modeled in LS-DYNA: a) Solid panel; b) Hollow panel

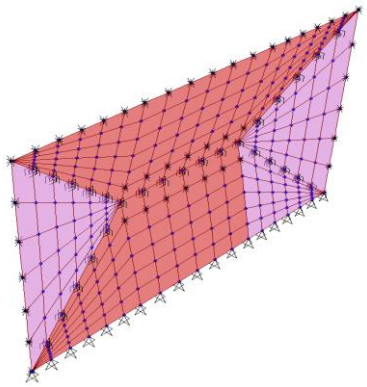

Figure C-4 Deformed shape of wall 2 in SAP2000

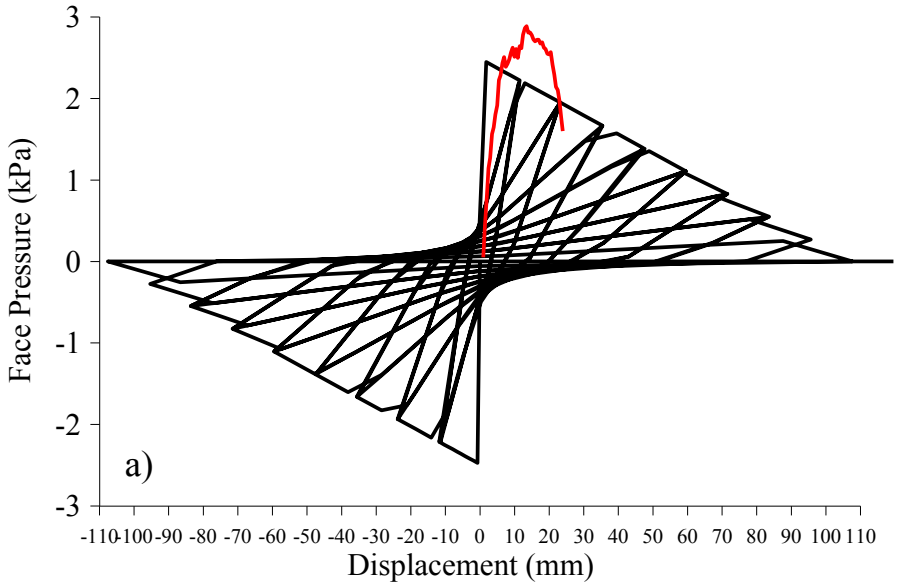

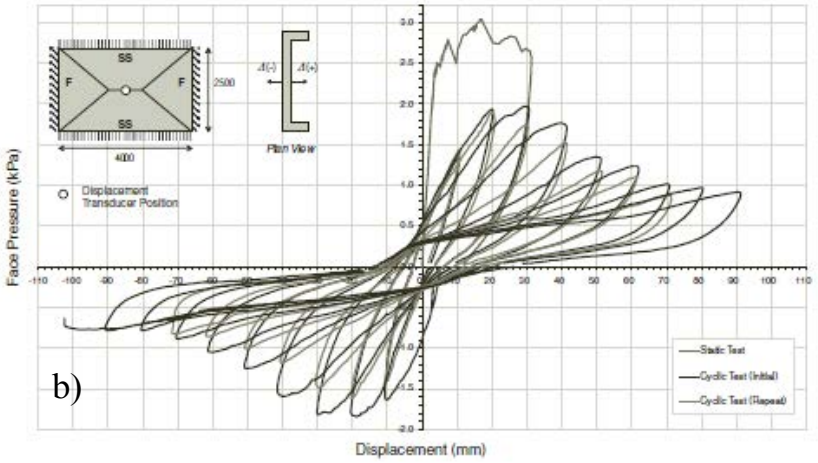

Figure C-5 Cyclic pressure-displacement relationship of Wall 2: a) Numerical response in SAP2000 (cyclic) and LS-DYNA (monotonic) and b) Experimental

Appendix D Structural Drawings of the Experimental Test Setup

CONTENT

GENERAL NOTES

STEEL:
1.All steel elements shall be GRADE

WOOD:
1. Wood elements shall be Douglas F or similar

MASONRY AND MORTAR:
1. Recycled old bricks
2.Mortar proportions: 1-2-9

PRODUCED BY AN AUTODESK EDUCATIONAL PRODUCT

PRODUCED BY AN AUTODESK EDUCATIONAL PRODUCT

CONTENT AND GENERAL NOTES	S.2 / S.12

PRODUCED BY AN AUTODESK EDUCATIONAL PRODUCT

MCEER Thrust Area 2
Sustainable and Resilient Buildings
Seismic Vulnerability of NYC Masonry Buildings

CONSTRUCTION DRAWINGS

UB Research Team

Faculty:
Andrew Whittaker,
Gilberto Mosqueda,

Graduate Student:
Juan Aleman

SEESL Technicial Staff:
Mark Pitman
Duane Kozlowski

External Collaborators

SEAoNY:
Chris Cerino
Michael Squarzini

DoB:
Dan Eschenasy

IMI:
Keith Lashway
David Sovinsky

PRODUCED BY AN AUTODESK EDUCATIONAL PRODUCT

PRODUCED BY AN AUTODESK EDUCATIONAL PRODUCT

PRODUCED BY AN AUTODESK EDUCATIONAL PRODUCT

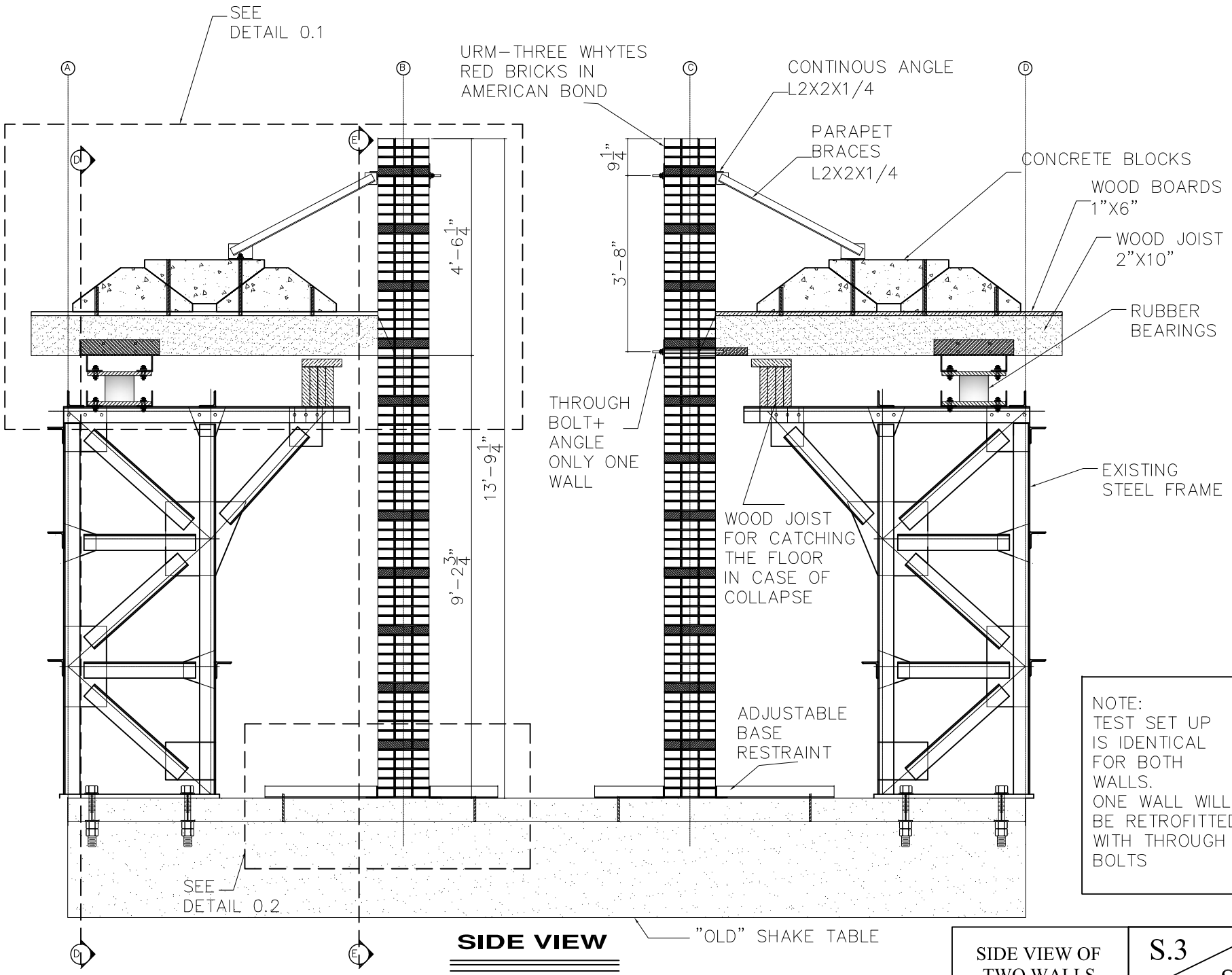

SIDE VIEW

SIDE VIEW OF TWO WALLS	S.3 / S.12

PRODUCED BY AN AUTODESK EDUCATIONAL PRODUCT

PRODUCED BY AN AUTODESK EDUCATIONAL PRODUCT

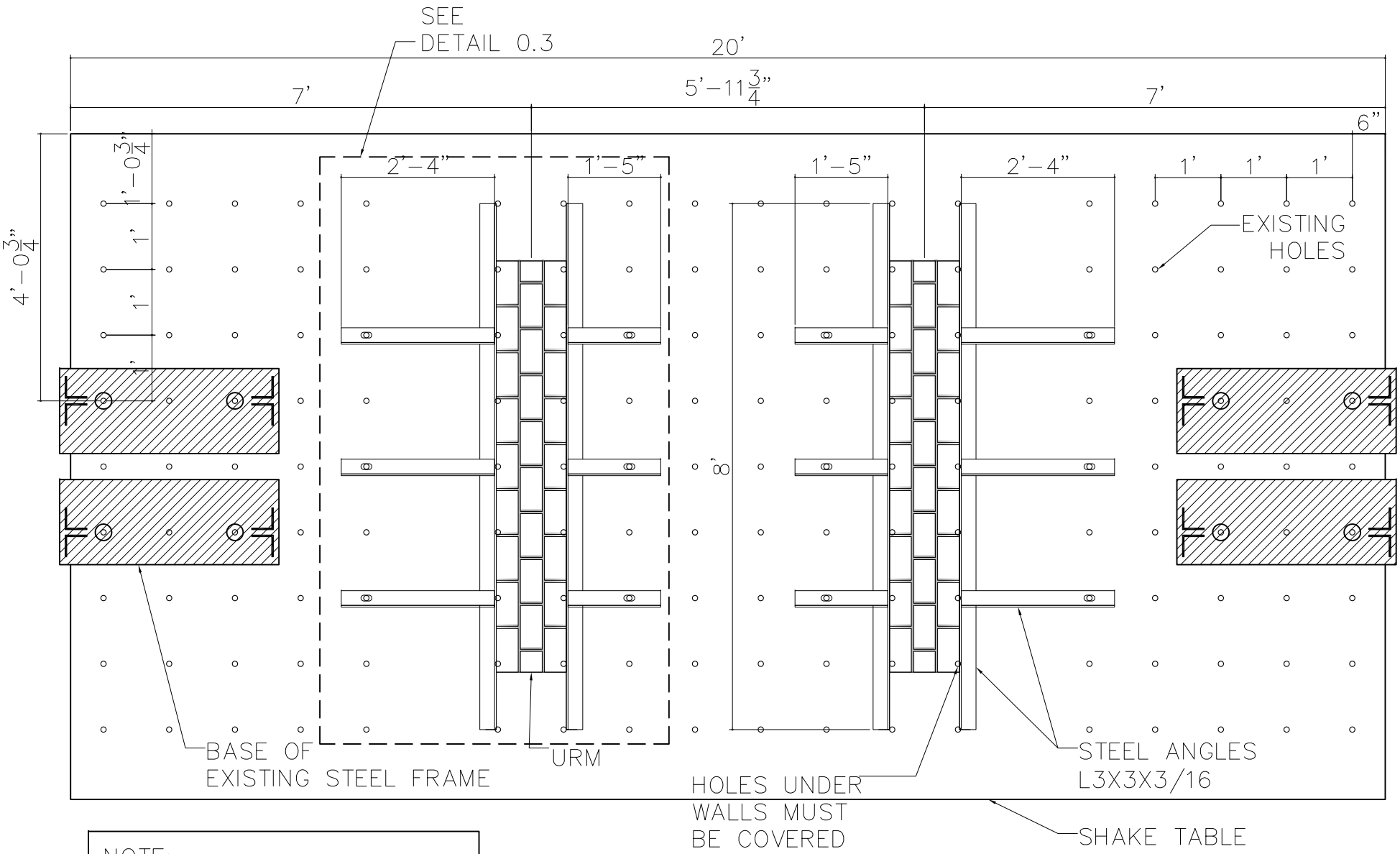

NOTE:
PROTECT THE SHAKE TABLE
AREA FROM MORTAR WASTE

PLAN VIEW

PLAN VIEW	S.4 / S.12

PRODUCED BY AN AUTODESK EDUCATIONAL PRODUCT

PRODUCED BY AN AUTODESK EDUCATIONAL PRODUCT

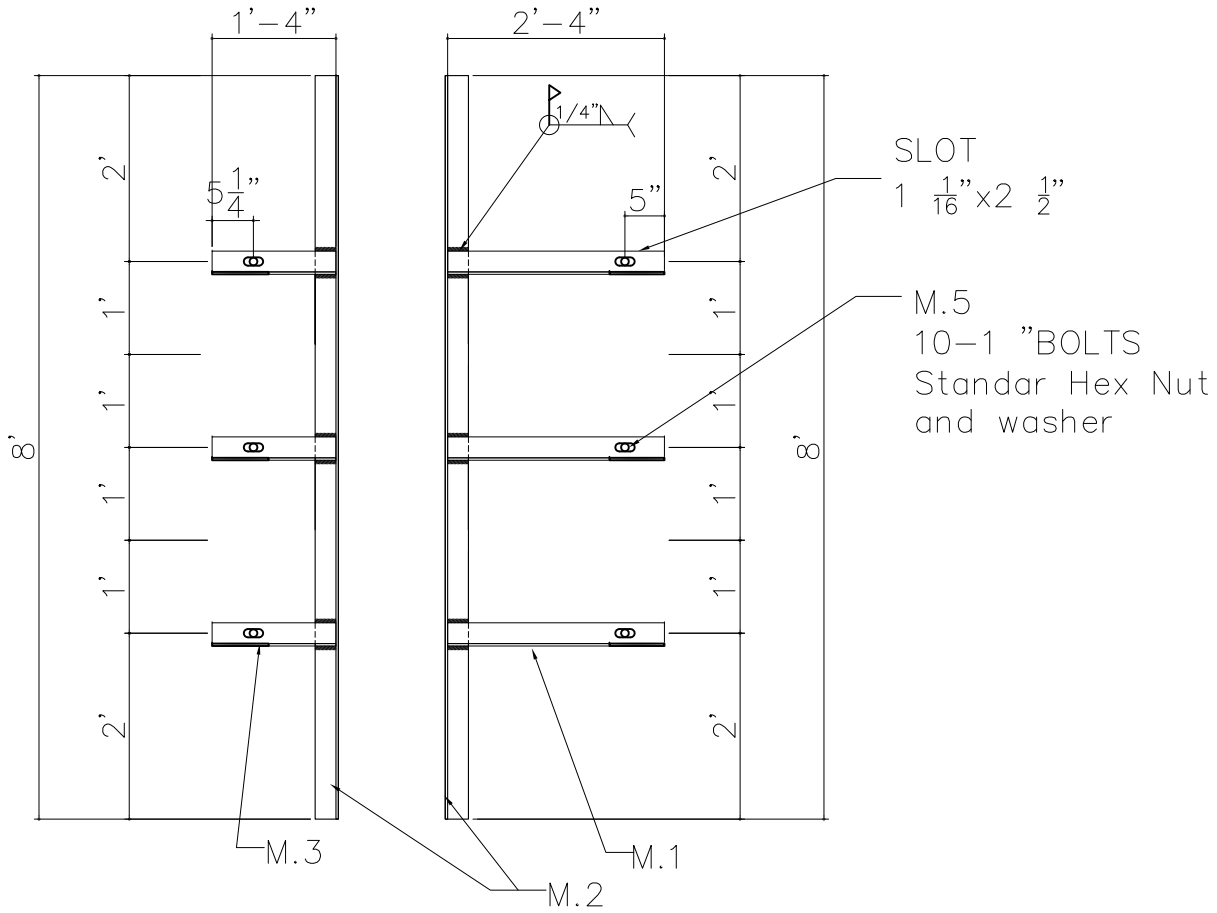

DETAIL 0.3

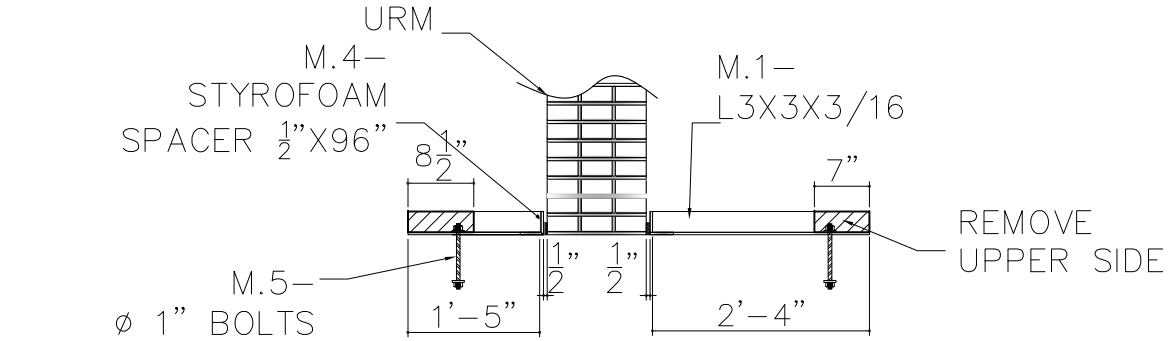

DETAIL 0.2

BILL OF MATERIAL FOR TWO (2) BASES					
ID	QTY	MATERIAL	LENGTH	WEIGHT	REMARKS
M.1	6	L3X3X3/16	28"		
M.2	4	L3X3X3/16	96"		
M.3	6	L3X3X3/16	16"		
M.4	4	STYROFOAM	96"		
M.5	12	1" BOLTS			

ADJUSTABLE STEEL BASE DETAILS	S.5 / S.12

PRODUCED BY AN AUTODESK EDUCATIONAL PRODUCT

PRODUCED BY AN AUTODESK EDUCATIONAL PRODUCT

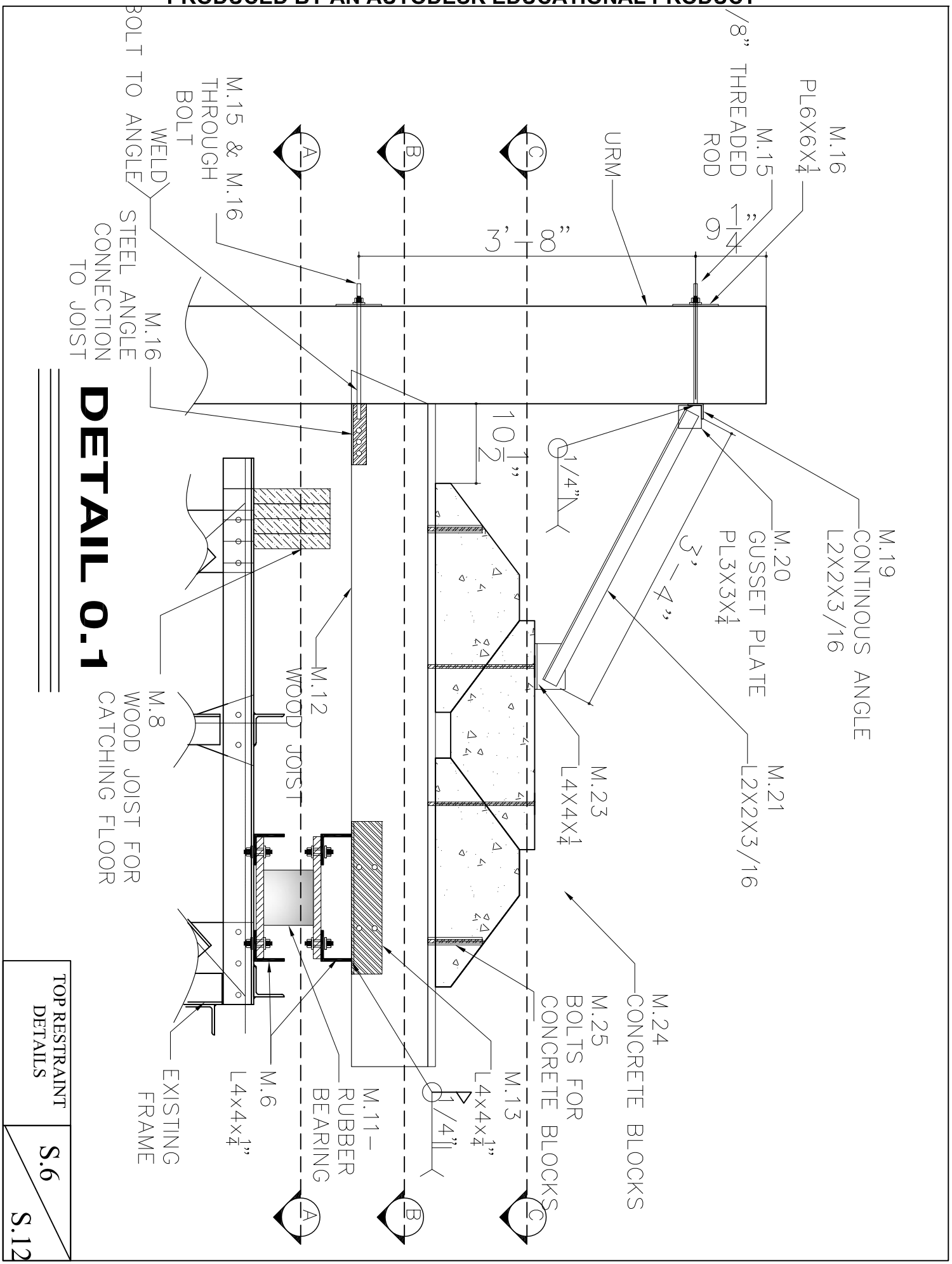

DETAIL 0.1

TOP RESTRAINT DETAILS

S.6

S.12

PRODUCED BY AN AUTODESK EDUCATIONAL PRODUCT

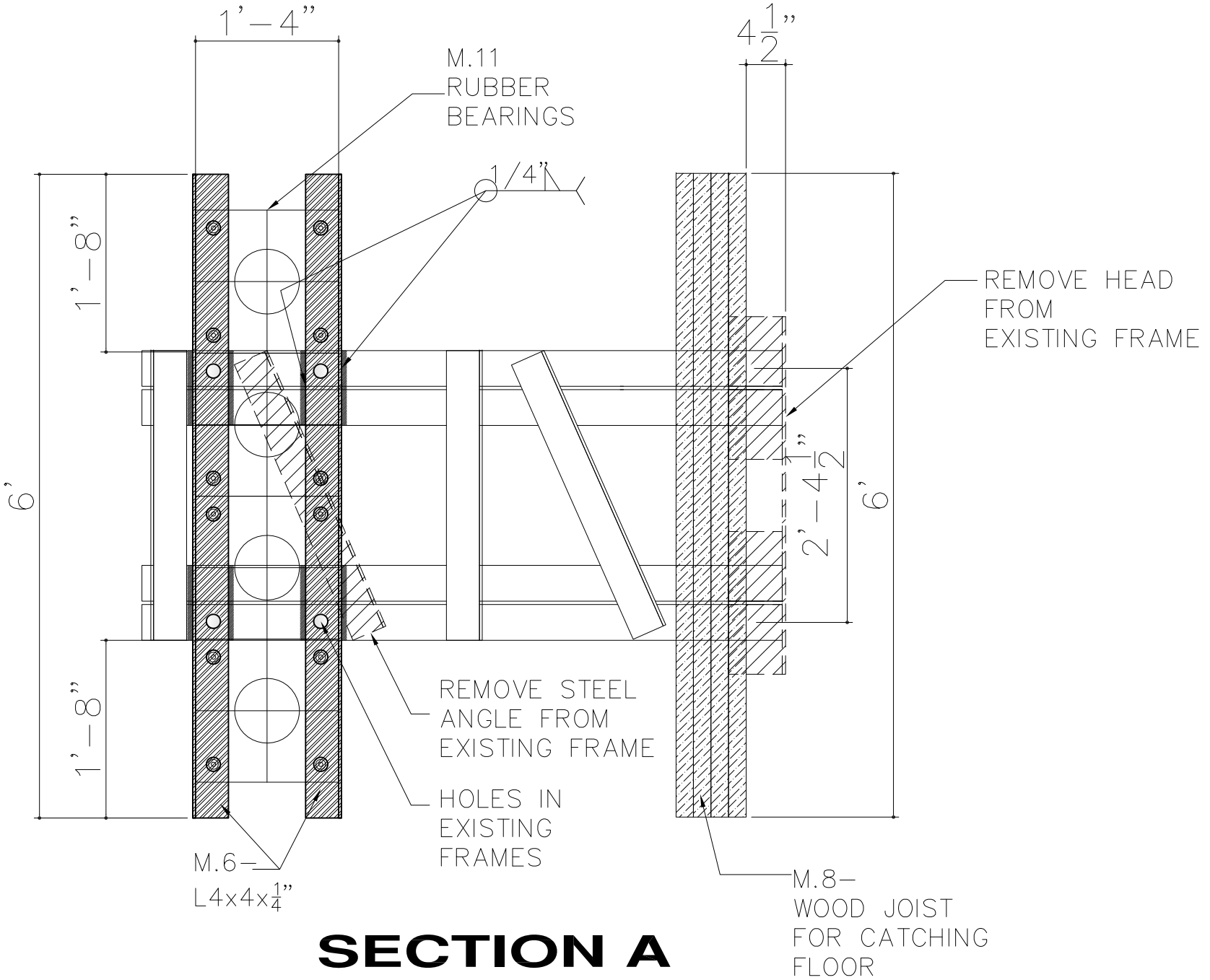

SECTION A

TOP RESTRAINT DETAILS	S.7 / S.12

PRODUCED BY AN AUTODESK EDUCATIONAL PRODUCT

SECTION B

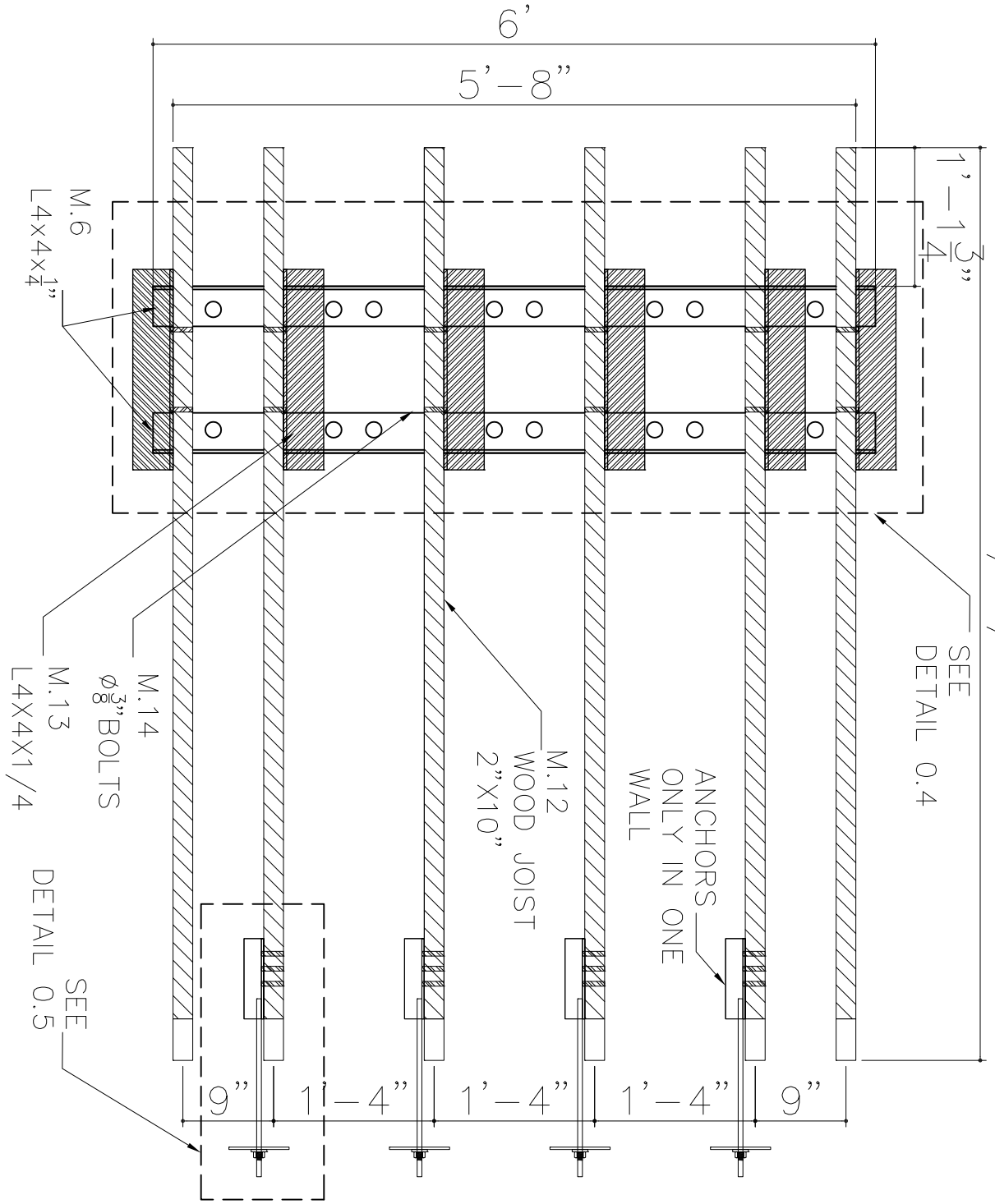

TOP RESTRAINT DETAILS

S.8

S.12

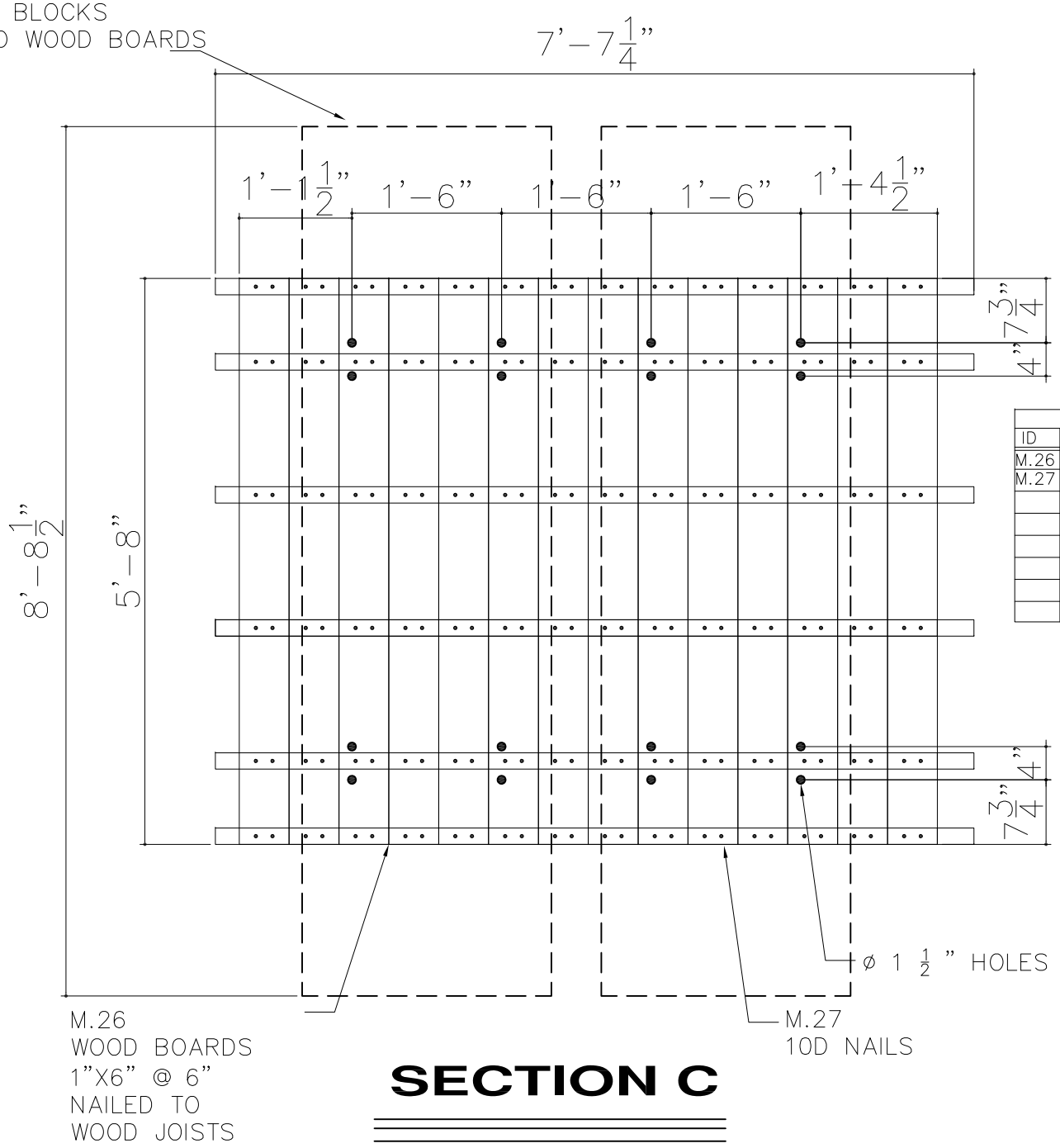

BILL OF MATERIAL FOR TWO(2) FRAMES					
ID	QTY	MATERIAL	LENGTH	WEIGHT	REMARKS
M.26	28	1X6 BOARD	68"		
M.27	5 LB	10D NAILS			COMMON

SECTION C

TOP RESTRAINT DETAILS

S.9 / S.12

PRODUCED BY AN AUTODESK EDUCATIONAL PRODUCT

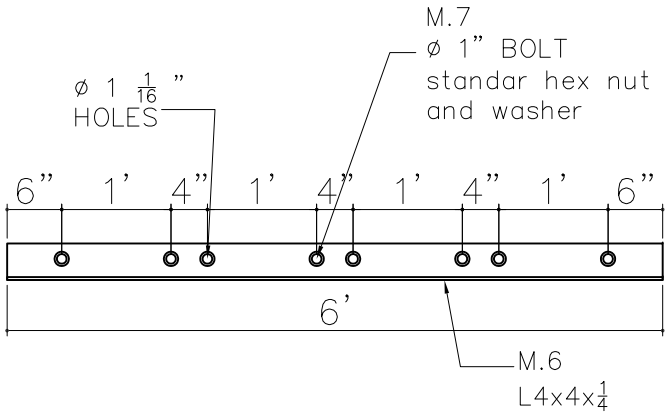

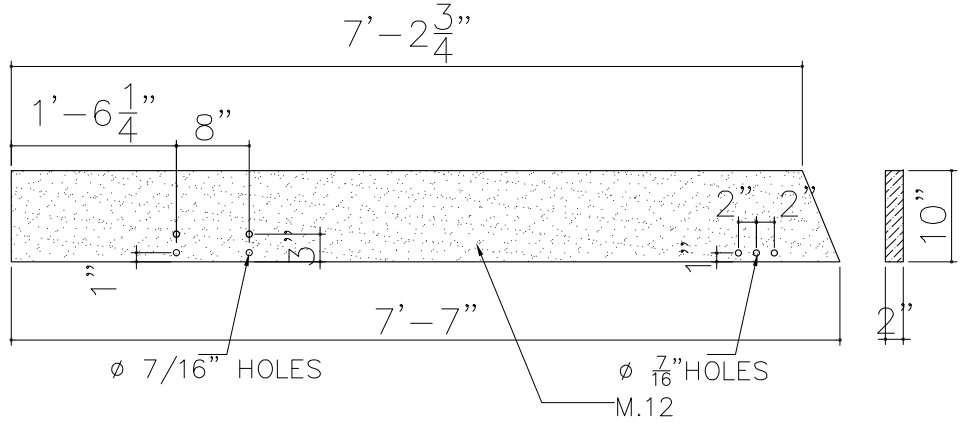

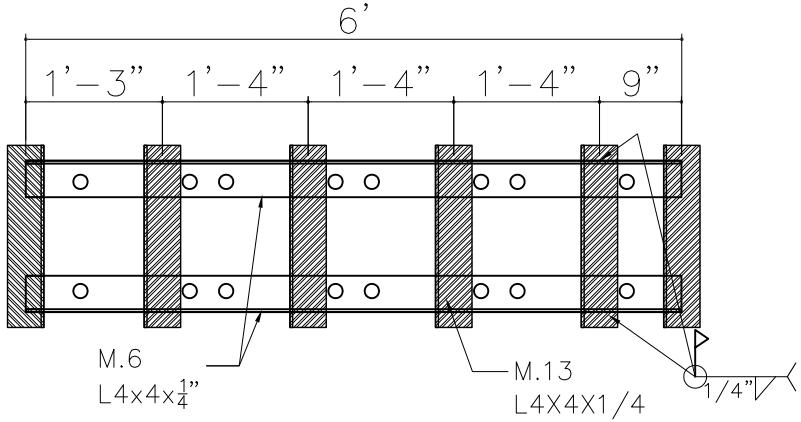

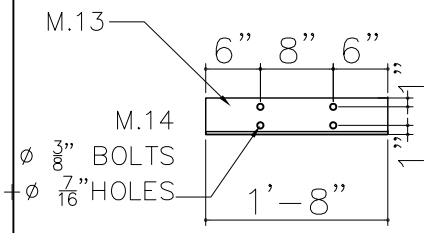

BILL OF MATERIAL FOR TWO(2) FRAMES					
ID	QTY	MATERIAL	LENGTH	WEIGHT	REMARKS
M.6	8	L4X4X1/4	72"		
M.7	64	1" BOLTS			@BEARINGS
M.11	8	BEARINGS			
M.12	12	2X10 JOIST	91"		
M.13	12	L4X4X1/4	17"		@BEARINGS
M.14	48	ø 3/8"BOLT			THREADED

DETAIL 0.4

TOP RESTRAINT DETAILS

S.10 / S.12

PRODUCED BY AN AUTODESK EDUCATIONAL PRODUCT

PRODUCED BY AN AUTODESK EDUCATIONAL PRODUCT

PRODUCED BY AN AUTODESK EDUCATIONAL PRODUCT

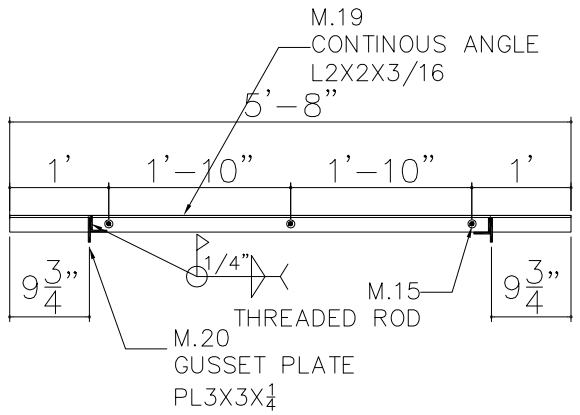

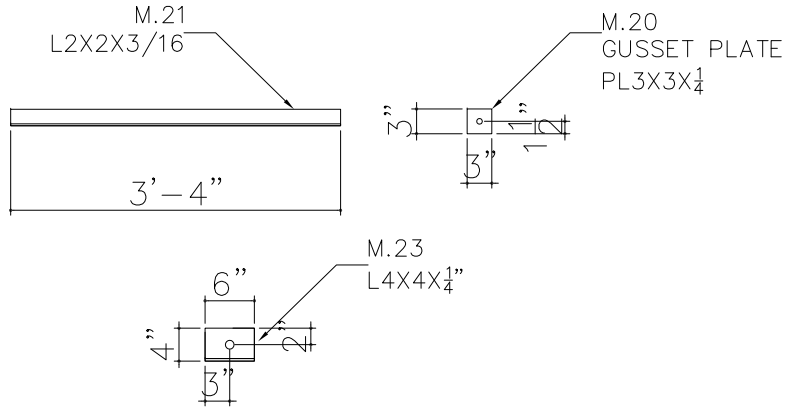

DETAIL 0.6

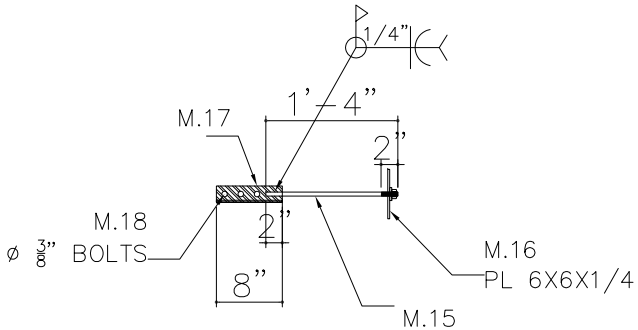

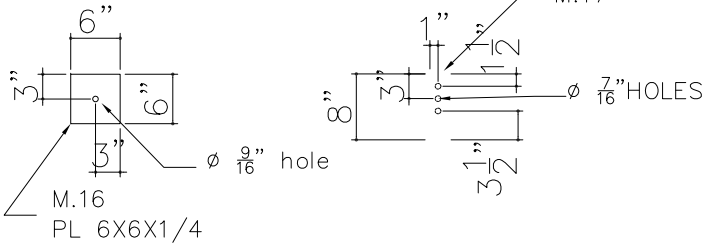

DETAIL 0.5

BILL OF MATERIAL FOR TWO(2) FRAMES					
ID	QTY	MATERIAL	LENGTH	WEIGHT	REMARKS
M.15	10	ø 5/8" ROD	16"	SIMPSON	STRONG-TIE
M.16	10	PL 6X6X1/4 "			
M.17	4	L 2X2X3/16	" 8"		
M.18	12	ø 3/8" BOLT	3"		THREADED
M.19	2	L 2X2X3/16	" 68"		
M.20	4	PL 3X3X1/4 "			
M.21	4	L 2X2X3/16	" 40"		
M.22					
M.23					
M.24	6	C.BLOCKS			
M.25		BOLTS			FOR BLOCKS

TOP RESTRAINT DETAILS

S.11 / S.12

PRODUCED BY AN AUTODESK EDUCATIONAL PRODUCT

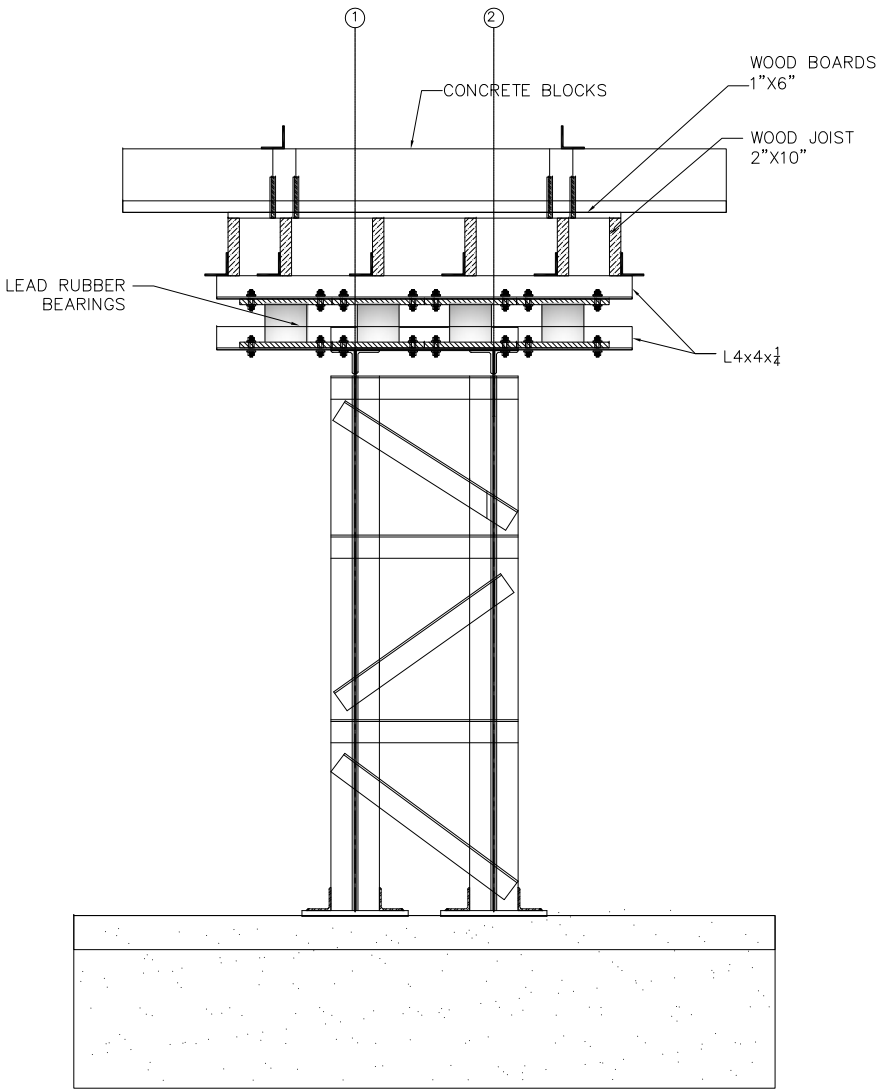

SECTION D

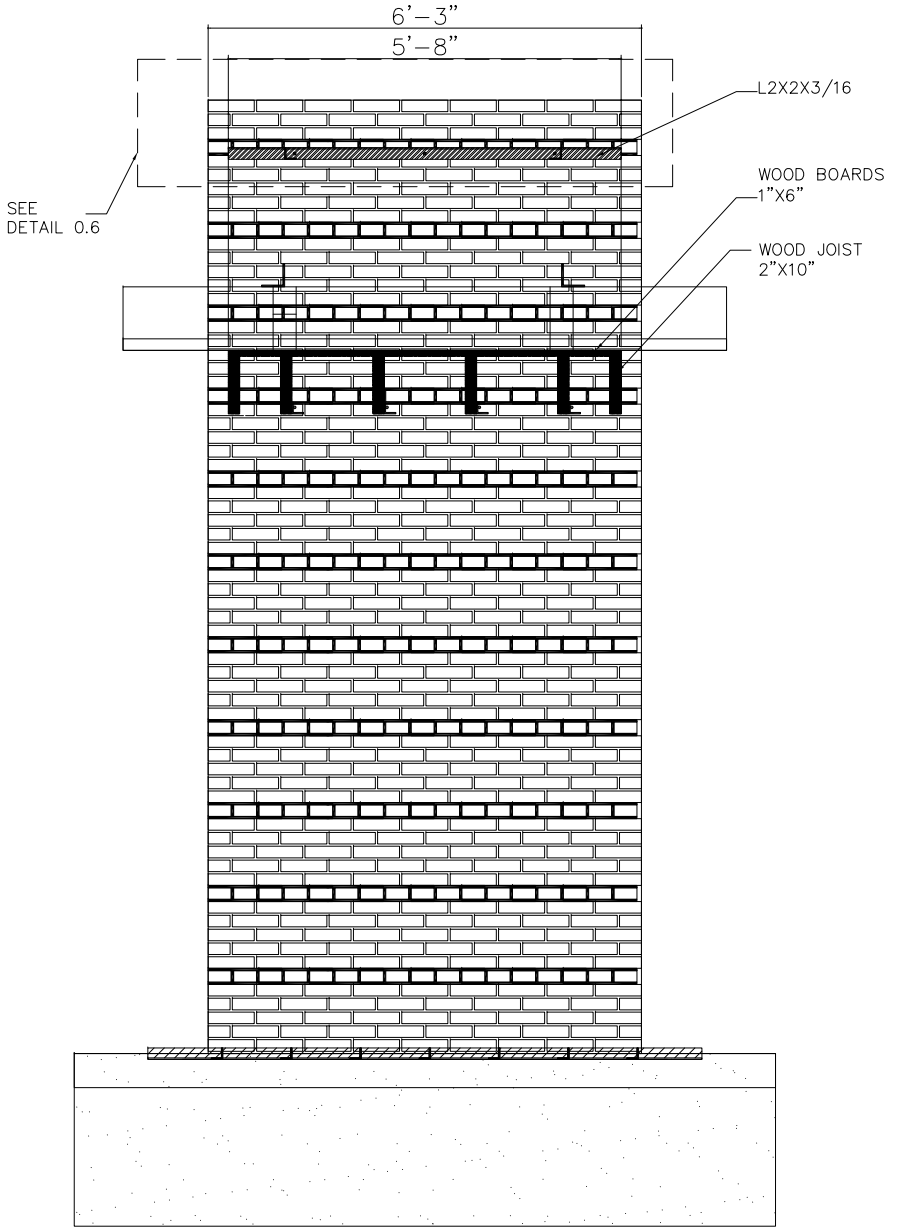

SECTION E

TOP RESTRAINT DETAILS	S.12 / S.12

PRODUCED BY AN AUTODESK EDUCATIONAL PRODUCT

PRODUCED BY AN AUTODESK EDUCATIONAL PRODUCT

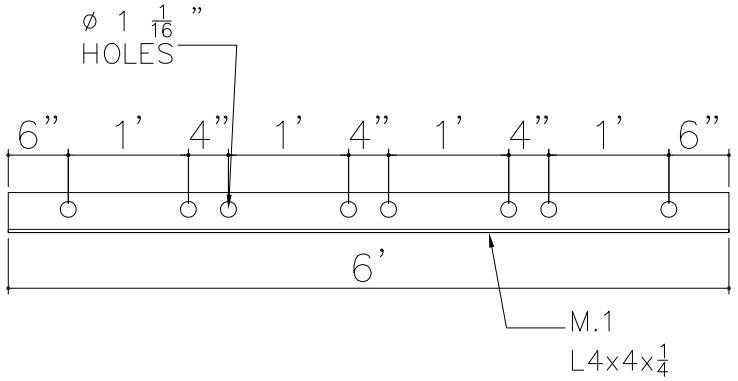

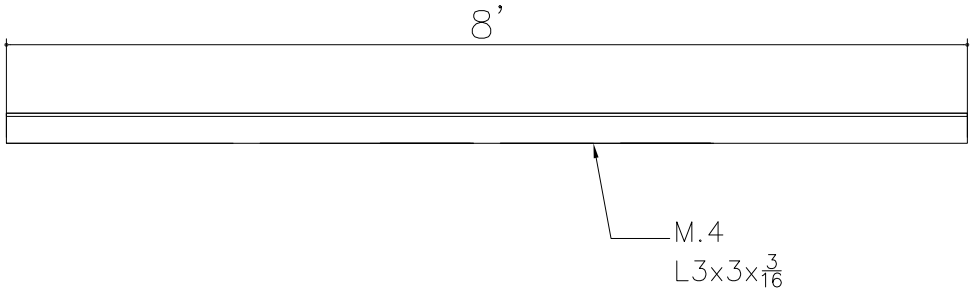

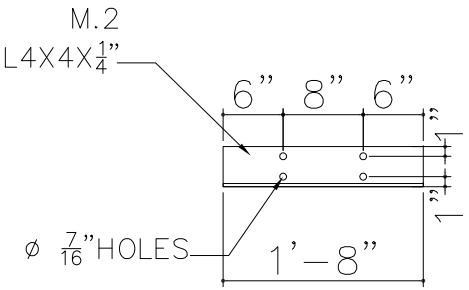

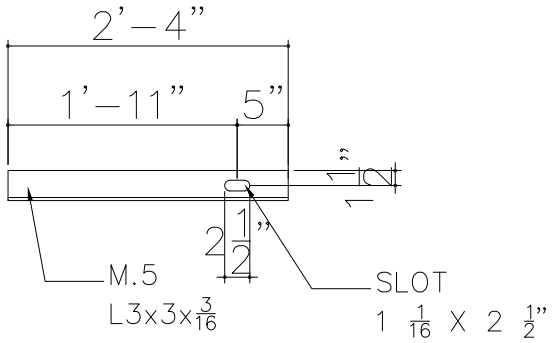

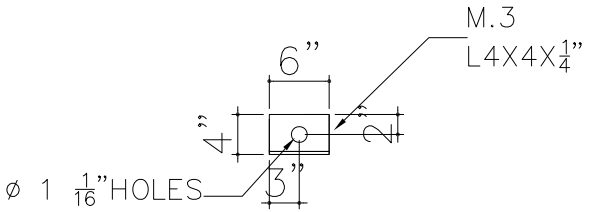

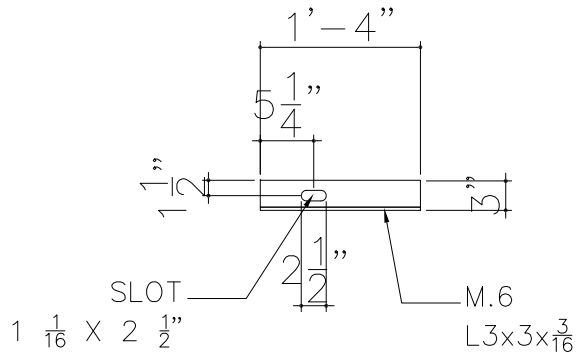

SHOP DRAWING	D.1 / D.3

PRODUCED BY AN AUTODESK EDUCATIONAL PRODUCT

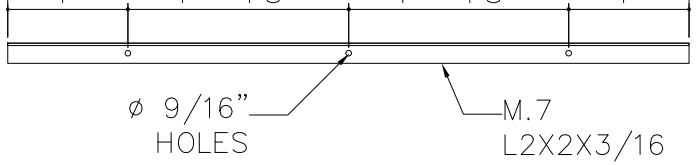

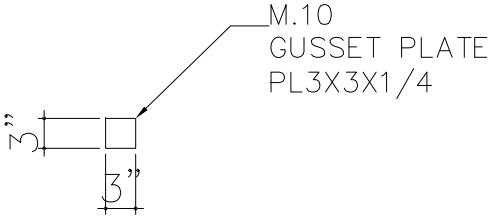

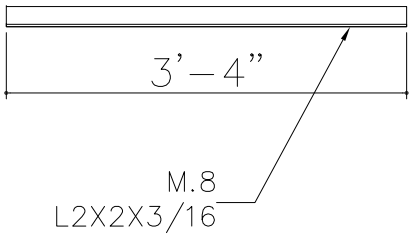

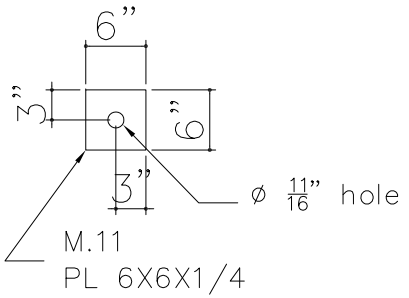

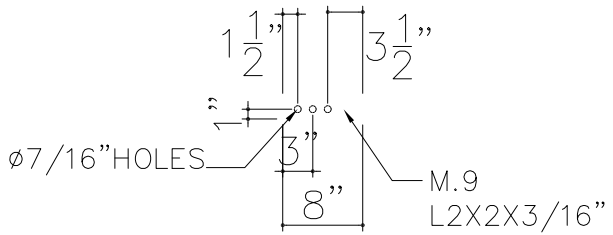

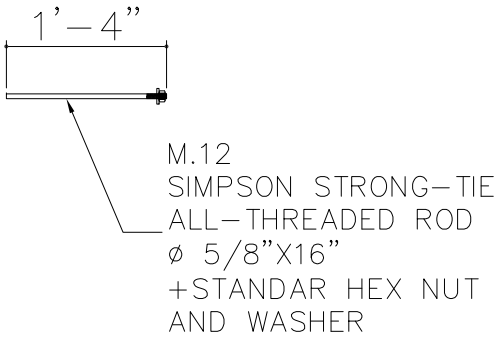

SHOP DRAWING	D.2 / D.3

PRODUCED BY AN AUTODESK EDUCATIONAL PRODUCT

SUMMARY–BILL OF MATERIALS	
QTY	MATERIAL FROM STEEL SHOP
4	L4X4X1/4–20'
3	L3X3X3/16–20'
2	L2X2X3/16–20'
4	PL3X3X1/4
10	PL6X6X1/4
	MATERIAL FROM HOME DEPOT
60	ø 3/8" BOLT–3"–GRADE 5
60	ø 3/8" HEX NUT–GRADE 5
120	ø 3/8" WASHERS
12	2X10"X8'–PREMIUM DOUGLAS FIR LUMBER
14	1X6"X12'–PINE BOARD
5LB	10D–BRIGHT COMMON NAILS
10	ALL–THREADED ROD ø 5/8"X16"–SIMPSON STRONG–TIE
4	PL3X3X1/4
10	PL6X6X1/4

DETAILED BILL OF MATERIALS–SHOP DRAWINGS					
ID	QTY	MATERIAL	LENGTH	WEIGHT	REMARKS
M.1	8	L4X4X1/4	72"		
M.2	12	L4X4X1/4	20"		
M.3	4	L4X4X1/4	6"		
M.4	4	L3X3X3/16	96"		
M.5	6	L3X3X3/16	28"		W/SLOT
M.6	6	L3X3X3/16	16"		W/SLOT
M.7	2	L2X2X3/16	68"		
M.8	4	L2X2X3/16	40"		
M.9	4	L2X2X3/16	8"		
M.10	4	PL3X3X1/4			
M.11	10	PL6X6X1/4			
M.12	10	ALL–THREADED ROD ø 5/8"X16"–SIMPSON STRONG–TIE			

SHOP DRAWING	D.3 / D.3

PRODUCED BY AN AUTODESK EDUCATIONAL PRODUCT

PRODUCED BY AN AUTODESK EDUCATIONAL PRODUCT

MCEER Technical Reports

MCEER publishes technical reports on a variety of subjects written by authors funded through MCEER. These reports are available from both MCEER Publications and the National Technical Information Service (NTIS). Requests for reports should be directed to MCEER Publications, MCEER, University at Buffalo, State University of New York, 133A Ketter Hall, Buffalo, New York 14260. Reports can also be requested through NTIS, P.O. Box 1425, Springfield, Virginia 22151. NTIS accession numbers are shown in parenthesis, if available.

NCEER-87-0001 "First-Year Program in Research, Education and Technology Transfer," 3/5/87, (PB88-134275, A04, MF-A01).

NCEER-87-0002 "Experimental Evaluation of Instantaneous Optimal Algorithms for Structural Control," by R.C. Lin, T.T. Soong and A.M. Reinhorn, 4/20/87, (PB88-134341, A04, MF-A01).

NCEER-87-0003 "Experimentation Using the Earthquake Simulation Facilities at University at Buffalo," by A.M. Reinhorn and R.L. Ketter, not available.

NCEER-87-0004 "The System Characteristics and Performance of a Shaking Table," by J.S. Hwang, K.C. Chang and G.C. Lee, 6/1/87, (PB88-134259, A03, MF-A01). This report is available only through NTIS (see address given above).

NCEER-87-0005 "A Finite Element Formulation for Nonlinear Viscoplastic Material Using a Q Model," by O. Gyebi and G. Dasgupta, 11/2/87, (PB88-213764, A08, MF-A01).

NCEER-87-0006 "Symbolic Manipulation Program (SMP) - Algebraic Codes for Two and Three Dimensional Finite Element Formulations," by X. Lee and G. Dasgupta, 11/9/87, (PB88-218522, A05, MF-A01).

NCEER-87-0007 "Instantaneous Optimal Control Laws for Tall Buildings Under Seismic Excitations," by J.N. Yang, A. Akbarpour and P. Ghaemmaghami, 6/10/87, (PB88-134333, A06, MF-A01). This report is only available through NTIS (see address given above).

NCEER-87-0008 "IDARC: Inelastic Damage Analysis of Reinforced Concrete Frame - Shear-Wall Structures," by Y.J. Park, A.M. Reinhorn and S.K. Kunnath, 7/20/87, (PB88-134325, A09, MF-A01). This report is only available through NTIS (see address given above).

NCEER-87-0009 "Liquefaction Potential for New York State: A Preliminary Report on Sites in Manhattan and Buffalo," by M. Budhu, V. Vijayakumar, R.F. Giese and L. Baumgras, 8/31/87, (PB88-163704, A03, MF-A01). This report is available only through NTIS (see address given above).

NCEER-87-0010 "Vertical and Torsional Vibration of Foundations in Inhomogeneous Media," by A.S. Veletsos and K.W. Dotson, 6/1/87, (PB88-134291, A03, MF-A01). This report is only available through NTIS (see address given above).

NCEER-87-0011 "Seismic Probabilistic Risk Assessment and Seismic Margins Studies for Nuclear Power Plants," by Howard H.M. Hwang, 6/15/87, (PB88-134267, A03, MF-A01). This report is only available through NTIS (see address given above).

NCEER-87-0012 "Parametric Studies of Frequency Response of Secondary Systems Under Ground-Acceleration Excitations," by Y. Yong and Y.K. Lin, 6/10/87, (PB88-134309, A03, MF-A01). This report is only available through NTIS (see address given above).

NCEER-87-0013 "Frequency Response of Secondary Systems Under Seismic Excitation," by J.A. HoLung, J. Cai and Y.K. Lin, 7/31/87, (PB88-134317, A05, MF-A01). This report is only available through NTIS (see address given above).

NCEER-87-0014 "Modelling Earthquake Ground Motions in Seismically Active Regions Using Parametric Time Series Methods," by G.W. Ellis and A.S. Cakmak, 8/25/87, (PB88-134283, A08, MF-A01). This report is only available through NTIS (see address given above).

NCEER-87-0015 "Detection and Assessment of Seismic Structural Damage," by E. DiPasquale and A.S. Cakmak, 8/25/87, (PB88-163712, A05, MF-A01). This report is only available through NTIS (see address given above).

NCEER-87-0016 "Pipeline Experiment at Parkfield, California," by J. Isenberg and E. Richardson, 9/15/87, (PB88-163720, A03, MF-A01). This report is available only through NTIS (see address given above).

NCEER-87-0017 "Digital Simulation of Seismic Ground Motion," by M. Shinozuka, G. Deodatis and T. Harada, 8/31/87, (PB88-155197, A04, MF-A01). This report is available only through NTIS (see address given above).

NCEER-87-0018 "Practical Considerations for Structural Control: System Uncertainty, System Time Delay and Truncation of Small Control Forces," J.N. Yang and A. Akbarpour, 8/10/87, (PB88-163738, A08, MF-A01). This report is only available through NTIS (see address given above).

NCEER-87-0019 "Modal Analysis of Nonclassically Damped Structural Systems Using Canonical Transformation," by J.N. Yang, S. Sarkani and F.X. Long, 9/27/87, (PB88-187851, A04, MF-A01).

NCEER-87-0020 "A Nonstationary Solution in Random Vibration Theory," by J.R. Red-Horse and P.D. Spanos, 11/3/87, (PB88-163746, A03, MF-A01).

NCEER-87-0021 "Horizontal Impedances for Radially Inhomogeneous Viscoelastic Soil Layers," by A.S. Veletsos and K.W. Dotson, 10/15/87, (PB88-150859, A04, MF-A01).

NCEER-87-0022 "Seismic Damage Assessment of Reinforced Concrete Members," by Y.S. Chung, C. Meyer and M. Shinozuka, 10/9/87, (PB88-150867, A05, MF-A01). This report is available only through NTIS (see address given above).

NCEER-87-0023 "Active Structural Control in Civil Engineering," by T.T. Soong, 11/11/87, (PB88-187778, A03, MF-A01).

NCEER-87-0024 "Vertical and Torsional Impedances for Radially Inhomogeneous Viscoelastic Soil Layers," by K.W. Dotson and A.S. Veletsos, 12/87, (PB88-187786, A03, MF-A01).

NCEER-87-0025 "Proceedings from the Symposium on Seismic Hazards, Ground Motions, Soil-Liquefaction and Engineering Practice in Eastern North America," October 20-22, 1987, edited by K.H. Jacob, 12/87, (PB88-188115, A23, MF-A01). This report is available only through NTIS (see address given above).

NCEER-87-0026 "Report on the Whittier-Narrows, California, Earthquake of October 1, 1987," by J. Pantelic and A. Reinhorn, 11/87, (PB88-187752, A03, MF-A01). This report is available only through NTIS (see address given above).

NCEER-87-0027 "Design of a Modular Program for Transient Nonlinear Analysis of Large 3-D Building Structures," by S. Srivastav and J.F. Abel, 12/30/87, (PB88-187950, A05, MF-A01). This report is only available through NTIS (see address given above).

NCEER-87-0028 "Second-Year Program in Research, Education and Technology Transfer," 3/8/88, (PB88-219480, A04, MF-A01).

NCEER-88-0001 "Workshop on Seismic Computer Analysis and Design of Buildings With Interactive Graphics," by W. McGuire, J.F. Abel and C.H. Conley, 1/18/88, (PB88-187760, A03, MF-A01). This report is only available through NTIS (see address given above).

NCEER-88-0002 "Optimal Control of Nonlinear Flexible Structures," by J.N. Yang, F.X. Long and D. Wong, 1/22/88, (PB88-213772, A06, MF-A01).

NCEER-88-0003 "Substructuring Techniques in the Time Domain for Primary-Secondary Structural Systems," by G.D. Manolis and G. Juhn, 2/10/88, (PB88-213780, A04, MF-A01).

NCEER-88-0004 "Iterative Seismic Analysis of Primary-Secondary Systems," by A. Singhal, L.D. Lutes and P.D. Spanos, 2/23/88, (PB88-213798, A04, MF-A01).

NCEER-88-0005 "Stochastic Finite Element Expansion for Random Media," by P.D. Spanos and R. Ghanem, 3/14/88, (PB88-213806, A03, MF-A01).

NCEER-88-0006 "Combining Structural Optimization and Structural Control," by F.Y. Cheng and C.P. Pantelides, 1/10/88, (PB88-213814, A05, MF-A01).

NCEER-88-0007 "Seismic Performance Assessment of Code-Designed Structures," by H.H-M. Hwang, J-W. Jaw and H-J. Shau, 3/20/88, (PB88-219423, A04, MF-A01). This report is only available through NTIS (see address given above).

NCEER-88-0008 "Reliability Analysis of Code-Designed Structures Under Natural Hazards," by H.H-M. Hwang, H. Ushiba and M. Shinozuka, 2/29/88, (PB88-229471, A07, MF-A01). This report is only available through NTIS (see address given above).

NCEER-88-0009 "Seismic Fragility Analysis of Shear Wall Structures," by J-W Jaw and H.H-M. Hwang, 4/30/88, (PB89-102867, A04, MF-A01).

NCEER-88-0010 "Base Isolation of a Multi-Story Building Under a Harmonic Ground Motion - A Comparison of Performances of Various Systems," by F-G Fan, G. Ahmadi and I.G. Tadjbakhsh, 5/18/88, (PB89-122238, A06, MF-A01). This report is only available through NTIS (see address given above).

NCEER-88-0011 "Seismic Floor Response Spectra for a Combined System by Green's Functions," by F.M. Lavelle, L.A. Bergman and P.D. Spanos, 5/1/88, (PB89-102875, A03, MF-A01).

NCEER-88-0012 "A New Solution Technique for Randomly Excited Hysteretic Structures," by G.Q. Cai and Y.K. Lin, 5/16/88, (PB89-102883, A03, MF-A01).

NCEER-88-0013 "A Study of Radiation Damping and Soil-Structure Interaction Effects in the Centrifuge," by K. Weissman, supervised by J.H. Prevost, 5/24/88, (PB89-144703, A06, MF-A01).

NCEER-88-0014 "Parameter Identification and Implementation of a Kinematic Plasticity Model for Frictional Soils," by J.H. Prevost and D.V. Griffiths, not available.

NCEER-88-0015 "Two- and Three- Dimensional Dynamic Finite Element Analyses of the Long Valley Dam," by D.V. Griffiths and J.H. Prevost, 6/17/88, (PB89-144711, A04, MF-A01).

NCEER-88-0016 "Damage Assessment of Reinforced Concrete Structures in Eastern United States," by A.M. Reinhorn, M.J. Seidel, S.K. Kunnath and Y.J. Park, 6/15/88, (PB89-122220, A04, MF-A01). This report is only available through NTIS (see address given above).

NCEER-88-0017 "Dynamic Compliance of Vertically Loaded Strip Foundations in Multilayered Viscoelastic Soils," by S. Ahmad and A.S.M. Israil, 6/17/88, (PB89-102891, A04, MF-A01).

NCEER-88-0018 "An Experimental Study of Seismic Structural Response With Added Viscoelastic Dampers," by R.C. Lin, Z. Liang, T.T. Soong and R.H. Zhang, 6/30/88, (PB89-122212, A05, MF-A01). This report is available only through NTIS (see address given above).

NCEER-88-0019 "Experimental Investigation of Primary - Secondary System Interaction," by G.D. Manolis, G. Juhn and A.M. Reinhorn, 5/27/88, (PB89-122204, A04, MF-A01).

NCEER-88-0020 "A Response Spectrum Approach For Analysis of Nonclassically Damped Structures," by J.N. Yang, S. Sarkani and F.X. Long, 4/22/88, (PB89-102909, A04, MF-A01).

NCEER-88-0021 "Seismic Interaction of Structures and Soils: Stochastic Approach," by A.S. Veletsos and A.M. Prasad, 7/21/88, (PB89-122196, A04, MF-A01). This report is only available through NTIS (see address given above).

NCEER-88-0022 "Identification of the Serviceability Limit State and Detection of Seismic Structural Damage," by E. DiPasquale and A.S. Cakmak, 6/15/88, (PB89-122188, A05, MF-A01). This report is available only through NTIS (see address given above).

NCEER-88-0023 "Multi-Hazard Risk Analysis: Case of a Simple Offshore Structure," by B.K. Bhartia and E.H. Vanmarcke, 7/21/88, (PB89-145213, A05, MF-A01).

NCEER-88-0024 "Automated Seismic Design of Reinforced Concrete Buildings," by Y.S. Chung, C. Meyer and M. Shinozuka, 7/5/88, (PB89-122170, A06, MF-A01). This report is available only through NTIS (see address given above).

NCEER-88-0025 "Experimental Study of Active Control of MDOF Structures Under Seismic Excitations," by L.L. Chung, R.C. Lin, T.T. Soong and A.M. Reinhorn, 7/10/88, (PB89-122600, A04, MF-A01).

NCEER-88-0026 "Earthquake Simulation Tests of a Low-Rise Metal Structure," by J.S. Hwang, K.C. Chang, G.C. Lee and R.L. Ketter, 8/1/88, (PB89-102917, A04, MF-A01).

NCEER-88-0027 "Systems Study of Urban Response and Reconstruction Due to Catastrophic Earthquakes," by F. Kozin and H.K. Zhou, 9/22/88, (PB90-162348, A04, MF-A01).

NCEER-88-0028 "Seismic Fragility Analysis of Plane Frame Structures," by H.H-M. Hwang and Y.K. Low, 7/31/88, (PB89-131445, A06, MF-A01).

NCEER-88-0029 "Response Analysis of Stochastic Structures," by A. Kardara, C. Bucher and M. Shinozuka, 9/22/88, (PB89-174429, A04, MF-A01).

NCEER-88-0030 "Nonnormal Accelerations Due to Yielding in a Primary Structure," by D.C.K. Chen and L.D. Lutes, 9/19/88, (PB89-131437, A04, MF-A01).

NCEER-88-0031 "Design Approaches for Soil-Structure Interaction," by A.S. Veletsos, A.M. Prasad and Y. Tang, 12/30/88, (PB89-174437, A03, MF-A01). This report is available only through NTIS (see address given above).

NCEER-88-0032 "A Re-evaluation of Design Spectra for Seismic Damage Control," by C.J. Turkstra and A.G. Tallin, 11/7/88, (PB89-145221, A05, MF-A01).

NCEER-88-0033 "The Behavior and Design of Noncontact Lap Splices Subjected to Repeated Inelastic Tensile Loading," by V.E. Sagan, P. Gergely and R.N. White, 12/8/88, (PB89-163737, A08, MF-A01).

NCEER-88-0034 "Seismic Response of Pile Foundations," by S.M. Mamoon, P.K. Banerjee and S. Ahmad, 11/1/88, (PB89-145239, A04, MF-A01).

NCEER-88-0035 "Modeling of R/C Building Structures With Flexible Floor Diaphragms (IDARC2)," by A.M. Reinhorn, S.K. Kunnath and N. Panahshahi, 9/7/88, (PB89-207153, A07, MF-A01).

NCEER-88-0036 "Solution of the Dam-Reservoir Interaction Problem Using a Combination of FEM, BEM with Particular Integrals, Modal Analysis, and Substructuring," by C-S. Tsai, G.C. Lee and R.L. Ketter, 12/31/88, (PB89-207146, A04, MF-A01).

NCEER-88-0037 "Optimal Placement of Actuators for Structural Control," by F.Y. Cheng and C.P. Pantelides, 8/15/88, (PB89-162846, A05, MF-A01).

NCEER-88-0038 "Teflon Bearings in Aseismic Base Isolation: Experimental Studies and Mathematical Modeling," by A. Mokha, M.C. Constantinou and A.M. Reinhorn, 12/5/88, (PB89-218457, A10, MF-A01). This report is available only through NTIS (see address given above).

NCEER-88-0039 "Seismic Behavior of Flat Slab High-Rise Buildings in the New York City Area," by P. Weidlinger and M. Ettouney, 10/15/88, (PB90-145681, A04, MF-A01).

NCEER-88-0040 "Evaluation of the Earthquake Resistance of Existing Buildings in New York City," by P. Weidlinger and M. Ettouney, 10/15/88, not available.

NCEER-88-0041 "Small-Scale Modeling Techniques for Reinforced Concrete Structures Subjected to Seismic Loads," by W. Kim, A. El-Attar and R.N. White, 11/22/88, (PB89-189625, A05, MF-A01).

NCEER-88-0042 "Modeling Strong Ground Motion from Multiple Event Earthquakes," by G.W. Ellis and A.S. Cakmak, 10/15/88, (PB89-174445, A03, MF-A01).

NCEER-88-0043 "Nonstationary Models of Seismic Ground Acceleration," by M. Grigoriu, S.E. Ruiz and E. Rosenblueth, 7/15/88, (PB89-189617, A04, MF-A01).

NCEER-88-0044 "SARCF User's Guide: Seismic Analysis of Reinforced Concrete Frames," by Y.S. Chung, C. Meyer and M. Shinozuka, 11/9/88, (PB89-174452, A08, MF-A01).

NCEER-88-0045 "First Expert Panel Meeting on Disaster Research and Planning," edited by J. Pantelic and J. Stoyle, 9/15/88, (PB89-174460, A05, MF-A01).

NCEER-88-0046 "Preliminary Studies of the Effect of Degrading Infill Walls on the Nonlinear Seismic Response of Steel Frames," by C.Z. Chrysostomou, P. Gergely and J.F. Abel, 12/19/88, (PB89-208383, A05, MF-A01).

NCEER-88-0047 "Reinforced Concrete Frame Component Testing Facility - Design, Construction, Instrumentation and Operation," by S.P. Pessiki, C. Conley, T. Bond, P. Gergely and R.N. White, 12/16/88, (PB89-174478, A04, MF-A01).

NCEER-89-0001 "Effects of Protective Cushion and Soil Compliancy on the Response of Equipment Within a Seismically Excited Building," by J.A. HoLung, 2/16/89, (PB89-207179, A04, MF-A01).

NCEER-89-0002 "Statistical Evaluation of Response Modification Factors for Reinforced Concrete Structures," by H.H-M. Hwang and J-W. Jaw, 2/17/89, (PB89-207187, A05, MF-A01).

NCEER-89-0003 "Hysteretic Columns Under Random Excitation," by G-Q. Cai and Y.K. Lin, 1/9/89, (PB89-196513, A03, MF-A01).

NCEER-89-0004 "Experimental Study of `Elephant Foot Bulge' Instability of Thin-Walled Metal Tanks," by Z-H. Jia and R.L. Ketter, 2/22/89, (PB89-207195, A03, MF-A01).

NCEER-89-0005 "Experiment on Performance of Buried Pipelines Across San Andreas Fault," by J. Isenberg, E. Richardson and T.D. O'Rourke, 3/10/89, (PB89-218440, A04, MF-A01). This report is available only through NTIS (see address given above).

NCEER-89-0006 "A Knowledge-Based Approach to Structural Design of Earthquake-Resistant Buildings," by M. Subramani, P. Gergely, C.H. Conley, J.F. Abel and A.H. Zaghw, 1/15/89, (PB89-218465, A06, MF-A01).

NCEER-89-0007 "Liquefaction Hazards and Their Effects on Buried Pipelines," by T.D. O'Rourke and P.A. Lane, 2/1/89, (PB89-218481, A09, MF-A01).

NCEER-89-0008 "Fundamentals of System Identification in Structural Dynamics," by H. Imai, C-B. Yun, O. Maruyama and M. Shinozuka, 1/26/89, (PB89-207211, A04, MF-A01).

NCEER-89-0009 "Effects of the 1985 Michoacan Earthquake on Water Systems and Other Buried Lifelines in Mexico," by A.G. Ayala and M.J. O'Rourke, 3/8/89, (PB89-207229, A06, MF-A01).

NCEER-89-R010 "NCEER Bibliography of Earthquake Education Materials," by K.E.K. Ross, Second Revision, 9/1/89, (PB90-125352, A05, MF-A01). This report is replaced by NCEER-92-0018.

NCEER-89-0011 "Inelastic Three-Dimensional Response Analysis of Reinforced Concrete Building Structures (IDARC-3D), Part I - Modeling," by S.K. Kunnath and A.M. Reinhorn, 4/17/89, (PB90-114612, A07, MF-A01). This report is available only through NTIS (see address given above).

NCEER-89-0012 "Recommended Modifications to ATC-14," by C.D. Poland and J.O. Malley, 4/12/89, (PB90-108648, A15, MF-A01).

NCEER-89-0013 "Repair and Strengthening of Beam-to-Column Connections Subjected to Earthquake Loading," by M. Corazao and A.J. Durrani, 2/28/89, (PB90-109885, A06, MF-A01).

NCEER-89-0014 "Program EXKAL2 for Identification of Structural Dynamic Systems," by O. Maruyama, C-B. Yun, M. Hoshiya and M. Shinozuka, 5/19/89, (PB90-109877, A09, MF-A01).

NCEER-89-0015 "Response of Frames With Bolted Semi-Rigid Connections, Part I - Experimental Study and Analytical Predictions," by P.J. DiCorso, A.M. Reinhorn, J.R. Dickerson, J.B. Radziminski and W.L. Harper, 6/1/89, not available.

NCEER-89-0016 "ARMA Monte Carlo Simulation in Probabilistic Structural Analysis," by P.D. Spanos and M.P. Mignolet, 7/10/89, (PB90-109893, A03, MF-A01).

NCEER-89-P017 "Preliminary Proceedings from the Conference on Disaster Preparedness - The Place of Earthquake Education in Our Schools," Edited by K.E.K. Ross, 6/23/89, (PB90-108606, A03, MF-A01).

NCEER-89-0017 "Proceedings from the Conference on Disaster Preparedness - The Place of Earthquake Education in Our Schools," Edited by K.E.K. Ross, 12/31/89, (PB90-207895, A012, MF-A02). This report is available only through NTIS (see address given above).

NCEER-89-0018 "Multidimensional Models of Hysteretic Material Behavior for Vibration Analysis of Shape Memory Energy Absorbing Devices, by E.J. Graesser and F.A. Cozzarelli, 6/7/89, (PB90-164146, A04, MF-A01).

NCEER-89-0019 "Nonlinear Dynamic Analysis of Three-Dimensional Base Isolated Structures (3D-BASIS)," by S. Nagarajaiah, A.M. Reinhorn and M.C. Constantinou, 8/3/89, (PB90-161936, A06, MF-A01). This report has been replaced by NCEER-93-0011.

NCEER-89-0020 "Structural Control Considering Time-Rate of Control Forces and Control Rate Constraints," by F.Y. Cheng and C.P. Pantelides, 8/3/89, (PB90-120445, A04, MF-A01).

NCEER-89-0021 "Subsurface Conditions of Memphis and Shelby County," by K.W. Ng, T-S. Chang and H-H.M. Hwang, 7/26/89, (PB90-120437, A03, MF-A01).

NCEER-89-0022 "Seismic Wave Propagation Effects on Straight Jointed Buried Pipelines," by K. Elhmadi and M.J. O'Rourke, 8/24/89, (PB90-162322, A10, MF-A02).

NCEER-89-0023 "Workshop on Serviceability Analysis of Water Delivery Systems," edited by M. Grigoriu, 3/6/89, (PB90-127424, A03, MF-A01).

NCEER-89-0024 "Shaking Table Study of a 1/5 Scale Steel Frame Composed of Tapered Members," by K.C. Chang, J.S. Hwang and G.C. Lee, 9/18/89, (PB90-160169, A04, MF-A01).

NCEER-89-0025 "DYNA1D: A Computer Program for Nonlinear Seismic Site Response Analysis - Technical Documentation," by Jean H. Prevost, 9/14/89, (PB90-161944, A07, MF-A01). This report is available only through NTIS (see address given above).

NCEER-89-0026 "1:4 Scale Model Studies of Active Tendon Systems and Active Mass Dampers for Aseismic Protection," by A.M. Reinhorn, T.T. Soong, R.C. Lin, Y.P. Yang, Y. Fukao, H. Abe and M. Nakai, 9/15/89, (PB90-173246, A10, MF-A02). This report is available only through NTIS (see address given above).

NCEER-89-0027 "Scattering of Waves by Inclusions in a Nonhomogeneous Elastic Half Space Solved by Boundary Element Methods," by P.K. Hadley, A. Askar and A.S. Cakmak, 6/15/89, (PB90-145699, A07, MF-A01).

NCEER-89-0028 "Statistical Evaluation of Deflection Amplification Factors for Reinforced Concrete Structures," by H.H.M. Hwang, J-W. Jaw and A.L. Ch'ng, 8/31/89, (PB90-164633, A05, MF-A01).

NCEER-89-0029 "Bedrock Accelerations in Memphis Area Due to Large New Madrid Earthquakes," by H.H.M. Hwang, C.H.S. Chen and G. Yu, 11/7/89, (PB90-162330, A04, MF-A01).

NCEER-89-0030 "Seismic Behavior and Response Sensitivity of Secondary Structural Systems," by Y.Q. Chen and T.T. Soong, 10/23/89, (PB90-164658, A08, MF-A01).

NCEER-89-0031 "Random Vibration and Reliability Analysis of Primary-Secondary Structural Systems," by Y. Ibrahim, M. Grigoriu and T.T. Soong, 11/10/89, (PB90-161951, A04, MF-A01).

NCEER-89-0032 "Proceedings from the Second U.S. - Japan Workshop on Liquefaction, Large Ground Deformation and Their Effects on Lifelines, September 26-29, 1989," Edited by T.D. O'Rourke and M. Hamada, 12/1/89, (PB90-209388, A22, MF-A03).

NCEER-89-0033 "Deterministic Model for Seismic Damage Evaluation of Reinforced Concrete Structures," by J.M. Bracci, A.M. Reinhorn, J.B. Mander and S.K. Kunnath, 9/27/89, (PB91-108803, A06, MF-A01).

NCEER-89-0034 "On the Relation Between Local and Global Damage Indices," by E. DiPasquale and A.S. Cakmak, 8/15/89, (PB90-173865, A05, MF-A01).

NCEER-89-0035 "Cyclic Undrained Behavior of Nonplastic and Low Plasticity Silts," by A.J. Walker and H.E. Stewart, 7/26/89, (PB90-183518, A10, MF-A01).

NCEER-89-0036 "Liquefaction Potential of Surficial Deposits in the City of Buffalo, New York," by M. Budhu, R. Giese and L. Baumgrass, 1/17/89, (PB90-208455, A04, MF-A01).

NCEER-89-0037 "A Deterministic Assessment of Effects of Ground Motion Incoherence," by A.S. Veletsos and Y. Tang, 7/15/89, (PB90-164294, A03, MF-A01).

NCEER-89-0038 "Workshop on Ground Motion Parameters for Seismic Hazard Mapping," July 17-18, 1989, edited by R.V. Whitman, 12/1/89, (PB90-173923, A04, MF-A01).

NCEER-89-0039 "Seismic Effects on Elevated Transit Lines of the New York City Transit Authority," by C.J. Costantino, C.A. Miller and E. Heymsfield, 12/26/89, (PB90-207887, A06, MF-A01).

NCEER-89-0040 "Centrifugal Modeling of Dynamic Soil-Structure Interaction," by K. Weissman, Supervised by J.H. Prevost, 5/10/89, (PB90-207879, A07, MF-A01).

NCEER-89-0041 "Linearized Identification of Buildings With Cores for Seismic Vulnerability Assessment," by I-K. Ho and A.E. Aktan, 11/1/89, (PB90-251943, A07, MF-A01).

NCEER-90-0001 "Geotechnical and Lifeline Aspects of the October 17, 1989 Loma Prieta Earthquake in San Francisco," by T.D. O'Rourke, H.E. Stewart, F.T. Blackburn and T.S. Dickerman, 1/90, (PB90-208596, A05, MF-A01).

NCEER-90-0002 "Nonnormal Secondary Response Due to Yielding in a Primary Structure," by D.C.K. Chen and L.D. Lutes, 2/28/90, (PB90-251976, A07, MF-A01).

NCEER-90-0003 "Earthquake Education Materials for Grades K-12," by K.E.K. Ross, 4/16/90, (PB91-251984, A05, MF-A05). This report has been replaced by NCEER-92-0018.

NCEER-90-0004 "Catalog of Strong Motion Stations in Eastern North America," by R.W. Busby, 4/3/90, (PB90-251984, A05, MF-A01).

NCEER-90-0005 "NCEER Strong-Motion Data Base: A User Manual for the GeoBase Release (Version 1.0 for the Sun3)," by P. Friberg and K. Jacob, 3/31/90 (PB90-258062, A04, MF-A01).

NCEER-90-0006 "Seismic Hazard Along a Crude Oil Pipeline in the Event of an 1811-1812 Type New Madrid Earthquake," by H.H.M. Hwang and C-H.S. Chen, 4/16/90, (PB90-258054, A04, MF-A01).

NCEER-90-0007 "Site-Specific Response Spectra for Memphis Sheahan Pumping Station," by H.H.M. Hwang and C.S. Lee, 5/15/90, (PB91-108811, A05, MF-A01).

NCEER-90-0008 "Pilot Study on Seismic Vulnerability of Crude Oil Transmission Systems," by T. Ariman, R. Dobry, M. Grigoriu, F. Kozin, M. O'Rourke, T. O'Rourke and M. Shinozuka, 5/25/90, (PB91-108837, A06, MF-A01).

NCEER-90-0009 "A Program to Generate Site Dependent Time Histories: EQGEN," by G.W. Ellis, M. Srinivasan and A.S. Cakmak, 1/30/90, (PB91-108829, A04, MF-A01).

NCEER-90-0010 "Active Isolation for Seismic Protection of Operating Rooms," by M.E. Talbott, Supervised by M. Shinozuka, 6/8/9, (PB91-110205, A05, MF-A01).

NCEER-90-0011 "Program LINEARID for Identification of Linear Structural Dynamic Systems," by C-B. Yun and M. Shinozuka, 6/25/90, (PB91-110312, A08, MF-A01).

NCEER-90-0012 "Two-Dimensional Two-Phase Elasto-Plastic Seismic Response of Earth Dams," by A.N. Yiagos, Supervised by J.H. Prevost, 6/20/90, (PB91-110197, A13, MF-A02).

NCEER-90-0013 "Secondary Systems in Base-Isolated Structures: Experimental Investigation, Stochastic Response and Stochastic Sensitivity," by G.D. Manolis, G. Juhn, M.C. Constantinou and A.M. Reinhorn, 7/1/90, (PB91-110320, A08, MF-A01).

NCEER-90-0014 "Seismic Behavior of Lightly-Reinforced Concrete Column and Beam-Column Joint Details," by S.P. Pessiki, C.H. Conley, P. Gergely and R.N. White, 8/22/90, (PB91-108795, A11, MF-A02).

NCEER-90-0015 "Two Hybrid Control Systems for Building Structures Under Strong Earthquakes," by J.N. Yang and A. Danielians, 6/29/90, (PB91-125393, A04, MF-A01).

NCEER-90-0016 "Instantaneous Optimal Control with Acceleration and Velocity Feedback," by J.N. Yang and Z. Li, 6/29/90, (PB91-125401, A03, MF-A01).

NCEER-90-0017 "Reconnaissance Report on the Northern Iran Earthquake of June 21, 1990," by M. Mehrain, 10/4/90, (PB91-125377, A03, MF-A01).

NCEER-90-0018 "Evaluation of Liquefaction Potential in Memphis and Shelby County," by T.S. Chang, P.S. Tang, C.S. Lee and H. Hwang, 8/10/90, (PB91-125427, A09, MF-A01).

NCEER-90-0019 "Experimental and Analytical Study of a Combined Sliding Disc Bearing and Helical Steel Spring Isolation System," by M.C. Constantinou, A.S. Mokha and A.M. Reinhorn, 10/4/90, (PB91-125385, A06, MF-A01). This report is available only through NTIS (see address given above).

NCEER-90-0020 "Experimental Study and Analytical Prediction of Earthquake Response of a Sliding Isolation System with a Spherical Surface," by A.S. Mokha, M.C. Constantinou and A.M. Reinhorn, 10/11/90, (PB91-125419, A05, MF-A01).

NCEER-90-0021 "Dynamic Interaction Factors for Floating Pile Groups," by G. Gazetas, K. Fan, A. Kaynia and E. Kausel, 9/10/90, (PB91-170381, A05, MF-A01).

NCEER-90-0022 "Evaluation of Seismic Damage Indices for Reinforced Concrete Structures," by S. Rodriguez-Gomez and A.S. Cakmak, 9/30/90, PB91-171322, A06, MF-A01).

NCEER-90-0023 "Study of Site Response at a Selected Memphis Site," by H. Desai, S. Ahmad, E.S. Gazetas and M.R. Oh, 10/11/90, (PB91-196857, A03, MF-A01).

NCEER-90-0024 "A User's Guide to Strongmo: Version 1.0 of NCEER's Strong-Motion Data Access Tool for PCs and Terminals," by P.A. Friberg and C.A.T. Susch, 11/15/90, (PB91-171272, A03, MF-A01).

NCEER-90-0025 "A Three-Dimensional Analytical Study of Spatial Variability of Seismic Ground Motions," by L-L. Hong and A.H.-S. Ang, 10/30/90, (PB91-170399, A09, MF-A01).

NCEER-90-0026 "MUMOID User's Guide - A Program for the Identification of Modal Parameters," by S. Rodriguez-Gomez and E. DiPasquale, 9/30/90, (PB91-171298, A04, MF-A01).

NCEER-90-0027 "SARCF-II User's Guide - Seismic Analysis of Reinforced Concrete Frames," by S. Rodriguez-Gomez, Y.S. Chung and C. Meyer, 9/30/90, (PB91-171280, A05, MF-A01).

NCEER-90-0028 "Viscous Dampers: Testing, Modeling and Application in Vibration and Seismic Isolation," by N. Makris and M.C. Constantinou, 12/20/90 (PB91-190561, A06, MF-A01).

NCEER-90-0029 "Soil Effects on Earthquake Ground Motions in the Memphis Area," by H. Hwang, C.S. Lee, K.W. Ng and T.S. Chang, 8/2/90, (PB91-190751, A05, MF-A01).

NCEER-91-0001 "Proceedings from the Third Japan-U.S. Workshop on Earthquake Resistant Design of Lifeline Facilities and Countermeasures for Soil Liquefaction, December 17-19, 1990," edited by T.D. O'Rourke and M. Hamada, 2/1/91, (PB91-179259, A99, MF-A04).

NCEER-91-0002 "Physical Space Solutions of Non-Proportionally Damped Systems," by M. Tong, Z. Liang and G.C. Lee, 1/15/91, (PB91-179242, A04, MF-A01).

NCEER-91-0003 "Seismic Response of Single Piles and Pile Groups," by K. Fan and G. Gazetas, 1/10/91, (PB92-174994, A04, MF-A01).

NCEER-91-0004 "Damping of Structures: Part 1 - Theory of Complex Damping," by Z. Liang and G. Lee, 10/10/91, (PB92-197235, A12, MF-A03).

NCEER-91-0005 "3D-BASIS - Nonlinear Dynamic Analysis of Three Dimensional Base Isolated Structures: Part II," by S. Nagarajaiah, A.M. Reinhorn and M.C. Constantinou, 2/28/91, (PB91-190553, A07, MF-A01). This report has been replaced by NCEER-93-0011.

NCEER-91-0006 "A Multidimensional Hysteretic Model for Plasticity Deforming Metals in Energy Absorbing Devices," by E.J. Graesser and F.A. Cozzarelli, 4/9/91, (PB92-108364, A04, MF-A01).

NCEER-91-0007 "A Framework for Customizable Knowledge-Based Expert Systems with an Application to a KBES for Evaluating the Seismic Resistance of Existing Buildings," by E.G. Ibarra-Anaya and S.J. Fenves, 4/9/91, (PB91-210930, A08, MF-A01).

NCEER-91-0008 "Nonlinear Analysis of Steel Frames with Semi-Rigid Connections Using the Capacity Spectrum Method," by G.G. Deierlein, S-H. Hsieh, Y-J. Shen and J.F. Abel, 7/2/91, (PB92-113828, A05, MF-A01).

NCEER-91-0009 "Earthquake Education Materials for Grades K-12," by K.E.K. Ross, 4/30/91, (PB91-212142, A06, MF-A01). This report has been replaced by NCEER-92-0018.

NCEER-91-0010 "Phase Wave Velocities and Displacement Phase Differences in a Harmonically Oscillating Pile," by N. Makris and G. Gazetas, 7/8/91, (PB92-108356, A04, MF-A01).

NCEER-91-0011 "Dynamic Characteristics of a Full-Size Five-Story Steel Structure and a 2/5 Scale Model," by K.C. Chang, G.C. Yao, G.C. Lee, D.S. Hao and Y.C. Yeh," 7/2/91, (PB93-116648, A06, MF-A02).

NCEER-91-0012 "Seismic Response of a 2/5 Scale Steel Structure with Added Viscoelastic Dampers," by K.C. Chang, T.T. Soong, S-T. Oh and M.L. Lai, 5/17/91, (PB92-110816, A05, MF-A01).

NCEER-91-0013 "Earthquake Response of Retaining Walls; Full-Scale Testing and Computational Modeling," by S. Alampalli and A-W.M. Elgamal, 6/20/91, not available.

NCEER-91-0014 "3D-BASIS-M: Nonlinear Dynamic Analysis of Multiple Building Base Isolated Structures," by P.C. Tsopelas, S. Nagarajaiah, M.C. Constantinou and A.M. Reinhorn, 5/28/91, (PB92-113885, A09, MF-A02).

NCEER-91-0015 "Evaluation of SEAOC Design Requirements for Sliding Isolated Structures," by D. Theodossiou and M.C. Constantinou, 6/10/91, (PB92-114602, A11, MF-A03).

NCEER-91-0016 "Closed-Loop Modal Testing of a 27-Story Reinforced Concrete Flat Plate-Core Building," by H.R. Somaprasad, T. Toksoy, H. Yoshiyuki and A.E. Aktan, 7/15/91, (PB92-129980, A07, MF-A02).

NCEER-91-0017 "Shake Table Test of a 1/6 Scale Two-Story Lightly Reinforced Concrete Building," by A.G. El-Attar, R.N. White and P. Gergely, 2/28/91, (PB92-222447, A06, MF-A02).

NCEER-91-0018 "Shake Table Test of a 1/8 Scale Three-Story Lightly Reinforced Concrete Building," by A.G. El-Attar, R.N. White and P. Gergely, 2/28/91, (PB93-116630, A08, MF-A02).

NCEER-91-0019 "Transfer Functions for Rigid Rectangular Foundations," by A.S. Veletsos, A.M. Prasad and W.H. Wu, 7/31/91, not available.

NCEER-91-0020 "Hybrid Control of Seismic-Excited Nonlinear and Inelastic Structural Systems," by J.N. Yang, Z. Li and A. Danielians, 8/1/91, (PB92-143171, A06, MF-A02).

NCEER-91-0021 "The NCEER-91 Earthquake Catalog: Improved Intensity-Based Magnitudes and Recurrence Relations for U.S. Earthquakes East of New Madrid," by L. Seeber and J.G. Armbruster, 8/28/91, (PB92-176742, A06, MF-A02).

NCEER-91-0022 "Proceedings from the Implementation of Earthquake Planning and Education in Schools: The Need for Change - The Roles of the Changemakers," by K.E.K. Ross and F. Winslow, 7/23/91, (PB92-129998, A12, MF-A03).

NCEER-91-0023 "A Study of Reliability-Based Criteria for Seismic Design of Reinforced Concrete Frame Buildings," by H.H.M. Hwang and H-M. Hsu, 8/10/91, (PB92-140235, A09, MF-A02).

NCEER-91-0024 "Experimental Verification of a Number of Structural System Identification Algorithms," by R.G. Ghanem, H. Gavin and M. Shinozuka, 9/18/91, (PB92-176577, A18, MF-A04).

NCEER-91-0025 "Probabilistic Evaluation of Liquefaction Potential," by H.H.M. Hwang and C.S. Lee," 11/25/91, (PB92-143429, A05, MF-A01).

NCEER-91-0026 "Instantaneous Optimal Control for Linear, Nonlinear and Hysteretic Structures - Stable Controllers," by J.N. Yang and Z. Li, 11/15/91, (PB92-163807, A04, MF-A01).

NCEER-91-0027 "Experimental and Theoretical Study of a Sliding Isolation System for Bridges," by M.C. Constantinou, A. Kartoum, A.M. Reinhorn and P. Bradford, 11/15/91, (PB92-176973, A10, MF-A03).

NCEER-92-0001 "Case Studies of Liquefaction and Lifeline Performance During Past Earthquakes, Volume 1: Japanese Case Studies," Edited by M. Hamada and T. O'Rourke, 2/17/92, (PB92-197243, A18, MF-A04).

NCEER-92-0002 "Case Studies of Liquefaction and Lifeline Performance During Past Earthquakes, Volume 2: United States Case Studies," Edited by T. O'Rourke and M. Hamada, 2/17/92, (PB92-197250, A20, MF-A04).

NCEER-92-0003 "Issues in Earthquake Education," Edited by K. Ross, 2/3/92, (PB92-222389, A07, MF-A02).

NCEER-92-0004 "Proceedings from the First U.S. - Japan Workshop on Earthquake Protective Systems for Bridges," Edited by I.G. Buckle, 2/4/92, (PB94-142239, A99, MF-A06).

NCEER-92-0005 "Seismic Ground Motion from a Haskell-Type Source in a Multiple-Layered Half-Space," A.P. Theoharis, G. Deodatis and M. Shinozuka, 1/2/92, not available.

NCEER-92-0006 "Proceedings from the Site Effects Workshop," Edited by R. Whitman, 2/29/92, (PB92-197201, A04, MF-A01).

NCEER-92-0007 "Engineering Evaluation of Permanent Ground Deformations Due to Seismically-Induced Liquefaction," by M.H. Baziar, R. Dobry and A-W.M. Elgamal, 3/24/92, (PB92-222421, A13, MF-A03).

NCEER-92-0008 "A Procedure for the Seismic Evaluation of Buildings in the Central and Eastern United States," by C.D. Poland and J.O. Malley, 4/2/92, (PB92-222439, A20, MF-A04).

NCEER-92-0009 "Experimental and Analytical Study of a Hybrid Isolation System Using Friction Controllable Sliding Bearings," by M.Q. Feng, S. Fujii and M. Shinozuka, 5/15/92, (PB93-150282, A06, MF-A02).

NCEER-92-0010 "Seismic Resistance of Slab-Column Connections in Existing Non-Ductile Flat-Plate Buildings," by A.J. Durrani and Y. Du, 5/18/92, (PB93-116812, A06, MF-A02).

NCEER-92-0011 "The Hysteretic and Dynamic Behavior of Brick Masonry Walls Upgraded by Ferrocement Coatings Under Cyclic Loading and Strong Simulated Ground Motion," by H. Lee and S.P. Prawel, 5/11/92, not available.

NCEER-92-0012 "Study of Wire Rope Systems for Seismic Protection of Equipment in Buildings," by G.F. Demetriades, M.C. Constantinou and A.M. Reinhorn, 5/20/92, (PB93-116655, A08, MF-A02).

NCEER-92-0013 "Shape Memory Structural Dampers: Material Properties, Design and Seismic Testing," by P.R. Witting and F.A. Cozzarelli, 5/26/92, (PB93-116663, A05, MF-A01).

NCEER-92-0014 "Longitudinal Permanent Ground Deformation Effects on Buried Continuous Pipelines," by M.J. O'Rourke, and C. Nordberg, 6/15/92, (PB93-116671, A08, MF-A02).

NCEER-92-0015 "A Simulation Method for Stationary Gaussian Random Functions Based on the Sampling Theorem," by M. Grigoriu and S. Balopoulou, 6/11/92, (PB93-127496, A05, MF-A01).

NCEER-92-0016 "Gravity-Load-Designed Reinforced Concrete Buildings: Seismic Evaluation of Existing Construction and Detailing Strategies for Improved Seismic Resistance," by G.W. Hoffmann, S.K. Kunnath, A.M. Reinhorn and J.B. Mander, 7/15/92, (PB94-142007, A08, MF-A02).

NCEER-92-0017 "Observations on Water System and Pipeline Performance in the Limón Area of Costa Rica Due to the April 22, 1991 Earthquake," by M. O'Rourke and D. Ballantyne, 6/30/92, (PB93-126811, A06, MF-A02).

NCEER-92-0018 "Fourth Edition of Earthquake Education Materials for Grades K-12," Edited by K.E.K. Ross, 8/10/92, (PB93-114023, A07, MF-A02).

NCEER-92-0019 "Proceedings from the Fourth Japan-U.S. Workshop on Earthquake Resistant Design of Lifeline Facilities and Countermeasures for Soil Liquefaction," Edited by M. Hamada and T.D. O'Rourke, 8/12/92, (PB93-163939, A99, MF-E11).

NCEER-92-0020 "Active Bracing System: A Full Scale Implementation of Active Control," by A.M. Reinhorn, T.T. Soong, R.C. Lin, M.A. Riley, Y.P. Wang, S. Aizawa and M. Higashino, 8/14/92, (PB93-127512, A06, MF-A02).

NCEER-92-0021 "Empirical Analysis of Horizontal Ground Displacement Generated by Liquefaction-Induced Lateral Spreads," by S.F. Bartlett and T.L. Youd, 8/17/92, (PB93-188241, A06, MF-A02).

NCEER-92-0022 "IDARC Version 3.0: Inelastic Damage Analysis of Reinforced Concrete Structures," by S.K. Kunnath, A.M. Reinhorn and R.F. Lobo, 8/31/92, (PB93-227502, A07, MF-A02).

NCEER-92-0023 "A Semi-Empirical Analysis of Strong-Motion Peaks in Terms of Seismic Source, Propagation Path and Local Site Conditions, by M. Kamiyama, M.J. O'Rourke and R. Flores-Berrones, 9/9/92, (PB93-150266, A08, MF-A02).

NCEER-92-0024 "Seismic Behavior of Reinforced Concrete Frame Structures with Nonductile Details, Part I: Summary of Experimental Findings of Full Scale Beam-Column Joint Tests," by A. Beres, R.N. White and P. Gergely, 9/30/92, (PB93-227783, A05, MF-A01).

NCEER-92-0025 "Experimental Results of Repaired and Retrofitted Beam-Column Joint Tests in Lightly Reinforced Concrete Frame Buildings," by A. Beres, S. El-Borgi, R.N. White and P. Gergely, 10/29/92, (PB93-227791, A05, MF-A01).

NCEER-92-0026 "A Generalization of Optimal Control Theory: Linear and Nonlinear Structures," by J.N. Yang, Z. Li and S. Vongchavalitkul, 11/2/92, (PB93-188621, A05, MF-A01).

NCEER-92-0027 "Seismic Resistance of Reinforced Concrete Frame Structures Designed Only for Gravity Loads: Part I - Design and Properties of a One-Third Scale Model Structure," by J.M. Bracci, A.M. Reinhorn and J.B. Mander, 12/1/92, (PB94-104502, A08, MF-A02).

NCEER-92-0028 "Seismic Resistance of Reinforced Concrete Frame Structures Designed Only for Gravity Loads: Part II - Experimental Performance of Subassemblages," by L.E. Aycardi, J.B. Mander and A.M. Reinhorn, 12/1/92, (PB94-104510, A08, MF-A02).

NCEER-92-0029 "Seismic Resistance of Reinforced Concrete Frame Structures Designed Only for Gravity Loads: Part III - Experimental Performance and Analytical Study of a Structural Model," by J.M. Bracci, A.M. Reinhorn and J.B. Mander, 12/1/92, (PB93-227528, A09, MF-A01).

NCEER-92-0030 "Evaluation of Seismic Retrofit of Reinforced Concrete Frame Structures: Part I - Experimental Performance of Retrofitted Subassemblages," by D. Choudhuri, J.B. Mander and A.M. Reinhorn, 12/8/92, (PB93-198307, A07, MF-A02).

NCEER-92-0031 "Evaluation of Seismic Retrofit of Reinforced Concrete Frame Structures: Part II - Experimental Performance and Analytical Study of a Retrofitted Structural Model," by J.M. Bracci, A.M. Reinhorn and J.B. Mander, 12/8/92, (PB93-198315, A09, MF-A03).

NCEER-92-0032 "Experimental and Analytical Investigation of Seismic Response of Structures with Supplemental Fluid Viscous Dampers," by M.C. Constantinou and M.D. Symans, 12/21/92, (PB93-191435, A10, MF-A03). This report is available only through NTIS (see address given above).

NCEER-92-0033 "Reconnaissance Report on the Cairo, Egypt Earthquake of October 12, 1992," by M. Khater, 12/23/92, (PB93-188621, A03, MF-A01).

NCEER-92-0034 "Low-Level Dynamic Characteristics of Four Tall Flat-Plate Buildings in New York City," by H. Gavin, S. Yuan, J. Grossman, E. Pekelis and K. Jacob, 12/28/92, (PB93-188217, A07, MF-A02).

NCEER-93-0001 "An Experimental Study on the Seismic Performance of Brick-Infilled Steel Frames With and Without Retrofit," by J.B. Mander, B. Nair, K. Wojtkowski and J. Ma, 1/29/93, (PB93-227510, A07, MF-A02).

NCEER-93-0002 "Social Accounting for Disaster Preparedness and Recovery Planning," by S. Cole, E. Pantoja and V. Razak, 2/22/93, (PB94-142114, A12, MF-A03).

NCEER-93-0003 "Assessment of 1991 NEHRP Provisions for Nonstructural Components and Recommended Revisions," by T.T. Soong, G. Chen, Z. Wu, R-H. Zhang and M. Grigoriu, 3/1/93, (PB93-188639, A06, MF-A02).

NCEER-93-0004 "Evaluation of Static and Response Spectrum Analysis Procedures of SEAOC/UBC for Seismic Isolated Structures," by C.W. Winters and M.C. Constantinou, 3/23/93, (PB93-198299, A10, MF-A03).

NCEER-93-0005 "Earthquakes in the Northeast - Are We Ignoring the Hazard? A Workshop on Earthquake Science and Safety for Educators," edited by K.E.K. Ross, 4/2/93, (PB94-103066, A09, MF-A02).

NCEER-93-0006 "Inelastic Response of Reinforced Concrete Structures with Viscoelastic Braces," by R.F. Lobo, J.M. Bracci, K.L. Shen, A.M. Reinhorn and T.T. Soong, 4/5/93, (PB93-227486, A05, MF-A02).

NCEER-93-0007 "Seismic Testing of Installation Methods for Computers and Data Processing Equipment," by K. Kosar, T.T. Soong, K.L. Shen, J.A. HoLung and Y.K. Lin, 4/12/93, (PB93-198299, A07, MF-A02).

NCEER-93-0008 "Retrofit of Reinforced Concrete Frames Using Added Dampers," by A. Reinhorn, M. Constantinou and C. Li, not available.

NCEER-93-0009 "Seismic Behavior and Design Guidelines for Steel Frame Structures with Added Viscoelastic Dampers," by K.C. Chang, M.L. Lai, T.T. Soong, D.S. Hao and Y.C. Yeh, 5/1/93, (PB94-141959, A07, MF-A02).

NCEER-93-0010 "Seismic Performance of Shear-Critical Reinforced Concrete Bridge Piers," by J.B. Mander, S.M. Waheed, M.T.A. Chaudhary and S.S. Chen, 5/12/93, (PB93-227494, A08, MF-A02).

NCEER-93-0011 "3D-BASIS-TABS: Computer Program for Nonlinear Dynamic Analysis of Three Dimensional Base Isolated Structures," by S. Nagarajaiah, C. Li, A.M. Reinhorn and M.C. Constantinou, 8/2/93, (PB94-141819, A09, MF-A02).

NCEER-93-0012 "Effects of Hydrocarbon Spills from an Oil Pipeline Break on Ground Water," by O.J. Helweg and H.H.M. Hwang, 8/3/93, (PB94-141942, A06, MF-A02).

NCEER-93-0013 "Simplified Procedures for Seismic Design of Nonstructural Components and Assessment of Current Code Provisions," by M.P. Singh, L.E. Suarez, E.E. Matheu and G.O. Maldonado, 8/4/93, (PB94-141827, A09, MF-A02).

NCEER-93-0014 "An Energy Approach to Seismic Analysis and Design of Secondary Systems," by G. Chen and T.T. Soong, 8/6/93, (PB94-142767, A11, MF-A03).

NCEER-93-0015 "Proceedings from School Sites: Becoming Prepared for Earthquakes - Commemorating the Third Anniversary of the Loma Prieta Earthquake," Edited by F.E. Winslow and K.E.K. Ross, 8/16/93, (PB94-154275, A16, MF-A02).

NCEER-93-0016 "Reconnaissance Report of Damage to Historic Monuments in Cairo, Egypt Following the October 12, 1992 Dahshur Earthquake," by D. Sykora, D. Look, G. Croci, E. Karaesmen and E. Karaesmen, 8/19/93, (PB94-142221, A08, MF-A02).

NCEER-93-0017 "The Island of Guam Earthquake of August 8, 1993," by S.W. Swan and S.K. Harris, 9/30/93, (PB94-141843, A04, MF-A01).

NCEER-93-0018 "Engineering Aspects of the October 12, 1992 Egyptian Earthquake," by A.W. Elgamal, M. Amer, K. Adalier and A. Abul-Fadl, 10/7/93, (PB94-141983, A05, MF-A01).

NCEER-93-0019 "Development of an Earthquake Motion Simulator and its Application in Dynamic Centrifuge Testing," by I. Krstelj, Supervised by J.H. Prevost, 10/23/93, (PB94-181773, A-10, MF-A03).

NCEER-93-0020 "NCEER-Taisei Corporation Research Program on Sliding Seismic Isolation Systems for Bridges: Experimental and Analytical Study of a Friction Pendulum System (FPS)," by M.C. Constantinou, P. Tsopelas, Y-S. Kim and S. Okamoto, 11/1/93, (PB94-142775, A08, MF-A02).

NCEER-93-0021 "Finite Element Modeling of Elastomeric Seismic Isolation Bearings," by L.J. Billings, Supervised by R. Shepherd, 11/8/93, not available.

NCEER-93-0022 "Seismic Vulnerability of Equipment in Critical Facilities: Life-Safety and Operational Consequences," by K. Porter, G.S. Johnson, M.M. Zadeh, C. Scawthorn and S. Eder, 11/24/93, (PB94-181765, A16, MF-A03).

NCEER-93-0023 "Hokkaido Nansei-oki, Japan Earthquake of July 12, 1993, by P.I. Yanev and C.R. Scawthorn, 12/23/93, (PB94-181500, A07, MF-A01).

NCEER-94-0001 "An Evaluation of Seismic Serviceability of Water Supply Networks with Application to the San Francisco Auxiliary Water Supply System," by I. Markov, Supervised by M. Grigoriu and T. O'Rourke, 1/21/94, (PB94-204013, A07, MF-A02).

NCEER-94-0002 "NCEER-Taisei Corporation Research Program on Sliding Seismic Isolation Systems for Bridges: Experimental and Analytical Study of Systems Consisting of Sliding Bearings, Rubber Restoring Force Devices and Fluid Dampers," Volumes I and II, by P. Tsopelas, S. Okamoto, M.C. Constantinou, D. Ozaki and S. Fujii, 2/4/94, (PB94-181740, A09, MF-A02 and PB94-181757, A12, MF-A03).

NCEER-94-0003 "A Markov Model for Local and Global Damage Indices in Seismic Analysis," by S. Rahman and M. Grigoriu, 2/18/94, (PB94-206000, A12, MF-A03).

NCEER-94-0004 "Proceedings from the NCEER Workshop on Seismic Response of Masonry Infills," edited by D.P. Abrams, 3/1/94, (PB94-180783, A07, MF-A02).

NCEER-94-0005 "The Northridge, California Earthquake of January 17, 1994: General Reconnaissance Report," edited by J.D. Goltz, 3/11/94, (PB94-193943, A10, MF-A03).

NCEER-94-0006 "Seismic Energy Based Fatigue Damage Analysis of Bridge Columns: Part I - Evaluation of Seismic Capacity," by G.A. Chang and J.B. Mander, 3/14/94, (PB94-219185, A11, MF-A03).

NCEER-94-0007 "Seismic Isolation of Multi-Story Frame Structures Using Spherical Sliding Isolation Systems," by T.M. Al-Hussaini, V.A. Zayas and M.C. Constantinou, 3/17/94, (PB94-193745, A09, MF-A02).

NCEER-94-0008 "The Northridge, California Earthquake of January 17, 1994: Performance of Highway Bridges," edited by I.G. Buckle, 3/24/94, (PB94-193851, A06, MF-A02).

NCEER-94-0009 "Proceedings of the Third U.S.-Japan Workshop on Earthquake Protective Systems for Bridges," edited by I.G. Buckle and I. Friedland, 3/31/94, (PB94-195815, A99, MF-A06).

NCEER-94-0010 "3D-BASIS-ME: Computer Program for Nonlinear Dynamic Analysis of Seismically Isolated Single and Multiple Structures and Liquid Storage Tanks," by P.C. Tsopelas, M.C. Constantinou and A.M. Reinhorn, 4/12/94, (PB94-204922, A09, MF-A02).

NCEER-94-0011 "The Northridge, California Earthquake of January 17, 1994: Performance of Gas Transmission Pipelines," by T.D. O'Rourke and M.C. Palmer, 5/16/94, (PB94-204989, A05, MF-A01).

NCEER-94-0012 "Feasibility Study of Replacement Procedures and Earthquake Performance Related to Gas Transmission Pipelines," by T.D. O'Rourke and M.C. Palmer, 5/25/94, (PB94-206638, A09, MF-A02).

NCEER-94-0013 "Seismic Energy Based Fatigue Damage Analysis of Bridge Columns: Part II - Evaluation of Seismic Demand," by G.A. Chang and J.B. Mander, 6/1/94, (PB95-18106, A08, MF-A02).

NCEER-94-0014 "NCEER-Taisei Corporation Research Program on Sliding Seismic Isolation Systems for Bridges: Experimental and Analytical Study of a System Consisting of Sliding Bearings and Fluid Restoring Force/Damping Devices," by P. Tsopelas and M.C. Constantinou, 6/13/94, (PB94-219144, A10, MF-A03).

NCEER-94-0015 "Generation of Hazard-Consistent Fragility Curves for Seismic Loss Estimation Studies," by H. Hwang and J-R. Huo, 6/14/94, (PB95-181996, A09, MF-A02).

NCEER-94-0016 "Seismic Study of Building Frames with Added Energy-Absorbing Devices," by W.S. Pong, C.S. Tsai and G.C. Lee, 6/20/94, (PB94-219136, A10, A03).

NCEER-94-0017 "Sliding Mode Control for Seismic-Excited Linear and Nonlinear Civil Engineering Structures," by J. Yang, J. Wu, A. Agrawal and Z. Li, 6/21/94, (PB95-138483, A06, MF-A02).

NCEER-94-0018 "3D-BASIS-TABS Version 2.0: Computer Program for Nonlinear Dynamic Analysis of Three Dimensional Base Isolated Structures," by A.M. Reinhorn, S. Nagarajaiah, M.C. Constantinou, P. Tsopelas and R. Li, 6/22/94, (PB95-182176, A08, MF-A02).

NCEER-94-0019 "Proceedings of the International Workshop on Civil Infrastructure Systems: Application of Intelligent Systems and Advanced Materials on Bridge Systems," Edited by G.C. Lee and K.C. Chang, 7/18/94, (PB95-252474, A20, MF-A04).

NCEER-94-0020 "Study of Seismic Isolation Systems for Computer Floors," by V. Lambrou and M.C. Constantinou, 7/19/94, (PB95-138533, A10, MF-A03).

NCEER-94-0021 "Proceedings of the U.S.-Italian Workshop on Guidelines for Seismic Evaluation and Rehabilitation of Unreinforced Masonry Buildings," Edited by D.P. Abrams and G.M. Calvi, 7/20/94, (PB95-138749, A13, MF-A03).

NCEER-94-0022 "NCEER-Taisei Corporation Research Program on Sliding Seismic Isolation Systems for Bridges: Experimental and Analytical Study of a System Consisting of Lubricated PTFE Sliding Bearings and Mild Steel Dampers," by P. Tsopelas and M.C. Constantinou, 7/22/94, (PB95-182184, A08, MF-A02).

NCEER-94-0023 “Development of Reliability-Based Design Criteria for Buildings Under Seismic Load,” by Y.K. Wen, H. Hwang and M. Shinozuka, 8/1/94, (PB95-211934, A08, MF-A02).

NCEER-94-0024 “Experimental Verification of Acceleration Feedback Control Strategies for an Active Tendon System,” by S.J. Dyke, B.F. Spencer, Jr., P. Quast, M.K. Sain, D.C. Kaspari, Jr. and T.T. Soong, 8/29/94, (PB95-212320, A05, MF-A01).

NCEER-94-0025 “Seismic Retrofitting Manual for Highway Bridges,” Edited by I.G. Buckle and I.F. Friedland, published by the Federal Highway Administration (PB95-212676, A15, MF-A03).

NCEER-94-0026 “Proceedings from the Fifth U.S.-Japan Workshop on Earthquake Resistant Design of Lifeline Facilities and Countermeasures Against Soil Liquefaction,” Edited by T.D. O’Rourke and M. Hamada, 11/7/94, (PB95-220802, A99, MF-E08).

NCEER-95-0001 "Experimental and Analytical Investigation of Seismic Retrofit of Structures with Supplemental Damping: Part 1 - Fluid Viscous Damping Devices," by A.M. Reinhorn, C. Li and M.C. Constantinou, 1/3/95, (PB95-266599, A09, MF-A02).

NCEER-95-0002 "Experimental and Analytical Study of Low-Cycle Fatigue Behavior of Semi-Rigid Top-And-Seat Angle Connections," by G. Pekcan, J.B. Mander and S.S. Chen, 1/5/95, (PB95-220042, A07, MF-A02).

NCEER-95-0003 "NCEER-ATC Joint Study on Fragility of Buildings," by T. Anagnos, C. Rojahn and A.S. Kiremidjian, 1/20/95, (PB95-220026, A06, MF-A02).

NCEER-95-0004 "Nonlinear Control Algorithms for Peak Response Reduction," by Z. Wu, T.T. Soong, V. Gattulli and R.C. Lin, 2/16/95, (PB95-220349, A05, MF-A01).

NCEER-95-0005 "Pipeline Replacement Feasibility Study: A Methodology for Minimizing Seismic and Corrosion Risks to Underground Natural Gas Pipelines," by R.T. Eguchi, H.A. Seligson and D.G. Honegger, 3/2/95, (PB95-252326, A06, MF-A02).

NCEER-95-0006 "Evaluation of Seismic Performance of an 11-Story Frame Building During the 1994 Northridge Earthquake," by F. Naeim, R. DiSulio, K. Benuska, A. Reinhorn and C. Li, not available.

NCEER-95-0007 "Prioritization of Bridges for Seismic Retrofitting," by N. Basöz and A.S. Kiremidjian, 4/24/95, (PB95-252300, A08, MF-A02).

NCEER-95-0008 "Method for Developing Motion Damage Relationships for Reinforced Concrete Frames," by A. Singhal and A.S. Kiremidjian, 5/11/95, (PB95-266607, A06, MF-A02).

NCEER-95-0009 "Experimental and Analytical Investigation of Seismic Retrofit of Structures with Supplemental Damping: Part II - Friction Devices," by C. Li and A.M. Reinhorn, 7/6/95, (PB96-128087, A11, MF-A03).

NCEER-95-0010 "Experimental Performance and Analytical Study of a Non-Ductile Reinforced Concrete Frame Structure Retrofitted with Elastomeric Spring Dampers," by G. Pekcan, J.B. Mander and S.S. Chen, 7/14/95, (PB96-137161, A08, MF-A02).

NCEER-95-0011 "Development and Experimental Study of Semi-Active Fluid Damping Devices for Seismic Protection of Structures," by M.D. Symans and M.C. Constantinou, 8/3/95, (PB96-136940, A23, MF-A04).

NCEER-95-0012 "Real-Time Structural Parameter Modification (RSPM): Development of Innervated Structures," by Z. Liang, M. Tong and G.C. Lee, 4/11/95, (PB96-137153, A06, MF-A01).

NCEER-95-0013 "Experimental and Analytical Investigation of Seismic Retrofit of Structures with Supplemental Damping: Part III - Viscous Damping Walls," by A.M. Reinhorn and C. Li, 10/1/95, (PB96-176409, A11, MF-A03).

NCEER-95-0014 "Seismic Fragility Analysis of Equipment and Structures in a Memphis Electric Substation," by J-R. Huo and H.H.M. Hwang, 8/10/95, (PB96-128087, A09, MF-A02).

NCEER-95-0015 "The Hanshin-Awaji Earthquake of January 17, 1995: Performance of Lifelines," Edited by M. Shinozuka, 11/3/95, (PB96-176383, A15, MF-A03).

NCEER-95-0016 "Highway Culvert Performance During Earthquakes," by T.L. Youd and C.J. Beckman, available as NCEER-96-0015.

NCEER-95-0017 "The Hanshin-Awaji Earthquake of January 17, 1995: Performance of Highway Bridges," Edited by I.G. Buckle, 12/1/95, not available.

NCEER-95-0018 "Modeling of Masonry Infill Panels for Structural Analysis," by A.M. Reinhorn, A. Madan, R.E. Valles, Y. Reichmann and J.B. Mander, 12/8/95, (PB97-110886, MF-A01, A06).

NCEER-95-0019 "Optimal Polynomial Control for Linear and Nonlinear Structures," by A.K. Agrawal and J.N. Yang, 12/11/95, (PB96-168737, A07, MF-A02).

NCEER-95-0020 "Retrofit of Non-Ductile Reinforced Concrete Frames Using Friction Dampers," by R.S. Rao, P. Gergely and R.N. White, 12/22/95, (PB97-133508, A10, MF-A02).

NCEER-95-0021 "Parametric Results for Seismic Response of Pile-Supported Bridge Bents," by G. Mylonakis, A. Nikolaou and G. Gazetas, 12/22/95, (PB97-100242, A12, MF-A03).

NCEER-95-0022 "Kinematic Bending Moments in Seismically Stressed Piles," by A. Nikolaou, G. Mylonakis and G. Gazetas, 12/23/95, (PB97-113914, MF-A03, A13).

NCEER-96-0001 "Dynamic Response of Unreinforced Masonry Buildings with Flexible Diaphragms," by A.C. Costley and D.P. Abrams," 10/10/96, (PB97-133573, MF-A03, A15).

NCEER-96-0002 "State of the Art Review: Foundations and Retaining Structures," by I. Po Lam, not available.

NCEER-96-0003 "Ductility of Rectangular Reinforced Concrete Bridge Columns with Moderate Confinement," by N. Wehbe, M. Saiidi, D. Sanders and B. Douglas, 11/7/96, (PB97-133557, A06, MF-A02).

NCEER-96-0004 "Proceedings of the Long-Span Bridge Seismic Research Workshop," edited by I.G. Buckle and I.M. Friedland, not available.

NCEER-96-0005 "Establish Representative Pier Types for Comprehensive Study: Eastern United States," by J. Kulicki and Z. Prucz, 5/28/96, (PB98-119217, A07, MF-A02).

NCEER-96-0006 "Establish Representative Pier Types for Comprehensive Study: Western United States," by R. Imbsen, R.A. Schamber and T.A. Osterkamp, 5/28/96, (PB98-118607, A07, MF-A02).

NCEER-96-0007 "Nonlinear Control Techniques for Dynamical Systems with Uncertain Parameters," by R.G. Ghanem and M.I. Bujakov, 5/27/96, (PB97-100259, A17, MF-A03).

NCEER-96-0008 "Seismic Evaluation of a 30-Year Old Non-Ductile Highway Bridge Pier and Its Retrofit," by J.B. Mander, B. Mahmoodzadegan, S. Bhadra and S.S. Chen, 5/31/96, (PB97-110902, MF-A03, A10).

NCEER-96-0009 "Seismic Performance of a Model Reinforced Concrete Bridge Pier Before and After Retrofit," by J.B. Mander, J.H. Kim and C.A. Ligozio, 5/31/96, (PB97-110910, MF-A02, A10).

NCEER-96-0010 "IDARC2D Version 4.0: A Computer Program for the Inelastic Damage Analysis of Buildings," by R.E. Valles, A.M. Reinhorn, S.K. Kunnath, C. Li and A. Madan, 6/3/96, (PB97-100234, A17, MF-A03).

NCEER-96-0011 "Estimation of the Economic Impact of Multiple Lifeline Disruption: Memphis Light, Gas and Water Division Case Study," by S.E. Chang, H.A. Seligson and R.T. Eguchi, 8/16/96, (PB97-133490, A11, MF-A03).

NCEER-96-0012 "Proceedings from the Sixth Japan-U.S. Workshop on Earthquake Resistant Design of Lifeline Facilities and Countermeasures Against Soil Liquefaction, Edited by M. Hamada and T. O'Rourke, 9/11/96, (PB97-133581, A99, MF-A06).

NCEER-96-0013 "Chemical Hazards, Mitigation and Preparedness in Areas of High Seismic Risk: A Methodology for Estimating the Risk of Post-Earthquake Hazardous Materials Release," by H.A. Seligson, R.T. Eguchi, K.J. Tierney and K. Richmond, 11/7/96, (PB97-133565, MF-A02, A08).

NCEER-96-0014 "Response of Steel Bridge Bearings to Reversed Cyclic Loading," by J.B. Mander, D-K. Kim, S.S. Chen and G.J. Premus, 11/13/96, (PB97-140735, A12, MF-A03).

NCEER-96-0015 "Highway Culvert Performance During Past Earthquakes," by T.L. Youd and C.J. Beckman, 11/25/96, (PB97-133532, A06, MF-A01).

NCEER-97-0001 "Evaluation, Prevention and Mitigation of Pounding Effects in Building Structures," by R.E. Valles and A.M. Reinhorn, 2/20/97, (PB97-159552, A14, MF-A03).

NCEER-97-0002 "Seismic Design Criteria for Bridges and Other Highway Structures," by C. Rojahn, R. Mayes, D.G. Anderson, J. Clark, J.H. Hom, R.V. Nutt and M.J. O'Rourke, 4/30/97, (PB97-194658, A06, MF-A03).

NCEER-97-0003 “Proceedings of the U.S.-Italian Workshop on Seismic Evaluation and Retrofit,” Edited by D.P. Abrams and G.M. Calvi, 3/19/97, (PB97-194666, A13, MF-A03).

NCEER-97-0004 "Investigation of Seismic Response of Buildings with Linear and Nonlinear Fluid Viscous Dampers," by A.A. Seleemah and M.C. Constantinou, 5/21/97, (PB98-109002, A15, MF-A03).

NCEER-97-0005 "Proceedings of the Workshop on Earthquake Engineering Frontiers in Transportation Facilities," edited by G.C. Lee and I.M. Friedland, 8/29/97, (PB98-128911, A25, MR-A04).

NCEER-97-0006 "Cumulative Seismic Damage of Reinforced Concrete Bridge Piers," by S.K. Kunnath, A. El-Bahy, A. Taylor and W. Stone, 9/2/97, (PB98-108814, A11, MF-A03).

NCEER-97-0007 "Structural Details to Accommodate Seismic Movements of Highway Bridges and Retaining Walls," by R.A. Imbsen, R.A. Schamber, E. Thorkildsen, A. Kartoum, B.T. Martin, T.N. Rosser and J.M. Kulicki, 9/3/97, (PB98-108996, A09, MF-A02).

NCEER-97-0008 "A Method for Earthquake Motion-Damage Relationships with Application to Reinforced Concrete Frames," by A. Singhal and A.S. Kiremidjian, 9/10/97, (PB98-108988, A13, MF-A03).

NCEER-97-0009 "Seismic Analysis and Design of Bridge Abutments Considering Sliding and Rotation," by K. Fishman and R. Richards, Jr., 9/15/97, (PB98-108897, A06, MF-A02).

NCEER-97-0010 "Proceedings of the FHWA/NCEER Workshop on the National Representation of Seismic Ground Motion for New and Existing Highway Facilities," edited by I.M. Friedland, M.S. Power and R.L. Mayes, 9/22/97, (PB98-128903, A21, MF-A04).

NCEER-97-0011 "Seismic Analysis for Design or Retrofit of Gravity Bridge Abutments," by K.L. Fishman, R. Richards, Jr. and R.C. Divito, 10/2/97, (PB98-128937, A08, MF-A02).

NCEER-97-0012 "Evaluation of Simplified Methods of Analysis for Yielding Structures," by P. Tsopelas, M.C. Constantinou, C.A. Kircher and A.S. Whittaker, 10/31/97, (PB98-128929, A10, MF-A03).

NCEER-97-0013 "Seismic Design of Bridge Columns Based on Control and Repairability of Damage," by C-T. Cheng and J.B. Mander, 12/8/97, (PB98-144249, A11, MF-A03).

NCEER-97-0014 "Seismic Resistance of Bridge Piers Based on Damage Avoidance Design," by J.B. Mander and C-T. Cheng, 12/10/97, (PB98-144223, A09, MF-A02).

NCEER-97-0015 “Seismic Response of Nominally Symmetric Systems with Strength Uncertainty,” by S. Balopoulou and M. Grigoriu, 12/23/97, (PB98-153422, A11, MF-A03).

NCEER-97-0016 “Evaluation of Seismic Retrofit Methods for Reinforced Concrete Bridge Columns,” by T.J. Wipf, F.W. Klaiber and F.M. Russo, 12/28/97, (PB98-144215, A12, MF-A03).

NCEER-97-0017 “Seismic Fragility of Existing Conventional Reinforced Concrete Highway Bridges,” by C.L. Mullen and A.S. Cakmak, 12/30/97, (PB98-153406, A08, MF-A02).

NCEER-97-0018 “Loss Asssessment of Memphis Buildings,” edited by D.P. Abrams and M. Shinozuka, 12/31/97, (PB98-144231, A13, MF-A03).

NCEER-97-0019 “Seismic Evaluation of Frames with Infill Walls Using Quasi-static Experiments,” by K.M. Mosalam, R.N. White and P. Gergely, 12/31/97, (PB98-153455, A07, MF-A02).

NCEER-97-0020 “Seismic Evaluation of Frames with Infill Walls Using Pseudo-dynamic Experiments,” by K.M. Mosalam, R.N. White and P. Gergely, 12/31/97, (PB98-153430, A07, MF-A02).

NCEER-97-0021 “Computational Strategies for Frames with Infill Walls: Discrete and Smeared Crack Analyses and Seismic Fragility,” by K.M. Mosalam, R.N. White and P. Gergely, 12/31/97, (PB98-153414, A10, MF-A02).

NCEER-97-0022 "Proceedings of the NCEER Workshop on Evaluation of Liquefaction Resistance of Soils," edited by T.L. Youd and I.M. Idriss, 12/31/97, (PB98-155617, A15, MF-A03).

MCEER-98-0001 "Extraction of Nonlinear Hysteretic Properties of Seismically Isolated Bridges from Quick-Release Field Tests," by Q. Chen, B.M. Douglas, E.M. Maragakis and I.G. Buckle, 5/26/98, (PB99-118838, A06, MF-A01).

MCEER-98-0002 "Methodologies for Evaluating the Importance of Highway Bridges," by A. Thomas, S. Eshenaur and J. Kulicki, 5/29/98, (PB99-118846, A10, MF-A02).

MCEER-98-0003 "Capacity Design of Bridge Piers and the Analysis of Overstrength," by J.B. Mander, A. Dutta and P. Goel, 6/1/98, (PB99-118853, A09, MF-A02).

MCEER-98-0004 "Evaluation of Bridge Damage Data from the Loma Prieta and Northridge, California Earthquakes," by N. Basoz and A. Kiremidjian, 6/2/98, (PB99-118861, A15, MF-A03).

MCEER-98-0005 "Screening Guide for Rapid Assessment of Liquefaction Hazard at Highway Bridge Sites," by T. L. Youd, 6/16/98, (PB99-118879, A06, not available on microfiche).

MCEER-98-0006 "Structural Steel and Steel/Concrete Interface Details for Bridges," by P. Ritchie, N. Kauhl and J. Kulicki, 7/13/98, (PB99-118945, A06, MF-A01).

MCEER-98-0007 "Capacity Design and Fatigue Analysis of Confined Concrete Columns," by A. Dutta and J.B. Mander, 7/14/98, (PB99-118960, A14, MF-A03).

MCEER-98-0008 "Proceedings of the Workshop on Performance Criteria for Telecommunication Services Under Earthquake Conditions," edited by A.J. Schiff, 7/15/98, (PB99-118952, A08, MF-A02).

MCEER-98-0009 "Fatigue Analysis of Unconfined Concrete Columns," by J.B. Mander, A. Dutta and J.H. Kim, 9/12/98, (PB99-123655, A10, MF-A02).

MCEER-98-0010 "Centrifuge Modeling of Cyclic Lateral Response of Pile-Cap Systems and Seat-Type Abutments in Dry Sands," by A.D. Gadre and R. Dobry, 10/2/98, (PB99-123606, A13, MF-A03).

MCEER-98-0011 "IDARC-BRIDGE: A Computational Platform for Seismic Damage Assessment of Bridge Structures," by A.M. Reinhorn, V. Simeonov, G. Mylonakis and Y. Reichman, 10/2/98, (PB99-162919, A15, MF-A03).

MCEER-98-0012 "Experimental Investigation of the Dynamic Response of Two Bridges Before and After Retrofitting with Elastomeric Bearings," by D.A. Wendichansky, S.S. Chen and J.B. Mander, 10/2/98, (PB99-162927, A15, MF-A03).

MCEER-98-0013 "Design Procedures for Hinge Restrainers and Hinge Sear Width for Multiple-Frame Bridges," by R. Des Roches and G.L. Fenves, 11/3/98, (PB99-140477, A13, MF-A03).

MCEER-98-0014 "Response Modification Factors for Seismically Isolated Bridges," by M.C. Constantinou and J.K. Quarshie, 11/3/98, (PB99-140485, A14, MF-A03).

MCEER-98-0015 "Proceedings of the U.S.-Italy Workshop on Seismic Protective Systems for Bridges," edited by I.M. Friedland and M.C. Constantinou, 11/3/98, (PB2000-101711, A22, MF-A04).

MCEER-98-0016 "Appropriate Seismic Reliability for Critical Equipment Systems: Recommendations Based on Regional Analysis of Financial and Life Loss," by K. Porter, C. Scawthorn, C. Taylor and N. Blais, 11/10/98, (PB99-157265, A08, MF-A02).

MCEER-98-0017 "Proceedings of the U.S. Japan Joint Seminar on Civil Infrastructure Systems Research," edited by M. Shinozuka and A. Rose, 11/12/98, (PB99-156713, A16, MF-A03).

MCEER-98-0018 "Modeling of Pile Footings and Drilled Shafts for Seismic Design," by I. PoLam, M. Kapuskar and D. Chaudhuri, 12/21/98, (PB99-157257, A09, MF-A02).

MCEER-99-0001 "Seismic Evaluation of a Masonry Infilled Reinforced Concrete Frame by Pseudodynamic Testing," by S.G. Buonopane and R.N. White, 2/16/99, (PB99-162851, A09, MF-A02).

MCEER-99-0002 "Response History Analysis of Structures with Seismic Isolation and Energy Dissipation Systems: Verification Examples for Program SAP2000," by J. Scheller and M.C. Constantinou, 2/22/99, (PB99-162869, A08, MF-A02).

MCEER-99-0003 "Experimental Study on the Seismic Design and Retrofit of Bridge Columns Including Axial Load Effects," by A. Dutta, T. Kokorina and J.B. Mander, 2/22/99, (PB99-162877, A09, MF-A02).

MCEER-99-0004 "Experimental Study of Bridge Elastomeric and Other Isolation and Energy Dissipation Systems with Emphasis on Uplift Prevention and High Velocity Near-source Seismic Excitation," by A. Kasalanati and M. C. Constantinou, 2/26/99, (PB99-162885, A12, MF-A03).

MCEER-99-0005 "Truss Modeling of Reinforced Concrete Shear-flexure Behavior," by J.H. Kim and J.B. Mander, 3/8/99, (PB99-163693, A12, MF-A03).

MCEER-99-0006 "Experimental Investigation and Computational Modeling of Seismic Response of a 1:4 Scale Model Steel Structure with a Load Balancing Supplemental Damping System," by G. Pekcan, J.B. Mander and S.S. Chen, 4/2/99, (PB99-162893, A11, MF-A03).

MCEER-99-0007 "Effect of Vertical Ground Motions on the Structural Response of Highway Bridges," by M.R. Button, C.J. Cronin and R.L. Mayes, 4/10/99, (PB2000-101411, A10, MF-A03).

MCEER-99-0008 "Seismic Reliability Assessment of Critical Facilities: A Handbook, Supporting Documentation, and Model Code Provisions," by G.S. Johnson, R.E. Sheppard, M.D. Quilici, S.J. Eder and C.R. Scawthorn, 4/12/99, (PB2000-101701, A18, MF-A04).

MCEER-99-0009 "Impact Assessment of Selected MCEER Highway Project Research on the Seismic Design of Highway Structures," by C. Rojahn, R. Mayes, D.G. Anderson, J.H. Clark, D'Appolonia Engineering, S. Gloyd and R.V. Nutt, 4/14/99, (PB99-162901, A10, MF-A02).

MCEER-99-0010 "Site Factors and Site Categories in Seismic Codes," by R. Dobry, R. Ramos and M.S. Power, 7/19/99, (PB2000-101705, A08, MF-A02).

MCEER-99-0011 "Restrainer Design Procedures for Multi-Span Simply-Supported Bridges," by M.J. Randall, M. Saiidi, E. Maragakis and T. Isakovic, 7/20/99, (PB2000-101702, A10, MF-A02).

MCEER-99-0012 "Property Modification Factors for Seismic Isolation Bearings," by M.C. Constantinou, P. Tsopelas, A. Kasalanati and E. Wolff, 7/20/99, (PB2000-103387, A11, MF-A03).

MCEER-99-0013 "Critical Seismic Issues for Existing Steel Bridges," by P. Ritchie, N. Kauhl and J. Kulicki, 7/20/99, (PB2000-101697, A09, MF-A02).

MCEER-99-0014 "Nonstructural Damage Database," by A. Kao, T.T. Soong and A. Vender, 7/24/99, (PB2000-101407, A06, MF-A01).

MCEER-99-0015 "Guide to Remedial Measures for Liquefaction Mitigation at Existing Highway Bridge Sites," by H.G. Cooke and J. K. Mitchell, 7/26/99, (PB2000-101703, A11, MF-A03).

MCEER-99-0016 "Proceedings of the MCEER Workshop on Ground Motion Methodologies for the Eastern United States," edited by N. Abrahamson and A. Becker, 8/11/99, (PB2000-103385, A07, MF-A02).

MCEER-99-0017 "Quindío, Colombia Earthquake of January 25, 1999: Reconnaissance Report," by A.P. Asfura and P.J. Flores, 10/4/99, (PB2000-106893, A06, MF-A01).

MCEER-99-0018 "Hysteretic Models for Cyclic Behavior of Deteriorating Inelastic Structures," by M.V. Sivaselvan and A.M. Reinhorn, 11/5/99, (PB2000-103386, A08, MF-A02).

MCEER-99-0019 "Proceedings of the 7th U.S.- Japan Workshop on Earthquake Resistant Design of Lifeline Facilities and Countermeasures Against Soil Liquefaction," edited by T.D. O'Rourke, J.P. Bardet and M. Hamada, 11/19/99, (PB2000-103354, A99, MF-A06).

MCEER-99-0020 "Development of Measurement Capability for Micro-Vibration Evaluations with Application to Chip Fabrication Facilities," by G.C. Lee, Z. Liang, J.W. Song, J.D. Shen and W.C. Liu, 12/1/99, (PB2000-105993, A08, MF-A02).

MCEER-99-0021 "Design and Retrofit Methodology for Building Structures with Supplemental Energy Dissipating Systems," by G. Pekcan, J.B. Mander and S.S. Chen, 12/31/99, (PB2000-105994, A11, MF-A03).

MCEER-00-0001 "The Marmara, Turkey Earthquake of August 17, 1999: Reconnaissance Report," edited by C. Scawthorn; with major contributions by M. Bruneau, R. Eguchi, T. Holzer, G. Johnson, J. Mander, J. Mitchell, W. Mitchell, A. Papageorgiou, C. Scaethorn, and G. Webb, 3/23/00, (PB2000-106200, A11, MF-A03).

MCEER-00-0002 "Proceedings of the MCEER Workshop for Seismic Hazard Mitigation of Health Care Facilities," edited by G.C. Lee, M. Ettouney, M. Grigoriu, J. Hauer and J. Nigg, 3/29/00, (PB2000-106892, A08, MF-A02).

MCEER-00-0003 "The Chi-Chi, Taiwan Earthquake of September 21, 1999: Reconnaissance Report," edited by G.C. Lee and C.H. Loh, with major contributions by G.C. Lee, M. Bruneau, I.G. Buckle, S.E. Chang, P.J. Flores, T.D. O'Rourke, M. Shinozuka, T.T. Soong, C-H. Loh, K-C. Chang, Z-J. Chen, J-S. Hwang, M-L. Lin, G-Y. Liu, K-C. Tsai, G.C. Yao and C-L. Yen, 4/30/00, (PB2001-100980, A10, MF-A02).

MCEER-00-0004 "Seismic Retrofit of End-Sway Frames of Steel Deck-Truss Bridges with a Supplemental Tendon System: Experimental and Analytical Investigation," by G. Pekcan, J.B. Mander and S.S. Chen, 7/1/00, (PB2001-100982, A10, MF-A02).

MCEER-00-0005 "Sliding Fragility of Unrestrained Equipment in Critical Facilities," by W.H. Chong and T.T. Soong, 7/5/00, (PB2001-100983, A08, MF-A02).

MCEER-00-0006 "Seismic Response of Reinforced Concrete Bridge Pier Walls in the Weak Direction," by N. Abo-Shadi, M. Saiidi and D. Sanders, 7/17/00, (PB2001-100981, A17, MF-A03).

MCEER-00-0007 "Low-Cycle Fatigue Behavior of Longitudinal Reinforcement in Reinforced Concrete Bridge Columns," by J. Brown and S.K. Kunnath, 7/23/00, (PB2001-104392, A08, MF-A02).

MCEER-00-0008 "Soil Structure Interaction of Bridges for Seismic Analysis," I. PoLam and H. Law, 9/25/00, (PB2001-105397, A08, MF-A02).

MCEER-00-0009 "Proceedings of the First MCEER Workshop on Mitigation of Earthquake Disaster by Advanced Technologies (MEDAT-1), edited by M. Shinozuka, D.J. Inman and T.D. O'Rourke, 11/10/00, (PB2001-105399, A14, MF-A03).

MCEER-00-0010 "Development and Evaluation of Simplified Procedures for Analysis and Design of Buildings with Passive Energy Dissipation Systems, Revision 01," by O.M. Ramirez, M.C. Constantinou, C.A. Kircher, A.S. Whittaker, M.W. Johnson, J.D. Gomez and C. Chrysostomou, 11/16/01, (PB2001-105523, A23, MF-A04).

MCEER-00-0011 "Dynamic Soil-Foundation-Structure Interaction Analyses of Large Caissons," by C-Y. Chang, C-M. Mok, Z-L. Wang, R. Settgast, F. Waggoner, M.A. Ketchum, H.M. Gonnermann and C-C. Chin, 12/30/00, (PB2001-104373, A07, MF-A02).

MCEER-00-0012 "Experimental Evaluation of Seismic Performance of Bridge Restrainers," by A.G. Vlassis, E.M. Maragakis and M. Saiid Saiidi, 12/30/00, (PB2001-104354, A09, MF-A02).

MCEER-00-0013 "Effect of Spatial Variation of Ground Motion on Highway Structures," by M. Shinozuka, V. Saxena and G. Deodatis, 12/31/00, (PB2001-108755, A13, MF-A03).

MCEER-00-0014 "A Risk-Based Methodology for Assessing the Seismic Performance of Highway Systems," by S.D. Werner, C.E. Taylor, J.E. Moore, II, J.S. Walton and S. Cho, 12/31/00, (PB2001-108756, A14, MF-A03).

MCEER-01-0001 "Experimental Investigation of P-Delta Effects to Collapse During Earthquakes," by D. Vian and M. Bruneau, 6/25/01, (PB2002-100534, A17, MF-A03).

MCEER-01-0002 "Proceedings of the Second MCEER Workshop on Mitigation of Earthquake Disaster by Advanced Technologies (MEDAT-2)," edited by M. Bruneau and D.J. Inman, 7/23/01, (PB2002-100434, A16, MF-A03).

MCEER-01-0003 "Sensitivity Analysis of Dynamic Systems Subjected to Seismic Loads," by C. Roth and M. Grigoriu, 9/18/01, (PB2003-100884, A12, MF-A03).

MCEER-01-0004 "Overcoming Obstacles to Implementing Earthquake Hazard Mitigation Policies: Stage 1 Report," by D.J. Alesch and W.J. Petak, 12/17/01, (PB2002-107949, A07, MF-A02).

MCEER-01-0005 "Updating Real-Time Earthquake Loss Estimates: Methods, Problems and Insights," by C.E. Taylor, S.E. Chang and R.T. Eguchi, 12/17/01, (PB2002-107948, A05, MF-A01).

MCEER-01-0006 "Experimental Investigation and Retrofit of Steel Pile Foundations and Pile Bents Under Cyclic Lateral Loadings," by A. Shama, J. Mander, B. Blabac and S. Chen, 12/31/01, (PB2002-107950, A13, MF-A03).

MCEER-02-0001 "Assessment of Performance of Bolu Viaduct in the 1999 Duzce Earthquake in Turkey" by P.C. Roussis, M.C. Constantinou, M. Erdik, E. Durukal and M. Dicleli, 5/8/02, (PB2003-100883, A08, MF-A02).

MCEER-02-0002 "Seismic Behavior of Rail Counterweight Systems of Elevators in Buildings," by M.P. Singh, Rildova and L.E. Suarez, 5/27/02. (PB2003-100882, A11, MF-A03).

MCEER-02-0003 "Development of Analysis and Design Procedures for Spread Footings," by G. Mylonakis, G. Gazetas, S. Nikolaou and A. Chauncey, 10/02/02, (PB2004-101636, A13, MF-A03, CD-A13).

MCEER-02-0004 "Bare-Earth Algorithms for Use with SAR and LIDAR Digital Elevation Models," by C.K. Huyck, R.T. Eguchi and B. Houshmand, 10/16/02, (PB2004-101637, A07, CD-A07).

MCEER-02-0005 "Review of Energy Dissipation of Compression Members in Concentrically Braced Frames," by K.Lee and M. Bruneau, 10/18/02, (PB2004-101638, A10, CD-A10).

MCEER-03-0001 "Experimental Investigation of Light-Gauge Steel Plate Shear Walls for the Seismic Retrofit of Buildings" by J. Berman and M. Bruneau, 5/2/03, (PB2004-101622, A10, MF-A03, CD-A10).

MCEER-03-0002 "Statistical Analysis of Fragility Curves," by M. Shinozuka, M.Q. Feng, H. Kim, T. Uzawa and T. Ueda, 6/16/03, (PB2004-101849, A09, CD-A09).

MCEER-03-0003 "Proceedings of the Eighth U.S.-Japan Workshop on Earthquake Resistant Design f Lifeline Facilities and Countermeasures Against Liquefaction," edited by M. Hamada, J.P. Bardet and T.D. O'Rourke, 6/30/03, (PB2004-104386, A99, CD-A99).

MCEER-03-0004 "Proceedings of the PRC-US Workshop on Seismic Analysis and Design of Special Bridges," edited by L.C. Fan and G.C. Lee, 7/15/03, (PB2004-104387, A14, CD-A14).

MCEER-03-0005 "Urban Disaster Recovery: A Framework and Simulation Model," by S.B. Miles and S.E. Chang, 7/25/03, (PB2004-104388, A07, CD-A07).

MCEER-03-0006 "Behavior of Underground Piping Joints Due to Static and Dynamic Loading," by R.D. Meis, M. Maragakis and R. Siddharthan, 11/17/03, (PB2005-102194, A13, MF-A03, CD-A00).

MCEER-04-0001 "Experimental Study of Seismic Isolation Systems with Emphasis on Secondary System Response and Verification of Accuracy of Dynamic Response History Analysis Methods," by E. Wolff and M. Constantinou, 1/16/04 (PB2005-102195, A99, MF-E08, CD-A00).

MCEER-04-0002 "Tension, Compression and Cyclic Testing of Engineered Cementitious Composite Materials," by K. Kesner and S.L. Billington, 3/1/04, (PB2005-102196, A08, CD-A08).

MCEER-04-0003 "Cyclic Testing of Braces Laterally Restrained by Steel Studs to Enhance Performance During Earthquakes," by O.C. Celik, J.W. Berman and M. Bruneau, 3/16/04, (PB2005-102197, A13, MF-A03, CD-A00).

MCEER-04-0004 "Methodologies for Post Earthquake Building Damage Detection Using SAR and Optical Remote Sensing: Application to the August 17, 1999 Marmara, Turkey Earthquake," by C.K. Huyck, B.J. Adams, S. Cho, R.T. Eguchi, B. Mansouri and B. Houshmand, 6/15/04, (PB2005-104888, A10, CD-A00).

MCEER-04-0005 "Nonlinear Structural Analysis Towards Collapse Simulation: A Dynamical Systems Approach," by M.V. Sivaselvan and A.M. Reinhorn, 6/16/04, (PB2005-104889, A11, MF-A03, CD-A00).

MCEER-04-0006 "Proceedings of the Second PRC-US Workshop on Seismic Analysis and Design of Special Bridges," edited by G.C. Lee and L.C. Fan, 6/25/04, (PB2005-104890, A16, CD-A00).

MCEER-04-0007 "Seismic Vulnerability Evaluation of Axially Loaded Steel Built-up Laced Members," by K. Lee and M. Bruneau, 6/30/04, (PB2005-104891, A16, CD-A00).

MCEER-04-0008 "Evaluation of Accuracy of Simplified Methods of Analysis and Design of Buildings with Damping Systems for Near-Fault and for Soft-Soil Seismic Motions," by E.A. Pavlou and M.C. Constantinou, 8/16/04, (PB2005-104892, A08, MF-A02, CD-A00).

MCEER-04-0009 "Assessment of Geotechnical Issues in Acute Care Facilities in California," by M. Lew, T.D. O'Rourke, R. Dobry and M. Koch, 9/15/04, (PB2005-104893, A08, CD-A00).

MCEER-04-0010 "Scissor-Jack-Damper Energy Dissipation System," by A.N. Sigaher-Boyle and M.C. Constantinou, 12/1/04 (PB2005-108221).

MCEER-04-0011 "Seismic Retrofit of Bridge Steel Truss Piers Using a Controlled Rocking Approach," by M. Pollino and M. Bruneau, 12/20/04 (PB2006-105795).

MCEER-05-0001 "Experimental and Analytical Studies of Structures Seismically Isolated with an Uplift-Restraint Isolation System," by P.C. Roussis and M.C. Constantinou, 1/10/05 (PB2005-108222).

MCEER-05-0002 "A Versatile Experimentation Model for Study of Structures Near Collapse Applied to Seismic Evaluation of Irregular Structures," by D. Kusumastuti, A.M. Reinhorn and A. Rutenberg, 3/31/05 (PB2006-101523).

MCEER-05-0003 "Proceedings of the Third PRC-US Workshop on Seismic Analysis and Design of Special Bridges," edited by L.C. Fan and G.C. Lee, 4/20/05, (PB2006-105796).

MCEER-05-0004 "Approaches for the Seismic Retrofit of Braced Steel Bridge Piers and Proof-of-Concept Testing of an Eccentrically Braced Frame with Tubular Link," by J.W. Berman and M. Bruneau, 4/21/05 (PB2006-101524).

MCEER-05-0005 "Simulation of Strong Ground Motions for Seismic Fragility Evaluation of Nonstructural Components in Hospitals," by A. Wanitkorkul and A. Filiatrault, 5/26/05 (PB2006-500027).

MCEER-05-0006 "Seismic Safety in California Hospitals: Assessing an Attempt to Accelerate the Replacement or Seismic Retrofit of Older Hospital Facilities," by D.J. Alesch, L.A. Arendt and W.J. Petak, 6/6/05 (PB2006-105794).

MCEER-05-0007 "Development of Seismic Strengthening and Retrofit Strategies for Critical Facilities Using Engineered Cementitious Composite Materials," by K. Kesner and S.L. Billington, 8/29/05 (PB2006-111701).

MCEER-05-0008 "Experimental and Analytical Studies of Base Isolation Systems for Seismic Protection of Power Transformers," by N. Murota, M.Q. Feng and G-Y. Liu, 9/30/05 (PB2006-111702).

MCEER-05-0009 "3D-BASIS-ME-MB: Computer Program for Nonlinear Dynamic Analysis of Seismically Isolated Structures," by P.C. Tsopelas, P.C. Roussis, M.C. Constantinou, R. Buchanan and A.M. Reinhorn, 10/3/05 (PB2006-111703).

MCEER-05-0010 "Steel Plate Shear Walls for Seismic Design and Retrofit of Building Structures," by D. Vian and M. Bruneau, 12/15/05 (PB2006-111704).

MCEER-05-0011 "The Performance-Based Design Paradigm," by M.J. Astrella and A. Whittaker, 12/15/05 (PB2006-111705).

MCEER-06-0001 "Seismic Fragility of Suspended Ceiling Systems," H. Badillo-Almaraz, A.S. Whittaker, A.M. Reinhorn and G.P. Cimellaro, 2/4/06 (PB2006-111706).

MCEER-06-0002 "Multi-Dimensional Fragility of Structures," by G.P. Cimellaro, A.M. Reinhorn and M. Bruneau, 3/1/06 (PB2007-106974, A09, MF-A02, CD A00).

MCEER-06-0003 "Built-Up Shear Links as Energy Dissipators for Seismic Protection of Bridges," by P. Dusicka, A.M. Itani and I.G. Buckle, 3/15/06 (PB2006-111708).

MCEER-06-0004 "Analytical Investigation of the Structural Fuse Concept," by R.E. Vargas and M. Bruneau, 3/16/06 (PB2006-111709).

MCEER-06-0005 "Experimental Investigation of the Structural Fuse Concept," by R.E. Vargas and M. Bruneau, 3/17/06 (PB2006-111710).

MCEER-06-0006 "Further Development of Tubular Eccentrically Braced Frame Links for the Seismic Retrofit of Braced Steel Truss Bridge Piers," by J.W. Berman and M. Bruneau, 3/27/06 (PB2007-105147).

MCEER-06-0007 "REDARS Validation Report," by S. Cho, C.K. Huyck, S. Ghosh and R.T. Eguchi, 8/8/06 (PB2007-106983).

MCEER-06-0008 "Review of Current NDE Technologies for Post-Earthquake Assessment of Retrofitted Bridge Columns," by J.W. Song, Z. Liang and G.C. Lee, 8/21/06 (PB2007-106984).

MCEER-06-0009 "Liquefaction Remediation in Silty Soils Using Dynamic Compaction and Stone Columns," by S. Thevanayagam, G.R. Martin, R. Nashed, T. Shenthan, T. Kanagalingam and N. Ecemis, 8/28/06 (PB2007-106985).

MCEER-06-0010 "Conceptual Design and Experimental Investigation of Polymer Matrix Composite Infill Panels for Seismic Retrofitting," by W. Jung, M. Chiewanichakorn and A.J. Aref, 9/21/06 (PB2007-106986).

MCEER-06-0011 "A Study of the Coupled Horizontal-Vertical Behavior of Elastomeric and Lead-Rubber Seismic Isolation Bearings," by G.P. Warn and A.S. Whittaker, 9/22/06 (PB2007-108679).

MCEER-06-0012 "Proceedings of the Fourth PRC-US Workshop on Seismic Analysis and Design of Special Bridges: Advancing Bridge Technologies in Research, Design, Construction and Preservation," Edited by L.C. Fan, G.C. Lee and L. Ziang, 10/12/06 (PB2007-109042).

MCEER-06-0013 "Cyclic Response and Low Cycle Fatigue Characteristics of Plate Steels," by P. Dusicka, A.M. Itani and I.G. Buckle, 11/1/06 06 (PB2007-106987).

MCEER-06-0014 "Proceedings of the Second US-Taiwan Bridge Engineering Workshop," edited by W.P. Yen, J. Shen, J-Y. Chen and M. Wang, 11/15/06 (PB2008-500041).

MCEER-06-0015 "User Manual and Technical Documentation for the REDARS^{TM} Import Wizard," by S. Cho, S. Ghosh, C.K. Huyck and S.D. Werner, 11/30/06 (PB2007-114766).

MCEER-06-0016 "Hazard Mitigation Strategy and Monitoring Technologies for Urban and Infrastructure Public Buildings: Proceedings of the China-US Workshops," edited by X.Y. Zhou, A.L. Zhang, G.C. Lee and M. Tong, 12/12/06 (PB2008-500018).

MCEER-07-0001 "Static and Kinetic Coefficients of Friction for Rigid Blocks," by C. Kafali, S. Fathali, M. Grigoriu and A.S. Whittaker, 3/20/07 (PB2007-114767).

MCEER-07-0002 "Hazard Mitigation Investment Decision Making: Organizational Response to Legislative Mandate," by L.A. Arendt, D.J. Alesch and W.J. Petak, 4/9/07 (PB2007-114768).

MCEER-07-0003 "Seismic Behavior of Bidirectional-Resistant Ductile End Diaphragms with Unbonded Braces in Straight or Skewed Steel Bridges," by O. Celik and M. Bruneau, 4/11/07 (PB2008-105141).

MCEER-07-0004 "Modeling Pile Behavior in Large Pile Groups Under Lateral Loading," by A.M. Dodds and G.R. Martin, 4/16/07(PB2008-105142).

MCEER-07-0005 "Experimental Investigation of Blast Performance of Seismically Resistant Concrete-Filled Steel Tube Bridge Piers," by S. Fujikura, M. Bruneau and D. Lopez-Garcia, 4/20/07 (PB2008-105143).

MCEER-07-0006 "Seismic Analysis of Conventional and Isolated Liquefied Natural Gas Tanks Using Mechanical Analogs," by I.P. Christovasilis and A.S. Whittaker, 5/1/07, not available.

MCEER-07-0007 "Experimental Seismic Performance Evaluation of Isolation/Restraint Systems for Mechanical Equipment – Part 1: Heavy Equipment Study," by S. Fathali and A. Filiatrault, 6/6/07 (PB2008-105144).

MCEER-07-0008 "Seismic Vulnerability of Timber Bridges and Timber Substructures," by A.A. Sharma, J.B. Mander, I.M. Friedland and D.R. Allicock, 6/7/07 (PB2008-105145).

MCEER-07-0009 "Experimental and Analytical Study of the XY-Friction Pendulum (XY-FP) Bearing for Bridge Applications," by C.C. Marin-Artieda, A.S. Whittaker and M.C. Constantinou, 6/7/07 (PB2008-105191).

MCEER-07-0010 "Proceedings of the PRC-US Earthquake Engineering Forum for Young Researchers," Edited by G.C. Lee and X.Z. Qi, 6/8/07 (PB2008-500058).

MCEER-07-0011 "Design Recommendations for Perforated Steel Plate Shear Walls," by R. Purba and M. Bruneau, 6/18/07, (PB2008-105192).

MCEER-07-0012 "Performance of Seismic Isolation Hardware Under Service and Seismic Loading," by M.C. Constantinou, A.S. Whittaker, Y. Kalpakidis, D.M. Fenz and G.P. Warn, 8/27/07, (PB2008-105193).

MCEER-07-0013 "Experimental Evaluation of the Seismic Performance of Hospital Piping Subassemblies," by E.R. Goodwin, E. Maragakis and A.M. Itani, 9/4/07, (PB2008-105194).

MCEER-07-0014 "A Simulation Model of Urban Disaster Recovery and Resilience: Implementation for the 1994 Northridge Earthquake," by S. Miles and S.E. Chang, 9/7/07, (PB2008-106426).

MCEER-07-0015 "Statistical and Mechanistic Fragility Analysis of Concrete Bridges," by M. Shinozuka, S. Banerjee and S-H. Kim, 9/10/07, (PB2008-106427).

MCEER-07-0016 "Three-Dimensional Modeling of Inelastic Buckling in Frame Structures," by M. Schachter and AM. Reinhorn, 9/13/07, (PB2008-108125).

MCEER-07-0017 "Modeling of Seismic Wave Scattering on Pile Groups and Caissons," by I. Po Lam, H. Law and C.T. Yang, 9/17/07 (PB2008-108150).

MCEER-07-0018 "Bridge Foundations: Modeling Large Pile Groups and Caissons for Seismic Design," by I. Po Lam, H. Law and G.R. Martin (Coordinating Author), 12/1/07 (PB2008-111190).

MCEER-07-0019 "Principles and Performance of Roller Seismic Isolation Bearings for Highway Bridges," by G.C. Lee, Y.C. Ou, Z. Liang, T.C. Niu and J. Song, 12/10/07 (PB2009-110466).

MCEER-07-0020 "Centrifuge Modeling of Permeability and Pinning Reinforcement Effects on Pile Response to Lateral Spreading," by L.L Gonzalez-Lagos, T. Abdoun and R. Dobry, 12/10/07 (PB2008-111191).

MCEER-07-0021 "Damage to the Highway System from the Pisco, Perú Earthquake of August 15, 2007," by J.S. O'Connor, L. Mesa and M. Nykamp, 12/10/07, (PB2008-108126).

MCEER-07-0022 "Experimental Seismic Performance Evaluation of Isolation/Restraint Systems for Mechanical Equipment – Part 2: Light Equipment Study," by S. Fathali and A. Filiatrault, 12/13/07 (PB2008-111192).

MCEER-07-0023 "Fragility Considerations in Highway Bridge Design," by M. Shinozuka, S. Banerjee and S.H. Kim, 12/14/07 (PB2008-111193).

MCEER-07-0024 "Performance Estimates for Seismically Isolated Bridges," by G.P. Warn and A.S. Whittaker, 12/30/07 (PB2008-112230).

MCEER-08-0001 "Seismic Performance of Steel Girder Bridge Superstructures with Conventional Cross Frames," by L.P. Carden, A.M. Itani and I.G. Buckle, 1/7/08, (PB2008-112231).

MCEER-08-0002 "Seismic Performance of Steel Girder Bridge Superstructures with Ductile End Cross Frames with Seismic Isolators," by L.P. Carden, A.M. Itani and I.G. Buckle, 1/7/08 (PB2008-112232).

MCEER-08-0003 "Analytical and Experimental Investigation of a Controlled Rocking Approach for Seismic Protection of Bridge Steel Truss Piers," by M. Pollino and M. Bruneau, 1/21/08 (PB2008-112233).

MCEER-08-0004 "Linking Lifeline Infrastructure Performance and Community Disaster Resilience: Models and Multi-Stakeholder Processes," by S.E. Chang, C. Pasion, K. Tatebe and R. Ahmad, 3/3/08 (PB2008-112234).

MCEER-08-0005 "Modal Analysis of Generally Damped Linear Structures Subjected to Seismic Excitations," by J. Song, Y-L. Chu, Z. Liang and G.C. Lee, 3/4/08 (PB2009-102311).

MCEER-08-0006 "System Performance Under Multi-Hazard Environments," by C. Kafali and M. Grigoriu, 3/4/08 (PB2008-112235).

MCEER-08-0007 "Mechanical Behavior of Multi-Spherical Sliding Bearings," by D.M. Fenz and M.C. Constantinou, 3/6/08 (PB2008-112236).

MCEER-08-0008 "Post-Earthquake Restoration of the Los Angeles Water Supply System," by T.H.P. Tabucchi and R.A. Davidson, 3/7/08 (PB2008-112237).

MCEER-08-0009 "Fragility Analysis of Water Supply Systems," by A. Jacobson and M. Grigoriu, 3/10/08 (PB2009-105545).

MCEER-08-0010 "Experimental Investigation of Full-Scale Two-Story Steel Plate Shear Walls with Reduced Beam Section Connections," by B. Qu, M. Bruneau, C-H. Lin and K-C. Tsai, 3/17/08 (PB2009-106368).

MCEER-08-0011 "Seismic Evaluation and Rehabilitation of Critical Components of Electrical Power Systems," S. Ersoy, B. Feizi, A. Ashrafi and M. Ala Saadeghvaziri, 3/17/08 (PB2009-105546).

MCEER-08-0012 "Seismic Behavior and Design of Boundary Frame Members of Steel Plate Shear Walls," by B. Qu and M. Bruneau, 4/26/08 . (PB2009-106744).

MCEER-08-0013 "Development and Appraisal of a Numerical Cyclic Loading Protocol for Quantifying Building System Performance," by A. Filiatrault, A. Wanitkorkul and M. Constantinou, 4/27/08 (PB2009-107906).

MCEER-08-0014 "Structural and Nonstructural Earthquake Design: The Challenge of Integrating Specialty Areas in Designing Complex, Critical Facilities," by W.J. Petak and D.J. Alesch, 4/30/08 (PB2009-107907).

MCEER-08-0015 "Seismic Performance Evaluation of Water Systems," by Y. Wang and T.D. O'Rourke, 5/5/08 (PB2009-107908).

MCEER-08-0016 "Seismic Response Modeling of Water Supply Systems," by P. Shi and T.D. O'Rourke, 5/5/08 (PB2009-107910).

MCEER-08-0017 "Numerical and Experimental Studies of Self-Centering Post-Tensioned Steel Frames," by D. Wang and A. Filiatrault, 5/12/08 (PB2009-110479).

MCEER-08-0018 "Development, Implementation and Verification of Dynamic Analysis Models for Multi-Spherical Sliding Bearings," by D.M. Fenz and M.C. Constantinou, 8/15/08 (PB2009-107911).

MCEER-08-0019 "Performance Assessment of Conventional and Base Isolated Nuclear Power Plants for Earthquake Blast Loadings," by Y.N. Huang, A.S. Whittaker and N. Luco, 10/28/08 (PB2009-107912).

MCEER-08-0020 "Remote Sensing for Resilient Multi-Hazard Disaster Response – Volume I: Introduction to Damage Assessment Methodologies," by B.J. Adams and R.T. Eguchi, 11/17/08 (PB2010-102695).

MCEER-08-0021 "Remote Sensing for Resilient Multi-Hazard Disaster Response – Volume II: Counting the Number of Collapsed Buildings Using an Object-Oriented Analysis: Case Study of the 2003 Bam Earthquake," by L. Gusella, C.K. Huyck and B.J. Adams, 11/17/08 (PB2010-100925).

MCEER-08-0022 "Remote Sensing for Resilient Multi-Hazard Disaster Response – Volume III: Multi-Sensor Image Fusion Techniques for Robust Neighborhood-Scale Urban Damage Assessment," by B.J. Adams and A. McMillan, 11/17/08 (PB2010-100926).

MCEER-08-0023 "Remote Sensing for Resilient Multi-Hazard Disaster Response – Volume IV: A Study of Multi-Temporal and Multi-Resolution SAR Imagery for Post-Katrina Flood Monitoring in New Orleans," by A. McMillan, J.G. Morley, B.J. Adams and S. Chesworth, 11/17/08 (PB2010-100927).

MCEER-08-0024 "Remote Sensing for Resilient Multi-Hazard Disaster Response – Volume V: Integration of Remote Sensing Imagery and VIEWS^{TM} Field Data for Post-Hurricane Charley Building Damage Assessment," by J.A. Womble, K. Mehta and B.J. Adams, 11/17/08 (PB2009-115532).

MCEER-08-0025 "Building Inventory Compilation for Disaster Management: Application of Remote Sensing and Statistical Modeling," by P. Sarabandi, A.S. Kiremidjian, R.T. Eguchi and B. J. Adams, 11/20/08 (PB2009-110484).

MCEER-08-0026 "New Experimental Capabilities and Loading Protocols for Seismic Qualification and Fragility Assessment of Nonstructural Systems," by R. Retamales, G. Mosqueda, A. Filiatrault and A. Reinhorn, 11/24/08 (PB2009-110485).

MCEER-08-0027 "Effects of Heating and Load History on the Behavior of Lead-Rubber Bearings," by I.V. Kalpakidis and M.C. Constantinou, 12/1/08 (PB2009-115533).

MCEER-08-0028 "Experimental and Analytical Investigation of Blast Performance of Seismically Resistant Bridge Piers," by S.Fujikura and M. Bruneau, 12/8/08 (PB2009-115534).

MCEER-08-0029 "Evolutionary Methodology for Aseismic Decision Support," by Y. Hu and G. Dargush, 12/15/08.

MCEER-08-0030 "Development of a Steel Plate Shear Wall Bridge Pier System Conceived from a Multi-Hazard Perspective," by D. Keller and M. Bruneau, 12/19/08 (PB2010-102696).

MCEER-09-0001 "Modal Analysis of Arbitrarily Damped Three-Dimensional Linear Structures Subjected to Seismic Excitations," by Y.L. Chu, J. Song and G.C. Lee, 1/31/09 (PB2010-100922).

MCEER-09-0002 "Air-Blast Effects on Structural Shapes," by G. Ballantyne, A.S. Whittaker, A.J. Aref and G.F. Dargush, 2/2/09 (PB2010-102697).

MCEER-09-0003 "Water Supply Performance During Earthquakes and Extreme Events," by A.L. Bonneau and T.D. O'Rourke, 2/16/09 (PB2010-100923).

MCEER-09-0004 "Generalized Linear (Mixed) Models of Post-Earthquake Ignitions," by R.A. Davidson, 7/20/09 (PB2010-102698).

MCEER-09-0005 "Seismic Testing of a Full-Scale Two-Story Light-Frame Wood Building: NEESWood Benchmark Test," by I.P. Christovasilis, A. Filiatrault and A. Wanitkorkul, 7/22/09 (PB2012-102401).

MCEER-09-0006 "IDARC2D Version 7.0: A Program for the Inelastic Damage Analysis of Structures," by A.M. Reinhorn, H. Roh, M. Sivaselvan, S.K. Kunnath, R.E. Valles, A. Madan, C. Li, R. Lobo and Y.J. Park, 7/28/09 (PB2010-103199).

MCEER-09-0007 "Enhancements to Hospital Resiliency: Improving Emergency Planning for and Response to Hurricanes," by D.B. Hess and L.A. Arendt, 7/30/09 (PB2010-100924).

MCEER-09-0008 "Assessment of Base-Isolated Nuclear Structures for Design and Beyond-Design Basis Earthquake Shaking," by Y.N. Huang, A.S. Whittaker, R.P. Kennedy and R.L. Mayes, 8/20/09 (PB2010-102699).

MCEER-09-0009 "Quantification of Disaster Resilience of Health Care Facilities," by G.P. Cimellaro, C. Fumo, A.M Reinhorn and M. Bruneau, 9/14/09 (PB2010-105384).

MCEER-09-0010 "Performance-Based Assessment and Design of Squat Reinforced Concrete Shear Walls," by C.K. Gulec and A.S. Whittaker, 9/15/09 (PB2010-102700).

MCEER-09-0011 "Proceedings of the Fourth US-Taiwan Bridge Engineering Workshop," edited by W.P. Yen, J.J. Shen, T.M. Lee and R.B. Zheng, 10/27/09 (PB2010-500009).

MCEER-09-0012 "Proceedings of the Special International Workshop on Seismic Connection Details for Segmental Bridge Construction," edited by W. Phillip Yen and George C. Lee, 12/21/09 (PB2012-102402).

MCEER-10-0001 "Direct Displacement Procedure for Performance-Based Seismic Design of Multistory Woodframe Structures," by W. Pang and D. Rosowsky, 4/26/10 (PB2012-102403).

MCEER-10-0002 "Simplified Direct Displacement Design of Six-Story NEESWood Capstone Building and Pre-Test Seismic Performance Assessment," by W. Pang, D. Rosowsky, J. van de Lindt and S. Pei, 5/28/10 (PB2012-102404).

MCEER-10-0003 "Integration of Seismic Protection Systems in Performance-Based Seismic Design of Woodframed Structures," by J.K. Shinde and M.D. Symans, 6/18/10 (PB2012-102405).

MCEER-10-0004 "Modeling and Seismic Evaluation of Nonstructural Components: Testing Frame for Experimental Evaluation of Suspended Ceiling Systems," by A.M. Reinhorn, K.P. Ryu and G. Maddaloni, 6/30/10 (PB2012-102406).

MCEER-10-0005 "Analytical Development and Experimental Validation of a Structural-Fuse Bridge Pier Concept," by S. El-Bahey and M. Bruneau, 10/1/10 (PB2012-102407).

MCEER-10-0006 "A Framework for Defining and Measuring Resilience at the Community Scale: The PEOPLES Resilience Framework," by C.S. Renschler, A.E. Frazier, L.A. Arendt, G.P. Cimellaro, A.M. Reinhorn and M. Bruneau, 10/8/10 (PB2012-102408).

MCEER-10-0007 "Impact of Horizontal Boundary Elements Design on Seismic Behavior of Steel Plate Shear Walls," by R. Purba and M. Bruneau, 11/14/10 (PB2012-102409).

MCEER-10-0008 "Seismic Testing of a Full-Scale Mid-Rise Building: The NEESWood Capstone Test," by S. Pei, J.W. van de Lindt, S.E. Pryor, H. Shimizu, H. Isoda and D.R. Rammer, 12/1/10 (PB2012-102410).

MCEER-10-0009 "Modeling the Effects of Detonations of High Explosives to Inform Blast-Resistant Design," by P. Sherkar, A.S. Whittaker and A.J. Aref, 12/1/10 (PB2012-102411).

MCEER-10-0010 "L'Aquila Earthquake of April 6, 2009 in Italy: Rebuilding a Resilient City to Withstand Multiple Hazards," by G.P. Cimellaro, I.P. Christovasilis, A.M. Reinhorn, A. De Stefano and T. Kirova, 12/29/10.

MCEER-11-0001 "Numerical and Experimental Investigation of the Seismic Response of Light-Frame Wood Structures," by I.P. Christovasilis and A. Filiatrault, 8/8/11 (PB2012-102412).

MCEER-11-0002 "Seismic Design and Analysis of a Precast Segmental Concrete Bridge Model," by M. Anagnostopoulou, A. Filiatrault and A. Aref, 9/15/11.

MCEER-11-0003 'Proceedings of the Workshop on Improving Earthquake Response of Substation Equipment," Edited by A.M. Reinhorn, 9/19/11 (PB2012-102413).

MCEER-11-0004 "LRFD-Based Analysis and Design Procedures for Bridge Bearings and Seismic Isolators," by M.C. Constantinou, I. Kalpakidis, A. Filiatrault and R.A. Ecker Lay, 9/26/11.

MCEER-11-0005 "Experimental Seismic Evaluation, Model Parameterization, and Effects of Cold-Formed Steel-Framed Gypsum Partition Walls on the Seismic Performance of an Essential Facility," by R. Davies, R. Retamales, G. Mosqueda and A. Filiatrault, 10/12/11.

MCEER-11-0006 "Modeling and Seismic Performance Evaluation of High Voltage Transformers and Bushings," by A.M. Reinhorn, K. Oikonomou, H. Roh, A. Schiff and L. Kempner, Jr., 10/3/11.

MCEER-11-0007 "Extreme Load Combinations: A Survey of State Bridge Engineers," by G.C. Lee, Z. Liang, J.J. Shen and J.S. O'Connor, 10/14/11.

MCEER-12-0001 "Simplified Analysis Procedures in Support of Performance Based Seismic Design," by Y.N. Huang and A.S. Whittaker.

MCEER-12-0002 "Seismic Protection of Electrical Transformer Bushing Systems by Stiffening Techniques," by M. Koliou, A. Filiatrault, A.M. Reinhorn and N. Oliveto, 6/1/12.

MCEER-12-0003 "Post-Earthquake Bridge Inspection Guidelines," by J.S. O'Connor and S. Alampalli, 6/8/12.

MCEER-12-0004 "Integrated Design Methodology for Isolated Floor Systems in Single-Degree-of-Freedom Structural Fuse Systems," by S. Cui, M. Bruneau and M.C. Constantinou, 6/13/12.

MCEER-12-0005 "Characterizing the Rotational Components of Earthquake Ground Motion," by D. Basu, A.S. Whittaker and M.C. Constantinou, 6/15/12.

MCEER-12-0006 "Bayesian Fragility for Nonstructural Systems," by C.H. Lee and M.D. Grigoriu, 9/12/12.

MCEER-12-0007 "A Numerical Model for Capturing the In-Plane Seismic Response of Interior Metal Stud Partition Walls," by R.L. Wood and T.C. Hutchinson, 9/12/12.

MCEER-12-0008 "Assessment of Floor Accelerations in Yielding Buildings," by J.D. Wieser, G. Pekcan, A.E. Zaghi, A.M. Itani and E. Maragakis, 10/5/12.

MCEER-13-0001 "Experimental Seismic Study of Pressurized Fire Sprinkler Piping Systems," by Y. Tian, A. Filiatrault and G. Mosqueda, 4/8/13.

MCEER-13-0002 "Enhancing Resource Coordination for Multi-Modal Evacuation Planning," by D.B. Hess, B.W. Conley and C.M. Farrell, 2/8/13.

MCEER-13-0003 "Seismic Response of Base Isolated Buildings Considering Pounding to Moat Walls," by A. Masroor and G. Mosqueda, 2/26/13.

MCEER-13-0004 "Seismic Response Control of Structures Using a Novel Adaptive Passive Negative Stiffness Device," by D.T.R. Pasala, A.A. Sarlis, S. Nagarajaiah, A.M. Reinhorn, M.C. Constantinou and D.P. Taylor, 6/10/13.

MCEER-13-0005 "Negative Stiffness Device for Seismic Protection of Structures," by A.A. Sarlis, D.T.R. Pasala, M.C. Constantinou, A.M. Reinhorn, S. Nagarajaiah and D.P. Taylor, 6/12/13.

MCEER-13-0006 "Emilia Earthquake of May 20, 2012 in Northern Italy: Rebuilding a Resilient Community to Withstand Multiple Hazards," by G.P. Cimellaro, M. Chiriatti, A.M. Reinhorn and L. Tirca, June 30, 2013.

MCEER-13-0007 "Precast Concrete Segmental Components and Systems for Accelerated Bridge Construction in Seismic Regions," by A.J. Aref, G.C. Lee, Y.C. Ou and P. Sideris, with contributions from K.C. Chang, S. Chen, A. Filiatrault and Y. Zhou, June 13, 2013.

MCEER-13-0008 "A Study of U.S. Bridge Failures (1980-2012)," by G.C. Lee, S.B. Mohan, C. Huang and B.N. Fard, June 15, 2013.

MCEER-13-0009 "Development of a Database Framework for Modeling Damaged Bridges," by G.C. Lee, J.C. Qi and C. Huang, June 16, 2013.

MCEER-13-0010 "Model of Triple Friction Pendulum Bearing for General Geometric and Frictional Parameters and for Uplift Conditions," by A.A. Sarlis and M.C. Constantinou, July 1, 2013.

MCEER-13-0011 "Shake Table Testing of Triple Friction Pendulum Isolators under Extreme Conditions," by A.A. Sarlis, M.C. Constantinou and A.M. Reinhorn, July 2, 2013.

MCEER-13-0012 "Theoretical Framework for the Development of MH-LRFD," by G.C. Lee (coordinating author), H.A Capers, Jr., C. Huang, J.M. Kulicki, Z. Liang, T. Murphy, J.J.D. Shen, M. Shinozuka and P.W.H. Yen, July 31, 2013.

MCEER-13-0013 "Seismic Protection of Highway Bridges with Negative Stiffness Devices," by N.K.A. Attary, M.D. Symans, S. Nagarajaiah, A.M. Reinhorn, M.C. Constantinou, A.A. Sarlis, D.T.R. Pasala, and D.P. Taylor, September 3, 2014.

MCEER-14-0001 "Simplified Seismic Collapse Capacity-Based Evaluation and Design of Frame Buildings with and without Supplemental Damping Systems," by M. Hamidia, A. Filiatrault, and A. Aref, May 19, 2014.

MCEER-14-0002 "Comprehensive Analytical Seismic Fragility of Fire Sprinkler Piping Systems," by Siavash Soroushian, Emmanuel "Manos" Maragakis, Arash E. Zaghi, Alicia Echevarria, Yuan Tian and Andre Filiatrault, August 26, 2014.

MCEER-14-0003 "Hybrid Simulation of the Seismic Response of a Steel Moment Frame Building Structure through Collapse," by M. Del Carpio Ramos, G. Mosqueda and D.G. Lignos, October 30, 2014.

MCEER-14-0004 "Blast and Seismic Resistant Concrete-Filled Double Skin Tubes and Modified Steel Jacketed Bridge Columns," by P.P. Fouche and M. Bruneau, June 30, 2015.

MCEER-14-0005 "Seismic Performance of Steel Plate Shear Walls Considering Various Design Approaches," by R. Purba and M. Bruneau, October 31, 2014.

MCEER-14-0006 "Air-Blast Effects on Civil Structures," by Jinwon Shin, Andrew S. Whittaker, Amjad J. Aref and David Cormie, October 30, 2014.

MCEER-14-0007 "Seismic Performance Evaluation of Precast Girders with Field-Cast Ultra High Performance Concrete (UHPC) Connections," by G.C. Lee, C. Huang, J. Song, and J. S. O'Connor, July 31, 2014.

MCEER-14-0008 "Post-Earthquake Fire Resistance of Ductile Concrete-Filled Double-Skin Tube Columns," by Reza Imani, Gilberto Mosqueda and Michel Bruneau, December 1, 2014.

MCEER-14-0009 "Cyclic Inelastic Behavior of Concrete Filled Sandwich Panel Walls Subjected to In-Plane Flexure," by Y. Alzeni and M. Bruneau, December 19, 2014.

MCEER-14-0010 "Analytical and Experimental Investigation of Self-Centering Steel Plate Shear Walls," by D.M. Dowden and M. Bruneau, December 19, 2014.

MCEER-15-0001 "Seismic Analysis of Multi-story Unreinforced Masonry Buildings with Flexible Diaphragms," by J. Aleman, G. Mosqueda and A.S. Whittaker, June 12, 2015.

ISSN 1520-295X